BRAIN ABNORMALITIES DUE TO GENETIC ALTERATIONS OR DEVELOPMENTAL EXPOSURE TO ENVIRONMENTAL FACTORS

EDITED BY: Kazuhiko Sawada, Atsushi Yoshiki and Shigeyoshi Saito

PUBLISHED IN: Frontiers in Neuroscience

frontiers Research Topics

frontiers

ISSN 1664-8714
ISBN 978-2-88976-876-9
DOI 10.3389/978-2-88976-876-9

About Frontiers

Frontiers is more than just an open-access publisher of scholarly articles: it is a pioneering approach to the world of academia, radically improving the way scholarly research is managed. The grand vision of Frontiers is a world where all people have an equal opportunity to seek, share and generate knowledge. Frontiers provides immediate and permanent online open access to all its publications, but this alone is not enough to realize our grand goals.

Frontiers Journal Series

The Frontiers Journal Series is a multi-tier and interdisciplinary set of open-access, online journals, promising a paradigm shift from the current review, selection and dissemination processes in academic publishing. All Frontiers journals are driven by researchers for researchers; therefore, they constitute a service to the scholarly community. At the same time, the Frontiers Journal Series operates on a revolutionary invention, the tiered publishing system, initially addressing specific communities of scholars, and gradually climbing up to broader public understanding, thus serving the interests of the lay society, too.

Dedication to Quality

Each Frontiers article is a landmark of the highest quality, thanks to genuinely collaborative interactions between authors and review editors, who include some of the world's best academicians. Research must be certified by peers before entering a stream of knowledge that may eventually reach the public - and shape society; therefore, Frontiers only applies the most rigorous and unbiased reviews.
Frontiers revolutionizes research publishing by freely delivering the most outstanding research, evaluated with no bias from both the academic and social point of view. By applying the most advanced information technologies, Frontiers is catapulting scholarly publishing into a new generation.

What are Frontiers Research Topics?

Frontiers Research Topics are very popular trademarks of the Frontiers Journals Series: they are collections of at least ten articles, all centered on a particular subject. With their unique mix of varied contributions from Original Research to Review Articles, Frontiers Research Topics unify the most influential researchers, the latest key findings and historical advances in a hot research area! Find out more on how to host your own Frontiers Research Topic or contribute to one as an author by contacting the Frontiers Editorial Office: frontiersin.org/about/contact

BRAIN ABNORMALITIES DUE TO GENETIC ALTERATIONS OR DEVELOPMENTAL EXPOSURE TO ENVIRONMENTAL FACTORS

Topic Editors:
Kazuhiko Sawada, Tsukuba International University, Japan
Atsushi Yoshiki, RIKEN BioResource Research Center (BRC), Japan
Shigeyoshi Saito, Osaka University, Japan

Citation: Sawada, K., Yoshiki, A., Saito, S., eds. (2022). Brain abnormalities due to genetic alterations or developmental exposure to environmental factors. Lausanne: Frontiers Media SA. doi: 10.3389/978-2-88976-876-9

Table of Contents

frontiers | Frontiers in Neuroscience

TYPE Editorial
PUBLISHED 26 July 2022
DOI 10.3389/fnins.2022.944861

OPEN ACCESS

EDITED AND REVIEWED BY
Josef P. Kapfhammer,
University of Basel, Switzerland

*CORRESPONDENCE
Kazuhiko Sawada
k-sawada@tius.ac.jp

SPECIALTY SECTION
This article was submitted to Neurodevelopment, a section of the journal Frontiers in Neuroscience

RECEIVED 16 May 2022
ACCEPTED 10 June 2022
PUBLISHED 26 July 2022

CITATION
Sawada K, Yoshiki A and Saito S (2022) Editorial: Brain abnormalities due to genetic alterations or developmental exposure to environmental factors. *Front. Neurosci.* 16:944861. doi: 10.3389/fnins.2022.944861

Editorial: Brain abnormalities due to genetic alterations or developmental exposure to environmental factors

Kazuhiko Sawada[1,2]*, Atsushi Yoshiki[2] and Shigeyoshi Saito[3,4]

[1]Department of Nutrition, Faculty of Medical and Health Sciences, Tsukuba International University, Tsuchiura, Japan, [2]Experimental Animal Division, RIKEN BioResource Research Center, Tsukuba, Japan, [3]Division of Health Sciences, Department of Medical Physics and Engineering, Graduate School of Medicine, Osaka University, Suita, Japan, [4]Department of Advanced Medical Technologies, National Cerebral and Cardiovascular Center, Research Institute, Suita, Japan

KEYWORDS

neurodevelopmental disorders, brain, cerebral cortex, cerebellum, neurogenesis, maldevelopment, epigenesis

Editorial on the Research Topic
Brain abnormalities due to genetic alterations or developmental exposure to environmental factors

The structural and functional development of the brain is altered by many genetic and environmental factors, including drugs, industrial chemicals, nutrition, infections, irradiation, prenatal stress, and maternal separation. These factors can influence various neurodevelopmental events, such as neurogenesis, neural differentiation, neural migration, apoptosis, axonal connections, and synaptogenesis, which can be triggered directly or *via* epigenetic dysregulation and can often cause irreversible changes in the brain. This Research Topic on "*Brain Abnormalities due to Genetic Alterations or Developmental Exposure to Environmental Factors*" comprises 12 papers published in Frontiers in Neuroscience, including three review articles and nine original articles focusing on the brain development abnormalities caused by various genetic and environmental factors.

Many studies in this research area have focused on the structural and functional maldevelopment of the brain in animal models for neurodevelopmental disorders. These papers emphasize multifaceted perspectives on maldevelopmental changes in the brain common to different neurodevelopmental disorders, studied using various research strategies. A review by Uchida and Suzuki mentioned the histoarchitecture and altered chemical phenotypes of neurons in the cerebrum in congenital hypothyroidism. The decreased parvalbumin expression in cortical neurons, shown in several mouse models of hypothyroidism, was reminiscent of the maldevelopment of cortical phenotypes in autism spectrum disorder (ASD) and schizophrenia. Original articles by Sethi et al. and Stietz et al. reveal that the behavioral characteristics and dendritic morphogenesis in the cerebrum were altered depending on the sex and neuronal

Ca^{2+} signaling-related gene variants in mice with developmental exposure to an endocrine disruptor, polychlorinated biphenyl (PCB). Since developmental PCB exposure confers a risk of neurodevelopmental disorders, including ASD and attention deficit hyperactivity disorder (ADHD), individual variabilities in genetic characteristics may modify the clinical phenotypes of these neurodevelopmental disorders. An original article by Zhou et al. reported that social interaction deficits were improved by modulating vasopressin pathways in ASD model rats developmentally exposed to valproic acid (VPA). These findings indicate the possibility of a clinical application of arginine vasopressin treatment to improve behavioral symptoms in patients with ASD. A review article by Ossola and Kalebic cited the involvement of subventricular zone (SVZ) progenitors in the malformation of cortical development in neurodevelopmental disorders. In particular, the proliferation and polarity of progenitors are key factors that are disrupted in the malformation of cortical development in gyrencephalic mammals. This hypothesis is supported by previous studies, which showed that manipulations of SVZ progenitor proliferation alter cortical folding (Rabe et al., 1985; Masuda et al., 2015; Sawada et al., 2021). An original article by Sawada et al. reinforces the supposition that the modification of neuronal progenitor proliferation is involved in brain maldevelopment. They revealed that the fate of hippocampal dentate gyrus progenitors was manipulated by developmental exposure to VPA. This study is unique in that it used ferrets as experimental animals as they are characterized by slow development and maturation of the brain, sustaining cerebral and cerebellar neurogenesis until early postnatal life, which is reminiscent of humans. The findings, along with other studies (Fujimura et al., 2016; Lauber et al., 2016; Sawada et al., 2021) facilitate a comprehensive understanding of brain maldevelopment in VPA-exposed ASD models. In an epidemiological study conducted by Deng et al., factors contributing to ADHD susceptibility have been epidemiologically identified in preschool-aged children in Beijing and Tangshan City. Notably, this study indicated that parental influences such as smoking, breastfeeding, and patience, during the prenatal and early postnatal periods, may increase the risk of ADHD susceptibility.

Other studies in this Research Topic focus on the impact of particular molecules or genes on brain maldevelopment. A review article by Hawkes summarizes the deformations of the cerebellar zone-and-stripe patterns in mice with spontaneous gene mutations or gene manipulations. We can study the cerebellar zone-and-stripe development that is organized by the interplay of two distinct developmental pathways, one for inhibitory Purkinje neurons and the second for excitatory granular neurons, by focusing on particular genes. An original article by Shabanipour et al. showed two alternative suppositions for the roles of neural cell adhesion molecule 1 in the inhibitory Purkinje cell developmental pathway. One is excessive Purkinje cell migration along the Bergmann glia, and the other is Purkinje cell monolayering. Original articles by Sun et al. and Wang et al. assessed the effect of gene knockout for *Plppr5*, a subclass of the lipid phosphate phosphatase superfamily, on developmental seizure-induced late-onset hypersensitivity and hypoxia-ischemia-induced cortical damage with long-term excitability. These changes may be mediated by the disruption of zinc- and mitochondria-dependent metabolic pathways. These findings suggest that different environmental stimuli for specific genes during development can result in diverse brain abnormalities. An original article by Tian et al. reported primary visual cortex atrophy with the reorganization of functional connectivity accompanied by strengthened connectivity to the default mode network in patients with chronic Leber's hereditary optic neuropathy. This report placed a focus on hereditary diseases carrying mutations in mitochondrial DNA in terms of "Brain Abnormalities due to Genetic Alterations," which is one of the themes of this Research Topic.

The articles on "models for neurodevelopmental disorders" and "impacts of particular molecules and/or genes" in brain maldevelopment have facilitated our understanding of the themes of the Research Topic, "*Brain Abnormalities due to Genetic Alterations or Developmental Exposure to Environmental Factors*." We hope that these findings will provide readers with new insights and baselines for investigating the normal and abnormal development of mammalian brain structures and functions.

Author contributions

All authors listed have made a substantial, direct, and intellectual contribution to the work and approved it for publication.

Acknowledgments

We wish to thank all authors, reviewers, and editors who contributed to this Research Topic.

Conflict of interest

The authors declare that the research was conducted in the absence of any commercial or financial relationships that could be construed as a potential conflict of interest.

Publisher's note

All claims expressed in this article are solely those of the authors and do not necessarily represent those of their affiliated

organizations, or those of the publisher, the editors and the reviewers. Any product that may be evaluated in this article, or claim that may be made by its manufacturer, is not guaranteed or endorsed by the publisher.

References

Fujimura, K., Mitsuhashi, T., Shibata, S., Shimozato, S., and Takahashi, T. (2016). *In utero* exposure to valproic acid induces neocortical dysgenesis via dysregulation of neural progenitor cell proliferation/differentiation. *J. Neurosci.* 36, 10908–10919. doi: 10.1523/JNEUROSCI.0229-16.2016

Lauber, E., Filice, F., and Schwaller, B. (2016). Prenatal valproate exposure differentially affects parvalbumin-expressing neurons and related circuits in the cortex and striatum of mice. *Front. Mol. Neurosci.* 9, 150. doi: 10.3389/fnmol.2016.00150

Masuda, K., Toda, T., and Shinmyo, Y. (2015). Pathophysiological analyses of cortical malformation using gyrencephalic mammals. *Sci. Rep.* 5, 15370. doi: 10.1038/srep15370

Rabe, A., Haddad, R., and Dumas,. R. (1985). Behavior and neurobehavioral teratology using the ferret. *Lab. Anim. Sci.* 35, 256–267.

Sawada, K., Kamiya, S., and Aoki, I. (2021). Neonatal valproic acid exposure produces altered gyrification related to increased parvalbumin-immunopositive neuron density with thickened sulcal floors. *PLoS ONE* 16, e0250262. doi: 10.1371/journal.pone.0250262

frontiers in Neuroscience

ORIGINAL RESEARCH
published: 27 August 2021
doi: 10.3389/fnins.2021.715555

PRG5 Knockout Precipitates Late-Onset Hypersusceptibility to Pilocarpine-Induced Juvenile Seizures by Exacerbating Hippocampal Zinc Signaling-Mediated Mitochondrial Damage

Dandan Wang[1,2†], Mei-fang Jin[1†], Lili Li[1†], Yueying Liu[3], Yuxiao Sun[1] and Hong Ni[1]*

[1] Division of Brain Science, Institute of Pediatric Research, Children's Hospital of Soochow University, Suzhou, China,
[2] Department of Pediatrics, First Affiliated Hospital of University of Science and Technology of China, Hefei, China,
[3] Department of Pediatrics, North Branch, Affiliated Hospital of Jiangnan University, Wuxi, China

OPEN ACCESS

Edited by:
Shigeyoshi Saito,
Osaka University, Japan

Reviewed by:
Ashwin S. Shetty,
Harvard University, United States
Mahmoud Elahdadi Salmani,
Damghan University, Iran

***Correspondence:**
Hong Ni
nhdoctor@163.com

† These authors have contributed equally to this work

Specialty section:
This article was submitted to Neurodevelopment, a section of the journal Frontiers in Neuroscience

Received: 27 May 2021
Accepted: 30 July 2021
Published: 27 August 2021

Citation:
Wang D, Jin M-f, Li L, Liu Y, Sun Y and Ni H (2021) PRG5 Knockout Precipitates Late-Onset Hypersusceptibility to Pilocarpine-Induced Juvenile Seizures by Exacerbating Hippocampal Zinc Signaling-Mediated Mitochondrial Damage. Front. Neurosci. 15:715555. doi: 10.3389/fnins.2021.715555

Introduction: Epileptogenesis is understood as the plastic process that produces a persistent reorganization of the brain's neural network after a precipitating injury (recurrent neonatal seizures, for instance) with a latent period, finally leading to neuronal hyperexcitability. Plasticity-related genes (PRGs), also known as lipid phosphate phosphatase-related proteins (PLPPRs), are regulators of mitochondrial membrane integrity and energy metabolism. This study was undertaken to determine whether PRG5 gene knockout contributes to the delayed hypersensitivity induced by developmental seizures and the aberrant sprouting of hippocampal mossy fibers, and to determine whether it is achieved through the mitochondrial pathway. Here, we developed a "twist" seizure model by coupling pilocarpine-induced juvenile seizures with later exposure to penicillin to test the long-term effects of PRG5 knockout on seizure latency through comparison with wild-type (WT) mice. Hippocampal mossy fiber sprouting (MFS) was detected by Timm staining. In order to clarify the mechanism of the adverse reactions triggered by PRG5 knockout, hippocampal HT22 neuronal cultures were exposed to glutamate, with or without PRG5 interference. Mitochondrial function, oxidative stress indicators and zinc ion content were detected.

Results: PRG5 gene knockout significantly reduced the seizure latency, and aggravated the lowered seizure threshold induced by developmental seizures. Besides, knockout of the PRG5 gene reduced the MFS scores to a certain extent. Furthermore, PRG5 gene silencing significantly increases the zinc ion content in hippocampal neurons, impairs

neuronal activity and mitochondrial function, and exacerbates glutamate-induced oxidative stress damage.

Conclusion: In summary, PRG5 KO is associated with significantly greater hypersusceptibility to juvenile seizures in PRG5$^{(-/-)}$ mice compared with WT mice. These effects may be related to the hippocampal zinc signaling. The effects do not appear to be related to changes in MFS because KO mice with juvenile seizures had the shortest seizure latencies but exhibited less MFS than WT mice with juvenile seizures.

Keywords: zinc signaling, hippocampal mossy fiber sprouting, hypersusceptibility, PRG5, developmental seizure

INTRODUCTION

Approximately 70 million people worldwide suffer from epilepsy, half of which are children, in whom the prevalence is approximately 0.5–0.8% (Málaga et al., 2019). Although many third-generation anti-seizure drugs (ASDs) (such as lacosamide, esikazepine acetate, brivaracetam, perampanel, retigabine, everolimus, and cannabidiol) have been included in clinical practice, only approximately 50% of newly diagnosed patients respond to the first anti-seizure drug prescribed, and approximately 30% of epilepsy patients continue to have seizures and have anti-seizure drug-refractory epilepsy (Málaga et al., 2019; Bresnahan et al., 2020). In pediatric neurology, many children who suffer from neonatal seizures develop epilepsy in adulthood. However, anticonvulsants aggravate brain damage, such as white matter damage (Kaushal et al., 2016). In recent years, significant progress has been made in understanding the effects of non-anticonvulsant drug treatment on epilepsy, particularly a ketogenic diet (KD) and autophagy modulators. The hippocampal phospholipase signaling pathway, especially the PRG family (plasticity-related genes, PRGs), may be a target for the protection of KD or autophagy inhibitors against long-term brain damage after developmental seizures (Ling et al., 2019; Zheng et al., 2020).

PRGs is a subclass of the lipid phosphate phosphatase (LPP-) superfamily (PRGs/LRPs, PRG1-5 or LPA1-5, Plppr1-5), which mediates lipid phosphate phosphatase activity and neuronal plasticity (Brauer and Nitsch, 2008; Trimbuch et al., 2009). PRG1 regulates bioactive lipids of postsynaptic density, is highly expressed at postsynaptic density during development and regeneration, and modulates the level of synaptic lysophosphatidic acid (LPA) (Brauer and Nitsch, 2008; Petzold et al., 2016). Notably, Trimbuch et al. (2009) described seizure generation in mice that lack PRG1. They found that deletion of PRG-1 in mice led to epileptic seizures and augmentation of EPSCs, suggesting an important role of PRG-1 in the modulatory control of hippocampal excitability related to epilepsy and brain damage. Our previous study also found that PRG-1 and ZnT-3 mRNA protein levels in the hippocampus were upregulated at 14 days after flurothyl-induced neonatal seizures, which is in parallel with seizure-induced hippocampal mossy fiber sprouting (MFS) and cognitive deficits (Ni et al., 2009, 2010). Subsequently, we examined the effects of E-64d (an autophagy inhibitor) on hippocampal aberrant MFS following penicillin-induced recurrent epilepticus. The results showed that, compared with the seizure group (EXP1) not treated with E64d, not only PRG1 but also PRG5 mRNA levels in the hippocampus of seizure rats pretreated with E-64d (EXP2) were significantly downregulated, which was in parallel with reduced MFS in the hippocampus (Ni et al., 2013). The cloning of PRG5 (also known as Plppr5) was reported by Broggini et al. (2010). PRG5 is only distributed in the nervous system. PRG5 is distributed in the plasma membrane of neurons and is specifically involved in filopodia and axon growth, as well as dendritic spine formation. siRNA-mediated knockdown of PRG5 hinders the growth of axons and interferes with the formation of filopodia (Broggini et al., 2010). However, the role of PRG5 in epileptogenesis, especially developmental-induced mossy fiber spouting and seizure susceptibility, has not been extensively studied.

Epileptogenesis is the plastic process that refers to the development and extension of tissue capable of generating spontaneous seizures, resulting in the development of an epileptic condition and/or progression of epilepsy after the condition is established. During epileptogenesis, the hippocampus, as the initiation area of many epilepsy patients, undergoes plasticity changes, which are mainly manifested in mossy fiber sprouting (MFS) and alterations in dendritic branching, spine density and shape (Sierra et al., 2015). Hippocampal MFS induced by developmental seizures is a typical phenomenon of aberrant axon growth in response to seizures, which could be detected by using a zinc-detecting histologic technique (Timm). Interestingly, MFS is an active phenomenon that is reversible. Mitophagy-mediated zinc homeostasis via mitochondrial activation may be a potential mechanism (Ni et al., 2016, 2019; Li et al., 2018). In addition, our previous studies have shown that developmental seizures cause long-term abnormal expression of hippocampal zinc transporters and plasticity-related genes (PRG1 and PRG-3), and the high correlation between these molecules is also destroyed (Ni et al., 2009, 2010; Tian et al., 2016), indicating that both PRG and zinc signaling are involved in the long-term hippocampal metabolic abnormalities after neonatal seizures. However, the effect of PRG5 on seizure-induced brain damage and its relationship with zinc ion signals remain unclear. Therefore, we also further revealed the internal connection between PRG5, mitochondrial damage and zinc ion signal through *in vitro* cell experiments. Here we report for the first time the segregation phenotype of PRG5$^{-/-}$ mice with seizure latency and aberrant sprouting of hippocampal mossy fibers. We performed a "twist" seizure model

to determine the seizure latency in PRG5$^{-/-}$ mice. Our results suggest a role for PRG5 and zinc signaling in the underlying mechanisms of epileptogenesis.

MATERIALS AND METHODS

Animal Preparation

The generation of PRG5 knockout mice was conducted at the Nanjing Biomedical Research Institute of Nanjing University (Nanjing, China). The gRNA was designed and transcribed *in vitro* using CRISPR/Cas9 technology. Then, Cas9 and gRNA were injected into fertilized mouse eggs at the same time (see **Table 1** for the sequence information for gRNA). The Cas9 protein binds to the target site under the guidance of gRNA, causing DNA double-strand breaks, resulting in the deletion of the base sequence of the target site and ultimately achieving systemic gene knockout (Sun et al., 2021). The strain backgrounds of PRG5 knockout mice and WT wild-type mice are both C57BL/6JNju (see **Table 2** for strain information of knockout mice).

We bred male heterozygous PRG5 knockout mice (PRG5±) and female heterozygous PRG5 knockout mice (PRG5±) in a 1:2 breeding cage. Both PRG5 knockout mice and littermate control wild-type mice were derived from the progeny of heterozygous PRG5 knockout mice. To identify whether the PRG5 protein is knocked out in KO mice, we first cut 3–5 mm tail tip tissue from the offspring mice born at the age of 3 days, and used PCR to perform genotype identification, and compare the size of the DNA products of the mice to be identified: Wild-type mice (PRG5$^{-/-}$) = 439 bp, homozygous PRG5 knockout mice (PRG5$^{-/-}$) = 414 bp, heterozygous PRG5 knockout mice (PRG5 ±) = 414 bp + 439 bp. (The process was completed by the Nanjing Institute of Biomedicine, Nanjing University) (Sun et al., 2021).

All procedures were reviewed and approved by the Institutional Animal Care and Use Committee of Soochow University. We took adequate measures to minimize animal suffering, and the sample size was based on the sample size used in our group's previous publications and other similar studies (Companys-Alemany et al., 2020).

Group Allocation

Thirty 25-day-old (P25) wild-type mice were randomly divided into two groups: WT group (n = 15) and WT + SE group (n = 15); another 30 25-day-old (P25) PRG5 knockout mice were randomly divided into 2 groups: KO group (n = 15) and KO + SE group (n = 15). (KO represents PRG5$^{-/-}$ mice without seizure injury, WT means wild-type mice without seizure injury, KO + SE represents PRG5$^{-/-}$ mice with seizure injury, WT + SE means wild-type mice with seizure injury).

A schematic diagram of the entire experiment is shown in **Figure 1**.

TABLE 1 | Sequence information of gRNA.

gRNA name	gRNA sequence	PAM
gRNAl	5′-ACCACTAGGCAG TAGAGACT-3′	GGG
gRNA2	5′-TGTGAGGACAATTGGCTCTA-3′	AGG
gRNA3	5′-GGG CTTTGTCGTGGGTG G C G-3′	GGG
gRNA4	5′-CACAGTCTCGTGGGAGGGCG-3′	GGG

TABLE 2 | Strain information of knockout mice.

Name	Code
Strain number	T004790
Source of strain	GemPharmatech Co., Ltd.
Strain name	B6/JNju-Plppr5em1Cd/Nju u
Strain background	C57BL/6JNJu
Strain type	Cas9-KO

Animal Model of Juvenile Seizure

The induction of juvenile seizures was performed as described previously (Ni et al., 2018). Each mouse in the WT + SE group and KO + SE group was injected with lithium chloride (127 mg/kg, i.p.) at P26. Then, after 24 h (P27), animals were injected with pilocarpine (320 mg/kg, i.p.) to induce juvenile seizure. Scopolamine methyl chloride hydrobromide was injected (1 mg/kg, i.p.) 30 min before the injection of pilocarpine to antagonize the peripheral effect of pilocarpine. The control mice in the WT group and KO group received saline injections at the same time and the same handling as the seizure groups. After the injection, the seizures were observed according to the Racine classification (Racine, 1972). Epileptic seizures reaching grade IV and above were considered successful induction, and the mice that did not reach grade IV were eliminated. All animals in the WT + SE group and KO + SE group reached Racine stage 4 or higher during the modeling process. After successful modeling, 12 survived in the WT + SE group (n = 12), and 10 survived in the KO + SE group (n = 10).

Seizure Latency

Seizure susceptibility was studied by exposing the mice to penicillin using a procedure modified from one previously described procedure (Ni et al., 2018). All mice from each group were injected with penicillin (5.1×10^6 U/kg/d, i.p.) on postnatal day 62. The time to the first seizure after penicillin injection was recorded, which was the seizure latency (min) (seizure latency). The observation time was 2 h.

Mice were anesthetized, and brains were removed for Timm staining/Western blotting as soon as the animals reached Racine Stage 4. Five mice in each group were randomly selected for Western blot detection, and five were used for Timm's staining.

Timm Staining

At the end of the seizure latency test on P62, five mice from each group were randomly selected and given i.p. injection of chloral hydrate at a dose of 1 ml/100 g. After the anesthesia was complete, each group was perfused through the heart with 0.9% saline followed in order by PBS solution, precooled Na2S-PBS solution, precooled 4% paraformaldehyde solution, and precooled Na2S-PBS solution. The method used for Timm

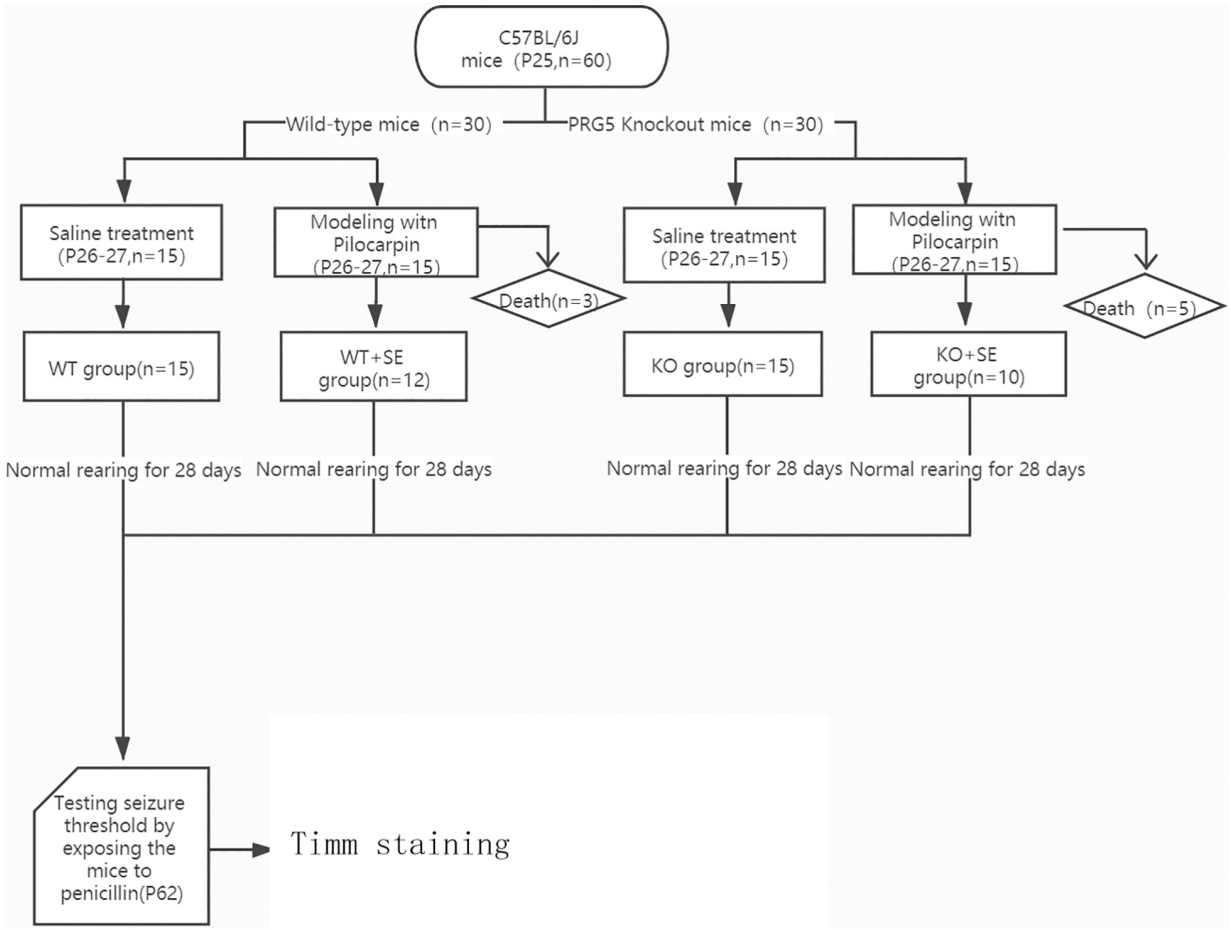

FIGURE 1 | Schematic diagram of the experimental process.

staining and semiquantitative scoring of the hippocampal CA3 area and dentate gyrus (DG) MFS has been described previously (Ni et al., 2009).

The person scoring the Timm staining was blind to the treatment group. The scoring criteria in the supragranular region of dentate gyrus or in the stratum pyramidal or stratum oriens of CA3 are divided into 6 levels from 0 to 5, 0: no granules; 1: occasional granules; 2: occasional to moderate granules; 3: prominent granules; 4: prominent granules in the stratum pyramidal or stratum oriens occurring in near-continuous distribution along the entire CA3 region, or highly concentrated band of granules appearing either in continuous or near-continuous distribution; 5: continuous or near continuous dense laminar band of granules in the stratum pyramidal or stratum oriens along the entire CA3 region, or continuous dense laminar band of granules from crest to tip of dentate (Sogawa et al., 2001).

Cell Lines

The HT22 mouse hippocampal neuron cell line was obtained from the Cell Bank of the Institute of Cell Biology, Chinese Academy of Sciences.

Cell Culture Conditions

HT22 cells were cultured in DMEM supplemented with 10% fetal bovine serum, 100 U/ml penicillin, and 100 mg/ml streptomycin in humidified air at 37°C with 5% CO_2.

Drug Treatment and Grouping

The shControl group, shControl + Glutamate group, shPRG5 group and shPRG5 + Glutamate group were established. Each group is processed as follows:

(a) shControl group: After 72 h of infecting cells with no-load lentivirus, change to normal medium. shControl source/sequence: 5′-TTCTCCGAACGTGTCACGT-3′.
(b) shControl + Glutamate group: 72 h after the cells are infected with no-load lentivirus, replaced with a culture medium containing 5 mM (Song et al., 2017) glutamic acid (with serum-containing medium configuration) and cultured for 24 h.
(c) shPRG5 group: 72 h after shPRG5 lentivirus infects the cells, change to normal medium. shPRG5 source/sequence: 5′-GCAATTAGCCACAAGAGAT-3′.

(d) shPRG5 + Glutamate group: 72 h after shPRG5 lentivirus infects the cells, replaced with 5 mM glutamate (serum-containing medium configuration) culture medium and cultured for 24 h.

Analysis of Mitochondrial Membrane Potentials Using JC-1

After the experimental grouping and treatment, the cells were collected by trypsin digestion, resuspended in 0.5 ml cell culture medium and added the mitochondrial membrane potential sensitive probe JC-1 (Beyotime, Shanghai, China) staining working solution 0.5 ml, shaking and mixing. Cells were incubated in an incubator for 30 min at a final concentration of 2 μM in PBS and washed twice with PBS. JC-1 aggregate was measured at the FL-2 channel, and green fluorescence (JC-1 monomer) was measured at the FL-1 channel. The data were analyzed using the FlowJo analysis software, and the results are displayed in a dot plot of J-aggregate red fluorescence (y-axis) against JC-1 green fluorescence (x-axis) (Ma et al., 2017).

Measurement of Intracellular Zinc Ions Concentration

The cells were seeded in a small confocal dish and cultured overnight. After washing the cells twice with HBSS in each group, 250 μl of 12 μM Zinquin ethyl ester solution (diluted in HBSS, Dojindo Molecular Technologies, Kumamoto, Japan) was added to the cells and incubated at 37°C for 1 h. After washing the cells twice with HBSS, a laser confocal microscope was used to detect the fluorescence intensity of the cells (Jin et al., 2018).

Statistical Analysis

The data were analyzed with two-way ANOVAs with *post hoc* Bonferroni's multiple comparisons tests using SPSS 23.0 software. Data are presented as the mean ± SD. Statistical significance was considered as $P < 0.05$.

RESULTS

Seizure Latency

The reduction in seizure latency represents an increase in brain excitability. At P62, all mice had seizures after penicillin injection. The seizure latencies of the two pilocarpine-treated groups were significantly lower than those of the corresponding control group (WT + SE vs. WT, KO + SE vs. KO) [two-way ANOVA; Genotype × Seizure $F(1, 48) = 0.047$, $P = 0.829$; Genotype $F(1, 48) = 40.056$, $P < 0.001$; Seizure $F(1, 48) = 140.012$, $P < 0.001$; *post hoc* Bonferroni's multiple comparisons test, $P < 0.05$; WT group: $n = 15$, KO group: $n = 15$, WT + SE group: $n = 12$, KO + SE group: $n = 10$]. This is consistent with previous studies, indicating that early developmental seizures increase brain excitability and susceptibility to epilepsy. Interestingly, the seizure latencies of the two knockout groups were significantly lower than those of the corresponding control group (KO vs. WT, KO + SE vs. WT + SE), suggesting that PRG5 knockout changes the balance of excitability and inhibitory activity in the brain by affecting plasticity signaling, making animals more prone to seizures (**Figure 2**).

Timm Staining

Timm staining showed that the mossy fibers in the WT + SE group grew significantly toward the pyramidal cell layer of the hippocampal CA3 area and the inner molecular layer of the granular cells of the dentate gyrus. The sprouting scoring analysis further showed that the scores of CA3 and DG areas of WT + SE group were significantly higher than those of the WT group [two-way ANOVA; CA3: Genotype × Seizure $F(1, 16) = 7.692$, $P = 0.014$; Genotype $F(1, 16) = 11.077$, $P = 0.004$; Seizure $F(1, 16) = 24.923$, $P < 0.001$. DG: Genotype × Seizure $F(1, 16) = 9.68$, $P = 0.007$; Genotype $F(1, 16) = 13.52$, $P = 0.002$; Seizure $F(1, 16) = 35.28$, $P < 0.001$, $n = 5$/each group]. PRG5 gene knockout significantly reduced the MFS score, which was specifically reflected in the fact that PRG5 gene knockout significantly reduced the postconvulsive Timm score of the KO + SE group compared with the WT + SE group [*post hoc* Bonferroni's multiple comparisons test, $P < 0.05$.]. In addition, although the MFS score of the KO group was not significantly different from that of the WT group, the MFS scores of the CA3 and DG areas of the KO group were 25 and 16.7% lower than those of the WT group, respectively (**Figures 3**, **4**).

Effect of PRG5 Gene Silencing on Glutamate-Induced Mitochondrial Membrane Potential Changes Using JC-1

The increase of mitochondrial membrane potential will cause JC-1 to accumulate in the mitochondrial matrix and produce red fluorescence. When the mitochondrial membrane potential

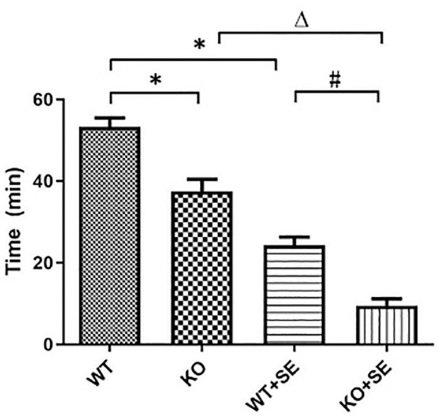

FIGURE 2 | PRG5 KO increased seizure susceptibility, as assessed in the seizure latency test, in which the seizure latencies of the two knockout groups were significantly lower than those of the corresponding control group (KO vs. WT, KO + SE vs. WT + SE). $^{*}P < 0.05$, compared to the WT group, $^{\Delta}P < 0.05$ compared to the KO group, $^{\#}P < 0.05$ compared to the WT + SE group.

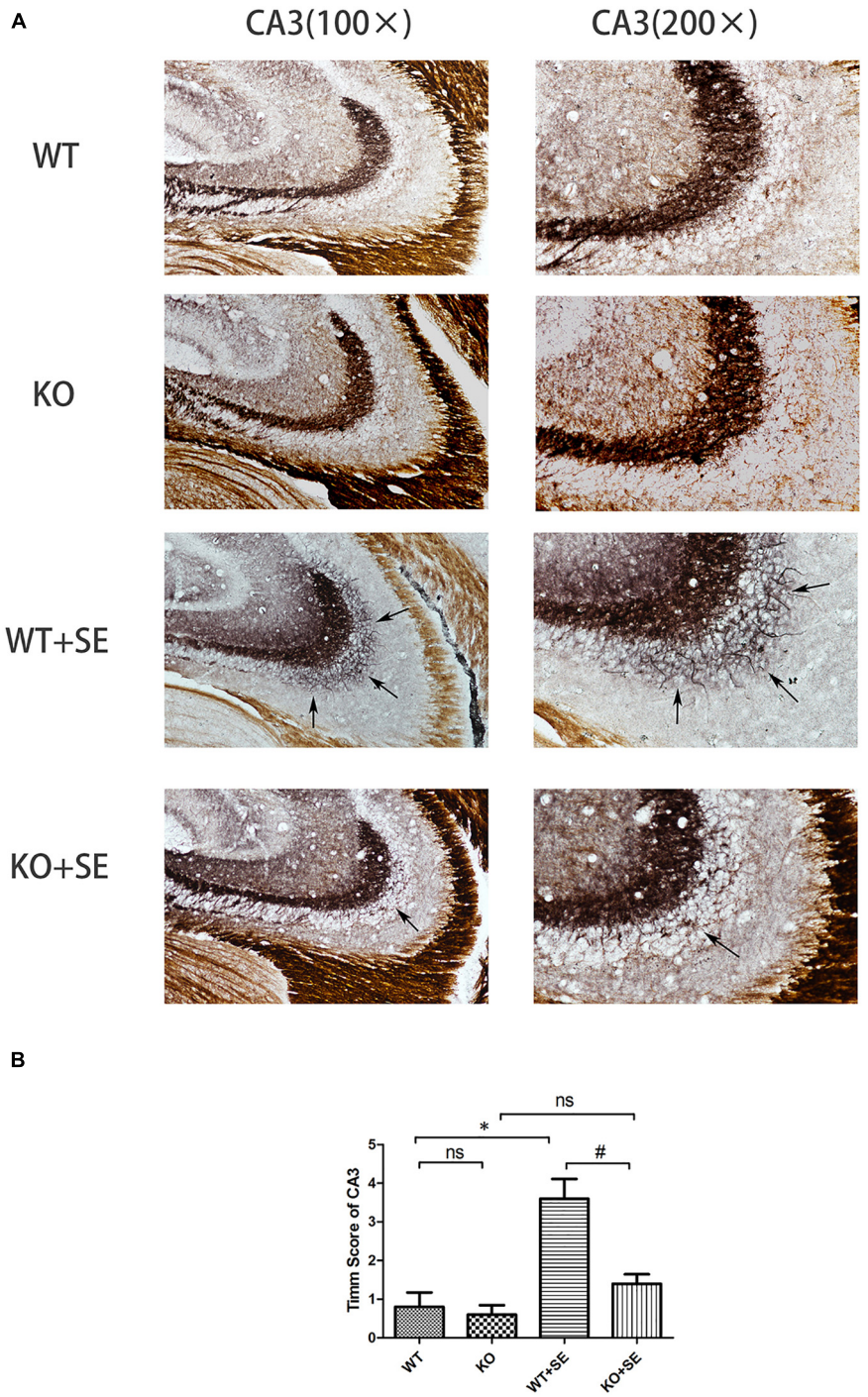

FIGURE 3 | Juvenile seizures increased mossy fiber sprouting (indicated by the arrows) in the pyramidal cell layer of the hippocampal CA3 area of WT mice, but this effect was attenuated in KO mice. **(A)** Timm staining in CA3 subfield; **(B)** Timm score analysis. $^{*}P < 0.05$, compared to WT group, $^{\#}P < 0.05$ compared to WT + SE group, ns means no statistical significance.

is low, JC-1 cannot accumulate in the mitochondrial matrix, resulting in green fluorescence. The change of JC-1 from red fluorescence to green fluorescence is an indicator of early cell apoptosis.

The results of flow cytometry showed that both plppr5 gene silencing and glutamate treatment significantly reduced the mitochondrial membrane potential when compared with the shControl group ($P < 0.05$). Moreover, the mitochondrial

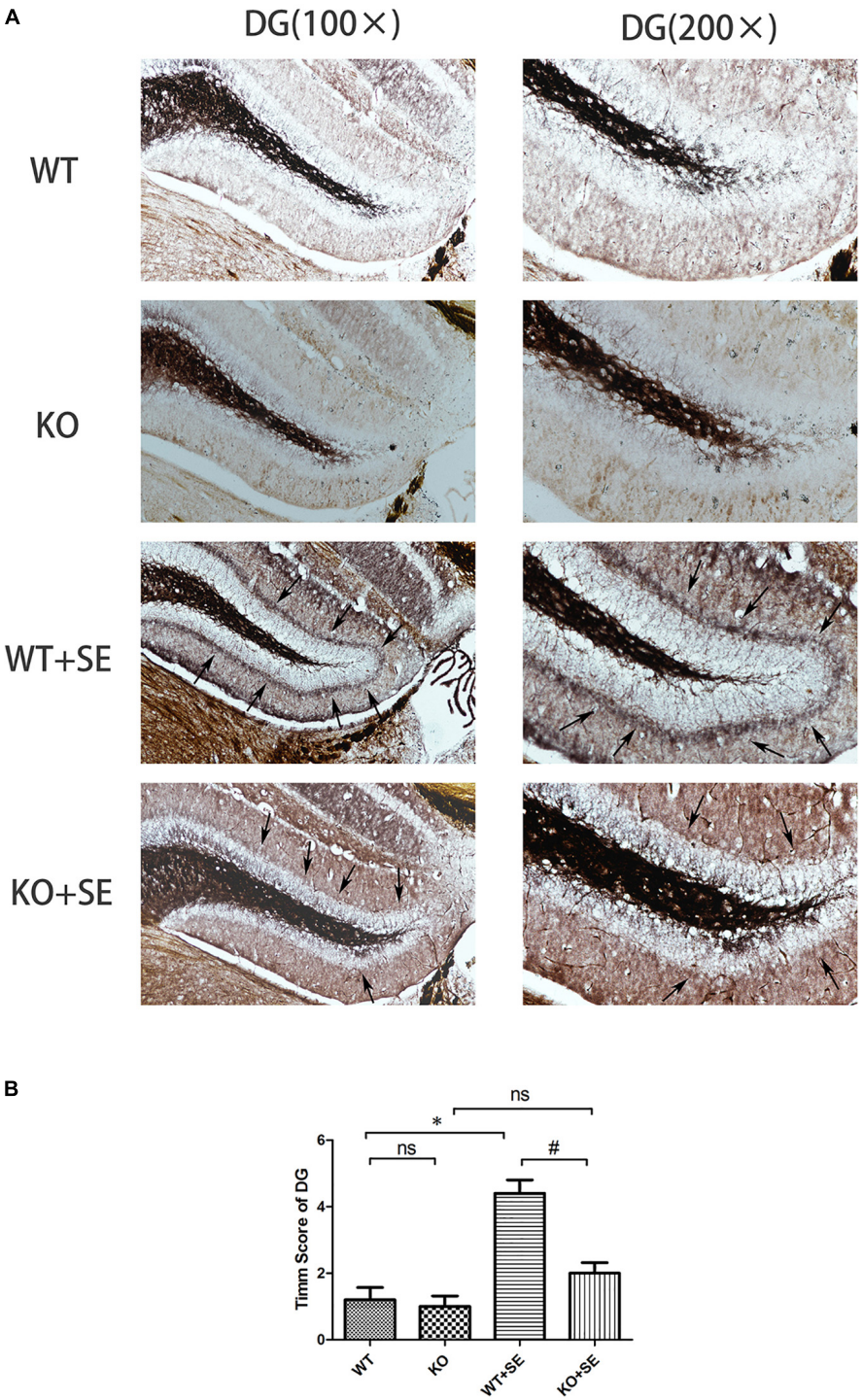

FIGURE 4 | Juvenile seizures increased mossy fiber sprouting (indicated by the arrows) in the inner molecular layer of the dentate gyrus of WT mice, but this effect was attenuated in KO mice. **(A)** Timm staining in dentate gyrus subfield; **(B)** Timm score analysis. $^{*}P < 0.05$, compared to WT group, $^{\#}P < 0.05$ compared to WT + SE group, ns means no statistical significance.

membrane potential of the shPRG5 + Glutamate group was significantly lower than that of the shControl + Glutamate ($P < 0.05$) and the shPRG5 + Glutamate group, indicating that PRG5 gene silencing can reduce the mitochondrial membrane potential of HT22 cells treated with glutamate (**Figure 5**).

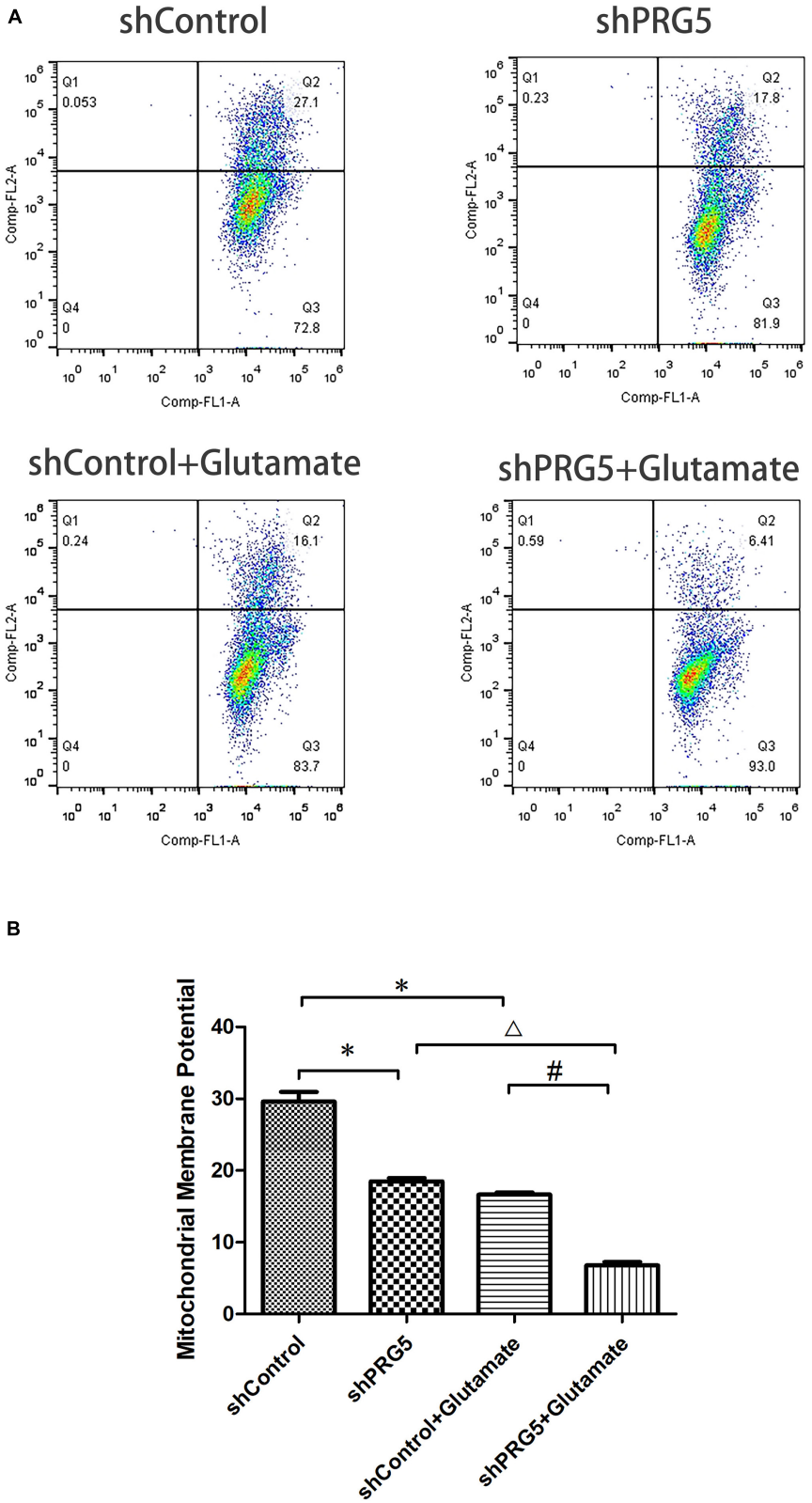

FIGURE 5 | The effect of PRG5 gene silencing and glutamate treatment on the changes of mitochondrial membrane potential by JC-1. **(A)** Flow cytometric diagram of cell mitochondrial membrane potential in each group. **(B)** Analysis of cell mitochondrial membrane potential in each group. $^{*}P < 0.05$ compared with shControl group, $^{\triangle}P < 0.05$ compared with shPRG5 group, $^{\#}P < 0.05$ compared with Control + Glutamate group ($n = 3$).

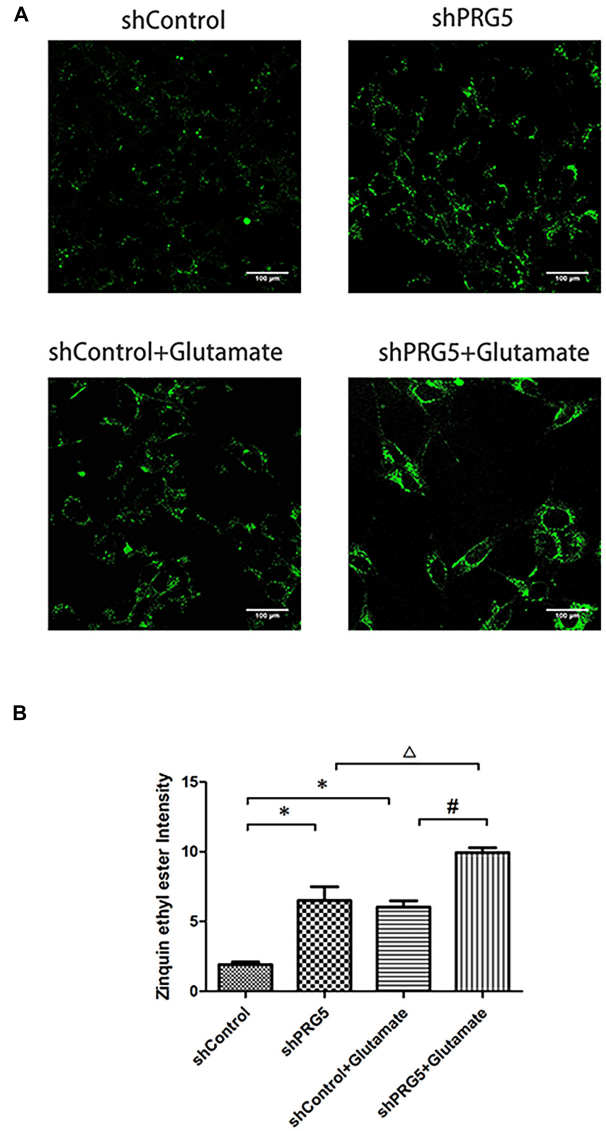

FIGURE 6 | The effect of PRG5 gene silencing and glutamate treatment on the cellular zinc ion levels in HT22 cells. **(A)** The fluorescence intensity of Zinquin ethyl ester in HT22 cells; **(B)** the quantitative analysis of the average fluorescence intensity of Zinquin ethyl ester in HT22 cells. $^{*}P < 0.05$ compared with shControl group, $^{\triangle}P < 0.05$ compared with shPlppr5 group, $^{\#}P < 0.05$ compared with Control + Glutamate group ($n = 3$).

Measurement of Intracellular Zinc Ions Concentration

PRG5 gene silencing and glutamic acid treatment both significantly increased the cellular zinc ion level. As shown in **Figure 6**, the zinc ion content in the shControl + Glutamate and shPRG5 + Glutamate groups was markedly higher than that in the corresponding shControl and shPRG5 groups, respectively ($P < 0.05$). Moreover, the zinc ion content was significantly elevated in the shPRG5 group compared to the shControl group ($P < 0.05$). Furthermore, the zinc ion content was significantly higher in the shPRG5 + Glutamate group than in the shControl + Glutamate ($P < 0.05$).

DISCUSSION

Here, our *in vivo* results describe the outcomes of wild-type (WT) and PRG5 KO mice in young adulthood following pilocarpine-induced juvenile seizures, focusing on seizure threshold and hippocampal MFS. The main findings were that PRG5 KO mice, relative to WT controls, had shorter seizure latency times following penicillin administration. Regardless of genotype, juvenile seizures reduced seizure latency. Interestingly, seizures increased MFS in the WT mice, but this effect was attenuated in the KO mice.

Of note, regardless of juvenile seizures, PRG5 knockout resulted in reduced seizure latency. Specifically, the seizure latency of the two gene knockout groups was significantly lower than that of the corresponding control group (KO vs. WT, KO + SE vs. WT + SE). Since shortened seizure latency indicates increased brain excitability, this result suggests that PRG5 gene knockout may change the balance of brain excitability and inhibitory activity by regulating plasticity-related signals, thereby making animals more prone to seizures. The key mechanism of PRG5's role in regulating brain excitability and seizure latency may be bioactive lipid phosphate. As shown by Trimbuch et al. (2009), PRG-1 regulates synaptic excitatory transmission through lipid phosphate-mediated signal transduction. There was previous report of aggravation of chronic stress effects on hippocampal neurogenesis and spatial memory in lysophosphatidic acid (LPA) receptor knockout mice (Castilla-Ortega et al., 2011). LPA also induced a decrease in mitochondrial membrane potential. Pretreatment of neurons with cyclosporin A protected against the LPA-induced decrease in mitochondrial membrane potential and neuronal apoptosis (Holtsberg et al., 1998). Moreover, we recently reported that cyclosporin A significantly reduced intracellular zinc ion content and corrected glutamate-induce cytotoxicity in mouse HT22 hippocampal neurons (Jin et al., 2018; Wang et al., 2019). Therefore, the bioactive lipid phosphates might play a key role in seizure latency in the PRG5 KO mouse brain after juvenile seizures, which merit further investigation by using PRG-5/LPA receptor-deficient animals.

The PRG family is a set of five brain-specific integral membrane proteins that are part of the lipid phosphate phosphatase superfamily. We previously examined the effect of E-64d (a calpain and autophagy inhibitor) on hippocampal aberrant MFS in a developmental rat model of penicillin-induced recurrent epilepticus. An interesting finding is that while E-64d obviously suppressed the aberrant MFS in the supragranular region of dentate gyrus and CA3 subfield of hippocampus, E-64d-pretreated seizure rats (EXP2) showed a significant downregulation of mRNA expression of PRG-1, PRG-3, and PRG-5 in hippocampus when compared with non-E64d-treated seizure rats. These results suggest that PRGs and sprouting may have some internal connection (Ni et al., 2013). PRG5, specifically, is involved in filopodia and axon growth, as well as dendritic spine formation (Broggini et al., 2010).

However, there is no report on the direct effect of PRG5 on sprouting. Here, we investigated for the first time the role of PRG5 in aberrant sprouting of hippocampal mossy fibers in PRG5$^{-/-}$ mice. We found that PRG5 knockout significantly reduced the postconvulsive MFS Timm staining score of wild-type mice (comparison between KO + SE group and WT + SE group); the MFS score of the non-seizure KO group with PRG5 knockout (KO) also decreased to a certain extent (compared with the WT group). This is consistent with the study of Broggini et al. (2010) They found that PRG5 promoted the formation of neurites and filopodia of primary neurons and that PRG5 silencing weakened the formation and growth of neurites (Broggini et al., 2010). These results highlight the possibility that PRG5 plays a role in promoting hippocampal mossy fiber axon regeneration. It should be mentioned that repeated sensory stimulation has been shown to lead to a transient decrease in the vesicular zinc content of neurons that can be visualized with histochemical techniques (Brown and Dyck, 2005). For example, Mitsuya et al. (2009) reported a transient decrease in Timm staining following kainic acid administration to the hippocampus. In our present study, brain tissues were collected on the same day as the seizure latency test. However, in this study, the animals in the four groups were immediately anesthetized for Timm staining and western blot analysis when the mouse first had Racine grade 4 seizures. We did not continue to observe grade 5 seizures. Therefore, there was no difference in the severity of seizures in this experiment. Thus, in this experiment, the effect of the seizure latency test on Timm stainable zinc was the same. The difference in MFS scores in each group still reflects the influence of pilocarpine-induced developmental seizures or PRG5 gene knockout.

Interestingly, treatment of hippocampal HT22 neuron cultures silenced by PRG5, with or without glutamate treatment, markedly elevated intracellular zinc ion levels, and reduced the mitochondrial membrane potential. It has been shown that malfunction or loss of enzymes involved in mitochondrial phospholipid biosynthesis lead to dysfunction of cell respiration, affect the assembly and stability of the mitochondrial protein import machinery and cause abnormal mitochondrial morphology or even lethality (Horvath and Daum, 2013). In addition, mitochondria defect can lead to high-level release of labile Zn2 + from mitochondrial, thereby high intracellular zinc ion level as well as oxidative stress (Turan and Tuncay, 2021). A correlation between epilepsy and cellular redox imbalance has been proposed. Seizure induces mitochondrial oxidative damage and neuronal loss, as well as affect neuronal water and ion balance, thus creating a vicious circle, thereby promoting neuronal hyperexcitability (Pecorelli et al., 2015). Hence, our finding, that PRG5 silencing leads to increased intracellular zinc ion content, and aggravates the damage of mitochondrial function, support the hypothesis that PRG5 knockout precipitates late-onset hypersusceptibility to pilocarpine-induced juvenile seizures by exacerbating hippocampal zinc signaling-mediated mitochondrial damage.

This study has some limitations. It is best to use isolated rat hippocampal neuron cultures combined with a fluorescent Zn2 + sensor and western blot analysis (Sanford et al., 2019) to study the effects of long-term Pgr5 knockdown on hippocampal imaging zinc and the expression changes of zinc transporters, so as to better understand the relationship between Pgr5 and zinc signaling Interaction.

Taken together, PRG5 KO may increase seizure susceptibility. This effect may be related to the hippocampal zinc signaling. The effects do not appear to be related to changes in MFS because KO mice with juvenile seizures had the shortest seizure latencies but exhibited less mossy fiber sprouting than WT mice with juvenile seizures. Further investigations are needed to address this issue.

DATA AVAILABILITY STATEMENT

The original contributions presented in the study are included in the article/**Supplementary Material**, further inquiries can be directed to the corresponding author/s.

ETHICS STATEMENT

The animal study was reviewed and approved by the Institutional Animal Care and Use Committee of Soochow University.

AUTHOR CONTRIBUTIONS

HN designed the study and wrote the manuscript. DW analyzed the data. DW, YL, LL, M-fJ, and YS were the operators of the experiment and responsible for the statistical analysis of the data. All authors contributed to the article and approved the submitted version.

FUNDING

This work was supported by the National Natural Science Foundation of China (81871024 and 81471337) and the Key Talent's Subsidy Project in Science and Education of Department of Public Health of Jiangsu Province (ZDRCC2016008).

SUPPLEMENTARY MATERIAL

The Supplementary Material for this article can be found online at: https://www.frontiersin.org/articles/10.3389/fnins.2021.715555/full#supplementary-material

REFERENCES

Brauer, A. U., and Nitsch, R. (2008). Plasticity-related genes (PRGs/LRPs): a brain-specific class of lysophospholipid-modifying proteins. *Biochim. Biophys. Acta* 1781, 595–600. doi: 10.1016/j.bbalip.2008.04.004

Bresnahan, R., Gianatsi, M., Maguire, M. J., Smith, C. T., and Marson, A. G. (2020). Vigabatrin add-on therapy for drug-resistant focal epilepsy. *Cochrane Database Syst. Rev.* 7:CD007302. doi: 10.1002/14651858.CD007302.pub3

Broggini, T., Nitsch, R., and Savaskan, N. E. (2010). Plasticity-related gene 5 (PRG5) induces filopodia and neurite growth and impedes lysophosphatidic

acid- and nogo-A-mediated axonal retraction. *Mol. Biol. Cell.* 21, 521–537. doi: 10.1091/mbc.e09-06-0506

Brown, C. E., and Dyck, R. H. (2005). Modulation of synaptic zinc in barrel cortex by whisker stimulation. *Neuroscience.* 134, 355–359. doi: 10.1016/j.neuroscience.2005.05.011

Castilla-Ortega, E., Hoyo-Becerra, C., Pedraza, C., Chun, J., Rodríguez, De Fonseca, F., et al. (2011). Aggravation of chronic stress effects on hippocampal neurogenesis and spatial memory in LPA_1 receptor knockout mice. *PLoS One.* 6:e25522. doi: 10.1371/journal.pone.0025522

Companys-Alemany, J., Turcu, A. L., Bellver-Sanchis, A., Loza, M. I., Brea, J. M., Canudas, A. M., et al. (2020). A novel NMDA receptor antagonist protects against cognitive decline presented by senescent mice. *Pharmaceutics.* 12:284. doi: 10.3390/pharmaceutics12030284

Holtsberg, F. W., Steiner, M. R., Keller, J. N., Mark, R. J., Mattson, M. P., and Steiner, S. M. (1998). Lysophosphatidic acid induces necrosis and apoptosis in hippocampal neurons. *J. Neurochem.* 70, 66–76. doi: 10.1046/j.1471-4159.1998.70010066.x

Horvath, S. E., and Daum, G. (2013). Lipids of mitochondria. *Prog. Lipid Res.* 52, 590–614. doi: 10.1016/j.plipres.2013.07.002

Jin, M. F., Ni, H., and Li, L. L. (2018). Leptin maintained zinc homeostasis against glutamate-induced excitotoxicity by preventing mitophagy-mediated mitochondrial activation in HT22 hippocampal neuronal cells. *Front. Neurol.* 9:322. doi: 10.3389/fneur.2018.00322

Kaushal, S., Tamer, Z., Opoku, F., and Forcelli, P. A. (2016). Anticonvulsant drug-induced cell death in the developing white matter of the rodent brain. *Epilepsia.* 57, 727–734. doi: 10.1111/epi.13365

Li, L. L., Jin, M. F., and Ni, H. (2018). Zinc/CaMK II associated-mitophagy signaling contributed to hippocampal mossy fiber sprouting and cognitive deficits following neonatal seizures and its regulation by chronic leptin treatment. *Front. Neurol.* 9:802. doi: 10.3389/fneur.2018.00802

Ling, Y., Wang, D., Sun, Y., Zhao, D., and Ni, H. (2019). Neuro-behavioral status and the hippocampal expression of metabolic associated genes in wild-type rat following a ketogenic diet. *Front. Neurol.* 10:65. doi: 10.3389/fneur.2019.00065

Ma, Y., Zhang, Z., Chen, Z., Ma, N., Sun, S., Zhang, J., et al. (2017). Suppression of inner mitochondrial membrane peptidase 2-like (IMMP2L) gene exacerbates hypoxia-induced neural death under high glucose condition. *Neurochem. Res.* 42, 1504–1514. doi: 10.1007/s11064-017-2207-y

Málaga, I., Sánchez-Carpintero, R., Roldán, S., Ramos-Lizana, J., and García-Peñas, J. J. (2019). New anti-epileptic drugs in Paediatrics. *Pediatrics* 91, 415.e1–415.e10. doi: 10.1016/j.anpedi.2019.09.008.

Mitsuya, K., Nitta, N., and Suzuki, F. (2009). Persistent zinc depletion in the mossy fiber terminals in the intrahippocampal kainite mouse model of mesial temporal lobe epilepsy. *Epilepsia* 50, 1979–1990. doi: 10.1111/j.1528-1167.2009.02055.x

Ni, H., Chen, S. H., Li, L. L., and Jin, M. F. (2018). Leptin treatment prevents long-term abnormalities in cognition, seizure latency, hippocampal mossy fiber sprouting and ZnT3/CB-D28k expression in a rat developmental "twist" seizure model. *Epilepsy Res.* 139, 164–170. doi: 10.1016/j.eplepsyres.2017.12.009

Ni, H., Jiang, Y. W., Tao, L. Y., Jin, M. F., and Wu, X. R. (2009). ZnT-1. ZnT-3, CaMKII, PRG-1 expressions in hippocampus following neonatal seizure-induced cognitive deficit in rats. *Toxicol. Lett.* 184, 145–150. doi: 10.1016/j.toxlet.2008.11.003

Ni, H., Jiang, Y. W., Xiao, Z. J., Tao, L. Y., and Wu, X. R. (2010). Dynamic pattern of gene expression of ZnT-1. ZnT-3 and PRG-1 in rat brain following flurothyl-induced recurrent neonatal seizures. *Toxicol. Lett.* 194, 86–93. doi: 10.1016/j.toxlet.2010.02.008

Ni, H., Kirschstein, T., Norwood, B. A., and Hsieh, C. L. (2019). Editorial: the developmental seizure-induced hippocampal mossy fiber sprouting: target for epilepsy therapies? *Front. Neurol.* 10:1212. doi: 10.3389/fneur.2019.01212

Ni, H., Ren, S. Y., Zhang, L. L., Sun, Q., Tian, T., and Feng, X. (2013). Expression profiles of hippocampal regenerative sprouting-related genes and their regulation by E-64d in a developmental rat model of penicillin-induced recurrent epilepticus. *Toxicol. Lett.* 217, 162–169. doi: 10.1016/j.toxlet.2012.12.010

Ni, H., Zhao, D. J., and Tian, T. (2016). Ketogenic diet change cPLA2/clusterin and autophagy related gene expression and correlate with cognitive deficits and hippocampal MFs sprouting following neonatal seizures. *Epilepsy Res.* 120, 13–18. doi: 10.1016/j.eplepsyres.2015.11.021

Pecorelli, A., Natrella, F., Belmonte, G., Miracco, C., Cervellati, F., Ciccoli, L., et al. (2015). NADPH oxidase activation and 4-hydroxy-2-nonenal/aquaporin-4 adducts as possible new players in oxidative neuronal damage presents in drug-resistant epilepsy. *Biochim. Biophys Acta* 1852, 507–519. doi: 10.1016/j.bbadis.2014.11.016

Petzold, S., Sommer, B., Kröber, A., Nitsch, R., Schwegler, H., Vogt, J., et al. (2016). NT-3 protein levels are enhanced in the hippocampus of PRG1-deficient mice but remain unchanged in PRG1/LPA2 double mutants. *Neurosci. Lett.* 612, 145–148. doi: 10.1016/j.neulet.2015.12.016

Racine, R. J. (1972). Modification of seizure activity by electrical stimulation. II. Motor seizure. *Electroencephalogr. Clin. Neurophysiol.* 32, 281–294. doi: 10.1016/0013-4694(72)90177-0

Sanford, L., Carpenter, M. C., and Palmer, A. E. (2019). Intracellular Zn2+ transients modulate global gene expression in dissociated rat hippocampal neurons. *Sci. Rep.* 9:9411. doi: 10.1038/s41598-019-45844-2

Sierra, A., Gröhn, O., and Pitkänen, A. (2015). Imaging microstructural damage and plasticity in the hippocampus during epileptogenesis. *Neuroscience* 309, 162–172. doi: 10.1016/j.neuroscience.2015.04.054

Sogawa, Y., Monokoshi, M., Silveira, D. C., Cha, B. H., Cilio, M. R., McCabe, B. K., et al. (2001). Timing of cognitive deficits following neonatal seizures: relationship to histological changes in the hippocampus. *Brain Res. Dev. Brain Res.* 131, 73–83. doi: 10.1016/s0165-3806(01)00265-6

Song, J. H., Kang, K. S., and Choi, Y. K. (2017). Protective effect of casuarinin against glutamate-induced apoptosis in HT22 cells through inhibition of oxidative stress- mediated MAPK phosphorylation. *Bioorg. Med. Chem. Lett.* 27, 5109–5113. doi: 10.1016/j.bmcl.2017.10.075

Sun, Y. X., Ma, L. Y., Jin, M. F., Zheng, Y. Q., Wang, D. D., and Ni, H. (2021). Effects of melatonin on neurobehavior and cognition in a cerebral palsy model of plppr5-/-mice. *Front. Endocrinol.* 12:598788. doi: 10.3389/fendo.2021.598788

Tian, T., Li, L. L., Zhang, S. Q., and Ni, H. (2016). Long-term effects of ketogenic diet on subsequent seizure-induced brain injury during early adulthood: relationship of seizure thresholds to zinc transporter-related gene expressions. *Biol. Trace Elem. Res.* 174, 369–376. doi: 10.1007/s12011-016-0730-3

Trimbuch, T., Beed, P., Vogt, J., Schuchmann, S., Maier, N., Kintscher, M., et al. (2009). Synaptic PRG-1 modulates excitatory transmission via lipid phosphate-mediated signaling. *Cell* 138, 1222–1235. doi: 10.1016/j.cell.2009.06.050

Turan, B., and Tuncay, E. (2021). The role of labile Zn(2+) and Zn(2+)-transporters in the pathophysiology of mitochondria dysfunction in cardiomyocytes. *Mol. Cell Biochem.* 476, 971–989. doi: 10.1007/s11010-020-03964-8

Wang, D. D., Jin, M. F., Zhao, D. J., and Ni, H. (2019). Reduction of Mitophagy-Related Oxidative Stress And Preservation Of Mitochondria Function Using Melatonin Therapy in an HT22 hippocampal neuronal cell model of glutamate-induced excitotoxicity. *Front Endocrinology* 2019:550. doi: 10.3389/fendo.2019.00550

Zheng, Y., Jin, M., Suo, G., Wu, Y., Sun, Y., and Ni, H. (2020). Proteomics for studying the effects of ketogenic diet against Lithium Chloride/Pilocarpine induced Epilepsy in rats. *Front. Neurosci.* 14:562853. doi: 10.3389/fnins.2020.562853

Conflict of Interest: The authors declare that the research was conducted in the absence of any commercial or financial relationships that could be construed as a potential conflict of interest.

Publisher's Note: All claims expressed in this article are solely those of the authors and do not necessarily represent those of their affiliated organizations, or those of the publisher, the editors and the reviewers. Any product that may be evaluated in this article, or claim that may be made by its manufacturer, is not guaranteed or endorsed by the publisher.

frontiers in Neuroscience

ORIGINAL RESEARCH
published: 28 September 2021
doi: 10.3389/fnins.2021.736313

The Proliferation of Dentate Gyrus Progenitors in the Ferret Hippocampus by Neonatal Exposure to Valproic Acid

Kazuhiko Sawada[1], Shiori Kamiya[1] and Ichio Aoki[2,3]*

[1] Department of Nutrition, Faculty of Medical and Health Sciences, Tsukuba International University, Tsuchiura, Japan, [2] Department of Molecular Imaging and Theranostics, National Institutes for Quantum Science and Technology, Chiba, Japan, [3] Institute for Quantum Life Science, National Institutes for Quantum Science and Technology, Chiba, Japan

OPEN ACCESS

Edited by:
Wassim Abou-Kheir, American University of Beirut, Lebanon

Reviewed by:
Farah Chamaa, American University of Beirut, Lebanon
Ariel A. Di Nardo, Centre National de la Recherche Scientifique (CNRS), France

***Correspondence:**
Kazuhiko Sawada
k-sawada@tius.ac.jp

Specialty section:
This article was submitted to Neurodevelopment, a section of the journal Frontiers in Neuroscience

Received: *05 July 2021*
Accepted: *30 August 2021*
Published: *28 September 2021*

Citation:
Sawada K, Kamiya S and Aoki I (2021) The Proliferation of Dentate Gyrus Progenitors in the Ferret Hippocampus by Neonatal Exposure to Valproic Acid. Front. Neurosci. 15:736313. doi: 10.3389/fnins.2021.736313

Prenatal and neonatal exposure to valproic acid (VPA) is associated with human autism spectrum disorder (ASD) and can alter the development of several brain regions, such as the cerebral cortex, cerebellum, and amygdala. Neonatal VPA exposure induces ASD-like behavioral abnormalities in a gyrencephalic mammal, ferret, but it has not been evaluated in brain regions other than the cerebral cortex in this animal. This study aimed to facilitate a comprehensive understanding of brain abnormalities induced by developmental VPA exposure in ferrets. We examined gross structural changes in the hippocampus and tracked proliferative cells by 5-bromo-2-deoxyuridine (BrdU) labeling following VPA administration to ferret infants on postnatal days (PDs) 6 and 7 at 200 μg/g of body weight. *Ex vivo* short repetition time/time to echo magnetic resonance imaging (MRI) with high spatial resolution at 7-T was obtained from the fixed brain of PD 20 ferrets. The hippocampal volume estimated using MRI-based volumetry was not significantly different between the two groups of ferrets, and optical comparisons on coronal magnetic resonance images revealed no differences in gross structures of the hippocampus between VPA-treated and control ferrets. BrdU-labeled cells were observed throughout the hippocampus of both two groups at PD 20. BrdU-labeled cells were immunopositive for Sox2 (>70%) and almost immunonegative for NeuN, S100 protein, and glial fibrillary acidic protein. BrdU-labeled Sox2-positive progenitors were abundant, particularly in the subgranular layer of the dentate gyrus (DG), and were denser in VPA-treated ferrets. When BrdU-labeled Sox2-positive progenitors were examined at 2 h after the second VPA administration on PD 7, their density in the granular/subgranular layer and hilus of the DG was significantly greater in VPA-treated ferrets compared to controls. The findings suggest that VPA exposure to ferret infants facilitates the proliferation of DG progenitors, supplying excessive progenitors for hippocampal adult neurogenesis to the subgranular layer.

Keywords: hippocampus, development, valproic acid, ferret, immunohistochemistry

INTRODUCTION

Valproic acid (VPA), a well-known antiepileptic/anticonvulsant drug, also acts as an inhibitor of histone deacetylases 1 and 2 (Göttlicher et al., 2001; Phiel et al., 2001). Many studies have reported autism spectrum disorder (ASD)-like behavioral abnormalities induced by VPA exposure during prenatal and neonatal periods in various mammalian species such as mice (Yochum et al., 2008; Burenkova et al., 2014), rats (Miyazaki et al., 2005; Mychasiuk et al., 2012; Favre et al., 2013), common marmosets (Yasue et al., 2018), and ferrets (Krahe et al., 2016). These behavioral abnormalities are believed to be associated with cerebral cortical abnormalities caused by developmental VPA exposure (Sabers et al., 2014; Wood et al., 2014; Fujimura et al., 2016; Lauber et al., 2016; Sawada et al., 2021). In contrast, prenatal and neonatal VPA exposure can alter the development of other brain regions, such as the hippocampus (Edalatmanesh et al., 2013; Juliandi et al., 2015; Wang et al., 2016; Hou et al., 2018; Win-Shwe et al., 2018), cerebellum (Hou et al., 2018; Mirza and Sharma, 2019), and amygdala (Olexová et al., 2016; Wang et al., 2016). In association with such VAP-induced brain abnormalities, VPA regulates neurogenesis; however, studies have reported inconsistent findings – facilitation of neuronal differentiation of rat adult hippocampal neuronal progenitors (Hsieh et al., 2004) and mouse embryonic stem cells (Juliandi et al., 2012) but inhibition of neuronal differentiation of cortical progenitors in mouse fetuses (Fujimura et al., 2016).

Ferrets are small laboratory animals that have morphological characteristics of the brain similar to humans, not found in rodents: for example, the gyrencephalic cerebral cortex (Sawada and Watanabe, 2012; Kroenke et al., 2014) and torque asymmetry of the cerebellum (Sawada et al., 2015, 2020). VPA exposure to ferret infants decreased gyrification with thickened cerebral cortex at the sulcal floors (Sawada et al., 2021) that is comparable to the cortical abnormality observed in a type of human ADS (Ecker et al., 2013; Libero et al., 2014, 2019). Such gyrification abnormalities were involved in the excess production of cortical neurons by promoting neurogenesis or proliferation of cortical progenitors in ferrets (Sawada et al., 2021). The effect of neonatal VPA exposure, however, has not yet been evaluated in brain regions other than the cerebral cortex in gyrencephalic mammals such as ferrets. This study aimed to facilitate a comprehensive understanding of the brain abnormalities induced by developmental VPA exposure. The hippocampus is known as a target region by developmental VPA exposure in rodents, both morphologically and functionally (Edalatmanesh et al., 2013; Juliandi et al., 2015; Wang et al., 2016; Hou et al., 2018; Win-Shwe et al., 2018). Therefore, we examined gross structural and histological changes in the hippocampus and tracked proliferative cells by BrdU labeling following VPA administration to ferret infants on postnatal days (PDs) 6 and 7.

MATERIALS AND METHODS

Animals

Fourteen male ferret pups naturally delivered by six pregnant ferrets were purchased from Japan SLC (Hamamatsu, Japan). The pups were reared with lactating mothers (4–6 pups/mother) in stainless-steel cages (80 cm × 50 cm × 35 cm) maintained at 21.5 ± 2.5°C under 12-h artificial illumination in the Facility of Animal Breeding, Nakaizu Laboratory, Japan SLC. All lactating mothers were fed a pellet diet (High-Density Ferret Diet 5L14; PMI Feeds, Inc., St. Louis, MO, United States) and tap water *ad libitum*.

Seven ferrets were intraperitoneally injected VPA on PDs 6 and 7 at 200 μg/0.01 ml/g body weight. 5-Bromo-2-deoxyuridine (BrdU; Sigma-Aldrich, St. Louis, MO, United States) was injected at 30 μg/0.01 ml/g body weight simultaneously with the last injection of VPA. As controls, seven ferrets were administered BrdU on PD 7. Two hours after BrdU injection, three pups in each group were perfused with 4% paraformaldehyde (PFA) in phosphate-buffered saline (PBS) under deep anesthesia with ∼2% isoflurane gas. The remaining four ferrets in each group were reared until PD 20 and then perfused with PFA under deep anesthesia.

Magnetic Resonance Imaging Measurements and Magnetic Resonance Imaging-Based Analysis

Three-dimensional (3D) magnetic resonance (MR) images were acquired from the fixed brains of PD 20 ferrets using a 7.0-T magnetic resonance imaging (MRI) system (magnet: 400 mm inner diameter bore; Kobelco and Jastec, Kobe, Japan; console: AVANCE-I; Bruker BioSpin, Ettlingen, Germany) according to the procedure reported previously (Sawada and Aoki, 2017).

The hippocampus was segmented semiautomatically on coronal (transaxial) MRIs based on image contrast as well as user knowledge of anatomy using the "Morpho" tool of the SliceOmatic software ver. 4.3 (TomoVision, Montreal, QC, Canada), according to the procedure reported previously (Sawada et al., 2013). The segmented images were used to calculate the hippocampal volume and to render the hippocampus in 3D using SliceOmatic software, as reported previously (Sawada et al., 2013).

Immunohistochemical Procedures

Cerebral hemispheres were immersed in 30% sucrose-PBS solution overnight and then embedded in optimal cutting temperature compound (Sakura Finetek Japan Co., Ltd., Tokyo, Japan) at −70°C. Coronal cryosections of the hemispheres at 100 μm thickness were made from PD 7 and PD 20 ferrets with or without neonatal VPA exposure using a Retratome (REM-700; Yamato Kohki Industrial Co., Ltd., Saitama, Japan) equipped with a refrigeration unit (Electro Freeze MC-802A, Yamato Kohki Industrial).

Immunofluorescence staining was performed on floating sections with identical staining conditions using the same sets of the solution by the slight modified procedures in the previous report (Sawada, 2019). The primary antibodies used were highly specific for ferret tissues and the endogenous antigen (BrdU) (Sawada, 2019; Kamiya and Sawada, 2021) and included rabbit antibodies to calbindin D-28k (1:1,000; CB38; Swant, Bellinzona, Switzerland), NeuN (1:1,000; ABN78;

Millipore, Billerica, CA, United States), and S100 protein (1:200; 942001; Immunostar, Hudson, WI, United States); mouse antibodies to glial fibrillary acidic protein (GFAP) (1:1,000, G3893, Sigma-Aldrich); a goat antibody to Sox2 (1:1,000; AF2018, R&D Systems Minneapolis, MN, United States); a rat antibody to phospho-histone H3 (PH3) (1:1,000; ab10543; Abcam, Cambridge, United Kingdom); and a sheep antibody to BrdU (1:500; ab1893, Abcam). Secondary antibodies included Alexa 488 donkey anti-rabbit IgG (1:500; A21206, Thermo Fisher Scientific, Waltham, MA, United States), Alexa 555 donkey anti-mouse IgG (1:500; A31570, Thermo Fisher Scientific), Alexa 555 donkey anti-goat IgG (1:500; A-21432, Thermo Fisher Scientific), Alexa 647 donkey anti-sheep IgG (1:500; ab150179, Abcam), and Alexa 555 goat anti-rat IgG (1:500; A21434, Thermo Fisher Scientific). All sections were stained using Hoechst, mounted on slides, and coverslipped with glycerin.

Estimation of Cell Density

Serial digital sectioning images (10 sections at 1 μm plane thickness) were obtained under a 20 × objective using an Axio Imager M2 ApoTome.2 microscope equipped with an AxioCam MRm camera (Zeiss, Gottingen, Germany) with Zen 2.3 blue edition software (Zeiss). Densities of immuno- and BrdU-labeled cells were calculated by the disector method using systematic random sampling, according to a previous report (Sawada, 2019). To estimate cell density, three consecutive sections at the coronal plane, including the caudal end of the splenium of the corpus callosum, were analyzed per animal. Frames with six square boxes (box size = 40 μm × 40 μm) were used to select systematically the region of interest (ROI) superimposed randomly on subregions of dorsal and/or ventral hippocampi. The percentage of immuno- or BrdU-labeled cells was estimated by summing the cells counted within all ROIs from six cerebral hemispheres of VPA-treated and control groups on PD 7, and eight hemispheres of both two groups on PD 20.

Statistical Analysis

Data from the left and right hippocampi were considered to be independent samples, since no significant the left- and right-side differences in any measurements were demonstrated by a paired sample *t*-test. One-way analysis of variance (ANOVA) followed by Student's *t*-tests was used to assess statistically the volume of the hippocampus between VPA-treated and control groups. A repeated-measures two-way ANOVA was used to assess the hippocampal region (dorsal or ventral)-related differences in immuno- and BrdU-labeled cell density. Scheffe's test was performed as *post hoc* testing when significant interactions were revealed by two-way repeated-measures ANOVA, followed by simple main effects at $P < 0.05$.

The Chi-square test was conducted to compare the proportions of immunolabeled cells positive for each marker to BrdU-labeled cells between two groups of ferrets. The total number of BrdU-labeled cells counted was defined as "*n*" for the Chi-square test.

RESULTS

Magnetic Resonance Imaging-Based Analysis of Postnatal Day 20 Ferret Hippocampi

The volume of the hippocampus was estimated based on MR images. The hippocampal volume was 27.3 ± 0.6 mm^3 in VPA-treated ferrets, not significantly different from that in control ferrets (27.4 ± 0.6 mm^3) (**Table 1**). Three-dimensional rendered images of the hippocampus with the cerebral cortex in the left hemisphere are depicted in **Figure 1A**. The hippocampus was situated in the deep portion of the posterior ectosylvian gyrus, corresponding to the auditory cortex. Gross structures of the hippocampus were not different between the VPA-treated and control ferrets. Coronal MR images of the hippocampus of VPA-treated ferrets and controls are shown in two identical planes, that is, the plane including the caudal end of the splenium of the corpus callosum (**Figure 1B**) and in the plane including the posterior commissure (**Figure 1C**). In coronal MR images at the caudal end of the splenium of the corpus callosum, the dorsal hippocampus began to descend in both groups (**Figure 1B**). A connection from the dorsal to ventral hippocampus was found in coronal MR images at the posterior commissure in VPA-treated and control ferrets (**Figure 1C**).

Immunohistochemical Analysis of Postnatal Day 20 Ferret Hippocampi

The dorsal hippocampus in the coronal plane including the caudal end of the splenium of the corpus callosum was depicted by calbindin D-28k immunofluorescence with BrdU labeling and Hoechst staining in both VPA-treated and control ferrets (**Figure 2A**). In the dentate gyrus (DG), the subgranular layer was distinguishable by an array of calbindin D-28k-negative Hoechst-stained cells beneath a layer consisting of calbindin D-28k-positive granular neurons. To assess the effect of neonatal VPA exposure, the densities of cells defined by marker antigens for neuronal progenitors, neurons, and glial cells were estimated. There were no differences in the densities of calbindin D-28k-positive granular neurons in the DG granular layer and calbindin D-28k-negative Hoechst-stained cells in the DG subgranular layer between VPA-treated and control ferrets (**Supplementary Figures 1A,B**).

5-Bromo-2-deoxyuridine -labeled cells were found throughout the hippocampus of PD 20 ferrets and were particularly abundant in the DG (**Figure 2A**). A significant effect on treatments [$F_{(1,14)} = 24.756$, $P < 0.001$], but not hippocampal regions (dorsal/ventral), was observed in the density of BrdU-labeled cells in the DG subgranular layer by repeated-measures two-way ANOVA. *Post hoc* testing indicated

TABLE 1 | Hippocampal volume in VPA-treated ferrets on PD 20.

	VPA (*n* = 8)	Control (*n* = 8)
Hippocampal volume (mm^3)	27.3 ± 0.6	27.4 ± 0.6

Data are represented as mean ± SEM of eight cerebral hemispheres.

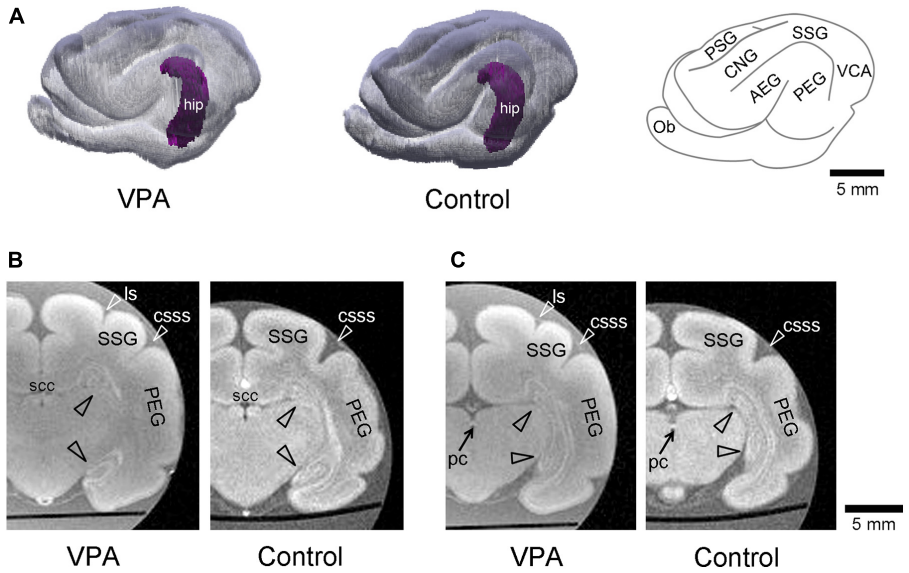

FIGURE 1 | Three-dimensional volume-rendered images in cerebrum with the hippocampus of the postnatal day (PD) 20 ferrets. **(A)** The left and moderate images are reconstructed images of the cerebral cortex and hippocampus (hip; purple) of the left hemisphere in valproic acid (VPA)-treated and control ferrets, respectively. A gyral map of the left hemisphere is shown on the right. **(B)** Coronal *ex vivo* magnetic resonance (MR) images [using RARE sequence with short repetition time (TR) and minimum time to echo (TE) setting] of cerebrum including the hippocampus at the caudal end of the splenium of corpus callosum from VPA-treated ferret (left) and control one (right). **(C)** Coronal *ex vivo* MR images of cerebrum including the hippocampus at the posterior commissure from VPA-treated ferret (left) and control one (right). AEG, anterior ectosylvian gyrus; CNG, coronal gyrus; csss, caudal suprasylvian sulcus; Ob, olfactory bulb; ls, lateral sulcus; pc, posterior commissure; PEG, posterior ectosylvian gyrus; PSG, posterior sigmoid gyrus; scc, splenium of the corpus callosum; SSG, suprasylvian gyrus; VCA, visual cortical area.

significantly denser BrdU-labeled cells in VPA-treated ferrets compared to controls in both the dorsal and ventral hippocampi (**Figure 3A**). Significantly denser BrdU-labeled cells in VPA-treated ferrets compared to controls were also detected in the DG granular layer of the dorsal hippocampus ($P < 0.001$; **Figure 3A**), following a significant effect on treatment [$F_{(1,14)} = 8.612$, $P < 0.05$] by repeated-measures two-way ANOVA. This meant a slight disarrangement of the DG granular layer of the dorsal hippocampus by mismigration of the tracked neonatal DG progenitors, although this disarrangement was difficult to define optically. In the CA1 and CA3 fields, there was no difference in the BrdU-labeled cell density between VPA-treated and controls (**Supplementary Figures 2A,C**).

Sox2-positive progenitors were distributed widely throughout the hippocampus in both VPA-treated ferrets and controls on PD 20. Multiple immunofluorescence staining revealed the presence of BrdU labeling in Sox2-positive progenitors (**Figure 2B**). More than 70% of BrdU labeling appeared in Sox2-positive progenitors in the DG (**Table 2**) and CA1 and CA3 fields (**Supplementary Tables 1, 2**) in both groups. The density of BrdU-labeled Sox2-progenitors was estimated in the subregions of the dorsal and ventral hippocampi. Repeated-measures two-way ANOVA revealed a significant effect of treatment [$F_{(1,14)} = 99.127$, $P < 0.001$] and hippocampal regions (dorsal/ventral) [$F_{(1,14)} = 13.057$, $P < 0.005$], and these two interactions [$F_{(1,14)} = 6.018$, $P < 0.05$] in the DG subgranular layers. *Post hoc* testing indicated significantly denser BrdU-labeled Sox2-progenitors in VPA-treated ferrets than in controls in the DG subgranular layer of both the dorsal and ventral hippocampi (**Figure 3B**). In the DG granular layer, significantly denser BrdU-labeled Sox-2-positive progenitors in VPA-treated ferrets compared to controls were detected in the dorsal hippocampus ($P < 0.001$; **Figure 3B**), following a significant effect on treatment [$F_{(1,14)} = 7.118$, $P < 0.05$] by repeated-measures two-way ANOVA. In other hippocampal regions examined, including the CA1 and CA3 fields, there was no difference in the BrdU-labeled Sox-2-positive progenitor density between VPA-treated and control ferrets (**Supplementary Figures 2B,D**).

Multiple immunofluorescence staining was conducted using neuronal and glial markers, that is, granular neurons in the DG and pyramidal neurons in the CA fields (calbindin D-28k-positive), neurons (NeuN-positive), and glial cells (S100-positive or GFAP-positive). NeuN-positive neurons were distributed sparsely in the hilus and molecular layer of the DG (**Figure 2C**), the strata radiatum and oriens of the CA1 and the CA3, and also aligned into the DG granular layer and the CA pyramidal layer. Calbindin D-28k immunostaining also appeared predominantly in DG granular neurons and CA pyramidal neurons (**Figures 2A,B**). While 5.9% of BrdU-labeled cells were unexpectedly NeuN-positive in the CA3 stratum radiatum, almost all NeuN-positive neurons and calbindin D-28k granular/pyramidal neurons in the hippocampus were not labeled with BrdU in both VPA-treated and control ferrets (**Figures 2B,C**, **Table 2** and **Supplementary Tables 1, 2**).

While S100-positive cells were distributed throughout the hippocampus, their alignment at the bottom of the DG subgranular layer was striking (**Figure 2D**). S100

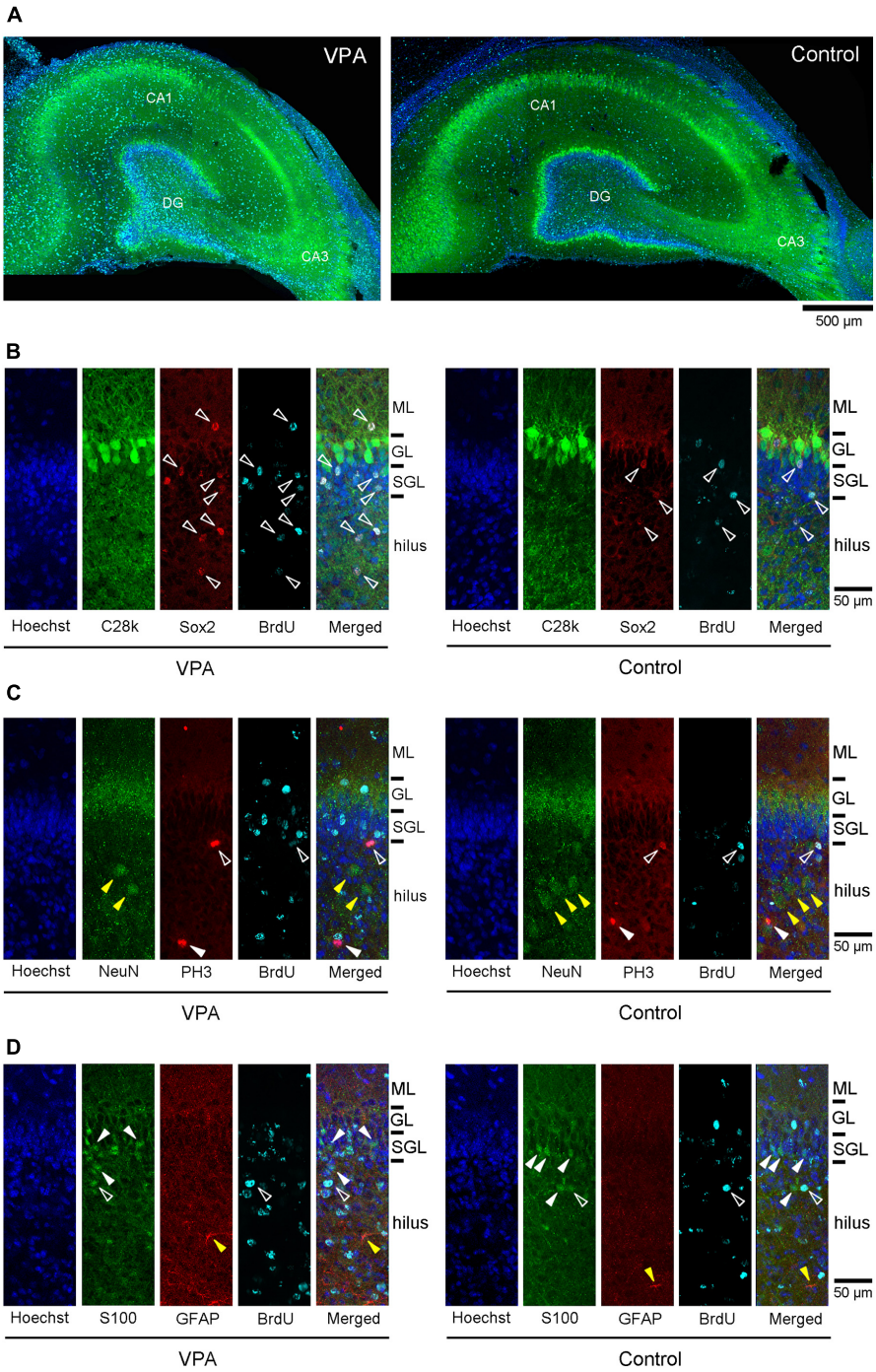

FIGURE 2 | Immunofluorescence images for antibodies against various marker antigens with 5-bromo-2-deoxyuridine (BrdU)-labeling and Hoechst staining in dorsal hippocampi of postnatal day (PD) 20 ferrets. **(A)** Low-magnification images of calbindin D-28k immunofluorescence with BrdU-labeling and Hoechst staining in the dorsal hippocampus at the coronal plane including the caudal end of the splenium of the corpus callosum in valproic acid (VPA)-treated (left) and control (right) ferrets. **(B)** High magnification images of double immunofluorescence for calbindin D-28k and Sox2 with BrdU-labeling and Hoechst staining in the dentate gyrus of the dorsal hippocampus in VPA-treated (left) and control (right) ferrets. White open arrowheads indicate BrdU-labeled Sox2-immunopositive progenitors located in the molecular layer (ML), subgranular layer (SGL), and hilus. **(C)** High-magnification images of double immunofluorescence for NeuN and PH3 with BrdU-labeling and Hoechst staining in the dentate gyrus of the dorsal hippocampus in VPA-treated (left) and control (right) ferrets. White open arrowheads indicate BrdU-labeled PH3-immunopositive cells. White closed arrowheads indicate PH3-single stained cells. Yellow closed arrowheads indicate NeuN-single stained neurons in the hilus. **(D)** High-magnification images of double immunofluorescence for S100 and glial fibrillary acidic protein (GFAP) with BrdU-labeling and Hoechst staining in the dentate gyrus of the dorsal hippocampus in VPA-treated (left) and control (right) ferrets. White open arrowheads indicate BrdU-labeled S100-immunopositive cells. White closed arrowheads indicate S100-single stained neurons in the SGL and hilus Yellow closed arrowheads indicate GFAP-single stained astrocytes in the hilus.

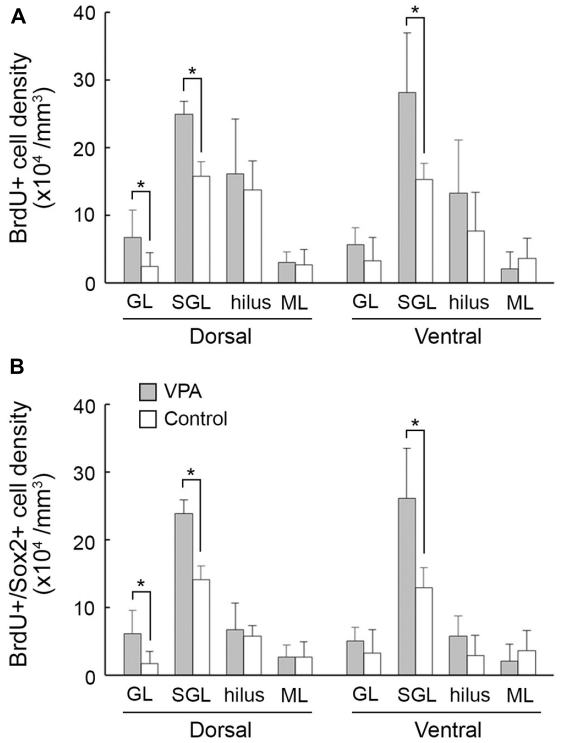

FIGURE 3 | The 5-bromo-2-deoxyuridine (BrdU)-labeled cell density and BrdU-labeled Sox2-immunopositive progenitor density in the dentate gyrus of dorsal and ventral hippocampi in postnatal day (PD) 20 ferrets. **(A)** BrdU-labeled cell density. **(B)** BrdU-labeled Sox2-immunopositive progenitor density. Data are shown as mean ± SEM. Significance is indicated using Scheffe's test at $*P < 0.001$; number of hippocampi = 8; GL, granular layer; ML, molecular layer; SGL, subgranular layer.

TABLE 2 | Percentages of cells immunostained for various markers in BrdU-labeled cells in dentate gyrus of hippocampus in VPA-treated ferrets on PD 20.

	Dorsal hippocampus		Ventral hippocampus	
	VPA	**Control**	**VPA**	**Control**
Granular layer				
% of Sox2+	90.0% (18/20)	71.4% (5/7)	88.2% (15/17)	100.0% (10/10)
% of C28k+	0% (0/20)	0% (0/7)	0% (0/17)	0% (0/10)
% of S100+	0% (0/25)	0% (0/23)	10.0% (2/10)	0% (0/13)
% of GFAP+	0% (0/25)	0% (0/23)	0% (0/10)	0% (0/13)
Subgranular layer				
% of Sox2+	96.0% (72/75)	89.4% (42/47)	92.9% (78/84)	84.8% (39/46)
% of S100+	15.3% (17/111)	7.0% (5/71)	10.9% (10/92)	2.1% (1/47)
% of GFAP+	0% (0/111)	0% (0/71)	0% (0/92)	0% (0/46)
Hilus				
% of Sox2+	89.1% (41/46)	85.4% (35/41)	89.7% (35/39)	78.3% (18/23)
% of NeuN+	0% (0/53)	5.6% (1/18)	0% (0/31)	6.3% (1/16)
% of S100+	6.5% (2/31)	4.2% (1/24)	4.8% (1/21)	0% (0/8)
% of GFAP+	0% (0/31)	0% (0/24)	0% (0/21)	0% (0/8)
Molecular layer				
% of Sox2+	88.9% (8/9)	100.0% (8/8)	100.0% (6/6)	100.0% (11/11)
% of NeuN+	0% (0/24)	0% (0/16)	0% (0/20)	0% (0/10)
% of S100+	8.3% (1/12)	13.3% (2/15)	0% (0/10)	0% (0/5)
% of GFAP+	0% (0/12)	0% (0/15)	0% (0/10)	0% (0/5)

Percentages are calculated by summing each immunolabeled cell counted within all ROIs from eight cerebral hemispheres. The number of each labeled cell for calculating the percentages is shown in parentheses. There were no significant difference in the incidence in any subregions of the dentate gyrus of both dorsal and ventral hippocampus between VPA-treated and control ferrets.

immunostaining was found in BrdU-labeled cells in the range of 0–15.3% in VPA-treated ferrets and from 0 to 13.3% in controls (**Table 2**). There was no difference in the incidence of S100 immunostaining in BrdU-labeled cells in any DG subregion between VPA-treated and controls. In contrast, no BrdU-positive cells expressed S100 immunostaining in the CA1 and CA3 fields in either group (**Supplementary Tables 1, 2**).

GFAP immunostaining mainly appeared in astrocytes sparsely distributed throughout the hippocampus (yellow closed arrowhead in **Figure 2D**) and was not observed in radial glia-like cells aligned in the DG granular through subgranular layers (**Figure 2D**), as seen in the adult ferret hippocampus (**Supplementary Figures 3A,B**). There were no BrdU-labeled GFAP-positive astrocytes in the hippocampal subregions, including the DG, except the stratum oriens in the CA1 and CA3 fields. GFAP-positive astrocytes were found in BrdU-labeled cells of the CA1 stratum oriens at 5.9% in the ventral hippocampus of VPA-treated ferrets and 12.5% in the dorsal hippocampus of control ferrets (**Supplementary Table 1**). In the CA3 stratum oriens, 21% of BrdU-labeled cells were GFAP-positive astrocytes in the dorsal hippocampus of VPA-treated ferrets (**Supplementary Table 2**). In any case, there was no difference in the incidence of GFAP-positive astrocytes in BrdU-labeled cells in all hippocampal subregions examined between VPA-treated and control ferrets.

Notably, immunostaining for PH3, a specific marker for mitosis, was found in a very small population of BrdU-labeled cells in the hippocampus (**Figure 2C**). Only 0.2 and 0.5% of BrdU-labeled cells distributed throughout the hippocampus were PH3-immunopositive in VPA-treated and control ferrets, respectively. The co-presence of PH3 immunostaining with BrdU labeling indicates the possibility that Sox2-positive progenitors distributed throughout the hippocampus may have mitotic potency.

Immunohistochemical Analysis of Postnatal Day 7 Ferret Premature Hippocampi

Immunofluorescence staining for Sox2 with BrdU labeling was performed in the premature hippocampus of VPA-treated ferrets and controls on PD 7, 2 h following BrdU injection simultaneously with the last VPA injection. BrdU-labeled Sox2-positive progenitors were abundant, particularly in the granular and subgranular layers and hilus of the DG in the premature hippocampus (**Figure 4**). As it was difficult to distinguish the border between granular and subgranular layers in the premature DG, the density of BrdU-labeled Sox2-positive progenitors was estimated in areas including either the granular layer

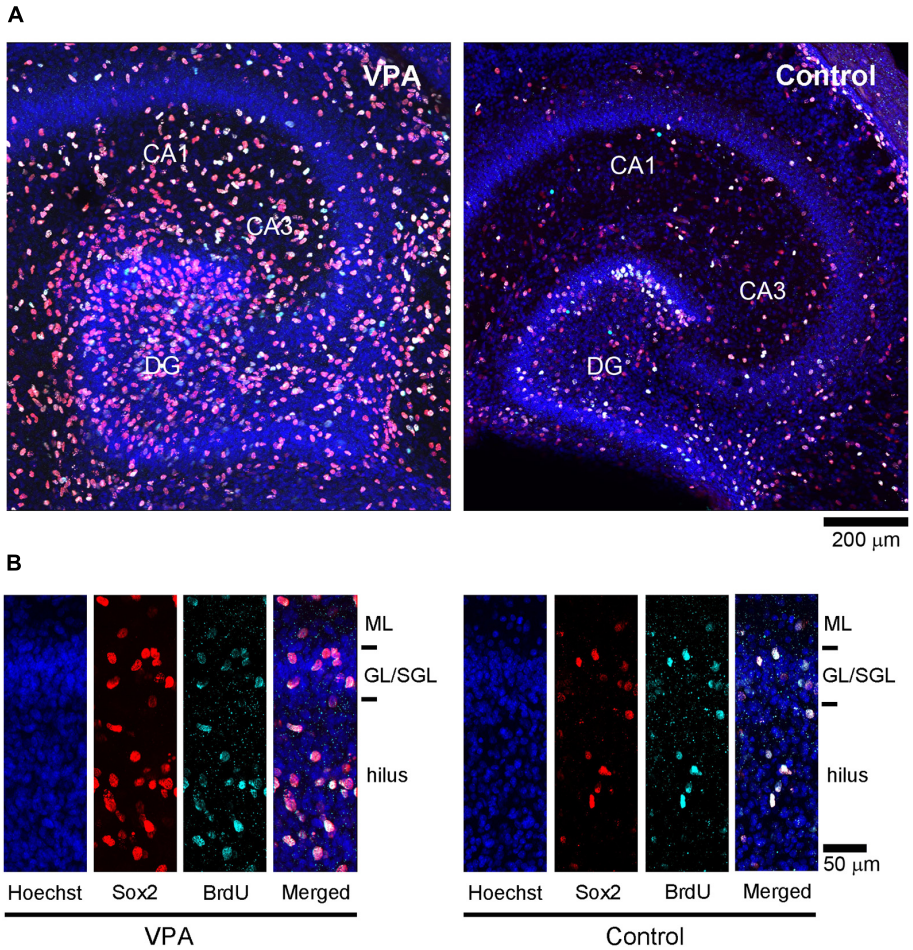

FIGURE 4 | Sox2 immunofluorescence with 5-bromo-2-deoxyuridine (BrdU)-labeling and Hoechst staining in premature hippocampus of postnatal day (PD) 7 ferrets. **(A)** Low-magnification images in the premature hippocampi of valproic acid (VPA)-treated (left) and control (right) ferrets. **(B)** High-magnification images of Sox2 immunofluorescence with BrdU-labeling and Hoechst staining in the dentate gyrus in VPA-treated (left) and control (right) ferrets. GL, granular layer; ML, molecular layer; SGL, subgranular layer.

or subgranular layer or the hilus. BrdU-labeled cells were significantly denser in both the granular/subgranular layers and hilus in VPA-treated ferrets than in controls (**Figure 5**). Sox2-positive progenitors were found in BrdU-labeled cells at 97.5% and 88.2% in the granular/subgranular layers and 94.6% and 91.7% in the hilus of VPA-treated and control ferrets, respectively (**Table 3**). The density of BrdU-labeled Sox2-positive progenitors was significantly greater in both the granular/subgranular layers and hilus of VPA-treated ferrets than those of controls (**Figure 5**). Thus, VPA exposure facilitated the proliferation of Sox2-positive progenitor pools in the DG of the premature hippocampus.

DISCUSSION

The effect of VPA on the developing hippocampus has been studied mainly during neural tube development. These findings are inconsistent; although a previous study has reported an increased density of neurons in the DG and CA fields in rats (Edalatmanesh et al., 2013), other studies have reported enhanced neurogenesis with decreased neuronal progenitor pools in mice (Juliandi et al., 2015) and reduced expression of GAD 67, an isoform of GABA synthetic enzyme, in rats (Hou et al., 2018; Win-Shwe et al., 2018). In contrast, there have been a few studies regarding the effect of VPA on the hippocampus during neonatal periods. Neonatal VPA exposure induced cell proliferation rather than neuronal differentiation in the hippocampal DG 24 h after VPA injection in rat infants (Wang et al., 2016). The current investigation consistently showed proliferation of Sox2-positive progenitors in the hippocampal DG of PD 7 ferrets immediately following VPA injection. The putative precursors of granular neurons appeared massively in the DG during the first week of postnatal age in mice (Nicola et al., 2015; Hevner, 2016). Therefore, stable results may be obtained by neonatal VPA exposure targeting DG progenitors rather than prenatal VPA exposure targeting neural tube development. It has been reported that DG progenitors are changed from

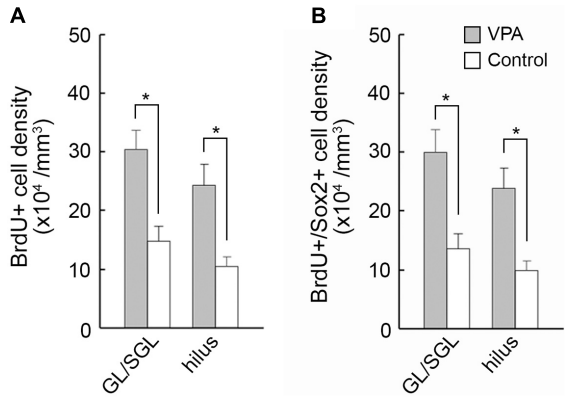

FIGURE 5 | The 5-bromo-2-deoxyuridine (BrdU)-labeled cell density and BrdU-labeled Sox2-immunopositive progenitor density in the dentate gyrus of premature hippocampi in postnatal day (PD) ferrets. **(A)** BrdU-labeled cell density. **(B)** BrdU-labeled Sox2-immunopositive progenitor density. Data are shown as mean ± SEM. Significance is indicated using Scheffe's test at $^*P < 0.001$; number of hippocampi = 8; GL, granular layer; SGL, subgranular layer.

TABLE 3 | Percentages of Sox2-immunopositive progenitors in BrdU-labeled cells in dentate gyrus of hippocampus in VPA-treated ferrets on PD 7.

	VPA	Control
Granular/subgranular layers	95.7% (67/70)	88.2% (30/34)
Hilus	94.6% (53/56)	91.7% (22/24)

Percentages are calculated by summing each immunolabeled cell counted within all ROIs from six cerebral hemispheres. The number of each labeled cell for calculating the percentages is shown in parentheses. There were no significant difference in the incidence in any subregions of the dentate gyrus of hippocampus between VPA-treated and control ferrets.

embryonic-type to adult-type during early postnatal ages in mice (Matsue et al., 2018). VPA has a proliferative effect on neonatal DG progenitors (embryonic-type) (Wang et al., 2016; present results); however, it facilitates adult neurogenesis of the DG progenitors (adult-type) (Hsieh et al., 2004). It may be interesting to note the factors responsible for the diverse effects of VPA on embryonic and adult forms of DG progenitor cells. Regarding the adult type, VPA-facilitated adult neurogenesis is mediated by inhibition of histone deacetylase activity in rats (Hsieh et al., 2004). One of the factors related to facilitating the proliferation of the embryonic-type DG progenitors may be the Wnt/β-catenin pathway, which was reportedly upregulated in the hippocampus of VPA-treated rat fetuses (Wang et al., 2010).

The present study tracked the DG progenitors of PD 7 ferret infants by labeling them with BrdU and examined their fates on PD 20 using neuronal and glial markers. Although tracked cells could not be fully characterized, they expressed Sox2 in the majority, but not neural (NeuN and calbindin D-28k) and glial (GFAP and S100) markers examined in both VPA-treated and control ferrets. Notably, the density of tracked cells expressing Sox2 in the subgranular layer was significantly increased by neonatal VPA exposure. This suggests that VPA promotes the proliferation of embryonic-type DG progenitors, resulting in increased adult-type DG progenitors, mainly in the DG subgranular layer. In contrast, GFAP-positive radial processes vertically across the DG granular and subgranular layers were found in young adult ferrets (PD 90), but not in prepubertal immature ferrets (PD 20). The DG progenitors had GFAP-positive radial processes, even if they were embryonic-type, in humans (Stagaard Janas et al., 1991), rats (Rickmann et al., 1987; Li et al., 2011), and mice (Matsue et al., 2018). Therefore, the chemical characteristics of embryonic and adult DG progenitors may be diverse among mammalian species. Embryonic DG progenitors may lack GFAP expression specifically in carnivores, and are still low in PD 20 ferrets.

The cerebral cortex was thickened and expanded its width at the posterior one-third when ferrets were exposed to VPA by an identical administration schedule to the current investigation (Sawada et al., 2021). The substantial effect of neonatal VPA exposure on the ferret hippocampus may increase adult-type DG progenitors in the DG subgranular layer in the present study. Prenatal VPA exposure has a long-term effect on DG progenitors, impairing adult neurogenesis and hippocampus-dependent learning and memory in mice (Juliandi et al., 2015). Impairment of social behaviors has been reported in ferrets exposed to neonatal VPA (Krahe et al., 2016), but not in hippocampus-related behavioral changes. The current findings revealed mitotic potency on tracked neonatal DG progenitors in both VPA-treated ferrets and controls on PD 20. Further studies are needed to evaluate neurogenesis of the tracked neonatal DG progenitors in the subgranular layer and hippocampal-related behaviors in VPA-treated ferrets.

CONCLUSION

Prenatal and neonatal exposure to VPA induces ASD-like behavioral abnormalities in various mammalian species (Miyazaki et al., 2005; Yochum et al., 2008; Mychasiuk et al., 2012; Favre et al., 2013; Burenkova et al., 2014; Yasue et al., 2018), including ferrets (Krahe et al., 2016). These behavioral abnormalities are believed to be associated with cerebral cortical abnormalities that have been reported as the effect of developmental VPA exposure in ferrets (Sawada et al., 2021) and other mammalian species (Wood et al., 2014; Fujimura et al., 2016; Lauber et al., 2016). In contrast, prenatal and neonatal VPA exposure can alter the development of various brain regions other than the cerebral cortex. The current findings revealed that neonatal VPA exposure alters the progenitors in the DG subgranular layers, which may be involved in hippocampal adult neurogenesis and its related behaviors. This will be helpful for a comprehensive understanding of brain abnormalities induced by neonatal VPA exposure.

DATA AVAILABILITY STATEMENT

The original contributions presented in the study are included in the article/**Supplementary Material**, further inquiries can be directed to the corresponding author.

ETHICS STATEMENT

The animal study was reviewed and approved by Institutional Animal Care and Use Committees of Tsukuba International University.

AUTHOR CONTRIBUTIONS

All authors had full access to all the data in the study and take responsibility for the integrity of the data and the accuracy of the data analysis. KS: study concept and design. KS, SK, and IA: acquisition of data and critical revision of the manuscript for important intellectual content. KS and IA: analysis and interpretation of data, drafting of the manuscript, and obtained funding.

FUNDING

This study was supported by a grant from Tsukuba International University. This research was supported by Program for Supporting Formation of Advanced Research Platforms (JST/MEXT).

SUPPLEMENTARY MATERIAL

The Supplementary Material for this article can be found online at: https://www.frontiersin.org/articles/10.3389/fnins.2021.736313/full#supplementary-material

REFERENCES

Burenkova, O. V., Aleksandrova, E. A., and Zaraiskaya, I. Y. (2014). Administration of histone deacetylase inhibitor during neonatal period changes emotionality of adult male 129Sv mice. *Bull. Exp. Biol. Med.* 156, 620–623. doi: 10.1007/s10517-014-2409-0

Ecker, C., Ronan, L., Feng, Y., Daly, E., Murphy, C., Ginestet, C. E., et al. (2013). Intrinsic gray-matter connectivity of the brain in adults with autism spectrum disorder. *Proc. Natl. Acad. Sci. U. S. A.* 110, 13222–13227. doi: 10.1073/pnas.1221880110

Edalatmanesh, M. A., Nikfarjam, H., Vafaee, F., and Moghadas, M. (2013). Increased hippocampal cell density and enhanced spatial memory in the valproic acid rat model of autism. *Brain Res.* 1526, 15–25. doi: 10.1016/j.brainres.2013.06.024

Favre, M. R., Barkat, T. R., Lamendola, D., Khazen, G., Markram, H., and Markram, K. (2013). General developmental health in the VPA-rat model of autism. *Front. Behav. Neurosci.* 7:88. doi: 10.3389/fnbeh.2013.00088

Fujimura, K., Mitsuhashi, T., Shibata, S., Shimozato, S., and Takahashi, T. (2016). In utero exposure to valproic acid induces neocortical dysgenesis via dysregulation of neural progenitor cell proliferation/differentiation. *J. Neurosci.* 36, 10908–10919. doi: 10.1523/JNEUROSCI.0229-16.2016

Göttlicher, M., Minucci, S., Zhu, P., Krämer, O. H., Schimpf, A., Giavara, S., et al. (2001). Valproic acid defines a novel class of HDAC inhibitors inducing differentiation of transformed cells. *EMBO J.* 20, 6969–6978. doi: 10.1093/emboj/20.24.6969

Hevner, R. F. (2016). Evolution of the mammalian dentate gyrus. *J. Comp. Neurol.* 524, 578–594. doi: 10.1002/cne.23851

Hou, Q., Wang, Y., Li, Y., Chen, D., Yang, F., and Wang, S. (2018). A developmental study of abnormal behaviors and altered GABAergic signaling in the VPA-treated rat model of autism. *Front. Behav. Neurosci.* 12:182. doi: 10.3389/fnbeh.2018.00182

Hsieh, J., Nakashima, K., Kuwabara, T., Mejia, E., and Gage, F. H. (2004). Histone deacetylase inhibition-mediated neuronal differentiation of multipotent adult neural progenitor cells. *Proc. Natl. Acad. Sci. U. S. A.* 101, 16659–16664. doi: 10.1073/pnas.0407643101

Juliandi, B., Abematsu, M., Sanosaka, T., Tsujimura, K., Smith, A., and Nakashima, K. (2012). Induction of superficial cortical layer neurons from mouse embryonic stem cells by valproic acid. *Neurosci. Res.* 72, 23–31. doi: 10.1016/j.neures.2011.09.012

Juliandi, B., Tanemura, K., Igarashi, K., Tominaga, T., Furukawa, Y., Otsuka, M., et al. (2015). Reduced adult hippocampal neurogenesis and cognitive impairments following prenatal treatment of the antiepileptic drug valproic acid. *Stem Cell Rep.* 5, 996–1009. doi: 10.1016/j.stemcr.2015.10.012

Kamiya, S., and Sawada, K. (2021). Immunohistochemical characterization of postnatal changes in cerebellar cortical cytoarchitectures in ferrets. *Anat. Rec. (Hoboken)* 304, 413–424. doi: 10.1002/ar.24420

Krahe, T. E., Filgueiras, C. C., and Medina, A. E. (2016). Effects of developmental alcohol and valproic acid exposure on play behavior of ferrets. *Int. J. Dev. Neurosci.* 52, 75–81. doi: 10.1016/j.ijdevneu.2016.03.007

Kroenke, C. D., Mills, B. D., Olavarria, J. F., and Neil, J. J. (2014). "Neuroanatomy of the ferret brain with focus on the cerebral cortex," in *Biology and Diseases of the Ferret*, 3rd Edn, eds J. G. Fox and R. P. Marini (Hoboken NJ: Wiley Blackwell), 69–80. doi: 10.1002/9781118782699.ch3

Lauber, E., Filice, F., and Schwaller, B. (2016). Prenatal valproate exposure differentially affects parvalbumin-expressing neurons and related circuits in the cortex and striatum of mice. *Front. Mol. Neurosci.* 9:150. doi: 10.3389/fnmol.2016.00150

Li, H., Jin, G., Qin, J., Yang, W., Tian, M., Tan, X., et al. (2011). Identification of neonatal rat hippocampal radial glia cells in vitro. *Neurosci. Lett.* 490, 209–214. doi: 10.1016/j.neulet.2010.12.054

Libero, L. E., DeRamus, T. P., Deshpande, H. D., and Kana, R. K. (2014). Surface-based morphometry of the cortical architecture of autism spectrum disorders: volume, thickness, area, and gyrification. *Neuropsychologia* 62, 1–10. doi: 10.1016/j.neuropsychologia.2014.07.001

Libero, L. E., Schaer, M., Li, D. D., Amaral, D. G., and Nordahl, C. W. (2019). Longitudinal study of local gyrification index in young boys with autism spectrum disorder. *Cereb. Cortex* 29, 2575–2587. doi: 10.1093/cercor/bhy126

Matsue, K., Minakawa, S., Kashiwagi, T., Toda, K., Sato, T., Shioda, S., et al. (2018). Dentate granule progenitor cell properties are rapidly altered soon after birth. *Brain Struct. Funct.* 223, 357–369. doi: 10.1007/s00429-017-1499-7

Mirza, R., and Sharma, B. (2019). Benefits of Fenofibrate in prenatal valproic acid-induced autism spectrum disorder related phenotype in rats. *Brain. Res. Bull.* 147, 36–46. doi: 10.1016/j.brainresbull.2019.02.003

Miyazaki, K., Narita, N., and Narita, M. (2005). Maternal administration of thalidomide or valproic acid causes abnormal serotonergic neurons in the offspring: implication for pathogenesis of autism. *Int. J. Dev. Neurosci.* 223, 287–297. doi: 10.1016/j.ijdevneu.2004.05.004

Mychasiuk, R., Richards, S., Nakahashi, A., Kolb, B., and Gibb, R. (2012). Effects of rat prenatal exposure to valproic acid on behaviour and neuro-anatomy. *Dev. Neurosci.* 34, 268–276. doi: 10.1159/000341786

Nicola, Z., Fabel, K., and Kempermann, G. (2015). Development of the adult neurogenic niche in the hippocampus of mice. *Front. Neuroanat.* 9:53. doi: 10.3389/fnana.2015.00053

Olexová, L., Štefánik, P., and Kršková, L. (2016). Increased anxiety-like behaviour and altered GABAergic system in the amygdala and cerebellum of VPA rats –

an animal model of autism. *Neurosci. Lett.* 629, 9–14. doi: 10.1016/j.neulet.2016.06.035

Phiel, C. J., Zhang, F., Huang, E. Y., Guenther, M. G., Lazar, M. A., and Klein, P. S. (2001). Histone deacetylase is a direct target of valproic acid, a potent anticonvulsant, mood stabilizer, and teratogen. *J. Biol. Chem.* 276, 36734–36741. doi: 10.1074/jbc.M101287200

Rickmann, M., Amaral, D. G., and Cowan, W. M. (1987). Organization of radial glial cells during the development of the rat dentate gyrus. *J. Comp. Neurol.* 264, 449–479. doi: 10.1002/cne.902640403

Sabers, A., Bertelsen, F. C., Scheel-Krüger, J., Nyengaard, J. R., and Møller, A. (2014). Long-term valproic acid exposure increases the number of neocortical neurons in the developing rat brain. A possible new animal model of autism. *Neurosci. Lett.* 580, 12–16. doi: 10.1016/j.neulet.2014.07.036

Sawada, K. (2019). Follow-up study of subventricular zone progenitors with multiple rounds of cell division during sulcogyrogenesis in the ferret cerebral cortex. *IBRO Rep.* 7, 42–51. doi: 10.1016/j.ibror.2019.07.1720

Sawada, K., and Aoki, I. (2017). Biphasic aspect of sexually dimorphic ontogenetic trajectory of gyrification in the ferret cerebral cortex. *Neuroscience* 364, 71–81. doi: 10.1016/j.neuroscience.2017.09.015

Sawada, K., Horiuchi-Hirose, M., Saito, S., and Aoki, I. (2013). MRI-based morphometric characterizations of sexual dimorphism of the cerebrum of ferrets (*Mustela putorius*). *Neuroimage* 83, 294–306. doi: 10.1016/j.neuroimage.2013.06.024

Sawada, K., Horiuchi-Hirose, M., Saito, S., and Aoki, I. (2015). Male prevalent enhancement of leftward asymmetric development of the cerebellar cortex in ferrets (*Mustela putorius*). *Laterality* 20, 723–737. doi: 10.1080/1357650X.2015.1047379

Sawada, K., Kamiya, S., and Aoki, I. (2020). Asymmetry of cerebellar lobular development in ferrets. *Symmetry* 12:735. doi: 10.3390/sym12091509

Sawada, K., Kamiya, S., and Aoki, I. (2021). Neonatal valproic acid exposure produces altered gyrification related to increased parvalbumin-immunopositive neuron density with thickened sulcal floors. *PLoS One* 16:e0250262. doi: 10.1371/journal.pone.0250262

Sawada, K., and Watanabe, M. (2012). Development of cerebral sulci and gyri in ferrets (*Mustela putorius*) *Congenit. Anom. (Kyoto)* 52, 168–175. doi: 10.1111/j.1741-4520.2012.00372.x

Stagaard Janas, M., Nowakowski, R. S., and Møllgård, K. (1991). Glial cell differentiation in neuron-free and neuron-rich regions. II. Early appearance of S-100 protein positive astrocytes in human fetal hippocampus. *Anat. Embryol. (Berl.).* 184, 559–569. doi: 10.1007/BF00942578

Wang, C. Y., Cheng, C. W., Wang, W. H., Chen, P. S., and Tzeng, S. F. (2016). Postnatal stress induced by injection with valproate leads to developing emotional disorders along with molecular and cellular changes in the hippocampus and amygdala. *Mol. Neurobiol.* 53, 6774–6785. doi: 10.1007/s12035-015-9600-9

Wang, Z., Xu, L., Zhu, X., Cui, W., Sun, Y., Nishijo, H., et al. (2010). Demethylation of specific Wnt/β-catenin pathway genes and its upregulation in rat brain induced by prenatal valproate exposure. *Anat. Rec. (Hoboken)* 293, 1947–1953. doi: 10.1002/ar.21232

Win-Shwe, T. T., Nway, N. C., Imai, M., Lwin, T. T., Mar, O., and Watanabe, H. (2018). Social behavior, neuroimmune markers and glutamic acid decarboxylase levels in a rat model of valproic acid-induced autism. *J. Toxicol. Sci.* 43, 631–643. doi: 10.2131/jts.43.631

Wood, A. G., Chen, J., Barton, S., Nadebaum, C., Anderson, V. A., Catroppa, C., et al. (2014). Altered cortical thickness following prenatal sodium valproate exposure. *Ann. Clin. Transl. Neurol.* 1, 497–501. doi: 10.1002/acn3.74

Yasue, M., Nakagami, A., Nakagaki, K., Ichinohe, N., and Kawai, N. (2018). Inequity aversion is observed in common marmosets but not in marmoset models of autism induced by prenatal exposure to valproic acid. *Behav. Brain Res.* 343, 36–40. doi: 10.1016/j.bbr.2018.01.013

Yochum, C. L., Dowling, P., Reuhl, K. R., Wagner, G. C., and Ming, X. (2008). VPA-induced apoptosis and behavioral deficits in neonatal mice. *Brain Res.* 1203, 126–132. doi: 10.1016/j.brainres.2008.01.055

Conflict of Interest: The authors declare that the research was conducted in the absence of any commercial or financial relationships that could be construed as a potential conflict of interest.

Publisher's Note: All claims expressed in this article are solely those of the authors and do not necessarily represent those of their affiliated organizations, or those of the publisher, the editors and the reviewers. Any product that may be evaluated in this article, or claim that may be made by its manufacturer, is not guaranteed or endorsed by the publisher.

frontiers in Neuroscience

ORIGINAL RESEARCH
published: 03 December 2021
doi: 10.3389/fnins.2021.766802

Sex and Genotype Modulate the Dendritic Effects of Developmental Exposure to a Human-Relevant Polychlorinated Biphenyls Mixture in the Juvenile Mouse

*Kimberly P. Keil Stietz[1†‡], Sunjay Sethi[1†], Carolyn R. Klocke[1†], Tryssa E. de Ruyter[1], Machelle D. Wilson[2], Isaac N. Pessah[1] and Pamela J. Lein[1]**

[1] Department of Molecular Biosciences, School of Veterinary Medicine, University of California, Davis, Davis, CA, United States, [2] Clinical and Translational Science Center, Division of Biostatistics, Department of Public Health Sciences, School of Medicine, University of California, Davis, Davis, CA, United States

OPEN ACCESS

Edited by:
Kazuhiko Sawada, Tsukuba International University, Japan

Reviewed by:
Eiki Kimura, University of Cincinnati, United States
Dora Sedmak, University of Zagreb, Croatia

***Correspondence:**
Pamela J. Lein
pjlein@ucdavis.edu

† These authors have contributed equally to this work and share first authorship

‡ Present address:
Kimberly P. Keil Stietz, Department of Comparative Biosciences, School of Veterinary Medicine, University of Wisconsin–Madison, Madison, WI, United States

Specialty section:
This article was submitted to Neurodevelopment, a section of the journal Frontiers in Neuroscience

Received: *30 August 2021*
Accepted: *04 November 2021*
Published: *03 December 2021*

Citation:
Keil Stietz KP, Sethi S, Klocke CR, de Ruyter TE, Wilson MD, Pessah IN and Lein PJ (2021) Sex and Genotype Modulate the Dendritic Effects of Developmental Exposure to a Human-Relevant Polychlorinated Biphenyls Mixture in the Juvenile Mouse. Front. Neurosci. 15:766802. doi: 10.3389/fnins.2021.766802

While many neurodevelopmental disorders (NDDs) are thought to result from interactions between environmental and genetic risk factors, the identification of specific gene-environment interactions that influence NDD risk remains a critical data gap. We tested the hypothesis that polychlorinated biphenyls (PCBs) interact with human mutations that alter the fidelity of neuronal Ca^{2+} signaling to confer NDD risk. To test this, we used three transgenic mouse lines that expressed human mutations known to alter Ca^{2+} signals in neurons: (1) gain-of-function mutation in ryanodine receptor-1 (T4826I-*RYR1*); (2) CGG-repeat expansion in the 5′ non-coding portion of the fragile X mental retardation gene 1 (*FMR1*); and (3) a double mutant (DM) that expressed both mutations. Transgenic and wildtype (WT) mice were exposed throughout gestation and lactation to the MARBLES PCB mix at 0.1, 1, or 6 mg/kg in the maternal diet. The MARBLES mix simulates the relative proportions of the twelve most abundant PCB congeners found in serum from pregnant women at increased risk for having a child with an NDD. Using Golgi staining, the effect of developmental PCB exposure on dendritic arborization of pyramidal neurons in the CA1 hippocampus and somatosensory cortex of male and female WT mice was compared to pyramidal neurons from transgenic mice. A multilevel linear mixed-effects model identified a main effect of dose driven by increased dendritic arborization of cortical neurons in the 1 mg/kg PCB dose group. Subsequent analyses with genotypes indicated that the MARBLES PCB mixture had no effect on the dendritic arborization of hippocampal neurons in WT mice of either sex, but significantly increased dendritic arborization of cortical neurons of WT males in the 6 mg/kg PCB dose group. Transgene expression increased sensitivity to the impact of developmental PCB exposure on dendritic arborization in a sex-, and brain region-dependent manner. In conclusion, developmental exposure to PCBs present in the gestational environment of at-risk humans interfered with normal dendritic

morphogenesis in the developing mouse brain in a sex-, genotype- and brain region-dependent manner. Overall, these observations provide proof-of-principle evidence that PCBs interact with heritable mutations to modulate a neurodevelopmental outcome of relevance to NDDs.

Keywords: FMR1 premutation, gene–environment interaction, Golgi stain, neurodevelopmental disorders, ryanodine receptor, Sholl analysis

INTRODUCTION

Despite a worldwide ban on the production of polychlorinated biphenyls (PCBs) since the early 2000's, PCBs remain a significant risk to the developing human brain. Pregnant women and children continue to be exposed to not only legacy PCBs released from hazardous waste sites and PCB-containing equipment and materials manufactured prior to the PCB production ban, but also contemporary PCBs produced as inadvertent byproducts of contemporary pigment and dye production or via environmental degradation of legacy PCBs (Koh et al., 2015; Granillo et al., 2019). Human (Schantz et al., 2003; Berghuis et al., 2015; Pessah et al., 2019) and animal (Sable and Schantz, 2006; Klocke and Lein, 2020) studies provide compelling evidence of PCB developmental neurotoxicity, while recent epidemiologic studies suggest that developmental PCB exposures confer risk for NDDs, including autism spectrum disorder (ASD) and attention-deficit/hyperactivity disorder (ADHD) (Lyall et al., 2017; Pessah et al., 2019; Xi and Wu, 2021).

The size and shape of the neuronal dendritic arbor is a key structural determinant of neuronal connectivity, and changes in dendritic morphology (increased or decreased dendrite number, branching and/or spine density) contribute to the altered patterns of neuronal connectivity observed in many NDDs (Coskun et al., 2013; Keown et al., 2013; Khan et al., 2015; Alaerts et al., 2016; Cooper et al., 2017). The dynamic structural remodeling of dendrites and synapses that occurs during development is driven in large part by Ca^{2+}-dependent signaling that mediates the influence of neural activity and other environmental factors on dendritic morphogenesis and plasticity (Cline, 2001; Konur and Ghosh, 2005; Chen and Nedivi, 2010). Many NDD risk genes encode proteins that regulate intracellular Ca^{2+} signals, are regulated by local fluctuations in Ca^{2+} concentrations and/or are involved in regulating dendritic growth and synaptogenesis (Krey and Dolmetsch, 2007; Pessah et al., 2010; Grove et al., 2019). Developmental exposure to Aroclor 1254, a commercial mixture of legacy PCBs, or to PCB 95 has been demonstrated to increase dendritic arborization in the hippocampus, cortex and cerebellum of experimental animal models (Roegge et al., 2006; Lein et al., 2007; Yang et al., 2009; Wayman et al., 2012b). *In vitro* studies have shown that the ryanodine receptor (RyR)-active PCB congeners PCB 95 and PCB 136 (Wayman et al., 2012b; Yang et al., 2014), and the lower chlorinated congener PCB 11 (Sethi et al., 2018), promote dendritic growth in primary hippocampal and cortical neurons via activation of Ca^{2+}-dependent signaling pathways (Wayman et al., 2012a; Sethi et al., 2018) that map onto Ca^{2+}-dependent signaling pathways implicated in the etiology of NDDs (Panesar et al., 2020). These observations suggest the possibility that PCBs amplify the risk and/or severity of NDDs by converging on signaling pathways altered by heritable defects in Ca^{2+}-dependent signaling pathways that regulate dendritic arborization and/or plasticity.

To test this hypothesis, we compared the effect of developmental exposure to a human-relevant PCB mixture on the dendritic morphology of pyramidal neurons in the hippocampus and somatosensory cortex of wildtype (WT) *vs.* transgenic mice that expressed heritable human mutations that modulate the fidelity of neuronal Ca^{2+} signaling. Specifically, we examined three transgenic lines: (1) mice that carried a human *RYR1* gain-of-function mutation (T4826I-*RYR1*) (Barrientos et al., 2012; Yuen et al., 2012); (2) mice that expressed a CGG repeat expansion in the 5′ non-coding region of the fragile X mental retardation gene 1 (*FMR1*) in the premutation range (55–200 repeats) (Willemsen et al., 2003); and (3) mice that expressed both mutations (double mutant; DM) (Keil et al., 2019b). RyR Ca^{2+} ion channels regulate intracellular Ca^{2+} stores (Pessah et al., 2010) and their activation is required for activity-dependent dendritic growth and synaptogenesis (Wayman et al., 2012b; Lesiak et al., 2014). A genome wide association study identified *RYR1* and *RYR2* as ASD candidate genes by using sex as an additional risk factor (Lu and Cantor, 2012). *FMR1* premutation is causally linked to fragile X-associated tremor/ataxia syndrome (FXTAS) and is the most prevalent monogenic NDD risk factor (Krueger and Bear, 2011; Chonchaiya et al., 2012; Leehey and Hagerman, 2012). Unlike *FMR1* knockout models, these mice exhibit reduced FMR1 protein (FMRP) expression and elevated *Fmr1* mRNA (Berman et al., 2012; Robin et al., 2017). In a study examining GWAS and genetic databases, approximately 10% of FMRP targets in the brain overlap with ASD candidate genes, many of which regulate neuronal connectivity (Fernandez et al., 2013). Studies of primary neurons derived from *FMR1* premutation knockin mice (referred to hereafter as CGG mice) demonstrate resting intracellular Ca^{2+} concentrations threefold higher than neurons derived from WT (Robin et al., 2017), and abnormal patterns of intracellular Ca^{2+} oscillations including increased number of spontaneous Ca^{2+} burst activity (Cao et al., 2012). iPSC-derived neurons from an *FMR1* premutation carrier also exhibited enhanced Ca^{2+} transients (Liu et al., 2012). Altered dendritic arborization and spine density are linked with these changes in Ca^{2+} dynamics in both primary neurons from *FMR1* premutation mice (Chen et al., 2010), and iPSC-derived neurons from humans with *FMR1* premutation (Liu et al., 2012).

In addition to the two transgenic lines expressing either a RYR1 gain-of-function mutation or *FMR1* premutation, we examined a transgenic line (DM) that expressed both mutations (Keil et al., 2019b). Expressed variants in RyR1 and FMR1

expansion repeats in the premutation range are relatively common mutations in the human population. Approximately 15% of the human population is estimated to carry one or more RYR1 genetic variants (Kim et al., 2013), whereas, the estimated prevalence of the FMR1 premutation in the human population is 1:209 in females and 1:430 in males (Tassone et al., 2012). Both mutations are phenotypically silent until triggered by halogenated anesthetics (RYR1 gain-of-function) or advancing age (*FMR1* premutation). Thus, while we are not aware of any clinical reports of human patients expressing mutations at both loci, there is a reasonable likelihood that there are individuals who carry both mutagens. Regardless, these DM mice were not created to mimic a human disease, but rather as an experimental model to investigate whether gene dosage influences the effects of developmental PCB exposures. In other words, is the phenotypic outcome amplified when two mutations that converge on calcium signaling and regulation of dendritic growth are expressed relative to expression of either mutation alone. The *RYR1* mutation was chosen as a direct target of PCBs (Ta and Pessah, 2007); whereas the FMR1 premutation was chosen because of its demonstrated role in translational control of calcium regulating proteins (Robin et al., 2017). Our earlier characterization of dendritic arborization in juvenile male and female mice from these three transgenic lines revealed significantly increased dendritic arborization of pyramidal neurons in the CA1 hippocampus of male T4826I-*RYR1* and, to a lesser extent, male CGG mice relative to male congenic WT mice. Dendritic arborization of pyramidal neurons in the somatosensory cortex was significantly enhanced in male and female CGG and DM mice compared to WT mice with the most pronounced differences seen in DM females (Keil et al., 2019b).

In this study, we exposed WT, T4826I, CGG and DM mice to vehicle or the MARBLES PCB mixture (Sethi et al., 2019) in the maternal diet throughout gestation and lactation. The MARBLES PCB mixture proportionally mimics the top twelve PCB congeners detected in the serum of pregnant women enrolled in the MARBLES cohort (Granillo et al., 2019; Sethi et al., 2019) who are at increased risk of having a child with an NDD (Hertz-Picciotto et al., 2018). We previously demonstrated that the MARBLES PCB mix has RyR activity *in vitro* at low micromolar concentrations, reflecting the small percentage of PCB congeners with potent RyR activity (Sethi et al., 2019). This is consistent with epidemiological evidence that RyR-active PCBs are associated with increased risk of ASD (Granillo et al., 2019). Our findings indicate that expression of heritable mutations that alter the fidelity of neuronal Ca^{2+} signals modulated the impact of PCB exposure on several parameters of dendritic arborization in a sex- and brain region-dependent manner.

MATERIALS AND METHODS

Materials

Organic unsalted peanut butter (Trader Joe's, Monrovia, CA, United States) and organic peanut oil (Spectrum Organic Products, LLC, Melville, NY, United States) were purchased from Trader Joe's (Davis, CA, United States). The individual PCB congeners (PCB 11, 28, 52, 84, 95, 101, 118, 135, 138, 149, 153, and 180) used to make the MARBLES PCB mix were synthesized and authenticated as previously described (Li et al., 2018; Sethi et al., 2019). The purity of all PCB congeners was > 99% pure (Sethi et al., 2019).

Animals

All procedures involving animals were conducted in accordance with the NIH Guide for the Care and Use of Laboratory Animals, conformed to the ARRIVE guidelines (Kilkenny et al., 2010), and were approved by the University of California, Davis Institutional Animal Care and Use Committee. Male and female mice were derived from transgenic mouse colonies maintained at UC Davis (Keil et al., 2019b), which included transgenic strains: (1) homozygous for the human gain-of-function mutation in *RYR1* (T4826I-*RYR1*) referred to as T4826I mice, (2) homozygous (female) or hemizygous (male) for the X-linked CGG repeat expansion in *FMR1* in the permutation range (170-200 repeats; referred to as CGG mice); and (3) DM mice that expressed both mutations (Keil et al., 2019b). C57Bl/6J and SVJ129 WT mice were purchased from Jackson Labs (Sacramento, CA, United States) and crossed to generate a 75% C57Bl/6J / 25% SVJ129 congenic WT line that matched the genetic background of the T4826I, CGG and DM animals as determined by single-nucleotide polymorphism (SNP) analysis (Keil et al., 2019b). Homo/hemizygous matings were used to generate the juvenile mice used for Golgi analyses, and all animals used in this study were genotyped as previously described (Keil et al., 2019b).

All animals were housed in clear plastic shoebox cages containing corn cob bedding and maintained on a 12 h light and dark cycle at 22 ± 2°C with 40–50% humidity. Feed (Diet 5058, LabDiet, Saint Louis, MO, United States) and water were available *ad libitum*. Two weeks prior to mating, nulliparous and previously unmated dams (>6 weeks of age) were singly housed and PCB dosing was initiated. Dams were placed with a genotype-matched male overnight for mating. Males and females were separated the next day and females were checked for the presence of a copulatory plug, which was considered gestational day 0. After mating, dams were housed singly prior to parturition and with their pups after parturition. At postnatal day 2 (P2), pups were culled or cross-fostered within genotype- and dose-matched litters to ensure all litters consisted of 4–8 pups. After weaning at P21, pups were group housed with same-sex littermates. Mice underwent self-grooming and social approach behavioral testing as part of a larger study, and then were euthanized on P27–31 to collect brains for Golgi analyses.

This study is part of an overall study designed to assess the effects of developmental exposure to the MARBLES PCB mixture on multiple developmental outcomes, including NDD-relevant behavioral phenotypes (data under review), the gut microbiome and intestinal physiology (Rude et al., 2019) and cytokine levels in the serum and hippocampus (Matelski et al., 2020). The data described in this study were collected from animals used for behavioral studies prior to being euthanized to harvest brains for morphometric analyses of dendritic arborization. We previously reported that developmental exposure to the MARBLES PCB

mixture had no effect on the length of time from mating to parturition and pregnancy rates across groups averaged 88% (Matelski et al., 2020). While dam weight at weaning was not altered by PCB exposure, there was a significant main effect of genotype, with DM dams weighing significantly more than WT dams, T4826I dams weighing significantly more than CGG dams, and CGG dams weighing significantly less than DM dams (Matelski et al., 2020). We also found that there were no effects of developmental PCB exposure or genotype on litter size or sex ratio within the litter (data under review).

Developmental Polychlorinated Biphenyls Exposures

The MARBLES PCB mixture was prepared to proportionally mimic the serum PCB congener profile of the twelve most prevalent PCB congeners detected in serum of pregnant women enrolled in the MARBLES human epidemiological cohort (Granillo et al., 2019; Sethi et al., 2019). These women are at increased risk for having a child with an NDD (Hertz-Picciotto et al., 2018). The PCB congeners included in the MARBLES PCB mixture and their final total percentage in the mixture was as follows: PCB 28 (48.2%), PCB 11 (24.3%), PCB 118 (4.9%), PCB 101 (4.5%), PCB 52 (4.5%), PCB 153 (3.1%), PCB 180 (2.8%), PCB 149 (2.1%), PCB 138 (1.7%), PCB 84 (1.5%), PCB 135 (1.3%), and PCB 95 (1.2%). The MARBLES PCB mix was solubilized in peanut oil and homogenously mixed into peanut butter to achieve concentrations of 0.025, 0.25, and 1.5 mg PCB/g peanut butter. A vehicle control (0 mg/g) was similarly prepared by mixing the equivalent amount of peanut oil needed to solubilize the highest concentration of MARBLES mix into peanut butter. Two weeks prior to mating, nulliparous dams (>6 weeks of age) were randomized to dose groups and PCB exposures were initiated. Dams were fed the MARBLES PCB mix in peanut butter at doses of either 0, 0.1, 1 or 6 mg/kg_{BW}/day daily until pups were weaned at P21. Similar doses of Aroclor 1254 were previously shown to result in PCB body burdens comparable to those observed in human tissues (Yang et al., 2009). At each daily dosing, dams were monitored to ensure complete ingestion of each dose of peanut butter.

Golgi Staining

Golgi staining, image acquisition, and analysis were performed as described previously (Keil et al., 2017, 2019b; Wilson et al., 2017). Parameters used to assess Golgi staining and criteria for selecting Golgi-stained neurons to trace were described previously (Lein et al., 2007; Keil et al., 2017). Briefly, P27–31 pups were euthanized with CO_2. Brains were carefully and quickly extracted from the skulls and processed for Golgi staining using the FD Rapid GolgiStain kit (FD NeuroTechnologies Inc. Columbia, MD, United States) according to the manufacturer's instructions. Brightfield image stacks of pyramidal neurons in the CA1 of the hippocampus and layers IV/V of the somatosensory cortex were captured using an Olympus IX-81 inverted confocal microscope (Olympus, Shinjuku, Japan) at 20X magnification using MetaMorph Advanced image analysis software (version 7.1, Molecular Devices, Sunnyvale, CA, United States). These brain regions were chosen because they contain easily identifiable pyramidal neurons and are implicated in the pathogenesis of neurodevelopmental disorders (Coskun et al., 2013; Khan et al., 2015; Cooper et al., 2017). Neuronal basilar dendritic arbors (N = 39–49 hippocampal neurons per group and N = 44–48 cortical neurons per group derived from six mice per sex, genotype, and exposure group) were hand-traced by a single individual blinded to experimental group using Neurolucida (version 11, MBF Bioscience, Williston, VT, United States). Basilar dendritic arbors in these regions were chosen for analysis because previous studies of PCB effects on dendritic arborization demonstrated the developmental exposure to Aroclor 1254 or PCB 95 altered basilar dendrites (Lein et al., 2007; Yang et al., 2009; Wayman et al., 2012b). Dendritic arbor complexity was quantified using automated Sholl (Neurolucida Explorer, version 11, MBF Bioscience) with 10-μm Sholl rings centered on the neuronal soma. Neuron tracings are publicly available on the NeuroMorpho.Org database[1].

Statistical Analyses

Sholl curves for each neuron were assessed using a multilevel linear mixed-effects model to determine effects of genotype, sex, dose or interactions on dendritic arborization; these analyses were conducted using SAS software (version 9.4, SAS Institute Inc., Cary, NC, United States) as described previously (Keil et al., 2017, 2019b; Wilson et al., 2017). In the multi-level linear mixed-effects modeling, genotype, sex, and dose were treated as fixed effects. A random intercept was included in the model to control for clustering of observations within a neuron and neurons within animals. Log transformation was applied when necessary (as indicated in **Tables 1**, **2**). **Tables 1**, **2** report tests for fixed effects and differences of least squares means for any fixed effects with $p \leq 0.05$ as well as for any fixed effects that were approaching significance ($p < 0.1$) and also had significant effects as identified in the differences of least squares means. **Supplementary Data** Files report the SAS output, including the solution for fixed effects, fixed effects, least squares means and differences of least squares means. Area under the curve (AUC), distance from soma of the peak dendritic intersections (Peak X), and maximum number of dendritic intersections (Peak Y) values were calculated for Sholl profiles using AUC analysis in GraphPad Prism Software (version 6 and 7, San Diego, CA, United States) for each neuron. To allow for comparisons to earlier studies that did not use mixed-effects models (Roegge et al., 2006; Lein et al., 2007; Yang et al., 2009; Wayman et al., 2012b), PCB-induced differences between neurons within sex and genotypes were independently examined using GraphPad Prism Software. These data were first assessed for normality using the Shapiro–Wilks, KS and D'Agostino and Pearson omnibus normality test, and homogeneity of variance using Bartlett's test. Within each sex and genotype, significant differences between PCB dose groups were determined using one-way ANOVA followed by Dunnett's or Tukey's multiple comparison test for approximately normal data. If data were normal but had unequal variance, group differences were determined using a

[1]www.neuromorpho.org

TABLE 1 | Summary of mixed model effects in pyramidal CA1 hippocampal neurons.

	Tests of fixed effects	***p*-value**	**Differences of least squares means**	***p*-value**
Sholl Profile	Sex	0.5		
	Genotype	0.4		
	Dose	0.5		
Peak X	Sex	0.5	**CGG > T4826I**	0.04
	Genotype	0.08	**CGG > WT**	0.03
	Dose	0.9		
Peak Y	Sex	0.9		
	Genotype	0.3	**DM < WT**	0.02
	Dose	**0.03**	**T4826I < WT**	0.008
Total area under Sholl curve	Sex	0.8		
	Genotype	0.4		
	Dose	0.5		
Proximal area under Sholl curve	Sex	0.9		
	Genotype	0.2		
	Dose	0.3		
Distal area under Sholl curve (log)	Sex	0.6		
	Genotype	0.4		
	Dose	0.8		
	Sex*Genotype	**0.03**	**CGG F > DM F**	0.04
			CGG F > WT F	0.01
			CGG F > CGG M	0.04
			CGG F > T4826I M	0.01
			DM M > T4826I M	0.03
			DM M > WT F	0.05
Number of dendrites	Sex	0.7		
	Genotype	**0.004**	**CGG < WT**	0.02
	Dose	0.4	**DM < WT**	0.0009
			T4826I < WT	0.003
Terminal dendritic tips	Sex	0.8	**T4826I < WT**	0.05
	Genotype	0.1		
	Dose	0.6		
Sum dendritic length	Sex	0.7		
	Genotype	0.3		
	Dose	0.5		
Tips per dendrite	Sex	0.8		
	Genotype	0.3		
	Dose	0.5		
Mean dendritic length	Sex	0.4		
	Genotype	0.2		
	Dose	0.4		
Nodes	Sex	0.9		
	Genotype	0.2		
	Dose	0.7		
Soma area	Sex	0.09		
	Genotype	**<0.0001**	**CGG > DM**	0.003
			CGG > T4826I	0.002
			CGG 0.1 < WT 0	<0.0001
			DM < WT	<0.0001
	Dose	0.4		
	Genotype*Dose	**0.03**	**T4826I < WT**	0.01

(Continued)

TABLE 1 | (Continued)

Tests of fixed effects	*p*-value	Differences of least squares means	*p*-value
		CGG 0.1 > DM 1	0.03
		CGG 1 > DM 1	0.02
		CGG 1 < WT 0	0.01
		CGG 6 > DM 0	0.05
		CGG 6 > DM 1	0.006
		CGG 6 > T4826I 1	0.04
		CGG 6 > T4826I 6	0.05
		CGG 6 < WT 0	0.04
		CGG 0 > DM 0	0.02
		CGG 0 > DM 0.1	0.04
		CGG 0 > DM 1	0.002
		CGG 0 > T4826I 1	0.02
		CGG 0 > T4826I 6	0.02
		DM 0.1 < WT 0.1	0.02
		DM 0.1 < WT 1	0.01
		DM 0.1 < WT 0	0.0002
		DM 1 < DM 6	0.01
		DM 1 < WT 0.1	0.001
		DM 1 < WT 1	0.0004
		DM 1 < WT 0	< 0.0001
		DM 6 < WT 0	0.03
		DM 0 < WT 0.1	0.01
		DM 0 < WT 1	0.006
		DM 0 < WT 0	< 0.0001
		T4826I 0.1 < WT 0.1	0.04
		T4826I 0.1 < WT 1	0.02
		T4826I 0.1 < WT 0	0.0004
		T4826I 1 < WT 0.1	0.009
		T4826I 1 < WT 1	0.004
		T4826I 1 < WT 0	< 0.0001
		T4826I 6 < WT 0.1	0.01
		T4826I 6 < WT 1	0.006
		T4826I 6 < WT 0	< 0.0001
		T4826I 0 < WT 0.1	0.05
		T4826I 0 < WT 1	0.03
		T4826I 0 < WT 0	0.0007
		WT 6 < WT 0.1	0.03
		WT 6 < WT 1	0.02
		WT 6 < WT 0	0.0004

Bold text indicates biologically relevant comparisons.

one-way ANOVA with Welch's correction followed by Dunnett's T3 multiple comparisons test. For non-normal data, differences were determined using a Kruskal–Wallis test followed by Dunn's multiple comparison test. We first focused on differences from vehicle control, if there were no differences from vehicle control then differences between PCB groups were examined. *P*-values ≤ 0.05 were considered statistically significant. In two instances, the p value of the Kruskal–Wallis tests were 0.0591 and 0.0565, Dunn's *post hoc* analysis revealed significant differences ($p = 0.04$ and $p = 0.03$), so these were reported in **Figures 2E**, **3A** respectively.

RESULTS

Pyramidal CA1 hippocampal neurons and layer IV/V pyramidal somatosensory cortical neurons were examined in this study because altered patterns of connectivity and dendritic morphology have been reported in these brain regions in individuals with ASD compared to neurotypical controls (Coskun et al., 2013; Keown et al., 2013; Khan et al., 2015; Cooper et al., 2017). Results from the multilevel, mixed-effects statistical model, which includes interactions and allows for the analysis of the Sholl plot as a whole, are summarized in

TABLE 2 | Summary of mixed model effects in pyramidal cortical neurons.

	Test of fixed effects	***p*-value**	**Differences of least squares means**	***p*-value**
Sholl profile	Sex	0.6		
	Genotype	0.8		
	Dose	**0.03**	**1 mg/kg > 6 mg/kg**	0.004
			1 mg/kg > 0 mg/kg	0.02
	Genotype*Dose	**0.01**	**CGG 6 < CGG 1**	0.05
			CGG 6 < CGG 0	0.003
			CGG 6 < WT 6	0.05
			CGG 6 < DM 1	0.0005
			CGG 6 < T4826I 0.1	0.04
			CGG 6 < T4826I 1	0.02
			CGG 0 > WT 0	0.01
			CGG 0 > DM 0	0.03
			CGG 0 > DM 0.1	0.01
			CGG 0 > DM 6	0.01
			CGG 0 > T4826I 0	0.008
			CGG 0 > T4826I 6	0.03
			DM 0.1 < T4826I 1	0.05
			DM 1 > DM 0.1	0.002
			DM 1 > DM 6	0.002
			DM 1 > DM 0	0.008
			DM 1 > WT 0.1	0.04
			DM1 > WT 1	0.02
			DM 1 > WT 0	0.002
			DM 1 > T4826I 6	0.008
			DM 1 > T4826I 0	0.001
			T4826I 1 > T4826I 0	0.03
			T4826I 1 > WT 0	0.04
			T4826I 1 > DM 6	0.04
Peak X	Sex	0.8		
	Genotype	0.5		
	Dose	0.6		
Peak Y	Sex	0.4		
	Genotype	0.6		
	Dose	**0.02**	**1 mg/kg > 0.1 mg/kg**	0.05
			1 mg/kg > 6 mg/kg	0.002
			1 mg/kg > 0 mg/kg	0.02
Total area under Sholl curve	Sex	0.7		
	Genotype	0.8		
	Dose	**0.02**	**1 mg/kg > 6 mg/kg**	0.003
			1 mg/kg > 0 mg/kg	0.02
	Genotype*Dose	**0.01**	**CGG 6 < CGG 1**	0.05
			CGG 6 < CGG 0	0.004
			CGG 6 < WT 6	0.05
			CGG 6 < DM 1	0.0007
			CGG 6 < T4826I 0.1	0.05
			CGG 6 < T4826I 1	0.02
			CGG 0 > WT 0	0.01
			CGG 0 > DM 0	0.03
			CGG 0 > DM 0.1	0.01
			CGG 0 > DM 6	0.007
			CGG 0 > T4826I 0	0.009
			CGG 0 > T4826I 6	0.04

(Continued)

TABLE 2 | (Continued)

	Test of fixed effects	*p*-value	Differences of least squares means	*p*-value
			DM 0.1 < T4826I 1	0.05
			DM 1 > DM 0.1	0.003
			DM 1 > DM 6	0.001
			DM 1 > DM 0	0.007
			DM 1 > WT 0.1	0.04
			DM 1 > WT 1	0.02
			DM 1 > WT 0	0.002
			DM 1 > T4826I 6	0.009
			DM 1 > T4826I 0	0.002
			T4826I 1 > T4826I 0	0.04
			T4826I 1 > WT 0	0.04
			T4826I 1 > DM 6	0.03
Proximal area under Sholl curve	Sex	0.4		
	Genotype	0.7		
	Dose	**0.02**	**1 mg/kg > 0.1 mg/kg**	0.05
			1 mg/kg > 6 mg/kg	0.003
			1 mg/kg > 0 mg/kg	0.03
	Genotype*Dose	**0.02**	CGG 1 > DM 6	0.03
			CGG 6 < CGG 1	0.03
			CGG 6 < CGG 0	0.004
			CGG 6 < WT 6	0.03
			CGG 6 < T4826I 0.1	0.05
			CGG 6 < T4826I 1	0.009
			CGG 6 < DM 1	0.002
			CGG 0 > WT 0	0.01
			CGG 0 > DM 0	0.04
			CGG 0 > DM 0.1	0.02
			CGG 0 > DM 6	0.003
			CGG 0 > T4826I 0	0.02
			CGG 0 > T4826I 6	0.05
			DM 1 > DM 0.1	0.009
			DM 1 > DM 6	0.002
			DM 1 > DM 0	0.02
			DM 1 > WT 0.1	0.05
			DM 1 > WT 1	0.05
			DM 1 > WT 0	0.007
			DM 1 > T4826I 6	0.03
			DM 1 > T4826I 0	0.008
			DM 6 < WT 6	0.03
			DM 6 < T4826I 0.1	0.05
			T4826I 1 > T4826I 0	0.03
			T4826I 1 > WT 0	0.03
			T4826I 1 > DM 0.1	0.04
			T4826I 1 > DM 6	0.008
Distal area under Sholl curve (log)	Sex	0.3		
	Genotype	0.7		
	Dose	0.3		
	Genotype*Dose	**0.06**	**CGG 6 < CGG 0**	0.03
			CGG 6 < DM 1	0.01
			CGG 0 > WT 1	0.03
			CGG 0 > DM 0	0.05

(Continued)

TABLE 2 | (Continued)

	Test of fixed effects	*p*-value	Differences of least squares means	*p*-value
			CGG 0 > DM 0.1	0.05
			CGG 0 > DM 6	0.05
			CGG 0 > T4826I 0	0.03
			CGG 0 > WT 0	0.03
			DM 1 > DM 0.1	0.02
			DM 1 > DM 6	0.02
			DM 1 > DM 0	0.02
			DM 1 > WT 1	0.01
			DM 1 > WT 0	0.01
			DM 1 > T4826I 6	0.05
			DM 1 > T4826I 0	0.01
Number of dendrites	Sex	0.7		
	Genotype	1		
	Dose	**0.01**	**0.1 mg/kg < 1 mg/kg**	0.05
			1 mg/kg > 6 mg/kg	0.005
			1 mg/kg > 0 mg/kg	0.003
Terminal dendritic tips	Sex	0.2		
	Genotype	0.8		
	Dose	**0.0007**	**0.1 mg/kg < 1 mg/kg**	0.003
			1 mg/kg > 6 mg/kg	0.0001
			1 mg/kg > 0 mg/kg	0.003
Sum dendritic length	Sex	0.6		
	Genotype	0.8		
	Dose	**0.01**	**0.1 mg/kg < 1 mg/kg**	0.05
			1 mg/kg > 6 mg/kg	0.002
			1 mg/kg > 0 mg/kg	0.01
	Genotype*Dose	**0.02**	CGG 0.1 < DM 1	0.05
			CGG 1 > DM 6	0.05
			CGG 6 < CGG 1	0.04
			CGG 6 < CGG 0	0.006
			CGG 6 < DM 1	0.0006
			CGG 6 < T4826I 1	0.02
			CGG 0 > WT 0	0.01
			CGG 0 > DM 0	0.04
			CGG 0 > DM 0.1	0.02
			CGG 0 > DM 6	0.008
			CGG 0 > T4826I 0	0.008
			CGG 0 > T4826I 6	0.04
			DM 0.1 < T4826I 1	0.05
			DM 1 > DM 0.1	0.002
			DM 1 > DM 6	0.0009
			DM 1 > DM 0	0.006
			DM 1 > WT 0.1	0.03
			DM 1 > WT 1	0.02
			DM 1 > WT 0	0.002
			DM 1 > T4826I 0	0.001
			DM 1 > T4826I 6	0.007
			DM 6 < T4826I 1	0.03
			T4826I 1 > T4826I 0	0.03
			T4826I 1 > WT 0	0.04

(Continued)

TABLE 2 | (Continued)

	Test of fixed effects	*p*-value	Differences of least squares means	*p*-value
Tips per dendrite	Sex	0.2		
	Genotype	0.3		
	Dose	0.1	**0.1 mg/kg < 1 mg/kg**	0.05
			1 mg/kg > 6 mg/kg	0.03
Mean dendritic length	Sex	0.7		
	Genotype	0.4		
	Dose	0.4		
Nodes	Sex	0.2		
	Genotype	0.6		
	Dose	**0.002**	**0.1 mg/kg < 1 mg/kg**	0.003
			1 mg/kg > 6 mg/kg	0.0004
			1 mg/kg > 0 mg/kg	0.02
Soma area	Sex	0.7		
	Genotype	**0.03**	**CGG > DM**	0.04
			CGG > T4826I	0.01
			T4826I < WT	0.03
	Dose	**0.05**	**0.1 mg/kg > 0 mg/kg**	0.008
			1 mg/kg > 0 mg/kg	0.04

Bold text indicates biologically relevant comparisons.

Tables 1, **2** with biologically relevant comparisons highlighted in bold. Within each subsection of the Results below, these results are discussed first. Subsequently, we describe PCB effects that are significantly different from vehicle control within each sex and genotype independently to allow for interpretation of PCB effects alone and to allow for comparisons to published studies that did not use mixed-effects models (Roegge et al., 2006; Lein et al., 2007; Yang et al., 2009; Wayman et al., 2012b).

Morphometric Effects of Polychlorinated Biphenyls and Genotype on Pyramidal CA1 Hippocampal Neurons

Sholl plots and representative images of basilar dendritic arbors of Golgi-stained pyramidal CA1 hippocampal neurons from male and female WT, T4826I, CGG and DM mice at P27-P31 are shown in **Figure 1** (see also **Supplementary Figures 1**, **2**; Neurolucida reconstructions are publicly available within the neuromorpho.org database). While the Sholl profile analysis revealed no significant effects (**Table 1**), other parameters extracted from the Sholl profile revealed sex and genotype effects. The distance from the soma of the maximum number of dendritic intersections (Peak X) was significantly greater in CGG mice than T4826I or WT mice (**Table 1**). There was an overall effect of genotype on the maximum number of dendritic intersections (Peak Y), with DM and T4826I mice exhibiting significantly fewer intersections than WT mice (**Table 1**). While the total area under the Sholl curve was not changed, there was a significant sex by genotype interaction for the distal AUC with this parameter being significantly greater in CGG female mice compared to WT and DM females or CGG males (**Table 1**). Distal area under the Sholl curve was also greater in DM males vs. T4826I males (**Table 1**). Overall, these results suggest pyramidal CA1 hippocampal neurons from CGG mice are more complex than those of WT mice, while pyramidal CA1 hippocampal neurons from T4826I and DM mice are less complex than their WT counterparts, and hippocampal neurons of DM males are more complex than T4826I males.

We next asked whether developmental PCB exposure alters dendritic arborization by focusing on PCB dose-response relationships within each sex and genotype independently (**Figure 2**). We focused on difference from vehicle control; if there were no difference from vehicle control then differences between PCB groups were analyzed. There were no effects of PCB exposure on distance from the soma of the maximum number of dendritic intersections (Peak X) in male or female hippocampal neurons of any genotype (**Figures 2A,B**). The maximum number of dendritic intersections (Peak Y) was increased in the 1 mg/kg PCB group *vs*. the 0.1 mg/kg PCB group in male CGG hippocampal neurons (**Figures 2C,D**). Total area under the Sholl curve was increased in the 6 mg/kg PCB dose group *vs*. vehicle control in male DM hippocampal neurons (**Figures 2E,F**). Differences in the proximal AUC of the Sholl plot were limited to female hippocampal neurons with a significant dose-dependent increase in DM female neurons in all PCB dose groups compared to vehicle controls (**Figure 2H**). There were no PCB effects in distal area under the Sholl curve for either sex in any genotype (**Figures 2I,J**). These results suggest that compared to vehicle control, PCBs increase dendritic complexity in DM mice only, an effect which is sex- and dose-dependent.

We also analyzed more detailed measures of dendritic arborization (Keil et al., 2017) that have previously been shown to be sensitive to PCBs (Lein et al., 2007; Yang et al., 2009; Wayman et al., 2012b). Based on the mixed-effect model

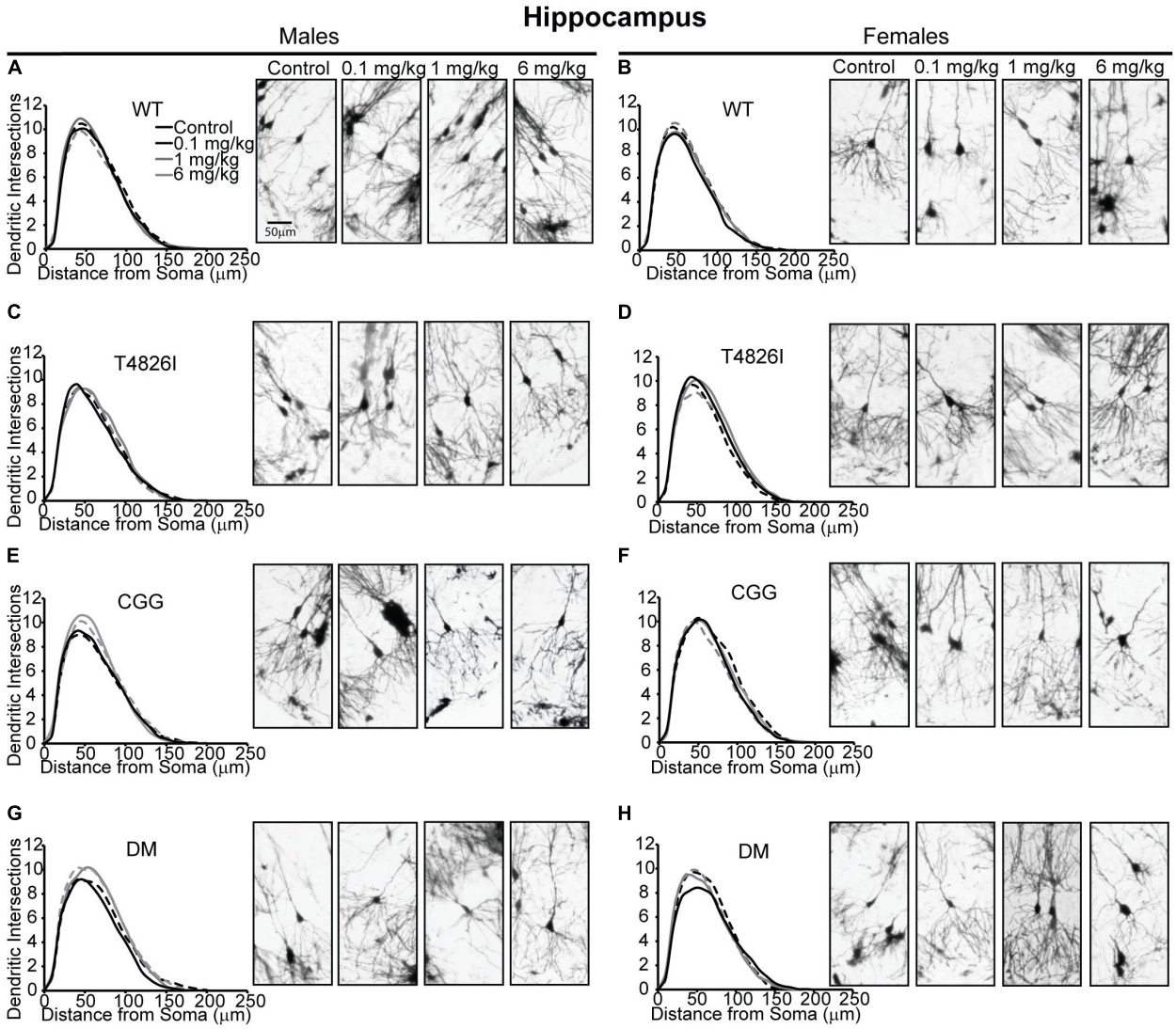

FIGURE 1 | Genotype influences the effect of PCBs on the dendritic morphology of pyramidal neurons in the CA1 hippocampus of juvenile mice. Sholl plots and representative images of the basilar dendritic arbors of Golgi-stained pyramidal CA1 hippocampal neurons derived from P27–31 male and female **(A,B)** WT, **(C,D)** T4826I, **(E,F)** CGG, or **(G,H)** DM mice exposed to the MARBLES PCB mixture in the maternal diet throughout gestation and lactation. *N* = 39–49 neurons from at least six independent mice per sex per genotype per dose. Also see **Supplementary Figure 1** for representative tracings of the basilar dendritic arbors of Golgi-stained pyramidal hippocampal neurons.

analysis, effects were limited to genotype for the total number of basilar dendrites with pyramidal CA1 hippocampal neurons of all transgenic mice having fewer dendrites compared to WT (**Table 1**). Examining each sex and genotype independently, there were no effects of developmental PCB exposure on the number of primary dendrites, dendritic tips, or the number of dendritic tips per primary dendrite (**Supplementary Figures 3A–F**). The sum length of all dendrites was increased in the 6 mg/kg male DM neurons vs. sex- and genotype-matched vehicle control (**Figures 3A,B**). Mean dendritic length was unchanged (**Figures 3C,D**). These results suggest that genotype alone decreases dendrite number and PCBs only increase sum dendritic length in DM males exposed to the highest PCB dose.

Soma area was the morphometric parameter most affected by both genotype and developmental PCB exposure in pyramidal CA1 hippocampal neurons. **Table 1** illustrates the statistically significant effect of genotype and significant genotype by dose interactions, with DM and T4826I mice displaying a smaller soma size than WT and CGG mice. Genotype by dose interactions were seen in WT neurons, with soma size significantly decreased in the 6 mg/kg group *vs*. WT vehicle control and other PCB dose groups (**Table 1**). T4826I and DM mice had smaller soma size than WT controls regardless of exposure (**Table 1**). Additionally, in DM mice, soma size was significantly decreased in the 1 mg/kg dose group compared to the 6 mg/kg group (**Table 1**). Soma size of CGG vehicle controls did not differ from WT vehicle controls, but

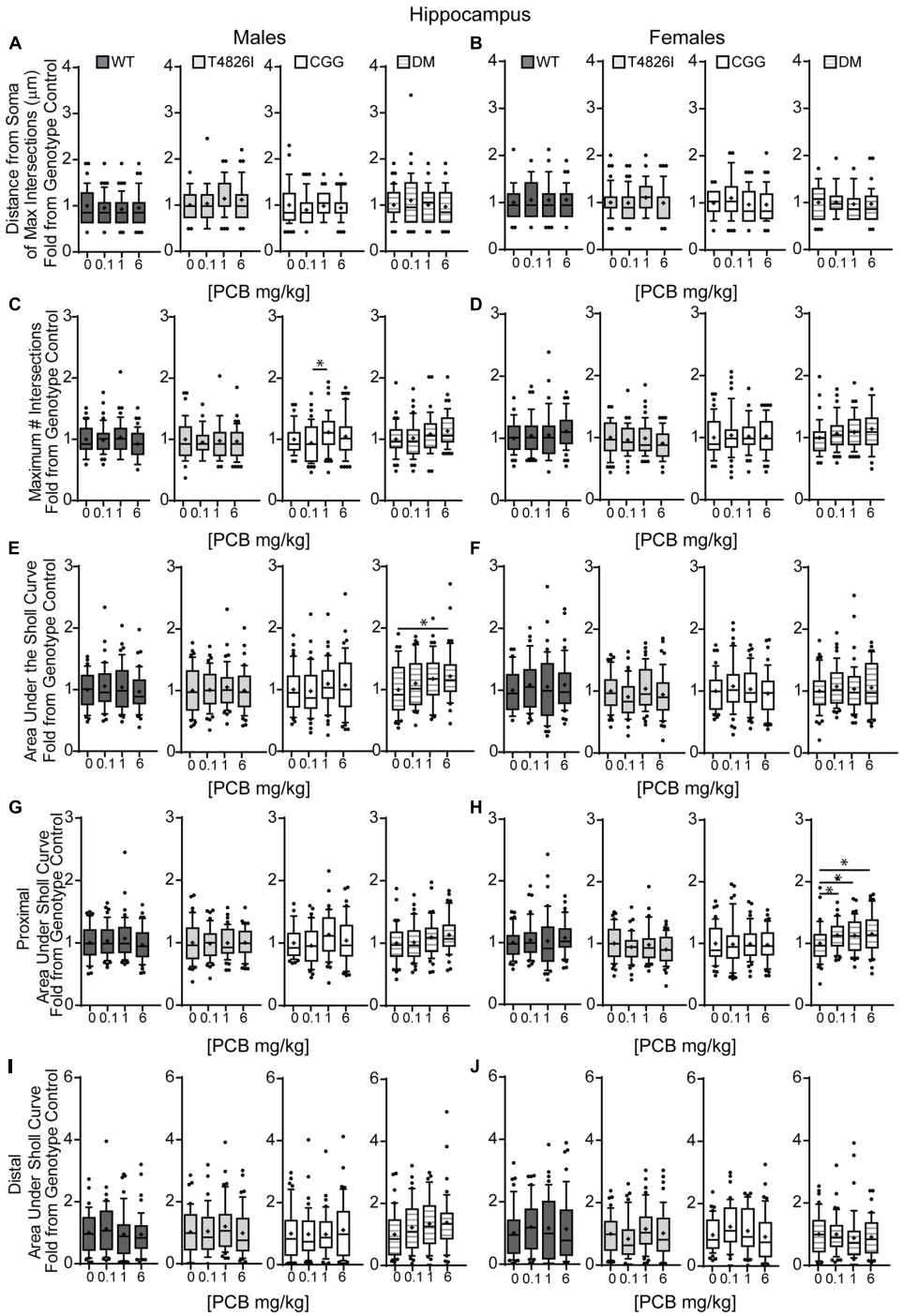

FIGURE 2 | Double mutant mice are more sensitive to effects of PCBs on the dendritic morphology of pyramidal neurons in the CA1 hippocampus of juvenile mice. Morphometric analyses of the basilar dendritic arbors of Golgi-stained pyramidal CA1 hippocampal neurons from P27–31 male and female WT, T4826I, CGG, or DM mice exposed to the MARBLES PCB mixture in the maternal diet throughout gestation and lactation. **(A,B)** The distance from the soma to the maximum number of dendritic intersections (Peak X). **(C,D)** The maximum number of dendritic intersections (Peak Y). **(E,F)** The total area under the curve of the Sholl plot (0–240 μm from the soma). **(G,H)** Proximal area under the curve of the Sholl plot (10–70 μm from the soma), and **(I,J)** distal area under the curve of the Sholl plot (80–140 μm from the soma). Data (N = 39–49 neurons from at least six independent mice per sex per genotype per dose) are presented as box plots, where the box indicates the lower (25th) to upper (75th) quartiles, the "+" indicates the mean, whiskers indicate the 10–90th percentile, and dots represent values outside the upper or lower fences. *Significantly different from control at $p \leq 0.05$ as determined by Kruskal–Wallis test followed by Dunn's multiple comparisons test. Average values of vehicle controls for WT, T4826I, CGG and DM, respectively, are **(A)** 46.9, 40.8, 47.9, 47.3 μm; **(B)** 42.3, 44.9, 48.5, 46.4 μm; **(C)** 11.9, 10.8, 10.8, 10.4 intersections; **(D)** 10.8, 11.3, 11.2, 10.1 intersections; **(E)** 773.8, 698.2, 727.7, 713.8 μm^2; **(F)** 721.1, 787.2, 807.8, 715.1 μm^2; **(G)** 493.7, 454.1, 456.9, 450.5 μm^2; **(H)** 466.7, 497.2, 492.1, 420.3 μm^2; **(I)** 192.2, 164.6, 188.6, 178.8 μm^2; and **(J)** 170.8, 197.4, 216.5, 202.6 μm^2.

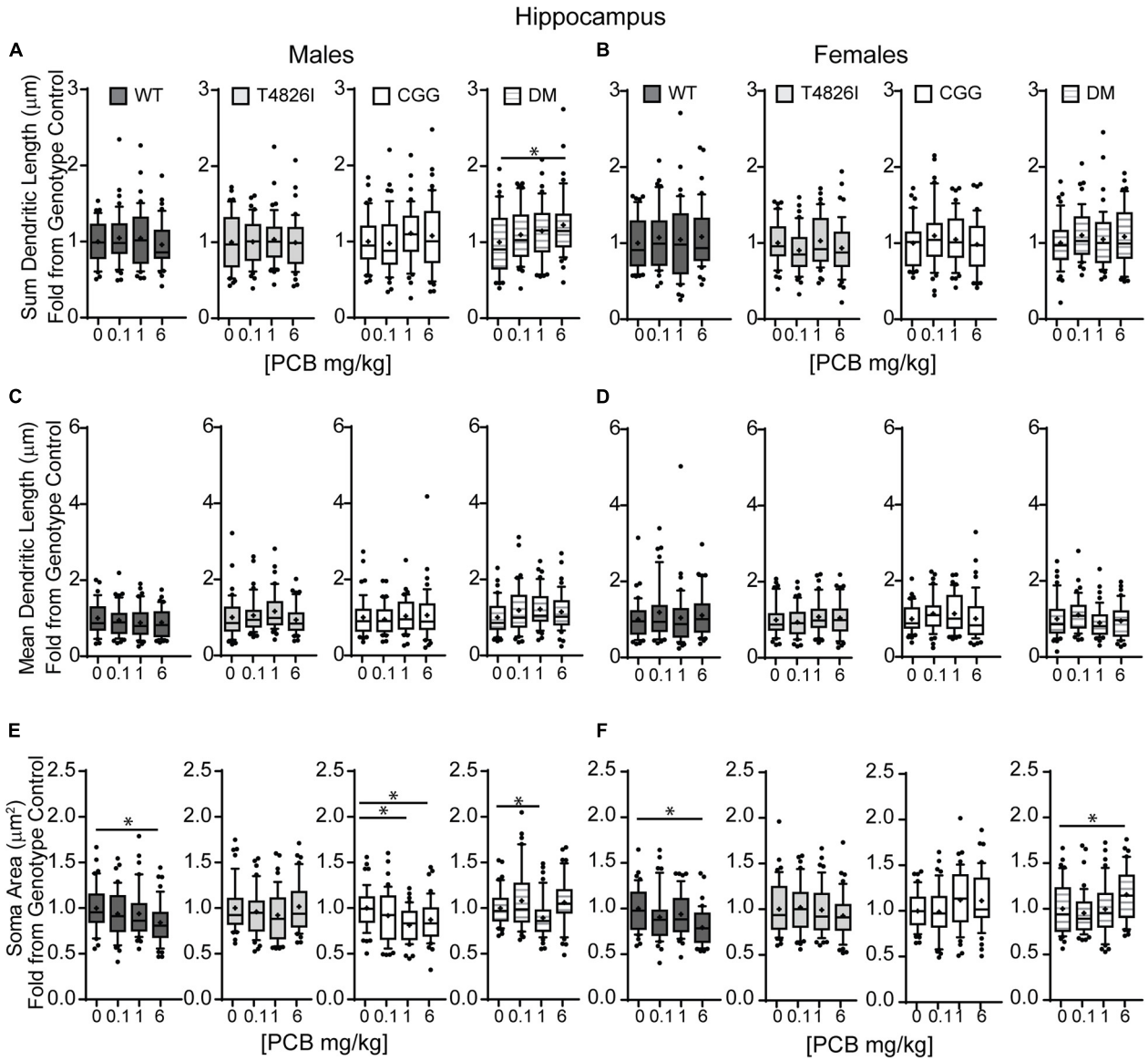

FIGURE 3 | Polychlorinated biphenyls effects on dendritic sum length are observed in DM male but not female mice and both genotype and PCB exposure impact soma area in both sexes. Dendritic morphology was assessed in basilar dendritic arbors of Golgi-stained pyramidal CA1 hippocampal neurons in P27–31 male and female WT, T4826I, CGG, or DM mice following gestational and lactational PCB exposure via the maternal diet. **(A,B)** Sum length of dendrites per neuron (μm). **(C,D)** Mean dendritic length per neuron (μm). **(E,F)** Cell body area per neuron (μm^2). Data (N = 39–49 neurons from at least six independent mice per sex per genotype per dose) are presented as box plots, where the box indicates the lower (25th) to upper (75th) quartiles, the "+" indicates the mean, whiskers indicate the 10–90th percentile, and dots represent values outside the upper or lower fences. Bar and asterisk indicate a significant difference between groups as determined by Kruskal–Wallis test followed by Dunn's multiple comparisons test, or (E-CGG) one-way ANOVA followed by Dunnett's multiple comparisons test with $p \leq 0.05$ considered statistically significant. Average values of vehicle controls for WT, T4826I, CGG, and DM, respectively, are **(A)** 898.8, 804.8, 833.2, 815.2 μm; **(B)** 833.1, 903.0, 909.5, 801.5 μm; **(C)** 256.4, 215.7, 236.5, 228.3 μm; **(D)** 214.4, 244.9, 241.9, 245.9 μm; **(E)** 283.2, 246.3, 284.5, 230.2 μm^2; and **(F)** 305.9, 240.3, 253.5, 238.8 μm^2.

hippocampal neurons of CGG mice at all PCB concentrations had smaller soma size than WT vehicle controls (**Table 1**). Overall, developmental PCB exposure or the T4826I and DM genotypes were associated with decreased hippocampal soma area.

Examining PCB effects in each sex and genotype independently, PCB exposure altered soma area in WT, CGG, and DM males, as well as in WT and DM females. In WT males, soma area was significantly reduced in the 6 mg/kg PCB dose group compared to WT male vehicle controls. In CCG males, soma area was significantly reduced in the 1 and 6 mg/kg dose groups relative to CGG vehicle controls (**Figure 3E**). Soma area was also significantly reduced in 1 mg/kg DM males in contrast to DM vehicle control males (**Figure 3E**). While PCBs generally decreased soma area in males across genotypes, this

effect was genotype-dependent in females. Like males, soma area of hippocampal neurons in WT females was significantly reduced in the 6 mg/kg dose group compared to WT female vehicle controls (**Figure 3F**). However, in DM females, soma area was significantly increased in the 6 mg/kg dose group vs. DM female vehicle controls (**Figure 3F**).

Morphometric Effects of Polychlorinated Biphenyls and Genotypes on Layer IV/V Pyramidal Somatosensory Cortical Neurons

Polychlorinated biphenyl dose effects were more pronounced in cortical neurons compared to hippocampal neurons. **Figure 4** illustrates Sholl plots and representative images of Golgi-stained pyramidal neurons in layer IV/V of the somatosensory cortical neurons from male and female WT, T4826I, CGG, and DM mice. There was a significant effect of dose on cortical Sholl profiles, with the 1 mg/kg PCB group exhibiting greater dendritic complexity than vehicle controls or the 6 mg/kg dose group (**Table 2**). There was also a significant genotype by dose interaction observed in the Sholl profiles (fully summarized in **Table 2**), identified as: (1) CGG vehicle control neurons were more complex than T4826I, DM, and WT vehicle control neurons; (2) 6 mg/kg CGG neurons were less complex than CGG vehicle control neurons; (3) 1 mg/kg T4826I neurons had greater complexity compared to T4826I and WT vehicle control neurons; and (4) 1 mg/kg DM neurons showed much greater complexity than DM vehicle controls, 0.1, or 6 mg/kg DM neurons, as well as increased complexity relative to WT vehicle controls, WT 1 mg/kg, or T4826I vehicle control groups. Distance from the soma of maximum dendritic intersections (Peak X) did not differ between dose groups, but there was a significant effect of dose on the maximum number of dendritic intersections (Peak Y), with the 1 mg/kg PCB dose group having increased intersections relative to all other dose groups (**Table 2**). There was a significant effect of dose on the total area under the Sholl curve, with 1 mg/kg PCB dose groups having increased area vs. vehicle controls or the 6 mg/kg PCB dose group as well as a significant genotype by dose effect driven by the same differences stated above for the Sholl profile analysis model (**Table 2**). For proximal area under the Sholl curve, there was a significant effect of dose with 1 mg/kg dose groups having greater area than all other dose groups, as well as a significant genotype by dose interaction driven by all differences listed above for the Sholl profile analysis with the addition of the DM 6 mg/kg PCB dose group having decreased proximal area compared to the WT 6 mg/kg PCB dose group (**Table 2**). In contrast, distal AUC showed fewer differences. CGG vehicle controls had greater distal AUC than WT, T4826I, or DM vehicle control neurons, and exposure to 6 mg/kg PCB decreased distal AUC in CGG neurons relative to CGG vehicle controls. The DM 1 mg/kg group showed greater distal AUC than DM vehicle controls, all other DM PCB dose groups, 1 mg/kg PCB WT mice, and vehicle controls from T4826I and WT mice (**Table 2**). Together, these results indicate a non-monotonic dose response, with exposure to the MARBLES PCB mix at 1 mg/kg promoting dendritic arborization, especially in T4826I and DM neurons. Vehicle-treated CGG animals have the greatest dendritic complexity compared to the other genotypes, and the highest PCB dose (6 mg/kg) decreased dendritic complexity within CGG neurons.

We next examined the effects of PCBs on dendritic growth when independently analyzed within sex and genotype (**Figure 5**). In WT mice, the distance from the soma of the maximum number of intersections (Peak X) was increased in the 6 mg/kg PCB dose group relative to vehicle controls in males, but not females (**Figures 5A,B**). PCB effects on the maximum number of dendritic intersections (Peak Y) were limited to female animals, where they were decreased in 6 mg/kg CGG neurons vs. CGG vehicle controls and in 6 mg/kg DM females relative to 1 mg/kg DM females (**Figure 5D**). PCB effects on the area under the Sholl curve were genotype- and sex-dependent. In WT animals, the total AUC was increased in the male 6 mg/kg dose group vs. WT male vehicle controls (**Figure 5E**). In T4826I animals, the total area under the Sholl curve was increased in the male 1 mg/kg dose group vs. T4826I male vehicle control (**Figure 5E**). Total area under the Sholl curve was also increased in DM males in the 1 mg/kg dose group vs. the 0.1 or 6 mg/kg dose group (**Figure 5E**). In contrast to males, total area under the Sholl curve was unchanged in WT female mice and was decreased in CGG 6 mg/kg females compared to CGG vehicle control females (**Figure 5F**). Like males, total area under the Sholl curve was greater in T4826I 1 mg/kg females compared to T4826I vehicle control females (**Figure 5F**) and total area under the Sholl curve was greater in DM 1 mg/kg females vs. the DM 6 mg/kg females (**Figure 5F**). For both males and females, most of the differences in AUC occurred in the proximal portion. Similar to total area under the Sholl curve, proximal area under the Sholl curve was increased in the 6 mg/kg dose group vs. vehicle control in WT males, and increased in the 1 mg/kg PCB dose group vs. vehicle control in T4826I and DM males (**Figure 5G**). In CGG males and females, proximal area under the Sholl curve was decreased in the 6 mg/kg PCB dose group vs. vehicle controls, compared to an increase in DM 1 mg/kg females compared to 0.1 or 6 mg/kg DM females (**Figure 5H**). The only significant difference in the distal area under the Sholl curve was found in DM males, with a significant increase in the 1 mg/kg PCB dose group relative to the 0.1 mg/kg group (**Figures 5I,J**). In summary, these results indicate that developmental exposure to the MARBLES PCB mixture increased dendritic complexity in WT male cortical neurons at 6 mg/kg, an effect that was influenced by genotype as T4826I and DM male cortical neurons had indices of increased dendritic complexity at the 1 mg/kg dose. In contrast, PCB exposure only affected female cortical neurons from T4826I and CGG genotypes when compared to vehicle controls, with increased complexity in T4826I cortical neurons at the 1 mg/kg dose but decreased complexity in CGG cortical neurons at the 6 mg/kg dose.

In other measures of dendritic arborization, effects were driven by PCB dose for the total number of basilar dendrites, terminal dendritic tips, dendritic length sum and the number of nodes, with the 1 mg/kg PCB dose groups having greater complexity than all other dose groups (**Table 2**). In addition, there was a significant genotype by dose interaction for total dendritic

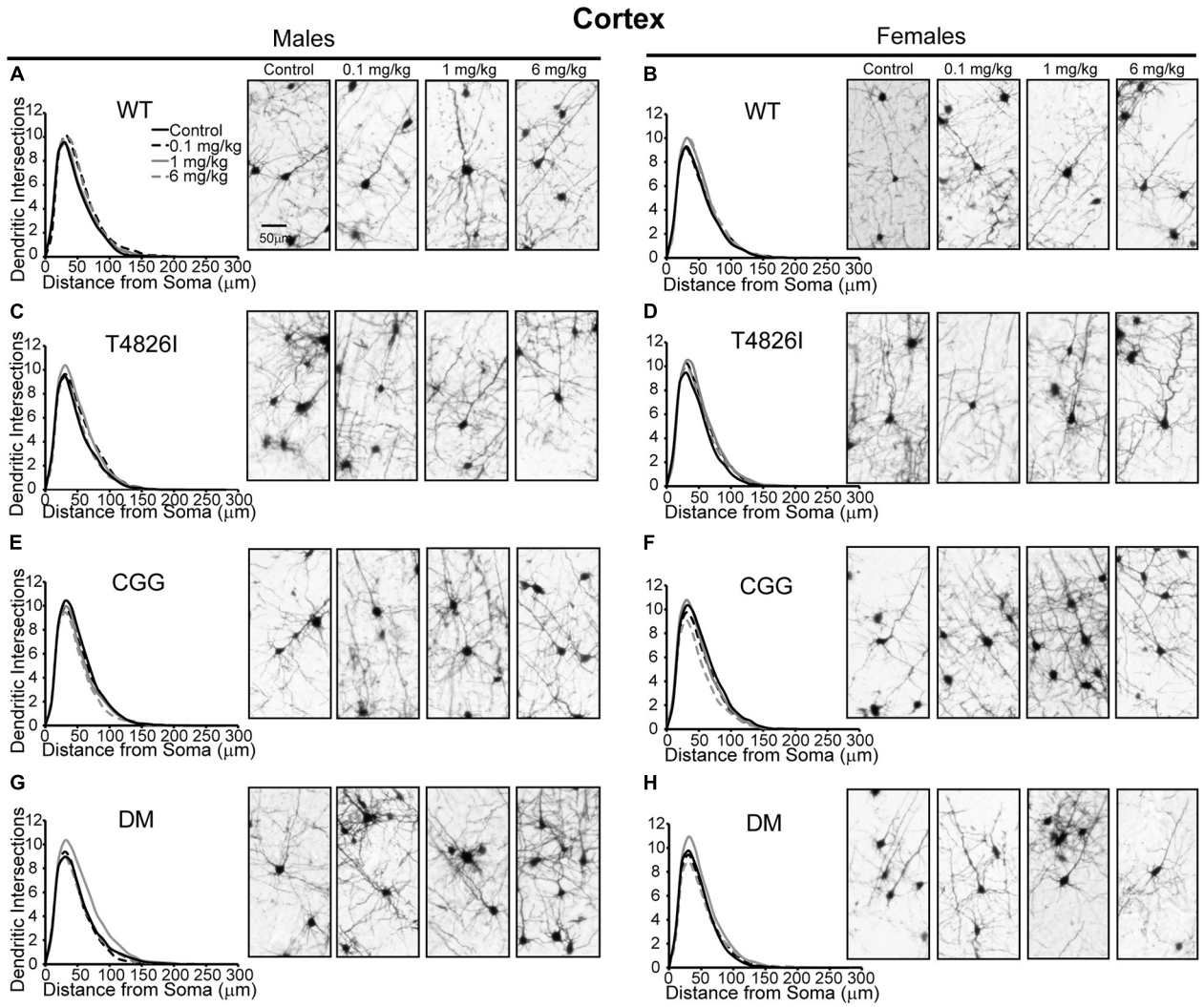

FIGURE 4 | Genotype influences the effect of PCBs on the dendritic morphology of pyramidal neurons in the somatosensory cortex of juvenile mice. Sholl plots of the basilar dendritic arbors of Golgi-stained layer IV/V pyramidal somatosensory cortical neurons in P27-31 male and female **(A,B)** WT, **(C,D)** T4826I, **(E,F)** CGG, or **(G,H)** DM mice. Mice were exposed to the MARBLES PCB mix in the maternal diet throughout gestation and lactation. *N* = 44–48 neurons from at least six independent mice per sex per genotype per dose. See also **Supplementary Figure 2** for representative tracings of the basilar arbors of Golgi-stained layer IV/V pyramidal somatosensory cortical neurons.

length, which was largely driven by differences highlighted above for the cortical Sholl profile analysis (**Table 2**). There was an increase in the number of dendritic tips per dendrite in the 1 mg/kg PCB dose vs. the 0.1 mg/kg or 6 mg/kg PCB dose groups; there were no effects of PCB exposure on mean dendritic length (**Table 2**). Together, these results indicate a non-monotonic dose response, with the 1 mg/kg PCB dose group having the greatest response and an overall tendency to increased dendritic complexity, especially in T4826I and DM neurons. In contrast, vehicle-treated CGG neurons were more complex than the other genotypes with the exception of the 6 mg/kg dose group, which exhibited decreased CGG neuron complexity.

Examining PCB dose effects in each sex and genotype independently, we observed differences in the number of primary dendrites were limited to CGG females, with the number of primary dendrites decreased in the 6 mg/kg dose group compared to the 1 mg/kg dose group (**Supplementary Figure 4A,B**). Effects of developmental PCB exposure on the number of dendritic tips were seen in offspring of both sexes, but to a greater extent in females. More specifically, the number of dendritic tips was increased in DM 1 mg/kg males vs. DM vehicle control males (**Supplementary Figure 4C**). However, in female neurons, the number of dendritic tips was increased in the T4826I 1 mg/kg dose group vs. vehicle control, decreased in the CGG 6 mg/kg dose group vs. vehicle control, and decreased in the DM 6 mg/kg dose group vs. the 1 mg/kg dose group (**Supplementary Figure 4D**). Dendritic tips in WT female neurons had a Kruskal–Wallis *p*-value of 0.05 however no differences compared to

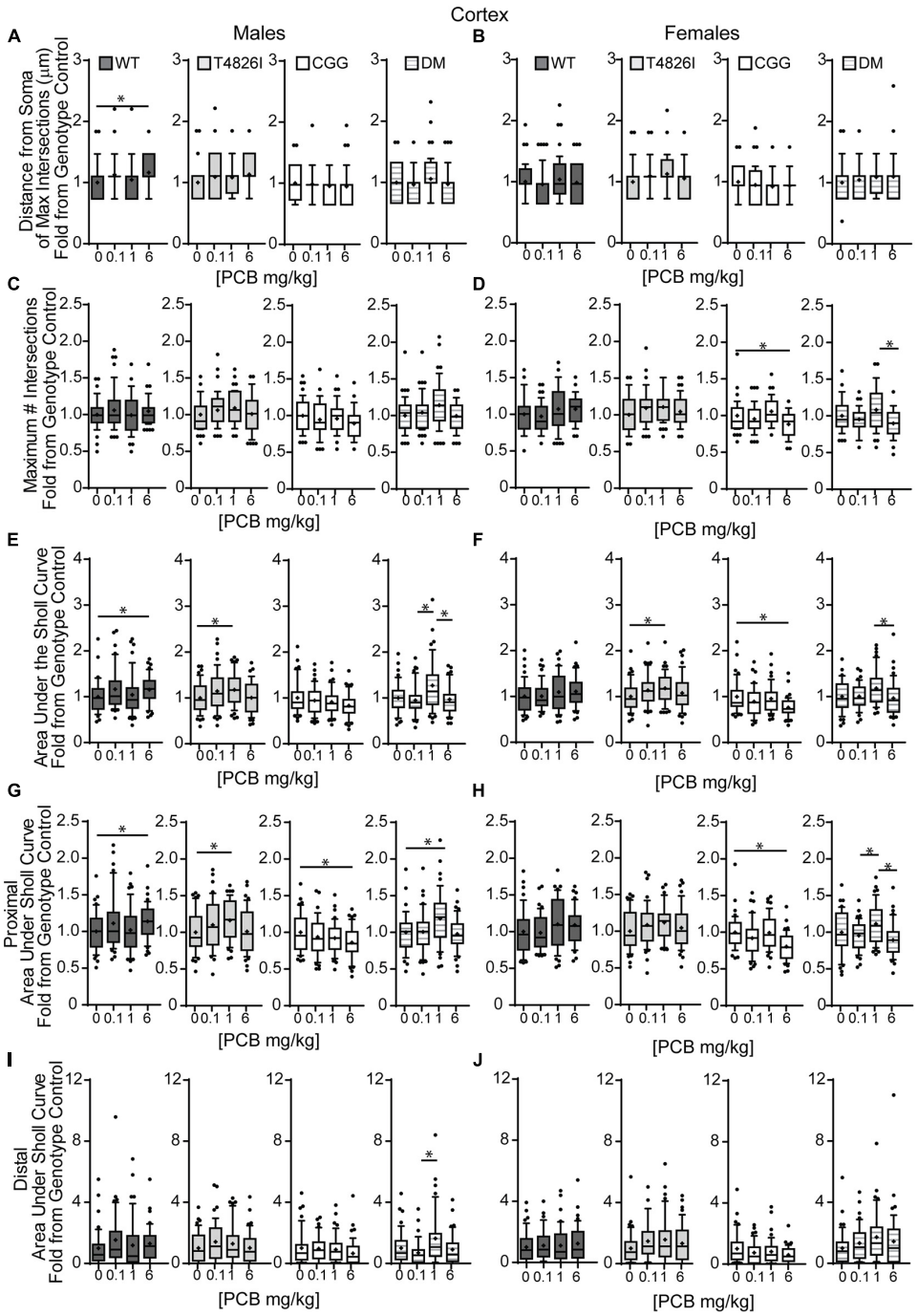

FIGURE 5 | Effects of PCBs on the dendritic morphology of pyramidal neurons in the somatosensory cortex of juvenile mice vary between genotypes and are dose and sex dependent. Morphometric analyses of the basilar dendritic arbors of Golgi-stained pyramidal CA1 hippocampal neurons from P27-31 male and female WT, T4826I, CGG, or DM mice exposed to the MARBLES PCB mixture in the maternal diet throughout gestation and lactation. **(A,B)** The distance from the soma to the maximum number of dendritic intersections (Peak X). **(C,D)** The maximum number of dendritic intersections (Peak Y). **(E,F)** The total area under the curve of the Sholl plot (0–280 μm from the soma). **(G,H)** Proximal area under the curve of the Sholl plot (10–70 μm from the soma). **(I,J)** Distal area under the curve of the Sholl plot (80–140 μm from the soma). Data (N = 44–48 neurons from at least six independent mice per sex per genotype per dose) are presented as box plots, where the box indicates the lower (25th) to upper (75th) quartiles, the "+" indicates the mean, whiskers indicate the 10–90th percentile, and dots represent values outside the upper or lower fences. Bar and asterisk indicate a significant difference between groups as determined by Kruskal–Wallis test followed by Dunn's multiple comparisons test, or (E-T4826I, G-CGG) one-way ANOVA followed by Dunnett's multiple comparisons test or (H-DM) Tukey's multiple comparisons test with $p \leq 0.05$ considered statistically significant. Average values of vehicle controls for WT, T4826I, CGG and DM, respectively, are **(A)** 27.2, 27.1, 30.8, 30.2 μm; **(B)** 31.0, 27.7, 31.9, 27.1 μm; **(C)** 10.1, 9.9, 11.0, 9.6 intersections; **(D)** 10.0, 9.9, 10.9, 10.5 intersections; **(E)** 504.0, 502.9, 603.5, 534.2 μm^2; **(F)** 522.7, 516.4, 642.1, 522.7 μm^2; **(G)** 403.8, 396.4, 466.4, 405.5 μm^2; **(H)** 407.9, 418.8, 477.8, 428.9 μm^2; **(I)** 52.7, 58.5, 81.4, 74.4 μm^2; and **(J)** 64.9, 52.8, 101.4, 47.2 μm^2.

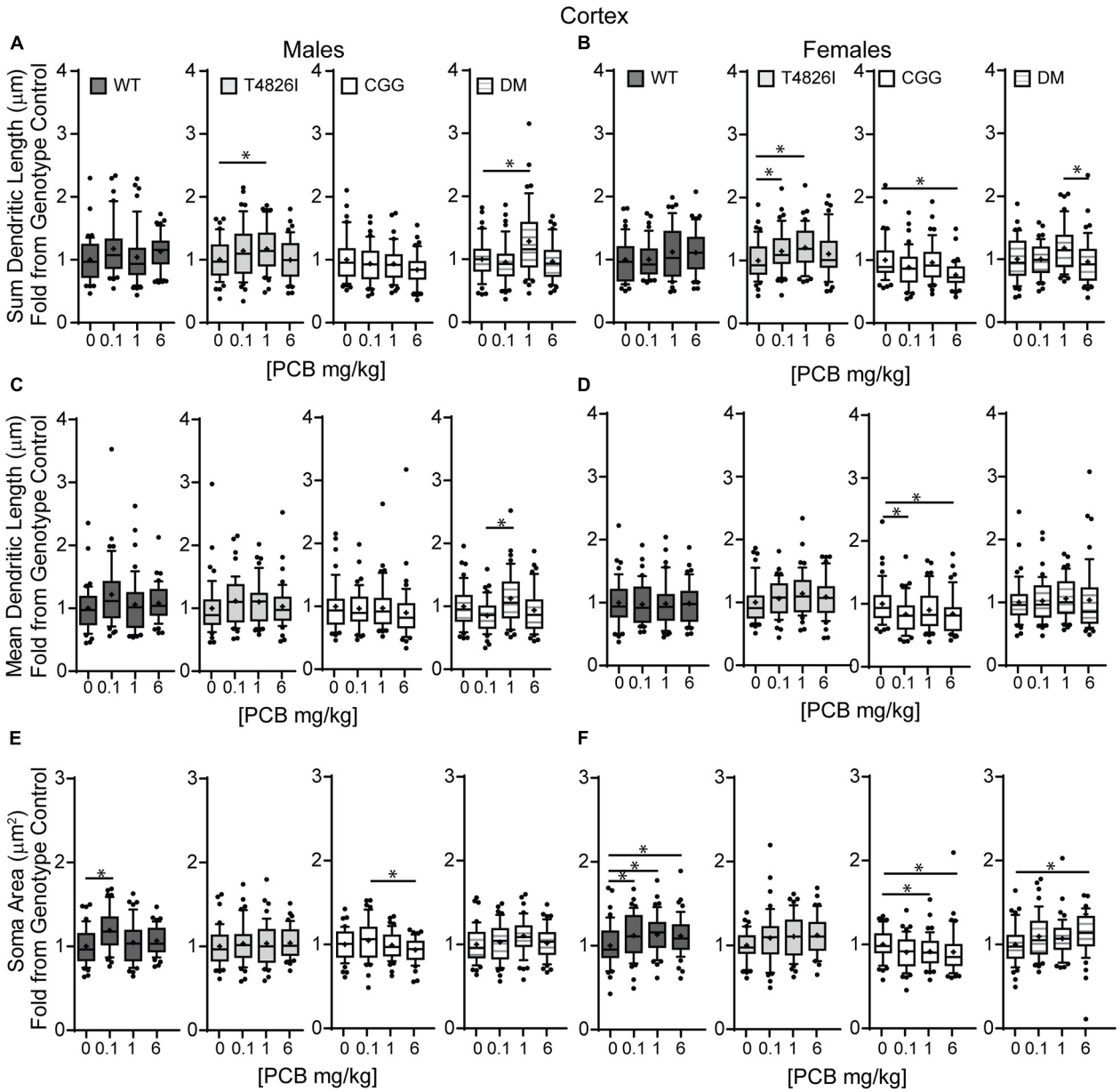

FIGURE 6 | Polychlorinated biphenyls effects on dendritic length and soma area are more prevalent in female vs. male pyramidal somatosensory cortical neurons. Morphometric analyses of the basilar dendritic arbors of Golgi-stained pyramidal CA1 hippocampal neurons from P27–31 male and female WT, T4826I, CGG, or DM mice exposed to the MARBLES PCB mixture in the maternal diet throughout gestation and lactation. **(A,B)** Sum length of dendrites per neuron (μm). **(C,D)** Mean dendritic length per neuron (μm). **(E,F)** Cell body area (μm^2). Data (N = 44–48 neurons from at least six independent mice per sex per genotype per dose) are presented as box plots, where the box indicates the lower (25th) to upper (75th) quartiles, the "+" indicates the mean, whiskers indicate the 10–90th percentile, and dots represent values outside the upper or lower fences. Bar and asterisk indicate a significant difference between groups as determined by Kruskal–Wallis test followed by Dunn's multiple comparisons test, or (A-T4826I, E-WT, DM) one-way ANOVA followed by Dunnett's multiple comparisons test or (E-CGG) one-way ANOVA with Welch's correction followed by Dunnett's T3 multiple comparison test with $p \leq 0.05$ considered statistically significant. Average values of vehicle controls for WT, T4826I, CGG and DM, respectively, are **(A)** 582.2, 583.0, 699.4, 617.5 μm; **(B)** 603.1, 591.4, 740.5, 612.1 μm; **(C)** 94.7, 96.9, 113.8, 110.5 μm; **(D)** 108.6, 99.8, 123.7, 100.2 μm; **(E)** 229.2, 228.0, 256.1, 235.1 μm^2; and **(F)** 233.2, 224.6, 267.3, 222.9 μm^2.

vehicle control were significantly different upon *post hoc* analysis (**Supplementary Figure 4D**). There were no differences in the number of dendritic tips normalized to primary dendrite number (**Supplementary Figures 4E,F**). Total dendritic length per neuron was increased in the 1 mg/kg dose group vs. vehicle control in T4826I and DM males and in the 1mg/kg and 0.1 mg/kg dose group in T4826I females (**Figures 6A,B**). Additionally, the total dendritic length was decreased in the female CGG 6 mg/kg dose group vs. vehicle control, and in the female DM 6 mg/kg dose group vs. 1 mg/kg dose group

(**Figure 6B**). Mean dendritic length per neuron was increased in male DM in the 1 mg/kg PC dose group vs. the 0.1 mg/kg dose group (**Figure 6C**), but was decreased in CGG females in the 0.1 mg/kg and 6 mg/kg dose groups vs. vehicle control (**Figure 6D**). In summary, PCBs at 1 mg/kg tended to increase complexity within DM and T4826I males and T4826I females vs. vehicle control, and PCBs at 6 mg/kg decreased dendritic complexity in CGG females.

Similar to hippocampal neurons, soma area of cortical neurons was significantly impacted by genotype and PCB exposure. CGG neurons had greater soma area than T4826I and DM neurons and T4826I neurons had reduced soma area relative to WT neurons (**Table 2**). There was also a dose effect for soma area, with the 0.1 mg/kg and 1 mg/kg PCB dose groups having greater area than vehicle control neurons (**Table 2**). Examining each sex and genotype independently, soma area was increased in the 0.1 mg/kg PCB dose group vs. vehicle control in WT male neurons (**Figure 6E**). There was also a decrease in soma area in the 6 mg/kg PCB dose group vs. the 0.1 mg/kg PCB dose group in male CGG neurons (**Figure 6E**). A greater number of PCB effects were observed in female neurons. Unlike WT hippocampal neurons, there was a significant increase in soma area in the 0.1, 1, and 6 mg/kg PCB dose groups vs. vehicle control in WT female neurons (**Figure 6F**). In CGG female neurons, there was a significant decrease in soma area in the 1mg/kg and 6 mg/kg dose group compared to vehicle control. In contrast, in DM female neurons, there was a significant increase in soma area in the 6 mg/kg PCB dose group vs. vehicle control (**Figure 6F**). In summary, PCBs increased soma area in WT cortical neurons in a sex- and dose-dependent manner, and this effect was affected by genotype since CGG female neurons had decreased soma area while DM female neurons had increased soma area at the 6 mg/kg PCB dose group relative to vehicle controls.

Table 3 summarizes data presented in **Figures 2**, **3**, **5**, **6** and **Supplementary Figures 3**, **4**, which are the PCB dose responses (indicated by arrows) within each sex and genotype relative to the vehicle control for each parameter of dendritic arborization that was measured in this study.

DISCUSSION

We describe novel data demonstrating that developmental exposure to a human-relevant PCB mixture alters dendritic arborization in the juvenile mouse brain; however, the dendritic outcome and dose-response relationship varied depending on sex, genotype, and brain region. These findings support the hypothesis that PCBs interact with heritable human mutations that alter the fidelity of neuronal Ca^{2+} signaling to confer NDD risk. This conclusion is based on two lines of evidence. First, dendritic arborization was significantly increased in cortical neurons of WT males in the 6 mg/kg PCB dose group. By comparison, the dendritic complexity of cortical neurons was significantly increased in T4826I and DM males in the 1 mg/kg PCB dose group, suggesting that expression of the T4826I-*RYR1* mutation, either alone or in combination with CGG mutation, increased sensitivity of male cortical neurons to the dendrite-promoting effects of the MARBLES PCB mixture, evident as a leftward shift of the dose-response relationship. This is consistent with previous reports that *RYR1* gain-of-function mutations confer heightened sensitivity to RyR-active PCBs *in vitro* (Ta and Pessah, 2007). Second, while developmental exposure of WT mice to the MARBLES PCB mixture had no significant effect on the dendritic morphology of male or female hippocampal neurons or female cortical neurons, it significantly altered the dendritic arborization of these neuronal cell types in mice that expressed one or more transgenes. Specifically, dendritic arborization of hippocampal neurons was significantly increased in DM males in the 6 mg/kg dose group and DM females in the 0.1, 1, and 6 mg/kg dose groups. The dendritic arbors of cortical neurons were more complex in T4826I females in the 1 mg/kg dose group, while dendritic arborization was decreased in CGG females in the 6 mg/kg dose group. Overall, these results add to a growing body of literature indicating that the genetic substrate can modulate the response to neurotoxic environmental chemicals.

Several interesting observations emerged from this study, including: (1) cortical neurons were more sensitive than hippocampal neurons to the dendritic effects of the MARBLES PCB mix; and (2) sex strongly influenced dendritic responses to PCB exposure. The observation of the differential sensitivity of cortical and hippocampal neurons is consistent with our earlier studies of dendritic arborization in the hippocampus and cortex of juvenile rats developmentally exposed to the commercial PCB mixture Aroclor 1254 (Lein et al., 2007; Yang et al., 2009). The observation regarding the influence of sex is also consistent with previous studies in which we demonstrated sex-dependent effects of PCB 95 and PCB 11 on the dendritic arborization of primary hippocampal and cortical neurons *in vitro* (Sethi et al., 2017; Keil et al., 2019a). The *in vivo* sex differences we observed in this study varied between genotypes. Specifically, PCB effects on dendritic arborization of cortical neurons were male-specific in WT and DM mice, but female-specific in CGG mice. Moreover, the direction of the dendritic response of cortical neurons to PCBs varied depending on sex, with male WT and DM cortical neurons exhibiting increased dendritic arborization and female CGG cortical neurons exhibiting decreased dendritic arborization. More subtle sex differences were observed in DM hippocampal neurons and T4826I cortical neurons: (1) female and male DM hippocampal neurons responded similarly to PCBs with increased dendritic arborization, but female neurons were more sensitive, responding to the MARBLES PCB mixtures at 0.1, 1, and 6 mg/kg/d while male neurons were affected only by the 6 mg/kg/d dose; and (2) while the direction of the dendritic response in DM hippocampal neurons and T4826I cortical neurons was similar between sexes, the specific parameters of dendritic arborization that were altered by PCBs differed. While it is widely posited that sex differences in dendritic arborization and neuronal connectivity contribute to the sex bias in the prevalence of a number of NDDs (Alaerts et al., 2016; McCarthy, 2016), our findings support an emerging literature suggesting that sex differences in the response to environmental neurotoxicant exposure may contribute to NDD sex bias.

TABLE 3 | Summary of PCB effects on neuron morphology within each sex and genotype.

Response to PCBs relative to genotype vehicle control	Hippocampus				Cortex			
	WT	**T4826I**	**CGG**	**DM**	**WT**	**T4826I**	**CGG**	**DM**
Distance from soma of max intersections (Peak X)	–	–	–	–	⬆ 6	–	–	–
Maximum # of intersections (Peak Y)	–	–	–	–	–	–	⇩ 6	–
Area under the Sholl curve (AUC)	–	–	–	⬆ 6	⬆ 6	⬆ 1 ⇧ 1	⇩ 6	–
Proximal AUC	–	–	–	⇧ 0.1,1,6	⬆ 6	⬆ 1	⇩ 6 ⇩ 6	⬆ 1
Distal AUC	–	–	–	–	–	–	–	–
Primary dendrites	–	–	–	–	–	–	–	–
Dendritic tips	–	–	–	–	–	⇧ 1	⇩ 6	⬆ 1
Dendritic tips/primary dendrites	–	–	–	–	–	–	–	–
Sum dendritic length	–	–	–	⬆ 6	–	⬆ 1 ⇧ 0.1,1	⇩ 6	⬆ 1
Mean dendritic length	–	–	–	–	–	–	⇩ 0.1,6	–
Soma area	⬇ 6 ⇩ 6	–	⬇ 1,6	⬇ 1 ⇧ 6	⬆ 0.1 ⇧ 0.1,1,6	–	⇩ 1, 6	⇧ 6

Black Arrow: Male, White Arrow: Female, Dash indicates no effect.

The biological basis for the differential susceptibility of females *vs*. males and hippocampal *vs*. cortical neurons is not known. One possibility is sex and regional differences in PCB toxicokinetics. PCBs tend to be lipophilic and thus would be predicted to be uniformly distributed throughout the brain in both sexes; however, this has yet to be demonstrated. Moreover, it is now appreciated that hydroxylated metabolites of PCBs can have neurotoxic properties that differ from those of the parent congener (Klocke and Lein, 2020), and expression of the cytochrome P450 enzymes that metabolize PCBs differ by sex and brain region (Stamou et al., 2014). Another non-mutually exclusive possibility is that PCB toxicodynamics vary according to sex and/or brain region. While addressing this possibility will require identification of the mechanism(s) that mediate the effects of the MARBLES PCB mixture on dendritic arborization, if RyR activity is involved, there is significant evidence in the literature that expression of RyRs and accessory proteins that regulate its gating properties are developmentally regulated and vary across brain regions (Pessah et al., 2010).

A novel observation of this study was the effect of the MARBLES PCB mixture on soma size, with PCB effects on this morphometric parameter observed in all but the T4826I genotype. Generally, developmental PCB exposure decreased hippocampal soma size but increased cortical soma size. The two exceptions to this generalization were increased soma size of female DM hippocampal neurons in the 6 mg/kg dose group and decreased soma size of female CGG cortical neurons in the 1 mg/kg and 6 mg/kg dose group. Interestingly, PCB effects on soma size in hippocampal neurons were phenocopied in the T4826I and DM genotypes, which had hippocampal neurons with smaller soma sizes relative to WT controls. PCB effects on soma size did not necessarily correlate with PCB effects on dendritic complexity. For example, while developmental exposure to the MARBLES PCB mix significantly decreased soma size of hippocampal neurons in male and female WT mice, male CGG mice, and male DM mice, dendritic arborization in these neuronal cell types was either unaffected (male and female WT mice and male CGG mice) or increased (male DM mice) relative to sex- and genotype- matched control. Moreover, PCBs significantly increased dendritic arborization of male and female T4826I cortical neurons, but had no significant effect on soma size in these neurons. These observations suggest that different mechanisms mediate the morphometric effects of PCBs on soma vs. dendrites, and that the PCB effects on

either morphometric parameter do not simply reflect general cellular hypertrophy.

Other environmental exposures have been reported to alter soma size. For example, developmental exposure to morphine was found to decrease or increase soma size of ventral tegmental area dopaminergic neurons depending on the brain region to which the neurons projected (Simmons et al., 2019). Soma size has been linked to cognitive ability, with increased hippocampal soma size in birds hypothesized to enhance spatial memory and survival in changing climate conditions (Freas et al., 2013). In a rat model of autism-like behavior, soma size of hippocampal CA1 pyramidal neurons was reduced in offspring developmentally exposed to valproic acid (Hajisoltani et al., 2019). The effects of reduced soma size on cognitive behavior may extend to humans, as hippocampal soma size is reduced in individuals with schizophrenia (Benes et al., 1991). Human iPSC cells with a knockdown of SHANK3, an autism-related gene, or neurons derived from iPSC from patients with Rett syndrome also exhibited reduced soma size (Marchetto et al., 2010; Huang et al., 2019). Conversely, there is evidence that increased soma size is associated with altered cognitive ability: mice lacking the FMR protein had increased neuronal somata (Selby et al., 2007). These observations suggest that either abnormally enlarged or reduced neuronal soma size may be detrimental to cognitive function, identifying another NDD-relevant outcome influenced by interactions between PCBs and human mutations associated with altered Ca^{2+}-dependent signaling and/or neuronal connectivity.

A question raised by this study is whether gene dosage affected dendritic arborization in the absence or presence of developmental PCB exposures. Gene dosage seemed to influence dendritic outcome independent of developmental PCB exposure as evidenced by the observation that male DM hippocampal neurons had significantly more complex dendritic arbors than male T4826I hippocampal neurons (assessed as distal area under the Sholl curve, **Table 1**). Gene dosage also seemed to influence sensitivity of hippocampal neurons to the dendritic effects of the MARBLES PCB mixture since PCB effects on this neuronal cell type were only observed in male and female DM mice. Assessing the influence of gene dosage on the response of cortical neurons to PCBs is more difficult because PCB effects on cortical neurons were more complex. Nonetheless, male DM cortical neurons were more sensitive to the dendrite-promoting activity of PCBs than male WT and CCG neurons. Conversely, the dendritic arborization of female DM cortical neurons was not altered by developmental PCB exposure compared to vehicle control, while female T4826I cortical neurons responded to PCBs with more complex dendritic arbors and female CGG cortical neurons responded with less complex dendritic arbors. Based on these observations, it is difficult to determine whether the T4826I and CGG genotypes contributed equally to the DM phenotype. In male cortical neurons, developmental PCB exposure increased the proximal area under the Sholl curve in both T4826I and DM mice in the 1 mg/kg dose group, but had no effect or reduced this parameter in male CGG cortical neurons, suggesting this phenotype in DM males was driven largely by the T4826I-*RYR1* mutation. However, in male hippocampal neurons, developmental PCB exposure decreased soma area in CGG and DM neurons of mice in the 1 mg/kg dose group but not in T4826I neurons, suggesting this PCB response is largely influenced by the CGG mutation. Yet in other cases, the DM response to PCBs was not phenocopied by either the T4826I or CGG genotype. For example, in hippocampal neurons, PCB responses were only seen in DM mice and not mice of the other genotypes. Additionally, in female cortical neurons, developmental PCB exposure increased dendritic complexity in T4826I mice in the 1mg/kg dose group, decreased dendritic arborization in CGG mice in the 6 mg/kg dose group, and had no effect on dendritic arborization in DM mice compared to vehicle controls. This latter scenario may reflect an additive effect of both genotypes. Collectively, these observations suggest that while the T4826I-*RYR1* and CGG mutations both alter the fidelity of Ca^{2+} signaling in neurons (Barrientos et al., 2012; Cao et al., 2012; Robin et al., 2017), the interactions between these mutations in the DM mice are complex, potentially reflecting mechanism(s) independent of Ca^{2+} signaling.

Several potential mechanisms by which MARBLES PCBs interact with the T4826I-*RYR1* and *FMR1* CGG repeat expansion mutations to modulate dendritic arborization include (1) PCB induced changes in the expression of RYR1 and FMR1/FMRP and/or (2) convergence on the same signaling systems dysregulated by these genetic factors at critical times during development. With respect to the former, we have previously demonstrated that gestational and lactational exposure to Aroclor 1254 in the maternal diet at 1 or 6 mg/kg/d dose-dependently increased RyR expression in the cerebellum of weanling pups (Yang et al., 2009). Whether the MARBLES mix similarly increases RyR expression and whether any PCB(s) increase expression of FMRP is not known, but should be the focus of future investigations. Several lines of evidence support a model in which PCBs and genetic factors converse on Ca^{2+}-dependent signaling pathways. First, the MARBLES PCB mixture has RyR activity as determined by equilibrium binding of [^{3}H]ryanodine to RyR1-enriched microsomes (Sethi et al., 2019). Moreover, two of the MARBLES PCB congeners, PCB 95 and PCB 11, promote dendritic growth in primary hippocampal and cortical neurons via activation of Ca^{2+}-dependent signaling pathways involving CREB, Wnt, miR132, and/or mTOR (Yang et al., 2009; Wayman et al., 2012a,b; Lesiak et al., 2014; Keil et al., 2018; Sethi et al., 2018). The signaling pathways activated by PCBs to increase dendritic arborization map onto Ca^{2+}-dependent signaling pathways altered in NDDs (Stamou et al., 2013; Panesar et al., 2020). Second, both the T4826I-*RYR1* gain of function mutation (Barrientos et al., 2012) and the *FMR1* CGG repeat expansion mutation (Cao et al., 2012; Robin et al., 2017) have been shown to increase resting intracellular Ca^{2+} concentrations and spontaneous Ca^{2+} oscillations in neuronal cells. Increased intracellular Ca^{2+} promotes dendritic growth via a CaMK-CREB-Wnt signaling pathway (Wayman et al., 2006) and dendritic spine formation via a CREB-miR132 pathway (Impey et al., 2010). Intracellular Ca^{2+} also regulates mTOR-dependent translational control of dendritic growth (Kumar et al., 2005; Urbanska et al., 2012). The *FMR1* CGG repeat expansion mutation results in decreased expression of

the translational repressor FMRP (Hagerman and Hagerman, 2013), which effectively alters mTOR signaling (Wang et al., 2012). FMRP also functions as a chaperone for miR132, but the effects of decreased FMRP on miR132 signaling are not known. Expression of either the *RYR1* gain of function mutation (Pessah, personal communication) or the *FMR1* CGG repeat expansion (Chen et al., 2010) have been shown to alter dendritic growth in primary neurons. We propose that at least a subset of PCB congeners in the MARBLES PCB mixture converge on these signaling pathways to amplify the effects of these gene mutations on dendritic arborization.

While further studies are required to confirm this model, it does provide a potential explanation for the observation that in contrast to previous studies of rats exposed developmentally to PCB 95 (Wayman et al., 2012b) or Aroclor 1254 (Lein et al., 2007; Yang et al., 2009), the MARBLES mix did not promote dendritic arborization in the CA1 pyramidal neurons in the hippocampus of WT mice. PCB 95 is among the most potent congener with respect to RyR sensitization (Pessah et al., 2010), and Aroclor 1254 contains a significant percentage of RyR-active PCB congeners, including PCB 95 (Howard et al., 2003). In contrast, PCB 95 comprised only 1.2% of the total mass in the MARBLES mixture. Moreover, a comparative analysis of the *in vitro* RyR potency of PCB 95 *vs*. the MARBLES mix showed that the MARBLES mix activates the RyR at micromolar concentrations with a maximal activation of 4-fold while PCB 95 activated the RyR at nanomolar concentrations and the maximal activation was 12-fold (Sethi et al., 2019). This earlier *in vitro* study compared the RyR potency of each of the individual PCB congeners in the MARBLES mix, and the results indicate that the most potent RyR sensitizing congeners comprise ∼9% of the MARBLES mix. Therefore, if RyR sensitization is the predominant mechanism driving PCB-induced dendritic arborization, it is perhaps not surprising that the MARBLES mix did not promote dendritic arborization in hippocampal neurons of WT animals. However, we did observe increased dendritic arborization of cortical neurons in WT animals, suggesting that the dose-dependency of PCB-induced dendritic growth varies between brain regions.

A model in which PCBs and genetic factors interact via convergence on Ca^{2+}-dependent signaling pathways also provides a potential explanation for the non-monotonic dose-related effect of the MARBLES PCB mix on dendritic arborization. Multilevel linear mixed-effects modeling identified a main effect of dose on the dendritic complexity of cortical neurons with the 1 mg/kg PCB dose group exhibiting significantly increased dendritic arborization compared to vehicle controls or the 0.1 and 6 mg/kg dose groups. A similar non-monotonic dose-response relationship has been reported in previous *in vivo* and *in vitro* studies of Aroclor 1254, PCB 95 and PCB 136 (Yang et al., 2009, 2014; Wayman et al., 2012b). The mechanism underlying this dose-response relationship is not known, but a possibility is suggested by *in vitro* studies demonstrating that moderate increases in Ca^{2+} promote dendritic growth whereas large increases cause dendritic retraction (Segal et al., 2000; Lohmann and Wong, 2005). Thus, if PCBs and the T4826I-*RYR1* and *FMR1* CGG repeat expansion mutations are modulating dendritic growth via increased levels of intracellular Ca^{2+}, then higher PCB doses, increased gene dosage, or the combination of PCBs and gene mutations may increase intracellular Ca^{2+} above concentrations that promote dendritic growth to levels that trigger dendritic retraction, perhaps via activation of calpain (Baudry et al., 2013) or preferential activation of CaMKIV (Redmond et al., 2002). This mechanism may also explain the observation that MARBLES PCBs decreased dendritic complexity of female CGG cortical neurons. Testing this hypothesis is an important area of future study, findings from which will expand our understanding of how environmental and genetic risk factors and potentially provide algorithms for predicting specific gene-environment interactions likely to increase the risk of adverse neurodevelopmental outcomes.

An outstanding question is whether effects of the MARBLES PCB mixture on dendritic arborization are linked to changes in behavior. The animals used in this study were assessed in tasks that measured social communication, repetitive behavior and sociability (data under review). While aberrant behavior was observed in PCB-exposed animals, there was not a one-to-one correlation between PCB effects on dendritic growth and behavior in terms of dose-response relationships or genotype effects. However, this does not negate the relevance of the dendritic findings since we may not have captured the neuroanatomic circuits that mediate the behaviors that were assessed. We believe the dendritic findings are relevant to human NDDs for several reasons. First, animals were exposed to a human-relevant PCB mixture that reflected the PCB congener profile in the gestational environment of at-risk individuals, and the PCB concentrations measured in brain tissue of exposed pups were within the range of PCB levels measured in human brain tissue (Sethi et al., under review)[2]. Second, both increased and decreased dendritic arborization are thought to contribute to the clinical phenotypes associated with many NDDs (Coskun et al., 2013; Keown et al., 2013; Khan et al., 2015; Alaerts et al., 2016; Cooper et al., 2017). In summary, these studies add to the growing body of literature implicating PCBs as NDD risk factors, and identify genetic mutations that may amplify the effects of neurotoxic PCBs on the developing brain.

DATA AVAILABILITY STATEMENT

The raw data supporting the conclusions of this article will be made available by the authors, without undue reservation.

ETHICS STATEMENT

The animal study was reviewed and approved by University of California, Davis Institutional Animal Care and Use Committee.

[2]Sethi, S., Keil Stietz, K. P., Valenzuela, A. E., Klocke, C. R., Silverman, J. L., Puschner, B., et al. (under review). Developmental exposure to a human-relevant PCB mixture causes behavioral phenotypes that vary by sex and genotype in juvenile mice expressing human mutations that modulate neuronal calcium. *Front. Neurosci.*

AUTHOR CONTRIBUTIONS

IP and PL conceptualized the project and obtained funding to support the work. PL supervised all aspects of this study. KK, SS, and PL designed the experiments. KK and SS maintained the mouse colony, dosed the animals, collected tissues for PCB quantitation, and conducted the statistical analysis of the independent PCB dose effects. KK, SS, TR, and CK conducted the Golgi analysis. MW conducted the mixed-effects modeling of the morphometric data. KK, SS, and CK composed the figures. KK drafted the initial manuscript. CK and PL made significant edits to the early versions of the manuscript. All authors listed have made a substantial, direct, and intellectual contribution to the work and approved it for publication.

FUNDING

This study was supported by the National Institute of Environmental Health (grant numbers R01 ES014901 to PL and IP, T32 ES007059 to SS, R00 ES029537 to KK and P30 ES023513) and by the Eunice Kennedy Shriver National Institute of Child Health and Human Development (grant number F32 HD088016 to KK). This project used core facilities supported by the MIND Institute Intellectual and Developmental Disabilities Research Center (grant number P50 HD103526), by the National Center for Advancing Translational Sciences, National Institutes of Health (grant number UL1 TR001860) and the UC Davis Environmental Health Sciences Center (grant number P30 ES023513). Synthesis of PCB congeners was supported by the Superfund Research Center at The University of Iowa (grant number P42 ES013661). The contents of this study do not necessarily represent the official views of the NIEHS or NICHD. The NIEHS and NICHD do not endorse the purchase of any commercial products or services mentioned in the publication.

ACKNOWLEDGMENTS

We would like to acknowledge Xueshu Li and Hans-Jaochim Lehmler (The University of Iowa) for providing the PCBs congeners used to make the MARBLES PCB mix used in this study.

SUPPLEMENTARY MATERIAL

The Supplementary Material for this article can be found online at: https://www.frontiersin.org/articles/10.3389/fnins.2021.766802/full#supplementary-material

REFERENCES

Alaerts, K., Swinnen, S. P., and Wenderoth, N. (2016). Sex differences in autism: a resting-state fMRI investigation of functional brain connectivity in males and females. *Soc. Cogn. Affect. Neurosci.* 11, 1002–1016. doi: 10.1093/scan/nsw027

Barrientos, G. C., Feng, W., Truong, K., Matthaei, K. I., Yang, T., Allen, P. D., et al. (2012). Gene dose influences cellular and calcium channel dysregulation in heterozygous and homozygous T4826I-RYR1 malignant hyperthermia-susceptible muscle. *J. Biol. Chem.* 287, 2863–2876. doi: 10.1074/jbc.M111.307926

Baudry, M., Chou, M. M., and Bi, X. (2013). Targeting calpain in synaptic plasticity. *Expert Opin. Ther. Targets* 17, 579–592. doi: 10.1517/14728222.2013.766169

Benes, F. M., Sorensen, I., and Bird, E. D. (1991). Reduced neuronal size in posterior hippocampus of schizophrenic patients. *Schizophr. Bull.* 17, 597–608. doi: 10.1093/schbul/17.4.597

Berghuis, S. A., Bos, A. F., Sauer, P. J., and Roze, E. (2015). Developmental neurotoxicity of persistent organic pollutants: an update on childhood outcome. *Arch. Toxicol.* 89, 687–709. doi: 10.1007/s00204-015-1463-3

Berman, R. F., Murray, K. D., Arque, G., Hunsaker, M. R., and Wenzel, H. J. (2012). Abnormal dendrite and spine morphology in primary visual cortex in the CGG knock-in mouse model of the fragile X premutation. *Epilepsia* 53, 150–160. doi: 10.1111/j.1528-1167.2012.03486.x

Cao, Z., Hulsizer, S., Tassone, F., Tang, H. T., Hagerman, R. J., Rogawski, M. A., et al. (2012). Clustered burst firing in FMR1 premutation hippocampal neurons: amelioration with allopregnanolone. *Hum. Mol. Genet.* 21, 2923–2935. doi: 10.1093/hmg/dds118

Chen, J. L., and Nedivi, E. (2010). Neuronal structural remodeling: is it all about access? *Curr. Opin. Neurobiol.* 20, 557–562. doi: 10.1016/j.conb.2010.06.002

Chen, Y., Tassone, F., Berman, R. F., Hagerman, P. J., Hagerman, R. J., Willemsen, R., et al. (2010). Murine hippocampal neurons expressing Fmr1 gene premutations show early developmental deficits and late degeneration. *Hum. Mol. Genet.* 19, 196–208. doi: 10.1093/hmg/ddp479

Chonchaiya, W., Au, J., Schneider, A., Hessl, D., Harris, S. W., Laird, M., et al. (2012). Increased prevalence of seizures in boys who were probands with the FMR1 premutation and co-morbid autism spectrum disorder. *Hum. Genet.* 131, 581–589. doi: 10.1007/s00439-011-1106-6

Cline, H. T. (2001). Dendritic arbor development and synaptogenesis. *Curr. Opin. Neurobiol.* 11, 118–126. doi: 10.1016/s0959-4388(00)00182-3

Cooper, R. A., Richter, F. R., Bays, P. M., Plaisted-Grant, K. C., Baron-Cohen, S., and Simons, J. S. (2017). Reduced hippocampal functional connectivity during episodic memory retrieval in autism. *Cereb. Cortex* 27, 888–902. doi: 10.1093/cercor/bhw417

Coskun, M. A., Loveland, K. A., Pearson, D. A., Papanicolaou, A. C., and Sheth, B. R. (2013). Functional assays of local connectivity in the somatosensory cortex of individuals with autism. *Autism Res.* 6, 190–200. doi: 10.1002/aur.1276

Fernandez, E., Rajan, N., and Bagni, C. (2013). The FMRP regulon: from targets to disease convergence. *Front. Neurosci.* 7:191. doi: 10.3389/fnins.2013.00191

Freas, C. A., Roth, T. C., LaDage, L. D., and Pravosudov, V. V. (2013). Hippocampal neuron soma size is associated with population differences in winter climate severity in food-caching chickadees. *Funct. Ecol.* 27, 1341–1349. doi: 10.1111/1365-2435.12125

Granillo, L., Sethi, S., Keil, K. P., Lin, Y., Ozonoff, S., Iosif, A. M., et al. (2019). Polychlorinated biphenyls influence on autism spectrum disorder risk in the MARBLES cohort. *Environ. Res.* 171, 177–184. doi: 10.1016/j.envres.2018.12.061

Grove, J., Ripke, S., Als, T. D., Mattheisen, M., Walters, R. K., Won, H., et al. (2019). Identification of common genetic risk variants for autism spectrum disorder. *Nat. Genet.* 51, 431–444. doi: 10.1038/s41588-019-0344-8

Hagerman, R., and Hagerman, P. (2013). Advances in clinical and molecular understanding of the FMR1 premutation and fragile X-associated tremor/ataxia syndrome. *Lancet Neurol.* 12, 786–798. doi: 10.1016/S1474-4422(13)70125-X

Hajisoltani, R., Karimi, S. A., Rahdar, M., Davoudi, S., Borjkhani, M., Hosseinmardi, N., et al. (2019). Hyperexcitability of hippocampal CA1 pyramidal neurons in male offspring of a rat model of autism spectrum disorder (ASD) induced by prenatal exposure to valproic acid: a possible involvement of Ih channel current. *Brain Res.* 1708, 188–199. doi: 10.1016/j.brainres.2018.12.011

Hertz-Picciotto, I., Schmidt, R. J., Walker, C. K., Bennett, D. H., Oliver, M., Shedd-Wise, K. M., et al. (2018). A prospective study of environmental exposures and early biomarkers in autism spectrum disorder: design, protocols, and preliminary data from the MARBLES study. *Environ. Health Perspect.* 126:117004. doi: 10.1289/EHP535

Howard, A. S., Fitzpatrick, R., Pessah, I., Kostyniak, P., and Lein, P. J. (2003). Polychlorinated biphenyls induce caspase-dependent cell death in cultured embryonic rat hippocampal but not cortical neurons *via* activation of the ryanodine receptor. *Toxicol. Appl. Pharmacol.* 190, 72–86. doi: 10.1016/s0041-008x(03)00156-x

Huang, G., Chen, S., Chen, X., Zheng, J., Xu, Z., Doostparast Torshizi, A., et al. (2019). Uncovering the functional link between SHANK3 deletions and deficiency in neurodevelopment Using iPSC-derived human neurons. *Front. Neuroanat.* 13:23. doi: 10.3389/fnana.2019.00023

Impey, S., Davare, M., Lasiek, A., Fortin, D., Ando, H., Varlamova, O., et al. (2010). An activity-induced microRNA controls dendritic spine formation by regulating Rac1-PAK signaling. *Mol. Cell Neurosci.* 43, 146–156. doi: 10.1016/j.mcn.2009.10.005

Keil, K. P., Miller, G. W., Chen, H., Sethi, S., Schmuck, M. R., Dhakal, K., et al. (2018). PCB 95 promotes dendritic growth in primary rat hippocampal neurons *via* mTOR-dependent mechanisms. *Arch. Toxicol.* 92, 3163–3173. doi: 10.1007/s00204-018-2285-x

Keil, K. P., Sethi, S., Wilson, M. D., Silverman, J. L. I, Pessah, N., and Lein, P. J. (2019b). Genetic mutations in Ca^{2+} signaling alter dendrite morphology and social approach in juvenile mice. *Genes Brain Behav.* 18:e12526. doi: 10.1111/gbb.12526

Keil, K. P., Sethi, S., and Lein, P. J. (2019a). Sex-Dependent Effects of 2,2',3,5',6-Pentachlorobiphenyl on Dendritic Arborization of Primary Mouse Neurons. *Toxicol. Sci.* 168, 95–109. doi: 10.1093/toxsci/kfy277

Keil, K. P., Sethi, S., Wilson, M. D., Chen, H., and Lein, P. J. (2017). *In vivo* and *in vitro* sex differences in the dendritic morphology of developing murine hippocampal and cortical neurons. *Sci. Rep.* 7:8486. doi: 10.1038/s41598-017-08459-z

Keown, C. L., Shih, P., Nair, A., Peterson, N., Mulvey, M. E., and Muller, R. A. (2013). Local functional overconnectivity in posterior brain regions is associated with symptom severity in autism spectrum disorders. *Cell Rep.* 5, 567–572. doi: 10.1016/j.celrep.2013.10.003

Khan, S., Michmizos, K., Tommerdahl, M., Ganesan, S., Kitzbichler, M. G., Zetino, M., et al. (2015). Somatosensory cortex functional connectivity abnormalities in autism show opposite trends, depending on direction and spatial scale. *Brain* 138, 1394–1409. doi: 10.1093/brain/awv043

Kilkenny, C., Browne, W. J. I, Cuthill, C., Emerson, M., and Altman, D. G. (2010). Improving bioscience research reporting: the ARRIVE guidelines for reporting animal research. *PLoS Biol.* 8:e1000412. doi: 10.1371/journal.pbio.1000412

Kim, J. H., Jarvik, G. P., Browning, B. L., Rajagopalan, R., Gordon, A. S., Rieder, M. J., et al. (2013). Exome sequencing reveals novel rare variants in the ryanodine receptor and calcium channel genes in malignant hyperthermia families. *Anesthesiology* 119, 1054–1065. doi: 10.1097/ALN.0b013e3182a8a998

Klocke, C., and Lein, P. J. (2020). Evidence Implicating Non-Dioxin-Like Congeners as the Key Mediators of Polychlorinated Biphenyl (PCB) Developmental Neurotoxicity. *Int. J. Mol. Sci.* 21:1013. doi: 10.3390/ijms21031013

Koh, W. X., Hornbuckle, K. C., and Thorne, P. S. (2015). Human Serum from Urban and Rural Adolescents and Their Mothers Shows Exposure to Polychlorinated Biphenyls Not Found in Commercial Mixtures. *Environ. Sci. Technol.* 49, 8105–8112. doi: 10.1021/acs.est.5b01854

Konur, S., and Ghosh, A. (2005). Calcium signaling and the control of dendritic development. *Neuron* 46, 401–405. doi: 10.1016/j.neuron.2005.04.022

Krey, J. F., and Dolmetsch, R. E. (2007). Molecular mechanisms of autism: a possible role for Ca2+ signaling. *Curr. Opin. Neurobiol.* 17, 112–119. doi: 10.1016/j.conb.2007.01.010

Krueger, D. D., and Bear, M. F. (2011). Toward fulfilling the promise of molecular medicine in fragile X syndrome. *Annu. Rev. Med.* 62, 411–429. doi: 10.1146/annurev-med-061109-134644

Kumar, V., Zhang, M. X., Swank, M. W., Kunz, J., and Wu, G. Y. (2005). Regulation of dendritic morphogenesis by Ras-PI3K-Akt-mTOR and Ras-MAPK signaling pathways. *J. Neurosci.* 25, 11288–11299. doi: 10.1523/JNEUROSCI.2284-05.2005

Leehey, M. A., and Hagerman, P. J. (2012). Fragile X-associated tremor/ataxia syndrome. *Handb. Clin. Neurol.* 103, 373–386. doi: 10.1016/B978-0-444-51892-7.00023-1

Lein, P. J., Yang, D., Bachstetter, A. D., Tilson, H. A., Harry, G. J., Mervis, R. F., et al. (2007). Ontogenetic alterations in molecular and structural correlates of dendritic growth after developmental exposure to polychlorinated biphenyls. *Environ. Health Perspect.* 115, 556–563. doi: 10.1289/ehp.9773

Lesiak, A., Zhu, M., Chen, H., Appleyard, S. M., Impey, S., Lein, P. J., et al. (2014). The environmental neurotoxicant PCB 95 promotes synaptogenesis *via* ryanodine receptor-dependent miR132 upregulation. *J. Neurosci.* 34, 717–725. doi: 10.1523/JNEUROSCI.2884-13.2014

Li, X., Holland, E. B., Feng, W., Zheng, J., Dong, Y. I, Pessah, N., et al. (2018). Authentication of synthetic environmental contaminants and their (bio)transformation products in toxicology: polychlorinated biphenyls as an example. *Environ. Sci. Pollut. Res. Int.* 25, 16508–16521. doi: 10.1007/s11356-017-1162-0

Liu, J., Koscielska, K. A., Cao, Z., Hulsizer, S., Grace, N., Mitchell, G., et al. (2012). Signaling defects in iPSC-derived fragile X premutation neurons. *Hum. Mol. Genet.* 21, 3795–3805. doi: 10.1093/hmg/dds207

Lohmann, C., and Wong, R. O. (2005). Regulation of dendritic growth and plasticity by local and global calcium dynamics. *Cell Calcium* 37, 403–409. doi: 10.1016/j.ceca.2005.01.008

Lu, A. T., and Cantor, R. M. (2012). Allowing for sex differences increases power in a GWAS of multiplex Autism families. *Mol. Psychiatry* 17, 215–222. doi: 10.1038/mp.2010.127

Lyall, K., Croen, L. A., Sjodin, A., Yoshida, C. K., Zerbo, O., Kharrazi, M., et al. (2017). Polychlorinated biphenyl and organochlorine pesticide concentrations in maternal mid-pregnancy serum samples: association with autism spectrum disorder and intellectual disability. *Environ. Health Perspect.* 125, 474–480. doi: 10.1289/EHP277

Marchetto, M. C., Carromeu, C., Acab, A., Yu, D., Yeo, G. W., Mu, Y., et al. (2010). A model for neural development and treatment of Rett syndrome using human induced pluripotent stem cells. *Cell* 143, 527–539. doi: 10.1016/j.cell.2010.10.016

Matelski, L., Keil Stietz, K. P., Sethi, S., Taylor, S. L., Van de Water, J., and Lein, P. J. (2020). The influence of sex, genotype, and dose on serum and hippocampal cytokine levels in juvenile mice developmentally exposed to a human-relevant mixture of polychlorinated biphenyls. *Curr. Res. Toxicol.* 1, 85–103. doi: 10.1016/j.crtox.2020.09.001

McCarthy, M. M. (2016). Sex differences in the developing brain as a source of inherent risk. *Dialogues Clin. Neurosci.* 18, 361–372. doi: 10.31887/dcns.2016.18.4/mmccarthy

Panesar, H. K., Kennedy, C. L., Keil Stietz, K. P., and Lein, P. J. (2020). Polychlorinated Biphenyls (PCBs): risk factors for autism spectrum disorder? *Toxics* 8:70. doi: 10.3390/toxics8030070

Pessah, I. N., Cherednichenko, G., and Lein, P. J. (2010). Minding the calcium store: ryanodine receptor activation as a convergent mechanism of PCB toxicity. *Pharmacol. Ther.* 125, 260–285. doi: 10.1016/j.pharmthera.2009.10.009

Pessah, I. N., Lein, P. J., Seegal, R. F., and Sagiv, S. K. (2019). Neurotoxicity of polychlorinated biphenyls and related organohalogens. *Acta Neuropathol.* 138, 363–387. doi: 10.1007/s00401-019-01978-1

Redmond, L., Kashani, A. H., and Ghosh, A. (2002). Calcium regulation of dendritic growth *via* CaM kinase IV and CREB-mediated transcription. *Neuron* 34, 999–1010. doi: 10.1016/s0896-6273(02)00737-7

Robin, G., Lopez, J. R., Espinal, G. M., Hulsizer, S., Hagerman, P. J., and Pessah, I. N. (2017). Calcium dysregulation and Cdk5-ATM pathway involved in a mouse model of fragile X-associated tremor/ataxia syndrome. *Hum. Mol. Genet.* 26, 2649–2666. doi: 10.1093/hmg/ddx148

Roegge, C. S., Morris, J. R., Villareal, S., Wang, V. C., Powers, B. E., Klintsova, A. Y., et al. (2006). Purkinje cell and cerebellar effects following developmental exposure to PCBs and/or MeHg. *Neurotoxicol. Teratol.* 28, 74–85. doi: 10.1016/j.ntt.2005.10.001

Rude, K. M., Pusceddu, M. M., Keogh, C. E., Sladek, J. A., Rabasa, G., Miller, E. N., et al. (2019). Developmental exposure to polychlorinated biphenyls (PCBs)

in the maternal diet causes host-microbe defects in weanling offspring mice. *Environ. Pollut.* 253, 708–721. doi: 10.1016/j.envpol.2019.07.066

Sable, H. J. K., and Schantz, S. L. (2006). "Executive function following developmental exposure to Polychlorinated Biphenyls (PCBs): what animal models have told us," in *Animal Models of Cognitive Impairment*, eds E. D. Levin and J. J. Buccafusco (Boca Raton: CRC Press), 22.

Schantz, S. L., Widholm, J. J., and Rice, D. C. (2003). Effects of PCB exposure on neuropsychological function in children. *Environ. Health Perspect.* 111, 357–576. doi: 10.1289/ehp.5461

Segal, I., Korkotian, I., and Murphy, D. D. (2000). Dendritic spine formation and pruning: common cellular mechanisms? *Trends Neurosci.* 23, 53–57. doi: 10.1016/s0166-2236(99)01499-x

Selby, L., Zhang, C., and Sun, Q. Q. (2007). Major defects in neocortical GABAergic inhibitory circuits in mice lacking the fragile X mental retardation protein. *Neurosci. Lett.* 412, 227–232. doi: 10.1016/j.neulet.2006.11.062

Sethi, S., Keil, K. P., and Lein, P. J. (2017). Species and Sex Differences in the Morphogenic Response of Primary Rodent Neurons to 3,3'-Dichlorobiphenyl (PCB 11). *Toxics* 6:4. doi: 10.3390/toxics6010004

Sethi, S., Keil, K. P., and Lein, P. J. (2018). 3,3'-Dichlorobiphenyl (PCB 11) promotes dendritic arborization in primary rat cortical neurons *via* a CREB-dependent mechanism. *Arch. Toxicol.* 92, 3337–3345. doi: 10.1007/s00204-018-2307-8

Sethi, S., Morgan, R. K., Feng, W., Lin, Y., Li, X., Luna, C., et al. (2019). Comparative analyses of the 12 most abundant PCB congeners detected in human maternal serum for activity at the thyroid hormone receptor and ryanodine receptor. *Environ. Sci. Technol.* 53, 3948–3958. doi: 10.1021/acs.est.9b00535

Simmons, S. C., Wheeler, K., and Mazei-Robison, M. S. (2019). Determination of circuit-specific morphological adaptations in ventral tegmental area dopamine neurons by chronic morphine. *Mol. Brain* 12:10. doi: 10.1186/s13041-019-0435-6

Stamou, M., Streifel, K. M., Goines, P. E., and Lein, P. J. (2013). Neuronal connectivity as a convergent target of gene x environment interactions that confer risk for Autism Spectrum Disorders. *Neurotoxicol. Teratol.* 36, 3–16. doi: 10.1016/j.ntt.2012.12.001

Stamou, M., Wu, X., Kania-Korwel, I., Lehmler, H. J., and Lein, P. J. (2014). Cytochrome p450 mRNA expression in the rodent brain: species-, sex-, and region-dependent differences. *Drug Metab. Dispos.* 42, 239–244. doi: 10.1124/dmd.113.054239

Ta, T. A., and Pessah, I. N. (2007). Ryanodine receptor type 1 (RyR1) possessing malignant hyperthermia mutation R615C exhibits heightened sensitivity to dysregulation by non-coplanar 2,2',3,5',6-pentachlorobiphenyl (PCB 95). *Neurotoxicology* 28, 770–779. doi: 10.1016/j.neuro.2006.08.007

Tassone, F., Iong, K. P., Tong, T. H., Lo, J., Gane, L. W., Berry-Kravis, E., et al. (2012). FMR1 CGG allele size and prevalence ascertained through newborn screening in the United States. *Genome Med.* 4:100. doi: 10.1186/gm401

Urbanska, M., Gozdz, A., Swiech, L. J., and Jaworski, J. (2012). Mammalian target of rapamycin complex 1 (mTORC1) and 2 (mTORC2) control the dendritic arbor morphology of hippocampal neurons. *J. Biol. Chem.* 287, 30240–30256. doi: 10.1074/jbc.M112.374405

Wang, T., Bray, S. M., and Warren, S. T. (2012). New perspectives on the biology of fragile X syndrome. *Curr. Opin. Genet. Dev.* 22, 256–263. doi: 10.1016/j.gde.2012.02.002

Wayman, G. A., Bose, D. D., Yang, D., Lesiak, A., Bruun, D., Impey, S., et al. (2012a). PCB-95 modulates the calcium-dependent signaling pathway responsible for activity-dependent dendritic growth. *Environ. Health Perspect.* 120, 1003–1009. doi: 10.1289/ehp.1104833

Wayman, G. A., Yang, D., Bose, D. D., Lesiak, A., Ledoux, V., Bruun, D., et al. (2012b). PCB-95 promotes dendritic growth *via* ryanodine receptor-dependent mechanisms. *Environ. Health Perspect.* 120, 997–1002. doi: 10.1289/ehp.1104832

Wayman, G. A., Impey, S., Marks, D., Saneyoshi, T., Grant, W. F., Derkach, V., et al. (2006). Activity-dependent dendritic arborization mediated by CaM-kinase I activation and enhanced CREB-dependent transcription of Wnt-2. *Neuron* 50, 897–909. doi: 10.1016/j.neuron.2006.05.008

Willemsen, R., Hoogeveen-Westerveld, M., Reis, S., Holstege, J., Severijnen, L. A. I, Nieuwenhuizen, M., et al. (2003). The FMR1 CGG repeat mouse displays ubiquitin-positive intranuclear neuronal inclusions; implications for the cerebellar tremor/ataxia syndrome. *Hum. Mol. Genet.* 12, 949–959. doi: 10.1093/hmg/ddg114

Wilson, M. D., Sethi, S., Lein, P. J., and Keil, K. P. (2017). Valid statistical approaches for analyzing sholl data: mixed effects versus simple linear models. *J. Neurosci. Methods* 279, 33–43. doi: 10.1016/j.jneumeth.2017.01.003

Xi, T., and Wu, J. (2021). A review on the mechanism between different factors and the occurrence of autism and ADHD. *Psychol. Res. Behav. Manag.* 14, 393–403. doi: 10.2147/PRBM.S304450

Yang, D., Kania-Korwel, I., Ghogha, A., Chen, H., Stamou, M., Bose, D. D. I, et al. (2014). PCB 136 atropselectively alters morphometric and functional parameters of neuronal connectivity in cultured rat hippocampal neurons *via* ryanodine receptor-dependent mechanisms. *Toxicol. Sci.* 138, 379–392. doi: 10.1093/toxsci/kft334

Yang, D., Kim, K. H., Phimister, A., Bachstetter, A. D., Ward, T. R., Stackman, R. W., et al. (2009). Developmental exposure to polychlorinated biphenyls interferes with experience-dependent dendritic plasticity and ryanodine receptor expression in weanling rats. *Environ. Health Perspect.* 117, 426–435. doi: 10.1289/ehp.11771

Yuen, B., Boncompagni, S., Feng, W., Yang, T., Lopez, J. R., Matthaei, K. I., et al. (2012). Mice expressing T4826I-RYR1 are viable but exhibit sex- and genotype-dependent susceptibility to malignant hyperthermia and muscle damage. *FASEB J.* 26, 1311–1322. doi: 10.1096/fj.11-197582

Conflict of Interest: The authors declare that the research was conducted in the absence of any commercial or financial relationships that could be construed as a potential conflict of interest.

Publisher's Note: All claims expressed in this article are solely those of the authors and do not necessarily represent those of their affiliated organizations, or those of the publisher, the editors and the reviewers. Any product that may be evaluated in this article, or claim that may be made by its manufacturer, is not guaranteed or endorsed by the publisher.

frontiers in Neuroscience

ORIGINAL RESEARCH
published: 06 December 2021
doi: 10.3389/fnins.2021.766826

OPEN ACCESS

Edited by:
Kazuhiko Sawada, Tsukuba International University, Japan

Reviewed by:
Sheila Fleming, Northeast Ohio Medical University, United States
Nadja R. Brun, University of Bergen, Norway

***Correspondence:**
Pamela J. Lein
pjlein@ucdavis.edu

† These authors have contributed equally to this work and share first authorship

‡Present address:
Kimberly P. Keil Stietz, Department of Comparative Biosciences, School of Veterinary Medicine, University of Wisconsin-Madison, Madison, WI, United States
Birgit Puschner, Department of Pathobiology and Diagnostic Investigation, College of Veterinary Medicine, Michigan State University, East Lansing, MI, United States

Specialty section:
This article was submitted to Neurodevelopment, a section of the journal Frontiers in Neuroscience

Received: *30 August 2021*
Accepted: *17 November 2021*
Published: *06 December 2021*

Citation:
Sethi S, Keil Stietz KP, Valenzuela AE, Klocke CR, Silverman JL, Puschner B, Pessah IN and Lein PJ (2021) Developmental Exposure to a Human-Relevant Polychlorinated Biphenyl Mixture Causes Behavioral Phenotypes That Vary by Sex and Genotype in Juvenile Mice Expressing Human Mutations That Modulate Neuronal Calcium. Front. Neurosci. 15:766826. doi: 10.3389/fnins.2021.766826

Developmental Exposure to a Human-Relevant Polychlorinated Biphenyl Mixture Causes Behavioral Phenotypes That Vary by Sex and Genotype in Juvenile Mice Expressing Human Mutations That Modulate Neuronal Calcium

Sunjay Sethi[1†], Kimberly P. Keil Stietz[1†‡], Anthony E. Valenzuela[1], Carolyn R. Klocke[1], Jill L. Silverman[2,3], Birgit Puschner[1‡], Isaac N. Pessah[1,3] and Pamela J. Lein[1,3]*

[1] Department of Molecular Biosciences, School of Veterinary Medicine, University of California, Davis, Davis, CA, United States, [2] Department of Psychiatry and Behavioral Sciences, School of Medicine, University of California, Davis, Davis, CA, United States, [3] The MIND Institute, University of California, Davis, Davis, CA, United States

Polychlorinated biphenyls (PCBs) are putative environmental risks for neurodevelopmental disorders. Here, we tested two hypotheses: (1) developmental exposure to a human-relevant PCB mixture causes behavioral phenotypes relevant to neurodevelopmental disorders; and (2) expression of human mutations that dysregulate neuronal Ca^{2+} homeostasis influence sensitivity to behavioral effects of developmental PCB exposures. To test these hypotheses, we used mice that expressed a gain-of-function mutation (T4826I) in ryanodine receptor 1 (*RYR1*), the X-linked fragile X mental retardation 1 (*FMR1*) CGG repeat expansion or both mutations (double mutant; DM). Transgenic mice and wildtype (WT) mice were exposed to the MARBLES PCB mix at 0, 0.1, 1, and 6 mg/kg/day in the maternal diet throughout gestation and lactation. The MARBLES PCB mix simulates the relative proportions of the 12 most abundant PCB congeners found in the serum of pregnant women at increased risk for having a child with a neurodevelopmental disorder. We assessed ultrasonic vocalizations at postnatal day 7 (P7), spontaneous repetitive behaviors at P25-P30, and sociability at P27-P32. Developmental PCB exposure reduced ultrasonic vocalizations in WT litters in all dose groups, but had no effect on ultrasonic vocalizations in transgenic litters. Developmental PCB exposure significantly increased self-grooming and decreased sociability in WT males in the 0.1 mg/kg dose group, but had no effect on WT females in any dose group. Genotype alone influenced ultrasonic vocalizations, self-grooming and to a lesser extent sociability. Genotype alone also influenced effects of PCBs on sociability. PCB levels in the brain tissue of pups increased in a dose-dependent manner, but within any dose group did not differ between genotypes. In summary, developmental PCB exposure phenocopied social behavior phenotypes observed in mice expressing

human mutations that modify intracellular Ca^{2+} dynamics, and expression of these mutations alleviated PCB effects on ultrasonic vocalizations and repetitive behavior, and modified the dose-response relationships and sex-dependent effects of PCB effects on social behavior. These findings suggest that: (1) developmental PCB exposure causes behavioral phenotypes that vary by sex and genotype; and (2) sex-specific responses to environmental factors may contribute to sex biases in the prevalence and/or severity of neurodevelopmental disorders.

Keywords: *FMR1* permutation, gene-environment interaction, neurodevelopmental disorders, ryanodine receptor, sex differences, social behavior, T4826I mutation, ultrasonic vocalization

INTRODUCTION

The prevalence of neurodevelopmental disorders, and in particular, autism spectrum disorder, is increasing worldwide (Landrigan et al., 2012; Baio et al., 2018), and several studies have documented that this is not due solely to increased awareness and expanded diagnostic criteria (Bishop et al., 2008; Coo et al., 2008; Hertz-Picciotto and Delwiche, 2009). The rapid rise in the prevalence of autism spectrum disorder coupled with evidence that single genetic factors alone account for only a percentage of cases (El-Fishawy and State, 2010; Herbert, 2010; Hallmayer et al., 2011; Weintraub, 2011; Landrigan et al., 2012) strongly support a role for environmental factors in determining individual risk and/or severity of these and other neurodevelopmental disorders (Sealey et al., 2016; Lyall et al., 2017). Given the social and economic burden of autism spectrum disorder and, more broadly, neurodevelopmental disorders, on individuals, families, and society (Barrett et al., 2012; Lavelle et al., 2014), there is significant interest in identifying factors that modify individual risk for neurodevelopmental disorders. In contrast to genetic risks, which are currently challenging to reverse, environmental factors are modifiable risk factors; therefore, identifying specific environmental factors that confer risk for neurodevelopmental disorders may provide rational approaches for mitigating the severity or preventing clinical outcomes.

Polychlorinated biphenyls (PCBs) are a class of persistent organic pollutants that are widely recognized as neurodevelopmental toxicants (Schantz et al., 2003; Boucher et al., 2009; Berghuis et al., 2015; Pessah et al., 2019). More recently, PCBs have been identified as environmental risk factors for neurodevelopmental disorders (reviewed in Pessah et al., 2019; Xi and Wu, 2021). Although PCB production was banned worldwide in the early 2000s, human exposures to these pollutants continue, in part because of the environmental persistence of the legacy PCBs found in the commercial PCB mixture, but also because of their release from PCB-containing hazardous waste sites, aging equipment, and building materials (Hornbuckle and Robertson, 2010; Klosterhaus et al., 2014; Grimm et al., 2015). Humans are also exposed to contemporary PCBs produced as inadvertent byproducts of contemporary pigment and dye production (Hu and Hornbuckle, 2010; Guo et al., 2014; Herkert et al., 2018). The predominant routes of human exposure to both legacy and contemporary PCBs are ingestion and inhalation (Ampleman et al., 2015), and women of childbearing age continue to have quantifiable PCB levels in their serum (Koh et al., 2015; Granillo et al., 2019).

One mechanism posited to explain how environmental factors interact with genes of susceptibility to increase risk for neurodevelopmental disorders is the convergence of environmental and genetic factors on signaling pathways that regulate phenotypes relevant to neurodevelopmental disorders (Lein, 2015). We previously demonstrated that a subset of non-dioxin-like PCB congeners that sensitize the ryanodine receptor (RyR) activate Ca^{2+}-dependent signaling pathways that normally mediate activity-induced dendritic growth and synapse formation, to increase dendritic arborization and synaptic density in primary rat hippocampal and cortical neurons (Yang et al., 2009, 2014; Wayman et al., 2012a; Lesiak et al., 2014). Interestingly, increased dendritic arborization and synapse density are common in many neurodevelopmental disorders (Engle, 2010; Penzes et al., 2011; Supekar et al., 2013), and a large number of risk genes for neurodevelopmental disorders regulate or are regulated by Ca^{2+}-dependent signaling and/or regulation of dendritogenesis and synaptogenesis (Krey and Dolmetsch, 2007; Stamou et al., 2013; Grove et al., 2019). Thus, the goal of this study was to test the hypotheses that (1) developmental exposure to a human-relevant PCB mixture causes behavioral phenotypes of relevance to neurodevelopmental disorders; and (2) expression of heritable mutations that alter Ca^{2+}-dependent signaling modulate the behavioral effects of developmental PCB exposure.

To test these hypotheses, we leveraged several mouse lines genetically engineered to express human mutations previously shown to alter the fidelity of neuronal Ca^{2+} signals (Keil et al., 2019b). The first is the T4826I-*RYR1* mouse, which expresses a human gain-of-function mutation in the gene that encodes *RYR1*, a transmembrane ion channel that is an essential regulator of intracellular Ca^{2+} stores (Barrientos et al., 2012; Yuen et al., 2012). Approximately 15% of the human population is estimated to carry one or more *RYR1* genetic variants (Kim et al., 2013). Gain-of-function mutations in the human *RYR1* gene underlie malignant hyperthermia susceptibility, which predisposes carriers to acute, potentially lethal, hyperthermia in response to heat stress, anesthetics, and other environmental stressors (Pessah et al., 2010; Dlamini et al., 2013). RyR1 activity is necessary for BDNF-induced remodeling of dendritic spines (Adasme et al., 2011), and activity-dependent dendritic growth and synaptogenesis (Wayman et al., 2012b; Lesiak et al., 2014). The second transgenic line we tested was the CGG mouse

strain, which expresses CGG repeat expansions in the 5′ non-coding region of the fragile X mental retardation gene 1 (*FMR1*) in the premutation range (55–200 CGG repeats) (Berman et al., 2014). Expansion mutations in the *FMR1* gene are the most prevalent monogenic risk factor for neurodevelopmental disorders (Krueger and Bear, 2011; Leehey and Hagerman, 2012). Estimated prevalence of the *FMR1* premutation in the human population is 1:209 in females and 1:430 in males (Tassone et al., 2012). Primary neurons derived from the CGG mouse strain were observed to have altered dendritic morphology compared to primary neurons from wildtype (WT) littermates (Chen et al., 2010), increased resting intracellular Ca^{2+} concentrations, and abnormal patterns of spontaneous Ca^{2+} oscillations (Cao et al., 2012; Robin et al., 2017), findings that have been corroborated in human iPSC-derived neurons from *FMR1* premutation patients (Liu et al., 2012). A third strain that expresses both mutations, referred to as the double mutant (DM) mouse, was developed to investigate gene dose and gene:gene interaction effects on neurodevelopmental outcomes (Keil et al., 2019b). We previously reported that juvenile male and female DM mice exhibited significantly decreased sociability relative to WT mice (Keil et al., 2019b).

In this study, we exposed these transgenic mice and WT control mice to the MARBLES PCB mix (Sethi et al., 2019) *via* the maternal diet throughout gestation and lactation. The MARBLES PCB mix was based on the PCB congener profile detected in the serum of pregnant women at increased risk of having a child with a neurodevelopmental disorder (Hertz-Picciotto et al., 2018; Sethi et al., 2019). We assessed ultrasonic vocalizations, self-grooming and social approach as a tailored behavioral battery relevant to clinical behavioral phenotypes in neurodevelopmental disorders (Silverman et al., 2010; Ey et al., 2011). The circulating thyroid hormone levels and PCB brain burden of developmentally exposed offspring were also examined.

MATERIALS AND METHODS

Materials

Organic peanut butter (Trader Joe's, Monrovia, CA) and organic peanut oil (Spectrum Organic Products, LLC, Melville, NY) were purchased from Trader Joe's (Davis, CA). The individual PCB congeners (PCB 11, 28, 52, 84, 95, 101, 118, 135, 138, 149, 153, and 180) used to make the MARBLES PCB mix were synthesized and authenticated as previously described (Li et al., 2018; Sethi et al., 2019). All PCB congeners were > 99% pure (Sethi et al., 2019). All organic solvents used for gas chromatography were of HPLC grade and obtained from Fisher Scientific (Fair Lawn, NJ, United States). PCB standards (PCB 11, 28, 52, 84, 95, 101, 118, 135, 138, 149, 153, and 180) were purchased from AccuStandard Inc. (New Haven, CT, USA). The ^{13}C12-labeled 2,2′,3′,4,5-pentachlorobiphenyl (^{13}C12-PCB-97) was purchased from Cambridge Isotope Laboratories (Tewksbury, MA, United States). Mirex was purchased from Sigma Aldrich (St. Louis, MO, United States). Solutions were diluted with isooctane to appropriate concentrations.

Animals

All procedures involving animals were conducted in accordance with the NIH Guide for the Care and Use of Laboratory Animals and were approved by the University of California, Davis, Animal Care and Use Committee. Protocols conformed to the ARRIVE guidelines (Kilkenny et al., 2010). Mice were derived from transgenic mouse colonies maintained at UC Davis (Keil et al., 2019b). These included mice homozygous for the human gain-of-function mutation in *RYR1* (T4826I-*RYR1*) referred to as T4826I mice, mice homozygous (female) or hemizygous (male) for the X-linked CGG repeat expansion in *FMR1* in the premutation range (170–200 repeats), referred to as CGG mice, and double mutant (DM) mice that expressed both mutations (Keil et al., 2019b). C57Bl/6J and SVJ129 WT mice were purchased from Jackson Labs (Sacramento, CA) and crossed to generate a 75% C57Bl/6J/25% SVJ129 hybrid WT line that was used to match the genetic background of the T4826I, CGG and DM animals as determined by single nucleotide polymorphism (SNP) analysis. All animals used in this study were genotyped as previously described (Keil et al., 2019b). To generate the juvenile mice used for behavioral phenotyping, homo/hemizygous matings were used as previously described (Keil et al., 2019b).

Two weeks prior to mating, nulliparous and previously unmated dams (>6 weeks of age) were singly housed and PCB dosing was initiated. Dams were placed with a genotype-matched male overnight for mating. Males and females were separated the next day and females were checked for the presence of a copulatory plug, which was considered gestational day 0. After mating, dams were housed singly prior to parturition and with their pups after parturition. At postnatal day 2 (P2), pups were culled or cross-fostered within genotype- and dose-matched litters to ensure all litters consisted of 4–8 pups. After weaning at P21, pups were group housed with same-sex littermates prior to behavioral testing, which has been reported to not alter social approach behavior (Yang et al., 2015). All mice were group-housed in clear plastic cages containing corncob bedding and maintained on a 12 h light and dark cycle at 22 ± 2°C and 40–50% humidity. Food (Diet 5058, LabDiet, Saint Louis, MO) and water were available *ad libitum*.

Developmental Polychlorinated Biphenyl Exposures

Humans are exposed to both higher- and lower-chlorinated PCBs *via* both ingestion and inhalation (Ampleman et al., 2015). Therefore, as the MARBLES mix included both higher- and lower-chlorinated congeners, we exposed dams to PCBs *via* the diet beginning 2 weeks prior to mating and continuing throughout gestation and lactation until pups were weaned at P21, at which time PCB exposure of the pups ceased. This timeframe corresponds to human brain development throughout gestation, e.g., rodent brain development during the first 3 weeks after birth corresponds to human brain development during the third trimester (Rice and Barone, 2000; Semple et al., 2013). The MARBLES mix was dissolved in peanut oil, which was then homogeneously mixed into peanut butter using a Bullet blender as previously described (Rude et al., 2019). Vehicle control

consisted of peanut oil mixed into peanut butter. Two weeks prior to meeting, dams were randomly assigned to a dose group and dosing was initiated. Dosing continued daily throughout gestation and lactation up to P21 *via* ingestion of peanut butter containing peanut oil or the MARBLES PCB mix at doses of 0.1, 1, or 6 mg/kg/day based on daily body weight. Each dam was weighed and the amount of PCB mixture was adjusted for body weight to ensure the appropriate dose was consumed, which typically occurred within 15–20 min.

Pup Ultrasonic Vocalizations

Ultrasonic vocalizations were recorded using Avisoft UltraSoundGate microphone and Avisoft Recorder USGH software (version 4.2, Avisoft Bioacoustics, Glienicke, Germany) and spectrograms were analyzed using Avisoft SASLab Pro software (version 5.2, Avisoft Bioacoustics) as previously described (Brielmaier et al., 2012; Berg et al., 2018). Since ultrasonic vocalizations can vary within a litter (Rieger and Dougherty, 2016), all pups in the litter were analyzed using litters of 6–8 animals. Briefly, pups at P7 were removed from their home cage, placed in a separate container of corn cob bedding within a sound attenuating chamber equipped with an Avisoft UltraSoundGate microphone. Ultrasonic vocalizations were recorded for a total of 3 min. After each recording period, body mass and temperature were recorded, after which pups were returned to their home cage. The temperature of the room was maintained at 22 ± 2°C. Ultrasonic calls were manually quantified by an experienced individual without knowledge of the experimental group. The total number of calls per pups over the 3-min recording period was averaged across all pups within the litter such that each litter was assigned a single total number of ultrasonic vocalizations that was used in statistical analyses.

Empty Cage Observations

Empty cage observations were conducted from P25-P30 as previously described (Ellegood et al., 2021; Haigh et al., 2021). Home cages were moved into the behavioral testing room (lux level 110) and allowed at least 1 h to acclimate prior to testing. One mouse was randomly chosen from each cage and placed into a separate empty plastic cage with a plastic lid, no bedding and without a top wire rack. The assay lasted 20 min, with the first 10 min considered the habituation phase, which was not scored. The last 10 min of the recording were scored by an experienced individual without knowledge of experimental group. The only behavior observed was self-grooming. The recorder sat approximately 2 m away from the testing cage and scored the cumulative amount of time spent grooming all body regions with a stopwatch. The testing cage was thoroughly cleaned with 70% ethanol to remove any scent cues and was allowed sufficient time to dry between each mouse. Once mice underwent the self-grooming test, they remained individually housed and were used 2 day later for social approach behavior.

Social Approach

Sociability was measured at P27-P32 using a three-chambered social box constructed from white plastic with removable doors as described previously (Silverman et al., 2010; Keil et al., 2019a). Mice were moved into the behavioral testing room (lux level 110) in their home cage and allowed at least 1 h acclimation prior to testing. The sociability assay consisted of three 10-min periods for a total of 30 min. First, animals were placed in the center of the three-chambered arena for a 10-min acclimation period. Second, in the habituation phase, the doors were removed and mice were allowed free exploration of the entire arena for 10 min. If an animal failed to explore during this time, they were removed from the study. Finally, during the last 10-min session, animals were allowed to interact with either an empty, upside-down wire pencil cup (object) or an identical cup containing a novel age- and sex-matched WT mouse. The two cups were placed on opposite sides of the arena. Placement of the object and mouse was counterbalanced between the left and right sides of the area to eliminate side bias. Both the area and the cups were cleaned with 70% ethanol and allowed to dry completely between each animal to eliminate scent cues. Animals used as novel mice were habituated to sitting under the wire cup for 10 min to avoid erratic behavior during the testing phase of the assay. Behavior was recorded and analyzed using Noldus EthoVision XT (version 11.0) automated tracking and analysis software (Noldus Information Technology Inc., Leesburg, VA).

Brain Polychlorinated Biphenyl Measurement

Following the conclusion of behavioral testing, animals that underwent behavioral testing and untested littermates were euthanized *via* CO_2 inhalation. Brains were rapidly dissected from the skull and sagittally bisected. One hemisphere was collected for PCB analyses and quickly flash-frozen in pre-washed glass vials and stored at −80°C until analysis. A 50-mg portion of the frozen brain tissue was placed in a microtube and homogenized in 800 μL acetonitrile using a Geno/Grinder bead homogenizer (SPEX SamplePrep LLC, Metuchen, NJ, United States). After homogenization, the tubes were vortexed, sonicated, and mechanically shaken to facilitate extraction of the PCBs. Samples were then centrifuged and the supernatant collected. The remaining pellet was resuspended and extracted twice more using a 50:50 solution of acetonitrile and isopropanol; 600 μL of the solution was used for the second extraction and 400 μL for the third. During each subsequent extraction, the tubes were vortexed, sonicated, shaken, centrifuged, and the supernatant collected. The three supernatants were filtered through a Phree Phospholipid Removal Plate (Phenomenex Inc., Torrance, CA, United States) to remove proteins and phospholipids, and then combined. The combined supernatant was evaporated under nitrogen, reconstituted in 50 μL isooctane, and then centrifuged to remove any residue. The resulting supernatant was loaded into an auto-sampler vial for GC/EI-MS/MS analysis.

An eight-point calibration curve at PCB concentrations of 2.5, 5, 10, 20, 30, 40, 60, and 80 ng/g was prepared by adding PCB analytical standards (AccuStandard Inc.) to 50 mg of untreated mouse brain homogenates derived from mice that had not undergone any experimental manipulations. Quality control (QC) samples at PCB concentrations of 12.5, 25 and 50 ng/g were

prepared in the same manner. Calibrators and QCs, as well as matrix blanks and reagent blanks, were processed following the same extraction method as samples. All samples, calibrators, QCs and blanks were internal standard-corrected with a ^{13}C-labeled PCB 97 internal standard (Cambridge Isotope Laboratories Inc.) at a concentration of 100 ng/g.

Extracted samples were then run as previously described (Lin et al., 2013; Sethi et al., 2017) using a Bruker Scion triple quadrupole mass spectrometer equipped with a Scion 456-GC and CP-8400 auto-sampler and series split/splitless injector (Bruker Scientific LLC, Billerica, MA, United States). The GC-MS/MS data were processed using Bruker Mass Spectrometry Working Station version 8.2 (Bruker). All analytes were quantified using the eight-point calibration curve. The peak areas were used for quantification following an internal algorithm. The limit of detection (LOD) and limit of quantification (LOQ) were defined based on signal-to-noise (S/N) ratio exceeding 3 and 10, respectively. Values found below the LOD were reported as "non-detected" (ND).

Thyroid Hormone Measurement

Following euthanasia, blood was collected *via* cardiac puncture. Blood was allowed to clot and then centrifuged at 5,200 × *g* for 10 min. The serum was collected and immediately frozen at −80°C until analysis. Serum was thawed for analysis, and 3,3′,5-triidothyronine (T3) and thyroxine (T4) were measured by ELISA (Calbiotech, El Cajon, CA) according to the manufacturer's protocol. Samples were run in technical duplicates with the average of the duplicates used for statistical analysis.

Statistical Analyses

Statistical analyses were performed using GraphPad Prism software (version 9.0). A one-way analysis of variance (ANOVA) or Kruskal Wallis test with *post hoc* Holm-Sidak's multiple comparisons test or Dunn's test, respectively, was used to assess PCB effects within each genotype, or genotype effects within vehicle groups of each sex for ultrasonic vocalizations, grooming behavior, thyroid hormone, and PCB brain burden data compared to sex-matched controls. Social approach data were assessed using an unpaired *t*-test for parametric data, unpaired *t*-test with Welch's correction for data with unequal variance, and a Mann-Whitney *U*-test for non-parametric data. Thyroid hormone and PCB tissue concentration data were analyzed using a one-way ANOVA, one-way ANOVA with Welch's correction or Kruskal Wallis test with Holm-Sidak's multiple comparisons test, Dunnett's T3 multiple comparisons test or Dunn's test, respectively, as indicated in the figure legends.

RESULTS

This study is part of an overall study designed to assess the effects of developmental exposure to the MARLES PCB mixture on multiple endpoints, including the gut microbiome and intestinal physiology (Rude et al., 2019), cytokine levels in the serum and hippocampus (Matelski et al., 2020), and dendritic arborization of hippocampal and cortical neurons (Keil Stietz et al., 2021). As reported previously, developmental PCB exposure had no effect on pregnancy rates across genotypes, which averaged 88%, or the length of time from mating to parturition (Matelski et al., 2020). While dam weight at weaning was not altered by PCB exposure, there was a significant main effect of genotype, with DM dams weighing significantly more than WT dams, T4826I dams weighing significantly more than CGG dams, and CGG dams weighing significantly less than DM dams (Matelski et al., 2020). There were no effects of developmental PCB exposure or genotype on litter size or sex ratio within the litter (**Supplementary Figure 1**).

Developmental Polychlorinated Biphenyl Exposure and Genotype Effects on Ultrasonic Vocalizations

Ultrasonic vocalizations are emitted by mouse pups following separation from the dam and littermates during the first 2 weeks of life, with call number beginning to rise around P2 through P5 and then gradually decreasing at P12. Thus, ultrasonic vocalizations can be used as a milestone to evaluate early postnatal development (Hahn et al., 1998; Rieger and Dougherty, 2016) and are used as a measure of social communication in rodent models of neurodevelopmental disorders (Scattoni et al., 2009; Ey et al., 2011). Therefore, we tested the effect on the number of ultrasonic calls at P7 of developmental exposure to the MARBLES PCB mix, expression of genetic mutations that alter the fidelity of calcium signaling, singly and combined environmental and genetic factors. Developmental exposure to the MARBLES PCB mix at 0.1, 1, or 6 mg/kg in the maternal diet caused a significant decrease in the number of ultrasonic calls made by WT mice, but had no effect on the number of calls made in any of the mice expressing knock-in mutations (**Figure 1A**). However, genotype alone had an effect. Within each genotype, the vehicle-control group emitted significantly fewer ultrasonic vocalizations than the WT vehicle control pups (**Figure 1A**). There were no PCB- or genotype-induced differences in body temperature at P7 (**Figure 1B**). Developmental PCB exposure also had no effect on body mass. In contrast, T4826I and CGG vehicle control mice had significantly lower body mass at P7 when compared to WT vehicle control pups (**Figure 1C**).

Developmental Polychlorinated Biphenyl Exposure or the T4826I Mutation Increased Repetitive Behavior

Self-grooming is typical behavior for mice that can be leveraged as a behavioral assay for measuring abnormal repetitive or stereotypic behavior. If mice groom for a significantly longer duration than what is considered typical, it is suggestive of repetitive behavior and this has been characterized in multiple mouse models of neurodevelopmental disorders (Ey et al., 2011; Ellegood et al., 2021; Haigh et al., 2021). Developmental exposure to the lowest dose of the MARBLES mix (0.1 mg/kg/d) caused a significant increase in time spent grooming in WT male mice (**Figure 2A**). In contrast, developmental exposure to the MARBLES PCB mix had no effect on WT females. Exposure

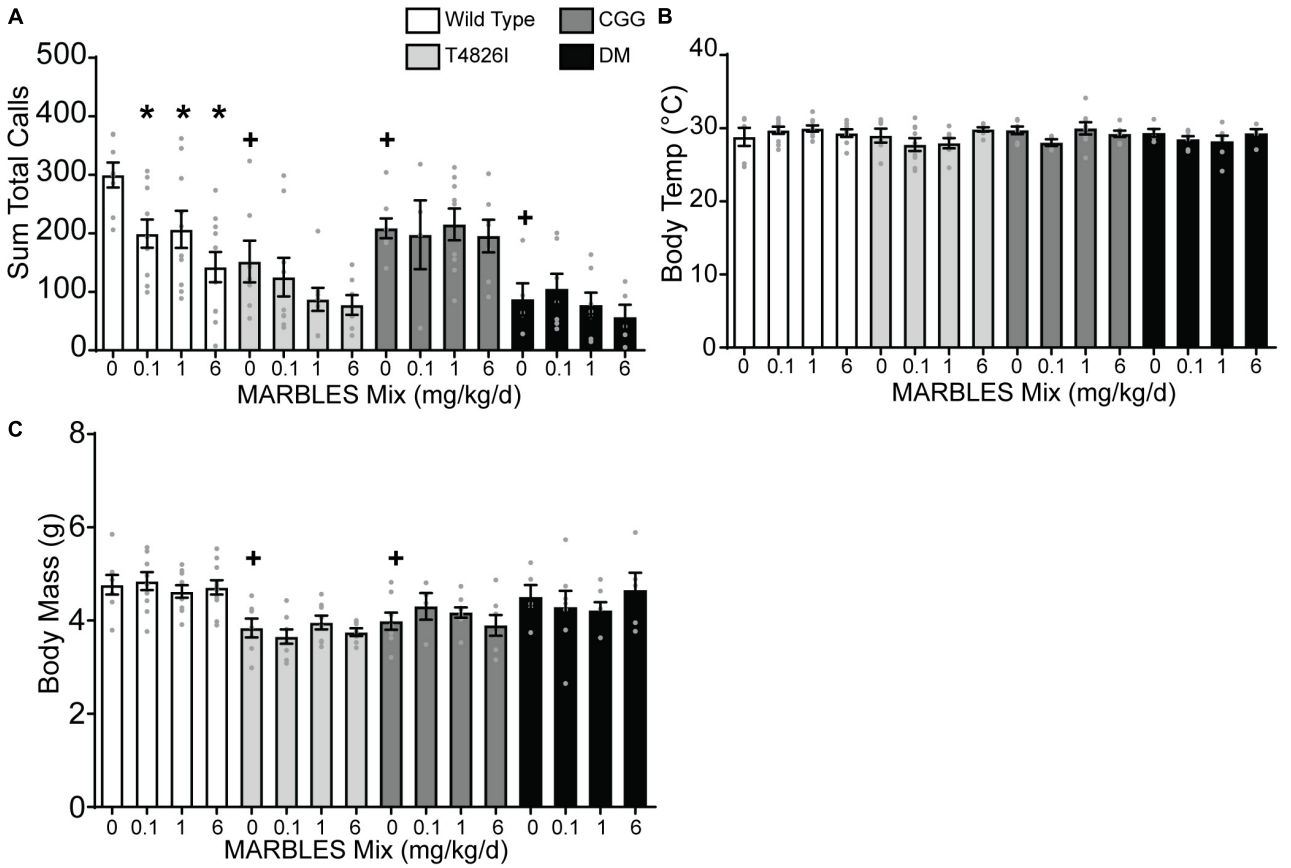

FIGURE 1 | Developmental PCB exposure or expression of mutations in calcium signaling decreased the number of ultrasonic vocalizations (USVs) emitted from pups at P7. **(A)** The sum total calls made during the 3-min testing period averaged per litter. **(B)** Body temperature during the testing period averaged per litter. **(C)** Body mass during the testing period averaged per litter. Only litters of 6–8 pups were used for analysis with n = 4–11 litters per group. Data are presented as mean ± SEM. *Indicates significantly different from vehicle control within a genotype, + indicates significantly different from WT vehicle control at $p < 0.05$ as determined using a one-way ANOVA or Kruskal Wallis test with *post hoc* Holm-Sidak's multiple comparisons test or Dunn's test, respectively.

to PCBs had little to no effect on the grooming behavior in any of the transgenic mice when compared to their sex- and genotype-matched vehicle controls (**Figures 2B–D**). However, both male and female T426I and DM mice spent significantly more time grooming when compared to their WT sex-matched controls (**Figure 2E**).

Developmental Polychlorinated Biphenyl Exposure and/or Genotype Alters Social Behavior

The three-chambered social approach task with automated data collection (Silverman et al., 2010; Yang et al., 2011) was used to assess changes in sociability, as deficits in this behavior are a component of multiple neurodevelopmental disorders. Vehicle control WT males and females displayed a preference for social behavior, evidenced by subjects spending significantly more time investigating a novel mouse vs. a novel object (**Figures 3A,C**), and by spending significantly more time in the novel mouse whole chamber side (**Figures 3B,D**). Developmental PCB exposure had no effect on sociability in WT females (**Figures 3C,D**); however, WT males in the 0.1 mg/kg/d MARBLES PCB mix dose group exhibited significantly reduced sociability (**Figures 3A,B**).

Vehicle control T4826I mice showed a preference for social behavior, with developmental exposure to the MARBLES mix having no effect on the sociability of either T4826I male and female mice (**Figure 4**). Vehicle control CGG mice also displayed a preference for social behavior. The sociability of CGG males was not affected by the MARBLES mix (**Figures 5A,B**). In contrast, CGG females in the 6 mg/kg/d MARBLES PCB dose group displayed reduced sociability (**Figures 5C,D**). Both male and female vehicle control DM mice displayed reduced social behavior (**Figure 6**). Developmental exposure to the MARBLES mix altered this phenotype, with females in the 0.1 and males in the 1 mg/kg dose groups exhibiting increased sociability (**Figures 6A–D**). There was also suggestive evidence that the 1 or 6 mg/kg doses increased sociability in DM females, but this varied depending on the parameter measured, e.g., close-proximity sniffing measure (**Figure 6C**) or time spent in the chamber side (**Figure 6D**). Changes in sociability were not due to differences in exploration, as there were no differences in total side entries for any genotype (**Supplementary Figure 2**),

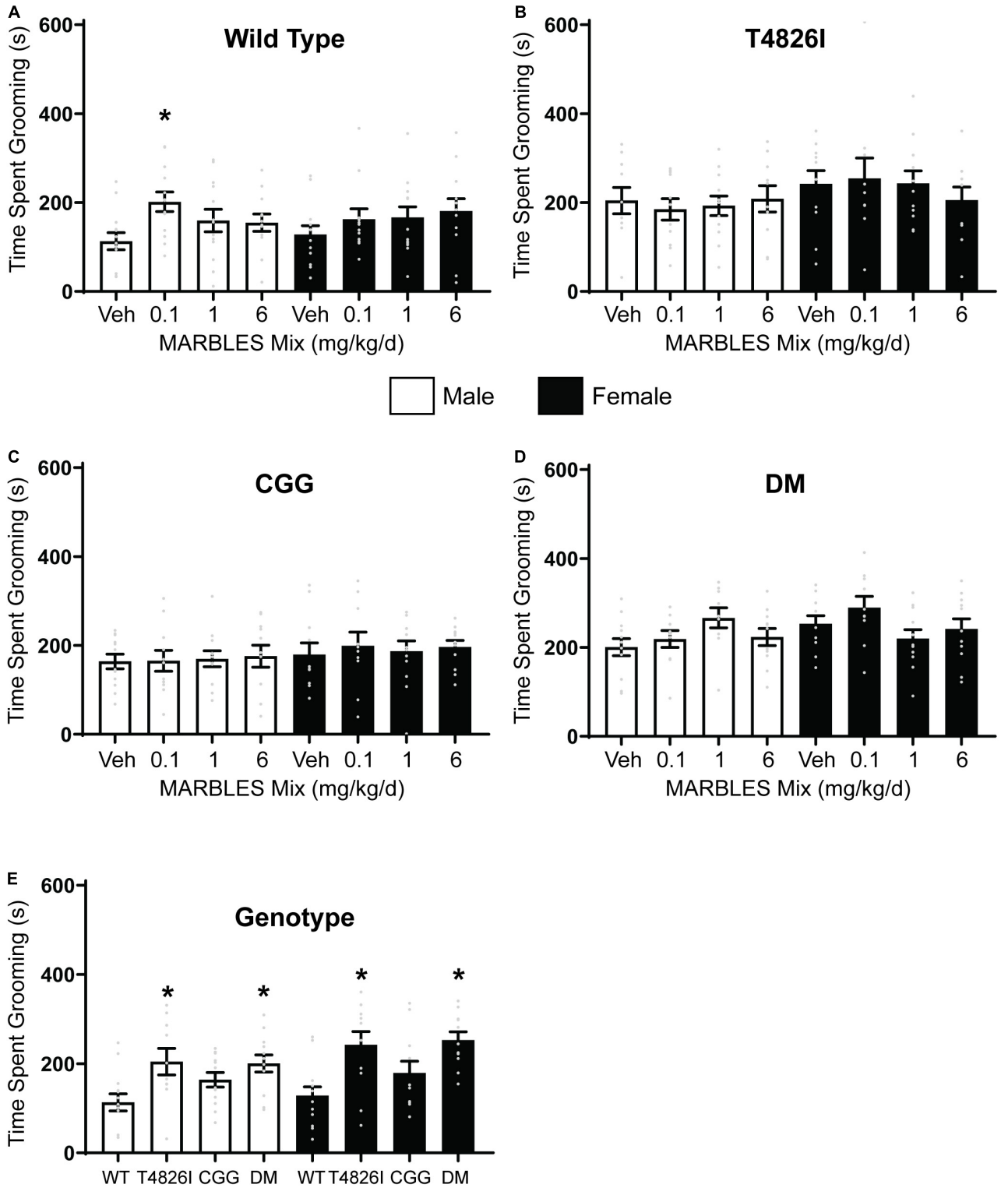

FIGURE 2 | Developmental PCB exposure or expression of expression of a gain-of-function RyR mutation (T4826I) increased repetitive behavior in P26-28 mice. Repetitive behavior was assessed in one male and one female per litter per experimental group by quantifying the time spent grooming in **(A)** WT, **(B)** T4826I, **(C)** CGG, or **(D)** DM mice during a 10-min period. **(E)** Time spent grooming in vehicle control mice of each genotype. Cumulative time spent grooming is presented as mean ± SEM (n = 10–13). * Indicates significantly different from sex-matched **(A–D)** vehicle control or **(E)** sex-matched WT at $p < 0.05$ as determined using a one-way ANOVA or Kruskal Wallis test with *post hoc* Holm-Sidak's multiple comparisons test or Dunn's test, respectively.

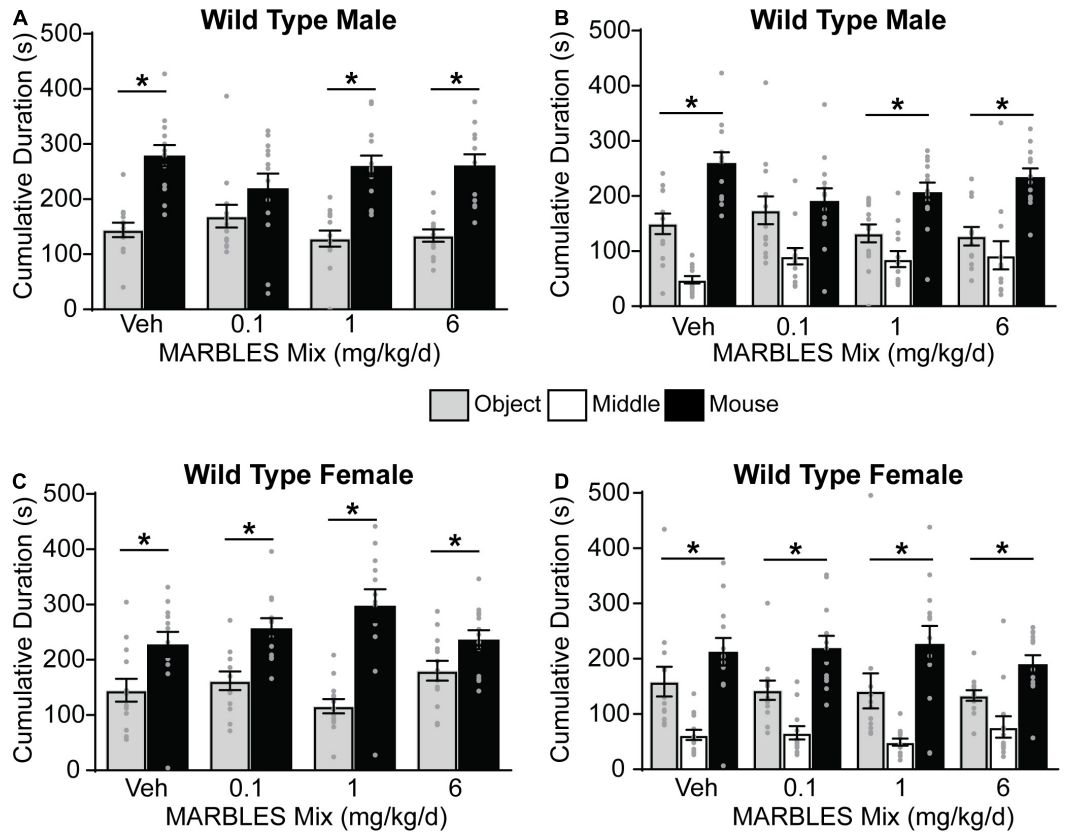

FIGURE 3 | Developmental exposure to 0.1 mg/kg of MARBLES PCB mix in the maternal diet decreased sociability in male WT mice. **(A,C)** The amount of time males **(A)** or females **(C)** spent sniffing either a novel sex- and age-matched mouse vs. a novel object. **(B,D)** The amount of time males **(B)** or females **(D)** spent on each chamber side. Data presented as mean ± SEM (n = 12–13). * Indicates significant difference between novel mouse vs. novel object at $p < 0.05$ as determined using an unpaired t-test or Mann-Whitney test.

a key motor control, which is often omitted from reports, leading to misinterpreted data (Silverman et al., 2020; Ellegood et al., 2021). Additionally, there were no differences in velocity amongst the groups (**Supplementary Figure 3**) indicating that the changes in behavior are unlikely due to changes in overall activity.

Differences in body mass or brain development could potentially contribute to differences in behavior. Changes in body mass observed at P7 are still apparent at P27-32, with both male and female T4826I and CGG mice having significantly less body mass than their sex -matched WT controls (**Supplementary Figure 4**). Similarly, DM male mice weighed less than male WT mice. T4826I and DM mice had significantly less brain mass than WT controls, but when brain mass was normalized to body weight, only T4826I males and CGG mice exhibited a significant difference in brain mass relative to body mass (**Supplementary Figure 4**). PCB exposure had no effect on body mass, brain mass or the ratio of brain to body mass in WT or DM pups (**Supplementary Figure 5**). However, PCB exposure significantly increased body mass and decreased the brain to body mass ratio in female T4826I females in the 1 and 6 mg/kg dose groups, and significant decreased the brain to body mass in CGG males in the 0.1 and 1 mg/kg dose groups (**Supplementary Figure 5**).

Developmental Polychlorinated Biphenyl Exposure Had Minimal Effect on T3 and T4 Levels

Thyroid hormone (TH) is a critical factor for normal neurodevelopment (Oppenheimer and Schwartz, 1997; Williams, 2008), and exposure to PCBs has been shown to decrease circulating T3 and/or T4 levels (Oppenheimer and Schwartz, 1997; Kato et al., 2003; Williams, 2008; Martin and Klaassen, 2010). Therefore, we assessed whether developmental exposure to the MARBLES PCB mix altered TH levels in juvenile mice. There were no significant effects of PCB exposure on T3 or T4 levels within each genotype and sex, with the exception of increased T3 levels in the 0.1 mg/kg WT males (**Figures 7A–D**). There were no significant effects of genotype on T3 or T4 levels relative to sex-matched WT vehicle controls (**Figure 7E**).

Total Polychlorinated Biphenyl Levels in Pup Brains Is Dose-Dependent and Not Affected by Genotype or Sex

Differences between groups in the total burden of PCBs in the brain could contribute to some of the group differences

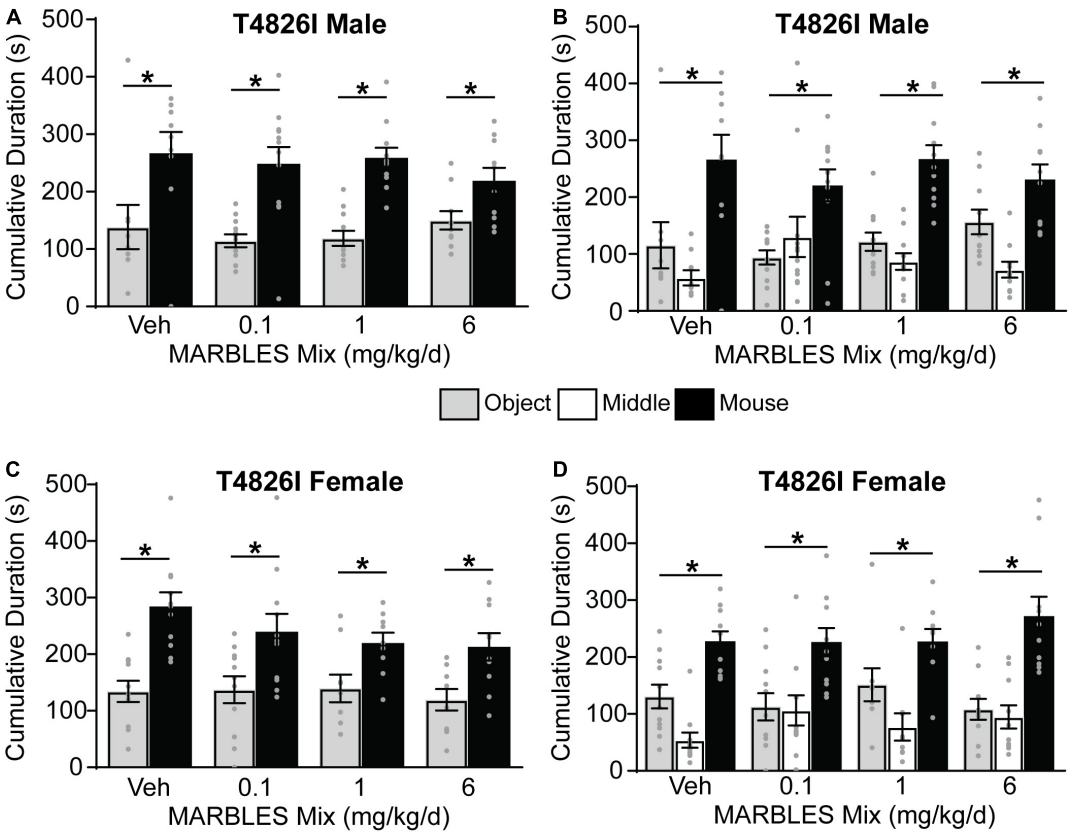

FIGURE 4 | Developmental exposure to the MARBLES PCB mix did not affect social behavior in T4826I mice. **(A,C)** The amount of time males **(A)** or females **(C)** spent sniffing either a novel sex- and age-matched mouse or a novel object. **(B,D)** The amount of time males **(B)** or females **(D)** spent on each chamber side. Data presented as mean ± SEM (n = 9–12). * Indicates significant difference between novel mouse vs. novel object at $p < 0.05$ as determined using an unpaired t-test, Mann-Whitney test or unpaired t-test with Welch's correction.

in behavior observed in this study. To address this possibility, we measured the PCB levels in P27-32 brain tissue. Only PCB congeners with a detection frequency greater than 70% in the 1 and 6 mg/kg dose groups were used to create a sum PCB value that was then used to assess PCB levels across groups. There is a clear dose response in each genotype, with the PCB brain burden significantly increasing as the MARBLES PCB dose increased (**Figures 8A–D**). There was no effect of genotype on PCB brain burden in the 1 or 6 mg/kg dose groups (**Figures 8F,G**); however, there was a significant increase in brain PCB levels in the 0.1 mg/kg DM males compared to 0.1 mg/kg WT males (**Figure 8E**). Detailed information on individual PCB congener content can be found in Excel spreadsheets in **Supplementary Material**.

DISCUSSION

It is widely posited that individual risk for many neurodevelopmental disorders is determined by complex interactions between genetic and environmental risk factors (Lyall et al., 2017; Bolte et al., 2019; Cheroni et al., 2020); however, the identification of specific gene-environment interactions that influence individual risk for neurodevelopmental disorders remains a significant data gap (Masini et al., 2020). To address this data gap, we leveraged the MARBLES PCB mix, the composition of which is based on the PCB congener profile detected in the serum of pregnant women at increased risk of having a child with a neurodevelopmental disorder (Sethi et al., 2019), and three lines of mice genetically altered to express human-relevant mutations that alter calcium signaling (Barrientos et al., 2012; Robin et al., 2017; Keil et al., 2019b) to test two hypotheses: (1) developmental exposure to the human-relevant MARBLES PCB mixture causes behavioral phenotypes relevant to neurodevelopmental disorders; and (2) expression of heritable mutations that alter Ca^{2+} signals modulate the behavioral effects of developmental PCB exposure. The data reported in this study support both hypotheses and add to the evidence implicating PCBs, and in particular RyR-active PCBs (Granillo et al., 2019), as environmental risk factors for neurodevelopmental disorders (Panesar et al., 2020).

The most direct evidence in support of the hypothesis that developmental PCB exposure results in behavioral phenotypes relevant to neurodevelopmental disorders is our observations of decreased ultrasonic vocalizations at P7, increased self-grooming at P25-P30, and lack of typical three-chambered sociability at

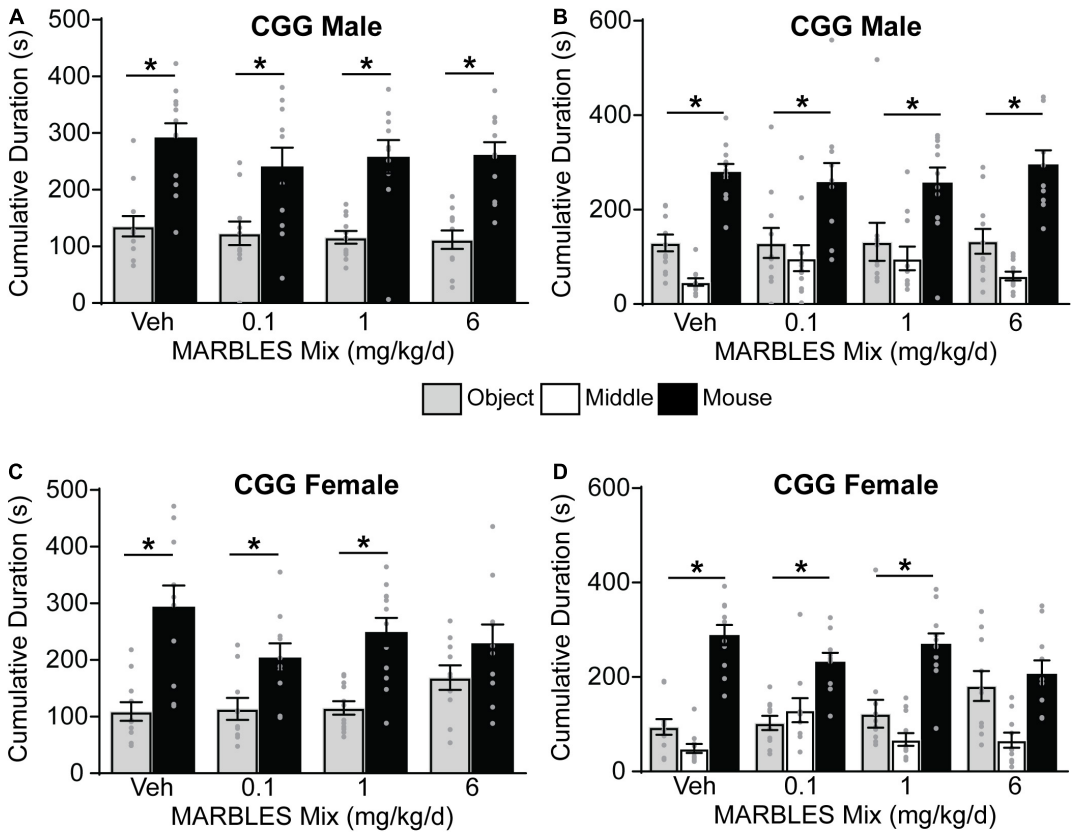

FIGURE 5 | Developmental exposure to MARBLES PCB mix at 6 mg/kg in the maternal diet decreased sociability in female CGG mice. **(A,C)** The amount of time males **(A)** or females **(C)** spent sniffing either a novel sex and age matched mouse or a novel object. **(B,D)** The amount of time males **(B)** or females **(D)** spent on each chamber side. Data presented as mean ± SEM (n = 10–12). * Indicates significant difference between novel mouse vs. novel object at $p < 0.05$ as determined using an unpaired t-test, Mann-Whitney test or unpaired t-test with Welch's correction.

P27-P32 in WT mice exposed to the MARBLES PCB mix in the maternal diet throughout gestation and lactation. While significant PCB effects on ultrasonic vocalizations were evident in WT mice in all PCB dose groups, significant PCB effects on grooming and social approach in WT mice were observed only in males in the 0.1 mg/kg PCB dose group. The mechanism(s) underlying this non-monotonic dose-response relationship are not known, but are consistent with previous reports of non-monotonic dose-related effects of developmental exposure to Aroclor 1254 (Yang et al., 2009) and PCB 95 (Wayman et al., 2012b), a RyR-active non-dioxin-like congener (Pessah et al., 2010), on dendritic arborization as well as spatial learning and memory in rats. The observation that deficits in social reciprocity and repetitive behavior were observed in PCB-exposed WT males but not WT females mimics the sex bias of autism spectrum disorder, which affects 4 times as many boys as girls, on average. This observation suggests that sex-specific responses to environmental factors may contribute to sex biases in the prevalence and/or severity of neurodevelopmental disorders. The relevance of these findings to the human condition is supported by several observations. First, these behavioral assays have face validity to core clinical signs of autism spectrum disorder; specifically, repetitive behavior and deficits in social reciprocity and communication (Silverman et al., 2010; Ey et al., 2011). Second, the PCB mixture to which mice were exposed reflects the PCB congener profile that actually exists in the gestational environment of at-risk individuals (Sethi et al., 2019). Third, the PCB brain burden in pups exposed to the MARBLES PCB mix at 0.1 mg/kg/d in the maternal diet, which ranged from 6.2 to 43.6 ng/g wet weight, is comparable to the range of PCB levels reported in human brain tissue (6–66 ng/g wet weight) (Chu et al., 2003; Hatcher-Martin et al., 2012; Klocke et al., 2020).

To the best of our knowledge, ultrasonic vocalizations in young pups have been investigated in only one other published study of PCB developmental neurotoxicity. Intraperitoneal injection of Aroclor 1221 into rat dams at 1 mg/kg on P16, P18, and P20 had no effect on affiliative ultrasonic vocalizations of offspring tested at P1-P3 (Bell et al., 2016). The discrepant finding between this study and ours likely reflects significant differences in study design (species, PCB dosing paradigm, ultrasonic vocalization testing protocol). In contrast, our observations that developmental PCB exposure increases grooming and decreases sociability in young male, but not female, WT mouse pups are largely consistent with previously published observations. For example, oral administration of PCB 126, a dioxin-like congener, to rat dams at 30 μg/kg on gestational day 15, significantly

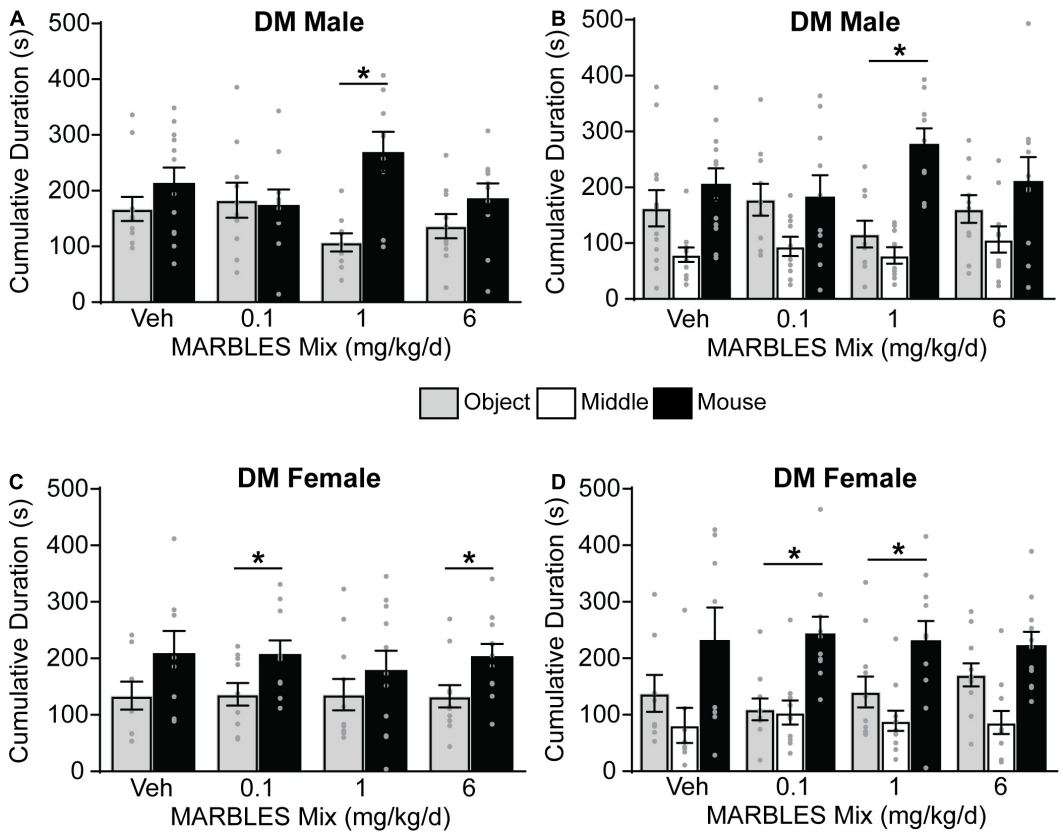

FIGURE 6 | Sociability in male and female DM mice was altered by genotype and PCB exposure. **(A,C)** The amount of time males **(A)** or females **(C)** mouse spent sniffing either a novel sex- and age-matched mouse or a novel object. **(B,D)** The amount time males **(B)** or females **(D)** spent in each chamber side. Data presented as mean ± SEM (n = 8–12). * Indicates significant difference between novel mouse vs. novel object at $p < 0.05$ as determined using an unpaired t-test, Mann-Whitney test or unpaired t-test with Welch's correction.

increased the time male offspring spent grooming (Orito et al., 2007). This same study (Orito et al., 2007), as well as another study of rats exposed developmentally to an equal mixture of PCB 47 and PCB 77, non-dioxin-like and dioxin-like congeners, respectively, at 12.5 or 25 mg/kg in maternal chow throughout gestation and lactation (Jolous-Jamshidi et al., 2010), reported decreased sociability in juvenile males. A study of the sociability of CD1 mice exposed to a mixture of six PCBs (28, 52, 101, 138, 153, and 180) in maternal chow at 10 or 1,000 ng/kg throughout gestation and lactation revealed PCB effects on not only males, evidenced as increased sociability at P50, but decreased sociability at P330, but also females, reported as increased sociability at P330. Given the significant differences in study design between this study and ours (mouse strain, PCB exposure and age at the time of testing), it is difficult to make direct comparisons; however, the collective data across all studies suggest that developmental PCB exposure alters social behavior, but the effect varies according to sex, species/strain, age of testing, and/or PCB congener/dose.

Consistent with the observation that species and/or strain influence the expression of behavioral phenotypes following developmental PCB exposures, we observed that genotype altered the behavioral effects of the MARBLES PCB mix. Specifically, in contrast to observations of WT mice, ultrasonic vocalizations were not significantly different in any PCB dose group in any of the three transgenic lines expressing heritable human mutations that modulate calcium signaling relative to genotype-matched vehicle controls. Similarly, PCB exposure had no effect on repetitive behavior in T4826I, CGG, or DM mice of either sex. However, PCB exposure decreased sociability in CGG females in the 6 mg/kg dose group and increased sociability in DM males in the 1 mg/kg group and DM females in the 0.1, 1 and 6 mg/kg groups. The differences in behavioral responses to the MARBLES PCB mix were likely not due to genotype-specific differences in PCB levels in the brain tissue of pups. While brain levels of PCBs varied in a dose-dependent manner, within any dose group, levels did not differ between genotypes with one exception: 0.1 mg/kg DM males had a higher PCB brain burden than 0.1 mg/kg WT males. Collectively, these data suggest that expression of a heritable mutation in Ca^{2+} signaling partially mitigated the impacts of developmental exposure to the MARBLES PCB mix on social behavior and repetitive behavior; whereas expression of more than one of these mutations altered PCB effects, both in terms of sex dependency and direction of effect.

Interestingly, expression of one or more heritable mutations that alter the fidelity of neuronal Ca^{2+} signals altered behavioral outcomes independent of developmental PCB exposures, and

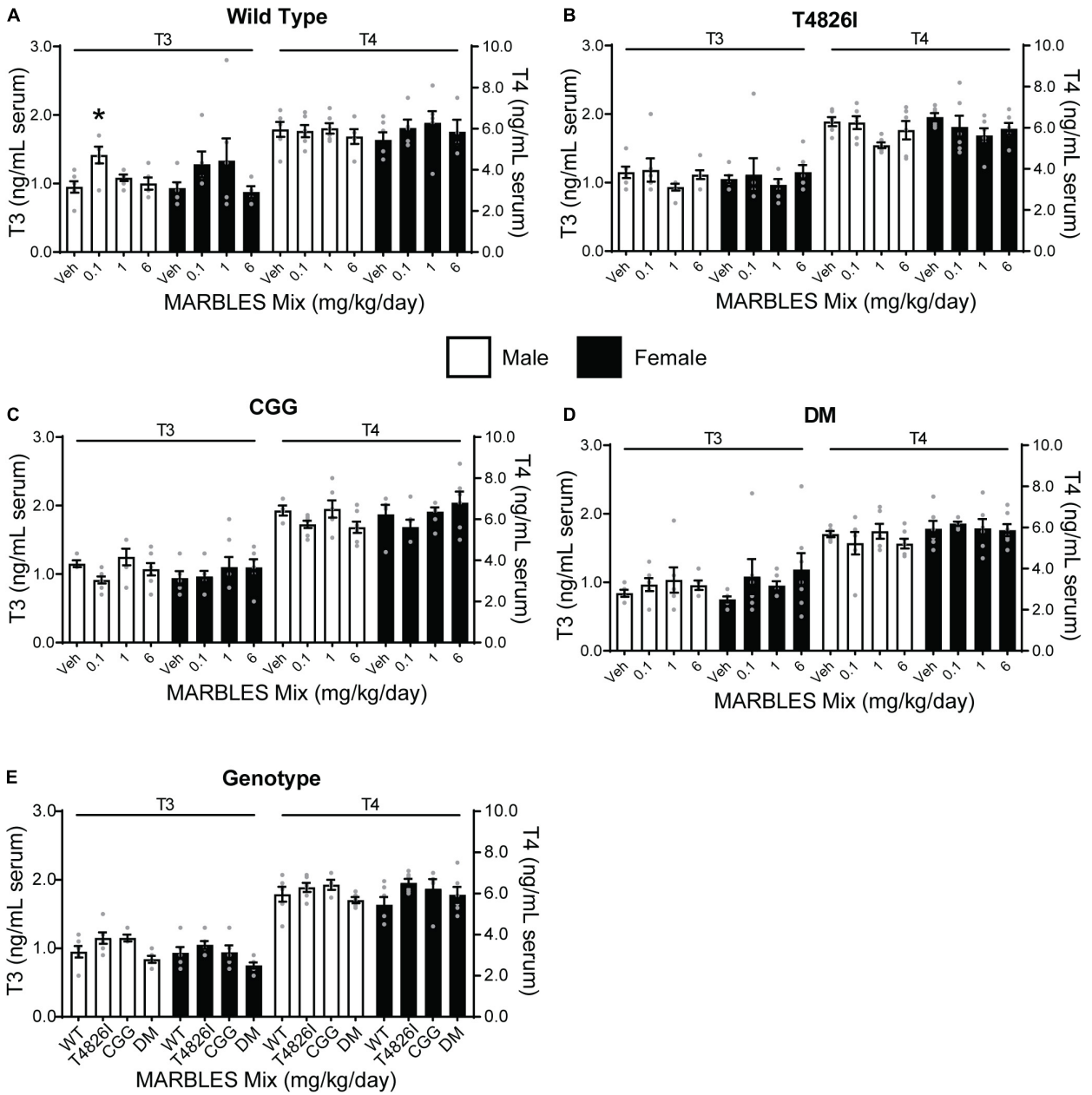

FIGURE 7 | Developmental PCB exposure and genotype had had minimal to no effect on thyroid hormone levels. **(A–D)** The serum levels of triiodothyronine (T3) and thyroxine (T4) in **(A)** WT, **(B)** T4826I, **(C)** CGG, and **(D)** DM mice developmentally exposed to varying doses of the MARBLES PCB mix in the maternal diet. **(E)** T3 and T4 levels in vehicle control mice of each genotype. Data presented as mean ± SEM (n = 4–7). * Indicates significant difference between sex-matched vehicle control at $p < 0.05$ as determined using a one-way ANOVA or Kruskal Wallis test with *post hoc* Holm-Sidak's multiple comparisons test or Dunn's test, respectively.

the outcome largely phenocopied PCB-induced behavioral phenotypes (**Table 1**). In all three genotypes, ultrasonic vocalizations were significantly decreased relative to WT vehicle control. In contrast, increased grooming was observed in T4826I and DM mice, but not CGG mice, suggesting that the gain-of-function *RYR1* mutation plays a predominant role in driving this behavioral phenotype. Decreased sociability was observed only in DM mice, consistent with our previous characterization of sociability in these same transgenic lines (Keil et al., 2019b), suggesting that gene dosage is an important determinant of this phenotype. The observation that increased repetitive behavior and deficits in sociability can be independently affected suggests that different molecular mechanisms contribute to each behavioral deficit. Interestingly, in contrast to PCB effects on WT mice, which were male-selective, the effect of genotype on grooming and sociability was observed in both sexes. The biological explanation for these genotype-dependent differences in sex bias remains to be determined.

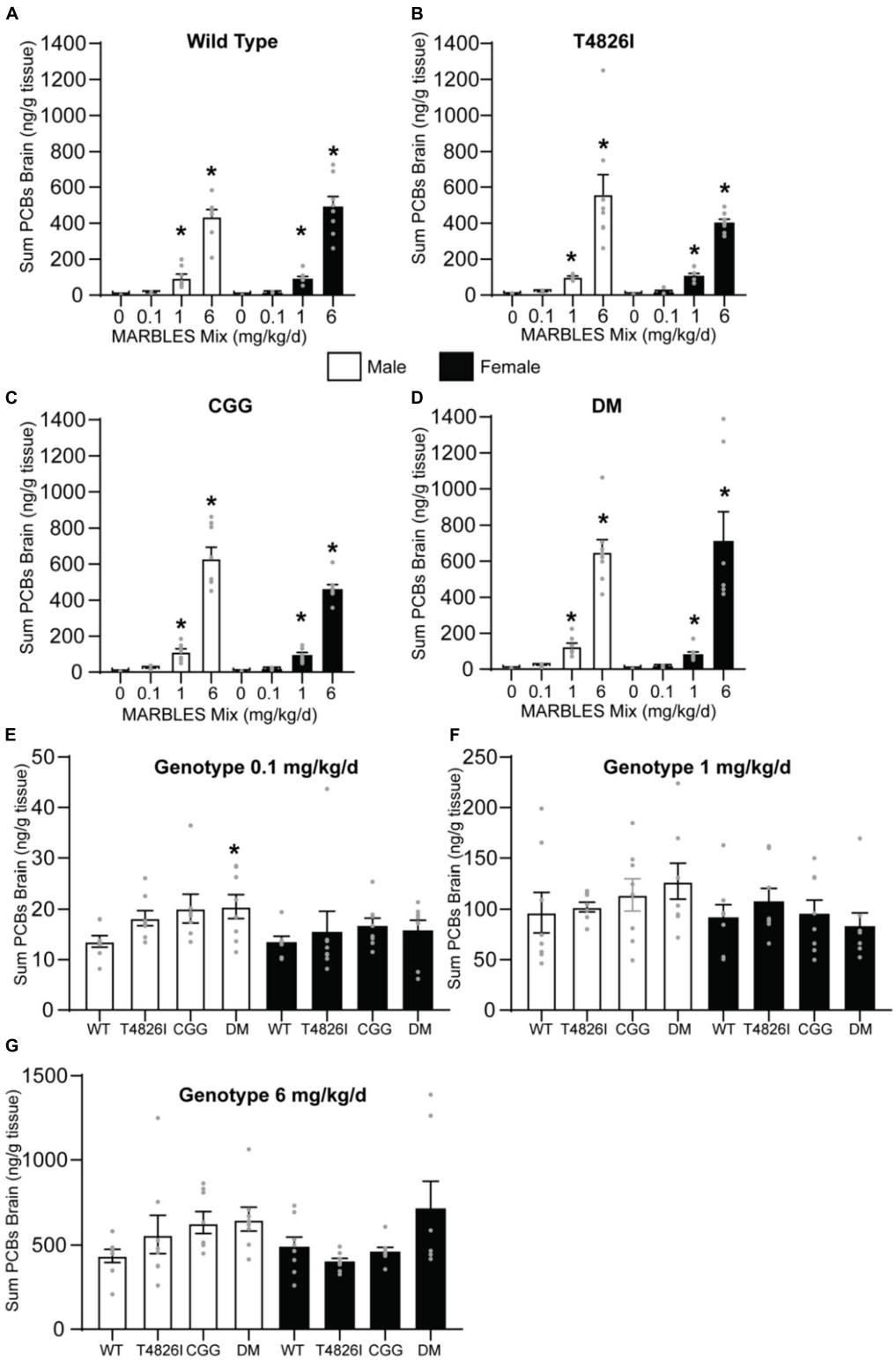

FIGURE 8 | PCB brain burden increased in a dose-dependent manner independent of genotype. **(A–D)** The sum PCB levels in brain tissue of **(A)** WT, **(B)** T4826I, **(C)** CGG, or **(D)** DM mice developmentally exposed to varying doses of the MARBLES PCB mix in the maternal diet. **(E)** The sum PCB levels in the brain tissue of each genotype at the 0.1, **(E)** 1, **(F),** or 6 **(G)** mg/kg/d exposure group. Data presented as mean ± SEM (n = 7–9). The sum of PCBs that were above 70% detection frequency in the 1 and 6 mg/kg/d groups were used and include PCB 28, 52, 101, 118, 138, 153, and 180. * Indicates significant difference from sex-matched vehicle control at *$p < 0.05$ as determined using a one-way ANOVA or Kruskal Wallis test with *post hoc* Holm-Sidak's multiple comparisons test or Dunn's test, respectively. Detailed information on individual PCB congener content can be found in Excel spreadsheets in **Supplementary Data Sheet 2**.

TABLE 1 | Summary of PCB and genotype effects on behavior compared to wildtype (WT) vehicle control mice.

	WT males (0.1 mg/kg/d)	T4826I* (vehicle)	CGG* (vehicle)	Double mutant* (vehicle)
USVs (communication)	Decrease	Decrease	Decrease	Decrease
Grooming (repetitive behavior)	Increase	Increase	No change	Increase
Social behavior	Decrease	Decrease	No change	Decrease

**Both sexes of the transgenic mice showed the same phenotype listed in this table.*

Our data suggest that environmentally relevant PCB exposures during brain development modulate molecular mechanisms targeted by the gain-of-function *RYR1* and CGG mutations to alter behavior. While diverse mechanisms have been proposed to mediate PCB developmental neurotoxicity, two of the more prevalent hypotheses include disruption of thyroid hormone homeostasis and altered fidelity of Ca^{2+} signaling (reviewed in Pessah et al., 2019; Klocke and Lein, 2020). Several lines of evidence from the current study provide weak support for the former, but strong support for the latter. First, we previously demonstrated that the PCB congeners that comprise the MARBLES PCB mixture neither agonize nor antagonize the thyroid hormone receptor singly or in combination; in contrast, the MARBLES PCB mixture has potent RyR activity as determined by equilibrium binding of [^{3}H]ryanodine to RyR1-enriched microsomes (Sethi et al., 2019). Second, developmental exposure to the MARBLES mixture in the maternal diet throughout gestation and lactation did not significantly alter serum T3 or T4 levels in WT or transgenic mice, with the exception of increased T3 in the 0.1 mg/kg WT males. Since this later group exhibited PCB effects on ultrasonic vocalizations, grooming and social behavior, we cannot rule out the possibility that increased T3 contributed to these behavioral phenotypes. However, while a few studies have shown changes in behavior linked to decreased T3 levels (Roman et al., 2013; Fetene et al., 2017), there are no data of which we are aware that demonstrate a link between excessive serum T3 levels and behavioral outcomes relevant to neurodevelopmental disorders. Moreover, there were no differences in T3 levels between vehicle control WT and DM mice despite striking genotype-specific differences in grooming behavior and sociability. Third, there was significant overlap in the behavioral phenotypes exhibited by WT mice developmentally exposed to PCBs and mice that expressed heritable mutations in Ca^{2+} signaling, particularly expression of the T4826I mutation in *RYR1*, singly or in combination with the CGG mutation. These observations suggest shared molecular mechanisms of Ca^{2+} dysregulation. In support of this hypothesis, multiple groups have shown that genetic alterations that dysregulate Ca^{2+} signaling caused deficits in social behaviors (Matsuo et al., 2009; Bader et al., 2011; Nakao et al., 2015; Kabir et al., 2017). In one of these studies, mice engineered to express mutant gain-of-function calcium channels also exhibited increased repetitive behaviors (Bader et al., 2011). In a separate study, reduced calcium signaling in astrocytes was also associated with increased grooming behavior in mice (Yu et al., 2018). An outstanding question is why expression of heritable mutations that increase Ca^{2+} signaling did not increase sensitivity to the developmental neurotoxicity of PCB congeners that similarly increase Ca^{2+} signaling, evident as a leftward shift in the dose-response curve. One potential explanation is that the genetically determined phenotypes are an all-or-none phenomenon, although the observation that DM mice, but not T4861I or CGG mice, exhibit decreased sociability argues against this possibility.

CONCLUSION

In conclusion, our studies demonstrated that developmental exposure to a human-relevant PCB mixture phenocopied social behavior phenotypes observed in mice expressing heritable human mutations that increase Ca^{2+} signaling, and that expression of these mutations altered the effects of developmental PCB exposure on sociability. One key difference between the PCB exposure vs. genotype effects was the sex-specificity of the outcome: PCB effects on repetitive behavior and sociability were male-specific, whereas genotype effects on these behaviors was sex-independent. These findings suggest that: (1) developmental PCB exposures can cause behavioral phenotypes of relevance to neurodevelopmental disorders, but this effect varies according to sex and genotype; and (2) sex-specific responses to environmental factors may contribute to sex biases in the prevalence and/or severity of neurodevelopmental disorders.

DATA AVAILABILITY STATEMENT

The original contributions presented in the study are included in the article/**Supplementary Material**, further inquiries can be directed to the corresponding author/s.

ETHICS STATEMENT

The animal study was reviewed and approved by University of California, Davis Institutional Animal Care and Use Committee.

AUTHOR CONTRIBUTIONS

IP and PL conceptualized the project and obtained funding to support the work. PL supervised all aspects of this study. JS oversaw the behavioral studies. BP oversaw the PCB analyses. SS, KK, JS, and PL designed the experiments. SS and KK maintained the mouse colony, dosed the animals, conducted the behavioral studies, collected tissues for PCB quantitation, and analyzed the behavioral data. SS, AV, and BP optimized the protocol for PCB quantitation. SS and AV conducted the PCB analyses. AV analyzed the PCB analyses data. CK facilitated the analysis of tissue samples for thyroid hormone levels. SS, KK, and CK composed the figures. SS wrote the initial manuscript draft. KK and PL made significant edits to the early versions of the manuscript. All authors reviewed and made final edits to the manuscript prior to submission.

FUNDING

This study was supported by the National Institute of Environmental Health (Grant Nos. R01 ES014901 to PL and IP, T32 ES007059 to SS, and R00 ES029537 to KK) and by the Eunice Kennedy Shriver National Institute of Child Health and Human Development (Grant No. F32 HD088016 to KK). This project used core facilities supported by the MIND Institute Intellectual and Developmental Disabilities Research Center (Grant No. P50 HD103526) and the UC Davis Environmental Health Sciences Center (Grant No. P30 ES023513). Synthesis of PCB congeners was supported by the Superfund Research Center at The University of Iowa (Grant No. P42 ES013661). The contents of this study do not necessarily represent the official views of the NIEHS or NICHD. The NIEHS and NICHD do not endorse the purchase of any commercial products or services mentioned in the publication.

ACKNOWLEDGMENTS

We would like to acknowledge Drs. Xueshu Li and Hans-Jaochim Lehmler (The University of Iowa) for providing the PCBs congeners used to make the MARBLES PCB mix used in this study. We also acknowledge Dr. Ingrid Gennity (University of California, Davis) for her assistance in developing the method used to determine the PCB levels in the brain tissue, and Dr. James Graham (University of California, Davis Mouse Phenotyping Core) for conducting the TH analyses.

SUPPLEMENTARY MATERIAL

The Supplementary Material for this article can be found online at: https://www.frontiersin.org/articles/10.3389/fnins.2021.766826/full#supplementary-material

REFERENCES

Adasme, T., Haeger, P., Paula-Lima, A. C., Espinoza, I., Casas-Alarcon, M. M., Carrasco, M. A., et al. (2011). Involvement of ryanodine receptors in neurotrophin-induced hippocampal synaptic plasticity and spatial memory formation. *Proc. Natl. Acad. Sci. U. S. A.* 108, 3029–3034. doi: 10.1073/pnas.1013580108

Ampleman, M. D., Martinez, A., DeWall, J., Rawn, D. F., Hornbuckle, K. C., and Thorne, P. S. (2015). Inhalation and dietary exposure to PCBs in urban and rural cohorts *via* congener-specific measurements. *Environ. Sci. Technol.* 49, 1156–1164. doi: 10.1021/es5048039

Bader, P. L., Faizi, M., Kim, L. H., Owen, S. F., Tadross, M. R., Alfa, R. W., et al. (2011). Mouse model of Timothy syndrome recapitulates triad of autistic traits. *Proc. Natl. Acad. Sci. U. S. A.* 108, 15432–15437. doi: 10.1073/pnas.1112667108

Baio, J., Wiggins, L., Christensen, D. L., Maenner, M. J., Daniels, J., Warren, Z., et al. (2018). Prevalence of Autism Spectrum Disorder Among Children Aged 8 Years - Autism and Developmental Disabilities Monitoring Network, 11 Sites, United States, 2014. *MMWR Surveill. Summ.* 67, 1–23. doi: 10.15585/mmwr.ss6706a1

Barrett, B., Byford, S., Sharac, J., Hudry, K., Leadbitter, K., Temple, K., et al. (2012). Service and wider societal costs of very young children with autism in the UK. *J. Autism Dev. Disord.* 42, 797–804. doi: 10.1007/s10803-011-1306-x

Barrientos, G. C., Feng, W., Truong, K., Matthaei, K. I., Yang, T., Allen, P. D., et al. (2012). Gene dose influences cellular and calcium channel dysregulation in heterozygous and homozygous T4826I-RYR1 malignant hyperthermia-susceptible muscle. *J. Biol. Chem.* 287, 2863–2876. doi: 10.1074/jbc.M111.307926

Bell, M. R., Thompson, L. M., Rodriguez, K., and Gore, A. C. (2016). Two-hit exposure to polychlorinated biphenyls at gestational and juvenile life stages: 1. Sexually dimorphic effects on social and anxiety-like behaviors. *Horm. Behav.* 78, 168–177. doi: 10.1016/j.yhbeh.2015.11.007

Berg, E. L., Copping, N. A., Rivera, J. K., Pride, M. C., Careaga, M., Bauman, M. D., et al. (2018). Developmental social communication deficits in the Shank3 rat model of phelan-mcdermid syndrome and autism spectrum disorder. *Autism Res.* 11, 587–601. doi: 10.1002/aur.1925

Berghuis, S. A., Bos, A. F., Sauer, P. J., and Roze, E. (2015). Developmental neurotoxicity of persistent organic pollutants: an update on childhood outcome. *Arch. Toxicol.* 89, 687–709. doi: 10.1007/s00204-015-1463-3

Berman, R. F., Buijsen, R. A., Usdin, K., Pintado, E., Kooy, F., Pretto, D., et al. (2014). Mouse models of the fragile X premutation and fragile X-associated tremor/ataxia syndrome. *J. Neurodev. Disord.* 6:25. doi: 10.1186/1866-1955-6-25

Bishop, D. V., Whitehouse, A. J., Watt, H. J., and Line, E. A. (2008). Autism and diagnostic substitution: evidence from a study of adults with a history of developmental language disorder. *Dev. Med. Child Neurol.* 50, 341–345. doi: 10.1111/j.1469-8749.2008.02057.x

Bolte, S., Girdler, S., and Marschik, P. B. (2019). The contribution of environmental exposure to the etiology of autism spectrum disorder. *Cell. Mol. Life Sci.* 76, 1275–1297. doi: 10.1007/s00018-018-2988-4

Boucher, O., Muckle, G., and Bastien, C. H. (2009). Prenatal exposure to polychlorinated biphenyls: a neuropsychologic analysis. *Environ. Health Perspect.* 117, 7–16. doi: 10.1289/ehp.11294

Brielmaier, J., Matteson, P. G., Silverman, J. L., Senerth, J. M., Kelly, S., Genestine, M., et al. (2012). Autism-relevant social abnormalities and cognitive deficits in engrailed-2 knockout mice. *PLoS One* 7:e40914. doi: 10.1371/journal.pone.0040914

Cao, Z., Hulsizer, S., Tassone, F., Tang, H. T., Hagerman, R. J., Rogawski, M. A., et al. (2012). Clustered burst firing in FMR1 premutation hippocampal neurons: amelioration with allopregnanolone. *Hum. Mol. Genet.* 21, 2923–2935. doi: 10.1093/hmg/dds118

Chen, Y., Tassone, F., Berman, R. F., Hagerman, P. J., Hagerman, R. J., Willemsen, R., et al. (2010). Murine hippocampal neurons expressing Fmr1 gene premutations show early developmental deficits and late degeneration. *Hum. Mol. Genet.* 19, 196–208. doi: 10.1093/hmg/ddp479

Cheroni, C., Caporale, N., and Testa, G. (2020). Autism spectrum disorder at the crossroad between genes and environment: contributions, convergences, and interactions in ASD developmental pathophysiology. *Mol. Autism* 11:69. doi: 10.1186/s13229-020-00370-1

Chu, S., Covaci, A., and Schepens, P. (2003). Levels and chiral signatures of persistent organochlorine pollutants in human tissues from Belgium. *Environ. Res.* 93, 167–176. doi: 10.1016/s0013-9351(03)00016-1

Coo, H., Ouellette-Kuntz, H., Lloyd, J. E., Kasmara, L., Holden, J. J., and Lewis, M. E. (2008). Trends in autism prevalence: diagnostic substitution revisited. *J. Autism Dev. Disord.* 38, 1036–1046. doi: 10.1007/s10803-007-0478-x

Dlamini, N., Voermans, N. C., Lillis, S., Stewart, K., Kamsteeg, E. J., Drost, G., et al. (2013). Mutations in RYR1 are a common cause of exertional myalgia and rhabdomyolysis. *Neuromuscul. Disord.* 23, 540–548. doi: 10.1016/j.nmd.2013.03.008

El-Fishawy, P., and State, M. W. (2010). The genetics of autism: key issues, recent findings, and clinical implications. *Psychiatr. Clin. North Am.* 33, 83–105. doi: 10.1016/j.psc.2009.12.002

Ellegood, J., Petkova, S. P., Kinman, A., Qiu, L. R., Adhikari, A., Wade, A. A., et al. (2021). Neuroanatomy and behavior in mice with a haploinsufficiency of AT-rich interactive domain 1B (ARID1B) throughout development. *Mol. Autism* 12:25. doi: 10.1186/s13229-021-00432-y

Engle, E. C. (2010). Human genetic disorders of axon guidance. *Cold Spring Harb. Perspect. Biol.* 2:a001784. doi: 10.1101/cshperspect.a001784

Ey, E., Leblond, C. S., and Bourgeron, T. (2011). Behavioral profiles of mouse models for autism spectrum disorders. *Autism Res.* 4, 5–16. doi: 10.1002/aur.175

Fetene, D. M., Betts, K. S., and Alati, R. (2017). Mechanisms in endocrinology: Maternal thyroid dysfunction during pregnancy and behavioural and psychiatric disorders of children: a systematic review. *Eur. J. Endocrinol.* 177, R261–R273. doi: 10.1530/EJE-16-0860

Granillo, L., Sethi, S., Keil, K. P., Lin, Y., Ozonoff, S., Iosif, A. M., et al. (2019). Polychlorinated biphenyls influence on autism spectrum disorder risk in the MARBLES cohort. *Environ. Res.* 171, 177–184. doi: 10.1016/j.envres.2018.12.061

Grimm, F. A., Hu, D., Kania-Korwel, I., Lehmler, H. J., Ludewig, G., Hornbuckle, K. C., et al. (2015). Metabolism and metabolites of polychlorinated biphenyls. *Crit. Rev. Toxicol.* 45, 245–272. doi: 10.3109/10408444.2014.999365

Grove, J., Ripke, S., Als, T. D., Mattheisen, M., Walters, R. K., Won, H., et al. (2019). Identification of common genetic risk variants for autism spectrum disorder. *Nat. Genet.* 51, 431–444. doi: 10.1038/s41588-019-0344-8

Guo, J., Capozzi, S. L., Kraeutler, T. M., and Rodenburg, L. A. (2014). Global distribution and local impacts of inadvertently generated polychlorinated biphenyls in pigments. *Environ. Sci. Technol.* 48, 8573–8580. doi: 10.1021/es502291b

Hahn, M. E., Karkowski, L., Weinreb, L., Henry, A., Schanz, N., and Hahn, E. M. (1998). Genetic and developmental influences on infant mouse ultrasonic calling. II. Developmental patterns in the calls of mice 2-12 days of age. *Behav. Genet.* 28, 315–325. doi: 10.1023/a:1021679615792

Haigh, J. L., Adhikari, A., Copping, N. A., Stradleigh, T., Wade, A. A., Catta-Preta, R., et al. (2021). Deletion of a non-canonical regulatory sequence causes loss of Scn1a expression and epileptic phenotypes in mice. *Genome Med.* 13:69. doi: 10.1186/s13073-021-00884-0

Hallmayer, J., Cleveland, S., Torres, A., Phillips, J., Cohen, B., Torigoe, T., et al. (2011). Genetic heritability and shared environmental factors among twin pairs with autism. *Arch. Gen. Psychiatry* 68, 1095–1102. doi: 10.1001/archgenpsychiatry.2011.76

Hatcher-Martin, J. M., Gearing, M., Steenland, K., Levey, A. I., Miller, G. W., and Pennell, K. D. (2012). Association between polychlorinated biphenyls and Parkinson's disease neuropathology. *Neurotoxicology* 33, 1298–1304. doi: 10.1016/j.neuro.2012.08.002

Herbert, M. R. (2010). Contributions of the environment and environmentally vulnerable physiology to autism spectrum disorders. *Curr. Opin. Neurol.* 23, 103–110. doi: 10.1097/WCO.0b013e328336a01f

Herkert, N. J., Jahnke, J. C., and Hornbuckle, K. C. (2018). Emissions of Tetrachlorobiphenyls (PCBs 47, 51, and 68) from Polymer Resin on Kitchen Cabinets as a Non-Aroclor Source to Residential Air. *Environ. Sci. Technol.* 52, 5154–5160. doi: 10.1021/acs.est.8b00966

Hertz-Picciotto, I., and Delwiche, L. (2009). The rise in autism and the role of age at diagnosis. *Epidemiology* 20, 84–90. doi: 10.1097/EDE.0b013e3181902d15

Hertz-Picciotto, I., Schmidt, R. J., Walker, C. K., Bennett, D. H., Oliver, M., Shedd-Wise, K. M., et al. (2018). A Prospective Study of Environmental Exposures and Early Biomarkers in Autism Spectrum Disorder: design, Protocols, and Preliminary Data from the MARBLES Study. *Environ. Health Perspect.* 126:117004. doi: 10.1289/EHP535

Hornbuckle, K., and Robertson, L. (2010). Polychlorinated biphenyls (PCBs): sources, exposures, toxicities. *Environ. Sci. Technol.* 44, 2749–2751. doi: 10.1021/es100801f

Hu, D., and Hornbuckle, K. C. (2010). Inadvertent polychlorinated biphenyls in commercial paint pigments. *Environ. Sci. Technol.* 44, 2822–2827. doi: 10.1021/es902413k

Jolous-Jamshidi, B., Cromwell, H. C., McFarland, A. M., and Meserve, L. A. (2010). Perinatal exposure to polychlorinated biphenyls alters social behaviors in rats. *Toxicol. Lett.* 199, 136–143. doi: 10.1016/j.toxlet.2010.08.015

Kabir, Z. D., Che, A., Fischer, D. K., Rice, R. C., Rizzo, B. K., Byrne, M., et al. (2017). Rescue of impaired sociability and anxiety-like behavior in adult cacna1c-deficient mice by pharmacologically targeting eIF2alpha. *Mol. Psychiatry* 22, 1096–1109. doi: 10.1038/mp.2017.124

Kato, Y., Haraguchi, K., Yamazaki, T., Ito, Y., Miyajima, S., Nemoto, K., et al. (2003). Effects of polychlorinated biphenyls, kanechlor-500, on serum thyroid hormone levels in rats and mice. *Toxicol. Sci.* 72, 235–241. doi: 10.1093/toxsci/kfg025

Keil, K. P., Sethi, S., and Lein, P. J. (2019a). Sex-Dependent Effects of 2,2′,3,5′,6-Pentachlorobiphenyl on Dendritic Arborization of Primary Mouse Neurons. *Toxicol. Sci.* 168, 95–109. doi: 10.1093/toxsci/kfy277

Keil, K. P., Sethi, S., Wilson, M. D., Silverman, J. L., Pessah, I. N., and Lein, P. J. (2019b). Genetic mutations in $Ca(^{2+})$ signaling alter dendrite morphology and social approach in juvenile mice. *Genes Brain Behav.* 18:e12526. doi: 10.1111/gbb.12526

Keil Stietz, K. P., Sethi, S., Klocke, C. R., de Ruyter, T. E., Wilson, M. D., Pessah, I. N., et al. (2021). Sex and genotype modulate the dendritic effects of developmental exposure to a human-relevant PCB mixture in the juvenile mouse. *Front Neurosci.* 15:766802. doi: 10.3389/fnins.2021.766802

Kilkenny, C., Browne, W. J., Cuthill, C. I., Emerson, M., and Altman, D. G. (2010). Improving bioscience research reporting: the ARRIVE guidelines for reporting animal research. *PLoS Biol.* 8:e1000412. doi: 10.1371/journal.pbio.1000412

Kim, J. H., Jarvik, G. P., Browning, B. L., Rajagopalan, R., Gordon, A. S., Rieder, M. J., et al. (2013). Exome sequencing reveals novel rare variants in the ryanodine receptor and calcium channel genes in malignant hyperthermia families. *Anesthesiology* 119, 1054–1065. doi: 10.1097/ALN.0b013e3182a8a998

Klocke, C., and Lein, P. J. (2020). Evidence Implicating Non-Dioxin-Like Congeners as the Key Mediators of Polychlorinated Biphenyl (PCB) Developmental Neurotoxicity. *Int. J. Mol. Sci.* 21:1013. doi: 10.3390/ijms21031013

Klocke, C., Sethi, S., and Lein, P. J. (2020). The developmental neurotoxicity of legacy vs. contemporary polychlorinated biphenyls (PCBs): similarities and differences. *Environ. Sci. Pollut. Res. Int.* 27, 8885–8896. doi: 10.1007/s11356-019-06723-5

Klosterhaus, S., McKee, L. J., Yee, D., Kass, J. M., and Wong, A. (2014). Polychlorinated biphenyls in the exterior caulk of San Francisco Bay Area buildings, California, USA. *Environ. Int.* 66, 38–43. doi: 10.1016/j.envint.2014.01.008

Koh, W. X., Hornbuckle, K. C., and Thorne, P. S. (2015). Human Serum from Urban and Rural Adolescents and Their Mothers Shows Exposure to Polychlorinated Biphenyls Not Found in Commercial Mixtures. *Environ. Sci. Technol.* 49, 8105–8112. doi: 10.1021/acs.est.5b01854

Krey, J. F., and Dolmetsch, R. E. (2007). Molecular mechanisms of autism: a possible role for Ca2+ signaling. *Curr. Opin. Neurobiol.* 17, 112–119. doi: 10.1016/j.conb.2007.01.010

Krueger, D. D., and Bear, M. F. (2011). Toward fulfilling the promise of molecular medicine in fragile X syndrome. *Annu. Rev. Med.* 62, 411–429. doi: 10.1146/annurev-med-061109-134644

Landrigan, P. J., Lambertini, L., and Birnbaum, L. S. (2012). A research strategy to discover the environmental causes of autism and neurodevelopmental disabilities. *Environ. Health Perspect.* 120, a258–a260. doi: 10.1289/ehp.1104285

Lavelle, T. A., Weinstein, M. C., Newhouse, J. P., Munir, K., Kuhlthau, K. A., and Prosser, L. A. (2014). Economic burden of childhood autism spectrum disorders. *Pediatrics* 133, e520–e529. doi: 10.1542/peds.2013-0763

Leehey, M. A., and Hagerman, P. J. (2012). Fragile X-associated tremor/ataxia syndrome. *Handb. Clin. Neurol.* 103, 373–386. doi: 10.1016/B978-0-444-51892-7.00023-1

Lein, P. J. (2015). "Overview of the role of environmental factors in neurodevelopmental disorders," in *Environmental Factors in Neurodevelopmental and Neurodegenerative Disorders*, eds L. G. Costa and M. Aschner (Oxford, UK: Elsevier, Inc), 3–20.

Lesiak, A., Zhu, M., Chen, H., Appleyard, S. M., Impey, S., Lein, P. J., et al. (2014). The environmental neurotoxicant PCB 95 promotes synaptogenesis *via* ryanodine receptor-dependent miR132 upregulation. *J. Neurosci.* 34, 717–725. doi: 10.1523/JNEUROSCI.2884-13.2014

Li, X., Holland, E. B., Feng, W., Zheng, J., Dong, Y., Pessah, N. I., et al. (2018). Authentication of synthetic environmental contaminants and their (bio)transformation products in toxicology: polychlorinated biphenyls as an example. *Environ. Sci. Pollut. Res. Int.* 25, 16508–16521. doi: 10.1007/s11356-017-1162-0

Lin, Y. P., Pessah, N. I., and Puschner, B. (2013). Simultaneous determination of polybrominated diphenyl ethers and polychlorinated biphenyls by gas chromatography-tandem mass spectrometry in human serum and plasma. *Talanta* 113, 41–48. doi: 10.1016/j.talanta.2013.04.001

Liu, J., Koscielska, K. A., Cao, Z., Hulsizer, S., Grace, N., Mitchell, G., et al. (2012). Signaling defects in iPSC-derived fragile X premutation neurons. *Hum. Mol. Genet.* 21, 3795–3805. doi: 10.1093/hmg/dds207

Lyall, K., Croen, L., Daniels, J., Fallin, M. D., Ladd-Acosta, C., Lee, B. K., et al. (2017). The Changing Epidemiology of Autism Spectrum Disorders. *Annu. Rev. Public Health* 38, 81–102. doi: 10.1146/annurev-publhealth-031816-044318

Martin, L., and Klaassen, C. D. (2010). Differential effects of polychlorinated biphenyl congeners on serum thyroid hormone levels in rats. *Toxicol. Sci.* 117, 36–44. doi: 10.1093/toxsci/kfq187

Masini, E., Loi, E., Vega-Benedetti, A. F., Carta, M., Doneddu, G., Fadda, R., et al. (2020). An Overview of the Main Genetic, Epigenetic and Environmental Factors Involved in Autism Spectrum Disorder Focusing on Synaptic Activity. *Int. J. Mol. Sci.* 21:8290. doi: 10.3390/ijms21218290

Matelski, L., Keil Stietz, K. P., Sethi, S., Taylor, S. L., Van de Water, J., and Lein, P. J. (2020). The influence of sex, genotype, and dose on serum and hippocampal cytokine levels in juvenile mice developmentally exposed to a human-relevant mixture of polychlorinated biphenyls. *Curr. Res. Toxicol.* 1, 85–103. doi: 10.1016/j.crtox.2020.09.001

Matsuo, N., Tanda, K., Nakanishi, K., Yamasaki, N., Toyama, K., Takao, K., et al. (2009). Comprehensive behavioral phenotyping of ryanodine receptor type 3 (RyR3) knockout mice: decreased social contact duration in two social interaction tests. *Front. Behav. Neurosci.* 3:3. doi: 10.3389/neuro.08.003.2009

Nakao, A., Miki, T., Shoji, H., Nishi, M., Takeshima, H., Miyakawa, T., et al. (2015). Comprehensive behavioral analysis of voltage-gated calcium channel beta-anchoring and -regulatory protein knockout mice. *Front. Behav. Neurosci.* 9:141. doi: 10.3389/fnbeh.2015.00141

Oppenheimer, J. H., and Schwartz, H. L. (1997). Molecular basis of thyroid hormone-dependent brain development. *Endocr. Rev.* 18, 462–475. doi: 10.1210/edrv.18.4.0309

Orito, K., Gotanda, N., Murakami, M., Ikeda, T., Egashira, N., Mishima, K., et al. (2007). Prenatal exposure to 3,3′,4,4′,5-pentachlorobiphenyl (PCB126) promotes anxiogenic behavior in rats. *Tohoku J. Exp. Med.* 212, 151–157. doi: 10.1620/tjem.212.151

Panesar, H. K., Kennedy, C. L., Keil Stietz, K. P., and Lein, P. J. (2020). Polychlorinated Biphenyls (PCBs): risk Factors for Autism Spectrum Disorder? *Toxics* 8:70. doi: 10.3390/toxics8030070

Penzes, P., Cahill, M. E., Jones, K. A., VanLeeuwen, J. E., and Woolfrey, K. M. (2011). Dendritic spine pathology in neuropsychiatric disorders. *Nat. Neurosci.* 14, 285–293. doi: 10.1038/nn.2741

Pessah, I. N., Cherednichenko, G., and Lein, P. J. (2010). Minding the calcium store: ryanodine receptor activation as a convergent mechanism of PCB toxicity. *Pharmacol. Ther.* 125, 260–285. doi: 10.1016/j.pharmthera.2009.10.009

Pessah, I. N., Lein, P. J., Seegal, R. F., and Sagiv, S. K. (2019). Neurotoxicity of polychlorinated biphenyls and related organohalogens. *Acta Neuropathol.* 138, 363–387. doi: 10.1007/s00401-019-01978-1

Rice, D., and Barone, S. Jr. (2000). Critical periods of vulnerability for the developing nervous system: evidence from humans and animal models. *Environ. Health Perspect.* 108, 511–533. doi: 10.1289/ehp.00108s3511

Rieger, M. A., and Dougherty, J. D. (2016). Analysis of within Subjects Variability in Mouse Ultrasonic Vocalization: pups Exhibit Inconsistent, State-Like Patterns of Call Production. *Front. Behav. Neurosci.* 10:182. doi: 10.3389/fnbeh.2016.00182

Robin, G., Lopez, J. R., Espinal, G. M., Hulsizer, S., Hagerman, P. J., and Pessah, I. N. (2017). Calcium dysregulation and Cdk5-ATM pathway involved in a mouse model of fragile X-associated tremor/ataxia syndrome. *Hum. Mol. Genet.* 26, 2649–2666. doi: 10.1093/hmg/ddx148

Roman, G. C., Ghassabian, A., Bongers-Schokking, J. J., Jaddoe, V. W., Hofman, A., de Rijke, Y. B., et al. (2013). Association of gestational maternal hypothroxinemia and increased autism risk. *Ann. Neurol.* 74, 733–742. doi: 10.1002/ana.23976

Rude, K. M., Pusceddu, M. M., Keogh, C. E., Sladek, J. A., Rabasa, G., Miller, E. N., et al. (2019). Developmental exposure to polychlorinated biphenyls (PCBs) in the maternal diet causes host-microbe defects in weanling offspring mice. *Environ. Pollut.* 253, 708–721. doi: 10.1016/j.envpol.2019.07.066

Scattoni, M. L., Crawley, J., and Ricceri, L. (2009). Ultrasonic vocalizations: a tool for behavioural phenotyping of mouse models of neurodevelopmental disorders. *Neurosci. Biobehav. Rev.* 33, 508–515. doi: 10.1016/j.neubiorev.2008.08.003

Schantz, S. L., Widholm, J. J., and Rice, D. C. (2003). Effects of PCB exposure on neuropsychological function in children. *Environ. Health Perspect.* 111, 357–576. doi: 10.1289/ehp.5461

Sealey, L. A., Hughes, B. W., Sriskanda, A. N., Guest, J. R., Gibson, A. D., Johnson-Williams, L., et al. (2016). Environmental factors in the development of autism spectrum disorders. *Environ. Int.* 88, 288–298. doi: 10.1016/j.envint.2015.12.021

Semple, B. D., Blomgren, K., Gimlin, K., Ferriero, D. M., and Noble-Haeusslein, L. J. (2013). Brain development in rodents and humans: identifying benchmarks of maturation and vulnerability to injury across species. *Prog. Neurobiol.* 10, 1–16. doi: 10.1016/j.pneurobio.2013.04.001

Sethi, S., Keil, K. P., Chen, H., Hayakawa, K., Li, X., Lin, Y., et al. (2017). Detection of 3,3′-Dichlorobiphenyl in Human Maternal Plasma and Its Effects on Axonal and Dendritic Growth in Primary Rat Neurons. *Toxicol. Sci.* 158, 401–411. doi: 10.1093/toxsci/kfx100

Sethi, S., Morgan, R. K., Feng, W., Lin, Y., Li, X., Luna, C., et al. (2019). Comparative Analyses of the 12 Most Abundant PCB Congeners Detected in Human Maternal Serum for Activity at the Thyroid Hormone Receptor and Ryanodine Receptor. *Environ. Sci. Technol.* 53, 3948–3958. doi: 10.1021/acs.est.9b00535

Silverman, J. L., Nithianantharajah, J., Der-Avakian, A., Young, J. W., and Sukoff Rizzo, S. J. (2020). Lost in translation: at the crossroads of face validity and translational utility of behavioral assays in animal models for the development of therapeutics. *Neurosci. Biobehav. Rev.* 116, 452–453. doi: 10.1016/j.neubiorev.2020.07.008

Silverman, J. L., Yang, M., Lord, C., and Crawley, J. N. (2010). Behavioural phenotyping assays for mouse models of autism. *Nat. Rev. Neurosci.* 11, 490–502. doi: 10.1038/nrn2851

Stamou, M., Streifel, K. M., Goines, P. E., and Lein, P. J. (2013). Neuronal connectivity as a convergent target of gene x environment interactions that confer risk for Autism Spectrum Disorders. *Neurotoxicol. Teratol.* 36, 3–16. doi: 10.1016/j.ntt.2012.12.001

Supekar, K., Uddin, L. Q., Khouzam, A., Phillips, J., Gaillard, W. D., Kenworthy, L. E., et al. (2013). Brain hyperconnectivity in children with autism and its links to social deficits. *Cell Rep.* 5, 738–747. doi: 10.1016/j.celrep.2013.10.001

Tassone, F., Iong, K. P., Tong, T. H., Lo, J., Gane, L. W., Berry-Kravis, E., et al. (2012). FMR1 CGG allele size and prevalence ascertained through newborn screening in the United States. *Genome Med.* 4:100. doi: 10.1186/gm401

Wayman, G. A., Bose, D. D., Yang, D., Lesiak, A., Bruun, D., Impey, S., et al. (2012a). PCB-95 modulates the calcium-dependent signaling pathway responsible for activity-dependent dendritic growth. *Environ. Health Perspect.* 120, 1003–1009. doi: 10.1289/ehp.1104833

Wayman, G. A., Yang, D., Bose, D. D., Lesiak, A., Ledoux, V., Bruun, D., et al. (2012b). PCB-95 promotes dendritic growth *via* ryanodine receptor-dependent mechanisms. *Environ. Health Perspect.* 120, 997–1002. doi: 10.1289/ehp.1104832

Weintraub, K. (2011). The prevalence puzzle: autism counts. *Nature* 479, 22–24. doi: 10.1038/479022a

Williams, G. R. (2008). Neurodevelopmental and neurophysiological actions of thyroid hormone. *J. Neuroendocrinol.* 20, 784–794. doi: 10.1111/j.1365-2826.2008.01733.x

Xi, T., and Wu, J. (2021). A Review on the Mechanism Between Different Factors and the Occurrence of Autism and ADHD. *Psychol. Res. Behav. Manag.* 14, 393–403. doi: 10.2147/PRBM.S304450

Yang, D., Kania-Korwel, I., Ghogha, A., Chen, H., Stamou, M., Bose, D. D, et al. (2014). PCB 136 atropselectively alters morphometric and functional parameters of neuronal connectivity in cultured rat hippocampal neurons *via* ryanodine receptor-dependent mechanisms. *Toxicol. Sci.* 138, 379–392. doi: 10.1093/toxsci/kft334

Yang, D., Kim, K. H., Phimister, A., Bachstetter, A. D., Ward, T. R., Stackman, R. W., et al. (2009). Developmental exposure to polychlorinated biphenyls interferes with experience-dependent dendritic plasticity and ryanodine receptor expression in weanling rats. *Environ. Health Perspect.* 117, 426–435. doi: 10.1289/ehp.11771

Yang, M., Lewis, F., Foley, G., and Crawley, J. N. (2015). In tribute to Bob Blanchard: divergent behavioral phenotypes of 16p11.2 deletion mice reared in same-genotype versus mixed-genotype cages. *Physiol. Behav.* 146, 16–27. doi: 10.1016/j.physbeh.2015.04.023

Yang, M., Silverman, J. L., and Crawley, J. N. (2011). Automated three-chambered social approach task for mice. *Curr. Protoc. Neurosci.* 8:8.26. doi: 10.1002/0471142301.ns0826s56

Yu, X., Taylor, A. M. W., Nagai, J., Golshani, P., Evans, C. J., Coppola, G., et al. (2018). Reducing Astrocyte Calcium Signaling *In Vivo* Alters Striatal Microcircuits and Causes Repetitive Behavior. *Neuron* 99, 1170–1187.e9. doi: 10.1016/j.neuron.2018.08.015

Yuen, B., Boncompagni, S., Feng, W., Yang, T., Lopez, J. R., Matthaei, K. I., et al. (2012). Mice expressing T4826I-RYR1 are viable but exhibit sex- and genotype-dependent susceptibility to malignant hyperthermia and muscle damage. *FASEB J.* 26, 1311–1322. doi: 10.1096/fj.11-197582

Conflict of Interest: The authors declare that the research was conducted in the absence of any commercial or financial relationships that could be construed as a potential conflict of interest.

Publisher's Note: All claims expressed in this article are solely those of the authors and do not necessarily represent those of their affiliated organizations, or those of the publisher, the editors and the reviewers. Any product that may be evaluated in this article, or claim that may be made by its manufacturer, is not guaranteed or endorsed by the publisher.

frontiers in Neuroscience

REVIEW
published: 08 December 2021
doi: 10.3389/fnins.2021.787425

Cerebellar Patterning Defects in Mutant Mice

*Richard Hawkes**

Department of Cell Biology, Cumming School of Medicine, Anatomy and Hotchkiss Brain Institute, University of Calgary, Calgary, AB, Canada

The cerebellar cortex is highly compartmentalized and serves as a remarkable model for pattern formation throughout the brain. In brief, the adult cerebellar cortex is subdivided into five anteroposterior units—transverse zones—and subsequently, each zone is divided into ∼20 parasagittal stripes. Zone-and-stripe pattern formation involves the interplay of two parallel developmental pathways—one for inhibitory neurons, the second for excitatory. In the inhibitory pathway, progenitor cells of the 4th ventricle generate the Purkinje cells and inhibitory interneurons. In the excitatory pathway, progenitor cells in the upper rhombic lip give rise to the external granular layer, and subsequently to the granular layer of the adult. Both the excitatory and inhibitory developmental pathways are spatially patterned and the interactions of the two generate the complex topography of the adult. This review briefly describes the cellular and molecular mechanisms that underly zone-and-stripe development with a particular focus on mutations known to interfere with normal cerebellar development and the light they cast on the mechanisms of pattern formation.

Keywords: cerebellar pattern formation Purkinje cell, granule cell, transverse zone, stripe, pattern formation, cerebellar development

OPEN ACCESS

Edited by:
Atsushi Yoshiki, RIKEN BioResource Research Center (BRC), Japan

Reviewed by:
Katsuhiko Ono, Kyoto Prefectural University of Medicine, Japan
Annalisa Buffo, University of Turin, Italy

***Correspondence:**
Richard Hawkes
rhawkes@ucalgary.ca

Specialty section:
This article was submitted to Neurodevelopment, a section of the journal Frontiers in Neuroscience

Received: *30 September 2021*
Accepted: *01 November 2021*
Published: *08 December 2021*

Citation:
Hawkes R (2021) Cerebellar Patterning Defects in Mutant Mice. Front. Neurosci. 15:787425. doi: 10.3389/fnins.2021.787425

INTRODUCTION

This review addresses the fundamental compartmentation of the cerebellar cortex into transverse zones and parasagittal stripes. On the other hand, the review does not address secondary aspects of patterning such as the lobulation of the cortex (e.g., Legué et al., 2015) and the regional restriction of the afferent terminal fields and various interneurons (e.g., Consalez and Hawkes, 2013). The key perspective is the light cast on patterning by mouse mutant phenotypes.

Briefly, the cerebellar cortex is highly patterned into hundreds, if not thousands, of genetically predetermined quanta (reviewed in Apps and Hawkes, 2009; Armstrong and Hawkes, 2014; Leto et al., 2016; Apps et al., 2018). The earliest pattern to form is an anteroposterior array of transverse zones defined by boundaries between Purkinje cell (PC) domains (Ozol et al., 1999). Five zones are reproducibly identified to date in all birds and mammals: the anterior zone (AZ), central zone (CZ—further subdivided into anterior and posterior domains: Marzban et al., 2008), posterior zone (PZ) and nodular zone (NZ). Similar transverse boundaries are also found in the granular layer.

Each transverse zone is subdivided from medial to lateral into parasagittal stripes. This patterning is most clearly seen in the adult in the PC expression patterns of numerous molecules. For example, the AZ and PZ show alternating striped arrays of PC expression for zebrin II/aldolase C (= zebrin II+, Brochu et al., 1990; Ahn et al., 1994) or the zebrin II- subset (e.g., phospholipase (PL)Cβ4 (Sarna et al., 2006) or the transcription factor Early B-cell Factor 2 (Ebf2, Croci et al., 2006). In contrast, the CZ and NZ are uniformly zebrin II + but stripes are seen in other expression patterns [e.g., heat shock protein (HSP)25±, Armstrong et al., 2001 or HNK-1,

Marzban et al., 2004]. In all zones, the zone-and-stripe patterns are highly reproducible between individuals and conserved across species (e.g., Sillitoe et al., 2005), but interspecific size differences are typical, reflecting a species' particular lifestyle. For example, mosaic evolution results in the CZ being especially large in bats (Kim et al., 2009), where it subserves echolocation and vision, whereas it is especially small in blind species such as the naked mole rat (Marzban et al., 2011) or star-nosed mole (Marzban et al., 2015; see also Legué et al., 2015). In parallel to the patterning of the PCs, the granular layer is similarly patterned into transverse domains that align with the PC transverse zones (e.g., Sillitoe et al., 2003).

In brief, the zone-and-stripe pattern forms during development via two separate but interacting pathways (reviewed in Leto et al., 2016). In brief, the inhibitory neurons—in particular the PCs—are born in the ventricular zone of the fourth ventricle (VZ: E10-E13 in mice). Postmitotic PCs migrate first to the cerebellar plate which subsequently disperses to form a stereotyped array of clusters (E14-E18), which are the topographic organizing centers that pattern the afferent connections and the interneurons (reviewed in Consalez and Hawkes, 2013; Apps et al., 2018). In parallel to the PC patterning, the granule cells are generated from granule cell precursors (G) in the upper rhombic lip (URL), which divide extensively and spread to cover the cerebellar anlage as the external granular layer (EGL) by E18. Thus, by birth the fundamental zone-and-stripe architecture has been laid down. Subsequently the embryonic cerebellum transforms into the adult: between ∼E18-P20 the granule cells in the EGL and the PC clusters all disperse to form the elaborate adult zone-and-stripe array.

Dozens of mutations are known that impede normal cerebellar development and many show abnormal morphology. The underlying disruptions are of two kinds: "patterning" defects—mutations that disturb normal pattern formation; and "patterned" defects—those which are secondary consequences of the underlying abnormal patterns. A pertinent analogy might be the bud and the flower. Mutations acting on bud formation might result, for example, in missing petals; in contrast, in mutations acting on the transformation of the bud to the flower, all the normal components would be present but in some way distorted. Almost all cerebellar mutants are of the second kind—all normal elements are present but disorganized. Indeed, it is arguable that mutations of the first kind have never been unambiguously identified.

PATTERNED PHENOTYPES IN THE INHIBITORY PURKINJE CELL DEVELOPMENT PATHWAY

PC pattern formation occurs in four distinct phases during which complexity steadily increases: PC birth in the ventricular zone of the VZ; migration to the cerebellar plate; dispersal of the cerebellar plate into a stereotypes array of PC clusters; and dispersal of the cluster array to reveal the mature zone-and-stripe architecture. In the interests of space, the patterning events that precede the formation of the cerebellar anlage (∼pre-E10) are not considered here (for an overview of PC patterning with numerous useful illustrations, see Leto et al., 2016).

Precisely when the zone-and-stripe pattern is first specified in cerebellar development is uncertain. There are several candidate stages at which aspects of the adult architecture might be specified: in the VZ; in the cerebellar plate; in the transformation of the cerebellar plate into the embryonic cluster array; and during the metamorphosis of the cluster array to the adult stripes. In all likelihood, stages in pattern formation involves several.

From Ventricular Zone to Cerebellar Plate

All PCs are generated between E10-E13 in a region of the 4th VZ, specified by the expression of the basic helix-loop-helix factor pancreatic transcription factor 1a (*Ptf1a*, Hoshino et al., 2005; reviewed in Dastjerdi et al., 2012). When *Ptf1a* is disrupted by a downstream transgene insertion (the mutant mouse *cerebelless*; *cbll*; Hoshino et al., 2005) the result is a comprehensive ablation of the entire cerebellar GABAergic phenotype. The newborn postmitotic PCs migrate dorsally from the VZ to form the cerebellar plate by about E13.

It is possible that some cerebellar patterning is already patterned in the VZ (a "protomap"; Rakic, 1988). Whether or not a protomap in present there are certainly mediolateral subdomains in the *Ptf1a* + VZ (e.g., Chizhikov et al., 2006; Zordan et al., 2008) but how, if at all, these relate to patterning, is unknown. The proposition that patterning of the cerebellar cortex starts early in development is supported by studies in mice null for the zinc finger protein Zfp423. *Zfp423* codes for a transcription factor with a link to the ciliopathy Joubert syndrome. *Zfp423* is expressed in the VZ from E11 onward and the consequences of its mutation include disruption of normal PC generation. In homozygous null alleles the cerebellum is deformed and has prominent vermian hypoplasia (Warming et al., 2006). Engineered mouse lines with targeted domain deletions (*notably Zfp423Δ9-20;* Casoni et al., 2017) show more subtle PC phenotypes. In particular, *Zfp423Δ9* shows a significant loss of PCs focussed on the late-born zebrin II-/Ebf2 + population. The upshot is that in *Zfp423Δ9-20* the adult PC stripe pattern is abnormal, with reduced size (but not number) of the zebrin II- stripes. In contrast, in the *Zfp423Δ28-30* allele there is also PC loss, but subtypes are not differentially affected.

Generally speaking, one aspect of the adult phenotype is certainly specified during the VZ-cerebellar plate (E10-E13) period—the adult PC zebrin II ± phenotype. In general, the future zebrin II + PCs are born first (∼E10-E11.5) followed by the zebrin II- population (∼E11.5-E13; Hashimoto and Mikoshiba, 2003). These two populations can already be distinguished in the cerebellar plate by expression data. For example, the transcription factor Ebf2 is a regulator of the zebrin II- PC phenotype (Croci et al., 2006; Chung et al., 2008). During development (from E12 to adult) *Ebf2* expression distinguishes two PC phenotypes, with the early born *Ebf2*- PCs becoming zebrin II + in the adult and the later-born *Ebf2* + PCs destined to become zebrin II-. The two PC subpopulations stack in the

cerebellar plate such that the Ebf2- PCs are preferentially located dorsally. The pathway to zebrin II ± phenotype specification is poorly understood. One model involves Neurogenin (*Neurog*)1/2 and evokes a *Ptf1a*→*Neurog1/2*→*Ebf2* regulatory network (reminiscent of frontal cortex development: e.g., Schuurmans et al., 2004; Zordan et al., 2008; Lundell et al., 2009). The hypothesis is that *Ptf1*a upregulates *Neurog1/2* in the late-born PC progenitors. In turn, *Neurog1/2* upregulates *Ebf2* and thereby downregulates the zebrin II + phenotype. Conversely, the early born PC cohort (E10-E11.5) expresses neither *Neurog1/2* nor *Ebf2* and therefore becomes zebrin II + in the adult. Consequently, in mice where *Ebf2* is ablated a complex cerebellar null phenotype results, in which some PCs die and many others undergo a transdifferentiation such that adult PC stripes that are normally Ebf2 + /zebrin II- ectopically express markers normally restricted to the zebrin II + stripes, resulting in an abnormal transdifferentiated Ebf2 + /zebrin II + phenotype; Croci et al., 2006; Chung et al., 2008). This suggests that PC subtype specification is achieved through *Ebf2* acting as a repressor of the zebrin II + phenotype. Indeed, the *Ebf2* null mutation is the only known genetic manipulation to subvert PC subtype specification. These data have two important implications for patterning. First, it is clear that at least two distinct PC classes (zebrin II + /Ebf2- and zebrin II-/Ebf2 +) are specified as soon as E13. Secondly, at least some positional information is also specified in in the sense that late-born Ebf2 + PCs reliably end up in the adult zebrin II- stripes.

From Cerebellar Plate to Embryonic Purkinje Cell Clusters

Between E14-E18 the cerebellar plate migrates dorsally and transforms into ∼54 reproducible PC clusters (Fujita et al., 2012; Vibulyaseck et al., 2017) with multiple expression profiles (Wassef and Sotelo, 1985; reviewed in Dastjerdi et al., 2012). PC clusters are the forerunners of the adult parasagittal stripes and also serve as organizing centers for the topography of other cerebellar components—interneurons, afferents etc. (e.g., Consalez and Hawkes, 2013; Apps et al., 2018). The quantitative relationship between individual clusters and stripes is complex. In some cases, a single cluster transforms into a single stripe but in other cases one cluster splits into multiple stripes (e.g., Armstrong et al., 2000; Armstrong and Hawkes, 2001; Sillitoe et al., 2009; see also Fujita et al., 2012; Vibulyaseck et al., 2017). Furthermore, several clusters may merge into a single stripe [although more likely, where several clusters combine, there are several contiguous stripes with similar marker expression—e.g., the zebrin II- stripes of the anterior vermis (Ozol et al., 1999; Marzban et al., 2007)]. Whatever the ultimate case, differential expression by PC cluster subtypes is seen already at E14 (e.g., the Olfactory Marker Protein-*lacZ* transgene: Nunzi et al., 1999) and by E18 multiple cerebellar PC phenotypes are present (e.g., reviewed in Dastjerdi et al., 2012; Armstrong and Hawkes, 2014). The mechanisms that convert the cerebellar plate into to the perinatal cluster array are not understood. There is some evidence that the transformation is guided by homophilic interactions between cadherins (e.g., Redies et al., 2011) and/or ephrins (which, in turn, are linked to the reelin signaling pathway—see below, e.g., Karam et al., 2000; Sentürk et al., 2011; reviewed in Dastjerdi et al., 2012). It is not clear if any mutations disrupt cluster formation. For example, the homeobox transcription factor *Engrailed* (*En2*) is expressed by a cluster subset from about E15 but *En2* deletion does not significantly disrupt the adult zone-and-stripe pattern: rather it seems to have subtle (probably secondary) effects on lobulation and the formation of mossy fiber afferent topography—Millen et al., 1994; Kuemerle et al., 1997; Sillitoe et al., 2010). One candidate for primary patterning defects is the lysosomal acid phosphatase null mutant (*Acp2-/-;* a.k.a. *Nax*), which appears to have missing stripes in both the AZ and CZ, consistent with abnormal cluster formation, but other explanations are equally plausible (Bailey et al., 2014). The boundaries between adjacent transverse zones are also apparent during this same temporal window (e.g., Ozol et al., 1999; Fujita et al., 2012; Armstrong and Hawkes, 2014). Thus, it is clear that the fundamental patterning of the cerebellar cortex—the bud of the cerebellar rose—is already established at birth.

From Clusters to Stripes

The transformation of the embryonic PC cluster array into the adult zone-and-stripe architecture occurs between E18 and P20. The transformation of the clusters (PCs plus affiliated interneurons, afferent terminals) into stripes is triggered by Reelin (Reln) signaling. Reln is a glycoprotein secreted in the cerebellar cortex by neurons of the rhombic lip migratory stream (reviewed in Nimura et al., 2019). Reln binds to a receptor complex on the PC surface comprising ApolipoproteinE Receptor 2 (ApoER2) and the Very-Low Density Lipoprotein Receptor (VLDLR: Trommsdorff et al., 1999; Hiesberger et al., 1999). The receptor signal is transduced via the phosphorylation by two tyrosine kinases—*Src* and *Fyn* (Howell et al., 1999) of the intracellular adaptor protein Disabled1 (*Dab1*: Howell et al., 1997: and its alleles *scrambler* (*Dab1*^{scm}) and *yotari* (*Dab1*^{yot}), Sheldon et al., 1997). The upshot is probably that PC-PC homophilic binding in the clusters is downregulated (as has been suggested for the cortex, Hoffarth et al., 1995), thereby facilitating cluster dispersal. The clusters disperse predominantly along the anteroposterior axis—roughly a 25-fold lengthening in the vermis—and thus the clusters in each transverse zone become the adult stripe arrays.

In mutations that block the Reln→Dab1 signaling pathway the PC clusters fail to form stripes and remain as ectopic clumps at the core of the cerebellar anlage. This was first reported in the naturally occurring ataxic mouse mutant *reeler* (*Reln*^{rl}; Falconer, 1951). Subsequently, the same reeler phenotype was found due to other mutations of elements that comprise the Reln→Dab1 pathway: for example, the double-deletion of *Apoer2/Vldlr* (Trommsdorff et al., 1999), the deletion of *Dab1* (Howell et al., 1997) and double mutants of *Fyn* and *Src* (Howell et al., 1999; reviewed in D'Arcangelo, 2014). In addition of these mutations, which disrupt all PC cluster dispersal, other mutations act selectively on PC subsets to yield patterned disruptions of the cerebellar cortex. The usual description of the Reln→Dab1 pathway assumes that Apoer2 and Vldlr combine in individual PCs to form a functional Reln receptor complex (Trommsdorff et al., 1999). Consistent with this, the *Apoer2−/−:Vldlr −/−* double null has a full *reeler* phenotype. However, single null

mutations show more complex phenotypes (Larouche et al., 2008). The single *Apoer2−/−* (a targeted disruption of *Apoer2* by a pol2*neo* cassette) has a few specific ectopic PC clusters, largely restricted to zebrin II- PCs located near the midline. Likewise, *Vldlr-/-* mice (with a disruption of exon 5) have only a small subset of ectopic PC clusters, some zebrin II +, others zebrin II-, suggesting differential subreceptor expression by PC subsets and hence patterned ectopias in the null phenotypes. However, while no PC ectopia is present in mice heterozygous for either receptor alone mutants double heterozygous for the two receptors (*Apoer2* ± :*Vldlr* ±) have a single small cluster of ectopic zebrin II- PCs.

PC cluster dispersal phenotypes are common. In addition to the full *reeler* phenotype in which all PC clusters fail to disperse, several naturally occurring mouse mutants show PC cluster dispersal phenotypes that are restricted to specific transverse zones. The best-understood are *rostral cerebellar malformation*, a spontaneous mutation of the netrin receptor gene (*Unc5c*^{rcm}, Ackerman et al., 1997), and *cerebellar deficient folia* (a mutation at the catenin alpha 2 (*Ctnna2)* locus, Beierbach et al., 2001). Both phenotypes show a massive failure of PC cluster dispersal in the AZ while the posterior clusters are only mildly affected (Eisenman and Brothers, 1998; Goldowitz et al., 2000). Selective failures of cluster dispersal are also seen in the *weaver* mouse (*Kcnj6*^{wv}: a mutation in the inwardly rectifying potassium channel GIRK2, Surmeier et al., 1996). In particular, the *wv/wv* homozygote shows a very specific PC dispersion defect in which a subset of zebrin II + /HSP25 + embryonic clusters located in the CZ fails to disperse normally and remains ectopic in their embryonic configuration (Armstrong and Hawkes, 2001).

Finally, multiple PC death mutants have been identified with patterned phenotypes that are restricted by the zone-and-stripe architecture. For example, a transgenic model of Niemann-Pick disease type A/B (an acid sphingomyelinase knockout (*Smpd1*^{tm1Esc}), Sarna et al., 2001) shows the selective loss of zebrin II- PCs. In most cases, PC death is postnatal, and the surviving PCs remain in their normal stripe and zone locations, indicating that the defect has no effect on pattern formation (i.e., a "patterned" defect rather than a "patterning defect": reviewed in Sarna and Hawkes, 2003). However, mutations that lead to embryonic PC death are less straightforward to interpret. For example, null mutations of *Ebf2* show a 30–40% loss in PCs, which happens prenatally (Croci et al., 2006, 2011). The result is a cerebellar hypoplasia with reduced lobulation, but more-or-less normal zone-and-stripe patterning, implying that the shortfall in PC numbers occurs during neurogenesis but before patterning begins [e.g., in the early VZ to cerebellar plate stage (E10-E11); also, see Kuemerle et al., 1997].

Whether PC death plays a role in refining the embryonic zone and patch pattern is unclear. On the one hand, here is evidence that PC death is concentrated at perinatal zone- and stripe boundaries, notably at the midline, consistent with a role in sculpting stripes and eliminating positional errors (Jankowski et al., 2011). In addition, there is some support for the idea that embryonic PC death might be transverse zone- or cluster-specific. For example, in the perinatal *Ebf2* null mouse, substantial embryonic PC apoptosis is concentrated in the AZ (Croci et al., 2011). However, suppression of perinatal PC death by deletion of the apoptosis-regulator BCL-Associated X-Protein (*Bax-/-)* results in a hypertrophic cerebellar cortex with 30% additional PCs but no patterning abnormalities (reviewed in Vogel, 2002), consistent with a role for apoptosis in size regulation rather than editing and fine tuning.

PATTERNING MUTATIONS IN THE EXCITATORY GRANULE CELL DEVELOPMENT PATHWAY

The patterning of the granule cell pathway happens in parallel to the PC VZ→cerebellar plate→cluster array→stripe formation pathway (a thorough review of granular layer patterning, together with useful cartoons, can be found in Consalez et al., 2021). All granule cells of the cerebellar cortex derive from *Atonal Transcription Factor 1* (*Atoh1:* a.k.a *Math1*) lineage in the URL, and deletion of *Atoh1* completely ablates the granular layer (Akazawa et al., 1995; Ben-Arie et al., 1997; reviewed in Consalez et al., 2021). GCPs migrate from the URL, starting at E10-E12, and proliferate and spread to cover the entire surface of the cerebellar anlage as the external granular layer (EGL) by E18. Starting around E18 postmitotic granule cells descend ventrally from the EGL, guided by Bergmann glial fibers through the dispersing PC clusters and the developing molecular layer, and settle in the nascent granular layer. Populating the granular layer proceeds until P20-P30, by which time the GCPs are spent, and the EGL has disappeared.

Within the URL, before the EGL is formed, there is already elaborate patterning as revealed by the expression of multiple transcription factors (Yeung et al., 2014), and by E18, the patterning of the EGL is established. Four EGL transverse domains that derive from distinct GCP populations are revealed by differences in gene expression, birthdates, lineage restriction and the consequences of mutations (reviewed in Consalez et al., 2021). Each transverse domain is aligned with its counterpart in the PC layer—the EGL-AZ (eAZ), eCZ, ePZ, and eNZ. This alignment presumably arises because the PC cluster architecture restricts the dispersal of different GCP lineages or the underlying PC clusters induce gene expression in the overlying EGL (e.g., Smeyne et al., 1995). In particular, multiple mutations result in defects with phenotypic abnormalities that are restricted at EGL transverse domain boundaries. These phenotypes are of two kinds: intrinsic defects that directly affect the GCPs [e.g., *meander tail* (*mea/mea*), Hamre and Goldowitz, 1997] and extrinsic defects due to abnormalities in the local environment (e.g., defective GCP production in sonic hedgehog (*Shh*) null mice, Lewis et al., 2004; PC defects in the Retinoid receptor-related Orphan Receptor (ROR)α mutant *staggerer* (*Rora*^{sg}), reviewed in Gold et al., 2003; Vitalis and Mariani, 2018). These are often difficult to distinguish in practice, and both intrinsic and extrinsic effects are often present concomitantly (e.g., *weaver*, Smeyne and Goldowitz, 1989).

The eAZ/eCZ boundary restricts the expression of several genes. For example, expression the homeodomain transcription factor *Otx1* (Frantz et al., 1994), fibroblast growth factor alpha,

Zic1 (Aruga et al., 1998), and protein tyrosine phosphatase rho (McAndrew et al., 1998), are all restricted predominantly to the EGL anterior to the eAZ/eCZ boundary. In contrast, expression of *Otx2* (Frantz et al., 1994) and the homeodomain transcription factor *Lmx1a* is restricted to the EGL posterior to the eAZ/eCZ boundary (and see below for the eCZ). The eAZ/eCZ is also a lineage-restriction boundary in embryonic stem cell chimeras, and hence in this case at least the EGL boundary is not secondary to induction by the underlying PC clusters (Hawkes et al., 2008).

Several mutant EGL phenotypes are restricted at the eAZ/eCZ boundary. The most prominent phenotype is the presence of an agranular AZ. This is seen in the *meander tail (mea/mea)* mutant (Ross et al., 1990), in *rostral cerebellar malformation* (*Unc5c*^{rcm}, Ackerman et al., 1997; Eisenman and Brothers, 1998), in the failure of the zebrin II- PC subpopulation in the cadherin receptor mutant *cerebellar deficient folia* (*Ctnna2*^{cdf}, Beierbach et al., 2001) and in the heterozygous *weaver* mutant (*wv*/+ , Eisenman et al., 1998; Armstrong and Hawkes, 2001). In contrast, a null mutation of the transcriptional activator gene *Neurogenic Differentiation 1* (*Neurod1*) results in a selective loss of GCPs posterior to the eAZ/eCZ boundary (Miyata et al., 1999; Cho and Tsai, 2006). As noted above, in the posterior EGL the GCPs are Lmx1a+, and consequently *Lmx1a* mutations (for instance, the deletion in the autosomal recessive mutant *dreher* (*Lmx1a* ^{drJ})) manifest EGL defects focused on the posterior vermis (Chizhikov et al., 2010: interestingly, in null mutations of *Lmx1a*, GCPs over-migrate into the anterior vermis, leading to posterior vermis hypoplasia). In addition, in the *dreher* mouse both roof plate and rhombic lip defects induce extreme deformities in the overall morphology including dramatic vermis distortion (Millonig et al., 2000; Chizhikov et al., 2010), presumably secondary to the switching of the *Lmx1a* + GCPs to an anterior (*Lmx1a*-) fate. However, despite the gross cortical deformities the underlying zone-and-stripe architecture is preserved (e.g., the HSP25 ± and zebrin II ± stripe arrays are intact, Sillitoe et al., 2014). Similarly, *Ebf2* is expressed transiently in the URL and the *Atoh1* + migratory stream between E12.5-E13.5 (Croci et al., 2006, 2011; Chung et al., 2008). Genetic fate mapping indicates that granule cells derived from *Ebf2* + precursors are restricted largely to the eAZ [Badaloni et al., 2019: the AZ is populated predominantly by early born GCs (Machold and Fishell, 2005), so this may account for their anterior location]. There is no obvious phenotype in the *Ebf2*−/− EGL. Finally, in *Dab1* null mutants a clear separation of anterior and posterior EGLs is found at the eAZ/eCZ boundary presumably secondary to the failure of PC cluster dispersal (Gallagher et al., 1998).

The evidence for a distinct eCZ/ePZ boundary and a specific eCZ domain is less clear cut. First, in chimeras of wildtype and the mutation *small eye* (*Pax6*$^{Sey/Sey}$) a lineage boundary is seen in lobules VII where the *Pax6* mutation preferentially affects the EGL anterior to the eCZ/ePZ boundary (Swanson and Goldowitz, 2011). Secondly, *Otx1/Otx2* expression reveals two boundaries in the EGL—the eAZ expresses only *Otx1* and the ePZ expresses *Otx2*. However, between the two the eCZ is revealed as a transverse domain of Co-expression (Frantz et al., 1994).

No *positive* markers of the third EGL transverse domain, the ePZ, are known. However, the ePZ can be defined as located between the posterior border of the eCZ and the anterior border of the eNZ. This is also a lineage boundary in chimeras at the same approximate location (Hawkes et al., 2008) and an expression boundary for zebrin II in the heterozygous mutant *Lurcher* (Tano et al., 1992), which has constitutive activation of the delta 2 ionotropic glutamate receptor (*Grid2*^{Lc}, Wollmuth et al., 2000). The posterior boundary of the ePZ is revealed by several positive markers of the eNZ. The clearest example is the restricted expression of the homeodomain transcription factor gene *Tlx3*, which clearly delineates the fourth EGL sub-domain aligned with the PC NZ (Logan et al., 2002). Expression of a neurotrophin-3-lacZ transgene is similarly restricted to the adult granular layer of the NZ, both during development and in the adult (Tojo et al., 1995), and the same boundary is seen when an *Atonal-cre* was used to eliminate *Neurod1* (Pan et al., 2009). Finally, a transverse discontinuity in the EGL is seen at the same approximate location in the heterozygous *weaver* mutant (*wv*/+, Eisenman et al., 1998; Armstrong and Hawkes, 2001).

The presence of transverse domains in the EGL is clear but evidence for parasagittal stripes is much less so. One candidate is in the young rabbit, where a monoclonal human granulocyte antibody B4,3 (= anti-CD15) reveals a striped expression pattern in the EGL (Marani and Tetteroo, 1983). Presumably this is a secondary induction via the underlying PC clusters or stripes. Another novel mediolateral pattern is seen in the evidence that one subgroup of GCPs in humans—concentrated in the hemispheres—is especially sensitive to *Shh* signaling and, perhaps as a result, is also more likely to give rise to medulloblastomas (Tan et al., 2018): how, if at all, this GCP mediolateral segregation relates to the anteroposterior EGL compartmentation, is unknown.

SUMMARY AND CONCLUSION

Mutant mice with cerebellar phenotypes have proved powerful tools to explore the mechanisms of pattern formation (Sidman et al., 1965). Abnormal patterns include missing cells, either never born (e.g., the *Zfp423Δ9-20* allele, Casoni et al., 2017; *Lmx1a*−/−, Chizhikov et al., 2010) or died (e.g., *Ebf2*−/−, Croci et al., 2006; Chung et al., 2008; selective granule cell death in *Neurod1*−/−: Miyata et al., 1999; Cho and Tsai, 2006), ectopias due to abnormal cell dispersal (e.g., for PCs, mutations in the Reln→Dab1 pathway or in *wv/wv*—Armstrong and Hawkes, 2001; for granule cells, examples include abnormal EGL migration in *Lmx1a*−/−, Chizhikov et al., 2010), and probably expression defects ("pattern defects" vs. "expression defects"; e.g., expression patterns induced by the local environment). These include 5′-nucleotidase expression by Bergmann glial cells induced by the local zebrin II + PCs (Scott, 1963; Eisenman and Hawkes, 1989) or abnormal tyrosine hydroxylase expression in *rolling mouse Nagoya* (*rol/rol*) a mutation in the α1 subunit of the calcium channel gene *Cacna1a* (Sawada et al., 1999), and the spontaneous *dilute-lethal* (*Myo5a*$^{d-l}$) mutant (Sawada et al., 1999).

It is remarkable how much light has been shed on cerebellar patterning and the mechanisms of pattern formation through

the analysis of mutant mouse strains. The mutant phenotypes reveal stages of patterning during development that become progressively complex. During PC generation and the formation of the cerebellar plate (E10–E13) there is at least some PC subtype specification, but whether the cerebellar plate contains a protomap is not known. From E14-E18, the cerebellar plate disperses into the embryonic PC cluster array. In parallel, during granule cell development, mutant phenotypes reveal reproducible boundaries within the EGL that arise often from distinct lineages in the URL (e.g., *rcm, cdf, mea* etc.). The transverse domains in the EGL and the zones in the PC layer become aligned during embryogenesis, but the mechanism that guides this is not well understood. As a result, by E18 the fundamental zone-and-stripe pattern is established. The embryonic bud is transformed into the adult flower during the first 3–4 postnatal weeks due to PC dispersal triggered by Reln→Dab1 signaling and granule cell migration from the EGL to the maturing granular layer. Finally, granular layer maturation reveals a further stage in cerebellar patterning—the subdivision of stripes into thousands of patches (e.g., Hawkes and Turner, 1994; Hawkes, 1997; Ozol and Hawkes, 1997; Sillitoe et al., 2003)—probably associated with inductive influences during the maturation of the mossy fiber projection maps (e.g., Shambes et al., 1978; Schilling et al., 1994).

AUTHOR CONTRIBUTIONS

The author confirms being the sole contributor of this work and has approved it for publication.

REFERENCES

Ackerman, S. L., Kozak, L. P., Przyborski, S. A., Rund, L. A., Boyer, B. B., and Knowles, B. B. (1997). The mouse rostral cerebellar malformation gene encodes an UNC-5-like protein. *Nature* 386, 838–842. doi: 10.1038/386838a0

Ahn, A. H., Dziennis, S., Hawkes, R., and Herrup, K. (1994). The cloning of zebrin II reveals its identity with aldolase C. *Development* 120, 2081–2090. doi: 10.1242/dev.120.8.2081

Akazawa, C., Ishibashi, M., Shimizu, C., Nakanishi, S., and Kageyama, R. (1995). A mammalian helix-loop-helix factor structurally related to the product of Drosophila proneural gene atonal is a positive transcriptional regulator expressed in the developing nervous system. *J. Biol. Chem.* 270, 8730–8738. doi: 10.1074/jbc.270.15.8730

Apps, R., and Hawkes, R. (2009). Cerebellar cortical organization: a one-map hypothesis. *Nat. Rev. Neurosci.* 10, 670–681. doi: 10.1038/nrn2698

Apps, R., Hawkes, R., Aoki, S., Bengtsson, F., and Brown, A. M. (2018). Cerebellar modules and their role as operational cerebellar processing units: a consensus paper. *Cerebellum* 17, 654–682. doi: 10.1007/s12311-018-0952-3

Armstrong, C. L., and Hawkes, R. (2014). *Pattern Formation in the Cerebellum.* San Rafael, CA: Morgan & Claypool, 138.

Armstrong, C. L., Krueger-Naug, A. M., Currie, R. W., and Hawkes, R. (2000). Constitutive expression of the 25-kDa heat shock protein Hsp25 reveals novel parasagittal bands of Purkinje cells in the adult mouse cerebellar cortex. *J. Comp. Neurol.* 416, 383–397. doi: 10.1002/(sici)1096-9861(20000117)416:3<383::aid-cne9>3.0.co;2-m

Armstrong, C. L., Krueger-Naug, A. M., Currie, R. W., and Hawkes, R. (2001). Expression of heat-shock protein Hsp25 in mouse Purkinje cells during development reveals novel features of cerebellar compartmentation. *J. Comp. Neurol.* 429, 7–21. doi: 10.1002/1096-9861(20000101)429:1<7::aid-cne2>3.0.co;2-q

Armstrong, C., and Hawkes, R. (2001). Selective purkinje cell ectopia in the cerebellum of the weaver mouse. *J. Comp. Neurol.* 439, 151–161. doi: 10.1002/cne.1339

Aruga, J., Minowea, O., Yaginuma, H., Kuno, J., Nagai, T., Noda, T., et al. (1998). Mouse Zic1 is involved in cerebellar development. *J. Neurosci.* 18, 284–293.

Badaloni, A., Casoni, F., Croci, L., Chiara, F., Bizzoca, A., Gennarini, G., et al. (2019). Dynamic expression and new functions of early B cell factor 2 in cerebellar development. *Cerebellum* 18, 999–1010. doi: 10.1007/s12311-019-01051-3

Bailey, K., Rahimi Balaei, M., Mannan, A., Del Bigio, M. R., and Marzban, H. (2014). Purkinje cell compartmentation in the cerebellum of the lysosomal acid phosphatase 2 mutant mouse (Nax - Naked-Ataxia mutant mouse). *PLoS One* 9:e94327. doi: 10.1371/journal.pone.0094327

Beierbach, E., Park, C., Ackerman, S. L., Goldowitz, D., and Hawkes, R. (2001). Abnormal dispersion of a Purkinje cell subset in the mouse cerebellar mutant cerebellar deficient folia (cdf). *J. Comp. Neurol.* 436, 42–51. doi: 10.1002/cne.1052

Ben-Arie, N., Bellen, H. J., Armstrong, D. L., McCall, A. E., Gordadze, P. R., Guo, Q., et al. (1997). Math1 is essential for genesis of cerebellar granule neurons. *Nature* 390, 169–172. doi: 10.1038/36579

Brochu, G., Maler, L., and Hawkes, R. (1990). Zebrin II: a polypeptide antigen expressed selectively by Purkinje cells reveals compartments in rat and fish cerebellum. *J. Comp. Neurol.* 291, 538–552. doi: 10.1002/cne.902910405

Casoni, F., Croci, L., Bosone, C., D'Ambrosio, R., Badaloni, A., Gaudesi, D., et al. (2017). Zfp423/ZNF423 regulates cell cycle progression, the mode of cell division and the DNA-damage response in Purkinje neuron progenitors. *Development* 144, 3686–3697. doi: 10.1242/dev.155077

Chizhikov, V. V., Lindgren, A. G., Currle, D. S., Rose, M. F., Monuki, E. S., Millen, K. J., et al. (2006). The roof plate regulates cerebellar cell-type specification and proliferation. *Development* 133, 2793–2804. doi: 10.1242/dev.02441

Chizhikov, V. V., Lindgren, A. G., Mishima, Y., Roberts, R. W., Aldinger, K. A., Miesegaes, G. R., et al. (2010). Lmx1a regulates fates and location of cells originating from the cerebellar rhombic lip and telencephalic cortical hem. *Proc. Natl. Acad. Sci. U.S.A.* 107, 10725–10730. doi: 10.1073/pnas.0910786107

Cho, J. H., and Tsai, M. J. (2006). Preferential posterior cerebellum defect in BETA2/NeuroD1 knockout mice is the result of differential expression of BETA2/NeuroD1 along anterior-posterior axis. *Dev. Biol.* 290, 125–138. doi: 10.1016/j.ydbio.2005.11.024

Chung, S. H., Marzban, H., Croci, L., Consalez, G. G., and Hawkes, R. (2008). Purkinje cell subtype specification in the cerebellar cortex: early B-cell factor 2 acts to repress the zebrin II-positive Purkinje cell phenotype. *Neuroscience* 153, 721–732. doi: 10.1016/j.neuroscience.2008.01.090

Consalez, G. G., and Hawkes, R. (2013). The compartmental restriction of cerebellar interneurons. *Front. Neural Circuits* 6:123.

Consalez, G. G., Goldowitz, D., Casoni, F., and Hawkes, R. (2021). Origins, development and compartmentation of the granule cells of the cerebellum. *Front. Neural Circuits* 14:6.

Croci, L., Barili, V., Chia, D., Massimino, L., Van Vugt, R., Masserdotti, G., et al. (2011). Local insulin-like growth factor i expression is essential for Purkinje neuron survival at birth. *Cell Death Differ.* 18, 48–59. doi: 10.1038/cdd.2010.78

Croci, L., Chung, S. H., Masserdotti, G., Gianola, S., Bizzoca, A., Gennarini, G., et al. (2006). A key role for the HLH transcription factor EBF2COE2,O/E-3 in Purkinje neuron migration and cerebellar cortical topography. *Development* 133, 2719–2729. doi: 10.1242/dev.02437

D'Arcangelo, G. (2014). Reelin in the years: controlling neuronal migration and maturation in the mammalian brain. *Adv. Neurosci.* 2014, 4–19.

Dastjerdi, F. V., Consalez, G. G., and Hawkes, R. (2012). Pattern formation during development of the embryonic cerebellum. *Front. Neuroanat.* 6:10.

Eisenman, L. M., and Brothers, R. (1998). Rostral cerebellar malformation (rcm/rcm): a murine mutant to study regionalization of the cerebellum. *J. Comp. Neurol.* 394, 106–117. doi: 10.1002/(sici)1096-9861(19980427)394:1<106::aid-cne8>3.0.co;2-4

Eisenman, L. M., and Hawkes, R. (1989). 5'-Nucleotidase and the mabQ113 antigen share a common distribution in the cerebellar cortex of the mouse. *Neuroscience* 31, 231–235. doi: 10.1016/0306-4522(89)90045-6

Eisenman, L. M., Gallagher, E., and Hawkes, R. (1998). Regionalization defects in the weaver mouse cerebellum. *J. Comp. Neurol.* 394, 431–444. doi: 10.1002/(sici)1096-9861(19980518)394:4<431::aid-cne3>3.0.co;2-2

Falconer, D. S. (1951). Two new mutants, "trembler" and "reeler", with neurological actions in the house mouse (*Mus musculus* L.). *J. Genet.* 50, 192–205. doi: 10.1007/bf02996215

Frantz, G. D., Weimann, J. M., Levin, M. E., and McConnell, S. K. (1994). Otx1 and Otx2 define layers and regions in developing cerebral cortex and cerebellum. *J. Neurosci.* 14, 5725–5740. doi: 10.1523/JNEUROSCI.14-10-05725.1994

Fujita, H., Morita, N., Furuichi, T., and Sugihara, I. (2012). Clustered fine compartmentalization of the mouse embryonic cerebellum and its rearrangement into the postnatal striped configuration. *J. Neurosci.* 32, 15688–15703. doi: 10.1523/JNEUROSCI.1710-12.2012

Gallagher, E., Howell, B. W., Soriano, P., Cooper, J. A., and Hawkes, R. (1998). Cerebellar abnormalities in the disabled (mdab1-1) mouse. *J. Comp. Neurol.* 402, 238–251. doi: 10.1002/(sici)1096-9861(19981214)402:2<238::aid-cne8>3.0.co;2-h

Gold, D. A., Baek, S. H., Schork, N. J., Rose, D. W., Larsen, D. D., Sachs, B. D., et al. (2003). RORα coordinates reciprocal signaling in cerebellar development through sonic hedgehog and calcium-dependent pathways. *Neuron* 40, 1119–1131. doi: 10.1016/s0896-6273(03)00769-4

Goldowitz, D., Hamre, K. M., Przyborski, S. A., and Ackerman, S. L. (2000). Granule cells and cerebellar boundaries: analysis of Unc5h3 mutant chimeras. *J. Neurosci.* 20, 4129–4137. doi: 10.1523/JNEUROSCI.20-11-04129.2000

Hamre, K. M., and Goldowitz, D. (1997). Meander tail acts intrinsic to granule cell precursors to disrupt cerebellar development: analysis of meander tail chimeric mice. *Development* 124, 4201–4212. doi: 10.1242/dev.124.21.4201

Hashimoto, M., and Mikoshiba, K. (2003). Mediolateral compartmentation of the cerebellum is determined on the "birth date" of Purkinje cells. *J. Neurosci.* 23, 11342–11351. doi: 10.1523/JNEUROSCI.23-36-11342.2003

Hawkes, R. (1997). An anatomical model of cerebellar modules. *Prog. Brain Res.* 114, 39–52. doi: 10.1016/s0079-6123(08)63357-9

Hawkes, R., and Turner, R. W. (1994). Compartmentation of NADPH-diaphorase activity in the mouse cerebellar cortex. *J. Comp. Neurol.* 346, 499–516. doi: 10.1002/cne.903460404

Hawkes, R., Beierbach, E., and Tan, S. S. (2008). Granule cell dispersion is restricted across transverse boundaries in mouse chimeras. *Eur. J. Neurosci.* 11, 3800–3808. doi: 10.1046/j.1460-9568.1999.00812.x

Hiesberger, T., Trommsdorff, M., Howell, B. W., Goffinet, A., Mumby, M. C., Cooper, J. A., et al. (1999). Direct binding of Reelin to VLDL receptor and ApoE receptor 2 induces tyrosine phosphorylation of disabled-1 and modulates tau phosphorylation. *Neuron* 24, 481–489. doi: 10.1016/s0896-6273(00)80861-2

Hoffarth, R. M., Johnston, J. G., Krushel, L. A., and van der Kooy, D. (1995). The mouse mutation reeler causes increased adhesion within a subpopulation of early postmitotic cortical neurons. *J. Neurosci.* 15, 4838–4850. doi: 10.1523/JNEUROSCI.15-07-04838.1995

Hoshino, M., Nakamura, S., Mori, K., Kawauchi, T., Terao, M., Nishimura, Y. V., et al. (2005). Ptf1a, a bHLH transcriptional gene, defines GABAergic neuronal fates in cerebellum. *Neuron* 47, 201–213. doi: 10.1016/j.neuron.2005.06.007

Howell, B. W., Hawkes, R., Soriano, P., and Cooper, J. A. (1997). Neuronal positioning in the developing brain is regulated by mouse disabled-1. *Nature* 389, 733–737. doi: 10.1038/39607

Howell, B. W., Herrick, T. M., and Cooper, J. A. (1999). Reelin-induced tyrosine phosphorylation of disabled 1 during neuronal positioning. *Genes Dev.* 13, 643–648. doi: 10.1101/gad.13.6.643

Jankowski, J., Miething, A., Schilling, K., Oberdick, J., and Baader, S. (2011). Cell death as a regulator of cerebellar histogenesis and compartmentation. *Cerebellum* 10, 373–392. doi: 10.1007/s12311-010-0222-5

Karam, S. D., Burrows, R. C., Logan, C., Koblar, S., Pasquale, E. B., and Bothwell, M. (2000). Eph receptors and ephrins in the developing chick cerebellum: relationship to sagittal patterning and granule cell migration. *J. Neurosci.* 20, 6488–6500. doi: 10.1523/JNEUROSCI.20-17-06488.2000

Kim, J. Y., Marzban, H., Chung, S., Watanabe, M., Eisenman, L. M., and Hawkes, R. (2009). Purkinje cell compartmentation of the cerebellum of microchiropteran bats. *J. Comp. Neurol.* 517, 193–219. doi: 10.1002/cne.22147

Kuemerle, B., Zanjani, H., Joyner, A., and Herrup, K. (1997). Pattern deformities and cell loss in Engrailed-2 mutant mice suggest two separate patterning events during cerebellar development. *J. Neurosci.* 17, 7881–7889. doi: 10.1523/JNEUROSCI.17-20-07881.1997

Larouche, M., Beffort, U., Herz, J., and Hawkes, R. (2008). The reelin receptors Apoer2 and Vldlr coordinate the patterning of Purkinje cell topography in the developing mouse cerebellum. *PLoS One* 3:e1653. doi: 10.1371/journal.pone.0001653

Legué, E., Riedel, E., and Joyner, A. L. (2015). Clonal analysis reveals granule cell behaviors and compartmentalization that determine the folded morphology of the cerebellum. *Development* 142, 1661–1671. doi: 10.1242/dev.120287

Leto, K., Arancillo, M., Becker, E. B., Buffo, A., Chiang, C., Ding, B., et al. (2016). Consensus paper: cerebellar development. *Cerebellum* 15, 789–828.

Lewis, P. M., Gritli-Linde, A., Smeyne, R., Kottmann, A., and McMahon, A. P. (2004). Sonic hedgehog signaling is required for expansion of granule neuron precursors and patterning of the mouse cerebellum. *Dev. Biol.* 270, 393–410. doi: 10.1016/j.ydbio.2004.03.007

Logan, C., Millar, C., Bharadia, V., and Rouleau, K. (2002). Onset of Tlx-3 expression in the chick cerebellar cortex correlates with the morphological development of fissures and delineates a posterior transverse boundary. *J. Comp. Neurol.* 448, 138–149. doi: 10.1002/cne.10234

Lundell, T. G., Zhou, Q., and Doughty, M. L. (2009). Neurogenin1 expression in cell lineages of the cerebellar cortex in embryonic and postnatal mice. *Dev. Dyn.* 238, 3310–3325. doi: 10.1002/dvdy.22165

Machold, R., and Fishell, G. (2005). Math1 is expressed in temporally discrete pools of cerebellar rhombic-lip neural progenitors. *Neuron* 48, 17–24. doi: 10.1016/j.neuron.2005.08.028

Marani, E., and Tetteroo, P. A. (1983). A longitudinal band-pattern for the monoclonal human granulocyte antibody B4,3 in the cerebellar external granular layer of the immature rabbit. *Histochemistry* 78, 157–161. doi: 10.1007/BF00489494

Marzban, H., Chung, S., Watanabe, M., and Hawkes, R. (2007). Phospholipase cß4 expression reveals the continuity of cerebellar topography through development. *J. Comp. Neurol.* 502, 857–871. doi: 10.1002/cne.21352

Marzban, H., Hoy, N., Aavani, T., Sarko, D. K., Catania, K. C., and Hawkes, R. (2011). Compartmentation of the cerebellar cortex in the naked mole-rat (*Heterocephalus glaber*). *Cerebellum* 10, 435–448. doi: 10.1007/s12311-011-0251-8

Marzban, H., Hoy, N., Buchok, M., Catania, K. C., and Hawkes, R. (2015). Compartmentation of the cerebellar cortex: adaptation to lifestyle in the star-nosed mole Condylura cristata. *Cerebellum* 14, 106–118. doi: 10.1007/s12311-014-0618-8

Marzban, H., Kim, C.-T., Doorn, D., Chung, S. H., and Hawkes, R. (2008). A novel transverse expression domain in the mouse cerebellum revealed by a neurofilament-associated antigen. *Neuroscience* 153, 1190–1201. doi: 10.1016/j.neuroscience.2008.02.036

Marzban, H., Sillitoe, R. V., Hoy, M., Chung, S.-H., Rafuse, V. F., and Hawkes, R. (2004). Abnormal HNK-1 expression in the cerebellum of an N-CAM null mouse. *J. Neurocytol.* 33, 117–130. doi: 10.1023/B:NEUR.0000029652.96456.0d

McAndrew, P. E., Frostholm, A., Evans, J. E., Zdilar, D., Goldowitz, D., Chiu, I. M., et al. (1998). Novel receptor protein tyrosine phosphatase (RPTPrho) and acidic fibroblast growth factor (FGF-1) transcripts delineate a rostrocaudal boundary in the granule cell layer of the murine cerebellar cortex. *J. Comp. Neurol.* 391, 444–455. doi: 10.1002/(sici)1096-9861(19980222)391:4<444::aid-cne3>3.0.co;2-0

Millen, K. J., Wurst, W., Herrup, K., and Joyner, A. L. (1994). Abnormal embryonic cerebellar development and patterning of postnatal foliation in two mouse Engrailed-2 mutants. *Development* 120, 695–706. doi: 10.1242/dev.120.3.695

Millonig, J. H., Millen, K. J., and Hatten, M. E. (2000). The mouse Dreher gene Lmx1a controls formation of the roof plate in the vertebrate CNS. *Nature* 403, 764–769. doi: 10.1038/35001573

Miyata, T., Maeda, T., and Lee, J. E. (1999). NeuroD is required for differentiation of the granule cells in the cerebellum and hippocampus. *Genes Dev.* 13, 1647–1652. doi: 10.1101/gad.13.13.1647

Nimura, T., Itoh, T., Hagio, H., Hasyashi, T., Donato, V. D., Takeuchi, M., et al. (2019). Role of reelin in cell positioning in the cerebellum and the cerebellum-like structure in zebrafish. *Dev. Biol.* 455, 393–408. doi: 10.1016/j.ydbio.2019.07.010

Nunzi, M. G., Grillo, M., Margolis, F. L., and Mugnaini, E. (1999). Compartmental organization of Purkinje cells in the mature and developing mouse cerebellum as revealed by an olfactory marker protein-lacZ transgene. *J. Comp. Neurol.* 404, 97–113. doi: 10.1002/(sici)1096-9861(19990201)404:1<97::aid-cne8>3.3.co;2-t

Ozol, K. O., and Hawkes, R. (1997). Compartmentation of the granular layer of the cerebellum. *Histol. Histopathol.* 12, 171–184.

Ozol, K., Hayden, J. M., Oberdick, J., and Hawkes, R. (1999). Transverse zones in the vermis of the mouse cerebellum. *J. Comp. Neurol.* 412, 95–111.

Pan, N., Jahan, I., Lee, J. E., and Fritzch, B. (2009). Defects in the cerebella of conditional Neurod1 null mice correlate with effective Tg(Atoh1-cre) recombination and granule cell requirements for Neurod1 for differentiation. *Cell Tissue Res.* 337, 407–428. doi: 10.1007/s00441-009-0826-6

Rakic, P. (1988). Specification of cerebral cortical areas. *Science* 241, 170–176. doi: 10.1126/science.3291116

Redies, C., Neudert, F., and Lin, J. (2011). Cadherins in cerebellar development: translation of embryonic patterning into mature functional compartmentalization. *Cerebellum* 10, 393–408. doi: 10.1007/s12311-010-0207-4

Ross, M. E., Fletcher, C., Mason, C. A., Hatten, M. E., and Heintz, N. (1990). Meander tail reveals a discrete developmental unit in the mouse cerebellum. *Proc. Natl. Acad. Sci. U.S.A.* 87, 4189–4192. doi: 10.1073/pnas.87.11.4189

Sarna, J. R., and Hawkes, R. (2003). Patterned Purkinje cell death in the cerebellum. *Prog. Neurobiol.* 70, 473–507. doi: 10.1016/s0301-0082(03)00114-x

Sarna, J. R., Marzban, H., Watanabe, M., and Hawkes, R. (2006). Complementary stripes of phospholipase Cß3 and Cß4 expression by Purkinje cell subsets in the mouse cerebellum. *J. Comp. Neurol.* 496, 303–313. doi: 10.1002/cne.20912

Sarna, J., Miranda, R. P., Schuchman, E. H., and Hawkes, R. (2001). Patterned cerebellar Purkinje cell death in a transgenic model of Niemann Pick Type A/B disease. *Eur. J. Neurosci.* 13, 1873–1880. doi: 10.1046/j.0953-816x.2001.01564.x

Sawada, K., Komatsu, S., Haga, H., Sun, X. Z., Hisano, S., and Fukui, Y. (1999). Abnormal expression of tyrosine hydroxylase immunoreactivity in the cerebellar cortex of ataxic mutant mice. *Brain Res.* 829, 107–112. doi: 10.1016/s0006-8993(99)01347-5

Schilling, K., Schmidt, H. H., and Baader, S. L. (1994). Nitric oxide synthase expression reveals compartments of cerebellar granule cells and suggests a role for mossy fibers in their development. *Neuroscience* 59, 893–903. doi: 10.1016/0306-4522(94)90293-3

Schuurmans, C., Armant, O., Nieto, M., Stenman, J. M., Britz, O., Klenin, N., et al. (2004). Sequential phases of cortical specification involve neurogenin-dependent and -independent pathways. *EMBO J.* 23, 2892–2902. doi: 10.1038/sj.emboj.7600278

Scott, T. G. (1963). A unique pattern of localization within the cerebellum. *Nature* 200:793. doi: 10.1038/200793a0

Sentürk, A., Pfennig, S., Weiss, A., Burk, K., and Acker-Palmer, A. (2011). Ephrin Bs are essential components of the reelin pathway to regulate neuronal migration. *Nature* 472, 356–360. doi: 10.1038/nature09874

Shambes, G. M., Gibson, J. M., and Welker, W. (1978). Fractured somatotopy in granule cell tactile areas of rat cerebellar hemispheres revealed by micromapping. *Brain Behav. Evol.* 15, 94–140. doi: 10.1159/000123774

Sheldon, M., Rice, D. S., D'Arcangelo, G., Yoneshima, H., Nakajima, K., Mikoshiba, K., et al. (1997). Scrambler and yotari disrupt the disabled gene and produce a reeler-like phenotype in mice. *Nature* 389, 730–733. doi: 10.1038/39601

Sidman, R. L., Green, M. C., and Appel, S. (1965). *Catalog of the Neurological Mutants of the Mouse*. Cambridge, MA: Harvard University Press.

Sillitoe, R. V., Benson, M. A., Blake, D. J., and Hawkes, R. (2003). Abnormal dysbindin expression in cerebellar mossy fiber synapses in the mdx mouse model of Duchenne muscular dystrophy. *J. Neurosci.* 23, 6576–6585. doi: 10.1523/JNEUROSCI.23-16-06576.2003

Sillitoe, R. V., George-Jones, N. A., Millen, K. J., and Hawkes, R. (2014). Purkinje cell compartmentalization in the cerebellum of the spontaneous mutant mouse dreher. *Brain Struct. Funct.* 219, 35–47. doi: 10.1007/s00429-012-0482-6

Sillitoe, R. V., Gopal, N., and Joyner, A. L. (2009). Embryonic origins of zebrinII parasagittal stripes and establishment of topographic Purkinje cell projections. *Neuroscience* 162, 574–588. doi: 10.1016/j.neuroscience.2008.12.025

Sillitoe, R. V., Marzban, H., Larouche, M., Zahedi, S., Affani, J., and Hawkes, R. (2005). Conservation of the architecture of the anterior lobe vermis of the cerebellum across mammalian species. *Prog. Brain Res.* 148, 283–297. doi: 10.1016/S0079-6123(04)48022-4

Sillitoe, R. V., Vogel, M. W., and Joyner, A. L. (2010). Engrailed homeobox genes regulate establishment of the cerebellar afferent circuit map. *J. Neurosci.* 30, 10015–10024. doi: 10.1523/JNEUROSCI.0653-10.2010

Smeyne, R. J., and Goldowitz, D. (1989). Development and death of external granular layer cells in the weaver mouse cerebellum: a quantitative study. *J. Neurosci.* 9, 1608–1620. doi: 10.1523/jneurosci.09-05-01608.1989

Smeyne, R. J., Chu, T., Lewin, A., Bian, F., Sanlioglu, S., Kunsch, C., et al. (1995). Local control of granule cell generation by cerebellar Purkinje cells. *Mol. Cell. Neurosci.* 6, 230–251.

Surmeier, D. J., Mermelstein, P. G., and Goldowitz, D. (1996). The weaver mutation of GIRK2 results in a loss of inwardly rectifying K+ current in cerebellar granule cells. *Proc. Natl. Acad. Sci. U.S.A.* 93, 11191–11195. doi: 10.1073/pnas.93.20.11191

Swanson, D. J., and Goldowitz, D. (2011). Experimental Sey mouse chimeras reveal the developmental deficiencies of Pax6-null granule cells in the postnatal cerebellum. *Dev. Biol.* 351, 1–12. doi: 10.1016/j.ydbio.2010.11.018

Tan, I. L., Wojcinski, A., Rallapalli, H., Lao, Z., Sanghrajka, R. M., Stephen, D., et al. (2018). Lateral cerebellum is preferentially sensitive to high sonic hedgehog signaling and medulloblastoma formation. *Proc. Natl. Acad. Sci. USA* 115, 3392–3397. doi: 10.1073/pnas.1717815115

Tano, D., Napieralski, J. A., Eisenman, L. M., Messer, A., Plummer, J., and Hawkes, R. (1992). Novel developmental boundary in the cerebellum revealed by zebrin II expression in the Lurcher (Lc/+) mutant mouse. *J. Comp. Neurol.* 323, 128–136. doi: 10.1002/cne.903230111

Tojo, H., Takami, K., Kaisho, Y., Nakata, M., Abe, T., Shiho, O., et al. (1995). Neurotrophin-3 is expressed in the posterior lobe of mouse cerebellum, but does not affect the cerebellar development. *Neurosci. Lett.* 192, 169–172. doi: 10.1016/0304-3940(95)11637-c

Trommsdorff, M., Gotthardt, M., Hiesberger, T., Shelton, J., Stockinger, W., Nimpf, J., et al. (1999). Reeler/Disabled-like disruption of neuronal migration in knockout mice lacking the VLDL receptor and ApoE receptor 2. *Cell* 97, 689–701. doi: 10.1016/s0092-8674(00)80782-5

Vibulyaseck, S., Fujita, H., Luo, Y., Tran, A. K., Oh-Nishi, A., Ono, Y., et al. (2017). Spatial rearrangement of Purkinje cell subsets forms the transverse and longitudinal compartmentalization in the mouse embryonic cerebellum. *J. Comp. Neurol.* 525, 2971–2990. doi: 10.1002/cne.24250

Vitalis, T., and Mariani, J. (2018). Retinoid receptor-related orphan receptor alpha: a key gene setting brain circuits. *Neural Regen. Res.* 13, 791–794. doi: 10.4103/1673-5374.232462

Vogel, M. W. (2002). Cell death, bcl-2, bax, and the cerebellum. *Cerebellum* 1, 277–287. doi: 10.1080/147342202320883588

Warming, S., Rivka, R. A., Jenkins, N. A., and Copeland, N. G. (2006). Zfp423 is required for normal cerebellar development. *Mol. Cell. Biol.* 26, 6913–6922. doi: 10.1128/MCB.02255-05

Wassef, M., and Sotelo, C. (1985). Transient biochemical compartmentalization of Purkinje cells during early cerebellar development. *Dev. Biol.* 111, 129–137.

Wollmuth, L. P., Kuner, T., Jatzke, C., Seeburg, P. H., Heintz, N., and Zuo, J. (2000). The Lurcher mutation identifies delta 2 as an AMPA/kainate receptor-like channel that is potentiated by Ca(2+). *J. Neurosci.* 20, 5973–5980. doi: 10.1523/JNEUROSCI.20-16-05973.2000

Yeung, J., Ha, T. J., Swanson, D. J., Choi, K., Tong, Y., and Goldowitz, D. (2014). Wls provides a new compartmental view of the rhombic lip in mouse cerebellar development. *J. Neurosci.* 34, 12527–12537. doi: 10.1523/JNEUROSCI.1330-14.2014

Zordan, P., Croci, L., Hawkes, R., and Consalez, G. G. (2008). A comparative analysis of proneural gene expression in the embryonic cerebellum. *Dev. Dyn.* 237, 1726–1735.

Conflict of Interest: The author declares that the research was conducted in the absence of any commercial or financial relationships that could be construed as a potential conflict of interest.

frontiers in Neuroscience

REVIEW
published: 09 December 2021
doi: 10.3389/fnins.2021.772382

Congenital Hypothyroidism and Brain Development: Association With Other Psychiatric Disorders

Katsuya Uchida[1] and Mao Suzuki[2]*

[1] *Laboratory of Information Biology, Graduate School of Information Sciences, Tohoku University, Sendai, Japan,*
[2] *Laboratory of Biomodeling, Graduate School of Information Sciences, Tohoku University, Sendai, Japan*

Thyroid hormones play an important role in brain development, and thyroid hormone insufficiency during the perinatal period results in severe developmental delays. Perinatal thyroid hormone deficiency is clinically known as congenital hypothyroidism, which is caused by dysgenesis of the thyroid gland or low iodine intake. If the disorder is not diagnosed or not treated early, the neuronal architecture is perturbed by thyroid hormone insufficiency, and neuropathological findings, such as abnormal synapse formation, defects in neuronal migration, and impairment of myelination, are observed in the brains of such patients. Furthermore, the expression of psychiatric disorder-related molecules, especially parvalbumin, is significantly decreased by thyroid hormone insufficiency during the perinatal period. Animal experiments using hypothyroidism models display decreased parvalbumin expression and abnormal brain architecture, and these experimental results show reproducibility and stability. These basic studies reinforce the results of epidemiological studies, suggesting the relevance of thyroid dysfunction in psychiatric disorders. In this review, we discuss the disruption of brain function associated with congenital hypothyroidism from the perspective of basic and clinical research.

Keywords: thyroid hormone, hypothyroid, developmental disorder, parvalbumin, psychiatric disorder, MeCP2

OPEN ACCESS

Edited by:
Kazuhiko Sawada, Tsukuba International University, Japan

Reviewed by:
Farimah Beheshti, Torbat Heydarieh University of Medical Sciences, Iran
Aaron Hanukoglu, Tel Aviv University, Israel

****Correspondence:***
Katsuya Uchida
uchida@m.tohoku.ac.jp

Specialty section:
This article was submitted to Neurodevelopment, a section of the journal Frontiers in Neuroscience

Received: *08 September 2021*
Accepted: *17 November 2021*
Published: *09 December 2021*

Citation:
Uchida K and Suzuki M (2021) Congenital Hypothyroidism and Brain Development: Association With Other Psychiatric Disorders. Front. Neurosci. 15:772382. doi: 10.3389/fnins.2021.772382

INTRODUCTION

Thyroid hormones are synthesized in and released by the thyroid gland, with thyroxine (T4) comprising the highest concentration of these hormones. T4 is released from the thyroid gland and converted to triiodothyronine (T3) by deiodinase; T3 is highly biologically active as a transcription factor that plays important roles in brain development. This includes its roles in glial myelination, neuronal migration, cortical layer formation, synaptogenesis, and neurogenesis (Nicholson and Altman, 1972; Oppenheimer and Schwartz, 1997; Koibuchi and Chin, 2000; Uchida et al., 2005). Therefore, thyroid hormones during the perinatal period are important for normal development of the brain, and congenital hypothyroidism causes serious developmental delay if proper treatment is not implemented immediately after birth in such patients (Morreale de Escobar et al., 1987; Rastogi and LaFranchi, 2010). Thyroid dysfunction can be clinically detected by mass screening immediately after birth, and developmental disorders can be avoided by treatment with levothyroxine (T4).

Therapy for thyroid dysfunction has been established; however, neuroscientific research using rodent models is still ongoing because thyroid hormones are involved in diverse aspects of neurodevelopment, and thyroid hormone research in turn has the potential to provide new insights. A typical neuropathological finding caused by thyroid hormone insufficiency is a decrease in the parvalbumin of GABAergic neurons. This phenomenon is of interest to many researchers because it is observed not only in thyroid hormone insufficiency, but also in the dysfunction of thyroid hormone receptors and iodothyronine deiodinase (Berbel et al., 1996; Gilbert et al., 2007; Wallis et al., 2008; Barez-Lopez et al., 2019). In other words, the decrease in parvalbumin in GABAergic neurons is closely linked to the thyroid system. In addition, in recent years, a decrease in parvalbumin has been observed in the postmortem brains of patients with autism and schizophrenia, reaffirming the importance of thyroid hormone research in these conditions (Hashimoto et al., 2003; Lawrence et al., 2010; Soghomonian et al., 2017). Furthermore, parvalbumin neurons are lost in the cerebral cortex of mice lacking methyl CpG binding protein 2 (MeCP2), the gene responsible for Rett syndrome (RTT) (Fukuda et al., 2005). Recently, abnormalities in thyroid function in RTT patients have also been reported (Stagi et al., 2015). Herein, we present the neuropathological findings observed in experimental hypothyroidism (animal study) and congenital hypothyroidism, discuss the relationship between some psychiatric disorders and hypothyroidism, and review the importance of thyroid hormones in brain development.

ROLE OF THYROID HORMONE ON THE BRAIN ARCHITECTURE

The role of thyroid hormones in brain development has long been studied, and numerous studies have been published to date. Congenital hypothyroidism that is not diagnosed or not treated early causes developmental delay, which, as mentioned above, is triggered by abnormalities in neural architecture during brain development. Notably, maternal hypothyroidism during pregnancy has long-lasting effects on the cortical morphology of their offspring, with specific effects reflecting both the severity and timing of maternal thyroid hormone insufficiency (Lischinsky et al., 2016). Furthermore, Cooper et al. (2019) reported that individuals with severe congenital hypothyroidism are at risk of developing white matter microstructural abnormalities, despite early detection and treatment. In congenital hypothyroidism, neuropathological features such as abnormalities in neuritogenesis of Purkinje cells in the cerebellum, myelin sheath hypoplasia in myelinated nerves, and dysgenesis of dendrite spine formation are observed in the developmental and mature brain. However, the effects of thyroid hormone deficiency are not only observed in local cellular structures, but also in neural architecture and signal transmission between the cerebral hemisphere *via* the corpus callosum (Berbel et al., 1993; Samadi et al., 2015). Although cell positioning during corticogenesis follows an inside-out pattern, radial neurogenic gradients are more diffuse than in normal animals. This difference in radial migration may be attributed to reduced reelin mRNA and protein in Cajal–Retzius cells observed in hypothyroid animals during the perinatal period. Since the administration of T3 to hypothyroid rats restores reelin mRNA expression both *in vitro* and *in vivo* (Alvarez-Dolado et al., 1999), the formation of radial neurogenic gradients may be highly dependent on thyroid hormones. Regarding the commissural fibers, the commissural neurons that form cortical layer II/III in the cortex are connected to the contralateral hemisphere *via* the corpus callosum. In general, retrograde neural tracers administered to the primary auditory cortex are widely distributed in the cortical layers of the contralateral side; however, in hypothyroid animals, tracer signals converge in cortical layers IV–V of the contralateral side of the primary auditory cortex (Berbel et al., 1993). Furthermore, Goodman and Gilbert (2007) reported that thyroid hormone insufficiency induced cellular malformation in the corpus callosum. Abnormalities in neural connections between the cerebral hemispheres, hence, would have a very strong impact on integrated brain functions (**Table 1**). In fact, abnormalities associated with commissural fibers have been observed not only in hypothyroidism but also in autism spectrum disorder (ASD) and attention deficit hyperactivity disorder (Casanova et al., 2011; Qiu et al., 2011; Ameis et al., 2016), indicating that defects in brain structures involved in functional integration affect behavioral expression. Thus, thyroid hormones participate in various aspects of the developing brain.

INVOLVEMENT OF THYROID HORMONE ON PARVALBUMIN EXPRESSION

Parvalbumin is a calcium-binding protein and a type of albumin with a small molecular weight (12 kD) (Arif, 2009). Parvalbumin is expressed in GABAergic neurons in the central nervous system, and parvalbumin-expressing neurons are mainly observed in the cortex, hippocampus, cerebellum, and reticular hypothalamic nucleus (Celio, 1986, 1990; Kosaka et al., 1987). Parvalbumin-expressing GABAergic neurons are generated from the medial ganglionic eminence and migrate tangentially to their respective destination areas (Danglot et al., 2006). In the cortex and hippocampus, the developmental expression of parvalbumin mRNA is observed from approximately postnatal day 10, and gradually increases daily (de Lecea et al., 1995). Parvalbumin neurons differentiate into basket and chandelier cells and function as fast-spiking interneurons (Hu et al., 2014).

Berbel et al. (1996) first reported the microstructural differences in parvalbumin neurons in adult hypothyroid rats. This report indicated that hypothyroid rats showed dysgenesis of parvalbumin-positive terminal puncta in the neocortex, while there were no differences observed in the number of parvalbumin neurons. Guadano-Ferraz et al. (2003) also reported that thyroid hormone receptor alpha 1-deficient mice displayed a decrease in the density of parvalbumin-positive terminals in the hippocampus. These two reports mainly showed the effect of hypothyroidism on the nerve endings of parvalbumin neurons. In contrast, a decrease in the number of parvalbumin neurons in the cortex and

TABLE 1 | Role of thyroid hormone on the brain architecture.

Species	State	References	Histological features
Human	Hypothyroidism	Lischinsky et al. (2016)	Cortical thinning and thickening
Human	Hypothyroidism	Cooper et al. (2019)	White matter microstructural abnormalities
Rat	Experimental hypothyroidism (MMI)	Berbel et al. (1993)	Dysgenesis of cortical layers and callosal connections
Human	Hypothyroidism	Samadi et al. (2015)	Dysgenesis of the corpus callosum
Rat	Experimental hypothyroidism (MMI)	Alvarez-Dolado et al. (1999)	Decreased in reelinRNA and protein
Rat	Experimental hypothyroidism (PTU)	Goodman and Gilbert (2007)	Cellular malformation in the corpus callosum

MMI, methimazole; PTU, propylthiouracil.

other regions has been shown in monocarboxylate transporter 8 (MCT8) and deiodinase type 2 (Dio2)-double deficient mice (Barez-Lopez et al., 2019). MCT8 actively transports a variety of iodothyronines, including thyroid hormones (T3 and T4) (Friesema et al., 2003), and Dio2 activates thyroid hormones by converting the prohormone T4 to bioactive T3 (Croteau et al., 1996). In mice, single mutations of MCT8 or Dio2 do not cause a significant decrease in the number of parvalbumin neurons due to compensatory effects. Therefore, double deficiency of MCT8 and Dio2 as well as severe thyroid hormone dysfunction may lead to a decrease in the number of parvalbumin neurons in mice. Gilbert et al. (2007) reported in detail the effects of thyroid hormone insufficiency on parvalbumin expression. Interestingly, animal models of congenital hypothyroidism display a significant decrease in the number of parvalbumin neurons during the juvenile phase, and the levels of parvalbumin expression slightly catch up with those of normal animals, with recovery of serum thyroid hormone levels after the termination of treatment with antithyroid agents. However, the degree of the decrease in parvalbumin neuron number and its subsequent recovery is dependent on the concentration of antithyroid agents, and significant recovery of the number of parvalbumin-expressing neurons was observed in the low concentration exposure group, but not in the high concentration exposure group. Thus, even though the levels of serum thyroid hormone completely recover in adulthood, animals that experience thyroid hormone deficiency during the perinatal period still retain the signatures of temporary hormonal defects in parvalbumin neurons in the adult brain. As a result of this occurrence, dysfunction of neuron-specific K(+)/Cl(−) co-transporter (KCC2) and a delayed onset of synaptic inhibition have been observed accordingly (Friauf et al., 2008; Yi et al., 2014). In general, during the first 2 weeks after birth, synaptic transmission *via* the inhibitory transmitter changes from excitatory depolarizing to inhibitory hyperpolarizing effects in GABAergic neurons (Cherubini et al., 1991; Rivera et al., 1999). Therefore, delay in the functional conversion of inhibitory neurons may significantly perturb the integrative function of inhibitory neural circuits in the hypothyroid brain.

On the other hand, just as treatment with levothyroxine avoids developmental delay accompanying congenital hypothyroidism in humans, thyroid hormone replacement immediately after birth can prevent a decrease in the number of parvalbumin neurons in rodents (Gilbert et al., 2007; Uchida et al., 2014, 2021). Thyroid hormone replacement after postnatal day 14 has no effect on the number of parvalbumin neurons, suggesting that a critical period of thyroid hormone sensitivity exists before this day (Gilbert et al., 2007; Uchida et al., 2014, 2021). Interestingly, a transient increase in blood thyroid hormone levels was observed around postnatal day 14 (Fishman et al., 1982; Calikoglu et al., 1996; Hadj-Sahraoui et al., 2000). Hence, the hormonal surge and/or the abundance of hormones in the early postnatal period might be important for normal neurodevelopment, including maturation of parvalbumin neurons. As mentioned above, parvalbumin expression and its morphogenesis have been observed to correlate with thyroid hormone levels; however, the direct or indirect action of TH on the transcription of PV genes remains unclear.

Similar to observations in patients with MCT8 mutations, loss of parvalbumin expression has been observed in the brains of patients with schizophrenia and autism (Hashimoto et al., 2003; Lopez-Espindola et al., 2014; Filice et al., 2020). Since these psychiatric disorders are observed in perturbation of executive functions, parvalbumin expression in the human prefrontal cortex has been preferentially analyzed accordingly. Although there are differences in the results among studies, a decrease in parvalbumin expression in the prefrontal cortex has been confirmed in schizophrenia and autism (Beasley and Reynolds, 1997; Hashemi et al., 2017; Ariza et al., 2018; Kaar et al., 2019) (**Table 2**). Therefore, a parvalbumin hypothesis for developmental delay has been proposed (Filice et al., 2020).

RELATIONSHIP BETWEEN THYROID DISEASE AND PSYCHIATRIC DISORDERS (SCHIZOPHRENIA AND AUTISM)

An increased prevalence of thyroid disorders has been noted in families of individuals with schizophrenia (DeLisi et al., 2000; Palha and Goodman, 2006; Radhakrishnan et al., 2013; Gyllenberg et al., 2016; Sharif et al., 2018). Radhakrishnan et al. (2013) reported that in a retrospective hospital-based study, hypothyroidism was observed in 25% of patients with schizophrenia. Sharif et al. (2018) also reported that the population of patients with schizophrenia in hypothyroid patients was higher than that in controls. Generally, the prevalence of schizophrenia is approximately 1%, but there is a twofold increase in the incidence rate of schizophrenia in

TABLE 2 | Morphological abnormalities of parvalbumin neurons in the brain.

Species	State	References	Histological features
Rat	Experimental hypothyroidism (MMI)	Berbel et al. (1996)	The density of nerve terminal ↓
Mouse	Thyroid hormone receptor alpha1 deficient	Guadano-Ferraz et al. (2003)	The density of nerve terminal ↓
Mouse	Mct8/Dio2 double KO	Barez-Lopez et al. (2019)	The number of PV neurons (signals)↓
Rat	Experimental hypothyroidism (PTU)	Gilbert et al. (2007)	The number of PV neurons (signals)↓
Mouse	Experimental hypothyroidism (MMI/perchlorate)	Uchida et al. (2021)	The number of PV neurons (signals)↓
Human	Mct8 mutation	Lopez-Espindola et al. (2014)	The number of PV neurons (signals)↓
Human	Schizophrenia	Hashemi et al. (2017)	The number of PV neurons (signals)↓
Human	Autism	Filice et al. (2020)	The number of PV neurons (signals)↓
Human	Schizophrenia	Beasley and Reynolds (1997)	The number of PV neurons (signals)↓
Human	Autism	Ariza et al. (2018)	The number of PV neurons (signals)↓
Human	Schizophrenia	Kaar et al. (2019)	The number of PV neurons (signals)↓

MMI, methimazole; PTU, propylthiouracil.

patients with hypothyroidism. These large-scale studies show a higher interaction between hypothyroidism and schizophrenia, although the functional relevance of these disorders remains unclear. Since antipsychotics affect thyroid hormone secretion and conversion of T4 toT3 (Terao et al., 1995; Langlois et al., 2001), it should also be considered whether medication affects thyroid status, so as to estimate the relationship between thyroid state and schizophrenia more accurately. According to Melamed et al. (2020), the increased rate of hypothyroidism in patients with schizophrenia after, but not before, the diagnosis of schizophrenia suggests that antipsychotic medications may affect thyroid hormone levels. However, the principal preoccupation is whether perinatal thyroid hormone deficiency is associated with the onset of schizophrenia. According to Gyllenberg et al. (2016), maternal hypothyroxinemia may be associated with an increased risk for the onset of schizophrenia, suggesting an association between low maternal thyroxine and increased odds of offspring schizophrenia. Therefore, congenital hypothyroidism (maternal hypothyroidism) is a potential risk factor for the onset of schizophrenia.

It has been reported that maternal hypothyroidism is associated with an increased risk of ASD (Roman et al., 2013; Chang and Shin, 2014; Getahun et al., 2018; Ge et al., 2020) and that hypothyroid animal models are useful for understanding the molecular mechanisms of ASD (Sadamatsu et al., 2006; Berbel et al., 2014). In a population-based study, there were no strong associations between neonatal thyroid hormones and ASD, but subgroups of newborns with the lowest T4 levels exhibited modestly increased ASD risk (Lyall et al., 2017). Although no significant differences were reported in the levels of serum T4, T3, and thyroid stimulating hormone (TSH) in patients with ASD compared to reference samples (Cohen et al., 1980), this study analyzed thyroid function in children aged 10–12 years with ASD in comparison to normal children. Since mild maternal thyroid hormone insufficiency during the perinatal period affects brain formation in fetuses and neonatal infants, measurement of postnatal hormone levels may provide a clue to its relevance to ASD. In fact, Lischinsky et al. (2016) reported that even mild variations in maternal thyroid hormones permanently affect the offspring cortex. Furthermore, although early treatment of congenital hypothyroidism prevents developmental delay, affected children still exhibit subtle persistent neurocognitive deficits, such as poor attention (Rovet and Hepworth, 2001). In an overall evaluation of offspring, there may be a rigid functional correlation between maternal hypothyroidism during the perinatal period and ASD in offspring (**Table 3**). In subsequent studies, single nucleotide polymorphisms in the ligand-binding domain of thyroid hormone receptors were found in patients with ASD (Kalikiri et al., 2017). Furthermore, alterations in thyroid hormone-dependent genes have been observed in the postmortem brains of humans with ASD (Khan et al., 2014). Hence, the risk of developing autism may be associated not only with an underactive the thyroid gland, but also with a defect in the process of hormone functioning or in the rate of transcribed products. More clinical studies and basic research using animal models are needed to better understand the detailed functional relationship between thyroid diseases and ASD.

THYROID FUNCTION DISORDERS AND RETT SYNDROME

The relationship between thyroid function disorders and RTT is unclear. RTT is a rare genetic disorder caused by mutations or deletions in a gene called MeCP2 on the X chromosome, resulting in severe mental and physical disabilities (Braddock et al., 1993; Gold et al., 2018). RTT is also rarely caused by abnormalities in the CDKL5 and FOXG1 genes (Guerrini and Parrini, 2012). Human autopsy brain tissue from with patients with RTT displays decreased in dendritic spines and neurotrophic factors (Belichenko and Dahlstrom, 1995; Lipani et al., 2000), and such histological impairment may be a leading cause of developmental delay. Partially common neuropathological findings are observed in both RTT and congenital hypothyroidism (Eayrs, 1960; Armstrong, 1997); this is of interest as a research subject for basic medical researchers. Currently, there are less than 10 publications on the relationship between RTT and thyroid state, and several papers have reported very interesting results. Cooke et al. (1995) were the first to report that patients with RTT have thyroid

TABLE 3 | Relationship between thyroid diseases and psychiatric disorders.

Species	State	References	Relationship
Human	Schizophrenia	DeLisi et al. (2000)	Increased prevalence of thyroid function disorders
Human	Schizophrenia	Radhakrishnan et al. (2013)	Increased prevalence of thyroid function disorders
Human	Schizophrenia	Gyllenberg et al. (2016)	Maternal hypothyroxinemia
Human	Hypothyroidism	Sharif et al. (2018)	Risk factor for schizophrenia
Human	Maternal hypothyroxinemia	Roman et al. (2013)	Risk factor for ASD
Human	Maternal hypothyroxinemia	Chang and Shin (2014)	Risk factor for ASD
Human	Maternal hypothyroxinemia	Getahun et al. (2018)	Risk factor for ASD
Human	Maternal hypothyroxinemia	Ge et al. (2020)	Risk factor for ASD
Human	Autism	Cohen et al. (1980)	No correlation of thyroid function disorders
Human	Newborns with low T4 levels	Lyall et al. (2017)	Risk factor for ASD
Human	Hypothyroidism	Rovet and Hepworth (2001)	Onset of attention deficit

ASD, Autism spectrum disorder.

TABLE 4 | Thyroid function disorders and RTT.

Species	State	References	Relationship
Human	RTT	Cooke et al. (1995)	T4 ↓
Human	RTT	Stagi et al. (2015)	T4/T3 ↑
Cell	MeCP2-knockout cells	de Souza et al. (2017)	IGF-1 ↓
Cell	MeCP2-knockout cells	de Souza et al. (2019)	Mct8 ↓
Mouse	Experimental hypothyroidism (MMI/perchlorate)	Uchida et al. (2021)	MeCP2 protein ↓
Mouse	Experimental hypothyroidism (PTU)	Bunker et al. (2017)	MeCP2 mRNA ↓

RTT, Rett syndrome; MMI, methimazole; PTU, propylthiouracil.

dysfunction, which displays a significant decrease in serum total T4 concentration compared to the reference range. Stagi et al. (2015) also reported abnormal thyroid function in RTT, showing that serum T4 levels are elevated in patients with RTT. These two studies have shown contradictory results regarding the serum T4 levels. We cannot describe whether the discrepancies depend on the blood sample or the technique, and these phenomena are of interest for the study of thyroid function on RTT. Future case reports are needed to better interpret the alterations in serum T4 levels with RTT. In contrast, the dysgenesis of neurite length in MeCP2-deficient cells was significantly restored by the administration of IGF-1, whereas IGF-1 concentration in culture media was enhanced by the administration of T3 (de Souza et al., 2017). Therefore, the neuropathological findings observed in RRTs may be due to a decrease in IGF-1 levels, and thyroid hormones may have an indirect effect. Furthermore, MeCP2-knockout cells show that thyroid hormone-related genes, such as hormone transporters and deiodinases, are altered in these cells as compared to normal cells (de Souza et al., 2019). Therefore, MeCP2 probably has a significant influence on the assembly of the thyroid system in the body. In contrast, experimental hypothyroidism leads to alterations in MeCP2 expression in the cortex and liver of rodents. Uchida et al. (2021) reported that hypothyroid pups indicated a decrease in MeCP2 staining signals in cortical layers II–IV; however, the expression of MeCP2 mRNA was not altered. In contrast, Bunker et al. (2017) showed that neonatal exposure to antithyroid agents led to a decrease in MeCP2 mRNA expression in the liver; however, translated products did not change. Although there is not a clear explanation regarding the behavior of MeCP2 transcripts and translated products differs between organs, these results suggest that thyroid hormones have a significant effect on the expression of MeCP2, at least, and the relationship between thyroid function and MeCP2 might be that of reciprocal interactions rather than one-way interactions (**Table 4**). Further studies are needed to clarify the molecular mechanisms by which thyroid hormones affect MeCP2 expression.

Fukuda et al. (2005) reported delayed corticogenesis in MeCP2-deficient mice. Interestingly, the cortex of MeCP2-deficient mice has no parvalbumin neurons at postnatal day 14, and its expression catches up at 6 weeks after birth (Fukuda et al., 2005). Parvalbumin-expressing neurons contribute to aspects of the RTT phenotype; genetically modified mice specifically defecting MeCP2 on parvalbumin neurons indicate distinct RTT-like phenotypes (Ito-Ishida et al., 2015). Hence, the functional defect of parvalbumin might have a profound causal relationship with the development of psychiatric disorders. Of course, this behavior of parvalbumin closely resembles that of histological alterations in thyroid hormone deficiency during the perinatal period. In addition, the article also reports immature cortical formation in the somatosensory cortex of MeCP2-deficient mice, a phenomenon also observed in hypothyroid mice. The histological abnormalities observed in MeCP2-deficient and hypothyroid mice share many similarities, suggesting that there are downstream overlapping molecular mechanisms. Further exploration of the common denominator with hypothyroidism may reveal the molecular mechanism of developmental delay in RTT.

CONCLUSION

In this review, we discussed the effects of thyroid hormones on the neural architecture of the brain, and then concisely mentioned their relationship with parvalbumin and/or MeCP2. The role of thyroid hormones in brain development has been studied since the early 20th century, and many studies have been published accordingly. Most of them are based on histomorphological evaluation by Nissl and Golgi staining, and the products of these histological studies have had a significant impact on the directionality of the current research. Furthermore, in recent years, researchers have been able to develop genetically modified mice with knockdown of target genes, and the importance of the thyroid system in brain development is becoming clearer. Nevertheless, just as the elementary processes of memory have been discovered, the mechanism of memory has not yet been elucidated, and the mechanism of developmental delay caused by congenital hypothyroidism has not been clarified. However, through animal experiments and clinical studies, a decrease in parvalbumin neurons has been reproducibly observed in hypothyroidism, and this phenomenon has also been observed in the postmortem brains of patients with schizophrenia and autism. Such comparative analysis with other psychiatric disorders may provide clues to the pathogenesis of developmental delay. In addition, since abnormal thyroid function is observed in patients with RTT, the onset of diseases associated with developmental disorders may have a common molecular mechanism. On the other hand, even though mild perinatal thyroid hormone deficiencies or even early treatment with levothyroxine, children who experience thyroid hormone deficiency during the perinatal period still retain the signatures of temporary hormonal defects in the adult brain. This case strongly indicates that thyroid hormones are essential for brain development. Hence, the study of congenital hypothyroidism and brain development remains a fascinating research topic.

AUTHOR CONTRIBUTIONS

KU wrote the manuscript. KU and MS collected the relevant research manuscript for the review. Both authors contributed to the article and approved the submitted version.

FUNDING

This work was supported by the JSPS KAKENHI Grant Numbers JP19K08969 and JP16H06276 (AdAMS).

ACKNOWLEDGMENTS

We would like to thank N. Katayama (Department of Humanities and Social Studies, Shokei Gakuin University) for advice on the manuscript. We would also like to thank Editage (http://www.editage.com) for English language editing.

REFERENCES

Alvarez-Dolado, M., Ruiz, M., Del Rio, J. A., Alcantara, S., Burgaya, F., Sheldon, M., et al. (1999). Thyroid hormone regulates reelin and dab1 expression during brain development. *J. Neurosci.* 19, 6979–6993. doi: 10.1523/JNEUROSCI.19-16-06979.1999

Ameis, S. H., Lerch, J. P., Taylor, M. J., Lee, W., Viviano, J. D., Pipitone, J., et al. (2016). A Diffusion Tensor Imaging Study in Children With ADHD, Autism Spectrum Disorder, OCD, and Matched Controls: distinct and Non-Distinct White Matter Disruption and Dimensional Brain-Behavior Relationships. *Am. J. Psychiatry* 173, 1213–1222. doi: 10.1176/appi.ajp.2016.15111435

Arif, S. H. (2009). A Ca(2+)-binding protein with numerous roles and uses: parvalbumin in molecular biology and physiology. *Bioessays* 31, 410–421. doi: 10.1002/bies.200800170

Ariza, J., Rogers, H., Hashemi, E., Noctor, S. C., and Martinez-Cerdeno, V. (2018). The Number of Chandelier and Basket Cells Are Differentially Decreased in Prefrontal Cortex in Autism. *Cereb. Cortex* 28, 411–420. doi: 10.1093/cercor/bhw349

Armstrong, D. D. (1997). Review of Rett syndrome. *J. Neuropathol. Exp. Neurol.* 56, 843–849.

Barez-Lopez, S., Grijota-Martinez, C., Auso, E., Fernandez-De Frutos, M., Montero-Pedrazuela, A., and Guadano-Ferraz, A. (2019). Adult Mice Lacking Mct8 and Dio2 Proteins Present Alterations in Peripheral Thyroid Hormone Levels and Severe Brain and Motor Skill Impairments. *Thyroid* 29, 1669–1682. doi: 10.1089/thy.2019.0068

Beasley, C. L., and Reynolds, G. P. (1997). Parvalbumin-immunoreactive neurons are reduced in the prefrontal cortex of schizophrenics. *Schizophr. Res.* 24, 349–355. doi: 10.1016/s0920-9964(96)00122-3

Belichenko, P. V., and Dahlstrom, A. (1995). Confocal laser scanning microscopy and 3-D reconstructions of neuronal structures in human brain cortex. *Neuroimage* 2, 201–207. doi: 10.1006/nimg.1995.1026

Berbel, P., Guadano-Ferraz, A., Martinez, M., Quiles, J. A., Balboa, R., and Innocenti, G. M. (1993). Organization of auditory callosal connections in hypothyroid adult rats. *Eur. J. Neurosci.* 5, 1465–1478. doi: 10.1111/j.1460-9568.1993.tb00214.x

Berbel, P., Marco, P., Cerezo, J. R., and Defelipe, J. (1996). Distribution of parvalbumin immunoreactivity in the neocortex of hypothyroid adult rats. *Neurosci. Lett.* 204, 65–68. doi: 10.1016/0304-3940(96)12318-1

Berbel, P., Navarro, D., and Roman, G. C. (2014). An evo-devo approach to thyroid hormones in cerebral and cerebellar cortical development: etiological implications for autism. *Front. Endocrinol.* 5:146. doi: 10.3389/fendo.2014.00146

Braddock, S. R., Braddock, B. A., and Graham, J. M. Jr. (1993). Rett syndrome. An update and review for the primary pediatrician. *Clin. Pediatr.* 32, 613–626. doi: 10.1177/000992289303201011

Bunker, S. K., Dandapat, J., Chainy, G. B. N., Sahoo, S. K., and Nayak, P. K. (2017). Neonatal Exposure to 6-n-Propyl-Thiouracil, an Anti-Thyroid Drug, Alters Expression of Hepatic DNA Methyltransferases, Methyl CpG-Binding Proteins, Gadd45a, p53, and PCNA in Adult Male Rats. *Eur. Thyroid J.* 6, 281–291. doi: 10.1159/000479681

Calikoglu, A. S., Gutierrez-Ospina, G., and D'ercole, A. J. (1996). Congenital hypothyroidism delays the formation and retards the growth of the mouse primary somatic sensory cortex (S1). *Neurosci. Lett.* 213, 132–136. doi: 10.1016/0304-3940(96)12836-6

Casanova, M. F., El-Baz, A., Elnakib, A., Switala, A. E., Williams, E. L., Williams, D. L., et al. (2011). Quantitative analysis of the shape of the corpus callosum in patients with autism and comparison individuals. *Autism* 15, 223–238. doi: 10.1177/1362361310386506

Celio, M. R. (1986). Parvalbumin in most gamma-aminobutyric acid-containing neurons of the rat cerebral cortex. *Science* 231, 995–997. doi: 10.1126/science.3945815

Celio, M. R. (1990). Calbindin D-28k and parvalbumin in the rat nervous system. *Neuroscience* 35, 375–475. doi: 10.1016/0306-4522(90)90091-h

Chang, K., and Shin, J. I. (2014). Association of gestational maternal hypothyroxinemia and increased autism risk: the role of brain-derived neurotrophic factor. *Ann. Neurol.* 75:971. doi: 10.1002/ana.24143

Cherubini, E., Gaiarsa, J. L., and Ben-Ari, Y. (1991). GABA: an excitatory transmitter in early postnatal life. *Trends Neurosci.* 14, 515–519. doi: 10.1016/0166-2236(91)90003-d

Cohen, D. J., Young, J. G., Lowe, T. L., and Harcherik, D. (1980). Thyroid hormone in autistic children. *J. Autism Dev. Disord.* 10, 445–450. doi: 10.1007/bf02414820

Cooke, D. W., Naidu, S., Plotnick, L., and Berkovitz, G. D. (1995). Abnormalities of thyroid function and glucose control in subjects with Rett syndrome. *Horm. Res.* 43, 273–278. doi: 10.1159/000184309

Cooper, H. E., Kaden, E., Halliday, L. F., Bamiou, D. E., Mankad, K., Peters, C., et al. (2019). White matter microstructural abnormalities in children with severe congenital hypothyroidism. *Neuroimage Clin.* 24:101980. doi: 10.1016/j.nicl.2019.101980

Croteau, W., Davey, J. C., Galton, V. A., and St Germain, D. L. (1996). Cloning of the mammalian type II iodothyronine deiodinase. A selenoprotein differentially expressed and regulated in human and rat brain and other tissues. *J. Clin. Invest.* 98, 405–417. doi: 10.1172/JCI118806

Danglot, L., Triller, A., and Marty, S. (2006). The development of hippocampal interneurons in rodents. *Hippocampus* 16, 1032–1060. doi: 10.1002/hipo.20225

de Lecea, L., del Rio, J. A., and Soriano, E. (1995). Developmental expression of parvalbumin mRNA in the cerebral cortex and hippocampus of the rat. *Brain Res. Mol. Brain Res.* 32, 1–13. doi: 10.1016/0169-328x(95)00056-x

de Souza, J. S., Carromeu, C., Torres, L. B., Araujo, B. H., Cugola, F. R., Maciel, R. M., et al. (2017). IGF1 neuronal response in the absence of MECP2 is dependent on TRalpha 3. *Hum. Mol. Genet.* 26, 270–281. doi: 10.1093/hmg/ddw384

de Souza, J. S., Ferreira, D. R., Herai, R., Carromeu, C., Torres, L. B., Araujo, B. H. S., et al. (2019). Altered Gene Expression of Thyroid Hormone Transporters and Deiodinases in iPS MeCP2-Knockout Cells-Derived Neurons. *Mol. Neurobiol.* 56, 8277–8295. doi: 10.1007/s12035-019-01645-2

DeLisi, L. E., Smith, A. B., Razi, K., Stewart, J., Wang, Z., Sandhu, H. K., et al. (2000). Investigation of a candidate gene for schizophrenia on Xq13 previously associated with mental retardation and hypothyroidism. *Am. J. Med. Genet.* 96, 398–403.

Eayrs, J. T. (1960). Influence of the thyroid on the central nervous system. *Br. Med. Bull.* 16, 122–127. doi: 10.1093/oxfordjournals.bmb.a069810

Filice, F., Janickova, L., Henzi, T., Bilella, A., and Schwaller, B. (2020). The Parvalbumin Hypothesis of Autism Spectrum Disorder. *Front. Cell. Neurosci.* 14:577525. doi: 10.3389/fncel.2020.577525

Fishman, R. H., Gaathon, A., and Yanai, J. (1982). Early barbiturate treatment eliminates peak serum thyroxine levels in neonatal mice and produces ultrastructural damage in the brains of adults. *Brain Res.* 281, 202–205. doi: 10.1016/0165-3806(82)90158-4

Friauf, E., Wenz, M., Oberhofer, M., Nothwang, H. G., Balakrishnan, V., Knipper, M., et al. (2008). Hypothyroidism impairs chloride homeostasis and onset of inhibitory neurotransmission in developing auditory brainstem and hippocampal neurons. *Eur. J. Neurosci.* 28, 2371–2380. doi: 10.1111/j.1460-9568.2008.06528.x

Friesema, E. C., Ganguly, S., Abdalla, A., Manning Fox, J. E., Halestrap, A. P., and Visser, T. J. (2003). Identification of monocarboxylate transporter 8 as a specific thyroid hormone transporter. *J. Biol. Chem.* 278, 40128–40135. doi: 10.1074/jbc.m300909200

Fukuda, T., Itoh, M., Ichikawa, T., Washiyama, K., and Goto, Y. (2005). Delayed maturation of neuronal architecture and synaptogenesis in cerebral cortex of Mecp2-deficient mice. *J. Neuropathol. Exp. Neurol.* 64, 537–544. doi: 10.1093/jnen/64.6.537

Ge, G. M., Leung, M. T. Y., Man, K. K. C., Leung, W. C., Ip, P., Li, G. H. Y., et al. (2020). Maternal Thyroid Dysfunction During Pregnancy and the Risk of Adverse Outcomes in the Offspring: a Systematic Review and Meta-Analysis. *J. Clin. Endocrinol. Metab.* 105:dgaa555. doi: 10.1210/clinem/dgaa555

Getahun, D., Jacobsen, S. J., Fassett, M. J., Wing, D. A., Xiang, A. H., Chiu, V. Y., et al. (2018). Association between maternal hypothyroidism and autism spectrum disorders in children. *Pediatr. Res.* 83, 580–588.

Gilbert, M. E., Sui, L., Walker, M. J., Anderson, W., Thomas, S., Smoller, S. N., et al. (2007). Thyroid hormone insufficiency during brain development reduces parvalbumin immunoreactivity and inhibitory function in the hippocampus. *Endocrinology* 148, 92–102. doi: 10.1210/en.2006-0164

Gold, W. A., Krishnarajy, R., Ellaway, C., and Christodoulou, J. (2018). Rett Syndrome: a Genetic Update and Clinical Review Focusing on Comorbidities. *ACS Chem. Neurosci.* 9, 167–176. doi: 10.1021/acschemneuro.7b00346

Goodman, J. H., and Gilbert, M. E. (2007). Modest thyroid hormone insufficiency during development induces a cellular malformation in the corpus callosum: a model of cortical dysplasia. *Endocrinology* 148, 2593–2597. doi: 10.1210/en.2006-1276

Guadano-Ferraz, A., Benavides-Piccione, R., Venero, C., Lancha, C., Vennstrom, B., Sandi, C., et al. (2003). Lack of thyroid hormone receptor alpha1 is associated with selective alterations in behavior and hippocampal circuits. *Mol. Psychiatry* 8, 30–38. doi: 10.1038/sj.mp.4001196

Guerrini, R., and Parrini, E. (2012). Epilepsy in Rett syndrome, and CDKL5- and FOXG1-gene-related encephalopathies. *Epilepsia* 53, 2067–2078. doi: 10.1111/j.1528-1167.2012.03656.x

Gyllenberg, D., Sourander, A., Surcel, H. M., Hinkka-Yli-Salomaki, S., Mckeague, I. W., and Brown, A. S. (2016). Hypothyroxinemia During Gestation and Offspring Schizophrenia in a National Birth Cohort. *Biol. Psychiatry* 79, 962–970. doi: 10.1016/j.biopsych.2015.06.014

Hadj-Sahraoui, N., Seugnet, I., Ghorbel, M. T., and Demeneix, B. (2000). Hypothyroidism prolongs mitotic activity in the post-natal mouse brain. *Neurosci. Lett.* 280, 79–82. doi: 10.1016/s0304-3940(00)00768-0

Hashemi, E., Ariza, J., Rogers, H., Noctor, S. C., and Martinez-Cerdeno, V. (2017). The Number of Parvalbumin-Expressing Interneurons Is Decreased in the Prefrontal Cortex in Autism. *Cereb. Cortex* 27, 1931–1943.

Hashimoto, T., Volk, D. W., Eggan, S. M., Mirnics, K., Pierri, J. N., Sun, Z., et al. (2003). Gene expression deficits in a subclass of GABA neurons in the prefrontal cortex of subjects with schizophrenia. *J. Neurosci.* 23, 6315–6326. doi: 10.1523/JNEUROSCI.23-15-06315.2003

Hu, H., Gan, J., and Jonas, P. (2014). Interneurons. Fast-spiking, parvalbumin(+) GABAergic interneurons: from cellular design to microcircuit function. *Science* 345:1255263.

Ito-Ishida, A., Ure, K., Chen, H., Swann, J. W., and Zoghbi, H. Y. (2015). Loss of MeCP2 in Parvalbumin-and Somatostatin-Expressing Neurons in Mice Leads to Distinct Rett Syndrome-like Phenotypes. *Neuron* 88, 651–658. doi: 10.1016/j.neuron.2015.10.029

Kaar, S. J., Angelescu, I., Marques, T. R., and Howes, O. D. (2019). Pre-frontal parvalbumin interneurons in schizophrenia: a meta-analysis of post-mortem studies. *J. Neural Transm.* 126, 1637–1651. doi: 10.1007/s00702-019-02080-2

Kalikiri, M. K., Mamidala, M. P., Rao, A. N., and Rajesh, V. (2017). Analysis and functional characterization of sequence variations in ligand binding domain of thyroid hormone receptors in autism spectrum disorder (ASD) patients. *Autism Res.* 10, 1919–1928. doi: 10.1002/aur.1838

Khan, A., Harney, J. W., Zavacki, A. M., and Sajdel-Sulkowska, E. M. (2014). Disrupted brain thyroid hormone homeostasis and altered thyroid hormone-dependent brain gene expression in autism spectrum disorders. *J. Physiol. Pharmacol.* 65, 257–272.

Koibuchi, N., and Chin, W. W. (2000). Thyroid hormone action and brain development. *Trends Endocrinol. Metab.* 11, 123–128. doi: 10.1016/s1043-2760(00)00238-1

Kosaka, T., Katsumaru, H., Hama, K., Wu, J. Y., and Heizmann, C. W. (1987). GABAergic neurons containing the Ca2+-binding protein parvalbumin in the rat hippocampus and dentate gyrus. *Brain Res.* 419, 119–130. doi: 10.1016/0006-8993(87)90575-0

Langlois, M. C., Beaudry, G., Zekki, H., Rouillard, C., and Levesque, D. (2001). Impact of antipsychotic drug administration on the expression of nuclear receptors in the neocortex and striatum of the rat brain. *Neuroscience* 106, 117–128. doi: 10.1016/s0306-4522(01)00248-2

Lawrence, Y. A., Kemper, T. L., Bauman, M. L., and Blatt, G. J. (2010). Parvalbumin-, calbindin-, and calretinin-immunoreactive hippocampal interneuron density in autism. *Acta Neurol. Scand.* 121, 99–108. doi: 10.1111/j.1600-0404.2009.01234.x

Lipani, J. D., Bhattacharjee, M. B., Corey, D. M., and Lee, D. A. (2000). Reduced nerve growth factor in Rett syndrome postmortem brain tissue. *J. Neuropathol. Exp. Neurol.* 59, 889–895. doi: 10.1093/jnen/59.10.889

Lischinsky, J. E., Skocic, J., Clairman, H., and Rovet, J. (2016). Preliminary Findings Show Maternal Hypothyroidism May Contribute to Abnormal

Cortical Morphology in Offspring. *Front. Endocrinol.* 7:16. doi: 10.3389/fendo.2016.00016

Lopez-Espindola, D., Morales-Bastos, C., Grijota-Martinez, C., Liao, X. H., Lev, D., Sugo, E., et al. (2014). Mutations of the thyroid hormone transporter MCT8 cause prenatal brain damage and persistent hypomyelination. *J. Clin. Endocrinol. Metab.* 99, E2799–E2804. doi: 10.1210/jc.2014-2162

Lyall, K., Anderson, M., Kharrazi, M., and Windham, G. C. (2017). Neonatal thyroid hormone levels in association with autism spectrum disorder. *Autism Res.* 10, 585–592.

Melamed, S. B., Farfel, A., Gur, S., Krivoy, A., Weizman, S., Matalon, A., et al. (2020). Thyroid function assessment before and after diagnosis of schizophrenia: a community-based study. *Psychiatry Res.* 293:113356. doi: 10.1016/j.psychres.2020.113356

Morreale de Escobar, G., Obregon, M. J., and Escobar del Rey, F. (1987). Fetal and maternal thyroid hormones. *Horm. Res.* 26, 12–27.

Nicholson, J. L., and Altman, J. (1972). Synaptogenesis in the rat cerebellum: effects of early hypo- and hyperthyroidism. *Science* 176, 530–532. doi: 10.1126/science.176.4034.530

Oppenheimer, J. H., and Schwartz, H. L. (1997). Molecular basis of thyroid hormone-dependent brain development. *Endocr. Rev.* 18, 462–475. doi: 10.1210/edrv.18.4.0309

Palha, J. A., and Goodman, A. B. (2006). Thyroid hormones and retinoids: a possible link between genes and environment in schizophrenia. *Brain Res. Rev.* 51, 61–71. doi: 10.1016/j.brainresrev.2005.10.001

Qiu, M. G., Ye, Z., Li, Q. Y., Liu, G. J., Xie, B., and Wang, J. (2011). Changes of brain structure and function in ADHD children. *Brain Topogr.* 24, 243–252.

Radhakrishnan, R., Calvin, S., Singh, J. K., Thomas, B., and Srinivasan, K. (2013). Thyroid dysfunction in major psychiatric disorders in a hospital based sample. *Indian J. Med. Res.* 138, 888–893.

Rastogi, M. V., and LaFranchi, S. H. (2010). Congenital hypothyroidism. *Orphanet J. Rare Dis.* 5:17.

Rivera, C., Voipio, J., Payne, J. A., Ruusuvuori, E., Lahtinen, H., Lamsa, K., et al. (1999). The K+/Cl- co-transporter KCC2 renders GABA hyperpolarizing during neuronal maturation. *Nature* 397, 251–255. doi: 10.1038/16697

Roman, G. C., Ghassabian, A., Bongers-Schokking, J. J., Jaddoe, V. W., Hofman, A., De Rijke, Y. B., et al. (2013). Association of gestational maternal hypothyroxinemia and increased autism risk. *Ann. Neurol.* 74, 733–742. doi: 10.1002/ana.23976

Rovet, J. F., and Hepworth, S. (2001). Attention problems in adolescents with congenital hypothyroidism: a multicomponential analysis. *J. Int. Neuropsychol. Soc.* 7, 734–744. doi: 10.1017/s135561770176609x

Sadamatsu, M., Kanai, H., Xu, X., Liu, Y., and Kato, N. (2006). Review of animal models for autism: implication of thyroid hormone. *Congenit. Anom.* 46, 1–9. doi: 10.1111/j.1741-4520.2006.00094.x

Samadi, A., Skocic, J., and Rovet, J. F. (2015). Children born to women treated for hypothyroidism during pregnancy show abnormal corpus callosum development. *Thyroid* 25, 494–502. doi: 10.1089/thy.2014.0548

Sharif, K., Tiosano, S., Watad, A., Comaneshter, D., Cohen, A. D., Shoenfeld, Y., et al. (2018). The link between schizophrenia and hypothyroidism: a population-based study. *Immunol. Res.* 66, 663–667. doi: 10.1007/s12026-018-9030-7

Soghomonian, J. J., Zhang, K., Reprakash, S., and Blatt, G. J. (2017). Decreased parvalbumin mRNA levels in cerebellar Purkinje cells in autism. *Autism Res.* 10, 1787–1796. doi: 10.1002/aur.1835

Stagi, S., Cavalli, L., Congiu, L., Scusa, M. F., Ferlini, A., Bigoni, S., et al. (2015). Thyroid function in Rett syndrome. *Horm. Res. Paediatr.* 83, 118–125. doi: 10.1159/000370066

Terao, T., Oga, T., Nozaki, S., Ohta, A., Otsubo, Y., Yamamoto, S., et al. (1995). Possible inhibitory effect of lithium on peripheral conversion of thyroxine to triiodothyronine: a prospective study. *Int. Clin. Psychopharmacol.* 10, 103–105. doi: 10.1097/00004850-199506000-00006

Uchida, K., Hasuoka, K., Fuse, T., Kobayashi, K., Moriya, T., Suzuki, M., et al. (2021). Thyroid hormone insufficiency alters the expression of psychiatric disorder-related molecules in the hypothyroid mouse brain during the early postnatal period. *Sci. Rep.* 11:6723. doi: 10.1038/s41598-021-86237-8

Uchida, K., Taguchi, Y., Sato, C., Miyazaki, H., Kobayashi, K., Kobayashi, T., et al. (2014). Amelioration of improper differentiation of somatostatin-positive interneurons by triiodothyronine in a growth-retarded hypothyroid mouse strain. *Neurosci. Lett.* 559, 111–116. doi: 10.1016/j.neulet.2013.11.052

Uchida, K., Yonezawa, M., Nakamura, S., Kobayashi, T., and Machida, T. (2005). Impaired neurogenesis in the growth-retarded mouse is reversed by T3 treatment. *Neuroreport* 16, 103–106. doi: 10.1097/00001756-200502080-00005

Wallis, K., Sjogren, M., Van Hogerlinden, M., Silberberg, G., Fisahn, A., Nordstrom, K., et al. (2008). Locomotor deficiencies and aberrant development of subtype-specific GABAergic interneurons caused by an unliganded thyroid hormone receptor alpha1. *J. Neurosci.* 28, 1904–1915. doi: 10.1523/JNEUROSCI.5163-07.2008

Yi, J., Zheng, J. Y., Zhang, W., Wang, S., Yang, Z. F., and Dou, K. F. (2014). Decreased pain threshold and enhanced synaptic transmission in the anterior cingulate cortex of experimental hypothyroidism mice. *Mol. Pain* 10:38. doi: 10.1186/1744-8069-10-38

Conflict of Interest: The authors declare that the research was conducted in the absence of any commercial or financial relationships that could be construed as a potential conflict of interest.

Publisher's Note: All claims expressed in this article are solely those of the authors and do not necessarily represent those of their affiliated organizations, or those of the publisher, the editors and the reviewers. Any product that may be evaluated in this article, or claim that may be made by its manufacturer, is not guaranteed or endorsed by the publisher.

frontiers in Neuroscience

REVIEW
published: 05 January 2022
doi: 10.3389/fnins.2021.817218

Roots of the Malformations of Cortical Development in the Cell Biology of Neural Progenitor Cells

*Chiara Ossola and Nereo Kalebic**

Human Technopole, Milan, Italy

The cerebral cortex is a structure that underlies various brain functions, including cognition and language. Mammalian cerebral cortex starts developing during the embryonic period with the neural progenitor cells generating neurons. Newborn neurons migrate along progenitors' radial processes from the site of their origin in the germinal zones to the cortical plate, where they mature and integrate in the forming circuitry. Cell biological features of neural progenitors, such as the location and timing of their mitoses, together with their characteristic morphologies, can directly or indirectly regulate the abundance and the identity of their neuronal progeny. Alterations in the complex and delicate process of cerebral cortex development can lead to malformations of cortical development (MCDs). They include various structural abnormalities that affect the size, thickness and/or folding pattern of the developing cortex. Their clinical manifestations can entail a neurodevelopmental disorder, such as epilepsy, developmental delay, intellectual disability, or autism spectrum disorder. The recent advancements of molecular and neuroimaging techniques, along with the development of appropriate *in vitro* and *in vivo* model systems, have enabled the assessment of the genetic and environmental causes of MCDs. Here we broadly review the cell biological characteristics of neural progenitor cells and focus on those features whose perturbations have been linked to MCDs.

Keywords: neural progenitor and stem cells, neurogenesis, cortical malformation, neocortex, neuronal migration

OPEN ACCESS

Edited by:
Kazuhiko Sawada, Tsukuba International University, Japan

Reviewed by:
Harvey B. Sarnat, University of Calgary, Canada
Maija Liisa Castrén, University of Helsinki, Finland
Madeline Andrews, University of California, San Francisco, United States

***Correspondence:**
Nereo Kalebic
nereo.kalebic@fht.org

Specialty section:
This article was submitted to Neurodevelopment, a section of the journal Frontiers in Neuroscience

Received: *17 November 2021*
Accepted: *14 December 2021*
Published: *05 January 2022*

Citation:
Ossola C and Kalebic N (2022) Roots of the Malformations of Cortical Development in the Cell Biology of Neural Progenitor Cells. Front. Neurosci. 15:817218. doi: 10.3389/fnins.2021.817218

HUMAN CORTICAL DEVELOPMENT

One of the most intriguing features that characterizes the human species is the exceptional size of the cerebral cortex, in particular the neocortex. Humans show a significant expansion in both radial and tangential direction of the cerebral cortex, which is involved in the increased cognitive abilities that we consider unique to humans. This expansion is a consequence of the increased neuronal production during the embryonic and fetal development, due to a prolonged neurogenic period and to an increased proliferative capacity of different neural progenitor cell types (Rakic, 2009; Geschwind and Rakic, 2013; Wilsch-Bräuninger et al., 2016; Sousa et al., 2017; Molnar et al., 2019; Kalebic and Huttner, 2020; Pattabiraman et al., 2020; Del Valle Anton and Borrell, 2021). In addition, the survival of newborn neurons also plays a role, as the inhibition of apoptosis was shown to increase brain size (Kuida et al., 1996, 1998; Rakic and Zecevic, 2000; Roth and D'Sa, 2001).

During mammalian evolution, the neocortex, which constitutes much of the cerebral cortex, shows the most significant expansion (Kriegstein et al., 2006; Lui et al., 2011; Borrell and Reillo, 2012). The developmental organization of the mammalian neocortex has been described by Rakic (1988, 2000, 2009) in radial unit and protomap hypotheses: it consists of columns positioned

tangentially to the cortical surface, generated by distinct proliferative units in the germinal zones (GZs), that form specialized regions with specific cytoarchitecture and function, called areas. Newborn excitatory neurons hence originate from progenitor cells located in the GZs and they migrate to their final location in the cortical plate (CP) along the processes of progenitor cells. In the radial dimension, the adult neocortex is organized in six layers (I-VI). The neocortex is built in an "inside-out" manner, with the deep layers (V–VI) generated first and the upper layers (II–IV) following subsequently (Angevine and Sidman, 1961; Rakic, 1988; Bayer and Altman, 1991; Molyneaux et al., 2007). The layer I, however, is formed by the earliest-born neurons that form a preplate which later splits into the marginal zone populated by Cajal-Retzius cells (Marin-Padilla, 1978; Zecevic and Rakic, 2001; Bielle et al., 2005) and the subplate (Kostovic, 2020). In contrast to excitatory neurons, cortical inhibitory interneurons are generated in the medial and caudal ganglionic eminences and undergo a tangential migration to reach the developing neocortex (Hu et al., 2017).

Developing mammalian brain exhibits apicobasal polarity with the apical side facing the lumen of the ventricles and the basal side facing the skull. The developing neocortex contains two principal GZs: the ventricular zone (VZ), situated along the ventricle, and the subventricular zone (SVZ), which is located more basally between the VZ and the intermediate zone (IZ). The latter is the layer through which newborn neurons migrate along the progenitors' scaffold toward the cortical plate (CP) (**Figure 1**). In contrast to lissencephalic mammals, whose brain is smooth, such as mouse, the gyrencephalic mammals, whose brain is folded, such as ferrets and primates, exhibit a massively enlarged SVZ that contains two cyto-architectonically specific sublayers, the inner and outer SVZ (iSVZ and oSVZ), separated by an axon-rich fiber layer (Smart et al., 2002; Reillo and Borrell, 2012; Dehay et al., 2015; Saito et al., 2018). Whereas the primate iSVZ is comparable to the mouse SVZ, with densely packed cells, the oSVZ cells have a radial arrangement similar to the VZ (Smart et al., 2002; Dehay et al., 2015).

The differences in neocortex size and complexity across mammals are widely considered to derive from the differences in the proliferative capacity and neurogenic potential of neural progenitor cells (Lui et al., 2011; Fernandez et al., 2016; de Juan Romero and Borrell, 2017; Molnar et al., 2019; Kalebic and Huttner, 2020). Neuroepithelial cells (NECs) are the first progenitor cells specifically devoted to neocortical development and the source of all other neocortical progenitors (Taverna et al., 2014). Before the onset of neurogenesis, NEC population is enlarged by symmetric proliferative divisions, which is prominent in primates, due to an extended period of proliferation (Rakic, 1995). At the beginning of neurogenesis NECs undergo asymmetric divisions to generate apical Radial Glia (aRG), a new pool of progenitor cells that replaces the NECs and populates the VZ (**Figure 1**). aRG maintain the epithelial apicobasal polarity, with an apical process that lines the ventricle and tightly seals the tissue with an adherens junction belt, and a basal process that contacts the basal lamina and provides a scaffold fundamental for the radial migration of newborn neurons to the CP (Rakic, 2003; Taverna et al., 2014). aRG can undergo self-amplifying symmetric proliferative divisions that increase their population and asymmetric divisions to produce more differentiated progenitor cell type called Basal Progenitors (BPs), or rarely a neuron. BPs delaminate from the apical belt of adherens junctions at the surface of the VZ and migrate basally to form the SVZ (Haubensak et al., 2004; Miyata et al., 2004; Noctor et al., 2004).

Basal Progenitors include two subtypes: basal intermediate progenitors (bIPs) and basal or outer Radial Glia (bRG or oRG) (**Figure 1**) (Taverna et al., 2014; Kalebic and Huttner, 2020). In species with a small and smooth brain, such as mouse, BPs usually divide only once to generate 2 neurons, whereas in species with an expanded and folded neocortex, such as ferret and primates, BPs have a greater proliferative capacity and they can undergo several proliferative divisions producing other BPs before finally generating neurons. This is particularly relevant for the bRG, whose abundance (up to 50% of all BPs) and proliferative capacity are significantly increased in humans, macaques and ferrets, compared to lissencephalic mammals (in mouse, bRG comprise up to 10% of BPs), suggesting a role in neocortical expansion (Fietz et al., 2010; Hansen et al., 2010; Reillo et al., 2011; Betizeau et al., 2013; Lewitus et al., 2014; Kalebic et al., 2019). Whereas the basal processes of both bRG and aRG are crucial for neuronal migration, bRG processes are considered particularly important for the tangential dispersion of newborn neurons, a key feature of folded brains (Borrell and Götz, 2014; Fernandez et al., 2016; Nowakowski et al., 2016; Kalebic and Huttner, 2020).

The complexity that characterizes human cortical development makes it particularly vulnerable to the effects of genetic mutations and environmental factors. The resulting alterations of the cortical development can lead to cortical malformations, defects that are considered to be a probable cause for neurological conditions such as epilepsy, autism spectrum disorder or intellectual disability (Pan et al., 2019).

MALFORMATIONS OF CORTICAL DEVELOPMENT

Malformations of cortical development are a heterogeneous group of disorders characterized by macroscopic alterations in the brain structure caused by genetic mutations or environmental factors that affect neocortical development (Sun and Hevner, 2014; Bizzotto and Francis, 2015; Desikan and Barkovich, 2016; Romero et al., 2018; Juric-Sekhar and Hevner, 2019; Subramanian et al., 2019; Klingler et al., 2021). Such alterations of brain structure can include abnormal brain size, layering, folding and presence of heterotopic gray matter. As the causative genetic mutations are highly diverse, the classification of MCDs is typically based on the neurological outcomes, whereas the diagnosis is mostly based on MRI data (Barkovich et al., 2012; Guarnieri et al., 2018; Severino et al., 2020). Three major groups of MCDs can be identified based on the affected developmental phase: (i) cell proliferation and survival, (ii) neuronal migration, (iii) post-migrational differentiation and circuits connectivity (Barkovich et al., 2012; Romero et al., 2018; Subramanian et al., 2019; Severino et al., 2020; Francis and Cappello, 2021).

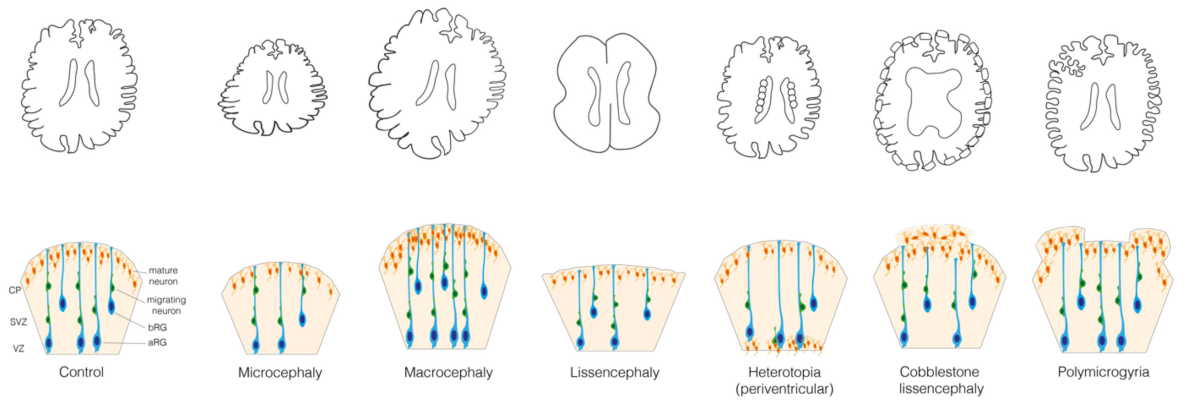

FIGURE 1 | Malformations of the cortical development. **(Upper)** Schematic representations of the control brain and brains affected by the following MCDs: microcephaly, macrocephaly, lissencephaly, periventricular nodular heterotopia, cobblestone lissencephaly and polymicrogyria. **(Lower)** Schematic representation of the mechanisms underlying these MCDs. In Control: VZ, ventricular zone; SVZ, subventricular zone; CP, cortical plate; aRG, apical radial glia; bRG, basal radial glia; migrating and mature neurons.

When cell proliferation or survival are affected, neurogenesis can be increased or reduced, which leads to an increase or reduction of the brain volume, that is megalencephaly or micrencephaly, respectively (Homem et al., 2015; Jayaraman et al., 2018). This in turn usually leads to a consequent modification of the entire head dimension, that is macrocephaly and microcephaly, respectively (**Figure 1**). Microcephaly is characterized by a reduction in the total number of neurons generated developmentally and is typically caused by a decreased neocortical progenitor pool size or an abnormal apoptosis. The former is accompanied by a premature differentiation of neurons and can most often be caused by various abnormalities of the mitotic phase and neural progenitor polarity (Jamuar and Walsh, 2015; Jayaraman et al., 2018). Instead, macrocephaly is typically characterized by a localized increase in the number or size of neurons and glial cells, which is usually due to mutations in key signaling pathways that regulate cell proliferation and growth (Mirzaa and Poduri, 2014; Hevner, 2015).

A disruption of the migration of newborn neurons from GZs to CP can lead to an aberrant localization of neocortical neurons and a failure in formation of cortical layers (Buchsbaum and Cappello, 2019; Castello and Gleeson, 2021). Such disruption can be a consequence of the primary defect in the migrating neuron or in the progenitor cell (aRG or bRG) whose processes are providing a scaffold for the migrating neurons. In this review we focus on the cell biology of neural progenitors. MCDs such as heterotopia and lissencephaly can arise when the neuronal migration is incomplete, whereas polymicrogyria and cobblestone lissencephaly are usually observed in relation to an excessive migration (**Figure 1**) (Francis and Cappello, 2021). Heterotopia is characterized by clusters of normal neurons in abnormal locations (Barkovich et al., 2012; Guerrini and Dobyns, 2014; Guarnieri et al., 2018) whose migration was arrested in different moments. In case of periventricular nodular heterotopia (**Figure 1**), the nodules or thick bands of gray matter are stuck at or near the ventricular surface, whereas in subcortical heterotopia newborn neurons remain in the white matter (Barkovich et al., 2012; Guerrini and Dobyns, 2014). Lissencephaly ("smooth brain", also known as classical or type I lissencephaly) is characterized by an abnormal gyral pattern accompanied by thickening and altered layering of the neocortex (Di Donato et al., 2017; Buchsbaum and Cappello, 2019). It includes a spectrum of conditions, ranging from broadening of few gyri, as in the case of pachygyria, to a complete absence thereof, as in the case of agyria. The latter, however, is extremely rare as it is observed almost only in Miller–Dieker syndrome (Blazejewski et al., 2018). Polymicrogyria refers to an overfolding of the neocortex with presence of abnormally small gyri that can be focal, multifocal, or affecting the entire neocortex, often characterized by dyslamination with displaced and disoriented neurons and discontinuities in the pial basement membrane (**Figure 1**) (Squier and Jansen, 2014; Stutterd and Leventer, 2014; Jansen et al., 2016; Diamandis et al., 2017; Sarnat and Flores-Sarnat, 2021). Cobblestone lissencephaly (also known as type II lissencephaly) shows a cobblestone-like brain surface due to an over-migration of neurons through 'gaps' in the pial basement membrane (**Figure 1**) (Devisme et al., 2012; Buchsbaum and Cappello, 2019). The MCDs characterized by incomplete or excessive migration are most often caused by mutations in genes related to cytoskeleton and cell adhesion (Moon and Wynshaw-Boris, 2013; Jamuar and Walsh, 2015; Romero et al., 2018).

The final step of neocortical development is the post-migrational differentiation with integration into neuronal circuits, which includes complex events like growth and maturation of axons and dendrites, synaptogenesis and synaptic pruning. MCDs arising at this stage usually lead to certain forms of focal cortical dysplasia (FCD) and dysgyria. FCD is characterized by disorganized cortical lamination, variability in cortical thickness and abnormal gyral pattern (Najm et al., 2018; Subramanian et al., 2019). Dysgyria refers to a dysmorphic cortex with abnormalities in gyral size and sulcal depth (Mutch et al., 2016; Romaniello et al., 2018). The main identified causes of MCDs affecting post-migrational differentiation and integration into neuronal circuits are mutations in signaling molecules and

cytoskeletal proteins (Jamuar and Walsh, 2015; Manikkam et al., 2018; Romaniello et al., 2018).

The MCD-causing mutations often arise *de novo* during gametogenesis or postzygotic development (Wilfert et al., 2017; Juric-Sekhar and Hevner, 2019). The timing of mutation is often associated with the severity of phenotype (Sarnat, 1987; Sarnat and Flores-Sarnat, 2014). In this context, somatic mutations have recently been found to exert and important contribution to MCDs with focal insult, such as in focal heterotopia, focal cortical dysplasia and hemimegalencephaly (Jamuar et al., 2014; Jansen et al., 2015; Gonzalez-Moron et al., 2017; Montier et al., 2019). Somatic mutations can be of type 1 or type 2, which cause a new heterozygous mutation or lead to a loss of heterozygosity, respectively (Qin et al., 2010; Jansen et al., 2015; Juric-Sekhar and Hevner, 2019).

The landscape of pathological conditions of MCDs is highly heterogeneous, as are the genetic variants and molecular pathways involved in the disease onset. However, the classifications of MCDs are mainly based on the neurological outcome and neuroimaging data. Furthermore, specific genetic mutations or events can impact the cortical development by affecting different cell types and/or different developmental phases, thus causing various MCDs (Sapir et al., 2019; Klingler et al., 2021). In this review we focus on the neural progenitor cells and their role in generation of neurons and supporting neuronal migration. To bridge across scales from genetic mutations to neurological outcomes, we focus on the cell biological level, as a key interaction point between genes and phenotypes.

CELL BIOLOGICAL BASIS OF MALFORMATIONS OF CORTICAL DEVELOPMENT IN NEURAL PROGENITORS

Below we discuss the cell biological features of neural progenitors involved in the onset of MCDs. We particularly focus on the progenitor proliferation and polarity as key aspects disrupted in MCDs. Tight regulation of mitosis is the key cell biological feature influencing the proliferation of neural progenitors. Hence, protein products of many MCD-causative genes are associated to the mitotic spindle. Various microtubule-associated proteins that operate at centrosome, kinetochore or that are involved in microtubule dynamics and severing have been implicated with MCDs. Similarly, actin-binding proteins that are important for the progression of mitosis and its fine regulation are also associated with MCDs. To correctly progress through the cell cycle, neural progenitors need to be able to receive extrinsic signals and to transduce this information *via* intracellular signaling pathways. Maintaining correct cell polarity is a fundamental cell biological feature that enables both the exposure to extrinsic signals and the neuronal migration. Various molecules operating in both the apical and the basal endfeet of aRG and bRG, adherens junctions, cell trafficking, cilium as well as components of the extracellular matrix and its receptors have been implicated in MCDs. Further, different receptors and molecules operating in pro-proliferative signaling pathways are often mutated in MCDs. Finally, several metabolic enzymes, transcription factors and epigenetic modifiers that promote proliferation of neural progenitors are found to be mutated in patients with MCDs. Considering that many molecules, whose mutations are associated with MCDs, operate in multiple cell biological domains, we typically discuss individual molecules within the cell biological context that is the most relevant for the disease aetiology.

Mitotic Spindle

The mitotic spindle is the key element involved in establishing the orientation of the cleavage plane, that is symmetric versus asymmetric cell division, and therefore is involved in determining the fate of the daughter cells (Lancaster and Knoblich, 2012; Taverna et al., 2014; Matsuzaki and Shitamukai, 2015; Kalebic and Namba, 2021). Hence, it is not surprising that the proteins implicated in the function of the mitotic spindle are often found mutated in microcephaly (Bond and Woods, 2006; Sun and Hevner, 2014) (**Figure 2A**). A notable example is ASPM (abnormal spindle-like microcephaly-associated protein), whose mutations are the most common cause of primary microcephaly (Bond et al., 2002; Thornton and Woods, 2009). Depletion of Aspm from mouse cortex results in a reduction of vertical symmetric proliferative division of apical progenitors (NECs and aRG) and subsequent depletion of the progenitor pool (Fish et al., 2006; Pulvers et al., 2010). However, the phenotypes observed in mutant mice were poorly recapitulating the extent of microcephaly in human patients (Pulvers et al., 2010) likely because mouse neural progenitors are less proliferative than the human progenitors. Interestingly, a knockout (KO) of *Aspm* in the developing ferret neocortex led to a premature detachment of aRG and generation of bRG, which in turn led to a severe microcephaly, similarly to what was observed in human patients (Johnson et al., 2018).

The second most common cause of primary microcephaly are mutations in WDR62 (WD repeat domain 62, also known as MCPH2), a scaffold protein associated with the spindle pole (Bilguvar et al., 2010; Nicholas et al., 2010). WDR62 mutants fail to localize to the spindle pole and cells transiently arrest in mitosis (Nicholas et al., 2010; Farag et al., 2013; Chen et al., 2014; Sgourdou et al., 2017). Depletion of Wdr62 in mice lead to microcephaly due to reduced proliferation of neural progenitors, spindle instability and abnormalities in centrosome inheritance (Chen et al., 2014; Sgourdou et al., 2017). Mechanistically, WDR62 has been shown to interact with JNK1/2 (c-Jun N-terminal kinase) and AURKA (Aurora kinase A) as well as AURKB (Aurora kinase B), which is likely regulating its localization to the spindle pole and cell cycle progression in neocortical progenitors (Chen et al., 2014; Lim N. R. et al., 2015; Sgourdou et al., 2017). Mutations in MCPH1 (microcephalin 1) are another notable cause of primary microcephaly (Jackson et al., 2002). Disruption of *Mcph1* in mice leads to a mitotic spindle misalignment and a premature shift from symmetric to asymmetric cell divisions (Gruber et al., 2011). Importantly, MCPH1 is further involved in chromatin condensation and DNA

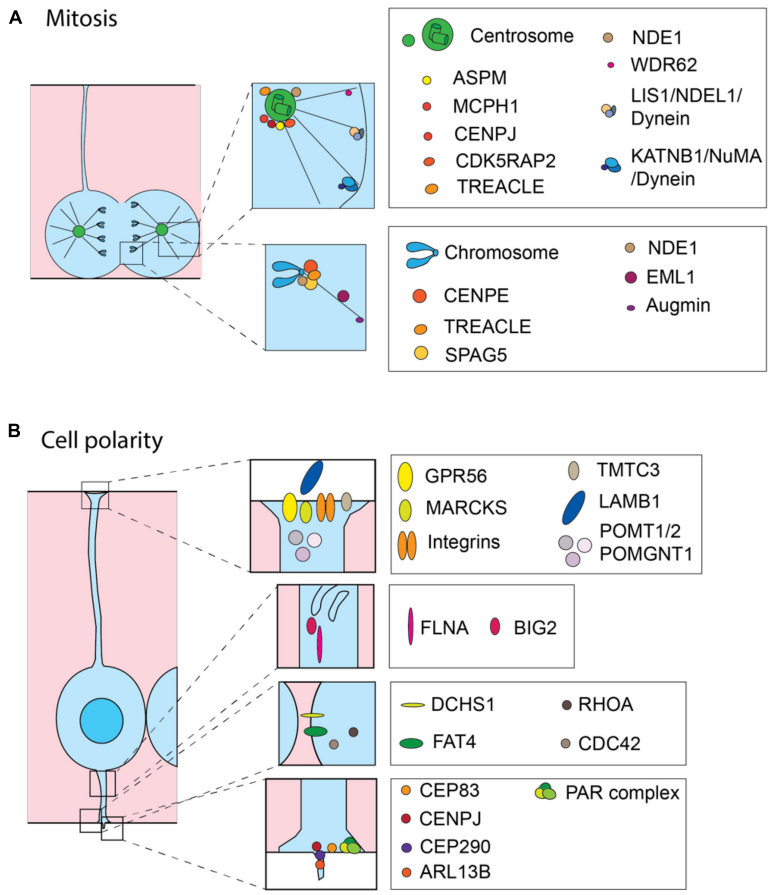

FIGURE 2 | Cell biological processes and molecules involved in the onset of MCDs. Schematic representation of proteins involved in MCDs. Most of the proteins are related to the precise regulation of mitosis **(A)** and maintaining correct cell polarity **(B)**. **(A)** During mitosis the MCD-involved proteins are mainly operating at the centrosome and astral microtubules (upper inset) or at the kinetochore (lower inset). **(B)** In interphase, MCD-involved proteins are operating at the basal endfoot (first inset from the top), intracellular trafficking (second inset from the top), adherens junctions (third inset from the top) and apical endfoot including cilium (the lowest inset) to maintain cell polarity.

damage repair with effects that span beyond the neocortex (Zhou et al., 2013; Pulvers et al., 2015; Houlard et al., 2021).

Various genes encoding for centrosomal proteins were found mutated in primary microcephaly (**Figure 2A**) (Bond et al., 2005; Gilmore and Walsh, 2013; Bizzotto and Francis, 2015). CDK5RAP2 (Cyclin Dependent Kinase 5 Regulatory Subunit Associated Protein 2; MCPH3) and CENPJ (Centromere protein J; MCPH6) are two notable examples (Bond et al., 2005). CDK5RAP2 mutant mice show thinning of the cerebral cortex with a reduction in late-born neurons, as a consequence of an early depletion of the progenitor pool due to the abnormal orientation of the mitotic spindle which leads to increased horizontal and reduced vertical cleavage planes (Lizarraga et al., 2010). CENPJ deletion in mice embryo also leads to a microcephaly, which in this case is a consequence of a progressive loss of centrioles in aRG and the subsequent detachment of progenitor cells from the VZ. Those detached progenitors continue proliferating, but exhibit a mitotic delay, which leads to an induction of apoptosis and a subsequent reduction in the number of progenitors (Insolera et al., 2014).

Similarly, *TCOF1*/TREACLE (Treacher Collins syndrome protein) is a centrosome- and kinetochore-associated protein that is required for mitotic progression and its mutation have been identified in patients with Treacher Collins syndrome who can exhibit microcephaly (Sakai et al., 2012). *Tcof1* mutant mice show abnormal spindle orientation, increased asymmetric cell division and defects in cell proliferation resulting in a smaller progenitor pool, fewer neurons and decreased brain size (Sakai et al., 2012). CENPE (Centromere protein E) is a core kinetochore component required for spindle microtubule capture and attachment at the kinetochore (Abrieu et al., 2000; Yao et al., 2000). Mutations in CENPE alter spindle dynamics and chromosome segregation leading to delayed mitotic progression and finally resulting in a microcephaly with a simplified gyral pattern (Mirzaa et al., 2014b).

During mitosis microtubules are generated by the centrosomal nucleation, chromatin-mediated nucleation and by nucleation from the surface of other microtubules (Meunier and Vernos, 2016). The latter mechanism is mediated by augmin that binds to the microtubule lattice, upon its generation by the centrosome-

and chromatin-dependant pathways, and promotes the growth of new microtubules as branches (Kamasaki et al., 2013). Conditional knockout of the augmin subunit Haus6 in aRG leads to spindle assembly defects, p53-mediated apoptosis and an increase in DNA damage, which in turn leads to a reduction of neurogenesis, disruption of tissue integrity and finally an abortion of the brain development (Viais et al., 2021).

Mutations in genes that encode for proteins involved in microtubule dynamics can also lead to abnormal spindle orientation and subsequent MCDs (**Figure 2A**). EML1 (echinoderm microtubule associated protein-like 1) is a microtubule-associated protein whose mutation leads to complex cortical malformations characterized by megalencephaly with a ribbon-like heterotopia and callosal agenesis (Kielar et al., 2014; Oegema et al., 2019). The spontaneously arisen mutant mice (HeCo mice) and KO mouse models recapitulate the heterotopia phenotype (Kielar et al., 2014; Collins et al., 2019). HeCo mice are characterized by a perturbation of microtubule dynamics and an increase in oblique cleavage orientations of aRG, that lead to ectopic proliferation of progenitor cells in IZ and CP (Kielar et al., 2014; Bizzotto et al., 2017). NDE1 (nudE neurodevelopment protein 1), whose mutations in human patients can lead to a severe microcephaly with lissencephaly, is involved in centrosome duplication and mitotic spindle assembly, attachment of microtubules to kinetochores and proper neuronal migration (Feng and Walsh, 2004; Vergnolle and Taylor, 2007; Alkuraya et al., 2011). Its ablation in the mouse neocortex induces microcephaly, due to abnormal orientation of cleavage plane, aberrant chromosome localization, mitotic delay and premature cell cycle exit (Feng and Walsh, 2004). Similarly, mutations observed in patients truncate the C-terminal domain, which is involved in the localization to the centrosome (Alkuraya et al., 2011). Consequently, they dysregulate cytoskeletal dynamics in mitosis, leading to spindle-structure defects that include tripolar spindles, misaligned mitotic chromosomes, nuclear fragmentation and abnormal microtubule organizations (Alkuraya et al., 2011). Deletion or mutations of LIS1 (Lissencephaly 1 protein; encoded by *PAFAH1B1*, Platelet activating factor acetylhydrolase 1b regulatory subunit 1) are the major cause of classical lissencephaly in humans (Reiner et al., 1993; Romero et al., 2018). Different rodent models have shown that LIS1 is important for both progenitor proliferation and neuronal migration (Cahana et al., 2001; Gambello et al., 2003; Tsai et al., 2005). LIS1 deletion leads to proliferation defects of apical progenitors due to misorientation of the mitotic spindle, reduced and weakened astral microtubules and increased apoptosis (Yingling et al., 2008). Mechanistically, Lis1 operates with Nde1 to target the cytoplasmic dynein complex, whereas the complex Lis1/Ndel1 (Nde1 like)/dynein is important for microtubule stability and cortical capture (Feng and Walsh, 2004; Yingling et al., 2008; McKenney et al., 2010; Moon et al., 2020). Lis1 and dynein are connected to the nuclear envelope through their interaction with the SUN- and KASH-domain proteins, SUN1/2 and Syne/Nesprin-1/2, which have a critical role in nuclear movement during neurogenesis and neuronal migration, as their ablation in mice leads to defects in cortical lamination and reduced brain size (Zhang et al., 2009).

Another protein involved in microtubule dynamics at mitosis, KATNB1 (B1 subunit of the microtubule severing enzyme katanin), has been associated with severe microcephaly with lissencephaly (Mishra-Gorur et al., 2015). KATNB1 plays an important role at the spindle pole together with cytoplasmic dynein and NuMA (nuclear mitotic apparatus protein), which tethers spindles at the poles and is fundamental for microtubule aster formation (Mishra-Gorur et al., 2015; Jin et al., 2017). Studies of various proteins involved in spindle positioning in both *Drosophila* neuroblasts and mammalian neocortical progenitors suggest an important role of spindle orientation for determination of cell fate, notably in generation of BPs (Lancaster and Knoblich, 2012; Matsuzaki and Shitamukai, 2015). For example, overexpression of Insc (Inscuteable) or a KO of LGN lead to an increase in BPs, that in case of LGN KO exhibit characteristics of bRG (Konno et al., 2008; Postiglione et al., 2011). Considering the importance of BPs, and in particular bRG, for the human cortical development, it is important to examine the mechanisms of bRG generation in order to better understand the MCD aetiology.

Actin Cytoskeleton and Cell Division

Several actin-binding proteins implicated in MCDs operate during the cell division of neural progenitors. Mutations in FLNA (Filamin A), which crosslinks actin filaments and links them to membrane proteins, can be a cause of periventricular heterotopia (Fox et al., 1998; Sheen et al., 2005). Knockout of FLNA in mice leads to prolongation of the cell cycle length by delaying the onset and progression through mitosis due to impaired regulation of cyclin B1 degradation which results in a decline in the progenitor numbers and a reduction of the brain size (Lian et al., 2012). Other actin-binding proteins were shown to be implicated in the neural progenitor division. For example, depletion of n-cofilin, which is involved in depolymerization of actin filaments, leads to an increased cell cycle exit of neural progenitors and a depletion of the progenitor pool (Bellenchi et al., 2007). PFN1 (Profilin-1) regulates actin polymerization and is associated with Miller–Dieker syndrome which is characterized by a lissencephaly (Kwiatkowski et al., 1990). In mutant mice model, absence of PFN1 leads to a change in cleavage plane orientation with an increase in horizontal divisions (Kullmann et al., 2020). This in turn led to an increase in bRG abundance and neuronal production during mid-neurogenesis and a formation of rudimentary neocortical folds. It hence remains important to examine the role of PFN1 and other actin-binding proteins for the proliferation of BPs in the developing human neocortex. Interestingly, a small GTPase Rac1 (Ras-related C3 botulinum toxin substrate 1), which regulates many cellular processes including cytoskeletal organization, is required for survival of neural progenitors and for the normal proliferation and differentiation of BPs, specifically (Leone et al., 2010). Deletion of Rac1 in telencephalon results in microcephaly with reduced size of both cerebral cortex and striatum (Chen et al., 2009), whereas its ablation in the progenitors situated in medial ganglionic eminence impairs their transition from G1 to S phase and leads to an impairment of GABAergic interneurons migration into the cortex (Vidaki et al., 2012).

Actin rearranges at the cell cortex and enhances cell membrane rigidity, which is important for proper anchorage of astral microtubules (Heng and Koh, 2010). DIAPH3 (Diaphanous three) is a member of the formin protein family that nucleate and elongate actin filaments and has a role in spindle assembly and cytokinesis. Two clinical studies point to *DIAPH3* as an autism susceptibility gene (Vorstman et al., 2011; Xie et al., 2016). DIAPH3 deficiency in mice induces centrosome abnormalities, disrupts the spindle and astral microtubules and leads to a loss of cortical progenitors, microcephaly, and autistic-like behavior (Lau et al., 2021). Depletion of DIAPH3 leads to downregulation of SPAG5, a kinetochore- and centrosome-associated protein that controls sister chromatid cohesion and recruitment of CDK5RAP2 to centrosome (Kodani et al., 2015). Knockdown of SPAG5 induces similar mitotic errors as the depletion of DIAPH3 and its overexpression rescues DIAPH3 knockdown phenotype (Kodani et al., 2015; Lau et al., 2021), emphasizing the importance of cooperation of actin and microtubule associated proteins in mitotic progression.

Cytokinesis

Cytokinesis is the final step in the mitosis. Cleavage furrow of aRG starts on the basal side and ingresses toward the apical membrane, a process which is mediated by anillin and actin-based cortex (Kosodo et al., 2008; Kosodo and Huttner, 2009). The midbody is formed at the end of the furrow as a structure that contains compacted microtubules. The midbody often relocates to the daughter cells containing the apical processes and is subsequently released into the ventricle (Dubreuil et al., 2007; Ettinger et al., 2011). Among the proteins involved in abscission are members of Kinesin-6 family. Interestingly, one of them, Kif20b, was found to be mutated in *magoo* mouse mutant which exhibits a fully penetrant microcephaly (Janisch et al., 2013). Kif20b mutants show changes in the midbody number, shape and position resulting in the disruption of the abscission step, which in turn causes apoptosis of neural progenitors and leads to a small cerebral cortex (Janisch et al., 2013).

Interphase Centrosome and Cilia

During interphase centrosomes are positioned in the apical endfeet of aRG, where they contribute to cell polarity, ciliogenesis and cell attachment (Taverna et al., 2014). Centrosome consists of two centrioles and upon a cell division, the older centriole is typically inherited by the proliferative daughter cell that remains an aRG, whereas the daughter centriole is inherited by the differentiating daughter cells (neuron or BP) (Wang et al., 2009). Previously mentioned microcephaly proteins ASPM and WDR62 during interphase localize to mother centrioles where they physically interact (Jayaraman et al., 2016). Loss of either of them or both leads to a defective centriole duplication and impaired cilia, resulting in premature delamination of progenitors and microcephaly (Jayaraman et al., 2016). It was shown recently that the mother centriole in aRG contains distal appendages that anchor it to the apical membrane and that CEP83 (centrosomal protein 83), a protein implicated in intellectual disabilities, is required for their maintenance (**Figure 2B**) (Shao et al., 2020). The elimination of CEP83 led to expansion of the progenitor pool which resulted in macrocephaly with abnormal folding. The rigidity of the apical membrane was affected, and the mechanically sensitive YAP (yes-associated protein) was activated, hence promoting progenitor proliferation (Shao et al., 2020). YAP was shown to promote proliferation of BPs in humans and ferrets, and it would hence be interesting to explore a possible role of this mechanism in human MCDs pertinent to BPs (Kostic et al., 2019). Importantly, AKNA, another protein that associates to mother centrioles, was shown to play a role not only in generation of BPs, but also in retaining cells in the SVZ, which again suggests to examine the role of centrosome-associated proteins in the context of BP cell biology (Camargo Ortega et al., 2019).

The mother centriole forms the basal body, a structure that makes the base of the primary cilium, an organelle involved in signaling, mechanotransduction and cell fate (Taverna et al., 2014). Interestingly, the ciliary membrane, which is endocytosed at the onset of mitosis along with the mother centriole, also tends to be inherited by the proliferative daughter cell (Paridaen et al., 2013). Perturbations of ciliary structure or function leads to ciliopathies such as Joubert and Bardet–Biedl syndromes, which can result in cortical disorganization and intellectual disabilities (Taverna et al., 2014; Bizzotto and Francis, 2015). Mutation in centrosomal proteins CENPJ and CEP290 (centrosomal protein 290) have been associated with ciliary phenotypes (**Figure 2B**). CEP290, which can be mutated in Joubert syndrome, is required for the function of Rab8, a protein involved in ciliogenesis (Valente et al., 2006; Kim et al., 2008). CENPJ has an important role in regulating cilia disassembly as its loss causes alterations in length of cilia, leading to delayed cell cycle, reduced cell proliferation, and increased cell apoptosis, all together resulting in microcephaly (Ding et al., 2019). ARL13B, mutated in Joubert syndrome, is a small GTPase specifically enriched in the cilium and required for ciliary structure and function. Knockout mice show inverted cell polarity with the cell body located on the pial surface and the basal endfoot positioned on the ventricular side (Higginbotham et al., 2013).

Cell Polarity

Cell polarity is a fundamental feature of neural progenitor cells. Whereas aRG exhibit a classical apicobasal polarity, with the apical pole lining the ventricular surface and the basal side contacting the pia, BPs show a greater heterogeneity in their cell polarities (Taverna et al., 2014; Kalebic et al., 2017). bIPs typically exhibit multipolar morphology in interphase, whereas bRG show polarized morphology, often containing the basal process contacting the pia, but not the apical polarity domain which can hence be termed pseudo-apicobasal polarity (Kalebic and Namba, 2021).

Apical progenitors contain a specialized apical polarity complex, which is fundamental for cell polarity, and it contains Par3 (Partitioning defective protein 3), Par6 (Partitioning defective protein 6), and aPKC (atypical protein kinase C) (Costa et al., 2008; Bultje et al., 2009; Hansen et al., 2017; Kalebic and Namba, 2021). Par-complex proteins are important for regulating aRG proliferation and differentiation in the developing cerebral cortex, as the inheritance of the apical domain is associated with

maintenance of stemness. Par complex contributes to regulating Notch signaling by enriching Notch on the plasma membrane of the daughter cells that inherited the apical domain and thereby enables that cell to maintain its stemness (Bultje et al., 2009; Kandachar and Roegiers, 2012). Overexpression of both Par3 and Par6 promoted generation of proliferative progenitors in the developing mouse neocortex (Costa et al., 2008). Loss of Par3 in developing mouse cortex causes severe MCD including increased volume and massive ribbon-like heterotopia (Liu et al., 2018). This was caused by temporally different progenitor behaviors in response to HIPPO and NOTCH signaling. During early phase of neurogenesis, the progenitor proliferation was increased at the expenses of production of deep-layer neurons, whereas at later stages the differentiation was increased leading to an increased production of upper layer neurons (Liu et al., 2018). The megalencephaly and heterotopia phenotypes were rescued by a simultaneous removal of the HIPPO pathway effectors YAP and TAZ (transcriptional coactivator with PDZ-binding motif), underlining again an important role of HIPPO pathway in cortical development (Liu et al., 2018).

Adherens Junctions

Adherens junctions play a key role in maintaining aRG polarity and VZ cohesion. Their disruption or instability can affect aRG morphology and lead to detrimental consequences on the cortical lamination and neuronal migration (**Figure 2B**) (Veeraval et al., 2020). The conditional knockout mouse of N-cadherin, a key junctional protein, displays a complete loss of cortical organization with mitotic and postmitotic cells scattered throughout the cortex and aRG that could not grow their processes (Kadowaki et al., 2007). Deletion of α-E-catenin in mouse cerebral cortex causes an uncoupling of adherens junctions with the intracellular actin fibers, which results in a loss of tissue polarity and formation of large subcortical band heterotopia, as migrating neurons fail to reach the cortical plate and accumulate in ectopic positions (Schmid et al., 2014). Similarly, inactivation of CDH2 (cadherin 2) or afadin, a junctional adaptor protein, results in a disruption of adherens junctions and an increase in progenitor proliferation, which again leads to a phenotype resembling subcortical band heterotopia (Gil-Sanz et al., 2014; Rakotomamonjy et al., 2017). Maintenance of cadherin-based adherens junctions requires Numb and Numbl (Numb-like) which localize to the apical end-foot. Their inactivation disrupts adherens junctions, causes premature progenitor depletion, abnormal progenitor dispersion and disorganized cortical lamination (Li et al., 2003; Petersen et al., 2004; Rasin et al., 2007).

Mutations in the receptor-ligand cadherin pair DCHS1 (Dachsous cadherin-related 1) and FAT4 (FAT Atypical Cadherin 4) have been associated with the Van Maldergem syndrome, which is characterized by a periventricular neuronal heterotopia (**Figure 2B**) (Cappello et al., 2013). Knockdown of those genes in the developing mouse neocortex results in increased progenitor cell numbers and reduced neuronal differentiation, which in turn leads to a heterotopic accumulation of cells below the neuronal layers (Cappello et al., 2013). Cerebral organoids derived from induced pluripotent stem cells (iPSCs) of patients with mutations in DCHS1 and FAT4 recapitulate the heterotopic phenotype, however, without a change in progenitor proliferation, highlighting the inter-species differences (Klaus et al., 2019). The phenotype of mutant organoids is due to a combination of changes in the morphology of neural progenitor cells and altered navigational system of some neurons, underscoring the importance of the neural progenitor cell biology for the neuronal migration also in the human model system (Klaus et al., 2019).

Rho GTPases are fundamental regulators of cytoskeleton organization and cell polarity during neocortical development. Conditional deletion of RhoA (Ras homolog family member A) in neural progenitors leads to the disruption of apical anchoring and mis-orientation of aRG processes which results in heterotopia underneath a thinner cortex, reminiscent of cobblestone lissencephaly (Cappello et al., 2012). Conditional deletion of Cdc42 (Cell Division Cycle 42) in mice leads to a gradual loss of adherens junctions, impairing the apically directed interkinetic nuclear migration, which results in progenitors undergoing mitoses at basal positions and acquiring the neurogenic fate of BPs (Cappello et al., 2006). Further, mice deficient in both DIAPH1 and 3, actin nucleators and Rho effectors, develop a periventricular dysplastic mass due to disruption of apical adherens junctions in aRG and impaired cell polarity (Thumkeo et al., 2011). Interestingly, a mutation in RhoA activator, PLEKHG6 (Pleckstrin homology and RhoGEF domain containing G6), was found in human heterotopia and it leads to the loss of a primate-specific isoform of this protein (O'Neill et al., 2018). Modulation of PLEKHG6 isoform in human cerebral organoids once again highlights the relevance of BPs and in particular bRG for the aetiology of human MCDs. Similarly, downregulation of another plecstrin homology domain protein, PLEKHA7 (Pleckstrin homology domain containing A7), which is adherens junction belt-specific, results in delamination of neural progenitors from the ventricular surface and conversion of aRG to bRG (Tavano et al., 2018). Furthermore, LGALS3BP (Galectin 3 binding protein), a secreted protein that interacts with components of the extracellular matrix, has been found mutated in patients with altered local gyrification and cortical thickness (Kyrousi et al., 2021). Analysis in electroporated mouse embryos and human organoids suggests that LGALS3BP, which is involved in the apical anchoring, is mediating BP delamination that in turn is critical for the proper neuronal migration and cortical folding (Kyrousi et al., 2021).

Intracellular Trafficking

Cell polarity is highly dependent on traffic through the secretory pathway and, interestingly, the pathological endoplasmic reticulum (ER) and the Golgi apparatus stress have been associated with MCDs, in particular microcephaly (**Figure 2B**) (Passemard et al., 2019). Some patients affected by microcephaly and periventricular heterotopia present mutations in the *ARFGEF2* (ADP-ribosylation factor guanine nucleotide-exchange factor-2), encoding for BIG2 [brefeldin A (BFA)-inhibited GEF2 protein]. BIG2 promotes the activation of ARF (ADP-ribosylation factor) proteins by guanine-nucleotide exchange, regulating Golgi vesicular budding and uncoating.

In vitro experiments show that inhibition of BIG2 decreases cell proliferation of mouse neural progenitors, possibly due to the aberrant intracellular localization of E-cadherin and β-catenin (Sheen et al., 2004). The other principal gene implicated in periventricular heterotopia, FLNA, is also implicated in intracellular trafficking, as it has been shown that FLNA facilitates trafficking of β1 integrin to the cell membrane (Kim et al., 2010). Further, deletion of BIG2 promotes phosphorylation of FLNA which in turn affects FLNA-actin binding affinity and changes the localization of FLNA, suggesting a cooperative action between actin and vesicle trafficking in the assembly of membrane proteins (Zhang et al., 2012, 2013). Considering the recently revealed novel features of the Golgi apparatus in apical versus basal progenitors and the differential contribution of Golgi to the apical versus basal process of the neural progenitors (Taverna et al., 2016; Taverna and Huttner, 2019), it is important in the future to better assess the importance of intracellular trafficking for the onset of MCDs.

Basal Attachment

Migration of newborn neurons from the site of their generation in GZ to their final position in the CP occurs along the basal processes of aRG and bRG that make a radial scaffold (Rakic, 2009; Geschwind and Rakic, 2013; Fernandez et al., 2016). In lissencephalic species, such as mouse, this scaffold is simpler, it consists mainly of the basal processes of aRG, as bRG are very rare in mouse, and it enables a radial migration of newborn neurons. In gyrencephalic species, such as human, ferret or macaque, this scaffold is more complex and apart of the radial migration, it enables also the tangential dispersion of neurons, which is required for correct folding (Fernandez et al., 2016; Kalebic and Huttner, 2020; Del Valle Anton and Borrell, 2021; Kalebic and Namba, 2021). Such complexity might be facilitated by the existence of bRG morphotypes with two basal processes, which were described in humans and ferrets, but not in mice (Kalebic et al., 2019). Further, at mid-neurogenic period human aRG become truncated, loose their basal processes and the migration of the late-born neurons is mediated only by the bRG-generated scaffold (Nowakowski et al., 2016).

Various cytoskeletal molecules have been implicated in maintenance of the basal processes. The attachment of the basal endfoot to the pia is mediated by various receptors and extracellular matrix (ECM) components. Many of these molecules have been associated with MCDs, most commonly because the defective radial scaffold leads to impairments in the migration of neurons (**Figure 2B**). Knockout mice for Marcks (myristoylated alanine-rich substrate protein), an actin cross-linking protein, disrupted basal end feet and led to a disorganization of the radial scaffold, which resulted in displacement of progenitors and heterotopia (Blackshear et al., 1997; Weimer et al., 2009). A deletion in the regulatory region of *GPR56* [guanine nucleotide-binding protein (G protein)-coupled receptor 56], was found in patients with polymicrogyria surrounding bilaterally the Sylvian fissure including Broca's area, the primary language area (Bae et al., 2014). Knockout mice show reduced cortical thickness and irregular cortical organization due to the defect in the progenitor proliferation (Bae et al., 2014). GPR56 localizes to the basal endfeet and binds to ECM components in the basal lamina, such as collagen III, which is considered to promote the proliferation of aRG and bRG (Singer et al., 2013). GPR56 functions together with α3β1 integrin, another major receptor of the ECM components (Jeong et al., 2013). The role of integrins in progenitor proliferation has been particularly highlighted in the context of BPs, and in particular bRG, in the gyrencephalic species (Fietz et al., 2010; Stenzel et al., 2014; Kalebic et al., 2019). Hence the disruption of the basal process is often linked to the perturbation of proliferation, in addition to migrational defects (Bizzotto and Francis, 2015; Kalebic and Huttner, 2020).

The most frequent cause of cobblestone lissencephaly are the mutations in genes which are required for the functional maturation of α-dystroglycan, another major ECM receptor (Devisme et al., 2012; Bizzotto and Francis, 2015). These genes include *POMT1* and *2* (Protein O-mannosyltransferase 1 and 2) (Beltran-Valero de Bernabe et al., 2002; van Reeuwijk et al., 2005), *POMGNT1* (Protein O-linked mannose *N*-acetylglucosaminyltransferase 1) (Yoshida et al., 2001), *LARGE* (LARGE xylosyl-and glucuronyltransferase 1) (van Reeuwijk et al., 2007), *TMEM5* (Transmembrane protein 5), *ISPD* (Isoprenoid synthase domain containing) (Vuillaumier-Barrot et al., 2012) and others. Finally, one-third of the cases of cobblestone lissencephaly are still unexplained, suggesting that other genes and pathways are involved (Devisme et al., 2012). Mutations in the transmembrane protein TMTC3 (transmembrane and tetratricopeptide repeat containing 3), which does not contain obvious functional connections to α-dystroglycan, have been found in patients with cobblestone lissencephaly (Jerber et al., 2016).

Mutations in the genes encoding for the components of the ECM can also lead to MCDs (**Figure 2B**). A notable example is *LAMB1* (laminin subunit β1) whose mutations were found in patients with cobblestone lissencephaly with severe cerebellar dysplasia, brainstem hypoplasia, and occipital encephalocele (Radmanesh et al., 2013). Enzymes involved in the production of ECM components have been associated with MCDs. ECE2 (endothelin-converting enzyme-2) has recently been found mutated in patients with periventricular heterotopia (Buchsbaum et al., 2020). Genetic manipulation in embryonic mouse neocortex and human cerebral organoids revealed that ECE2 is important for apicobasal cell polarity, apical belt integrity, actin and microtubule cytoskeleton dynamics and production of ECM components (Buchsbaum et al., 2020).

Pro-proliferative Signaling

Various signaling pathways are involved in promoting proliferation of neural progenitor cells. Notch, Shh, Wnt, PDGF, FGF, ECM-integrin, ERK, Hippo, PI3K-AKT, and mTOR are some of the most notable examples (Penisson et al., 2019; Ferent et al., 2020; Kalebic and Huttner, 2020). Many of the components of those pathways have been implicated in MCDs. Among the receptor tyrosine kinases, fibroblast growth factor receptors (FGFRs), are particularly relevant associated with the syndromes characterized by brain malformations. Apert syndrome, in which brain malformation is considered secondary

to the cranial abnormalities, is caused by mutations in FGFR2 (Aldridge et al., 2010). Instead, a mutation in FGFR3, which leads to a constitutive activity of the receptor, causes thanatophoric dysplasia (Hevner, 2005; Pannier et al., 2009). This disease is characterized by a combination of cortical abnormalities, which affects most severely the temporal lobe (Hevner, 2005). Mouse model of the thanatophoric dysplasia successfully recapitulated the megalencephaly phenotype, but not the other abnormalities (Lin et al., 2003). Instead the ferret model recapitulated all the other phenotypes found in human patients, such as polymicrogyria (Masuda et al., 2015), periventricular nodular heterotopia (Matsumoto et al., 2017a) and leptomeningeal glioneuronal heterotopia (Matsumoto et al., 2018). Similarly to FGF signaling, insulin growth factor (IGF) signaling through IGF1R (type 1 IGF receptor) stimulates progenitor proliferation and mutations in IGF1R were detected in patients with brain overgrowth (Faivre et al., 2002; Joseph D'Ercole and Ye, 2008).

Notch signaling pathway plays an essential role in neurogenesis through the process of lateral inhibition (Fortini, 2009; Pierfelice et al., 2011). In mammalian neocortex, Notch ligands are expressed by neurons and intermediate progenitors which signal back to aRG and bRG (Hansen et al., 2010; Nelson et al., 2013). The different combinations of Notch signaling molecules are involved in maintenance and likely diversification of the progenitor pool (Nelson et al., 2013). Further, Notch signaling can be amplified by reelin, a glycoprotein secreted by Cajal–Retzius cells. In addition to controlling neuronal migration and neocortical lamination, reelin promotes symmetric proliferative division of radial glia modulating thus the rate of neurogenesis (Lakoma et al., 2011; Hirota and Nakajima, 2017). Mutation in *RELN*, the gene encoding for reelin, have been shown to be associated with autosomal recessive lissencephaly as well as various neuropsychiatric disorders, such as schizophrenia (Hong et al., 2000; Fatemi, 2001; Ishii et al., 2016).

Recent studies have shown that diverse forms of brain overgrowth are often caused by mutations in the PI3K (phosphatidylinositol-3-kinase)–AKT signaling pathway (Hevner, 2015). Activating mutations of PI3K-AKT can cause hemimegalencephaly, dysplastic megalencephaly, heterotopia, polymicrogyria, pachygyria, and focal aggregates of small undifferentiated cells. Mildly activating variants, that are usually constitutional or germline, are associated with diffuse megalencephaly with intellectual disability and/or autism spectrum disorder, while moderately and strongly activating variants emerge as mosaic mutations and they are associated with mosaic megalencephaly, hemimegalencephaly and focal cortical dysplasia (Lee et al., 2012; Poduri et al., 2012; Riviere et al., 2012; Hevner, 2015; Jansen et al., 2015; Alcantara et al., 2017; Dobyns and Mirzaa, 2019). Mouse mutants for *Akt3* and *Pten* (phosphatase and tensin homolog) showed significant enlargement of the brain, but could not recapitulate the phenotypes pertinent to cortical folding (Groszer et al., 2001; Tokuda et al., 2011). Interestingly, when *PTEN* was deleted in human brain organoids, the subsequent activation of the PI3K-AKT pathway and increased proliferation of neural progenitors led to an increase in organoid size and the onset of organoid folding (Li et al., 2017). Mutations in the small GTPase gene RAB39b are associated with macrocephaly, autism spectrum disorder and intellectual disability (Woodbury-Smith et al., 2017). Deletion of RAB39b promotes PI3K–AKT signaling and leads to increased progenitor proliferation and macrocephaly in mouse model and increased organoid size in human *in vitro* model (Zhang et al., 2020).

PI3K-AKT signaling inhibits the activity of GSK3 (glycogen synthase kinase 3), a fundamental regulator of radial glia polarity. GSK3 inhibition in mouse aRG disrupts the radial organization of cell processes impairing thus the scaffold system that allows neuronal migration and affecting the progenitor proliferation (Yokota et al., 2010). Similarly, chronic inhibition of GSK3 in human cortical organoids increased the proliferation of neural progenitors (Lopez-Tobon et al., 2019). Some cases of megalencephaly and polymicrogyria are caused by mutations in *CCND2* (cyclin D2), a protein implicated in the cell cycle progression and a target of GSK3 (Kida et al., 2007; Mirzaa et al., 2014a). *In utero* electroporation of mutant *CCND2* into embryonic mouse cortex resulted in an increase in neural progenitor proliferation, likely explaining the brain enlargement of human patients (Mirzaa et al., 2014a).

Mammalian target of rapamycin (mTOR) signaling, also modulated by PI3K-AKT, is on the most important biological pathways and it is implicated in various diseases ranging from cancer to neurodevelopmental pathologies (Dobyns and Mirzaa, 2019). Mutations that affect mTOR are a common cause of focal cortical dysplasia and brain overgrowth along with the associated intellectual disabilities (Mirzaa et al., 2016; Marsan and Baulac, 2018; Kumari et al., 2020). Focal cortical dysplasia type II, which is the main cause of refractory epilepsy, is often caused by brain somatic mutations in mTOR kinase that lead to its hyperactivation (Lim J. S. et al., 2015). Indeed, overexpression of mutant mTOR by *in utero* electroporation in mice disrupts neuronal migration and causes spontaneous seizures, whereas the inhibition of mTOR can supress the seizures (Lim J. S. et al., 2015). Somatic mutations in genes involved in mTOR pathway, that occur in an early cell cycle of neocortical progenitors can lead to a more detrimental phenotype, that is hemimegalencephaly (Sarnat and Flores-Sarnat, 2014). The pathological phenotype can be a consequence of either a rare disruptive event causing hyperactivation of the pathway, or through the collective effects of many common alleles (Reijnders et al., 2017). Such activation of the pathway typically leads to over-proliferation of neural progenitors and subsequent increase in brain size (Dobyns and Mirzaa, 2019).

The pathway PI3K-AKT-mTOR is particularly interesting as mTOR pathway seem to be enriched in bRG (Nowakowski et al., 2017; Andrews et al., 2020) and PI3K-AKT is highly upregulated upon forced proliferation of mouse BPs (Kalebic et al., 2019). This suggests that PI3K-AKT-mTOR might play a specific role in promoting proliferation of BPs in species with an expanded cortex, such as human, and that the perturbations of its activity could have particularly relevant consequences for the proliferation of human bRG. Hence, a better understanding of the cellular processes impaired by PI3K-AKT-mTOR mutation would be fundamental for providing early diagnosis and appropriate therapy based on pathway inhibitors.

Cell Metabolism

Neocortical progenitor metabolism is emerging as an important player for progenitor proliferation and cortical expansion and its dysregulation can lead to various neurodevelopmental disorders (Namba et al., 2021). Mitochondrial activity has a fundamental role in regulating the proliferation of progenitors and the deficiency of mitochondrial function can cause MCDs. For example, Amish lethal microcephaly is caused by a mutation of the *SLC25A19* (Solute carrier family 25 member 19), coding for a mitochondrial thiamine pyrophosphate carrier, which is a coenzyme for α-ketoglutarate dehydrogenase that operates in the TCA (tricarboxylic acid) cycle, (Kelley et al., 2002; Rosenberg et al., 2002). Interestingly, it appears that glutaminolysis, which provides α-ketoglutarate, is required for the proliferation of neural progenitors. MCPH1, which can be located also on the mitochondria, interacts with VDAC1, an ion channel on the outer membrane, and stimulates the mitochondrial activity *via* glutaminolysis, increasing the mitochondrial calcium concentration (Journiac et al., 2020). When *MCPH1* is mutated, the defects in mitochondrial structure and metabolism lead to a reduction in cell proliferation and survival and finally to microcephaly (Journiac et al., 2020). Furthermore, glutaminolysis has been identified as the principal mechanism that the human-specific ARHGAP11B utilizes to promote BP proliferation (Namba et al., 2020). Together, this suggests that the glutaminolysis might have an important role in both brain evolution and the onset of MCDs. Enzymes involved in asparagine and serine synthesis have been also implicated in microcephaly (Ruzzo et al., 2013; Acuna-Hidalgo et al., 2014). For example, mutations in *ASNS*, which encodes asparagine synthetase, have also been identified in patients characterized by congenital microcephaly, intellectual disability, progressive cerebral atrophy and intractable seizures (Ruzzo et al., 2013). ASNS mutant mice have structural brain abnormalities, including enlarged ventricles, reduced cortical thickness, deficits in learning and memory (Ruzzo et al., 2013).

In addition, defects in fatty acid metabolism and transport have been shown to cause microcephaly. A microcephalic patient has been identified carrying a deletion of *BBOX1* (butyrobetaine-gamma 2-oxoglutarate dioxygenase 1), that encodes an enzyme involved in carnitine synthesis (Rashidi-Nezhad et al., 2014). Carnitine shuttle system is required for the transport of long-chain fatty acids into mitochondria. Cpt1a (carnitine palmitoyltransferase 1A), an essential protein in the carnitine shuttle system, is involved in maintaining the proliferation of neural progenitors (Knobloch et al., 2017). MFSD2A (major facilitator superfamily domain–containing 2a) is a transporter required for the uptake of docosahexanoic acid (DHA) in the brain. Inactivating mutations in this gene cause a lethal microcephaly syndrome due to inadequate uptake of the essential omega-3 fatty acid (Guemez-Gamboa et al., 2015). Lipid metabolism might be particularly important for the proliferation of BPs since palmitoylation, a reversible lipidation with profound roles in the development and function of the nervous system (Fukata and Fukata, 2010), has been recently shown to be required for maintaining the proliferation of BPs in the human cortical tissue (Kalebic et al., 2019).

DISCUSSION

Genetic linkage studies have been the basis for understanding the mechanisms underlying the MCDs so far. In contrast, their diagnosis and classification are mainly based on the neurological outcomes at the tissue and organ levels. Hence, understanding the cell biological context in which these molecules operate is key in order to improve the mechanistic knowledge and better bridge between genes and phenotypes. This is particularly relevant for the neural progenitors, as their cell biology often appears to be the *fons et origo* of many MCDs. Disrupted proliferation of neural progenitors can lead to microcephaly and macrocephaly, whereas impaired polarity and/or detachment from the apical and basal pole of the tissue can lead to lissencephaly or heterotopia. The situation, however, is more complex since various cell types, principally migrating neurons, can have a dominant role in specific MCDs. It is further known that mutations in the same genes can exert different roles in progenitors and neurons. Further complexity of MCDs is characteristic of the genetic and phenotypic levels. MCDs can have both monogenic and polygenic causes, whereas genetic mutations can have both convergent and divergent relations with the final phenotypes (Klingler et al., 2021). In addition to genomic mutations, there are various environmental factors that have been implicated in MCDs: alcohol, stress, nicotine, cocaine, hypoxia, and various viral infections, notably ZIKA and SARS-Cov-2 (Luhmann, 2016; Sarieva and Mayer, 2021). To tackle the mechanisms through which all of these contribute to the onset of MCDs, it is important to understand the affected features at the cell biological level. For example, prenatal exposure to alcohol can cause impaired neuronal migration, reduced proliferation and altered morphology of neural progenitors (Hirai et al., 1999; Mooney et al., 2004; Cuzon et al., 2008; Luhmann, 2016). Particularly strong effects were observed on production and migration of GABAergic interneurons (Cuzon et al., 2008; Boa-Amponsem et al., 2020). ZIKA virus causes microcephaly by reducing neural progenitor proliferation and inducing cell death. The phenotypes were recapitulated in both mouse models and cerebral organoids with the organoids revealing a potentially key role of bRG in this process (Faizan et al., 2016; Qian et al., 2016; Watanabe et al., 2017; Sutarjono, 2019).

We have above listed key cell biological features in neural progenitors implicated in the emergence of MCDs and we can broadly split them into two groups: (1) fine regulation of mitosis and (2) maintenance of the correct cell polarity (**Figure 2**). Mitosis and notably the orientation of the mitotic spindle are important in determining the fate of the daughter cells, whereas the correct polarity (i) allows the access to the pro-proliferative signals at the apical and basal sides of the tissue and (ii) it enables the neuronal migration along the basal fibers of aRG and bRG. It is important to note that in addition to those principal groups various other cell biological processes are implicated. We have discussed some of the key signaling pathways and the emerging role of the cell metabolism in the onset of MCDs. Importantly, various molecules involved in the regulation of gene expression have been implicated in the emergence of MCD. Transcription factors, notably PAX6, TBR2, EMX2, FOXG1, ARX, DMRTA2,

and others (Mallamaci et al., 2000; Kitamura et al., 2002; Ligon et al., 2003; Baala et al., 2007; Asami et al., 2011; Baek et al., 2015; Urquhart et al., 2016), as well as epigenetic mechanisms, including histone modifications, chromatin remodeling and RNA-level regulation, have been shown to play an important role in the onset of MCDs (Qiao et al., 2016; Silver, 2016; Albert and Huttner, 2018; Doan et al., 2018; Gabriele et al., 2018; Franz et al., 2019; Ciptasari and van Bokhoven, 2020; Vaid and Huttner, 2020; Reichard and Zimmer-Bensch, 2021; Wilson et al., 2021).

In light of the fact that the BPs, and in particular bRG, are the key cell type implicated in the development and evolution of the human brain (Lui et al., 2011; Borrell and Reillo, 2012; Florio and Huttner, 2014; Dehay et al., 2015; Llinares-Benadero and Borrell, 2019; Kalebic and Huttner, 2020), it is becoming increasingly important to examine the emergence of MCDs particularly in the context of those cells. As discussed above, the recent efforts suggest that both in the context of mitosis and especially of cell polarity, BPs might have specific roles with a substantial influence on the emergence of MCDs. To better understand those mechanisms, it is vital to use model systems that faithfully recapitulate both the phenotypes of diseases and the cell biological underpinnings. Mouse, and to a much lesser extent rat, have been very helpful in understanding the basic molecular roles of genes involved in MCDs. They, however, do not faithfully recapitulate certain phenotypic characteristics of MCDs that are pertinent to an expanded cortex, such as cortical folding, nor some of the developmental features that might have a key role in the disease, such as presence of the outer subventricular zone with a high abundance of proliferative bRG. To overcome those limitations two main directions have been undertaken: (i) use of human *in vitro* models, such as cerebral organoids and (ii) use of animals with the expanded cortex, such as macaques and ferrets.

Cerebral organoids, together with the recently developed assembloids, are three-dimensional *in vitro* structures that show great potential for investigating complex human genetic states and modeling aspects of human neurodevelopmental pathologies (Quadrato and Arlotta, 2017; Chiaradia and Lancaster, 2020; Sidhaye and Knoblich, 2021). Organoid models of human MCDs can be generated either by introducing the disease-causing mutations into otherwise wild type IPSCs or by directly using patient-derived IPSCs (Adegbola et al., 2017; Iefremova et al., 2017; Li et al., 2017; Fiddes et al., 2018; Klaus et al., 2019; Lopez-Tobon et al., 2019; Dhaliwal et al., 2021; Kyrousi et al., 2021; Wegscheid et al., 2021), with the latter being instrumental in personalized medicine. Among the animal models, macaques are particularly interesting as they recapitulate many of the cell biological features of human BPs (Betizeau et al., 2013). First transgenic macaques, with mutated *MCPH1* and modeling human microcephaly, have been recently generated (Ke et al., 2016; Shi et al., 2019). Ferrets are ethically and logistically a more suitable model for various human diseases including some MCDs (Gilardi and Kalebic, 2021). Ferrets well recapitulate the key features of the expanded cortex such as folding and the presence of the outer subventricular zone and proliferative bRG (Borrell and Reillo, 2012; Kawasaki, 2014; Gilardi and Kalebic, 2021). Ferret models of MCDs can be generated through a pharmacological or genetic manipulation, with the latter being possible through *in utero* electroporation and transgenesis. Pharmacological inhibition of mitosis is used to generate a ferret model of cortical dysplasia (Noctor et al., 1999, 2001). *In utero* electroporation of ferrets (Kawasaki et al., 2012, 2013; Kalebic et al., 2020), which has been used to deliver human-specific genes and thereby further enforce ferret's potential to model human brain characteristics (Kalebic et al., 2018), has been used to model lissencephaly (Shinmyo et al., 2017) and thanatophoric dysplasia (Masuda et al., 2015; Matsumoto et al., 2017a,b, 2018). Transgenic ferrets with a germline knockout of *Aspm* were generated as a model for microcephaly (Johnson et al., 2018). In addition to recapitulating the human microcephaly better than the mouse modes, *Aspm* KO ferrets show a displacement of aRG to the oSVZ where they resemble bRG, suggesting an evolutionary mechanism by which ASPM regulates cortical expansion by controlling the ratio between aRG and bRG (Johnson et al., 2018).

Because bRG are emerging as important in both the aetiology of MCDs and the evolution of the mammalian brain, it is tempting to discuss the co-evolution of MCD genes and the mammalian brain evolution. This is particularly relevant for the genes associated with microcephaly that display a strong signature of adaptive evolution in primates, cetaceans, and other mammalian orders with expanded brains (Montgomery and Mundy, 2014; Doan et al., 2018). For example, *MCPH1* has been positively selected in the primate lineage (Pulvers et al., 2015), whereas in anthropoid primates (monkeys and apes), the rates of evolution of *ASPM* and *CDK5RAP2* are associated with variation in brain size (Montgomery and Mundy, 2014). However, a recent study could not detect any human-specific adaptive evolution of microcephaly genes (Pervaiz et al., 2021).

In conclusion, the multi-level complexity of MCDs is a key factor preventing a better link between the genes and phenotypes, which in turn is fundamental to provide the patients with better diagnostic and therapeutic perspectives. Addressing some of this complexity at the cell biological level of neural progenitor cells is highly needed. The current efforts in utilizing more suitable model systems, that faithfully recapitulate key cell biological features of the disease onset, are an important step forward in creating improved diagnostic and therapeutic options and the personalized approaches.

AUTHOR CONTRIBUTIONS

Both authors wrote the manuscript, approved it for publication, and agreed to be accountable for the content of the work.

ACKNOWLEDGMENTS

We thank Elena Taverna (HT) and Takashi Namba (University of Helsinki) for critical reading of the manuscript. CO is a Ph.D. student within the European School of Molecular Medicine (SEMM).

REFERENCES

Abrieu, A., Kahana, J. A., Wood, K. W., and Cleveland, D. W. (2000). CENP-E as an essential component of the mitotic checkpoint *in vitro*. *Cell* 102, 817–826. doi: 10.1016/s0092-8674(00)00070-2

Acuna-Hidalgo, R., Schanze, D., Kariminejad, A., Nordgren, A., Kariminejad, M. H., Conner, P., et al. (2014). Neu-Laxova syndrome is a heterogeneous metabolic disorder caused by defects in enzymes of the L-serine biosynthesis pathway. *Am. J. Hum. Genet.* 95, 285–293. doi: 10.1016/j.ajhg.2014.07.012

Adegbola, A., Bury, L. A., Fu, C., Zhang, M., and Wynshaw-Boris, A. (2017). Concise review: induced pluripotent stem cell models for neuropsychiatric diseases. *Stem Cells Transl. Med.* 6, 2062–2070. doi: 10.1002/sctm.17-0150

Albert, M., and Huttner, W. B. (2018). Epigenetic and transcriptional pre-patterning-an emerging theme in cortical neurogenesis. *Front. Neurosci.* 12:359. doi: 10.3389/fnins.2018.00359

Alcantara, D., Timms, A. E., Gripp, K., Baker, L., Park, K., Collins, S., et al. (2017). Mutations of AKT3 are associated with a wide spectrum of developmental disorders including extreme megalencephaly. *Brain* 140, 2610–2622. doi: 10.1093/brain/awx203

Aldridge, K., Hill, C. A., Austin, J. R., Percival, C., Martinez-Abadias, N., Neuberger, T., et al. (2010). Brain phenotypes in two FGFR2 mouse models for Apert syndrome. *Dev. Dyn.* 239, 987–997. doi: 10.1002/dvdy.22218

Alkuraya, F. S., Cai, X., Emery, C., Mochida, G. H., Al-Dosari, M. S., Felie, J. M., et al. (2011). Human mutations in NDE1 cause extreme microcephaly with lissencephaly [corrected]. *Am. J. Hum. Genet.* 88, 536–547. doi: 10.1016/j.ajhg.2011.04.003

Andrews, M. G., Subramanian, L., and Kriegstein, A. R. (2020). mTOR signaling regulates the morphology and migration of outer radial glia in developing human cortex. *eLife* 9:e58737. doi: 10.7554/eLife.58737

Angevine, J. B. J., and Sidman, R. L. (1961). Autoradiographic study of cell migration during histogenesis of cerebral cortex in the mouse. *Nature* 192, 766–768. doi: 10.1038/192766b0

Asami, M., Pilz, G. A., Ninkovic, J., Godinho, L., Schroeder, T., Huttner, W. B., et al. (2011). The role of Pax6 in regulating the orientation and mode of cell division of progenitors in the mouse cerebral cortex. *Development* 138, 5067–5078. doi: 10.1242/dev.074591

Baala, L., Briault, S., Etchevers, H. C., Laumonnier, F., Natiq, A., Amiel, J., et al. (2007). Homozygous silencing of T-box transcription factor EOMES leads to microcephaly with polymicrogyria and corpus callosum agenesis. *Nat. Genet.* 39, 454–456. doi: 10.1038/ng1993

Bae, B. I., Tietjen, I., Atabay, K. D., Evrony, G. D., Johnson, M. B., Asare, E., et al. (2014). Evolutionarily dynamic alternative splicing of GPR56 regulates regional cerebral cortical patterning. *Science* 343, 764–768. doi: 10.1126/science.1244392

Baek, S. T., Copeland, B., Yun, E. J., Kwon, S. K., Guemez-Gamboa, A., Schaffer, A. E., et al. (2015). An AKT3-FOXG1-reelin network underlies defective migration in human focal malformations of cortical development. *Nat. Med.* 21, 1445–1454. doi: 10.1038/nm.3982

Barkovich, A. J., Guerrini, R., Kuzniecky, R. I., Jackson, G. D., and Dobyns, W. B. (2012). A developmental and genetic classification for malformations of cortical development: update 2012. *Brain* 135, 1348–1369. doi: 10.1093/brain/aws019

Bayer, S. A., and Altman, J. (1991). *Neocortical Development*. New York: Raven Press.

Bellenchi, G. C., Gurniak, C. B., Perlas, E., Middei, S., Ammassari-Teule, M., and Witke, W. (2007). N-cofilin is associated with neuronal migration disorders and cell cycle control in the cerebral cortex. *Genes Dev.* 21, 2347–2357. doi: 10.1101/gad.434307

Beltran-Valero de Bernabe, D., Currier, S., Steinbrecher, A., Celli, J., van Beusekom, E., van der Zwaag, B., et al. (2002). Mutations in the O-mannosyltransferase gene POMT1 give rise to the severe neuronal migration disorder Walker-Warburg syndrome. *Am. J. Hum. Genet.* 71, 1033–1043. doi: 10.1086/342975

Betizeau, M., Cortay, V., Patti, D., Pfister, S., Gautier, E., Bellemin-Meìnard, A., et al. (2013). Precursor diversity and complexity of lineage relationships in the outer subventricular zone of the primate. *Neuron* 80, 442–457. doi: 10.1016/j.neuron.2013.09.032

Bielle, F., Griveau, A., Narboux-Neme, N., Vigneau, S., Sigrist, M., Arber, S., et al. (2005). Multiple origins of Cajal-Retzius cells at the borders of the developing pallium. *Nat. Neurosci.* 8, 1002–1012. doi: 10.1038/nn1511

Bilguvar, K., Ozturk, A. K., Louvi, A., Kwan, K. Y., Choi, M., Tatli, B., et al. (2010). Whole-exome sequencing identifies recessive WDR62 mutations in severe brain malformations. *Nature* 467, 207–210. doi: 10.1038/nature09327

Bizzotto, S., and Francis, F. (2015). Morphological and functional aspects of progenitors perturbed in cortical malformations. *Front. Cell. Neurosci.* 9:30. doi: 10.3389/fncel.2015.00030

Bizzotto, S., Uzquiano, A., Dingli, F., Ershov, D., Houllier, A., Arras, G., et al. (2017). Eml1 loss impairs apical progenitor spindle length and soma shape in the developing cerebral cortex. *Sci. Rep.* 7:17308. doi: 10.1038/s41598-017-15253-4

Blackshear, P. J., Silver, J., Nairn, A. C., Sulik, K. K., Squier, M. V., Stumpo, D. J., et al. (1997). Widespread neuronal ectopia associated with secondary defects in cerebrocortical chondroitin sulfate proteoglycans and basal lamina in MARCKS-deficient mice. *Exp. Neurol.* 145, 46–61. doi: 10.1006/exnr.1997.6475

Blazejewski, S. M., Bennison, S. A., Smith, T. H., and Toyo-Oka, K. (2018). Neurodevelopmental genetic diseases associated with microdeletions and microduplications of chromosome 17p13.3. *Front. Genet.* 9:80. doi: 10.3389/fgene.2018.00080

Boa-Amponsem, O., Zhang, C., Burton, D., Williams, K. P., and Cole, G. J. (2020). Ethanol and cannabinoids regulate zebrafish GABAergic neuron development and behavior in a sonic hedgehog and fibroblast growth factor-dependent mechanism. *Alcohol. Clin. Exp. Res.* 44, 1366–1377. doi: 10.1111/acer.14383

Bond, J., Roberts, E., Mochida, G. H., Hampshire, D. J., Scott, S., Askham, J. M., et al. (2002). ASPM is a major determinant of cerebral cortical size. *Nat. Genet.* 32, 316–320. doi: 10.1038/ng995

Bond, J., Roberts, E., Springell, K., Lizarraga, S. B., Scott, S., Higgins, J., et al. (2005). A centrosomal mechanism involving CDK5RAP2 and CENPJ controls brain size. *Nat. Genet.* 37, 353–355. doi: 10.1038/ng1539

Bond, J., and Woods, C. G. (2006). Cytoskeletal genes regulating brain size. *Curr. Opin. Cell Biol.* 18, 95–101. doi: 10.1016/j.ceb.2005.11.004

Borrell, V., and Götz, M. (2014). Role of radial glial cells in cerebral cortex folding. *Curr. Opin. Neurobiol.* 27, 39–46. doi: 10.1016/j.conb.2014.02.007

Borrell, V., and Reillo, I. (2012). Emerging roles of neural stem cells in cerebral cortex development and evolution. *Dev. Neurobiol.* 72, 955–971. doi: 10.1002/dneu.22013

Buchsbaum, I. Y., and Cappello, S. (2019). Neuronal migration in the CNS during development and disease: insights from *in vivo* and *in vitro* models. *Development* 146:dev163766. doi: 10.1242/dev.163766

Buchsbaum, I. Y., Kielkowski, P., Giorgio, G., O'Neill, A. C., Di Giaimo, R., Kyrousi, C., et al. (2020). ECE2 regulates neurogenesis and neuronal migration during human cortical development. *EMBO Rep.* 21:e48204. doi: 10.15252/embr.201948204

Bultje, R. S., Castaneda-Castellanos, D. R., Jan, L. Y., Jan, Y. N., Kriegstein, A. R., and Shi, S. H. (2009). Mammalian Par3 regulates progenitor cell asymmetric division *via* notch signaling in the developing neocortex. *Neuron* 63, 189–202. doi: 10.1016/j.neuron.2009.07.004

Cahana, A., Escamez, T., Nowakowski, R. S., Hayes, N. L., Giacobini, M., von Holst, A., et al. (2001). Targeted mutagenesis of Lis1 disrupts cortical development and LIS1 homodimerization. *Proc. Natl. Acad. Sci. U.S.A.* 98, 6429–6434. doi: 10.1073/pnas.101122598

Camargo Ortega, G., Falk, S., Johansson, P. A., Peyre, E., Broix, L., Sahu, S. K., et al. (2019). The centrosome protein AKNA regulates neurogenesis *via* microtubule organization. *Nature* 567, 113–117. doi: 10.1038/s41586-019-0962-4

Cappello, S., Attardo, A., Wu, X., Iwasato, T., Itohara, S., Wilsch-Brauninger, M., et al. (2006). The Rho-GTPase cdc42 regulates neural progenitor fate at the apical surface. *Nat. Neurosci.* 9, 1099–1107. doi: 10.1038/nn1744

Cappello, S., Bohringer, C. R., Bergami, M., Conzelmann, K. K., Ghanem, A., Tomassy, G. S., et al. (2012). A radial glia-specific role of RhoA in double cortex formation. *Neuron* 73, 911–924. doi: 10.1016/j.neuron.2011.12.030

Cappello, S., Gray, M. J., Badouel, C., Lange, S., Einsiedler, M., Srour, M., et al. (2013). Mutations in genes encoding the cadherin receptor-ligand pair DCHS1 and FAT4 disrupt cerebral cortical development. *Nat. Genet.* 45, 1300–1308. doi: 10.1038/ng.2765

Castello, M. A., and Gleeson, J. G. (2021). Insight into developmental mechanisms of global and focal migration disorders of cortical development. *Curr. Opin. Neurobiol.* 66, 77–84. doi: 10.1016/j.conb.2020.10.005

Chen, J. F., Zhang, Y., Wilde, J., Hansen, K. C., Lai, F., and Niswander, L. (2014). Microcephaly disease gene Wdr62 regulates mitotic progression of

embryonic neural stem cells and brain size. *Nat. Commun.* 5:3885. doi: 10.1038/ncomms4885

Chen, L., Melendez, J., Campbell, K., Kuan, C. Y., and Zheng, Y. (2009). Rac1 deficiency in the forebrain results in neural progenitor reduction and microcephaly. *Dev. Biol.* 325, 162–170. doi: 10.1016/j.ydbio.2008.10.023

Chiaradia, I., and Lancaster, M. A. (2020). Brain organoids for the study of human neurobiology at the interface of *in vitro* and *in vivo*. *Nat. Neurosci.* 23, 1496–1508. doi: 10.1038/s41593-020-00730-3

Ciptasari, U., and van Bokhoven, H. (2020). The phenomenal epigenome in neurodevelopmental disorders. *Hum. Mol. Genet.* 29, R42–R50. doi: 10.1093/hmg/ddaa175

Collins, S. C., Uzquiano, A., Selloum, M., Wendling, O., Gaborit, M., Osipenko, M., et al. (2019). The neuroanatomy of Eml1 knockout mice, a model of subcortical heterotopia. *J. Anat.* 235, 637–650. doi: 10.1111/joa.13013

Costa, M. R., Wen, G., Lepier, A., Schroeder, T., and Gotz, M. (2008). Par-complex proteins promote proliferative progenitor divisions in the developing mouse cerebral cortex. *Development* 135, 11–22. doi: 10.1242/dev.009951

Cuzon, V. C., Yeh, P. W., Yanagawa, Y., Obata, K., and Yeh, H. H. (2008). Ethanol consumption during early pregnancy alters the disposition of tangentially migrating GABAergic interneurons in the fetal cortex. *J. Neurosci.* 28, 1854–1864. doi: 10.1523/JNEUROSCI.5110-07.2008

de Juan Romero, C., and Borrell, V. (2017). Genetic maps and patterns of cerebral cortex folding. *Curr. Opin. Cell Biol.* 49, 31–37. doi: 10.1016/j.ceb.2017.11.009

Dehay, C., Kennedy, H., and Kosik, K. S. (2015). The outer subventricular zone and primate-specific cortical complexification. *Neuron* 85, 683–694. doi: 10.1016/j.neuron.2014.12.060

Del Valle Anton, L., and Borrell, V. (2021). Folding brains: from development to disease modeling. *Physiol. Rev.* [Epub ahead of print]. doi: 10.1152/physrev.00016.2021

Desikan, R. S., and Barkovich, A. J. (2016). Malformations of cortical development. *Ann. Neurol.* 80, 797–810.

Devisme, L., Bouchet, C., Gonzales, M., Alanio, E., Bazin, A., Bessieres, B., et al. (2012). Cobblestone lissencephaly: neuropathological subtypes and correlations with genes of dystroglycanopathies. *Brain* 135, 469–482. doi: 10.1093/brain/awr357

Dhaliwal, N., Choi, W. W. Y., Muffat, J., and Li, Y. (2021). Modeling PTEN overexpression-induced microcephaly in human brain organoids. *Mol. Brain* 14:131. doi: 10.1186/s13041-021-00841-3

Di Donato, N., Chiari, S., Mirzaa, G. M., Aldinger, K., Parrini, E., Olds, C., et al. (2017). Lissencephaly: expanded imaging and clinical classification. *Am. J. Med. Genet. A* 173, 1473–1488. doi: 10.1002/ajmg.a.38245

Diamandis, P., Chitayat, D., Toi, A., Blaser, S., and Shannon, P. (2017). The pathology of incipient polymicrogyria. *Brain Dev.* 39, 23–39. doi: 10.1016/j.braindev.2016.06.005

Ding, W., Wu, Q., Sun, L., Pan, N. C., and Wang, X. (2019). Cenpj regulates cilia disassembly and neurogenesis in the developing mouse cortex. *J. Neurosci.* 39, 1994–2010. doi: 10.1523/JNEUROSCI.1849-18.2018

Doan, R. N., Shin, T., and Walsh, C. A. (2018). Evolutionary changes in transcriptional regulation: insights into human behavior and neurological conditions. *Annu. Rev. Neurosci.* 41, 185–206. doi: 10.1146/annurev-neuro-080317-062104

Dobyns, W. B., and Mirzaa, G. M. (2019). Megalencephaly syndromes associated with mutations of core components of the PI3K-AKT-MTOR pathway: PIK3CA, PIK3R2, AKT3, and MTOR. *Am. J. Med. Genet. C Semin. Med. Genet.* 181, 582–590. doi: 10.1002/ajmg.c.31736

Dubreuil, V., Marzesco, A. M., Corbeil, D., Huttner, W. B., and Wilsch-Brauninger, M. (2007). Midbody and primary cilium of neural progenitors release extracellular membrane particles enriched in the stem cell marker prominin-1. *J. Cell Biol.* 176, 483–495. doi: 10.1083/jcb.200608137

Ettinger, A. W., Wilsch-Brauninger, M., Marzesco, A. M., Bickle, M., Lohmann, A., Maliga, Z., et al. (2011). Proliferating versus differentiating stem and cancer cells exhibit distinct midbody-release behaviour. *Nat. Commun.* 2:503. doi: 10.1038/ncomms1511

Faivre, L., Gosset, P., Cormier-Daire, V., Odent, S., Amiel, J., Giurgea, I., et al. (2002). Overgrowth and trisomy 15q26.1-qter including the IGF1 receptor gene: report of two families and review of the literature. *Eur. J. Hum. Genet.* 10, 699–706. doi: 10.1038/sj.ejhg.5200879

Faizan, M. I., Abdullah, M., Ali, S., Naqvi, I. H., Ahmed, A., and Parveen, S. (2016). Zika virus-induced microcephaly and its possible molecular mechanism. *Intervirology* 59, 152–158. doi: 10.1159/000452950

Farag, H. G., Froehler, S., Oexle, K., Ravindran, E., Schindler, D., Staab, T., et al. (2013). Abnormal centrosome and spindle morphology in a patient with autosomal recessive primary microcephaly type 2 due to compound heterozygous WDR62 gene mutation. *Orphanet J. Rare Dis.* 8:178. doi: 10.1186/1750-1172-8-178

Fatemi, S. H. (2001). Reelin mutations in mouse and man: from reeler mouse to schizophrenia, mood disorders, autism and lissencephaly. *Mol. Psychiatry* 6, 129–133. doi: 10.1038/sj.mp.4000129

Feng, Y., and Walsh, C. A. (2004). Mitotic spindle regulation by Nde1 controls cerebral cortical size. *Neuron* 44, 279–293. doi: 10.1016/j.neuron.2004.09.023

Ferent, J., Zaidi, D., and Francis, F. (2020). Extracellular control of radial glia proliferation and scaffolding during cortical development and pathology. *Front. Cell Dev. Biol.* 8:578341. doi: 10.3389/fcell.2020.578341

Fernandez, V., Llinares-Benadero, C., and Borrell, V. (2016). Cerebral cortex expansion and folding: what have we learned? *EMBO J.* 35, 1021–1044. doi: 10.15252/embj.201593701

Fiddes, I. T., Lodewijk, G. A., Mooring, M., Bosworth, C. M., Ewing, A. D., Mantalas, G. L., et al. (2018). Human-specific NOTCH2NL genes affect notch signaling and cortical neurogenesis. *Cell* 173, 1356–1369. doi: 10.1016/j.cell.2018.03.051

Fietz, S. A., Kelava, I., Vogt, J., Wilsch-Brauninger, M., Stenzel, D., Fish, J. L., et al. (2010). OSVZ progenitors of human and ferret neocortex are epithelial-like and expand by integrin signaling. *Nat. Neurosci.* 13, 690–699. doi: 10.1038/nn.2553

Fish, J. L., Kosodo, Y., Enard, W., Paabo, S., and Huttner, W. B. (2006). Aspm specifically maintains symmetric proliferative divisions of neuroepithelial cells. *Proc. Natl. Acad. Sci. U.S.A.* 103, 10438–10443. doi: 10.1073/pnas.0604066103

Florio, M., and Huttner, W. B. (2014). Neural progenitors, neurogenesis and the evolution of the neocortex. *Development* 141, 2182–2194. doi: 10.1242/dev.090571

Fortini, M. E. (2009). Notch signaling: the core pathway and its posttranslational regulation. *Dev. Cell* 16, 633–647. doi: 10.1016/j.devcel.2009.03.010

Fox, J. W., Lamperti, E. D., Eksioglu, Y. Z., Hong, S. E., Feng, Y., Graham, D. A., et al. (1998). Mutations in filamin 1 prevent migration of cerebral cortical neurons in human periventricular heterotopia. *Neuron* 21, 1315–1325. doi: 10.1016/s0896-6273(00)80651-0

Francis, F., and Cappello, S. (2021). Neuronal migration and disorders - an update. *Curr. Opin. Neurobiol.* 66, 57–68. doi: 10.1016/j.conb.2020.10.002

Franz, H., Villarreal, A., Heidrich, S., Videm, P., Kilpert, F., Mestres, I., et al. (2019). DOT1L promotes progenitor proliferation and primes neuronal layer identity in the developing cerebral cortex. *Nucleic Acids Res.* 47, 168–183. doi: 10.1093/nar/gky953

Fukata, Y., and Fukata, M. (2010). Protein palmitoylation in neuronal development and synaptic plasticity. *Nat. Rev. Neurosci.* 11, 161–175. doi: 10.1038/nrn2788

Gabriele, M., Lopez Tobon, A., D'Agostino, G., and Testa, G. (2018). The chromatin basis of neurodevelopmental disorders: rethinking dysfunction along the molecular and temporal axes. *Prog. Neuropsychopharmacol. Biol. Psychiatry* 84, 306–327. doi: 10.1016/j.pnpbp.2017.12.013

Gambello, M. J., Darling, D. L., Yingling, J., Tanaka, T., Gleeson, J. G., and Wynshaw-Boris, A. (2003). Multiple dose-dependent effects of Lis1 on cerebral cortical development. *J. Neurosci.* 23, 1719–1729. doi: 10.1523/JNEUROSCI.23-05-01719.2003

Geschwind, D. H., and Rakic, P. (2013). Cortical evolution: judge the brain by its cover. *Neuron* 80, 633–647. doi: 10.1016/j.neuron.2013.10.045

Gilardi, C., and Kalebic, N. (2021). The ferret as a model system for neocortex development and evolution. *Front. Cell Dev. Biol.* 9:661759. doi: 10.3389/fcell.2021.661759

Gilmore, E. C., and Walsh, C. A. (2013). Genetic causes of microcephaly and lessons for neuronal development. *Wiley Interdiscip. Rev. Dev. Biol.* 2, 461–478. doi: 10.1002/wdev.89

Gil-Sanz, C., Landeira, B., Ramos, C., Costa, M. R., and Muller, U. (2014). Proliferative defects and formation of a double cortex in mice lacking Mltt4 and Cdh2 in the dorsal telencephalon. *J. Neurosci.* 34, 10475–10487. doi: 10.1523/JNEUROSCI.1793-14.2014

Gonzalez-Moron, D., Vishnopolska, S., Consalvo, D., Medina, N., Marti, M., Cordoba, M., et al. (2017). Germline and somatic mutations in cortical

malformations: molecular defects in Argentinean patients with neuronal migration disorders. *PLoS One* 12:e0185103. doi: 10.1371/journal.pone.0185103

Groszer, M., Erickson, R., Scripture-Adams, D. D., Lesche, R., Trumpp, A., Zack, J. A., et al. (2001). Negative regulation of neural stem/progenitor cell proliferation by the Pten tumor suppressor gene *in vivo*. *Science* 294, 2186–2189. doi: 10.1126/science.1065518

Gruber, R., Zhou, Z., Sukchev, M., Joerss, T., Frappart, P. O., and Wang, Z. Q. (2011). MCPH1 regulates the neuroprogenitor division mode by coupling the centrosomal cycle with mitotic entry through the Chk1-Cdc25 pathway. *Nat. Cell Biol.* 13, 1325–1334. doi: 10.1038/ncb2342

Guarnieri, F. C., de Chevigny, A., Falace, A., and Cardoso, C. (2018). Disorders of neurogenesis and cortical development. *Dialog. Clin. Neurosci.* 20, 255–266. doi: 10.31887/DCNS.2018.20.4/ccardoso

Guemez-Gamboa, A., Nguyen, L. N., Yang, H., Zaki, M. S., Kara, M., Ben-Omran, T., et al. (2015). Inactivating mutations in MFSD2A, required for omega-3 fatty acid transport in brain, cause a lethal microcephaly syndrome. *Nat. Genet.* 47, 809–813. doi: 10.1038/ng.3311

Guerrini, R., and Dobyns, W. B. (2014). Malformations of cortical development: clinical features and genetic causes. *Lancet Neurol.* 13, 710–726. doi: 10.1016/S1474-4422(14)70040-7

Hansen, A. H., Duellberg, C., Mieck, C., Loose, M., and Hippenmeyer, S. (2017). Cell polarity in cerebral cortex development-cellular architecture shaped by biochemical networks. *Front. Cell. Neurosci.* 11:176. doi: 10.3389/fncel.2017.00176

Hansen, D. V., Lui, J. H., Parker, P. R., and Kriegstein, A. R. (2010). Neurogenic radial glia in the outer subventricular zone of human neocortex. *Nature* 464, 554–561. doi: 10.1038/nature08845

Haubensak, W., Attardo, A., Denk, W., and Huttner, W. B. (2004). Neurons arise in the basal neuroepithelium of the early mammalian telencephalon: a major site of neurogenesis. *Proc. Natl. Acad. Sci. U.S.A.* 101, 3196–3201. doi: 10.1073/pnas.0308600100

Heng, Y. W., and Koh, C. G. (2010). Actin cytoskeleton dynamics and the cell division cycle. *Int. J. Biochem. Cell Biol.* 42, 1622–1633. doi: 10.1016/j.biocel.2010.04.007

Hevner, R. F. (2005). The cerebral cortex malformation in thanatophoric dysplasia: neuropathology and pathogenesis. *Acta Neuropathol.* 110, 208–221. doi: 10.1007/s00401-005-1059-8

Hevner, R. F. (2015). Brain overgrowth in disorders of RTK-PI3K-AKT signaling: a mosaic of malformations. *Semin. Perinatol.* 39, 36–43. doi: 10.1053/j.semperi.2014.10.006

Higginbotham, H., Guo, J., Yokota, Y., Umberger, N. L., Su, C. Y., Li, J., et al. (2013). Arl13b-regulated cilia activities are essential for polarized radial glial scaffold formation. *Nat. Neurosci.* 16, 1000–1007. doi: 10.1038/nn.3451

Hirai, K., Yoshioka, H., Kihara, M., Hasegawa, K., Sawada, T., and Fushiki, S. (1999). Effects of ethanol on neuronal migration and neural cell adhesion molecules in the embryonic rat cerebral cortex: a tissue culture study. *Brain Res. Dev. Brain Res.* 118, 205–210. doi: 10.1016/s0165-3806(99)00159-5

Hirota, Y., and Nakajima, K. (2017). Control of neuronal migration and aggregation by reelin signaling in the developing cerebral cortex. *Front. Cell Dev. Biol.* 5:40. doi: 10.3389/fcell.2017.00040

Homem, C. C., Repic, M., and Knoblich, J. A. (2015). Proliferation control in neural stem and progenitor cells. *Nat. Rev. Neurosci.* 16, 647–659.

Hong, S. E., Shugart, Y. Y., Huang, D. T., Shahwan, S. A., Grant, P. E., Hourihane, J. O., et al. (2000). Autosomal recessive lissencephaly with cerebellar hypoplasia is associated with human RELN mutations. *Nat. Genet.* 26, 93–96. doi: 10.1038/79246

Houlard, M., Cutts, E. E., Shamim, M. S., Godwin, J., Weisz, D., Aiden, A. P., et al. (2021). MCPH1 inhibits condensin II during interphase by regulating its SMC2-kleisin interface. *eLife* 10:e73348. doi: 10.7554/eLife.73348

Hu, J. S., Vogt, D., Sandberg, M., and Rubenstein, J. L. (2017). Cortical interneuron development: a tale of time and space. *Development* 144, 3867–3878. doi: 10.1242/dev.132852

Iefremova, V., Manikakis, G., Krefft, O., Jabali, A., Weynans, K., Wilkens, R., et al. (2017). An organoid-based model of cortical development identifies non-cell-autonomous defects in wnt signaling contributing to Miller-Dieker syndrome. *Cell Rep.* 19, 50–59. doi: 10.1016/j.celrep.2017.03.047

Insolera, R., Bazzi, H., Shao, W., Anderson, K. V., and Shi, S. H. (2014). Cortical neurogenesis in the absence of centrioles. *Nat. Neurosci.* 17, 1528–1535. doi: 10.1038/nn.3831

Ishii, K., Kubo, K. I., and Nakajima, K. (2016). Reelin and neuropsychiatric disorders. *Front. Cell. Neurosci.* 10:229. doi: 10.3389/fncel.2016.00229

Jackson, A. P., Eastwood, H., Bell, S. M., Adu, J., Toomes, C., Carr, I. M., et al. (2002). Identification of microcephalin, a protein implicated in determining the size of the human brain. *Am. J. Hum. Genet.* 71, 136–142. doi: 10.1086/341283

Jamuar, S. S., Lam, A. T., Kircher, M., D'Gama, A. M., Wang, J., Barry, B. J., et al. (2014). Somatic mutations in cerebral cortical malformations. *N. Engl. J. Med.* 371, 733–743.

Jamuar, S. S., and Walsh, C. A. (2015). Genomic variants and variations in malformations of cortical development. *Pediatr. Clin. North Am.* 62, 571–585. doi: 10.1016/j.pcl.2015.03.002

Janisch, K. M., Vock, V. M., Fleming, M. S., Shrestha, A., Grimsley-Myers, C. M., Rasoul, B. A., et al. (2013). The vertebrate-specific Kinesin-6, Kif20b, is required for normal cytokinesis of polarized cortical stem cells and cerebral cortex size. *Development* 140, 4672–4682. doi: 10.1242/dev.093286

Jansen, A. C., Robitaille, Y., Honavar, M., Mullatti, N., Leventer, R. J., Andermann, E., et al. (2016). The histopathology of polymicrogyria: a series of 71 brain autopsy studies. *Dev. Med. Child Neurol.* 58, 39–48. doi: 10.1111/dmcn.12840

Jansen, L. A., Mirzaa, G. M., Ishak, G. E., O'Roak, B. J., Hiatt, J. B., Roden, W. H., et al. (2015). PI3K/AKT pathway mutations cause a spectrum of brain malformations from megalencephaly to focal cortical dysplasia. *Brain* 138, 1613–1628. doi: 10.1093/brain/awv045

Jayaraman, D., Bae, B. I., and Walsh, C. A. (2018). The genetics of primary microcephaly. *Annu. Rev. Genom. Hum. Genet.* 19, 177–200.

Jayaraman, D., Kodani, A., Gonzalez, D. M., Mancias, J. D., Mochida, G. H., Vagnoni, C., et al. (2016). Microcephaly Proteins Wdr62 and aspm define a mother centriole complex regulating centriole biogenesis, apical complex, and cell fate. *Neuron* 92, 813–828. doi: 10.1016/j.neuron.2016.09.056

Jeong, S. J., Luo, R., Singer, K., Giera, S., Kreidberg, J., Kiyozumi, D., et al. (2013). GPR56 functions together with alpha3beta1 integrin in regulating cerebral cortical development. *PLoS One* 8:e68781. doi: 10.1371/journal.pone.0068781

Jerber, J., Zaki, M. S., Al-Aama, J. Y., Rosti, R. O., Ben-Omran, T., Dikoglu, E., et al. (2016). Biallelic mutations in TMTC3, encoding a transmembrane and TPR-containing protein, lead to cobblestone lissencephaly. *Am. J. Hum. Genet.* 99, 1181–1189. doi: 10.1016/j.ajhg.2016.09.007

Jin, M., Pomp, O., Shinoda, T., Toba, S., Torisawa, T., Furuta, K., et al. (2017). Katanin p80, NuMA and cytoplasmic dynein cooperate to control microtubule dynamics. *Sci. Rep.* 7:39902. doi: 10.1038/srep39902

Johnson, M. B., Sun, X., Kodani, A., Borges-Monroy, R., Girskis, K. M., Ryu, S. C., et al. (2018). Aspm knockout ferret reveals an evolutionary mechanism governing cerebral cortical size. *Nature* 556, 370–375. doi: 10.1038/s41586-018-0035-0

Joseph, D., Ercole, A., and Ye, P. (2008). Expanding the mind: insulin-like growth factor I and brain development. *Endocrinology* 149, 5958–5962. doi: 10.1210/en.2008-0920

Journiac, N., Gilabert-Juan, J., Cipriani, S., Benit, P., Liu, X., Jacquier, S., et al. (2020). Cell metabolic alterations due to Mcph1 mutation in microcephaly. *Cell Rep.* 31:107506. doi: 10.1016/j.celrep.2020.03.070

Juric-Sekhar, G., and Hevner, R. F. (2019). Malformations of cerebral cortex development: molecules and mechanisms. *Annu. Rev. Pathol.* 14, 293–318. doi: 10.1146/annurev-pathmechdis-012418-012927

Kadowaki, M., Nakamura, S., Machon, O., Krauss, S., Radice, G. L., and Takeichi, M. (2007). N-cadherin mediates cortical organization in the mouse brain. *Dev. Biol.* 304, 22–33. doi: 10.1016/j.ydbio.2006.12.014

Kalebic, N., Gilardi, C., Albert, M., Namba, T., Long, K. R., Kostic, M., et al. (2018). Human-specific ARHGAP11B induces hallmarks of neocortical expansion in developing ferret neocortex. *eLife* 7:e41241. doi: 10.7554/eLife.41241

Kalebic, N., Gilardi, C., Stepien, B., Wilsch-Brauninger, M., Long, K. R., Namba, T., et al. (2019). Neocortical expansion due to increased proliferation of basal progenitors is linked to changes in their morphology. *Cell Stem Cell* 24, 535–550. doi: 10.1016/j.stem.2019.02.017

Kalebic, N., and Huttner, W. B. (2020). Basal progenitor morphology and neocortex evolution. *Trends Neurosci.* 43, 843–853. doi: 10.1016/j.tins.2020.07.009

Kalebic, N., Langen, B., Helppi, J., Kawasaki, H., and Huttner, W. B. (2020). *In vivo* targeting of neural progenitor cells in ferret neocortex by in utero electroporation. *J. Vis. Exp.* 159:61171. doi: 10.3791/61171

Kalebic, N., Long, K., and Huttner, W. B. (2017). "Neocortex expansion in development and evolution: the cell biology of neural stem and progenitor cells and the impact of human-specific gene expression," in *Evolution of Nervous Systems*, 2 Edn, ed. J. Kaas (Oxford: Elsevier), 73–89. doi: 10.1016/b978-0-12-804042-3.00136-6

Kalebic, N., and Namba, T. (2021). Inheritance and flexibility of cell polarity: a clue for understanding human brain development and evolution. *Development* 148:dev199417. doi: 10.1242/dev.199417

Kamasaki, T., O'Toole, E., Kita, S., Osumi, M., Usukura, J., McIntosh, J. R., et al. (2013). Augmin-dependent microtubule nucleation at microtubule walls in the spindle. *J. Cell Biol.* 202, 25–33. doi: 10.1083/jcb.201304031

Kandachar, V., and Roegiers, F. (2012). Endocytosis and control of Notch signaling. *Curr. Opin. Cell Biol.* 24, 534–540. doi: 10.1016/j.ceb.2012.06.006

Kawasaki, H. (2014). Molecular investigations of the brain of higher mammals using gyrencephalic carnivore ferrets. *Neurosci. Res.* 86, 59–65. doi: 10.1016/j.neures.2014.06.006

Kawasaki, H., Iwai, L., and Tanno, K. (2012). Rapid and efficient genetic manipulation of gyrencephalic carnivores using in utero electroporation. *Mol. Brain* 5:24. doi: 10.1186/1756-6606-5-24

Kawasaki, H., Toda, T., and Tanno, K. (2013). *In vivo* genetic manipulation of cortical progenitors in gyrencephalic carnivores using in utero electroporation. *Biol. Open* 2, 95–100. doi: 10.1242/bio.20123160

Ke, Q., Li, W., Lai, X., Chen, H., Huang, L., Kang, Z., et al. (2016). TALEN-based generation of a cynomolgus monkey disease model for human microcephaly. *Cell Res.* 26, 1048–1061. doi: 10.1038/cr.2016.93

Kelley, R. I., Robinson, D., Puffenberger, E. G., Strauss, K. A., and Morton, D. H. (2002). Amish lethal microcephaly: a new metabolic disorder with severe congenital microcephaly and 2-ketoglutaric aciduria. *Am. J. Med. Genet.* 112, 318–326. doi: 10.1002/ajmg.10529

Kida, A., Kakihana, K., Kotani, S., Kurosu, T., and Miura, O. (2007). Glycogen synthase kinase-3beta and p38 phosphorylate cyclin D2 on Thr280 to trigger its ubiquitin/proteasome-dependent degradation in hematopoietic cells. *Oncogene* 26, 6630–6640. doi: 10.1038/sj.onc.1210490

Kielar, M., Tuy, F. P., Bizzotto, S., Lebrand, C., de Juan Romero, C., Poirier, K., et al. (2014). Mutations in Eml1 lead to ectopic progenitors and neuronal heterotopia in mouse and human. *Nat. Neurosci.* 17, 923–933. doi: 10.1038/nn.3729

Kim, H., Nakamura, F., Lee, W., Hong, C., Perez-Sala, D., and McCulloch, C. A. (2010). Regulation of cell adhesion to collagen *via* beta1 integrins is dependent on interactions of filamin A with vimentin and protein kinase C epsilon. *Exp. Cell Res.* 316, 1829–1844. doi: 10.1016/j.yexcr.2010.02.007

Kim, J., Krishnaswami, S. R., and Gleeson, J. G. (2008). CEP290 interacts with the centriolar satellite component PCM-1 and is required for Rab8 localization to the primary cilium. *Hum. Mol. Genet.* 17, 3796–3805. doi: 10.1093/hmg/ddn277

Kitamura, K., Yanazawa, M., Sugiyama, N., Miura, H., Iizuka-Kogo, A., Kusaka, M., et al. (2002). Mutation of ARX causes abnormal development of forebrain and testes in mice and X-linked lissencephaly with abnormal genitalia in humans. *Nat. Genet.* 32, 359–369. doi: 10.1038/ng1009

Klaus, J., Kanton, S., Kyrousi, C., Ayo-Martin, A. C., Di Giaimo, R., Riesenberg, S., et al. (2019). Altered neuronal migratory trajectories in human cerebral organoids derived from individuals with neuronal heterotopia. *Nat. Med.* 25, 561–568. doi: 10.1038/s41591-019-0371-0

Klingler, E., Francis, F., Jabaudon, D., and Cappello, S. (2021). Mapping the molecular and cellular complexity of cortical malformations. *Science* 371:eaba4517. doi: 10.1126/science.aba4517

Knobloch, M., Pilz, G. A., Ghesquiere, B., Kovacs, W. J., Wegleiter, T., Moore, D. L., et al. (2017). A fatty acid oxidation-dependent metabolic shift regulates adult neural stem cell activity. *Cell Rep.* 20, 2144–2155. doi: 10.1016/j.celrep.2017.08.029

Kodani, A., Yu, T. W., Johnson, J. R., Jayaraman, D., Johnson, T. L., Al-Gazali, L., et al. (2015). Centriolar satellites assemble centrosomal microcephaly proteins to recruit CDK2 and promote centriole duplication. *eLife* 4:e07519. doi: 10.7554/eLife.07519

Konno, D., Shioi, G., Shitamukai, A., Mori, A., Kiyonari, H., Miyata, T., et al. (2008). Neuroepithelial progenitors undergo LGN-dependent planar divisions to maintain self-renewability during mammalian neurogenesis. *Nat. Cell Biol.* 10, 93–101. doi: 10.1038/ncb1673

Kosodo, Y., and Huttner, W. B. (2009). Basal process and cell divisions of neural progenitors in the developing brain. *Dev. Growth Differ.* 51, 251–261. doi: 10.1111/j.1440-169X.2009.01101.x

Kosodo, Y., Toida, K., Dubreuil, V., Alexandre, P., Schenk, J., Kiyokage, E., et al. (2008). Cytokinesis of neuroepithelial cells can divide their basal process before anaphase. *EMBO J.* 27, 3151–3163. doi: 10.1038/emboj.2008.227

Kostic, M., Paridaen, J., Long, K. R., Kalebic, N., Langen, B., Grubling, N., et al. (2019). YAP activity is necessary and sufficient for basal progenitor abundance and proliferation in the developing neocortex. *Cell Rep.* 27, 1103–1118. doi: 10.1016/j.celrep.2019.03.091

Kostovic, I. (2020). The enigmatic fetal subplate compartment forms an early tangential cortical nexus and provides the framework for construction of cortical connectivity. *Prog. Neurobiol.* 194:101883. doi: 10.1016/j.pneurobio.2020.101883

Kriegstein, A., Noctor, S., and Martinez-Cerdeno, V. (2006). Patterns of neural stem and progenitor cell division may underlie evolutionary cortical expansion. *Nat. Rev. Neurosci.* 7, 883–890. doi: 10.1038/nrn2008

Kuida, K., Haydar, T. F., Kuan, C. Y., Gu, Y., Taya, C., Karasuyama, H., et al. (1998). Reduced apoptosis and cytochrome c-mediated caspase activation in mice lacking caspase 9. *Cell* 94, 325–337. doi: 10.1016/s0092-8674(00)81476-2

Kuida, K., Zheng, T. S., Na, S., Kuan, C., Yang, D., Karasuyama, H., et al. (1996). Decreased apoptosis in the brain and premature lethality in CPP32-deficient mice. *Nature* 384, 368–372. doi: 10.1038/384368a0

Kullmann, J. A., Meyer, S., Pipicelli, F., Kyrousi, C., Schneider, F., Bartels, N., et al. (2020). Profilin1-dependent F-actin assembly controls division of apical radial glia and neocortex development. *Cereb. Cortex* 30, 3467–3482. doi: 10.1093/cercor/bhz321

Kumari, K., Sharma, M. C., Kakkar, A., Malgulwar, P. B., Pathak, P., Suri, V., et al. (2020). mTOR pathway activation in focal cortical dysplasia. *Ann. Diagn. Pathol.* 46:151523.

Kwiatkowski, D. J., Aklog, L., Ledbetter, D. H., and Morton, C. C. (1990). Identification of the functional profilin gene, its localization to chromosome subband 17p13.3, and demonstration of its deletion in some patients with Miller-Dieker syndrome. *Am. J. Hum. Genet.* 46, 559–567.

Kyrousi, C., O'Neill, A. C., Brazovskaja, A., He, Z., Kielkowski, P., Coquand, L., et al. (2021). Extracellular LGALS3BP regulates neural progenitor position and relates to human cortical complexity. *Nat. Commun.* 12:6298. doi: 10.1038/s41467-021-26447-w

Lakoma, J., Garcia-Alonso, L., and Luque, J. M. (2011). Reelin sets the pace of neocortical neurogenesis. *Development* 138, 5223–5234. doi: 10.1242/dev.063776

Lancaster, M. A., and Knoblich, J. A. (2012). Spindle orientation in mammalian cerebral cortical development. *Curr. Opin. Neurobiol.* 22, 737–746. doi: 10.1016/j.conb.2012.04.003

Lau, E. O., Damiani, D., Chehade, G., Ruiz-Reig, N., Saade, R., Jossin, Y., et al. (2021). DIAPH3 deficiency links microtubules to mitotic errors, defective neurogenesis, and brain dysfunction. *eLife* 10:e61974. doi: 10.7554/eLife.61974

Lee, J. H., Huynh, M., Silhavy, J. L., Kim, S., Dixon-Salazar, T., Heiberg, A., et al. (2012). De novo somatic mutations in components of the PI3K-AKT3-mTOR pathway cause hemimegalencephaly. *Nat. Genet.* 44, 941–945. doi: 10.1038/ng.2329

Leone, D. P., Srinivasan, K., Brakebusch, C., and McConnell, S. K. (2010). The rho GTPase Rac1 is required for proliferation and survival of progenitors in the developing forebrain. *Dev. Neurobiol.* 70, 659–678. doi: 10.1002/dneu.20804

Lewitus, E., Kelava, I., Kalinka, A. T., Tomancak, P., and Huttner, W. B. (2014). An adaptive threshold in mammalian neocortical evolution. *PLoS Biol.* 12:e1002000. doi: 10.1371/journal.pbio.1002000

Li, H. S., Wang, D., Shen, Q., Schonemann, M. D., Gorski, J. A., Jones, K. R., et al. (2003). Inactivation of Numb and Numblike in embryonic dorsal forebrain impairs neurogenesis and disrupts cortical morphogenesis. *Neuron* 40, 1105–1118. doi: 10.1016/s0896-6273(03)00755-4

Li, Y., Muffat, J., Omer, A., Bosch, I., Lancaster, M. A., Sur, M., et al. (2017). Induction of expansion and folding in human cerebral organoids. *Cell Stem Cell* 20, 385–396. doi: 10.1016/j.stem.2016.11.017

Lian, G., Lu, J., Hu, J., Zhang, J., Cross, S. H., Ferland, R. J., et al. (2012). Filamin a regulates neural progenitor proliferation and cortical size through

Wee1-dependent Cdk1 phosphorylation. *J. Neurosci.* 32, 7672–7684. doi: 10.1523/JNEUROSCI.0894-12.2012

Ligon, K. L., Echelard, Y., Assimacopoulos, S., Danielian, P. S., Kaing, S., Grove, E. A., et al. (2003). Loss of Emx2 function leads to ectopic expression of Wnt1 in the developing telencephalon and cortical dysplasia. *Development* 130, 2275–2287. doi: 10.1242/dev.00421

Lim, J. S., Kim, W. I., Kang, H. C., Kim, S. H., Park, A. H., Park, E. K., et al. (2015). Brain somatic mutations in MTOR cause focal cortical dysplasia type II leading to intractable epilepsy. *Nat. Med.* 21, 395–400. doi: 10.1038/nm.3824

Lim, N. R., Yeap, Y. Y., Zhao, T. T., Yip, Y. Y., Wong, S. C., Xu, D., et al. (2015). Opposing roles for JNK and Aurora A in regulating the association of WDR62 with spindle microtubules. *J. Cell Sci.* 128, 527–540. doi: 10.1242/jcs.157537

Lin, T., Sandusky, S. B., Xue, H., Fishbein, K. W., Spencer, R. G., Rao, M. S., et al. (2003). A central nervous system specific mouse model for thanatophoric dysplasia type II. *Hum. Mol. Genet.* 12, 2863–2871. doi: 10.1093/hmg/ddg309

Liu, W. A., Chen, S., Li, Z., Lee, C. H., Mirzaa, G., Dobyns, W. B., et al. (2018). PARD3 dysfunction in conjunction with dynamic HIPPO signaling drives cortical enlargement with massive heterotopia. *Genes Dev.* 32, 763–780. doi: 10.1101/gad.313171.118

Lizarraga, S. B., Margossian, S. P., Harris, M. H., Campagna, D. R., Han, A. P., Blevins, S., et al. (2010). Cdk5rap2 regulates centrosome function and chromosome segregation in neuronal progenitors. *Development* 137, 1907–1917. doi: 10.1242/dev.040410

Llinares-Benadero, C., and Borrell, V. (2019). Deconstructing cortical folding: genetic, cellular and mechanical determinants. *Nat. Rev. Neurosci.* 20, 161–176. doi: 10.1038/s41583-018-0112-2

Lopez-Tobon, A., Villa, C. E., Cheroni, C., Trattaro, S., Caporale, N., Conforti, P., et al. (2019). Human cortical organoids expose a differential function of GSK3 on cortical neurogenesis. *Stem Cell Rep.* 13, 847–861. doi: 10.1016/j.stemcr.2019.09.005

Luhmann, H. J. (2016). Models of cortical malformation–Chemical and physical. *J. Neurosci. Methods* 260, 62–72. doi: 10.1016/j.jneumeth.2015.03.034

Lui, J. H., Hansen, D. V., and Kriegstein, A. R. (2011). Development and evolution of the human neocortex. *Cell* 146, 18–36. doi: 10.1016/j.cell.2011.06.030

Mallamaci, A., Mercurio, S., Muzio, L., Cecchi, C., Pardini, C. L., Gruss, P., et al. (2000). The lack of Emx2 causes impairment of Reelin signaling and defects of neuronal migration in the developing cerebral cortex. *J. Neurosci.* 20, 1109–1118. doi: 10.1523/JNEUROSCI.20-03-01109.2000

Manikkam, S. A., Chetcuti, K., Howell, K. B., Savarirayan, R., Fink, A. M., and Mandelstam, S. A. (2018). Temporal lobe malformations in achondroplasia: expanding the brain imaging phenotype associated with FGFR3-related skeletal dysplasias. *AJNR Am. J. Neuroradiol.* 39, 380–384. doi: 10.3174/ajnr.A5468

Marin-Padilla, M. (1978). Dual origin of the mammalian neocortex and evolution of the cortical plate. *Anat. Embryol.* 152, 109–126. doi: 10.1007/BF00315920

Marsan, E., and Baulac, S. (2018). Review: mechanistic target of rapamycin (mTOR) pathway, focal cortical dysplasia and epilepsy. *Neuropathol. Appl. Neurobiol.* 44, 6–17. doi: 10.1111/nan.12463

Masuda, K., Toda, T., Shinmyo, Y., Ebisu, H., Hoshiba, Y., Wakimoto, M., et al. (2015). Pathophysiological analyses of cortical malformation using gyrencephalic mammals. *Sci. Rep.* 5:15370. doi: 10.1038/srep15370

Matsumoto, N., Hoshiba, Y., Morita, K., Uda, N., Hirota, M., Minamikawa, M., et al. (2017a). Pathophysiological analyses of periventricular nodular heterotopia using gyrencephalic mammals. *Hum. Mol. Genet.* 26, 1173–1181. doi: 10.1093/hmg/ddx038

Matsumoto, N., Shinmyo, Y., Ichikawa, Y., and Kawasaki, H. (2017b). Gyrification of the cerebral cortex requires FGF signaling in the mammalian brain. *eLife* 6:e29285. doi: 10.7554/eLife.29285

Matsumoto, N., Kobayashi, N., Uda, N., Hirota, M., and Kawasaki, H. (2018). Pathophysiological analyses of leptomeningeal heterotopia using gyrencephalic mammals. *Hum. Mol. Genet.* 27, 985–991. doi: 10.1093/hmg/ddy014

Matsuzaki, F., and Shitamukai, A. (2015). Cell division modes and cleavage planes of neural progenitors during mammalian cortical development. *Cold Spring Harb. Perspect. Biol.* 7:a015719. doi: 10.1101/cshperspect.a015719

McKenney, R. J., Vershinin, M., Kunwar, A., Vallee, R. B., and Gross, S. P. (2010). LIS1 and NudE induce a persistent dynein force-producing state. *Cell* 141, 304–314. doi: 10.1016/j.cell.2010.02.035

Meunier, S., and Vernos, I. (2016). Acentrosomal microtubule assembly in mitosis: the where, when, and how. *Trends Cell Biol.* 26, 80–87. doi: 10.1016/j.tcb.2015.09.001

Mirzaa, G. M., Campbell, C. D., Solovieff, N., Goold, C., Jansen, L. A., Menon, S., et al. (2016). Association of MTOR mutations with developmental brain disorders, including megalencephaly, focal cortical dysplasia, and pigmentary mosaicism. *JAMA Neurol.* 73, 836–845. doi: 10.1001/jamaneurol.2016.0363

Mirzaa, G. M., Parry, D. A., Fry, A. E., Giamanco, K. A., Schwartzentruber, J., Vanstone, M., et al. (2014a). De novo CCND2 mutations leading to stabilization of cyclin D2 cause megalencephaly-polymicrogyria-polydactyly-hydrocephalus syndrome. *Nat. Genet.* 46, 510–515. doi: 10.1038/ng.2948

Mirzaa, G. M., Vitre, B., Carpenter, G., Abramowicz, I., Gleeson, J. G., Paciorkowski, A. R., et al. (2014b). Mutations in CENPE define a novel kinetochore-centromeric mechanism for microcephalic primordial dwarfism. *Hum. Genet.* 133, 1023–1039. doi: 10.1007/s00439-014-1443-3

Mirzaa, G. M., and Poduri, A. (2014). Megalencephaly and hemimegalencephaly: breakthroughs in molecular etiology. *Am. J. Med. Genet. C Semin. Med. Genet.* 166C, 156–172. doi: 10.1002/ajmg.c.31401

Mishra-Gorur, K., Caglayan, A. O., Schaffer, A. E., Chabu, C., Henegariu, O., Vonhoff, F., et al. (2015). Mutations in KATNB1 cause complex cerebral malformations by disrupting asymmetrically dividing neural progenitors. *Neuron* 85:228.

Miyata, T., Kawaguchi, A., Saito, K., Kawano, M., Muto, T., and Ogawa, M. (2004). Asymmetric production of surface-dividing and non-surface-dividing cortical progenitor cells. *Development* 131, 3133–3145. doi: 10.1242/dev.01173

Molnar, Z., Clowry, G. J., Sestan, N., Alzu'bi, A., Bakken, T., Hevner, R. F., et al. (2019). New insights into the development of the human cerebral cortex. *J. Anat.* 235, 432–451. doi: 10.1111/joa.13055

Molyneaux, B. J., Arlotta, P., Menezes, J. R., and Macklis, J. D. (2007). Neuronal subtype specification in the cerebral cortex. *Nat. Rev. Neurosci.* 8, 427–437. doi: 10.1038/nrn2151

Montgomery, S. H., and Mundy, N. I. (2014). Microcephaly genes evolved adaptively throughout the evolution of eutherian mammals. *BMC Evol. Biol.* 14:120. doi: 10.1186/1471-2148-14-120

Montier, L., Haneef, Z., Gavvala, J., Yoshor, D., North, R., Verla, T., et al. (2019). A somatic mutation in MEN1 gene detected in periventricular nodular heterotopia tissue obtained from depth electrodes. *Epilepsia* 60, e104–e109. doi: 10.1111/epi.16328

Moon, H. M., Hippenmeyer, S., Luo, L., and Wynshaw-Boris, A. (2020). LIS1 determines cleavage plane positioning by regulating actomyosin-mediated cell membrane contractility. *eLife* 9:e51512. doi: 10.7554/eLife.51512

Moon, H. M., and Wynshaw-Boris, A. (2013). Cytoskeleton in action: lissencephaly, a neuronal migration disorder. *Wiley Interdiscip. Rev. Dev. Biol.* 2, 229–245. doi: 10.1002/wdev.67

Mooney, S. M., Siegenthaler, J. A., and Miller, M. W. (2004). Ethanol induces heterotopias in organotypic cultures of rat cerebral cortex. *Cereb. Cortex* 14, 1071–1080. doi: 10.1093/cercor/bhh066

Mutch, C. A., Poduri, A., Sahin, M., Barry, B., Walsh, C. A., and Barkovich, A. J. (2016). Disorders of microtubule function in neurons: imaging correlates. *AJNR Am. J. Neuroradiol.* 37, 528–535. doi: 10.3174/ajnr.A4552

Najm, I. M., Sarnat, H. B., and Blumcke, I. (2018). Review: the international consensus classification of Focal Cortical Dysplasia - a critical update 2018. *Neuropathol. Appl. Neurobiol.* 44, 18–31. doi: 10.1111/nan.12462

Namba, T., Doczi, J., Pinson, A., Xing, L., Kalebic, N., Wilsch-Brauninger, M., et al. (2020). Human-specific ARHGAP11B acts in mitochondria to expand neocortical progenitors by glutaminolysis. *Neuron* 105, 867–881. doi: 10.1016/j.neuron.2019.11.027

Namba, T., Nardelli, J., Gressens, P., and Huttner, W. B. (2021). Metabolic regulation of neocortical expansion in development and evolution. *Neuron* 109, 408–419. doi: 10.1016/j.neuron.2020.11.014

Nelson, B. R., Hodge, R. D., Bedogni, F., and Hevner, R. F. (2013). Dynamic interactions between intermediate neurogenic progenitors and radial glia in embryonic mouse neocortex: potential role in Dll1-Notch signaling. *J. Neurosci.* 33, 9122–9139. doi: 10.1523/JNEUROSCI.0791-13.2013

Nicholas, A. K., Khurshid, M., Desir, J., Carvalho, O. P., Cox, J. J., Thornton, G., et al. (2010). WDR62 is associated with the spindle pole and is mutated in human microcephaly. *Nat. Genet.* 42, 1010–1014. doi: 10.1038/ng.682

Noctor, S. C., Martinez-Cerdeno, V., Ivic, L., and Kriegstein, A. R. (2004). Cortical neurons arise in symmetric and asymmetric division zones and migrate through specific phases. *Nat. Neurosci.* 7, 136–144. doi: 10.1038/nn1172

Noctor, S. C., Palmer, S. L., Hasling, T., and Juliano, S. L. (1999). Interference with the development of early generated neocortex results in disruption of radial glia and abnormal formation of neocortical layers. *Cereb. Cortex* 9, 121–136. doi: 10.1093/cercor/9.2.121

Noctor, S. C., Palmer, S. L., McLaughlin, D. F., and Juliano, S. L. (2001). Disruption of layers 3 and 4 during development results in altered thalamocortical projections in ferret somatosensory cortex. *J. Neurosci.* 21, 3184–3195. doi: 10.1523/JNEUROSCI.21-09-03184.2001

Nowakowski, T. J., Bhaduri, A., Pollen, A. A., Alvarado, B., Mostajo-Radji, M. A., Di Lullo, E., et al. (2017). Spatiotemporal gene expression trajectories reveal developmental hierarchies of the human cortex. *Science* 358, 1318–1323. doi: 10.1126/science.aap8809

Nowakowski, T. J., Pollen, A. A., Sandoval-Espinosa, C., and Kriegstein, A. R. (2016). Transformation of the radial glia scaffold demarcates two stages of human cerebral cortex development. *Neuron* 91, 1219–1227. doi: 10.1016/j.neuron.2016.09.005

Oegema, R., McGillivray, G., Leventer, R., Le Moing, A. G., Bahi-Buisson, N., Barnicoat, A., et al. (2019). EML1-associated brain overgrowth syndrome with ribbon-like heterotopia. *Am. J. Med. Genet. C Semin. Med. Genet.* 181, 627–637. doi: 10.1002/ajmg.c.31751

O'Neill, A. C., Kyrousi, C., Klaus, J., Leventer, R. J., Kirk, E. P., Fry, A., et al. (2018). A primate-specific isoform of PLEKHG6 regulates neurogenesis and neuronal migration. *Cell Rep.* 25, 2729.e6–2741.e6. doi: 10.1016/j.celrep.2018.11.029

Pan, Y. H., Wu, N., and Yuan, X. B. (2019). Toward a better understanding of neuronal migration deficits in autism spectrum disorders. *Front. Cell Dev. Biol.* 7:205. doi: 10.3389/fcell.2019.00205

Pannier, S., Martinovic, J., Heuertz, S., Delezoide, A. L., Munnich, A., Schibler, L., et al. (2009). Thanatophoric dysplasia caused by double missense FGFR3 mutations. *Am. J. Med. Genet. A* 149A, 1296–1301. doi: 10.1002/ajmg.a.32880

Paridaen, J. T., Wilsch-Brauninger, M., and Huttner, W. B. (2013). Asymmetric inheritance of centrosome-associated primary cilium membrane directs ciliogenesis after cell division. *Cell* 155, 333–344. doi: 10.1016/j.cell.2013.08.060

Passemard, S., Perez, F., Gressens, P., and El Ghouzzi, V. (2019). Endoplasmic reticulum and Golgi stress in microcephaly. *Cell Stress* 3, 369–384. doi: 10.15698/cst2019.12.206

Pattabiraman, K., Muchnik, S. K., and Sestan, N. (2020). The evolution of the human brain and disease susceptibility. *Curr. Opin. Genet. Dev.* 65, 91–97. doi: 10.1016/j.gde.2020.05.004

Penisson, M., Ladewig, J., Belvindrah, R., and Francis, F. (2019). Genes and mechanisms involved in the generation and amplification of basal radial glial cells. *Front. Cell. Neurosci.* 13:381. doi: 10.3389/fncel.2019.00381

Pervaiz, N., Kang, H., Bao, Y., and Abbasi, A. A. (2021). Molecular evolutionary analysis of human primary microcephaly genes. *BMC Ecol. Evol.* 21:76. doi: 10.1186/s12862-021-01801-0

Petersen, P. H., Zou, K., Krauss, S., and Zhong, W. (2004). Continuing role for mouse Numb and Numbl in maintaining progenitor cells during cortical neurogenesis. *Nat. Neurosci.* 7, 803–811. doi: 10.1038/nn1289

Pierfelice, T., Alberi, L., and Gaiano, N. (2011). Notch in the vertebrate nervous system: an old dog with new tricks. *Neuron* 69, 840–855. doi: 10.1016/j.neuron.2011.02.031

Poduri, A., Evrony, G. D., Cai, X., Elhosary, P. C., Beroukhim, R., Lehtinen, M. K., et al. (2012). Somatic activation of AKT3 causes hemispheric developmental brain malformations. *Neuron* 74, 41–48. doi: 10.1016/j.neuron.2012.03.010

Postiglione, M. P., Juschke, C., Xie, Y., Haas, G. A., Charalambous, C., and Knoblich, J. A. (2011). Mouse inscuteable induces apical-basal spindle orientation to facilitate intermediate progenitor generation in the developing neocortex. *Neuron* 72, 269–284. doi: 10.1016/j.neuron.2011.09.022

Pulvers, J. N., Bryk, J., Fish, J. L., Wilsch-Brauninger, M., Arai, Y., Schreier, D., et al. (2010). Mutations in mouse Aspm (abnormal spindle-like microcephaly associated) cause not only microcephaly but also major defects in the germline. *Proc. Natl. Acad. Sci. U.S.A.* 107, 16595–16600. doi: 10.1073/pnas.1010494107

Pulvers, J. N., Journiac, N., Arai, Y., and Nardelli, J. (2015). MCPH1: a window into brain development and evolution. *Front. Cell. Neurosci.* 9:92. doi: 10.3389/fncel.2015.00092

Qian, X., Nguyen, H. N., Song, M. M., Hadiono, C., Ogden, S. C., Hammack, C., et al. (2016). Brain-region-specific organoids using mini-bioreactors for modeling ZIKV exposure. *Cell* 165, 1238–1254. doi: 10.1016/j.cell.2016.04.032

Qiao, Y., Yang, X., and Jing, N. (2016). Epigenetic regulation of early neural fate commitment. *Cell Mol. Life Sci.* 73, 1399–1411. doi: 10.1007/s00018-015-2125-6

Qin, W., Chan, J. A., Vinters, H. V., Mathern, G. W., Franz, D. N., Taillon, B. E., et al. (2010). Analysis of TSC cortical tubers by deep sequencing of TSC1, TSC2 and KRAS demonstrates that small second-hit mutations in these genes are rare events. *Brain Pathol.* 20, 1096–1105. doi: 10.1111/j.1750-3639.2010.00416.x

Quadrato, G., and Arlotta, P. (2017). Present and future of modeling human brain development in 3D organoids. *Curr. Opin. Cell Biol* 49, 47–52. doi: 10.1016/j.ceb.2017.11.010

Radmanesh, F., Caglayan, A. O., Silhavy, J. L., Yilmaz, C., Cantagrel, V., Omar, T., et al. (2013). Mutations in LAMB1 cause cobblestone brain malformation without muscular or ocular abnormalities. *Am. J. Hum. Genet.* 92, 468–474. doi: 10.1016/j.ajhg.2013.02.005

Rakic, P. (1988). Specification of cerebral cortical areas. *Science* 241, 170–176.

Rakic, P. (1995). A small step for the cell, a giant leap for mankind: a hypothesis of neocortical expansion during evolution. *Trends Neurosci.* 18, 383–388. doi: 10.1016/0166-2236(95)93934-p

Rakic, P. (2000). Radial unit hypothesis of neocortical expansion. *Novartis Found. Symp.* 228, 30–42. doi: 10.1002/0470846631.ch3

Rakic, P. (2003). Developmental and evolutionary adaptations of cortical radial glia. *Cereb. Cortex* 13, 541–549. doi: 10.1093/cercor/13.6.541

Rakic, P. (2009). Evolution of the neocortex: a perspective from developmental biology. *Nat. Rev. Neurosci.* 10, 724–735. doi: 10.1038/nrn2719

Rakic, S., and Zecevic, N. (2000). Programmed cell death in the developing human telencephalon. *Eur. J. Neurosci.* 12, 2721–2734. doi: 10.1046/j.1460-9568.2000.00153.x

Rakotomamonjy, J., Brunner, M., Juschke, C., Zang, K., Huang, E. J., Reichardt, L. F., et al. (2017). Afadin controls cell polarization and mitotic spindle orientation in developing cortical radial glia. *Neural Dev.* 12:7. doi: 10.1186/s13064-017-0085-2

Rashidi-Nezhad, A., Talebi, S., Saebnouri, H., Akrami, S. M., and Reymond, A. (2014). The effect of homozygous deletion of the BBOX1 and Fibin genes on carnitine level and acyl carnitine profile. *BMC Med. Genet.* 15:75. doi: 10.1186/1471-2350-15-75

Rasin, M. R., Gazula, V. R., Breunig, J. J., Kwan, K. Y., Johnson, M. B., Liu-Chen, S., et al. (2007). Numb and Numbl are required for maintenance of cadherin-based adhesion and polarity of neural progenitors. *Nat. Neurosci.* 10, 819–827. doi: 10.1038/nn1924

Reichard, J., and Zimmer-Bensch, G. (2021). The epigenome in neurodevelopmental disorders. *Front. Neurosci.* 15:776809. doi: 10.3389/fnins.2021.776809

Reijnders, M. R. F., Kousi, M., van Woerden, G. M., Klein, M., Bralten, J., Mancini, G. M. S., et al. (2017). Variation in a range of mTOR-related genes associates with intracranial volume and intellectual disability. *Nat. Commun.* 8:1052. doi: 10.1038/s41467-017-00933-6

Reillo, I., and Borrell, V. (2012). Germinal zones in the developing cerebral cortex of ferret: ontogeny, cell cycle kinetics, and diversity of progenitors. *Cereb. Cortex* 22, 2039–2054. doi: 10.1093/cercor/bhr284

Reillo, I., de Juan Romero, C., Garcia-Cabezas, M. A., and Borrell, V. (2011). A role for intermediate radial glia in the tangential expansion of the mammalian cerebral cortex. *Cereb. Cortex* 21, 1674–1694. doi: 10.1093/cercor/bhq238

Reiner, O., Carrozzo, R., Shen, Y., Wehnert, M., Faustinella, F., Dobyns, W. B., et al. (1993). Isolation of a Miller-Dieker lissencephaly gene containing G protein beta-subunit-like repeats. *Nature* 364, 717–721. doi: 10.1038/364717a0

Riviere, J. B., Mirzaa, G. M., O'Roak, B. J., Beddaoui, M., Alcantara, D., Conway, R. L., et al. (2012). De novo germline and postzygotic mutations in AKT3, PIK3R2 and PIK3CA cause a spectrum of related megalencephaly syndromes. *Nat. Genet.* 44, 934–940. doi: 10.1038/ng.2331

Romaniello, R., Arrigoni, F., Fry, A. E., Bassi, M. T., Rees, M. I., Borgatti, R., et al. (2018). Tubulin genes and malformations of cortical development. *Eur. J. Med. Genet.* 61, 744–754. doi: 10.1016/j.ejmg.2018.07.012

Romero, D. M., Bahi-Buisson, N., and Francis, F. (2018). Genetics and mechanisms leading to human cortical malformations. *Semin. Cell Dev. Biol.* 76, 33–75. doi: 10.1016/j.semcdb.2017.09.031

Rosenberg, M. J., Agarwala, R., Bouffard, G., Davis, J., Fiermonte, G., Hilliard, M. S., et al. (2002). Mutant deoxynucleotide carrier is associated with congenital microcephaly. *Nat. Genet.* 32, 175–179. doi: 10.1038/ng948

Roth, K. A., and D'Sa, C. (2001). Apoptosis and brain development. *Ment. Retard. Dev. Disabil. Res. Rev.* 7, 261–266.

Ruzzo, E. K., Capo-Chichi, J. M., Ben-Zeev, B., Chitayat, D., Mao, H., Pappas, A. L., et al. (2013). Deficiency of asparagine synthetase causes congenital microcephaly and a progressive form of encephalopathy. *Neuron* 80, 429–441. doi: 10.1016/j.neuron.2013.08.013

Saito, K., Mizuguchi, K., Horiike, T., Dinh Duong, T. A., Shinmyo, Y., and Kawasaki, H. (2018). Characterization of the inner and outer fiber layers in the developing cerebral cortex of gyrencephalic ferrets. *Cereb. Cortex* 29, 4303–4311. doi: 10.1093/cercor/bhy312

Sakai, D., Dixon, J., Dixon, M. J., and Trainor, P. A. (2012). Mammalian neurogenesis requires Treacle-Plk1 for precise control of spindle orientation, mitotic progression, and maintenance of neural progenitor cells. *PLoS Genet.* 8:e1002566. doi: 10.1371/journal.pgen.1002566

Sapir, T., Barakat, T. S., Paredes, M. F., Lerman-Sagie, T., Aronica, E., Klonowski, W., et al. (2019). Building bridges between the clinic and the laboratory: a meeting review - brain malformations: a roadmap for future research. *Front. Cell. Neurosci.* 13:434. doi: 10.3389/fncel.2019.00434

Sarieva, K., and Mayer, S. (2021). The effects of environmental adversities on human neocortical neurogenesis modeled in brain organoids. *Front. Mol. Biosci.* 8:686410. doi: 10.3389/fmolb.2021.686410

Sarnat, H. B. (1987). Disturbances of late neuronal migrations in the perinatal period. *Am. J. Dis. Child* 141, 969–980. doi: 10.1001/archpedi.1987.04460090046022

Sarnat, H. B., and Flores-Sarnat, L. (2014). Morphogenesis timing of genetically programmed brain malformations in relation to epilepsy. *Prog. Brain Res.* 213, 181–198. doi: 10.1016/B978-0-444-63326-2.00010-7

Sarnat, H. B., and Flores-Sarnat, L. (2021). Excitatory/inhibitory synaptic ratios in polymicrogyria and down syndrome help explain epileptogenesis in malformations. *Pediatr. Neurol.* 116, 41–54. doi: 10.1016/j.pediatrneurol.2020.11.001

Schmid, M. T., Weinandy, F., Wilsch-Brauninger, M., Huttner, W. B., Cappello, S., and Gotz, M. (2014). The role of alpha-E-catenin in cerebral cortex development: radial glia specific effect on neuronal migration. *Front. Cell. Neurosci.* 8:215. doi: 10.3389/fncel.2014.00215

Severino, M., Geraldo, A. F., Utz, N., Tortora, D., Pogledic, I., Klonowski, W., et al. (2020). Definitions and classification of malformations of cortical development: practical guidelines. *Brain* 143, 2874–2894. doi: 10.1093/brain/awaa174

Sgourdou, P., Mishra-Gorur, K., Saotome, I., Henagariu, O., Tuysuz, B., Campos, C., et al. (2017). Disruptions in asymmetric centrosome inheritance and WDR62-Aurora kinase B interactions in primary microcephaly. *Sci. Rep.* 7:43708. doi: 10.1038/srep43708

Shao, W., Yang, J., He, M., Yu, X. Y., Lee, C. H., Yang, Z., et al. (2020). Centrosome anchoring regulates progenitor properties and cortical formation. *Nature* 580, 106–112. doi: 10.1038/s41586-020-2139-6

Sheen, V. L., Ganesh, V. S., Topcu, M., Sebire, G., Bodell, A., Hill, R. S., et al. (2004). Mutations in ARFGEF2 implicate vesicle trafficking in neural progenitor proliferation and migration in the human cerebral cortex. *Nat. Genet.* 36, 69–76.

Sheen, V. L., Jansen, A., Chen, M. H., Parrini, E., Morgan, T., Ravenscroft, R., et al. (2005). Filamin A mutations cause periventricular heterotopia with Ehlers-Danlos syndrome. *Neurology* 64, 254–262. doi: 10.1212/01.WNL.0000149512.79621.DF

Shi, L., Luo, X., Jiang, J., Chen, Y., Liu, C., Hu, T., et al. (2019). Transgenic rhesus monkeys carrying the human MCPH1 gene copies show human-like neoteny of brain development. *Natl. Sci. Rev.* 6, 480–493. doi: 10.1093/nsr/nwz043

Shinmyo, Y., Terashita, Y., Dinh Duong, T. A., Horiike, T., Kawasumi, M., Hosomichi, K., et al. (2017). Folding of the cerebral cortex requires Cdk5 in upper-layer neurons in gyrencephalic mammals. *Cell Rep.* 20, 2131–2143. doi: 10.1016/j.celrep.2017.08.024

Sidhaye, J., and Knoblich, J. A. (2021). Brain organoids: an ensemble of bioassays to investigate human neurodevelopment and disease. *Cell Death Differ.* 28, 52–67. doi: 10.1038/s41418-020-0566-4

Silver, D. L. (2016). Genomic divergence and brain evolution: how regulatory DNA influences development of the cerebral cortex. *Bioessays* 38, 162–171. doi: 10.1002/bies.201500108

Singer, K., Luo, R., Jeong, S. J., and Piao, X. (2013). GPR56 and the developing cerebral cortex: cells, matrix, and neuronal migration. *Mol. Neurobiol.* 47, 186–196. doi: 10.1007/s12035-012-8343-0

Smart, I. H., Dehay, C., Giroud, P., Berland, M., and Kennedy, H. (2002). Unique morphological features of the proliferative zones and postmitotic compartments of the neural epithelium giving rise to striate and extrastriate cortex in the monkey. *Cereb. Cortex* 12, 37–53. doi: 10.1093/cercor/12.1.37

Sousa, A. M. M., Meyer, K. A., Santpere, G., Gulden, F. O., and Sestan, N. (2017). Evolution of the human nervous system function, structure, and development. *Cell* 170, 226–247. doi: 10.1016/j.cell.2017.06.036

Squier, W., and Jansen, A. (2014). Polymicrogyria: pathology, fetal origins and mechanisms. *Acta Neuropathol. Commun.* 2:80. doi: 10.1186/s40478-014-0080-3

Stenzel, D., Wilsch-Brauninger, M., Wong, F. K., Heuer, H., and Huttner, W. B. (2014). Integrin alphavbeta3 and thyroid hormones promote expansion of progenitors in embryonic neocortex. *Development* 141, 795–806. doi: 10.1242/dev.101907

Stutterd, C. A., and Leventer, R. J. (2014). Polymicrogyria: a common and heterogeneous malformation of cortical development. *Am. J. Med. Genet. C Semin. Med. Genet.* 166C, 227–239. doi: 10.1002/ajmg.c.31399

Subramanian, L., Calcagnotto, M. E., and Paredes, M. F. (2019). Cortical malformations: lessons in human brain development. *Front. Cell. Neurosci.* 13:576. doi: 10.3389/fncel.2019.00576

Sun, T., and Hevner, R. F. (2014). Growth and folding of the mammalian cerebral cortex: from molecules to malformations. *Nat. Rev. Neurosci.* 15, 217–232. doi: 10.1038/nrn3707

Sutarjono, B. (2019). Can we better understand how zika leads to microcephaly? A systematic review of the effects of the zika virus on human brain organoids. *J. Infect. Dis.* 219, 734–745. doi: 10.1093/infdis/jiy572

Tavano, S., Taverna, E., Kalebic, N., Haffner, C., Namba, T., Dahl, A., et al. (2018). Insm1 induces neural progenitor delamination in developing neocortex *via* downregulation of the adherens junction belt-specific protein Plekha7. *Neuron* 97, 1299–1314. doi: 10.1016/j.neuron.2018.01.052

Taverna, E., Götz, M., and Huttner, W. B. (2014). The cell biology of neurogenesis: toward an understanding of the development and evolution of the neocortex. *Annu. Rev. Cell Dev. Biol.* 30, 465–502. doi: 10.1146/annurev-cellbio-101011-155801

Taverna, E., and Huttner, W. B. (2019). The golgi apparatus in polarized neuroepithelial stem cells and their progeny: canonical and noncanonical features. *Results Probl. Cell Differ.* 67, 359–375. doi: 10.1007/978-3-030-23173-6_15

Taverna, E., Mora-Bermudez, F., Strzyz, P. J., Florio, M., Icha, J., Haffner, C., et al. (2016). Non-canonical features of the Golgi apparatus in bipolar epithelial neural stem cells. *Sci. Rep.* 6:21206. doi: 10.1038/srep21206

Thornton, G. K., and Woods, C. G. (2009). Primary microcephaly: do all roads lead to Rome? *Trends Genet.* 25, 501–510. doi: 10.1016/j.tig.2009.09.011

Thumkeo, D., Shinohara, R., Watanabe, K., Takebayashi, H., Toyoda, Y., Tohyama, K., et al. (2011). Deficiency of mDia, an actin nucleator, disrupts integrity of neuroepithelium and causes periventricular dysplasia. *PLoS One* 6:e25465. doi: 10.1371/journal.pone.0025465

Tokuda, S., Mahaffey, C. L., Monks, B., Faulkner, C. R., Birnbaum, M. J., Danzer, S. C., et al. (2011). A novel Akt3 mutation associated with enhanced kinase activity and seizure susceptibility in mice. *Hum. Mol. Genet.* 20, 988–999. doi: 10.1093/hmg/ddq544

Tsai, J. W., Chen, Y., Kriegstein, A. R., and Vallee, R. B. (2005). LIS1 RNA interference blocks neural stem cell division, morphogenesis, and motility at multiple stages. *J. Cell Biol.* 170, 935–945. doi: 10.1083/jcb.200505166

Urquhart, J. E., Beaman, G., Byers, H., Roberts, N. A., Chervinsky, E., O'Sullivan, J., et al. (2016). DMRTA2 (DMRT5) is mutated in a novel cortical brain malformation. *Clin. Genet.* 89, 724–727. doi: 10.1111/cge.12734

Vaid, S., and Huttner, W. B. (2020). Transcriptional regulators and human-specific/primate-specific genes in neocortical neurogenesis. *Int. J. Mol. Sci.* 21:4614. doi: 10.3390/ijms21134614

Valente, E. M., Silhavy, J. L., Brancati, F., Barrano, G., Krishnaswami, S. R., Castori, M., et al. (2006). Mutations in CEP290, which encodes a centrosomal protein, cause pleiotropic forms of Joubert syndrome. *Nat. Genet.* 38, 623–625. doi: 10.1038/ng1805

van Reeuwijk, J., Grewal, P. K., Salih, M. A., Beltran-Valero de Bernabe, D., McLaughlan, J. M., Michielse, C. B., et al. (2007). Intragenic deletion in the LARGE gene causes Walker-Warburg syndrome. *Hum. Genet.* 121, 685–690. doi: 10.1007/s00439-007-0362-y

van Reeuwijk, J., Janssen, M., van den Elzen, C., Beltran-Valero de Bernabe, D., Sabatelli, P., Merlini, L., et al. (2005). POMT2 mutations cause alpha-dystroglycan hypoglycosylation and Walker-Warburg syndrome. *J. Med. Genet.* 42, 907–912. doi: 10.1136/jmg.2005.031963

Veeraval, L., O'Leary, C. J., and Cooper, H. M. (2020). Adherens junctions: guardians of cortical development. *Front. Cell Dev. Biol.* 8:6. doi: 10.3389/fcell.2020.00006

Vergnolle, M. A., and Taylor, S. S. (2007). Cenp-F links kinetochores to Ndel1/Nde1/Lis1/dynein microtubule motor complexes. *Curr. Biol.* 17, 1173–1179. doi: 10.1016/j.cub.2007.05.077

Viais, R., Farina-Mosquera, M., Villamor-Paya, M., Watanabe, S., Palenzuela, L., Lacasa, C., et al. (2021). Augmin deficiency in neural stem cells causes p53-dependent apoptosis and aborts brain development. *eLife* 10:e67989. doi: 10.7554/eLife.67989

Vidaki, M., Tivodar, S., Doulgeraki, K., Tybulewicz, V., Kessaris, N., Pachnis, V., et al. (2012). Rac1-dependent cell cycle exit of MGE precursors and GABAergic interneuron migration to the cortex. *Cereb. Cortex* 22, 680–692. doi: 10.1093/cercor/bhr145

Vorstman, J. A., van Daalen, E., Jalali, G. R., Schmidt, E. R., Pasterkamp, R. J., de Jonge, M., et al. (2011). A double hit implicates DIAPH3 as an autism risk gene. *Mol. Psychiatry* 16, 442–451. doi: 10.1038/mp.2010.26

Vuillaumier-Barrot, S., Bouchet-Seraphin, C., Chelbi, M., Devisme, L., Quentin, S., Gazal, S., et al. (2012). Identification of mutations in TMEM5 and ISPD as a cause of severe cobblestone lissencephaly. *Am. J. Hum. Genet.* 91, 1135–1143. doi: 10.1016/j.ajhg.2012.10.009

Wang, X., Tsai, J. W., Imai, J. H., Lian, W. N., Vallee, R. B., and Shi, S. H. (2009). Asymmetric centrosome inheritance maintains neural progenitors in the neocortex. *Nature* 461, 947–955. doi: 10.1038/nature08435

Watanabe, M., Buth, J. E., Vishlaghi, N., de la Torre-Ubieta, L., Taxidis, J., Khakh, B. S., et al. (2017). Self-organized cerebral organoids with human-specific features predict effective drugs to combat zika virus infection. *Cell Rep.* 21, 517–532. doi: 10.1016/j.celrep.2017.09.047

Wegscheid, M. L., Anastasaki, C., Hartigan, K. A., Cobb, O. M., Papke, J. B., Traber, J. N., et al. (2021). Patient-derived iPSC-cerebral organoid modeling of the 17q11.2 microdeletion syndrome establishes CRLF3 as a critical regulator of neurogenesis. *Cell Rep.* 36:109315. doi: 10.1016/j.celrep.2021.109315

Weimer, J. M., Yokota, Y., Stanco, A., Stumpo, D. J., Blackshear, P. J., and Anton, E. S. (2009). MARCKS modulates radial progenitor placement, proliferation and organization in the developing cerebral cortex. *Development* 136, 2965–2975. doi: 10.1242/dev.036616

Wilfert, A. B., Sulovari, A., Turner, T. N., Coe, B. P., and Eichler, E. E. (2017). Recurrent de novo mutations in neurodevelopmental disorders: properties and clinical implications. *Genome Med.* 9:101. doi: 10.1186/s13073-017-0498-x

Wilsch-Bräuninger, M., Florio, M., and Huttner, W. B. (2016). Neocortex expansion in development and evolution - from cell biology to single genes. *Curr. Opin. Neurobiol.* 39, 122–132. doi: 10.1016/j.conb.2016.05.004

Wilson, K. D., Porter, E. G., and Garcia, B. A. (2021). Reprogramming of the epigenome in neurodevelopmental disorders. *Crit. Rev. Biochem. Mol. Biol.* [Epub ahead of print]. doi: 10.1080/10409238.2021.1979457

Woodbury-Smith, M., Deneault, E., Yuen, R. K. C., Walker, S., Zarrei, M., Pellecchia, G., et al. (2017). Mutations in RAB39B in individuals with intellectual disability, autism spectrum disorder, and macrocephaly. *Mol. Autism* 8:59. doi: 10.1186/s13229-017-0175-3

Xie, J., Li, H., Zhu, H., Huang, L., Li, H., Zhang, X., et al. (2016). [Analysis of DIAPH3 gene mutation in a boy with autism spectrum disorder]. *Zhonghua Yi Xue Yi Chuan Xue Za Zhi* 33, 481–484. doi: 10.3760/cma.j.issn.1003-9406.2016.04.011

Yao, X., Abrieu, A., Zheng, Y., Sullivan, K. F., and Cleveland, D. W. (2000). CENP-E forms a link between attachment of spindle microtubules to kinetochores and the mitotic checkpoint. *Nat. Cell Biol.* 2, 484–491. doi: 10.1038/35019518

Yingling, J., Youn, Y. H., Darling, D., Toyo-Oka, K., Pramparo, T., Hirotsune, S., et al. (2008). Neuroepithelial stem cell proliferation requires LIS1 for precise spindle orientation and symmetric division. *Cell* 132, 474–486. doi: 10.1016/j.cell.2008.01.026

Yokota, Y., Eom, T. Y., Stanco, A., Kim, W. Y., Rao, S., Snider, W. D., et al. (2010). Cdc42 and Gsk3 modulate the dynamics of radial glial growth, inter-radial glial interactions and polarity in the developing cerebral cortex. *Development* 137, 4101–4110. doi: 10.1242/dev.048637

Yoshida, A., Kobayashi, K., Manya, H., Taniguchi, K., Kano, H., Mizuno, M., et al. (2001). Muscular dystrophy and neuronal migration disorder caused by mutations in a glycosyltransferase, POMGnT1. *Dev. Cell* 1, 717–724. doi: 10.1016/s1534-5807(01)00070-3

Zecevic, N., and Rakic, P. (2001). Development of layer I neurons in the primate cerebral cortex. *J. Neurosci.* 21, 5607–5619. doi: 10.1523/JNEUROSCI.21-15-05607.2001

Zhang, J., Neal, J., Lian, G., Hu, J., Lu, J., and Sheen, V. (2013). Filamin A regulates neuronal migration through brefeldin A-inhibited guanine exchange factor 2-dependent Arf1 activation. *J. Neurosci.* 33, 15735–15746. doi: 10.1523/JNEUROSCI.1939-13.2013

Zhang, J., Neal, J., Lian, G., Shi, B., Ferland, R. J., and Sheen, V. (2012). Brefeldin A-inhibited guanine exchange factor 2 regulates filamin A phosphorylation and neuronal migration. *J. Neurosci.* 32, 12619–12629. doi: 10.1523/JNEUROSCI.1063-12.2012

Zhang, W., Ma, L., Yang, M., Shao, Q., Xu, J., Lu, Z., et al. (2020). Cerebral organoid and mouse models reveal a RAB39b-PI3K-mTOR pathway-dependent dysregulation of cortical development leading to macrocephaly/autism phenotypes. *Genes Dev.* 34, 580–597. doi: 10.1101/gad.332494.119

Zhang, X., Lei, K., Yuan, X., Wu, X., Zhuang, Y., Xu, T., et al. (2009). SUN1/2 and Syne/Nesprin-1/2 complexes connect centrosome to the nucleus during neurogenesis and neuronal migration in mice. *Neuron* 64, 173–187. doi: 10.1016/j.neuron.2009.08.018

Zhou, Z. W., Tapias, A., Bruhn, C., Gruber, R., Sukchev, M., and Wang, Z. Q. (2013). DNA damage response in microcephaly development of MCPH1 mouse model. *DNA Repair* 12, 645–655. doi: 10.1016/j.dnarep.2013.04.017

Conflict of Interest: The authors declare that the research was conducted in the absence of any commercial or financial relationships that could be construed as a potential conflict of interest.

Publisher's Note: All claims expressed in this article are solely those of the authors and do not necessarily represent those of their affiliated organizations, or those of the publisher, the editors and the reviewers. Any product that may be evaluated in this article, or claim that may be made by its manufacturer, is not guaranteed or endorsed by the publisher.

frontiers in Neuroscience

ORIGINAL RESEARCH
published: 21 January 2022
doi: 10.3389/fnins.2021.804402

Upregulation of Neural Cell Adhesion Molecule 1 and Excessive Migration of Purkinje Cells in Cerebellar Cortex

*Shahin Shabanipour[1], Xiaodan Jiao[1], Maryam Rahimi-Balaei[1], Mohamad Reza Aghanoori[2], Seung H. Chung[3], Saeid Ghavami[1], G. Giacomo Consalez[4] and Hassan Marzban[1,5]**

[1] Department of Human Anatomy and Cell Science, Max Rady College of Medicine, Rady Faculty of Health Sciences, University of Manitoba, Winnipeg, MB, Canada, [2] Department of Pharmacology and Therapeutics, Max Rady College of Medicine, Rady Faculty of Health Sciences, University of Manitoba, Winnipeg, MB, Canada, [3] Department of Oral Biology, University of Illinois Chicago, Chicago, IL, United States, [4] Division of Neuroscience, San Raffaele Scientific Institute, Vita-Salute San Raffaele University, Milan, Italy, [5] The Children's Hospital Research Institute of Manitoba (CHRIM), Max Rady College of Medicine, Rady Faculty of Health Sciences, University of Manitoba, Winnipeg, MB, Canada

Purkinje cells (PCs) are large GABAergic projection neurons of the cerebellar cortex, endowed with elaborate dendrites that receive a multitude of excitatory inputs. Being the only efferent neuron of the cerebellar cortex, PCs project to cerebellar nuclei and control behaviors ranging from movement to cognition and social interaction. Neural cell adhesion molecule 1 (NCAM1) is widely expressed in the embryonic and postnatal development of the brain and plays essential roles in neuronal migration, axon pathfinding and synapse assembly. However, despite its high expression levels in cerebellum, little is known to date regarding the role(s) of NCAM1 in PCs development. Among other aspects, elucidating how the expression of NCAM1 in PCs could impact their postnatal migration would be a significant achievement. We analyzed the Acp2 mutant mouse (*nax*: naked and ataxia), which displays excessive PC migration into the molecular layer, and investigated how the excessive migration of PCs along Bergmann glia could correlate to NCAM1 expression pattern in early postnatal days. Our Western blot and RT-qPCR analysis of the whole cerebellum show that the protein and mRNA of NCAM1 in wild type are not different during PC dispersal from the cluster stage to monolayer formation. However, RT-qPCR analysis from FACS-based isolated PCs shows that Ncam1 is significantly upregulated when PCs fail to align and instead overmigrate into the molecular layer. Our results suggest two alternative interpretations: (1) NCAM1 promotes excessive PC migration along Bergmann glia, or (2) NCAM1 upregulation is an attempt to prevent PCs from invading the molecular layer. If the latter scenario proves true, NCAM1 may play a key role in PC monolayer formation.

Keywords: Bergmann glia, *nax*, neuronal migration, Purkinje cell cluster, mice

OPEN ACCESS

Edited by:
Kazuhiko Sawada, Tsukuba International University, Japan

Reviewed by:
Joaquín Martí-Clúa, Universitat Autònoma de Barcelona, Spain
Cristián Gutiérrez-Ibáñez, University of Alberta, Canada

****Correspondence:***
Hassan Marzban
Hassan.marzban@umanitoba.ca

Specialty section:
This article was submitted to Neurodevelopment, a section of the journal Frontiers in Neuroscience

Received: *29 October 2021*
Accepted: *17 December 2021*
Published: *21 January 2022*

Citation:
Shabanipour S, Jiao X, Rahimi-Balaei M, Aghanoori MR, Chung SH, Ghavami S, Consalez GG and Marzban H (2022) Upregulation of Neural Cell Adhesion Molecule 1 and Excessive Migration of Purkinje Cells in Cerebellar Cortex. Front. Neurosci. 15:804402. doi: 10.3389/fnins.2021.804402

INTRODUCTION

Neuronal migration and positioning are critical steps of development mediated by several cellular and molecular interactions that promote the assembly of neuronal circuits, a process that is fundamental for brain function (Rahimi-Balaei et al., 2018). The cerebellum is critical for motor control and cognitive function and is comprised of a few distinct neuronal subtypes. The cerebellar

three-layer cortex consists of the molecular layer, Purkinje cells (PC) layer, and granule cell layer. The main cells in the PC layer are a single row of PC somata, which are intermingled with bodies of Bergmann glial cells (BGCs). PCs are the sole output neuron of the cerebellar cortex and are arranged in an elaborate monolayer throughout the entire cerebellar cortex (Voogd, 1992).

During embryonic development, the cerebellar primordium contains two distinct germinal zones: the ventricular zone and the rhombic lip (Englund et al., 2006; Fink et al., 2006). PCs are derived from the ventricular zone, and complete their final mitotic division at E10–13 in mice (Miale and Sidman, 1961; Wang and Zoghbi, 2001; Marzban et al., 2014). At the post-mitotic stage, PCs start migrating a short distance from their site of origin in the ventricular zone and accumulate in the PC Plate. The migration of PCs from the ventricular zone is described as the glial-guided as PCs migrate along radial glial fibres during early embryonic cerebellar development (Li et al., 2014; Sergaki and Ibanez, 2017; Rahimi-Balaei et al., 2018; Schilling, 2018). PCs eventually change their position and reside as a cluster in the cerebellum during perinatal development. Finally, a new wave of PC migration initiates at around postnatal day (P)2, during which the PC clusters disperse and finally line up in the PC monolayer by P7 (Rahimi-Balaei et al., 2018).

At P2, the BGC bodies colocalize with the PCs in the cluster. BGCs are astrocytes originated from radial glia progenitors (Das, 1976). The movement of BGCs in the developing cerebellum at around P2 coincides with PC dispersal. By P7, both cells ultimately reside in a linear shape conformation called the PC layer. Several studies have shown that BGCs play a crucial role in regulating the movement of granule cell progenitors from the external germinal zone (EGZ) to the granular layer. BGCs have been suggested to share similar interactions with other neurons such as PCs and promote their migration (Higuera et al., 2017). Therefore, the PCs-BGCs intercellular crosstalk at P2-P7, is a likely prerequisite for a coupled migration and for the ability to form a definitive PC layer (Rahimi-Balaei et al., 2018).

Further studies also suggested the presence of intracellular junctions between BGCs and PCs (Bellamy, 2006; Elias et al., 2007; Famulski et al., 2010) that with variation would effectively set a specific spatiotemporal pattern for migration of both cells. It has been shown that the interactions between neuron, glia and extracellular matrix (ECM) would impact not only the migration of PCs but also the function of neural cell adhesion molecule 1 (NCAM1) which is one of the most typical member of cell adhesion molecules of the immunoglobulin superfamily (IgSF CAMs) (Mendis et al., 1994; Kearns et al., 2003; Sergaki and Ibanez, 2017). NCAM1 plays essential roles in migration of precursor cells and pathfinding of axons (Maar et al., 1998; Huang et al., 2006; Stoeckli, 2010). Studies on NCAM1 deficient mice and cerebellar explants showed that the lack of NCAM1 in PCs enhances their migration in the embryonic cerebellum (Rakic and Komuro, 1995; Schmid and Maness, 2008; Sergaki and Ibanez, 2017). PSA (polysialic acid) -NCAM1 interactions direct migration and differentiation of neural precursors during development (Schmid and Maness, 2008; Sergaki and Ibanez, 2017).

In this study, we investigated the expression pattern of NCAM1 in the whole cerebellum and the isolated PCs and BGCs during the PC dispersal period. For this purpose, *Acp2* (acid phosphatase 2, lysosomal) mutant mice (aka; *nax*, naked and ataxia) exhibiting excessive PCs migration were examined and the transcription of *Ncam1* was evaluated. Our results show a significant increase in *Ncam1* transcription in PCs and BGCs of the *nax* cerebellum. *Nax* PCs express abnormally high levels of *Ncam1* and yet feature excessive migration, while, in the wild type cerebellum, low *Ncam1* expression levels are sufficient to arrest PCs migration at the PC layer (Sergaki and Ibanez, 2017). BGCs also upregulate *Ncam1* in the *nax* cerebellum. Our data suggest that NCAM1 may be responsible for fine-tuning PC migration and alignment in the cerebellum. The potential role of *Ncam1* in the context of PC migration will be discussed below.

MATERIALS AND METHODS

Animal Protocol

In this study, the naked ataxia (*nax*; *Acp2* −/−) mice were used for investigating abnormal PC and BGC positioning in the cerebellar cortex. All the animal experiments were submitted and approved by institutional regulations and *the Guide to the Care and Use of Experimental Animals* from the Canadian Council for Animal Care (CCAC). This study was approved by the University of Manitoba Animal Care Committee (ACC) and efforts were made to minimize the number of animals that we needed for our experiments. Immunohistochemistry, Western blotting and RT-qPCR (tissue and sorted cells) examination were performed at least in three animal trials per each age (P2 and P7).

Animal

Acp2 mutant mice (nax mice) were obtained by importing the *nax* mutant embryos from the Institute of Human Genetics in the University Medical Center, Georg-August University, Gottingen, Germany followed by establishing the colony in the Genetic model center of University of Manitoba (Bailey et al., 2014). An average of 3–4 mice from each strain were housed per home cage under standard 12 h light/dark cycle. For immunohistochemistry experiment, the perfusion of mice was carried out with 4% PFA, after which the brain was removed from the skull and immersed in the same fixing solution. The brain tissue was washed with 1×PBS (phosphate-buffered saline) and frozen embedded in OCT. Using the cryotome, 25 μm-thick tissue sections were obtained.

Immunohistochemistry

To demonstrate the expression pattern of the NCAM1 in developing cerebellum at P2 and P7, brain tissue sections were processed through immunohistochemistry and co-labeled with PCs, BGCs markers and the NCAM1. Cerebella of at least three mice for each strain were collected and at least seven sections from cerebellar vermis were analyzed in each animal. During immunohistochemistry process, the tissues sections were blocked with NGS (Normal goat serum 10% including 0.3% triton × 100) for an hour at room

temperature (RT) and then incubated with the following primary antibodies: Rabbit polyclonal anti-calbindin D-28K antiserum CALB1 (Swant Cat# CB38, RRID:AB_10000340, 1:5,000), mouse monoclonal anti-S-100 (β-Subunit) antibody (Sigma-Aldrich Cat# S2532, RRID:AB_477499, 1:500) and mouse monoclonal_anti-NCAM1 (DSHB Cat# 5b8, RRID:AB_528393, 1:100) overnight at 4°C. After washing with PBS 1×, the sections were incubated 1 h with secondary antibodies: Polyclonal Alexa 488-conjugated goat-anti-mouse IgG (Thermo Fisher Scientific Cat# A-11029, RRID:AB_2534088 1:1,000) and Polyclonal Alexa 549-conjugated goat-anti-mouse IgG (Thermo Fisher Scientific Cat# A-11012, RRID:AB_2534079 1:1,000). The florescent labeled sections were mounted with Fluor Save Reagent, Fluorsave (Calbiochem: Cat# 345789) and visualized with Zeiss Light Sheet Z.1 microscope (Zeiss, Toronto, ON, Canada) equipped with a camera. The imaging of the immunostained sections from each group were carried out under similar lightening conditions. Adobe Photoshop CS5 Version 12 was used to edit, crop, and correct contrast and brightness of the images.

Western Blotting

The protein analysis of NCAM1 using Western blot was carried out on both *nax* and *wt* samples comprised of 3 cerebella for each strain. The collected samples were covered with lysis buffer (composed of protease inhibitor cocktail (Life Science, Cat# M250) and phosphatase inhibitor (Sigma Aldrich, Cat# P5726)) and homogenized by sonication. For immunostaining, membranes were blocked for 1 h in 5% skim milk in TBS + 0.1% Triton X-100 (TBST). Membranes were incubated with the mouse monoclonal anti-NCAM1 (DSHB Cat# 5b8, RRID:AB_528393, 1:100) primary antibody at 4°C overnight with gentle agitation. Blots were washed with PBS 1× and incubated with secondary antibodies HRP conjugated polyclonal goat anti-mouse IgG (Millipore Cat# AP308P, RRID:AB_92635, 1:7,500) and developed with Clarity Western ECL Substrate (Bio-Rad, Cat# 170506).

Fluorescence Activated Cell Sorting (FACS) of Purkinje Cells and Bergmann Glial Cells

Mice were selected from both *wt* and *nax* strains each at two different times (P2 and P7). At the day of the experiment, mice were anesthetized, and the dissected brains were immediately transferred into ice-cold 1× Hank's balanced salt solution (HBSS, Gibco 14185-052) and washed by changing the buffer 3×. Afterward, tissues were transferred to the dissection medium (1× HBSS containing gentamicin 10 μg/mL) for cerebellum isolation.

Following the cerebella isolation, washing steps of the collected samples were carried out (Centrifuge at 300 *g*, 4°C and change supernatant) in cold Dulbecco's modified Eagle medium: nutrient mixture F-12 (DMEM/F12, Lonza 12-719F) 3× 1 min, and then incubated in trypsin (Gibco 15090-046) (37°C) for about 12 min. The trypsin was inactivated with 10% FBS (fetal bovine serum) – DMEM/F12 media and washed 3× 5 min.

The pellets were mildly triturated with the 3.5 mL of DNase working solution (1 mL of DNase I stock solution [0.05% DNase (Roche 11284932001) + 12 mM $MgSO_4$ + 1 × HBSS] in 500 μL of heat-inactivated FBS and 2 mL of DMEM/F12) to get a homogenous mixture of cells as a result.

The collected cells were counted (1×10^6) and blocked with NGS 10% without triton X100 at RT for 15 min. The cells were then incubated at RT for 30 in primary antibodies: Mouse monoclonal anti- Kirrel2/NEPH3 (R and D Systems Cat# MAB2564, RRID:AB_2130844, 1:200) for PCs and Rabbit polyclonal anti- EAAT1/GLAST-1/SLC1A3 (Novus Cat# NB100-1869SS, 1:200) for BGC, and afterward were washed 3× with staining buffer. Followed by incubation with secondary antibodies: Polyclonal Alexa488-conjugated goat-anti-rabbit IgG (Thermo Fisher Scientific Cat# A32728, RRID:AB_2633277, 1:500) and Polyclonal Alexa 647-conjugated goat-anti-mouse IgG (Life Technologies, Catalog No., 1:500) for 30 min and counterstaining with DAPI, the final pellet of cells was re-suspended in staining buffer. The staining buffer (1× PBS, FBS 1%, 25 mM HEPES, 1 mM EDTA) was used for diluting antibodies and washing steps during immunohistochemistry. Cell sorting was performed on BD FACS Aria-III cell sorter. Cells were sorted with 100-micron nozzle at the concentration of 15 million cells per ml in purity mode. PCs and BGCs were collected in 15 ml Falcon tubes without any buffer. The next step after sorting the cells would be immediate RNA extraction. Data were acquired on a CytoFlex-LX flow cytometer (Beckman Coulter) equipped with 355, 375, 405, 488, 561, 638, and 808 Laser lines using the CytExpert software, and analyzed with Flow Jo software (version 10) (Treestar, San Carlos, CA, United States) at the University of Manitoba flow cytometry core facility. Cellular debris was excluded using forward light scatter/side scatter plot.

RNA Extraction From Sorted Purkinje Cells and Bergmann Glial Cells and RT-qPCR Analysis

The average number of sorted cells per each sample that were used for RNA extraction were about 50×10^3. Sorted cells were collected in tubes with the least volume of PBS 1×. After a short spin, the supernatant was removed and immediately the lysis buffer from Qiagen RNeasy Plus Mini Kit was added to the pellet. The rest of the steps were followed according to the instruction of the kit to have the high yield of RNA extraction and avoid contaminations as much as possible (QIAGEN: Cat#/ID: 74134). The cDNA synthesis was performed by 0.25 ng of RNA in a qScript cDNA SuperMix kit (Cat# 95048-100). The reaction mixture contained 10 μL PowerUp™ SYBR™ Green Master Mix (Cat# A25742), 2 μL cDNA template and 1.2 μL of each forward and reverse primers in a total reaction volume of 20 μl. Thermocycling parameters were: 95°C for 3 min followed by 40 cycles of 95°C for 30 s, 55°C for 60 s, 72°C for 60 s. The primer sequences are NCAM1 forward: 5′-TGGTTCCGAGATGGTCAGTT-3′ and NCAM1 reverse: 5′-GGATGGAGAAGACGGTGTGT-3′, GAPDH forward: 5′-GGTGAAGGTCGGTGTGAACG-3′ and GAPDH reverse: 5′-CTCGCTCCTGGAAGATGGTG-3′. All

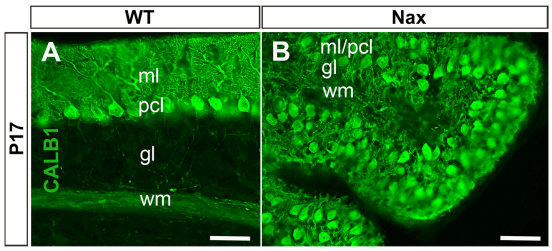

FIGURE 1 | Sagittal sections at P17 of the *wt* and *nax* cerebellum. **(A)** Immunostaining with anti-calbindin (CALB1) in a section through the cerebellum of the *wt* sibling showing the dendrites of PCs in the molecular layer (ml) and Purkinje cell (PC) soma in the Purkinje cell layer (PCl). **(B)** In the *nax* cerebellum showing that the PCs fail to form a uniform monolayer and PCs soma are intermingled in the ml; labeled as pcl/ml. gl, Granular layer; wm, white matter. Scale bar: $A = 50$ μm; $B = 50$ μm.

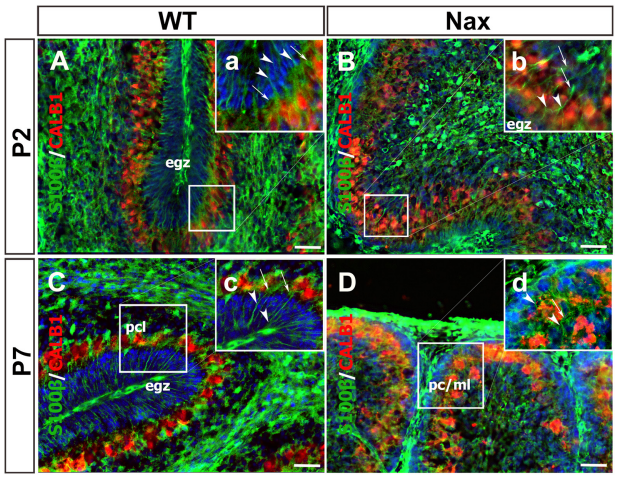

FIGURE 2 | Close relation of BGCs and PCs at P2 and P7 in *wt* and *nax* littermate cerebellum. **(A–D)** Sagittal section of the cerebellum at P2, and P7 were immunofluorescence labeled with anti-calbindin (red) (CALB1; specific marker for PCs) and anti-S100β (green) (specific marker of BGCs). **(A,B)** Images show multiple layers of PCs and the BGC soma at P2 in both *wt* **(A)** and *nax* **(B)** cerebellum. The BGC fibers (arrowhead in high magnifications **a,b**) are extended from basal end and pass the cluster of PCs' (arrow in high magnifications **a,b**) intercellular space where BGC soma is located. In other word, the extension ends in pial surface and the BGC soma are located in PCs cluster. **(C,D)** The location of BGCs (arrowhead in high magnifications **a,b**) is shown at P7 among PCs in PC layer of *wt* cerebellum **(C)**. BGCs and their fibers are located in *nax* cerebellar sections in PC/molecular layer close to EGZ **(D)**. The BGC fibers in *nax* cerebellum are not well organised as in *wt* cerebellum, but still basal end are connected to the pia matter through their fiber extensions. PCs, Purkinje cells; BGCs, Bergman glia cells; pcl, Purkinje cell layer; ml, Molecular layer. Scale bars: 100 μm (applies to panels **A–D**); 50 μm (applied to panels **a–d**).

reactions were performed in duplicate, and gene expression values were normalized with respect to the reference gene, GAPDH, and utilizing the $2^{-\Delta\Delta ct}$ method. Data are presented as means ± SEM.

RNA Isolation and RNA Sequencing of *nax* and *wt* Cerebellum

The cerebella of *nax* (P5; $n = 2$ and P7; $n = 3$) and *wt* littermates (P5; $n = 3$ and P7; $n = 3$) were isolated and RNA extraction was carried using the RNeasy Plus Mini Kit (Cat# 74134, QIAGEN, Toronto, ON, Canada). The RNA concentration of the collected samples was measured by Nano-Drop ND-1000 UV-Vis Spectrophotometer (Thermo Fisher Scientific, Waltham, MA, United States). The samples were frozen in −80 and sent to the McGill University and Genome Quebec Innovation Centre (MUGQIC) for RNA sequencing. The outcome analyzing (Jiao et al., 2021), raw data from RNA sequencing was the "Reads Per Kilobase of transcript, per Million mapped reads" (RPKM) calculated for each gene.

Statistical Methods

All experiments were repeated at least 3 times per each selected age of the strain. The raw quantitative (Western blot and RT-qPCR) results of each gene were then analyzed based on comparing the two variances of time point and strain in ANOVA. The analysis and figure preparations were carried out using ANOVA multiple comparisons testing in Prism GraphPad V7.05 and the $p \leq 0.05$ was considered significant.

RESULTS

Excessive Purkinje Cell Migration and Bergmann Glial Cell Positioning in the *nax* Cerebellar Cortex

To demonstrate the close relationship of PCs and BGCs during postnatal PCs migration, we used the *nax* cerebellum, which features excessive PC migration in the molecular layer. Multilayered PCs in the molecular layer of the *nax* cerebellum at P17, immunostained with anti-calbindin (Calb1) indicate an impairment of PC cluster dispersal to form monolayer during early postnatal development (**Figures 1A,B**; Bailey et al., 2014). To visualize the arrangement of PCs and BGCs, the cerebellar cortex was immunostained by anti-Calb1 and S100B, respectively, at P2, corresponding to the PC cluster stage, and P7, when PCs are dispersed and organized as a monolayer. In the mouse cerebellum, Calb1 is a specific marker of PCs (e.g., Baimbridge and Miller, 1982; Shabanipour et al., 2019), while S100B was used as a marker of both mature BGCs and their precursors (Raponi et al., 2007; Koirala and Corfas, 2010). At P2, a double immunofluorescence staining with anti- Calb1 and anti- S100B in both the *wt* (**Figure 2A**) and *nax* (**Figure 2B**) cerebellum shows that PCs form a multicellular cluster. The S100B immunopositive BGC somata (**Figures 2A,a,2B,b**; arrow) at this point colocalize with PC bodies, while their fibers extend toward pial surface in both the *wt* (**Figures 2A,a**; arrowhead) and *nax* (**Figures 2B,b**; arrowhead) cerebellum. At P7, in the *wt* cerebellum, PCs are found in the PC layer and are accompanied by BGC somata with their fiber extending into the EGZ (**Figures 2C,c**; higher magnification in the inset). In contrast, in the *nax* cerebellum, PCs are arranged in a

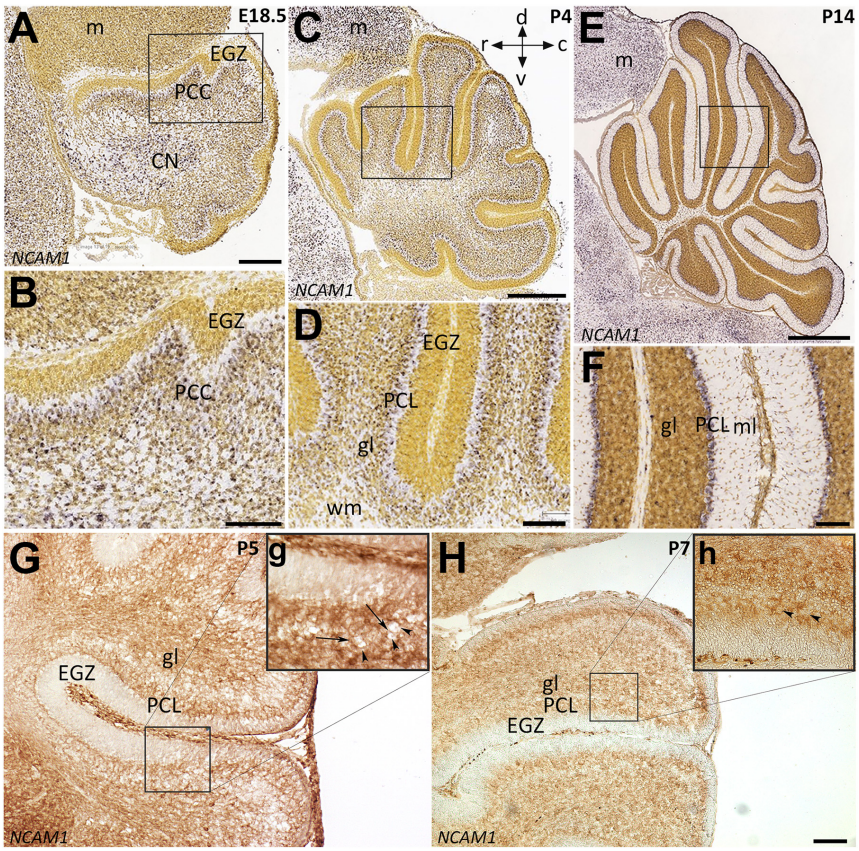

FIGURE 3 | Distribution of NCAM1 in sagittal sections hybridized *in situ* with antisense riboprobes specific for NCAM1 and immunoperoxidase staining in the cerebellum during development. Positive territories are labeled black. **(A–D)** NCAM1 expression at E18.5 and P4 is localized generally in whole cerebellum mostly in PC cluster and CN, except in EGZ and VZ (E18.5; **A** and P4; **C**, and higher magnification in **B,D**). **(E,F)** At P14, NCAM1 expression is localized in PC layer and clearly in PC soma (**E**, and higher magnification in **F**). Image credit: Allen Institute. © 2008 Allen Institute for Brain Science. Allen Developing Mouse Brain Atlas. Available online at: https://developingmouse.brain-map.org/. **(G,H)** Sagittal sections of P5 and P7 *wt* mouse cerebella immunostained with NCAM1 show the expression of NCAM1 is distributed in the granular layer and in PC layer, but not in EGZ, higher magnification provided in **(g,h)**. CN, cerebellar nuclei; EGZ, external germinal zone; gl, granular layer; m, mesencephalon; ml, molecular layer, NTZ, nuclear transitory zone; PCL, Purkinje cell layer; PCP, Purkinje cell plate; RL, upper rhombic lip; VZ, ventricular zone; WM, white matter. Scale Bars = *A* = 198 μm (applies to panels **A–F**); *H* = 100 μm (applies to panels **G,H**).

multilayer that invades the molecular layer, and fail to align in a monolayer (**Figures 2D,d**; higher magnification in the inset). Despite the impairment in migration and positioning, PC somata are still intermingling with BGC (**Figures 2D,d**; arrow). The colocalization of PCs and BGC even when PCs become ectopic (i.e., excessive migration to the molecular layer in *nax* cerebellum) may suggest the existence of cell-cell interactions during migration.

Neural Cell Adhesion Molecule 1 Expression Pattern in the Cerebellar Cortex

Neural cell adhesion molecule 1 is a member of the IgCAM (immunoglobulin cell adhesion molecule) superfamily broadly expressed in the neuroglia network not only during embryonic development but also in adults (Reyes et al., 1991; Huang et al., 2006; Magdaleno et al., 2006). To determine the distribution of the *NCAM1* in the cerebellum during PCs monolayer formation, we used *in situ* hybridization data from "Allen Developing Mouse Brain Atlas" [Image credit: Allen Institute.] and, in parallel, performed immunoperoxidase staining in cerebellar sections. The *Ncam1* expression pattern in sagittal sections during cerebellar development showed dynamic expression from E18 to P14. At E18 and P4, *Ncam1* is expressed in the PCs cluster region with low abundance in the EGZ (**Figures 3A–D**). At P14, NCAM1 expression is clearly localized in the PC layer, with scattered immunoreactivity in the granular layer (**Figures 3E,F**). Immunoperoxidase staining at P5 and P7 shows a similar pattern, as revealed by *in situ* hybridization, as well as localization in the PC layer (**Figures 3G,g,H,h**).

To examine whether NCAM1 colocalizes with PCs, cerebellar sections were double-stained using anti-NCAM1 and anti-Calb1. At P2, *NCAM1* expression is localized in the PCs cluster region of *wt* (**Figures 4A,a**; arrowhead) and *nax* cerebellum (**Figures 4B,b**; white arrowhead) highlighting the intercellular spaces. Similarly, at P7, *NCAM1* is expressed in the PC layer

in the *wt* (**Figures 4C,c**) while in the *nax* cerebellum it is found in the area where the multilayered PCs are located, including the molecular layer (**Figures 4D,d**; arrow). NCAM1 immunoreactivity is also strong in the leptomeninges of the *nax* cerebellum (**Figure 4D**).

Neural Cell Adhesion Molecule 1 Expression Patterns Are Altered in the Purkinje Cells and Bergmann Glial Cells of *nax* Cerebellum

To examine the NCAM1 protein expression pattern during postnatal cerebellar development, Western blotting was carried out using anti-NCAM1 antibody on *wt* and *nax* cerebella at P2 and P7 (**Figure 5A**). NCAM1 expression did not change by age between P2 and P7 in either the *nax* or *wt* mice cerebellum. Moreover, the expression levels of *NCAM1* were not significantly different between *nax* and *wt* littermate cerebella at P2 and P7 (**Figure 5B** and **Supplementary Figure 1**). In order to elucidate the correlation between NCAM1 protein and mRNA data, total *Ncam1* RNA of cerebellum was analyzed with RT-qPCR as well (**Figure 5C**) and the results were compared to the collected NCAM1 data. Although the total mRNA results did not reach statistical significance, their levels also showed a downward trend at P2 to P7. RNA-seq data was shown no significant differences in the expression of Ncam1 between wt and nax littermates (**Figure 5D**).

To better characterize *Ncam1* mRNA levels in isolated PCs and BGCs, we used FACS. To this end, PCs and BGCs were isolated from the cerebellum at P2 and P7, both in *nax* and *wt* littermates (**Supplementary Figure 2**), and RNA was extracted for RT-qPCR analysis. Results showed that *Ncam1* mRNA levels in both PCs (**Figure 5E**) and BGCs (**Figure 5F**) are substantially enhanced in the *nax* cerebellum as compared to the *wt* cerebellum ($^{*}p < 0.05$, $^{**}p < 0.01$, $^{***}p < 0.001$), a difference that was not revealed by the analysis of total lysates. The observed increase of *Ncam1* levels in *nax* PCs and BGCs may underlie their excessive migration toward the pial surface and failure of proper alignment into a mature PC layer.

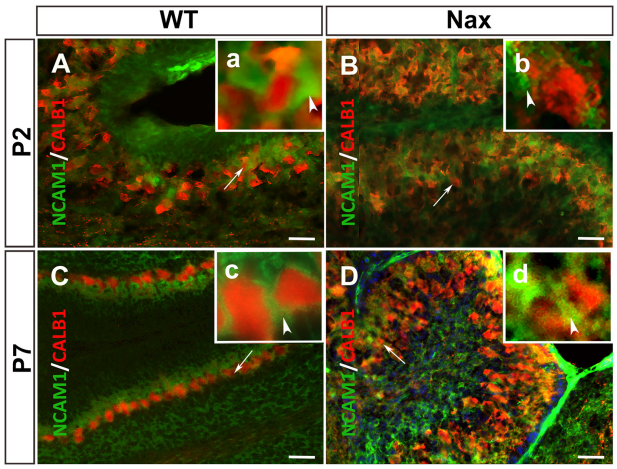

FIGURE 4 | PCs and the expression of NCAM1 in *wt* and *nax* cerebellar cortex. **(A,B)** Sagittal sections through the cerebellum immunostained with anti- calbindin (red) and anti-NCAM1 (green) shows the colocalization of PCs (red arrowhead in higher magnification **a**) and NCAM1 (arrowhead in higher magnification **b**) at P2 in both *wt* **(A)** and *nax* **(B)** cerebellum. **(C,D)** Images at P7 similarly shows the intercellular expression of NCAM1 not only in PC layer of *wt* **(C)** cerebellum but also in *nax* **(D)** cerebellum where the multilayer PCs are invaded into the molecular layer; **(c,d)** Higher magnification of the local NCAM1 expression. PCs, Purkinje cells. Scale bars: $A = 50\ \mu m$ (applies to panels **A–D**).

DISCUSSION

The PC layer consists of a single row of PC somata, which are intermingled with BGC bodies. PCs complete their final mitotic division at E10–13 in mice (Miale and Sidman, 1961; Marzban et al., 2014). At the post-mitotic stage, PCs start migrating a short distance from their site of origin in the ventricular zone and accumulate in the PC plate. Then, clustered PCs initiate their dispersal at around P2 to establish the PC monolayer by P7 (Rahimi-Balaei et al., 2018). Several studies have shown the interdependency of PCs and BGCs for their origins during embryonic development, and continued differentiation until postnatal days has been reported (Fisher, 1984; Bellamy, 2006). During prenatal cerebellar development, the migration of PCs is suggested to be guided by radial glial fibres and the interaction between these two cell types is mediated by cell adhesion molecules, including NCAM1 (Yuasa et al., 1991; Sergaki and Ibanez, 2017).

In the present study, we describe the effects of the *Acp2* gene mutation in the *nax* cerebellum, in which PCs with excessive migration invade the molecular layer (Bailey et al., 2014; Rahimi Balaei et al., 2016). Immunostaining shows that PC somata and BGCs bodies are attached together; in the normal cerebellum (coupled in the PC layer), and in the *nax* cerebellum (in the molecular layer, which is invaded by PCs due to excessive migration). In addition, NCAM1 expression shows adhesion between PCs and BGC in the *wt* PC layer and in *nax* cerebellum's molecular layer.

The protein and mRNA analysis of NCAM1 in total cerebellum from both *nax* and *wt* mice does not show a significant difference between *strains* and ages (P2 and P7). In contrast, RT-PCR results from sorted cells show that NCAM1 expression in both PCs and BGCs of the *nax* cerebellum is significantly higher than *wt* littermate cerebellum. Comparing the RT-qPCR results from total tissue to the sorted cells counterpart may suggest the following:

1. The majority of NCAM1 expression in *wt* cerebellum takes place in cells other than PCs and BGCs. This may reflect the high requirement of many cells for this adhesion molecule during cerebella development and PC dispersal.
2. The *wt* PCs and BGCs normally have low NCAM1 expression levels. *In situ* hybridization results reveal that *Ncam1* mRNA is detected in *wt* PCs not only at embryonic stages (E18) but also around PC layer formation and even weeks after PCs migration has completed (P14). Moreover,

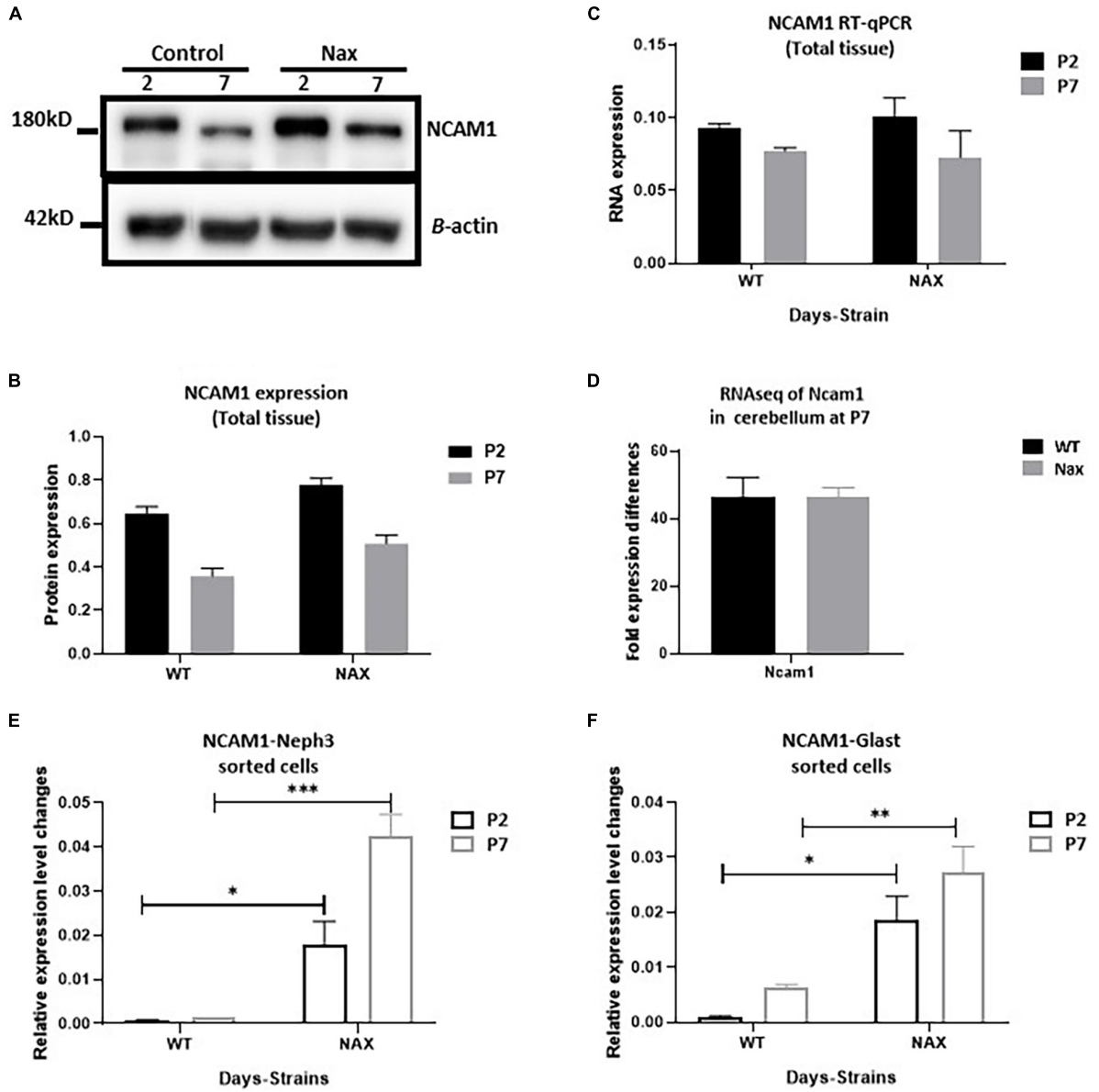

FIGURE 5 | Transcription of NCAM1 in *nax* PCs and BGCs significantly increases. **(A–C)** NCAM1 expression and transcription in the whole cerebellum tissue is measured by Western blot **(A,B)** and RT-qPCR **(C)** at P2 and P7. The NCAM1 protein and mRNA values does not show significant difference between *wt* and *nax* cerebellum (blot image of P2, P5, and P7 in **Supplementary Figure 1**). **(D)** RNAseq analysis of *nax* and wt cerebellum at P5/P7 to confirm total cerebellum RT-qPCR results; Ncam1 transcription shows the same value in both *nax* and *wt* cerebellum. **(E,F)** RT-qPCR of RNA collected from isolated PCs and BGCs from *nax* and *wt* cerebellum at P2 and P7. The mRNA value of NCAM1 in *nax* cerebellum from both P2 and P7 is significantly higher than the *wt* littermate. This experiment was repeated over three different litters for each postnatal day in *nax* and *wt* littermate (*wt*; $n = 3$ and *nax*; $n = 3$). The data in the bar graph are presented as the mean ± SEM, and statistical analysis was performed using multiple comparison ANOVA (*$p < 0.05$, **$p < 0.01$, ***$p < 0.001$). PCs, Purkinje cells; BGCs, Bergman glia cells. Scale bars: $A = 50$ μm (applies to panels **A–D**).

mRNA analysis of sorted cells shows low expression of NCAM1 in PCs and BGCs of *wt* cerebellum. It is well established that the cell–matrix or cell–cell adhesions can be modulated through a change in NCAM1 expression (Gorain et al., 2019). If there is any NCAM1 mediated interaction to be established between PCs and BGCs/ECM and start a new wave of migration, low expression of NCAM1 at P2 is reasonable. Maintaining the low expression of NCAM1 in PCs might be the proper way to tune the cell migration until PCs are settled in the PC layer. In *wt* BGCs, however, NCAM1 transcription increases at P7. It is believed that this increase, would accelerate the NCAM1 interactions with ECM components such as integrin and prevent further movement of PCs from PC layer. In line with these results, several *in vitro* and *in vivo* studies have suggested that NCAM1 expression inhibits the

migration of glioma cells (Edvardsen et al., 1994; Gratsa et al., 1997).

It is also well known that the ECM of the cerebellar cortex is enriched with laminin and collagen regions (Sur et al., 2014). The interaction of NCAM and Integrin β-1 with laminin might increase cell motility (Miyamoto et al., 1995; Tulla et al., 2008). In our studies, the RT-qPCR analysis of NCAM1 in *nax* cerebellum suggests that the post-mutation upregulation of NCAM1 expression in BGCs may trigger the NCAM1-integrin interaction and promote the migration of BGCs toward the pial surface. Our RNAseq data shows a significant increase in mRNA expression of Itgα3 and Itgα5 in the whole *nax* cerebellum at P5/P7 compared to the *wt* littermate (**Supplementary Figure 3**). Increasing the expression of integrins at P5/P7 may promote cells migration for *nax* PCs. Unlike integrins, increasing the NCAM1 mRNA level in *nax* PCs compared to *wt* might be an unsuccessful attempt to compensate for PCs failing to stop at the PC layer. This raises the possibility that changing ECM components at P7 in the *nax* cerebellar cortex is the main reason of initiating NCAM1 compensatory mechanism and PCs excessive migration. Other studies showed that removing PSA from NCAM1 in PCs can adversely affect their migration (Sergaki and Ibanez, 2017). It is possible that both *nax* PCs and BGCs respond to removing PSA from NCAM1 by upregulating NCAM1 expression in these cells. Our study shows that the connection of PCs and BGCs during postnatal migration in cerebellum needs to be further investigated.

Currently, it is believed that the position of PC cluster changes along with cerebellar surface development, which is extended rostrocaudally and mediolaterally and arranged in a monolayer because of cerebellar expansion (Butts et al., 2014). It is also suggested that granule cells are major players in the migration and positioning of PCs postnatally (Jensen et al., 2002). However, several reports have shown that despite granule cells defects (such as hypoplasia and agenesis), PCs respond differently to these anomalies. In most cases, each affected cerebellum comprises several small percentages of PCs population, which are either in different ectopic locations or arranged in monolayer positions in cerebellar cortex. For example, three populations of ectopic PCs were described in a study of the Atoh1 null-mutant mouse, in which the external granular layer does not form (Jensen et al., 2002). In addition, the scrambler (mutation in Dab1, Reelin adaptor protein) cerebellum is small because the size of the granule cell population is severely decreased by ∼80% and around 95% of PCs (not all) fail to complete their migration (Goldowitz et al., 1997; Reeber et al., 2013). Furthermore, Cxcr4 (a chemokine receptor) deficiency results in fewer granule cells in the cerebellum and partially disorganized ectopic PCs (Huang et al., 2014), which is almost similar to the phenotype described in Weaver mouse (Chen et al., 2009). It has been suggested that protein tyrosine phosphatase, non-receptor type 11 (Ptpn11) regulates formation of the laminar cerebellar cortex by controlling granule cell migration via mediating Cxcl12/Cxcr4 signaling (Hagihara et al., 2009). However, removing Ptpn11 in the external granular layer has no distinct effect on cerebellar corticogenesis (Li et al., 2014). Despite the important role of granule cells, they are not the main player in PCs migration and organization during cerebellar postnatal development. Therefore, such an elaborate PC monolayer organization cannot be explained by surface expansion and granule cells development alone, and this strongly indicates a phenomenon that is precisely regulated by an active cellular and molecular process rather than by passive expansion. Our study suggests that PCs move under molecular changes and regulations assisted BGCs to establish elaborated PC monolayer organization. In particular, our results indicate that NCAM1 in PCs and BGCs may function as a cell movement tuning mechanism that is required at early postnatal days of PCs migration. Finally, our results may also suggest that other molecules such as integrins (Itgα3 and Itgα5) in the ECM, may contribute to NCAM1 upregulation in *nax* PCs and BGCs and promote excessive PCs migration at P7.

CONCLUSION

In this study, we describe the spatiotemporal distribution of NCAM1 in PCs and BGCs during early postnatal development. We showed that the relationship between PCs and BGCs is greatly affected by gene mutation (*ACP2−/−*) and time. The close relationship between PCs and BGCs causes these two cell types to stay tightly coupled during their postnatal migration. In the *nax* cerebellum, changes in BGC position toward molecular layer are accompanied by excessive PCs migration. NCAM1 expression pattern in the *nax* cerebellum fits the criteria for excessive coupled migration of PCs and BGCs. NCAM1 overexpression in PCs and BGCs may increase the cell-ECM connections and drag the cells to an ectopic location toward pial surface and suggest that NCAM1 is an essential regulator during PCs dispersal and monolayer formation.

DATA AVAILABILITY STATEMENT

The original contributions presented in the study are included in the article/**Supplementary Material**, further inquiries can be directed to the corresponding author/s.

ETHICS STATEMENT

The animal study was reviewed and approved by the study was conducted according to the guidelines of the institutional regulations and the Guide to the Care and Use of Experimental Animals from the Canadian Council on Animal Care, and approved by local authorities "the Bannatyne Campus Animal Care Committee," University of Manitoba (approved protocol # 15066; 2017).

AUTHOR CONTRIBUTIONS

HM designed the research and experiments, supervised the research, and wrote the manuscript. SS, XJ, MR-B, MA, SC, SG, GC, and HM analyzed the data and co-wrote the manuscript. SS, XJ, MR-B, and MA performed the

experiments. All authors have read and agreed to the published version of the manuscript.

FUNDING

This study was supported by grants from the Natural Sciences and Engineering Research Council (HM: NSERC Discovery Grant # RGPIN-2018-06040), The Children's Hospital Research Institute of Manitoba (HM: CHRIM Grant # 320035), and Research Manitoba Tri-Council Bridge Funding Program (HM: Grant # 47955).

ACKNOWLEDGMENTS

We would like to thank Marc Del Bigio for his valuable comments and suggestions during this project.

SUPPLEMENTARY MATERIAL

The Supplementary Material for this article can be found online at: https://www.frontiersin.org/articles/10.3389/fnins.2021.804402/full#supplementary-material

Supplementary Figure 1 | Expression of NCAM1 at P2, P5, and P7 in both *wt* and *nax* cerebellum by using Western blot; NCAM expression in *wt* and *nax* cerebellum is downregulated at P5 and P7.

Supplementary Figure 2 | (A–D) FACS analysis of NEPH3 positive (Purkinje cells) and GLAST1 positive (Bergmann glia cells) from *nax* and *wt* mice cerebellum at the age of P2 **(A,B)** and P7 **(C,D)**. **(E)** We used cells incubated with secondary antibodies and DAPI only to set up the cut off levels for accurate sorting of the cells. The very low percentage of the cells were double positive (DP) which were excluded from mRNA extraction and the rest are double negative cells which are most of the cerebellar cells in both strains.

Supplementary Figure 3 | The RNAseq data sets from the cerebellum at P5/P7 shows significant difference in expression of *Itgα3* and *Itgα5* between *nax* and *wt* littermate (**$p < 0.01$, ***$p < 0.001$).

REFERENCES

Bailey, K., Rahimi Balaei, M., Mannan, A., Del Bigio, M. R., and Marzban, H. (2014). Purkinje cell compartmentation in the cerebellum of the lysosomal acid phosphatase 2 mutant mouse (nax - naked-ataxia mutant mouse). *PLoS One* 9:e94327. doi: 10.1371/journal.pone.0094327

Baimbridge, K. G., and Miller, J. J. (1982). Immunohistochemical localization of calcium-binding protein in the cerebellum, hippocampal formation and olfactory bulb of the rat. *Brain Res.* 245, 223–229. doi: 10.1016/0006-8993(82)90804-6

Bellamy, T. C. (2006). Interactions between Purkinje neurones and Bergmann glia. *Cerebellum* 5, 116–126. doi: 10.1080/14734220600724569

Butts, T., Green, M. J., and Wingate, R. J. (2014). Development of the cerebellum: simple steps to make a 'little brain'. *Development* 141, 4031–4041. doi: 10.1242/dev.106559

Chen, K. A., Lanuto, D., Zheng, T., and Steindler, D. A. (2009). Transplantation of embryonic and adult neural stem cells in the granuloprival cerebellum of the weaver mutant mouse. *Stem Cells* 27, 1625–1634. doi: 10.1002/stem.83

Das, G. D. (1976). Differentiation of Bergmann glia cells in the cerebellum: a golgi study. *Brain Res.* 110, 199–213. doi: 10.1016/0006-8993(76)90397-8

Edvardsen, K., Pedersen, P. H., Bjerkvig, R., Hermann, G. G., Zeuthen, J., Laerum, O. D., et al. (1994). Transfection of glioma cells with the neural-cell adhesion molecule NCAM: effect on glioma-cell invasion and growth in vivo. *Int. J. Cancer* 58, 116–122. doi: 10.1002/ijc.2910580119

Elias, L. A., Wang, D. D., and Kriegstein, A. R. (2007). Gap junction adhesion is necessary for radial migration in the neocortex. *Nature* 448, 901–907. doi: 10.1038/nature06063

Englund, C., Kowalczyk, T., Daza, R. A., Dagan, A., Lau, C., Rose, M. F., et al. (2006). Unipolar brush cells of the cerebellum are produced in the rhombic lip and migrate through developing white matter. *J. Neurosci.* 26, 9184–9195. doi: 10.1523/JNEUROSCI.1610-06.2006

Famulski, J. K., Trivedi, N., Howell, D., Yang, Y., Tong, Y., Gilbertson, R., et al. (2010). Siah regulation of Pard3A controls neuronal cell adhesion during germinal zone exit. *Science* 330, 1834–1838. doi: 10.1126/science.1198480

Fink, A. J., Englund, C., Daza, R. A., Pham, D., Lau, C., Nivison, M., et al. (2006). Development of the deep cerebellar nuclei: transcription factors and cell migration from the rhombic lip. *J. Neurosci.* 26, 3066–3076. doi: 10.1523/JNEUROSCI.5203-05.2006

Fisher, M. (1984). Neuronal influence on glial enzyme expression: evidence from mutant mouse cerebella. *Proc. Natl. Acad. Sci. U.S.A.* 81, 4414–4418. doi: 10.1073/pnas.81.14.4414

Goldowitz, D., Cushing, R. C., Laywell, E., D'Arcangelo, G., Sheldon, M., Sweet, H. O., et al. (1997). Cerebellar disorganization characteristic of reeler in scrambler mutant mice despite presence of reelin. *J. Neurosci.* 17, 8767–8777. doi: 10.1523/JNEUROSCI.17-22-08767.1997

Gorain, B., Bhattamishra, S. K., Choudhury, H., Nandi, U., Pandey, M., and Kesharwani, P. (2019). "Chapter 3–Overexpressed receptors and proteins in lung cancer," in *Nanotechnology-Based Targeted Drug Delivery Systems for Lung Cancer*, ed. P. Kesharwani (Cambridge, MA: Academic Press), 39–75. doi: 10.1016/b978-0-12-815720-6.00003-4

Gratsa, A., Rooprai, H. K., Rogers, J. P., Martin, K. K., and Pilkington, G. J. (1997). Correlation of expression of NCAM and GD3 ganglioside to motile behaviour in neoplastic glia. *Anticancer Res.* 17, 4111–4117.

Hagihara, K., Zhang, E. E., Ke, Y. H., Liu, G., Liu, J. J., Rao, Y., et al. (2009). Shp2 acts downstream of SDF-1alpha/CXCR4 in guiding granule cell migration during cerebellar development. *Dev. Biol.* 334, 276–284. doi: 10.1016/j.ydbio.2009.07.029

Higuera, G. A., Iaffaldano, G., Bedar, M., Shpak, G., Broersen, R., Munshi, S. T., et al. (2017). An expandable embryonic stem cell-derived Purkinje neuron progenitor population that exhibits in vivo maturation in the adult mouse cerebellum. *Sci. Rep.* 7:8863. doi: 10.1038/s41598-017-09348-1

Huang, G. J., Edwards, A., Tsai, C. Y., Lee, Y. S., Peng, L., Era, T., et al. (2014). Ectopic cerebellar cell migration causes maldevelopment of Purkinje cells and abnormal motor behaviour in Cxcr4 null mice. *PLoS One* 9:e86471. doi: 10.1371/journal.pone.0086471

Huang, J., Sakai, R., and Furuichi, T. (2006). The docking protein Cas links tyrosine phosphorylation signaling to elongation of cerebellar granule cell axons. *Mol. Biol. Cell* 17, 3187–3196. doi: 10.1091/mbc.e05-12-1122

Jensen, P., Zoghbi, H. Y., and Goldowitz, D. (2002). Dissection of the cellular and molecular events that position cerebellar Purkinje cells: a study of the math1 null-mutant mouse. *J. Neurosci.* 22, 8110–8116. doi: 10.1523/JNEUROSCI.22-18-08110.2002

Jiao, X., Rahimi Balaei, M., Abu-El-Rub, E., Casoni, F., Pezeshgi Modarres, H., Dhingra, S., et al. (2021). Reduced granule cell proliferation and molecular dysregulation in the cerebellum of lysosomal acid phosphatase 2 (ACP2) mutant mice. *Int. J. Mol. Sci.* 22:2994. doi: 10.3390/ijms22062994

Kearns, S. M., Laywell, E. D., Kukekov, V. K., and Steindler, D. A. (2003). Extracellular matrix effects on neurosphere cell motility. *Exp. Neurol.* 182, 240–244. doi: 10.1016/s0014-4886(03)00124-9

Koirala, S., and Corfas, G. (2010). Identification of novel glial genes by single-cell transcriptional profiling of Bergmann glial cells from mouse cerebellum. *PLoS One* 5:e9198. doi: 10.1371/journal.pone.0009198

Li, K., Leung, A. W., Guo, Q., Yang, W., and Li, J. Y. (2014). Shp2-dependent ERK signaling is essential for induction of Bergmann glia and foliation of the cerebellum. *J. Neurosci.* 34, 922–931. doi: 10.1523/JNEUROSCI.3476-13.2014

Maar, T. E., Lund, T. M., Gegelashvili, G., Hartmann-Petersen, R., Moran, J., Pasantes-Morales, H., et al. (1998). Effects of taurine depletion on cell migration and NCAM expression in cultures of dissociated mouse cerebellum and N2A cells. *Amino Acids* 15, 77–88. doi: 10.1007/BF01345281

Magdaleno, S., Jensen, P., Brumwell, C. L., Seal, A., Lehman, K., Asbury, A., et al. (2006). BGEM: an in situ hybridization database of gene expression in the embryonic and adult mouse nervous system. *PLoS Biol.* 4:e86. doi: 10.1371/journal.pbio.0040086

Marzban, H., Del Bigio, M. R., Alizadeh, J., Ghavami, S., Zachariah, R. M., and Rastegar, M. (2014). Cellular commitment in the developing cerebellum. *Front. Cell. Neurosci.* 8:450. doi: 10.3389/fncel.2014.00450

Mendis, D. B., Shahin, S., Gurd, J. W., and Brown, I. R. (1994). Developmental expression in the rat cerebellum of SC1, a putative brain extracellular matrix glycoprotein related to SPARC. *Brain Res.* 633, 197–205. doi: 10.1016/0006-8993(94)91540-7

Miale, I. L., and Sidman, R. L. (1961). An autoradiographic analysis of histogenesis in the mouse cerebellum. *Exp. Neurol.* 4, 277–296. doi: 10.1016/0014-4886(61)90055-3

Miyamoto, S., Akiyama, S. K., and Yamada, K. M. (1995). Synergistic roles for receptor occupancy and aggregation in integrin transmembrane function. *Science* 267, 883–885. doi: 10.1126/science.7846531

Rahimi Balaei, M., Jiao, X., Ashtari, N., Afsharinezhad, P., Ghavami, S., and Marzban, H. (2016). Cerebellar expression of the neurotrophin receptor p75 in naked-ataxia mutant mouse. *Int. J. Mol. Sci.* 17:115. doi: 10.3390/ijms17010115

Rahimi-Balaei, M., Bergen, H., Kong, J., and Marzban, H. (2018). Neuronal migration during development of the cerebellum. *Front. Cell. Neurosci.* 12:484. doi: 10.3389/fncel.2018.00484

Rakic, P., and Komuro, H. (1995). The role of receptor/channel activity in neuronal cell migration. *J. Neurobiol.* 26, 299–315.

Raponi, E., Agenes, F., Delphin, C., Assard, N., Baudier, J., Legraverend, C., et al. (2007). S100B expression defines a state in which GFAP-expressing cells lose their neural stem cell potential and acquire a more mature developmental stage. *Glia* 55, 165–177. doi: 10.1002/glia.20445

Reeber, S. L., Loeschel, C. A., Franklin, A., and Sillitoe, R. V. (2013). Establishment of topographic circuit zones in the cerebellum of scrambler mutant mice. *Front. Neural Circuits* 7:122. doi: 10.3389/fncir.2013.00122

Reyes, A. A., Small, S. J., and Akeson, R. (1991). At least 27 alternatively spliced forms of the neural cell adhesion molecule mRNA are expressed during rat heart development. *Mol. Cell Biol.* 11, 1654–1661. doi: 10.1128/mcb.11.3.1654-1661.1991

Schilling, K. (2018). Moving into shape: cell migration during the development and histogenesis of the cerebellum. *Histochem. Cell Biol.* 150, 13–36. doi: 10.1007/s00418-018-1677-6

Schmid, R. S., and Maness, P. F. (2008). L1 and NCAM adhesion molecules as signaling coreceptors in neuronal migration and process outgrowth. *Curr. Opin. Neurobiol.* 18, 245–250. doi: 10.1016/j.conb.2008.07.015

Sergaki, M. C., and Ibanez, C. F. (2017). GFRalpha1 regulates Purkinje cell migration by counteracting NCAM function. *Cell Rep.* 18, 367–379. doi: 10.1016/j.celrep.2016.12.039

Shabanipour, S., Dalvand, A., Jiao, X., Rahimi Balaei, M., Chung, S. H., Kong, J., et al. (2019). Primary culture of neurons isolated from embryonic mouse cerebellum. *J. Vis. Exp.* 152:e60168. doi: 10.3791/60168

Stoeckli, E. T. (2010). Neural circuit formation in the cerebellum is controlled by cell adhesion molecules of the contactin family. *Cell Adh. Migr.* 4, 523–526. doi: 10.4161/cam.4.4.12733

Sur, S., Guler, M. O., Webber, M. J., Pashuck, E. T., Ito, M., Stupp, S. I., et al. (2014). Synergistic regulation of cerebellar Purkinje neuron development by laminin epitopes and collagen on an artificial hybrid matrix construct. *Biomater. Sci.* 2, 903–914. doi: 10.1039/C3BM60228A

Tulla, M., Lahti, M., Puranen, J. S., Brandt, A. M., Kapyla, J., Domogatskaya, A., et al. (2008). Effects of conformational activation of integrin alpha 1I and alpha 2I domains on selective recognition of laminin and collagen subtypes. *Exp. Cell Res.* 314, 1734–1743. doi: 10.1016/j.yexcr.2008.01.025

Voogd, J. (1992). The morphology of the cerebellum the last 25 years. *Eur. J. Morphol.* 30, 81–96.

Wang, V. Y., and Zoghbi, H. Y. (2001). Genetic regulation of cerebellar development. *Nat. Rev. Neurosci.* 2, 484–491. doi: 10.1038/35081558

Yuasa, S., Kawamura, K., Ono, K., Yamakuni, T., and Takahashi, Y. (1991). Development and migration of Purkinje cells in the mouse cerebellar primordium. *Anat. Embryol.* 184, 195–212. doi: 10.1007/BF01673256

Conflict of Interest: The authors declare that the research was conducted in the absence of any commercial or financial relationships that could be construed as a potential conflict of interest.

Publisher's Note: All claims expressed in this article are solely those of the authors and do not necessarily represent those of their affiliated organizations, or those of the publisher, the editors and the reviewers. Any product that may be evaluated in this article, or claim that may be made by its manufacturer, is not guaranteed or endorsed by the publisher.

frontiers in Neuroscience

ORIGINAL RESEARCH
published: 31 January 2022
doi: 10.3389/fnins.2021.709374

Identification and Characterization of Influential Factors in Susceptibility to Attention Deficit Hyperactivity Disorder Among Preschool-Aged Children

Xiangling Deng[1,2], Min Yang[1,2], Shunan Wang[1,2], Bo Zhou[1,2], Kundi Wang[2], Zhixin Zhang[3,4]* and Wenquan Niu[3,4]**

[1] Graduate School, Beijing University of Chinese Medicine, Beijing, China, [2] Department of Pediatrics, China-Japan Friendship Hospital, Beijing, China, [3] International Medical Services, China-Japan Friendship Hospital, Beijing, China, [4] China-Japan Friendship Hospital, Institute of Clinical Medical Sciences, Beijing, China

OPEN ACCESS

Edited by:
Shigeyoshi Saito, Osaka University, Japan

Reviewed by:
Kazuhiko Sawada, Tsukuba International University, Japan
Ishanu Chattopadhyay, University of Chicago, United States

***Correspondence:**
Kundi Wang
kundi523@163.com
Zhixin Zhang
zhangzhixin032@163.com
Wenquan Niu
niuwenquan_shcn@163.com

Specialty section:
This article was submitted to Neurodevelopment, a section of the journal Frontiers in Neuroscience

Received: *13 May 2021*
Accepted: *23 December 2021*
Published: *31 January 2022*

Citation:
Deng X, Yang M, Wang S, Zhou B, Wang K, Zhang Z and Niu W (2022) Identification and Characterization of Influential Factors in Susceptibility to Attention Deficit Hyperactivity Disorder Among Preschool-Aged Children. Front. Neurosci. 15:709374. doi: 10.3389/fnins.2021.709374

Attention deficit hyperactivity disorder (ADHD) is the most common childhood-onset neurodevelopmental disorder. Currently, increasing amounts of attention have been focused on the epidemiologic profiling of ADHD in children, viewed as a continuously distributed risk dimension throughout the whole lifespan. This study aimed to identify and characterize potential influential factors susceptible to ADHD-related symptoms among preschool-aged children. A comprehensive questionnaire was self-designed for both children and their parents or guardians and was distributed to 30 kindergartens from Beijing and Hebei, collecting potential influential factors in susceptibility to ADHD. ADHD was assessed by the Conner's Abbreviated Symptom Questionnaire (C-ASQ), and 7,938 children were analyzed. Least absolute shrinkage and selection operator (LASSO) regression and hierarchical degree of adjustment were used to control possible covariates. Five factors, namely, children's secondhand smoking exposure, breastfeeding duration, sleep mode, maternal pregnancy smoking exposure, and parental self-rating for patience, were identified to be independently and significantly associated with ADHD susceptibility. Meanwhile, dose–response relationships were observed between breastfeeding duration, parental self-rating for patience, and ADHD-related symptoms. Finally, a nomogram model was created for predicting ADHD susceptibility based on significant and conventional attributes under each criterion.

Keywords: preschool-aged children, ADHD related symptoms, risk factor, C-ASQ, nomogram model

INTRODUCTION

Attention deficit hyperactivity disorder (ADHD) is the most common childhood-onset neurodevelopmental disorder, and it is characterized by developmentally inappropriate levels of overactivity, inattention, and impulsivity (Thapar and Cooper, 2016). Currently, increasing amounts of attention have been focused on the epidemiologic profiling of ADHD in children, viewed as a continuously distributed risk dimension throughout the whole lifespan, with pooled

prevalence rates ranging from 2.73 to 4.27% in children younger than 7 years (Vasileva et al., 2020) and at 3.40% in children and adolescents (Polanczyk et al., 2015).

Longitudinal data have shown that early onset ADHD is consistently associated with emotional problems throughout childhood (Stern et al., 2020), and it exerts a significant impact on functioning during adulthood (Harstad et al., 2020). Cohort studies revealed hyperactive, impulsive, and inattention symptoms as risk factors for adult intimate partner violence (Buitelaar et al., 2020). In addition, suicidality (Garas and Balazs, 2020), automobile crashes, traffic fatalities (Aduen et al., 2018), and even conviction and incarceration (Mohr-Jensen et al., 2019) have been reported to be significantly associated with ADHD symptoms. Meanwhile, ADHD places a major burden on health and healthcare costs. National annual healthcare costs in the United States ranged from $143 billion to $266 billion a decade ago (Doshi et al., 2012). Due to these severe circumstances, the concept of ADHD has been developed and refined in response to its clinical nature and structure over the past several decades. Nonetheless, many children and youth diagnosed with ADHD still receive no treatment or insufficient treatment (Manos et al., 2017), especially in low-income and middle-income countries (Thapar and Cooper, 2016).

The exploration of risk factors has proven to be beneficial for the development of preventive and intervention strategies to curb this global burden. It is widely recognized that ADHD is a highly heritable and multifactorial disorder to which multiple inherited and non-inherited factors contribute individually and interactively (Biederman and Faraone, 2005). Environmental profiles, including prenatal and perinatal factors, environmental toxins, dietary factors, and psychosocial factors, have been reported to be associated with ADHD risk (Thapar et al., 2013). It is of great importance to construct a prediction model by incorporating multiple established influential environmental factors for childhood ADHD symptoms.

To shed some light on this issue and yield more information for further studies, we conducted a cross-sectional investigation among preschool-aged children enrolled from 20 kindergartens in Beijing and 10 kindergartens in Tangshan city to identify promising factors that can predict the risk of childhood ADHD, and to enhance the magnitude of predicting ADHD susceptibility, and further we established a nomogram model by regressing individual attributes that were significantly associated with ADHD.

MATERIALS AND METHODS

Study Design

A population-based cross-sectional survey, in accordance with the principles of the Declaration of Helsinki, was conducted in Beijing and Tangshan city (Hebei province) between September and December 2020. This survey was reviewed and approved by the Ethics Committee of China-Japan Friendship Hospital.

Study Subjects

Preschool-aged children (3–7 years old) who attended junior to senior kindergarten classes were surveyed in this study. Utilizing a stratified cluster random sampling strategy, 5 out of 16 districts in Beijing and 1 city (Tangshan) in Hebei, a total of 30 public kindergartens were randomly selected.

Basic Characteristics

To collect potential influential factors for ADHD susceptibility, a comprehensive electronic questionnaire was designed for both children and their parents or guardians.

For the children, basic characteristics including age, sex, region, birth weight, ABO blood type, delivery mode, breastfeeding duration, daily sleep duration, daily sleep initiation time, secondhand smoke exposure, vitamin D supplement duration, probiotics supplementary, and average daily screen time were recorded. Children's body weight (to the nearest 0.1 kg) and height (to the nearest 0.1 cm) were measured by trained health physicians. The hyperactivity and inattention domains of the children were assessed using the Conner's Abbreviated Symptom Questionnaire (C-ASQ).

For the parents or guardians, sex and self-reported data, including age, weight, height, education, family income, maternal prepregnancy weight, gestational weight gain (GWG), maternal pregnancy smoking exposure, and parental self-rating for their patience with their children, which ranged from 0 to 10 scores, were recorded.

Sample Size Estimation

According to the method proposed by Riley et al. (2020), in this present study, the estimation of sample size is based on the conditions that overall proportion of children with ADHD susceptibility is 0.05, the number of candidate predictor parameters is 24, and the recommended max Cox-Snell R squared statistic (R^2_{cs}) value is 0.33. Assuming that the new model can explain 15% of the variability, the anticipated R^2_{cs} value should be 0.15×0.33, equivalent to 0.05. On the basis of the above parameters, the sample size is estimated to be 4,199, corresponding to 210 events and an events per candidate predictor parameter of 8.75.

In the present study, the aforementioned self-designed questionnaires were sent to the parents or guardians of 10,441 children, who read and signed an informed consent form prior to participation, and 98% of them (n = 10,230) returned the questionnaires within the scheduled time. After excluding 1,810 questionnaires that had no C-ASQ, 8,420 valid questionnaires were obtained within the specified time frame, the number exceeding the estimated sample size 4,199.

Quality Control

After training by medical and epidemiological researchers in advance, the kindergarten teachers were responsible for contacting parents or guardians to introduce the questionnaires in detail. All missing/uncertain records were checked by the epidemiological researchers who were responsible for this study, and the kindergarten teachers were contacted to reconfirm

the records. Data were exported from electronic questionnaires to a Microsoft Office Excel™ spreadsheet, and were cross-checked by trained staff. After excluding situations with no comprehensive information, incorrect filling and inability to be reconfirmed, mothers who suffered from prenatal and perinatal diseases, and children with a history of disease, including chronic kidney disease, hypothyroidism, congenital heart disease, chronic respiratory diseases, and inherited metabolic diseases, were also eliminated. Finally, 7,938 of the completed questionnaires were deemed eligible for analysis.

Conner's Abbreviated Symptom Questionnaire-Defined Attention Deficit Hyperactivity Disorder Susceptibility

The Conner's Abbreviated Symptom Questionnaire (C-ASQ), a global measure of psychopathology, is not a specific indicator of ADHD diagnosis (Conners, 1989), yet it has a high diagnostic ability in distinguishing children with and without ADHD (Chang et al., 2016). The information obtained from C-ASQ can facilitate the process of determining the requirements for a more comprehensive evaluation. The C-ASQ contains 10 identical items for parent and teacher rating scales, with each item being rated on a 4-point scale of frequency from never or rarely (0) to very often (3). The continuous measure of total ADHD symptoms is calculated as the sum of the score of each item. In this study, we defined children with a point >10 as the propensity of hyperactivity, called C-ASQ-defined ADHD susceptibility (Xiangdong, 1993).

Daily sleep duration was calculated as the sum of both break time during the day and sleep time at night, combining the time on working days × 5 and the corresponding time on weekends × 2 divided by 7. Daily sleep initiation time was grouped into before and after 23:00. Sleep mode was defined according to both sleep duration and daily sleep initiation time and was divided into 4 stages. Sleep mode was encoded as the number "4" if the sleep duration was less than 10 h per day and fall asleep time was after 23:00, as the number "3" if sleep duration was more than 10 h per day and the daily sleep initiation time was after 23:00, as the number "2" if sleep duration was less than 10 h and the daily sleep initiation time was before 23:00, and as the number "1" if the sleep duration was more than 10 h and the daily sleep initiation time was before 23:00. The children's average daily screen time was calculated as for the daily sleep duration. Secondhand smoking exposure meant that guardians living with the child were long-time smokers, and it was divided into 1–5 cigarettes per day, 5–10 cigarettes per day, and > 10 cigarettes per day. Vitamin D supplement duration was classified into ≤ 3 months, 3–6 months, 6–12 months, and > 12 months.

GWG was calculated from antepartum weight minus the prepregnancy weight, and it included three classes: adequate GWG (weight gain of 12.5–18.0 kg in underweight mothers, 11.5–16.0 kg in normal-weight mothers, 7.0–11.5 kg in overweight mothers, and 5.0–9.0 kg in obese mothers), inadequate GWG (less than the lower limits of adequate levels), and excessive GWG (greater than the upper limits of adequate levels). All reference criteria were based on the recommendations of the Institute of Medicine (2009) (Council, 2010).

Family income (RMB per year) was classified into ≤ 100,000, 100,000–300,000, 300,000–600,000, 600,000–900,000, and >1,000,000. Parent education was defined as a high school degree or below, college degree, master's degree, and doctor's degree and above. Smoking exposure during maternal pregnancy included secondhand smoke exposure on the mother and the mother smoking. Scores of parent self-rating about their patience with their children ranged from 0 to 10. A score of 0 indicates no patience. Stages of parent self-rating for the patience were classified into four stages based on the parent self-rating scores: stage 1 (scores = 0–3); stage 2 (scores = 4–6); stage 3 (scores = 7–9); and stage 4 (score = 10).

Statistical Analyses

The STATA software (version 14.0, Stata Corp., TX) and the R programming environment (version 4.1.0) were used for statistical analyses. All continuous variables were tested for normality and were log-transformed as appropriate, and the mean (SD) was calculated from the raw/non-log-transformed data. Skewed continuous variables were expressed as median (interquartile range). The intraclass correlation coefficient (ICC) was calculated to assess the possibility of non-random measurement error for factors under study collected from 30 public kindergartens. The ICC ranges from 0 to 1, and an ICC of 0 indicates that the variance in factors under study is not due to variation between the kindergartens.

Univariate analyses, specifically the *t*-test or rank-sum test for continuous variables and the chi-square for discrete variables, respectively, were performed for baseline characteristics' comparison. All statistical tests were two-sided with 0.05 significance levels. Dose–response relationships between children's breastfeeding duration and C-ASQ-defined ADHD susceptibility were investigated using restricted cubic spline models.

To identify the contribution of all possible factors, the least absolute shrinkage and selection operator (LASSO) model (Tibshirani, 1996), a regression-based methodology permitting a large number of covariates, was used to reduce the likelihood of overfitting and to remove unnecessary/uninfluential covariates. We utilized the "glmnet" package (version 2.0–16) to fit the logistic LASSO regression and used 10-fold cross-validation to select the penalty term, λ. Then, we identified statistically significant factors selected from the logistic LASSO model that were further adjusted for the age of the children, their sex, parents' age and education, and family income. Effect size estimates were denoted as odds ratios (ORs) and 95% CIs.

We searched for predictors of ADHD symptoms that were repeatedly reported in studies or systematic reviews, which included family income, screen time, low birth weight, probiotic supplementation, and parental education (Banerjee et al., 2007; Russell et al., 2016; Tamana et al., 2019;

Hartel et al., 2020). These factors were included in the basic model, and some baseline characteristics, including sex, age, region, BMI, parents' age at birth, parents' BMI, delivery mode, GWG, children's probiotic supplementation, and vitamin D supplement duration, were also included in the basic model. The Akaike information criterion (AIC), Bayesian information criterion (BIC), the −2 log likelihood ratio test, and Hosmer–Lemeshow goodness-of-fit test were used to appraise how closely the prediction probability was obtained by adding significant predictors selected by logistic LASSO regression. Integrated discrimination improvement (IDI) and the area under the receiver operating characteristic (AUROC) curve were used to determine whether the addition of significant predictors can differentiate preschool-aged children with C-ASQ-defined ADHD susceptibility.

The R programming environment (version 4.1.0) "rms" package was used to create a prediction nomogram model for the early identification of C-ASQ-defined ADHD susceptibility. The concordance index or C-index, defined as the AUROC curve, was used to quantify the model predictive accuracy.

Sample size was estimated using the "pmsampsize" package in the STATA software (version 14.0, Stata Corp., TX), which was developed by Riley et al. (2020). Meanwhile, study power was estimated using the PS-Power Simple Size software (version 3.1.2).

RESULTS

Baseline Characteristics

The flow diagram to selection of study children could be found in **Supplementary Figure 1**. The distributions of demographic, prenatal, and perinatal factors and environmental-related factor data from 7,938 children are shown in **Table 1**.

In addition, as study children were from 30 public kindergartens, the potential bias arising from different kindergartens was evaluated using the ICC. For 24 factors under study, ICC values ranged from 0.001 to 0.02, indicating a low likelihood of potential bias.

Identification of Contributing Predictors

The λ values for the logistic LASSO regression ranged from 0.000388 to 0.074940, and the selected λ value was 0.006509 in our study (**Supplementary Figure 2**). Originally, there were 10 variables in the LASSO regression model, including age, sex, maternal age at birth, paternal age at birth, secondhand smoking exposure, delivery mode, breastfeeding duration, sleep mode, maternal pregnancy smoking exposure, and parental self-rating for patience. These variables were further adjusted and corrected. Finally, five factors, namely, children's secondhand smoking exposure (OR: 1.24; 95% CI: 1.16–1.32; $p < 0.001$), breastfeeding duration (OR: 0.98; 95% CI: 0.98–0.99; $p < 0.001$), sleep mode (OR: 1.22; 95% CI: 1.17–1.28; $p < 0.001$), maternal pregnancy smoking exposure (OR: 1.28; 95% CI: 1.13–1.46; $p < 0.001$), and parental self-rating for patience (OR: 0.51; 95% CI: 0.47–0.56; $p < 0.001$), were independently identified by the multiple

TABLE 1 | Baseline characteristics of study participants in this study.

Characteristics	C-ASQ-defined ADHD susceptibility		P
	No (*n* = 6,366)	Yes (*n* = 1,573)	
For children			
Age, years			0.002
3–5 years	4,008 (60.3%)	1,057 (67.2%)	
5–7 years	2,357 (37.0%)	516 (32.8%)	
Boys	3,157 (49.6%)	949 (60.3%)	<0.001
Region			<0.001
Beijing	3,563 (56.0%)	1,082 (68.9%)	
Hebei	2,796 (44.0%)	489 (31.1%)	
ABO blood types			0.770
A	977 (28.0%)	264 (26.8%)	
B	1,172 (33.5%)	347 (35.2%)	
O	1,041 (29.8%)	288 (29.2%)	
AB	303 (8.7%)	87 (8.8%)	
Birth weight (kg)	3.3 (3.0, 3.6)	3.3 (3.0, 3.6)	0.529
Delivery mode			0.008
Natural delivery	3,229 (50.7%)	857 (54.5%)	
Artificial midwifery	3,137 (49.3%)	716 (45.5%)	
BMI (kg/m^2)	15.5 (14.5, 16.8)	15.5 (14.5, 16.7)	0.148
Breastfeeding duration (months)	12.0 (7.0, 18.0)	12.0 (8.0, 18.0)	<0.001
Fall asleep time (hours)			0.012
Before 23:00 pm	6,241 (98.0%)	1,526 (97.0%)	
After 23:00 pm	125 (2.0%)	47 (3.0%)	
Sleep duration	10.0 (9.0, 10.3)	10.0 (9.0, 10.6)	<0.001
Secondhand smoke exposure			<0.001
No	3,537 (55.6%)	757 (48.1%)	
1–5 cigarettes per day	1,907 (29.9%)	493 (31.3%)	
5–10 cigarettes per day	553 (8.7%)	195 (12.4%)	
> 10 cigarettes per day	369 (5.8%)	128 (8.1%)	
Vitamin D supplement duration			0.001
≤ 3 months	1,450 (26.8%)	317 (22.4%)	
3–6 months	969 (17.9%)	240 (16.9%)	
6–12 months	1,061 (19.6%)	304 (21.5%)	
> 12 months	1,935 (35.7%)	556 (39.2%)	
Probiotics supplemented			<0.001
Yes	2,079 (32.7%)	395 (25.1%)	
No	4,287 (67.3%)	1,178 (74.9%)	
Screen time (h/per day)	1.0 (0.6, 1.6)	1.0 (0.9, 2.0)	<0.001
For parents or guardians			
Family income (RMB per year)			<0.001
≤100,000	2,636 (41.4%)	546 (34.7%)	
100,000–300,000	2,382 (37.4%)	678 (43.1%)	
300,000–600,000	995 (15.6%)	261 (16.6%)	
600,000–900,000	229 (3.6%)	61 (3.9%)	
>1,000,000	124 (2.0%)	27 (1.7%)	
Maternal education			<0.001

(Continued)

TABLE 1 | (Continued)

Characteristics	C-ASQ-defined ADHD susceptibility		P
	No (*n* = 6,366)	Yes (*n* = 1,573)	
High school degree or below	2,600 (40.8%)	474 (30.1%)	
College degree	3,220 (50.6%)	971 (61.7%)	
Master degree	485 (7.6%)	113 (7.2%)	
Doctor degree and above	61 (1.0%)	15 (1.0%)	
Paternal education			<0.001
High school degree or below	2,845 (44.7%)	574 (36.5%)	
College degree	2,933 (46.1%)	847 (53.8%)	
Master degree	492 (7.7%)	126 (8.0%)	
Doctor degree and above	96 (1.5%)	26 (1.7%)	
Maternal BMI (kg/m^2)	22.3 (20.3, 24.8)	22.5 (20.5, 24.8)	0.084
Paternal BMI (kg/m^2)	25.4 (22.9, 28.4)	25.3 (22.9, 27.8)	0.045
Maternal age while children birth	28.5 (26.3, 31.2)	29.0 (26.8, 32.1)	<0.001
Paternal age while children birth	29.4 (27.1, 32.5)	30.0 (27.5, 33.5)	<0.001
Gestational weight gain (kg/m^2)			0.011
Inadequate	154 (24.3%)	380 (24.2%)	
Adequate	2,159 (33.9%)	477 (30.3%)	
Excessive	2,661 (41.8%)	716 (45.5%)	
Maternal pregnancy smoking			<0.001
Yes	3,766 (59.2%)	1,051 (66.8%)	
No	2,600 (40.8%)	522 (33.2%)	
Parental self-rating for patience			<0.001
1–3 points	254 (4%)	131 (8.3%)	
4–6 points	1,775 (27.9%)	653 (41.5%)	
7–9 points	3,526 (55.4%)	722 (45.9%)	
10 points	811 (12.7%)	67 (4.3%)	

Abbreviations: BMI, body mass index. Data are expressed as median (interquartile range) or count (percent). P value was calculated by the rank-sum test or the χ^2 test, where appropriate.

adjustment to be significantly associated with C-ASQ-defined ADHD susceptibility (**Figure 1** and **Table 2**).

On the basis of the above effect-size estimates, the minimal power to detect the significant association of the above five factors with ADHD risk was over 81.3%.

Dose–Response Analysis

We found a dose–response relationship between childhood breastfeeding duration and C-ASQ-defined ADHD susceptibility (**Figure 2**). Six months of breastfeeding duration was such a dramatic threshold; children seemed more likely to suffer from ADHD symptoms if the breastfeeding duration was less than 6 months.

In terms of sleep model, we found that in children that fell asleep before 23:00 and had a sleep duration of more than 8 h but less than 10 h, their odds ratio for ADHD susceptibility was 1.27 (95% CI: 1.13–1.44, $p < 0.001$) compared to those who fell asleep before 23:00 combined with sleep duration of more than 10 h. Likewise, serious trends were observed for a shorter sleep duration and a later sleep time [falling asleep time < 23:00 and sleep duration ≤ 8 h (OR: 1.54; 95% CI: 1.25–1.89; $p < 0.001$); falling asleep time ≥ 23:00 and sleep duration > 10 h (OR: 0.94; 95% CI: 0.52–1.72; $p = 0.85$); fall asleep time ≥ 23:00 and 8 h < sleep duration < 10 h (OR: 2.19; 95% CI: 1.32–3.62; $p = 0.002$); fall asleep time ≥ 23:00 and sleep duration ≤ 8 h (OR: 3.59; 95% CI: 1.62–7.94; $p = 0.002$)] (**Supplementary Table 1**). These results were adjusted by other variables investigated in this survey.

TABLE 2 | Risk prediction of five significant factors for C-ASQ-defined ADHD susceptibility.

Variables	C-ASQ-defined ADHD susceptibility		
	OR	95% CI	P
Unadjusted			
Secondhand smoke exposure	1.21	1.14–1.28	<0.001
Parental self-rating for patience	0.56	0.52–0.60	<0.001
Breastfeeding duration	0.98	0.98–0.99	<0.001
Maternal pregnancy smoking	1.39	1.24–1.56	<0.001
Sleep mode	1.23	1.17–1.28	<0.001
Partial adjustment*			
Secondhand smoke exposure	1.23	1.16–1.31	<0.001
Parental self-rating for patience	0.52	0.48–0.56	<0.001
Breastfeeding duration	0.98	0.98–0.99	<0.001
Maternal pregnancy smoking	1.31	1.15–1.48	<0.001
Sleep mode	1.22	1.17–1.28	<0.001
Multiple adjustment**			
Secondhand smoke exposure	1.24	1.16–1.32	<0.001
Parental self-rating for patience	0.51	0.47–0.56	<0.001
Breastfeeding duration	0.98	0.98–0.99	<0.001
Maternal pregnancy smoking	1.28	1.13–1.46	<0.001
Sleep mode	1.22	1.17–1.28	<0.001

*Abbreviations: OR, odds ratio; 95% CI, 95% confidence interval. *Partial adjustment contained sex, age, region, BMI (body mass index), family income, maternal education, and paternal education. **Multiple adjustment additionally included ABO blood types of children, children's birth weight, delivery mode, probiotics supplemented, Vitamin D supplement duration, parents' age while children birth, parents' BMI, gestational weight gain.*

Meanwhile, the risk of having ADHD-related symptoms was proportional to cigarette exposure of the children. Compared to never exposure, the risk ratio of children's exposure to 1–5 cigarettes per day was 1.20, with a 95% CI ranging from 0.98 to 1.46 ($p = 0.08$), while for those exposed to 5–10 and > 10 cigarettes per day, the risk ratio increased (OR: 1.48; 95% CI: 1.12–1.94; $p = 0.005$ and OR: 1.45; 95% CI: 1.04–2.02; $p = 0.03$, respectively).

For parental self-rating for patience, we concluded that children had ADHD-related symptoms when decreasing the stages of the self-rating. Compared with stage 1, the odds ratio was 0.62 (95% CI: 0.42–0.92; $p = 0.02$) in stage 2, 0.35 (95% CI: 0.24–0.52; $p < 0.001$) in stage 3, and 0.14 (95% CI: 0.08–0.24; $p < 0.001$) in stage 4.

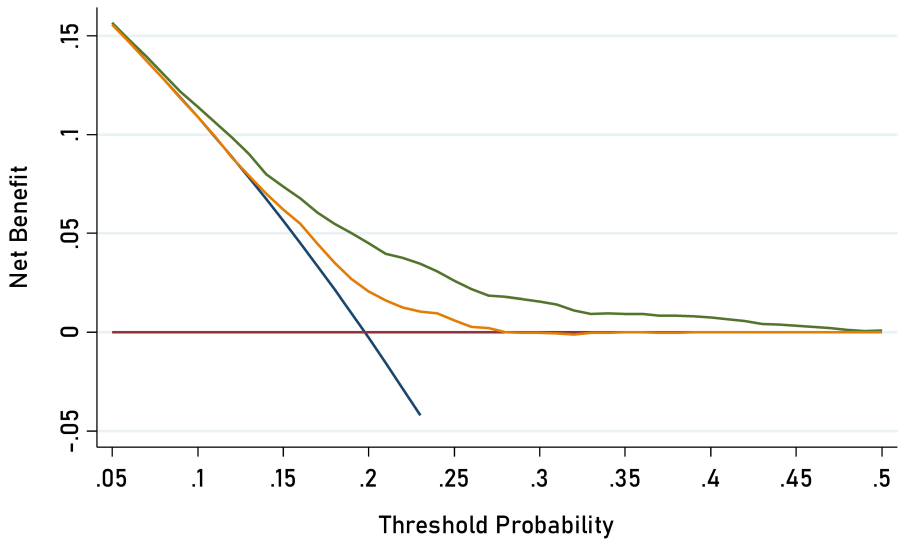

FIGURE 1 | Decision curve analysis for C-ASQ-defined ADHD susceptibility by adding significant factors to the basic model. The orange solid line corresponds to the basic model that includes sex, age, region, BMI (body mass index), family income, maternal education, and parental education, parent's age while children birth, parent's BMI, delivery mode gestational weight gain, probiotics supplemented, vitamin D supplement duration, screen time. The green solid line corresponds to the full model that includes both factors in the basic model and the five newly- identified significant factors including children's second hand smoking exposure, and parental self-rating patience. Larger area between the two lines represents better accuracy of the full prediction model.

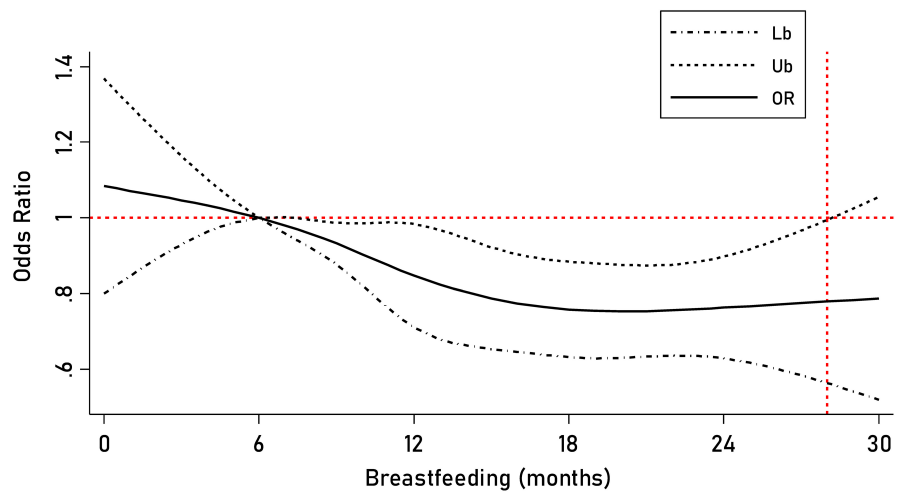

FIGURE 2 | Prediction of the breastfeeding duration for C-ASQ-defined ADHD susceptibility. The solid line represents the odd ratio (OR) for C-ASQ-defined ADHD susceptibility as the breastfeeding duration increases, and the black dashed line represents the corresponding 95% confident interval of the odd ratio.

Prediction Accuracy Assessment

A basic model and a full model were constructed to synthetically assess the prediction accuracy of the five significant factors. The full model included all variables investigated in this survey, and the basic model included all variables except the five factors. As shown in **Table 3**, the prediction accuracy gained by adding five significant factors associated with C-ASQ-defined ADHD susceptibility in preschool children was separately assessed by calibration and discrimination statistics. Compared with the basic model, the prediction accuracy was significantly improved in the full model and the difference was significant for the prediction performance in parallel.

Prediction Nomogram Model

A prediction nomogram model is necessary for extensive preliminary application of the C-ASQ-defined ADHD susceptibility in preschool children. Combining the five significant factors and the children's age and sex, we created a nomogram model (**Figure 3A**), with a concordance index (C-index) of 71% ($p < 0.05$), and good predictive accuracy (**Figure 3B**).

TABLE 3 | Prediction accuracy gained by adding five significant factors associated with C-ASQ-defined ADHD susceptibility in pre-school children.

Statistics	C-ASQ-defined ADHD susceptibility	
	Basic model	**Full model**
Calibration		
AIC	7480.1	7131.0
BIC	7556.4	7242.0
LR test (χ^2)	354.02	
LR test (*P*-value)	<0.0001	
Discrimination		
NRI	<0.0001	
IDI	<0.0001	
AUROC curves (*P*-value)	<0.0001	

Abbreviations: AIC, Akaike information criterion; BIC, Bayesian information criterion; LR, likelihood ratio; NRI, net reclassification improvement; IDI, integrated discrimination improvement; ROC, area under the receiver operating characteristic. Basic model included sex, age, region, BMI (body mass index), family income, maternal education, and paternal education, parents' age while children birth, parents' BMI, delivery mode, gestational weight gain, probiotics supplemented, vitamin D supplement duration, screen time.

An example to enhance its practical application is as follows: assume a boy (25 points) aged 5 years old (18 points), who falls asleep after 23:00 each day (24 points), with a sleep duration of 10 h (34 points), exposed to secondhand smoking 5–10 cigarettes per day (17 points), with a breastfeeding duration of 5 months (20 points), maternal pregnancy smoking exposed (20 points), and stage 4 of parental self-rating for practice being 1–3 (100 points). Since the total point is 258, the probability of developing ADHD-related symptoms is estimated to be approximately 64%.

DISCUSSION

Using a cross-sectional representative survey, annexed with robust statistical techniques, we aimed to identify and characterize prenatal and perinatal factors and environmental-related factors for C-ASQ-defined ADHD susceptibility among 7,938 preschool-aged children. The key point of our study is that five significant factors, namely, children's secondhand smoking exposure, breastfeeding duration, sleep mode, maternal pregnancy smoking exposure, and parental self-rating for patients, were independently associated with ADHD susceptibility assessed by Conner's ASQ. To our knowledge, this study is the first investigation about screening for ADHD-related symptoms in preschool-aged children in China.

In China, great efforts are being made to improve children's mental health, and the prevalence estimates of ADHD in mainland China, Hong Kong, and Taiwan were 6.5, 6.4, and 4.2%, respectively (Liu et al., 2018), which were derived from 67 studies covering 642,266 Chinese children and adolescents. However, little is known about the prevalence of ADHD in children aged 3–7 years. Due to the rapid physical, emotional, behavior, and cognitive development that young children experience, their emotional and behavior problems are often considered transient problems rather than mental disorders (Angold and Egger, 2004). However, many studies have proposed that preschoolers' temperaments and patterns of temperament traits could be linked to increased risks for later psychiatric disorders (Hirshfeld-Becker et al., 2003), and the rates of common childhood psychiatric disorders in preschoolers are similar to those seen in later childhood (Egger and Angold, 2006). Screening for ADHD susceptibility as well as searching for influential factors is necessary for the early detection, prevention, and intervention of childhood ADHD, as studies have demonstrated that children who did not undergo screening had a higher incidence of cognitive and behavior problems than those who did (Burakevych et al., 2016).

A growing number of studies have examined the risk factors associated with ADHD-related symptoms, yet the results are often not reproducible. For example, some studies have shown a significant association between maternal exposure to smoking and ADHD (Sourander et al., 2019), whereas others have failed to support this claim (Gustavson et al., 2017), with different sample sizes and regions, and possible incomplete adjustment of measured or unmeasured covariates.

The present study accounted for this aspect and undertook logistic LASSO regression and a hierarchical degree of adjustment for possible covariates, and added to existing evidence that co-exposure to prenatal and perinatal factors and environmental related factors significantly influenced ADHD-related outcomes. First, we found that smoking exposure was a severe risk factor, including maternal pregnancy exposure to smoking and children directly exposed to secondhand smoking. Many studies, including umbrella reviews, have proposed a relationship between nicotine exposure during pregnancy and offspring ADHD and have found a dose–response relationship (Thakur et al., 2013; Sourander et al., 2019; Kim et al., 2020). Meanwhile, a meta-analysis illustrated that postnatal exposure to secondhand smoking increased the risk of ADHD in children (OR: 1.60; 95% CI: 1.37–1.87) (Huang et al., 2021). These findings are highly consistent with our results.

Second, in terms of sleep mode, many studies have concluded that a short sleep duration is significantly linked to ADHD compared with an average sleep duration (Lee et al., 2019), especially in early childhood (Tso et al., 2019). Cremone-Caira et al. (2020) suggested that a sleep extension intervention improves inhibitory control in children with ADHD. Some studies have also illustrated that children's sleep onset latency, bedtime resistance, and sleep onset difficulties are significantly higher in children with ADHD (Cortese et al., 2009). In our study, we sought an interactive relationship between sleep duration and sleep initiation time, and found that the risk for ADHD susceptibility rose dramatically with a short sleep duration and a later bedtime.

Protective factors were also prominent in our study. A breastfeeding duration over 6 months is associated with lower conduct disorders. In early 1998, the World Health Organization (WHO) Expert Consultation recommended that infants be exclusively breastfed during the first 6 months of life (World Health Organization, 1998). Prolonged breastfeeding of infants may promote their mental health later in childhood, particularly by reducing the risk for inattention/hyperactivity

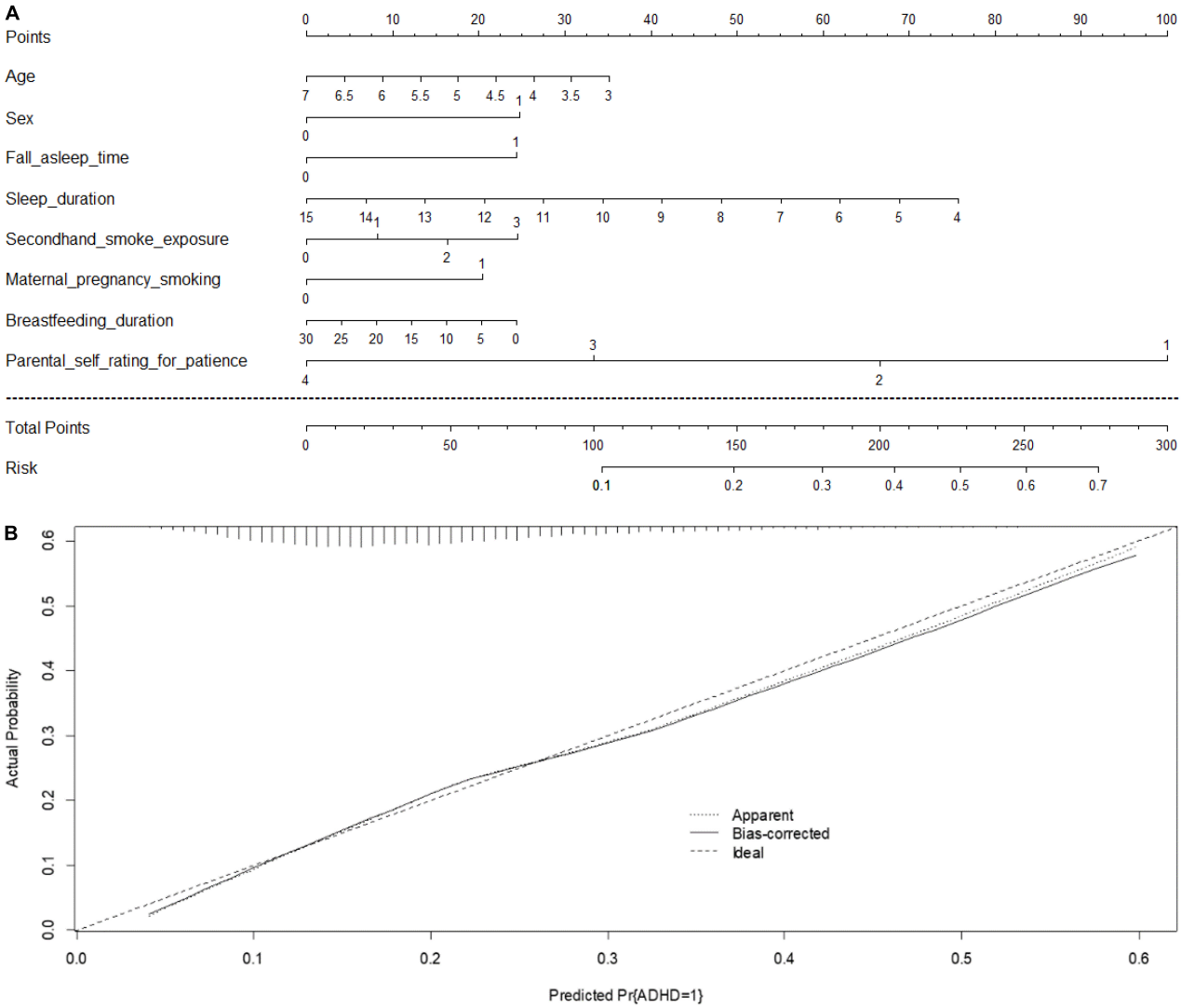

FIGURE 3 | (A) Prediction nomogram for C-ASQ-defined ADHD susceptibility. An individual's value is located on each variable axis, and a line is drawn upward to determine the number of points received for each variable value. The sum of these numbers is located on the "Total points" axis, and a line is drawn downward to the "Risk" axis to determine the likelihood of C-ASQ-defined ADHD susceptibility. **(B)** Calculation curves for C-ASQ-defined ADHD susceptibility. Nomogram-predicted probability of C-ASQ defined ADHD susceptibility plotted on the x- axis; actual probability of C-ASQ defined ADHD- susceptibility on the y- axis. The plots depict model performance in terms of agreement between predicted and actual probability of C-ASQ defined ADHD susceptibility. Prediction is represented by the 45 degree line.

and conduct disorders (Hartel et al., 2020). Breastfeeding could foster immune–microbiome interplay and promote mother–child interactions as well as improve long-term neurobehavior outcomes (Agostoni et al., 2017; Boucher et al., 2017; Tseng et al., 2019). Similarly, parents' patience is a significant factor for childhood development, especially for mental health. In our study, a higher parental self-rating for patience was associated with a lower risk of suffering from ADHD susceptibility. Multiple studies have shown that ADHD is linked to parent–child conflicts (Pelham and Fabiano, 2008; Williamson and Johnston, 2016), and ineffective, inconsistent, negligent parenting was found to exacerbate ADHD symptoms and be predictive of later disruptive behavior disorders (Ullsperger et al., 2016).

Finally, a risk prediction nomogram model for C-ASQ-defined ADHD susceptibility was created to enhance the practical applications of our findings. This model has excellent forecast precision and will be useful for conducting preliminary screening. However, several limitations of our study merit special consideration. First, since it is a cross-sectional study, it precludes further comments on the cause–effect relationship. We could not ascertain whether short sleep duration was a risk factor or a consequence of ADHD in this study, but we argued from an epidemiological perspective that sleep duration has an effect on preschool-aged children's ADHD susceptibility. Second, ADHD is a clinical diagnosis requiring a detailed evaluation of current and previous symptoms and a functional impairment, and full

family, gestational, and developmental history should be taken (Barkley, 2002). The key point of the present study focused on preliminary screening, and further diagnosis requires repeated evaluations. Third, objectively monitored variables such as sleep duration were self-reported by parents, and hence, recall bias could not be ruled out. Finally, some important items such as a family history of ADHD and the number of siblings were not surveyed in this study. In subsequent studies, we will pay more attention to hereditary factors.

In summary, *via* an analysis of survey data from 7,938 preschool-aged children and their parents or guardians, we identified five factors independently and consistently associated with children's C-ASQ-defined ADHD susceptibility, and a risk prediction nomogram model was established.

CONCLUSION

In general, five factors, namely, children's secondhand smoking exposure, breastfeeding duration, sleep mode, maternal pregnancy smoking exposure, and parental patience self-rating, were independently associated with ADHD susceptibility. These findings will help with developing intervention strategies for preventing ADHD susceptibility by promoting parental patience and encouraging a longer sleep duration and an earlier bedtime, a sufficient breastfeeding duration, and no secondhand smoking exposure.

DATA AVAILABILITY STATEMENT

The raw data supporting the conclusions of this article will be made available by the authors, without undue reservation.

ETHICS STATEMENT

The studies involving human participants were reviewed and approved by the Ethics Committee of China-Japan Friendship Hospital. Written informed consent to participate in this study was provided by the participants' legal guardian/next of kin.

AUTHOR CONTRIBUTIONS

KW, ZZ, and WN conceived and designed the experiments. XD and MY performed the experiments. XD and WN analyzed the data and wrote the manuscript. XD, MY, and BZ contributed materials and analysis tools. All authors read and approved the final manuscript prior to submission.

SUPPLEMENTARY MATERIAL

The Supplementary Material for this article can be found online at: https://www.frontiersin.org/articles/10.3389/fnins.2021.709374/full#supplementary-material

REFERENCES

Aduen, P. A., Kofler, M. J., Sarver, D. E., Wells, E. L., Soto, E. F., and Cox, D. J. (2018). ADHD, depression, and motor vehicle crashes: a prospective cohort study of continuously-monitored, real-world driving. *J. Psychiatr. Res.* 101, 42–49. doi: 10.1016/j.jpsychires.2018.02.026

Agostoni, C., Mazzocchi, A., Leone, L., Ciappolino, V., Delvecchio, G., Altamura, C. A., et al. (2017). The first model of keeping energy balance and optimal psycho affective development: breastfed infants. *J. Affect. Disord.* 224, 10–15. doi: 10.1016/j.jad.2017.01.001

Angold, A., and Egger, H. L. (2004). "Psychiatric diagnosis in preschool children," in *Handbook of Infant, Toddler, and Preschool Mental Health Assessment*, eds D. W. Rebecca and S. C. Alice (Oxford: Oxford University Press), 123–139.

Banerjee, T. D., Middleton, F., and Faraone, S. V. (2007). Environmental risk factors for attention-deficit hyperactivity disorder. *Acta Paediatr.* 96, 1269–1274.

Barkley, R. A. (2002). Major life activity and health outcomes associated with attention-deficit/hyperactivity disorder. *J. Clin. Psychiatry* 63, 10–15.

Biederman, J., and Faraone, S. V. (2005). Attention-deficit hyperactivity disorder. *Lancet* 366, 237–248.

Boucher, O., Julvez, J., Guxens, M., Arranz, E., Ibarluzea, J., Sanchez De Miguel, M., et al. (2017). Association between breastfeeding duration and cognitive development, autistic traits and ADHD symptoms: a multicenter study in Spain. *Pediatr. Res.* 81, 434–442. doi: 10.1038/pr.2016.238

Buitelaar, N. J. L., Posthumus, J. A., and Buitelaar, J. K. (2020). ADHD in Childhood and/or Adulthood as a Risk Factor for Domestic Violence or Intimate Partner Violence: a Systematic Review. *J. Atten. Disord.* 24, 1203–1214. doi: 10.1177/1087054715587099

Burakevych, N., Mckinlay, C. J., Alsweiler, J. M., Wouldes, T. A., and Harding, J. E. (2016). Pre-school screening for developmental and emotional health: comparison with neurodevelopmental assessment. *J. Paediatr. Child Health* 52, 600–607. doi: 10.1111/jpc.13169

Chang, L. Y., Wang, M. Y., and Tsai, P. S. (2016). Diagnostic Accuracy of Rating Scales for Attention-Deficit/Hyperactivity Disorder: a Meta-analysis. *Pediatrics* 137:e20152749. doi: 10.1542/peds.2015-2749

Conners, C. K. (1989). *Conners' Rating Scales: Conners' Teacher Rating Scales, Conners' Parent Rating Scales*. Toronto: Multi-Health Systems, Incorporated.

Cortese, S., Faraone, S. V., Konofal, E., and Lecendreux, M. (2009). Sleep in children with attention-deficit/hyperactivity disorder: meta-analysis of subjective and objective studies. *J. Am. Acad. Child Adolesc. Psychiatry* 48, 894–908. doi: 10.1097/CHI.0b013e3181ac09c9

Council, N. R. (2010). *Weight Gain During Pregnancy: Reexamining the Guidelines*. Washington, DC: National Academies Press.

Cremone-Caira, A., Root, H., Harvey, E. A., Mcdermott, J. M., and Spencer, R. M. C. (2020). Effects of Sleep Extension on Inhibitory Control in Children With ADHD: a Pilot Study. *J. Atten. Disord.* 24, 601–610. doi: 10.1177/1087054719851575

Doshi, J. A., Hodgkins, P., Kahle, J., Sikirica, V., Cangelosi, M. J., Setyawan, J., et al. (2012). Economic impact of childhood and adult attention-deficit/hyperactivity disorder in the United States. *J. Am. Acad. Child Adolesc. Psychiatry* 51:e1002. doi: 10.1016/j.jaac.2012.07.008

Egger, H. L., and Angold, A. (2006). Common emotional and behavioral disorders in preschool children: presentation, nosology, and epidemiology. *J. Child Psychol. Psychiatry* 47, 313–337. doi: 10.1111/j.1469-7610.2006.01618.x

Garas, P., and Balazs, J. (2020). Long-Term Suicide Risk of Children and Adolescents With Attention Deficit and Hyperactivity Disorder-A Systematic Review. *Front. Psychiatry* 11:557909. doi: 10.3389/fpsyt.2020.557909

Gustavson, K., Ystrom, E., Stoltenberg, C., Susser, E., Suren, P., Magnus, P., et al. (2017). Smoking in Pregnancy and Child ADHD. *Pediatrics* 139:e20162509.

Harstad, E. B., Katusic, S., Sideridis, G., Weaver, A. L., Voigt, R. G., and Barbaresi, W. J. (2020). Children With ADHD Are at Risk for a Broad Array of Adverse Adult Outcomes That Cross Functional Domains: results From a Population-Based Birth Cohort Study. *J. Atten. Disord.* 26, 3–14. doi: 10.1177/1087054720964578

Hartel, C., Spiegler, J., Fortmann, I., Astiz, M., Oster, H., Siller, B., et al. (2020). Breastfeeding for 3 Months or Longer but Not Probiotics Is Associated with Reduced Risk for Inattention/Hyperactivity and Conduct Problems in Very-Low-Birth-Weight Children at Early Primary School Age. *Nutrients* 12:3278. doi: 10.3390/nu12113278

Hirshfeld-Becker, D. R., Biederman, J., Calltharp, S., Rosenbaum, E. D., Faraone, S. V., and Rosenbaum, J. F. (2003). Behavioral inhibition and disinhibition as hypothesized precursors to psychopathology: implications for pediatric bipolar disorder. *Biol. Psychiatry* 53, 985–999. doi: 10.1016/s0006-3223(03)00316-0

Huang, A., Wu, K., Cai, Z., Lin, Y., Zhang, X., and Huang, Y. (2021). Association between postnatal second-hand smoke exposure and ADHD in children: a systematic review and meta-analysis. *Environ. Sci. Pollut. Res. Int.* 28, 1370–1380. doi: 10.1007/s11356-020-11269-y

Kim, J. H., Kim, J. Y., Lee, J., Jeong, G. H., Lee, E., Lee, S., et al. (2020). Environmental risk factors, protective factors, and peripheral biomarkers for ADHD: an umbrella review. *Lancet Psychiatry* 7, 955–970. doi: 10.1016/S2215-0366(20)30312-6

Lee, S. H., Kim, H. B., and Lee, K. W. (2019). Association between sleep duration and attention-deficit hyperactivity disorder: a systematic review and meta-analysis of observational studies. *J. Affect. Disord.* 256, 62–69. doi: 10.1016/j.jad.2019.05.071

Liu, A., Xu, Y., Yan, Q., and Tong, L. (2018). The Prevalence of Attention Deficit/Hyperactivity Disorder among Chinese Children and Adolescents. *Sci. Rep.* 8:11169. doi: 10.1038/s41598-018-29488-2

Manos, M. J., Giuliano, K., and Geyer, E. (2017). ADHD: overdiagnosed and overtreated, or misdiagnosed and mistreated? *Cleve Clin. J. Med.* 84, 873–880. doi: 10.3949/ccjm.84a.15051

Mohr-Jensen, C., Muller Bisgaard, C., Boldsen, S. K., and Steinhausen, H. C. (2019). Attention-Deficit/Hyperactivity Disorder in Childhood and Adolescence and the Risk of Crime in Young Adulthood in a Danish Nationwide Study. *J. Am. Acad. Child Adolesc. Psychiatry* 58, 443–452. doi: 10.1016/j.jaac.2018.11.016

Pelham, W. E. Jr., and Fabiano, G. A. (2008). Evidence-based psychosocial treatments for attention-deficit/hyperactivity disorder. *J. Clin. Child Adolesc. Psychol.* 37, 184–214.

Polanczyk, G. V., Salum, G. A., Sugaya, L. S., Caye, A., and Rohde, L. A. (2015). Annual research review: a meta-analysis of the worldwide prevalence of mental disorders in children and adolescents. *J. Child Psychol. Psychiatry* 56, 345–365. doi: 10.1111/jcpp.12381

Riley, R. D., Ensor, J., Snell, K. I. E., Harrell, F. E. Jr., Martin, G. P., Reitsma, J. B., et al. (2020). Calculating the sample size required for developing a clinical prediction model. *BMJ* 368:m441. doi: 10.1136/bmj.m441

Russell, A. E., Ford, T., Williams, R., and Russell, G. (2016). The Association Between Socioeconomic Disadvantage and Attention Deficit/Hyperactivity Disorder (ADHD): a Systematic Review. *Child Psychiatry Hum. Dev.* 47, 440–458. doi: 10.1007/s10578-015-0578-3

Sourander, A., Sucksdorff, M., Chudal, R., Surcel, H. M., Hinkka-Yli-Salomaki, S., Gyllenberg, D., et al. (2019). Prenatal Cotinine Levels and ADHD Among Offspring. *Pediatrics* 143:e20183144. doi: 10.1542/peds.2018-3144

Stern, A., Agnew-Blais, J. C., Danese, A., Fisher, H. L., Matthews, T., Polanczyk, G. V., et al. (2020). Associations between ADHD and emotional problems from childhood to young adulthood: a longitudinal genetically sensitive study. *J. Child Psychol. Psychiatry* 61, 1234–1242. doi: 10.1111/jcpp.13217

Tamana, S. K., Ezeugwu, V., Chikuma, J., Lefebvre, D. L., Azad, M. B., Moraes, T. J., et al. (2019). Screen-time is associated with inattention problems in preschoolers: results from the CHILD birth cohort study. *PLoS One* 14:e0213995. doi: 10.1371/journal.pone.0213995

Thakur, G. A., Sengupta, S. M., Grizenko, N., Schmitz, N., Page, V., and Joober, R. (2013). Maternal smoking during pregnancy and ADHD: a comprehensive clinical and neurocognitive characterization. *Nicotine Tob. Res.* 15, 149–157. doi: 10.1093/ntr/nts102

Thapar, A., and Cooper, M. (2016). Attention deficit hyperactivity disorder. *Lancet* 387, 1240–1250.

Thapar, A., Cooper, M., Eyre, O., and Langley, K. (2013). What have we learnt about the causes of ADHD? *J. Child Psychol. Psychiatry* 54, 3–16. doi: 10.1111/j.1469-7610.2012.02611.x

Tibshirani, R. (1996). Regression shrinkage and selection via the lasso. *J. R. Stat. Soc. Series B Stat. Methodol.* 58, 267–288. doi: 10.1111/j.2517-6161.1996.tb02080.x

Tseng, P. T., Yen, C. F., Chen, Y. W., Stubbs, B., Carvalho, A. F., Whiteley, P., et al. (2019). Maternal breastfeeding and attention-deficit/hyperactivity disorder in children: a meta-analysis. *Eur. Child Adolesc. Psychiatry* 28, 19–30. doi: 10.1007/s00787-018-1182-4

Tso, W., Chan, M., Ho, F. K., Rao, N., Li, A. M., Chan, K. L., et al. (2019). Early sleep deprivation and attention-deficit/hyperactivity disorder. *Pediatr. Res.* 85, 449–455. doi: 10.1038/s41390-019-0280-4

Ullsperger, J. M., Nigg, J. T., and Nikolas, M. A. (2016). Does Child Temperament Play a Role in the Association Between Parenting Practices and Child Attention Deficit/Hyperactivity Disorder? *J. Abnorm. Child Psychol.* 44, 167–178. doi: 10.1007/s10802-015-9982-1

Vasileva, M., Graf, R. K., Reinelt, T., Petermann, U., and Petermann, F. (2020). Research review: a meta-analysis of the international prevalence and comorbidity of mental disorders in children between 1 and 7 years. *J. Child Psychol. Psychiatry* 62, 372–381. doi: 10.1111/jcpp.13261

Williamson, D., and Johnston, C. (2016). Marital and Coparenting Relationships: associations With Parent and Child Symptoms of ADHD. *J. Atten. Disord.* 20, 684–694. doi: 10.1177/1087054712471717

World Health Organization (1998). *Evidence for the Ten Steps to Successful Breastfeeding*. Geneva: World Health Organization.

Xiangdong, W. (1993). *In Rating Scales for Mental Health*. Beijing: Chinese Mental Health Journal.

Conflict of Interest: The authors declare that the research was conducted in the absence of any commercial or financial relationships that could be construed as a potential conflict of interest.

Publisher's Note: All claims expressed in this article are solely those of the authors and do not necessarily represent those of their affiliated organizations, or those of the publisher, the editors and the reviewers. Any product that may be evaluated in this article, or claim that may be made by its manufacturer, is not guaranteed or endorsed by the publisher.

frontiers in Neuroscience

ORIGINAL RESEARCH
published: 24 March 2022
doi: 10.3389/fnins.2022.751489

Genetic Inhibition of Plppr5 Aggravates Hypoxic-Ischemie-Induced Cortical Damage and Excitotoxic Phenotype

Yuxiao Sun[1,2†], Mei-fang Jin[1†], Lili Li[1†], Yueying Liu[3], Dandan Wang[1] and Hong Ni[1]*

[1] Division of Brain Science, Institute of Pediatric Research, Children's Hospital of Soochow University, Suzhou, China, [2] The First Affiliated Hospital of Zhejiang University School of Medicine, Hangzhou, China, [3] Department of Pediatrics, Affiliated Hospital of Jiangnan University, Wuxi, China

Hypoxia-ischemia (HI) is the most common acute brain threat in neonates and a leading cause of neurodevelopmental impairment. Exploring the new molecular mechanism of HI brain injury has important clinical translational significance for the next clinical intervention research. Lipid phosphatase-related proteins (PLPPRs) are regulators of mitochondrial membrane integrity and energy metabolism. We recently found that *Plppr5* knockout exacerbated HI impairment in some aspects and partially attenuated the neuroprotective effects of melatonin, suggesting that *Plppr5* may be a novel intervention target for HI. The present study aimed to determine the long-term effects of gene knockout of *Plppr5* on HI brain injury, focusing on the neuronal excitability phenotype, and to determine the effect of *Plppr5* gene silencing on neuronal zinc metabolism and mitochondrial function *in vitro*. 10-day-old wild type (WT) mice and *Plppr5*-deficient (*Plppr5*$^{-/-}$) mice were subjected to hypoxia-ischemia. Lesion volumes and HI-induced neuroexcitotoxic phenotypes were quantified together with ZnT1 protein expression in hippocampus. In addition, HT22 (mouse hippocampal neuronal cells) cell model was established by oxygen–glucose deprivation/reoxygenation (OGD/R) treatment and was treated with medium containing LV-sh_*Plppr5* or control virus. Mitochondrial oxidative stress indicator ROS, mitochondrial ZnT1 protein expression and zinc ion content were detected.

Results: *Plppr5*-deficient mice subjected to hypoxia-ischemia at postnatal day 10 present significantly higher cerebral infarction. *Plppr5*-deficient mice were endowed with a more pronounced superexcitability phenotype at 4 weeks after HI, manifested as a reduced seizure threshold. ZnT1 protein was also found reduced in *Plppr5*-deficient mice as well as in mice subjected to HI excitotoxicity. *Plppr5* knockout *in vivo* exacerbates HI brain injury phenotypes, including infarct volume and seizure threshold. In addition, knockout of the *Plppr5* gene reduced the MFS score to some extent. *In vitro Plppr5* silencing directly interferes with neuronal zinc metabolism homeostasis and exacerbates hypoxia-induced mitochondrial oxidative stress damage. Taken together, our findings demonstrate for the first time that *Plppr5*-deficient mouse pups exposed

OPEN ACCESS

Edited by:
Kazuhiko Sawada, Tsukuba International University, Japan

Reviewed by:
Junjia Tang, Shanghai First People's Hospital, China
Sergei V. Fedorovich, Belarusian State University, Belarus

***Correspondence:**
Hong Ni
nhdoctor@163.com

† These authors have contributed equally to this work

Specialty section:
This article was submitted to Neurodevelopment, a section of the journal Frontiers in Neuroscience

Received: *07 January 2022*
Accepted: *28 February 2022*
Published: *24 March 2022*

Citation:
Sun Y, Jin M-f, Li L, Liu Y, Wang D and Ni H (2022) Genetic Inhibition of Plppr5 Aggravates Hypoxic-Ischemie-Induced Cortical Damage and Excitotoxic Phenotype. Front. Neurosci. 16:751489. doi: 10.3389/fnins.2022.751489

to neuronal hypoxia and ischemia exhibit aggravated acute brain injury and long-term brain excitability compared with the same treated WT pups, which may be related to the disruption of zinc and mitochondria-dependent metabolic pathways in the hippocampus. These data support further investigation into novel approaches targeting *Plppr5*-mediated zinc and mitochondrial homeostasis in neonatal HIE.

Keywords: plppr5, knockout, excitotoxic, hypoxic-ischemia, neonatal

INTRODUCTION

Neonatal Hypoxic-Ischemic Brain Damage (HIBD) refers to neonatal brain damage caused by cerebral hypoxia and ischemia, mostly caused by neonatal asphyxia that occurs in the perinatal period. The incidence of HIBD in live births is about 3‰∼6‰, of which about 18% die in the neonatal period, and about 25% of surviving children also have permanent neurological damage (Horn et al., 2013). Every year, more than 2 million babies die or develop permanent sequelae due to HIBD in the world (Martínez-Orgado et al., 2020). A report by The Lancet showed that about 75% of children with HIBD had seizures, and some children developed epilepsy (Gluckman et al., 2005). At present, several types of drugs commonly used in clinical treatment of convulsions caused by HIBD have many adverse consequences (Mitra et al., 2016). The HIBD animal model will help to reveal the mechanism of HIBD-induced epileptogenesis and provide new clues for early intervention.

The molecular and biochemical mechanisms of acute neonatal hypoxic-ischemic brain injury mainly include intracellular free radical/ion-mediated cell death/survival gene expression and mitochondrial dysfunction. However, the long-term effects of hypoxia-ischemia on brain function, especially on brain excitability and epileptogenesis, are still poorly investigated. Epileptogenesis refers to the pathophysiological process from the initial stimulation of brain injury to the final formation of spontaneous epilepsy (Pitkänen and Lukasiuk, 2009). The classic neuroplasticity change during the incubation period after the initial brain injury is the abnormal distribution and enhancement of active zinc ion staining (Timm staining) in hippocampal mossy fibers (MFs) (regenerative sprouting) (Rakhade and Jensen, 2009). The brain is rich in zinc, which is an important trace metal element in the central nervous network system. The normal survival and development of cells depend on zinc homeostasis. Zinc has two sides to brain mitochondrial function. Physiological concentration of zinc might be beneficial in protecting mitochondrial antioxidants from oxidative stress damage (Adebayo et al., 2016). However, glutamate-induced zinc release and dyshomeostasis contributed to HT22 neuronal mitochondrial injury (Jin et al., 2018).

Plasticity-Related Gene (also known as Phospholipid Phosphatase Related, PLPPR) is a new member of the brain-specific lipid phosphatase superfamily, including plasticity-related gene family 1-5 (PLPPR1-5) (Peeva et al., 2006; Sigal et al., 2007; Bräuer and Nitsch, 2008; Tang and Brindley, 2020). Our previous study demonstrated long-term abnormal expression of hippocampal zinc ion transporter 1 (ZnT-1), zinc ion transporter 3 (ZnT3), PLPPR4, and PLPPR1 induced by developmental seizures, and the high correlation among these molecules is also destroyed (Ni et al., 2009a,b), indicating that both PLPPR and zinc ion transporter signals are involved in the regulation of long-term hippocampal MF sprouting following neonatal seizures. However, the effect of *Plppr5* on neonatal hypoxic-ischemic brain damage and its relationship with zinc ion signal remains unclear.

The aim of this study was to compare *Plppr5*$^{-/-}$ mice and their littermate wild-type mice at 4 weeks after HIBD treatment. The main observation parameters include the seizure threshold, the distribution and intensity of active zinc ion staining (Timm staining, sprouting) of hippocampal mossy fibers, and the level of ZnT-1 protein expression. We also further revealed the internal connection between *Plppr5*, mitochondrial damage and zinc ion signal through *in vitro* cell experiments, providing new ideas for the clinical treatment of HIBD.

MATERIALS AND METHODS

Experimental Animals

The generation of *Plppr5* knockout mice was conducted in the GemPharmatech Co., Ltd. (Nanjing, China) using CRISPR/Cas9 technology as has been reported before (Sun et al., 2021). KO and littermate wildtype (WT) mice of 10 days were used in our experiments and only male mice were used. All experiments were conducted with approval of the University of Soochow University Animal Care and Use Committee (ethical code:SUDA20201020A01). Mice were tested blindly for genotype. Hypoxic-Ischemic Brain Damage (HIBD) is based on the mature Rice Vannucci model (Rice et al., 1981). Briefly, 10-day old mice were anesthetized, then, the left common carotid artery was carefully separated and cut in the middle after double ligation with a 5–0 suture. Lastly, the skin was sutured. The entire procedure took no more than 6 min. The mice were returned to the dam to recover for one hour and then placed in a hypoxic chamber for two hours (37°C, 8% oxygen, 92% nitrogen). The sham-operated (Sham) mice were only treated by isolating the left common carotid artery without ligation, and placed in a similar equipment without hypoxic (**Figure 1**). A total of thirty male WT mice and thirty *Plppr5*$^{-/-}$ mice were randomly selected and divided into the following four groups (fifteen in each group): WT group (wild-type sham operation group, $n = 15$), KO group (*Plppr5*$^{-/-}$ mice with sham operation group, $n = 15$), WT + HIBD group (wild-type mice with hypoxic-ischemic group, $n = 15$), KO + HIBD group (*Plppr5*$^{-/-}$ mice with hypoxic-ischemic group, $n = 15$).

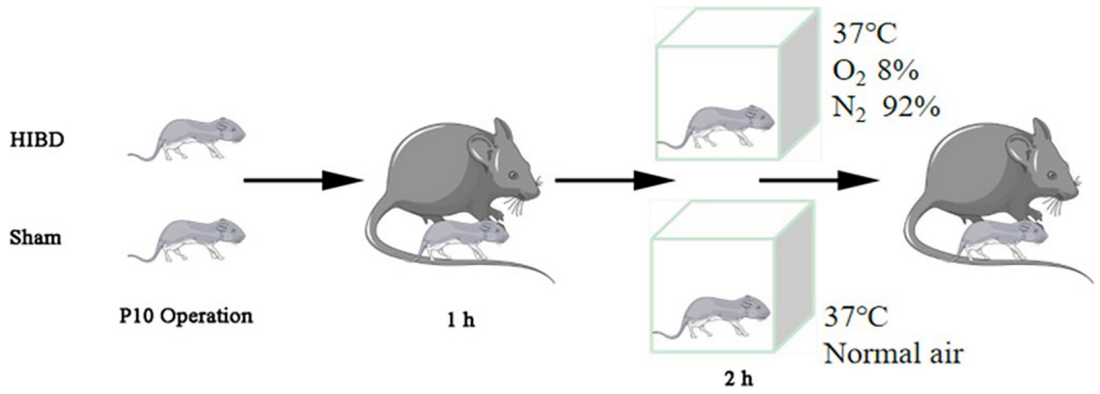

FIGURE 1 | HIBD model making.

Measurement of Infarct Volume

Three mice in each group were anesthetized and executed 24 h after HIBD. The brains were removed and sliced coronally into 2-mm-thick sections and incubated in 1% 2,3,5-triphenyltetrazolium chloride (TTC) (Sigma, St. Louis, MO, United States) at 37°C in the dark for 10 min. Then fixed overnight in 4% formaldehyde solution. The TTC-stained brain sections were photographed and the infarct volumes were measured by Image J (an image analysis software, United States). The degree of cerebral infarction is presented as the percentage of infarction volume to total brain volume (Wang et al., 2016; Wong et al., 2018; Omur et al., 2019).

Determination of Seizure Threshold

To explore the difference of the seizure latency (seizure threshold) between hypoxic-ischemic brain injury and sham operation, and the effect of *Plppr5* knockout.

Four weeks after HIBD, six mice in each group were randomly selected to test. The specific operation refers to the literature (Jin et al., 2018): the mice were injected with penicillin (5.1×10^6U/kg/d, i.p.), and the time from the injection of penicillin to the convulsive seizure of the mouse were recorded. The observation time was 90 min. The intensity of epilepsy was determined according to the Racine classification (Racine, 1972). Briefly, stage 1, stereotype mouth movement, eye blinking and/or mild facial clonus; stage 2, head nodding and/or sever facial clonus; stage 3, unilateral forelimb clonic twitching, but no hindlimb erection; stage 4, clonic convulsions in the forelimbs with rearing; and stage 5, generalized tonic-clonic seizures with falls, loss of postural control. Moreover, after the seizure started, the mouse was injected with 4% chloral hydrate immediately.

Neo-Timm's Staining

The neo-Timm's staining is based on the sulfide/silver method. Three mice were randomly selected from each group four weeks after HIBD. After anesthesia, they were fixed in the supine position. The chest was opened along the midline and the heart was exposed. Then, PBS, 0.4% Na_2S, 4% paraformaldehyde, 0.4% Na_2S were injected into the heart in turn. Then removed the brain and put into 4% paraformaldehyde for fixation, and selected according to the hippocampal positioning of Wiqas et al. (2020). The section with the largest area of the dorsal hippocampus (Bregma-1.3 to -3.7 mm, The mouse brain in stereotaxic coordinates. Amsterdam, the Netherlands, Boston, MA: Elsevier/Academic Press.). Incubate the Timm staining solution (90 ml of 50% gum Arabic with 7.65 g of citric acid, 7.05 g of sodium citrate in 22 ml ddH_20, 1.5 ml of 17% $AgNO_3$, 5.3 g of hydroquinone in 90 ml ddH_2O) at 37°C for 50 min in the dark. After the incubation, rinse it in running water and pass the 70%, 80%, 90% and 100% staining solution one by one. It is dehydrated in ethanol solution and mounted with neutral resin (Hsu and Buzsáki, 1993; Ni et al., 2009b; Yang et al., 2013). After drying, observe and take pictures under a light microscope. Semi-quantitative scoring of mossy fiber sprouting (MFS) in hippocampal DG and CA3 regions was performed (the scoring was done by persons who did not know the experimental group), and 5 consecutive brain slices were observed for each brain tissue CA3 area and DG area (Holmes et al., 1999; Ni et al., 2009b).

Cell Culture

HT22 cells (neuronal line of mouse hippocampus) were obtained from the Cell Bank of the Institute of Cell Biology, Chinese Academy of Sciences. Cells were cultured in medium composed of DMEM, 10% FBS, 100U/mL penicillin, and 100mg/mL streptomycin in the cell culture incubator at 37°C with 5% CO_2.

Viral Infecton and Oxygen Glucose Deprivation/Reoxygenation (OGD/R) of HT22 Cells

For viral infection *in vitro*, when cells grew to 60–70% confluency, the HT22 cells were transfected with medium containing LV-*Plppr5*-RNAi (MOI = 100), and empty plasmids LV-control-RNAi (normal control;MOI = 100; Genechem). After 24 hours of transfection, serum-free transfer solution was replaced by complete medium to culture for 48 h. The cells were cultured for 3 days and then subjected to OGD/R. Oxygen and glucose

deprivation/reoxygenation (OGD/R) is an accepted *in vitro* model for simulating HIBD. First, HT22 cells were cultured in glucose-free DMEM in a hypoxia incubator chamber (Billups-Rothenberg, Inc.) with 1% O_2, 5% CO_2, and 37°C for 6 h. Then, the medium was replaced with complete DMEM and the cells were incubated in an incubator with 5% CO_2 at 37°C for another 4h to simulated the reperfusion. Cells in the control group were treated identically except that they were not exposed to OGD (Wei et al., 2017). Briefly, it was divided into four groups: Sh-control, Sh-*Plppr5*, Sh-control + OGD/R, Sh-*Plppr5* + OGD/R.

Western Blot

Brain tissues from the left hippocampus region of the mice or cells were collected and added with RIPA lysis buffer (Beyotime Biotechnology, China) (Rafało-Ulińska et al., 2020). Lyse on ice for 1 h after shaking. The supernatant was collected after centrifugation at 4°C and 12,000 × g for 30 min. Protein concentrations were determined with BCA protein assay kit (Beyotime Biotechnology, China). Next, the protein extracts were boiled at 100°C for 10 min. Equal amount of protein from each sample was resolved on SDS–PAGE, trans-blotted onto polyvinylidene fluoride membranes (Millipore), and subjected to immunoblot assay by primary antibodies followed by secondary antibodies. The following antibodies were used for western blotting: rabbit polyclonal anti-ZnT1 (SLC30A1) antibody (1:1000; allomone labs, AZT-011), and mouse monoclonal beta actin antibody (1:5000; proteintech,66009-1-Ig) (Rafalo-Ulinska et al., 2016). The bands were visualized by an ECL detection kit (Beyotime Biotechnology, China) using AmerSham Imager 600 (GE, United States). β-actin was used as a loading control.

Biochemical Detection

Index of oxidative injury (lipoperoxidative damage) was determined by malondialdehyde (MDA) and antioxidant capacity was estimated by superoxide dismutase (SOD). After treatment, the cells were collected to detect MDA and SOD levels using a MDA (A003-2) or SOD (A001-1) kit (Nanjing Jiancheng Biotechnology Research Institute, Jiangsu, China) according to the manufacturer recommendations (Dai et al., 2018; Yan et al., 2019).

Mitochondrial Reactive Oxygen Species Detection

The intramitochondrial production of ROS in live HT22 cells was detected using the fluorescent MitoSox probe (M36008;Invitrogen) (Roelofs et al., 2015; Chen et al., 2019). The cells were reacted with a 5 μM working solution of MitoSOX Red for 10 min at 37°C, and then carefully washed twice with HBSS. Then, cells were stained with the Hoechst 33342 (1 mg/ml, Beyotime Biotechnology, China) dye for 10 min at 37°C and washed twice with HBSS. Images were obtained with a Laser Scanning Confocal Microscope (OLYMPUS, Japan), and the fluorescence intensity was evaluated with the Image J software (National Institutes of Health, MD, United States). The data are shown as the mean intensities.

Detection of Mitochondrial Membrane Potential (MMP, $\Delta\psi$m) Using JC-1

MMP was estimated by flow cytometry after staining with JC-1 fluorescent dye (Beyotime Biotechnology, China). MMP is high and JC-1 predominantly appears as red fluorescence when the cell is in a normal state. When the cell is in an apoptotic or necrotic state, the MMP is reduced and JC-1 appears as a monomer indicated by green fluorescence. Approximately 1×10^5 cells in 6-well plates were treated separately. The cells were then washed with PBS and incubated with JC-1 working solution for 20 min at 37°C in the dark. After the incubation, the supernatant was discarded after centrifugation at 600 g/min at 4°C for 3 min and resuspended in 500 μl JC-1 staining buffer. The stained cells were analyzed by flow cytometry to determine the change in the florescence from red to green (Jin et al., 2018).

Detection of Intracellular Zinc Ions Concentration

Zinquin ethyl ester is thought to be TSQ analog and can form a fluorescent complex with zinc ions to detect intracellular free zinc (Grabrucker et al., 2014). The cells were cultured in confocal microplates and treated separately 500 μl of 2.4 μM Zinquin ethyl ester solution (diluted in DMEM, Dojindo Molecular Technologies, Kumamoto, Japan) was added to the cells and incubated for 60 min at 37°C and washed twice with HBSS. Images were obtained with a Laser Scanning Confocal Microscope, and the fluorescence intensity was evaluated with the Image J software (National Institutes of Health, MD, United States). The data are shown as the mean intensities.

Statistical Analysis

All data in this study were statistically analyzed using SPSS 23.0 software. The measurement data is represented by the mean ± standard deviation, and the normality of the Shapiro-Wilk test is used. T test or analysis of variance was used for comparison between groups for normal distribution; the rank sum test was used for comparison between groups for abnormal distribution. The chi-square test was used to compare the count data between groups. $^*P < 0.05$, $^{**}P < 0.01$ indicates that the difference is statistically significant. The data are all obtained by more than three independent experiments. All statistical images are produced using GraphPad Prism version 8.0 software.

RESULTS

Determination of Infarct Volume

Both WT and *Plppr5*$^{-/-}$ mice showed obvious infarct on the left side of the brain 24 h after HIBD, and the infarct volume of *Plppr5*$^{-/-}$ mice was larger than WT mice (**Figures 2A,B**).

Determination of Seizure Threshold

Results show that mice in each group had seizures successively. No mice died in the WT group, two mice died in KO group and WT + HIBD group, respectively (mortality rate of 33.3%),

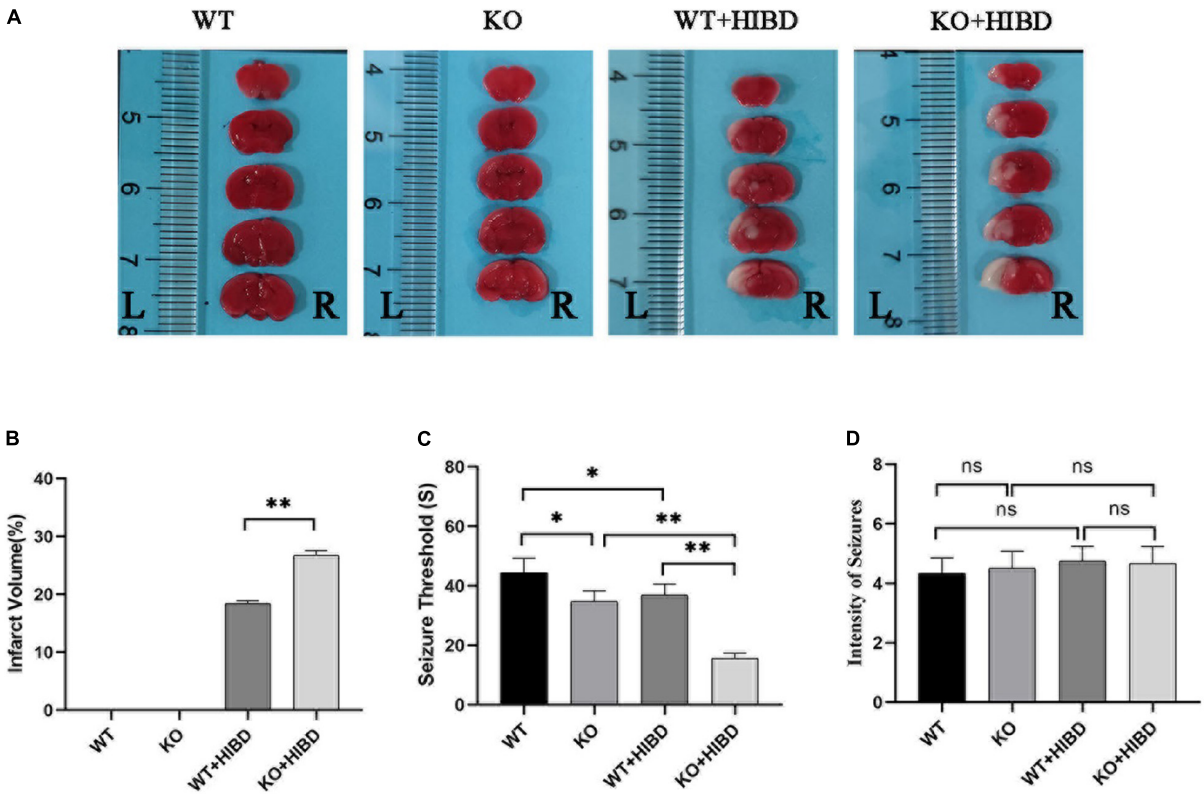

FIGURE 2 | TTC staining, penicillin-induced seizure threshold and intensity of seizure**. (A)** Results of TTC staining. **(B)** Results of infarct volume (*t* test, $n = 3$). **(C)** Seizure threshold (*t*-test, $n = 6$). **(D)** Intensity of seizure (Kruskal-Wallis, $n = 6$). Error bars represent mean ± SD. Ns, not significantly; $^{*}P < 0.05$; $^{**}P < 0.01$.

three mice died in KO + HIBD group (mortality rate of 50%). Fisher exact test (2 × C) showed that there was no significant difference in mortality among the four groups ($P = 0.392$). The seizure threshold of *Plppr5*$^{-/-}$ mice was significantly lower than that of WT mice ($P = 0.0102$), which shows that *Plppr5* knockout decreased the seizure threshold induced by penicillin in mice. After HIBD treatment, both WT mice and *Plppr5*$^{-/-}$ mice had a lower seizure threshold than the corresponding sham group ($P < 0.01$). Hypoxic-ischemic injury can also reduce the seizure threshold and *Plppr5*$^{-/-}$ mice were more likely to have convulsion ($P < 0.01$), *Plppr5* knockout can aggravate the lower degree of convulsion threshold induced by HIBD. However, there was no significant difference in the intensity of seizures among all groups ($P > 0.05$) (**Figures 2C,D**).

Timm Staining

As can be seen from the results of Timm staining, for WT mice, four weeks after HIBD, the mossy fiber sprouting (MFS) scores in bilateral hippocampus CA3 and DG were higher than the sham group ($P < 0.05$). For Plppr5$^{-/-}$ mice, four weeks after HIBD, the MFS scores in bilateral hippocampus DG were higher than the sham group ($P < 0.05$). Furthermore, the MFS scores in bilateral hippocampus CA3 were higher in KO + HIBD group than in WT + HIBD group (KO + HIBD vs. WT + HIBD, $P < 0.05$) (**Figure 3**).

Western Blot

Western blot results showed that the expression level of ZnT1 was significantly decreased in Plppr5$^{-/-}$ mice with sham treatment than WT mice ($P < 0.05$). And the expression level of ZnT1 in WT mice and Plppr5$^{-/-}$ mice four weeks after HIBD treatment were significantly higher than those in mice treated with sham operation ($P < 0.05$). Four weeks after HIBD treatment, Plppr5$^{-/-}$ mice had higher expression of ZnT1 than WT mice (KO + HIBD vs. WT + HIBD, $P < 0.05$) (**Figure 4A** and **Supplementary Figures 1S1,S2**). We found the same results at the cellular level (**Figure 4B** and **Supplementary Figures 1S3,S4**).

Measurement of Intracellular Zinc Ions Concentration

In Sh-*Plppr5* group, the intracellular free zinc content was significantly higher than those in Sh-control. OGD/R treatment can increase the intracellular free zinc in both groups. However, the content of intracellular free zinc in Sh-*Plppr5* + OGD/R group was higher than that in Sh-control + OGD/R group, but the difference was not statistically significant (**Figure 4C**).

Mitochondrial Reactive Oxygen Species Detection

Plppr5 knock out can significantly increase the content of ROS in HT22 cells (Sh-*Plppr5* vs. Sh-control, $P < 0.01$). Meanwhile, after

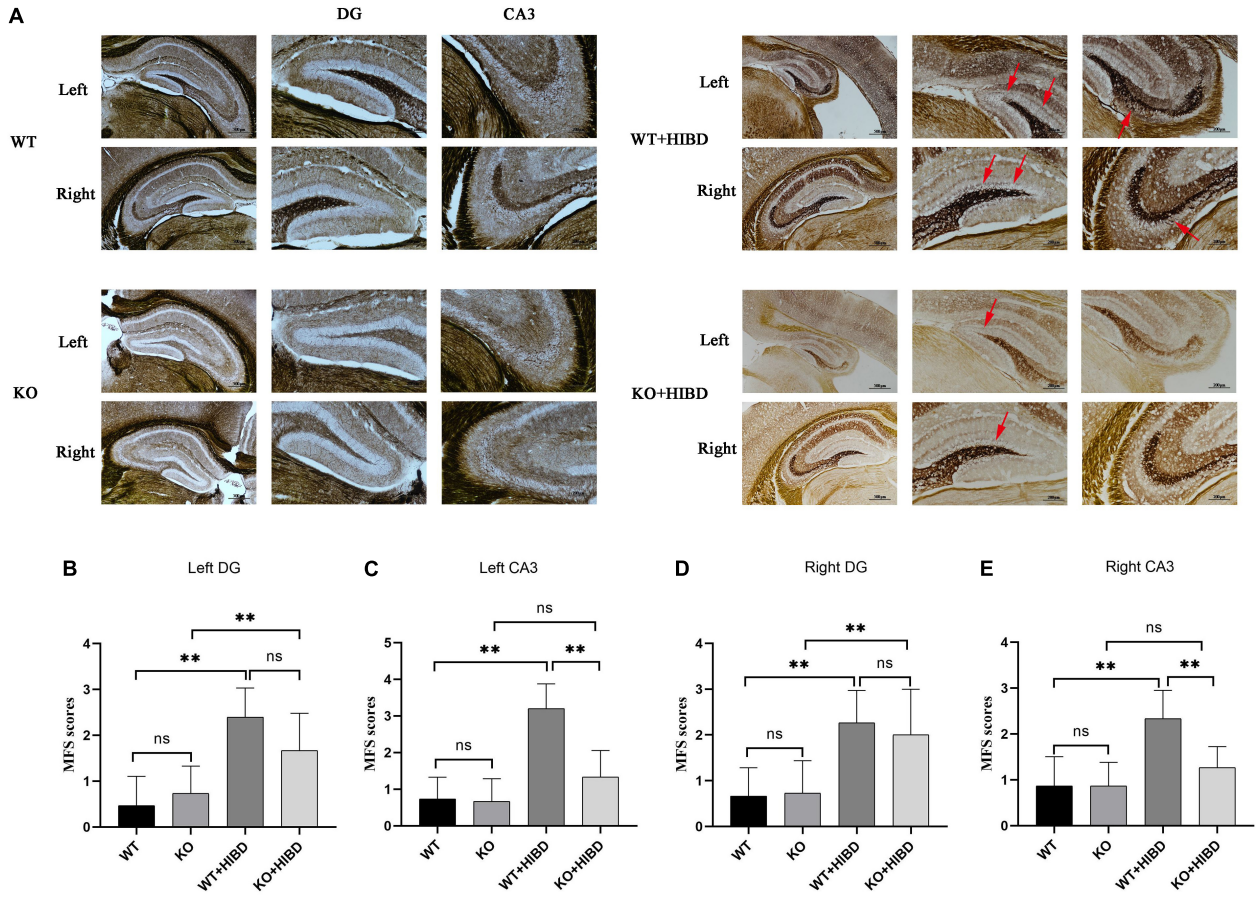

FIGURE 3 | Timm staining. **(A)** Timm staining results. **(B)** MFS scores in DG region of the left hippocampus. **(C)** MFS score in CA3 region of the left hippocampus. **(D)** MFS score in DG region of the right hippocampus. **(E)** MFS score in CA3 region of the right hippocampus. The arrows show where the moss fibers sprouting. Error bars represent mean ± SD. Ns, not significantly; $^{*}P < 0.05$; $^{**}P < 0.01$. (Kruskal-Wallis with Bonferroni *post hoc* tests, $n = 3$).

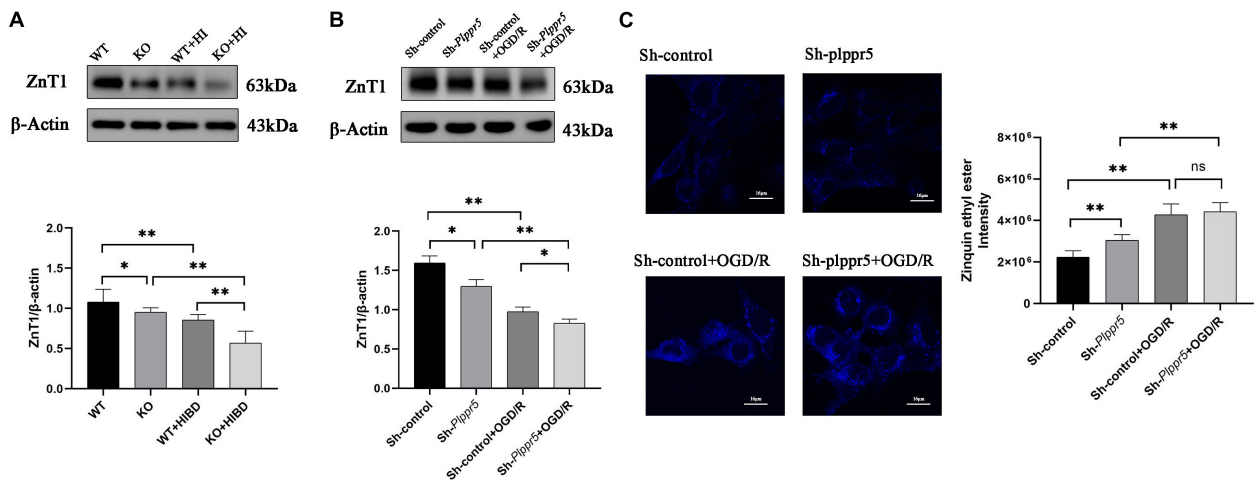

FIGURE 4 | Expression of ZnT1 in mice and HT22 cells and intracellular zinc ions concentration in HT22 cells. **(A)** Expression of ZnT1 in mice of each group; **(B)** Expression of ZnT1 in HT22 cells of each group; **(C)** Intracellular zinc ions concentration. Error bars represent mean ± SD, ns, not significantly; $^{*}P < 0.05$; $^{**}P < 0.01$ (*t*-test, $n = 3$).

OGD/R treatment, the content of ROS was significantly higher than that in the respective control group in Sh-*Plppr5* and Sh-control group ($P < 0.01$). What's more, after OGD/R treatment, the content in Sh-*Plppr5* group increased more significantly than that in Sh-control group (**Figure 5A**).

Detection of Mitochondrial Membrane Potential

The experimental results showed that the mitochondrial membrane potential of Sh-*Plppr5* group was significantly higher than that of Sh-control group. After OGD/R treatment, the mitochondrial membrane potential was significantly lower than that in the respective control group in Sh-*Plppr5* and Sh-control group. Furthermore, the decrease degree of Sh-*Plppr5* group after OGD/R was more obvious than that of Sh-control group (**Figure 5B**).

Biochemical Detection

Results showed that there was no statistical difference in MDA content between Sh-control group and Sh-*Plppr5* group ($P = 0.188$). However, OGD/R treatment can significantly increase the MDA content in both groups, especially in Sh-*Plppr5* group (**Figure 5C**, sh-control vs. sh-control + OGD/R, $P = 0.023$; sh-*Plppr5* vs. sh-*Plppr5* + OGD/R, $P = 0.0017$).

Knockdown of *Plppr5* decreased the activity of SOD. Compared with Sh-control group, SOD activity in Sh-*Plppr5* group was significantly decreased ($P = 0.0154$). Meanwhile, the SOD activity were decreased after OGD/R treatment in both groups and the decrease was more obvious in the Sh-*Plppr5* group (**Figure 5D**, sh-control vs. sh-control + OGD/R, $P = 0.022$; sh-*Plppr5* vs. sh-*Plppr5* + OGD/R, $P = 0.0013$).

DISCUSSION

In this study, we explored the long-term effects of *Plppr5* knockout on the seizure threshold, hippocampal MF regenerative sprouting, and ZnT1 protein expression after HIBD. In addition, by using an *in vitro* oxygen glucose deprivation reperfusion (OGD/R) HT22 cell model, we further analyzed the effects of knocking down *Plppr5* on mitochondrial function, mitochondrial oxidative stress levels, intracellular free zinc content and ZnT1 protein expression. We found that *Plppr5* knockout aggravated hypoxic-ischemic brain damage in mice. This damage effect may be mediated by hippocampal mitochondrial oxidative stress and zinc homeostasis signals. In summary, our data shows a previously unexplored mechanism that *Plppr5* exerts its neuroprotective effect after HIBD by maintaining zinc signal-mediated mitochondrial homeostasis.

Epilepsy is one of the common long-term sequelae of HIBD (Tekgul et al., 2006; Rafało-Ulińska et al., 2020). Basic research has also proved that HIBD in the neonatal period can induce long-term brain spontaneous EEG seizures (Hu et al., 2017). It was found that whether or not they have experienced neonatal hypoxic-ischemic injury, knocking out *Plppr5* can shorten the seizure latency. Specifically, the seizure latency of the two knockout groups was significantly lower than the corresponding control group (KO vs. WT; KO + HIBD vs. WT + HIBD). Since the decrease in the latency of seizure represents an increase in brain excitability, this result indicates that knocking out *Plppr5* can change the excitability of the brain, making animals more prone to seizures. Therefore, *Plppr5* is essential for maintaining the balance of brain excitability and inhibitory activity. We previously found that the reduction of the seizure threshold is related to the up-regulation of the expression of c-fos, a marker for the level of metabolic activity of hippocampal neurons (Sharp et al., 1993; Ni et al., 2005). Mitochondria are the key organelle for metabolic regulation. It has been demonstrated that phosphatidic acid can directly regulate the homeostasis of mitochondrial membrane potential. Pretreatment with autophagy inhibitor cyclosporin A can prevent phosphatidic acid-induced decline in mitochondrial membrane potential and neuronal apoptosis (Holtsberg et al., 1998). This may explain why PRG-1 regulates synaptic excitatory transmission through lipid phosphate-mediated signal transduction (Trimbuch et al., 2009). Therefore, it is reasonable to speculate that *Plppr5*, as a new type of phosphatidic acid phosphatase, may regulate the seizure threshold by regulating mitochondrial homeostasis of hippocampal neurons, which merit further investigation.

In order to further reveal the underlying molecular mechanism, we subsequently examined the expression of ZnT1 protein in the hippocampus by Western blot analysis. Interestingly, compared with the two corresponding sham operation control groups (WT, KO), the two hypoxic-ischemic injury groups (WT + HIBD, KO + HIBD) significantly reduced ZnT1 protein levels, while *Plppr5* gene knockout further down-regulated ZnT1 expression (KO + HIBD and WT + HIBD). It is worth noting that the expression of ZnT1 is also statistically different between the WT and KO groups, which mean that the expression trend of ZnT1 is completely consistent with the changes in seizure threshold. Therefore, it is reasonable to speculate that ZnT1 is related to the reduction of seizure latency caused by *Plppr5* gene knockout. In addition to the role of ZnT1 in transporting zinc from the intracellular to the extracellular space, ZnT1 is also critical to the integrity of the postsynaptic density (PSD) (Doboszewska et al., 2019). ZnT1 directly binds to the cytoplasmic tail of the GluN2A subunit of NMDAR at the PSD of hippocampal neurons and forms a new NMDAR binding protein (Popescu, 2015). Overexpression of zinc-sensitive ProSAP1/Shank2 or ProSAP2/Shank3 can lead to an increase in synaptic density, while the depletion of synaptic zinc, along with the knockdown of zinc-insensitive Shank1, which is insensitive to zinc, lead to the rapid disintegration of PSD and the loss of several postsynaptic molecules including the N-methyl-D-aspartate receptor (NMDAR) (Grabrucker et al., 2011). Therefore, it is reasonable to speculate that ZnT1 plays a more critical role in the long-term seizure threshold reduction caused by neonatal hypoxic-ischemic injury by regulating postsynaptic protein, which merit further investigation.

Interestingly, treatment of hippocampal HT22 neuron cultures silenced by *Plppr5*, with or without OGD/R treatment, markedly decreased the expression of mitochondrial ZnT1 protein. Furthermore, the silencing of *Plppr5* gene directly increased intracellular zinc ion levels, and reduced the

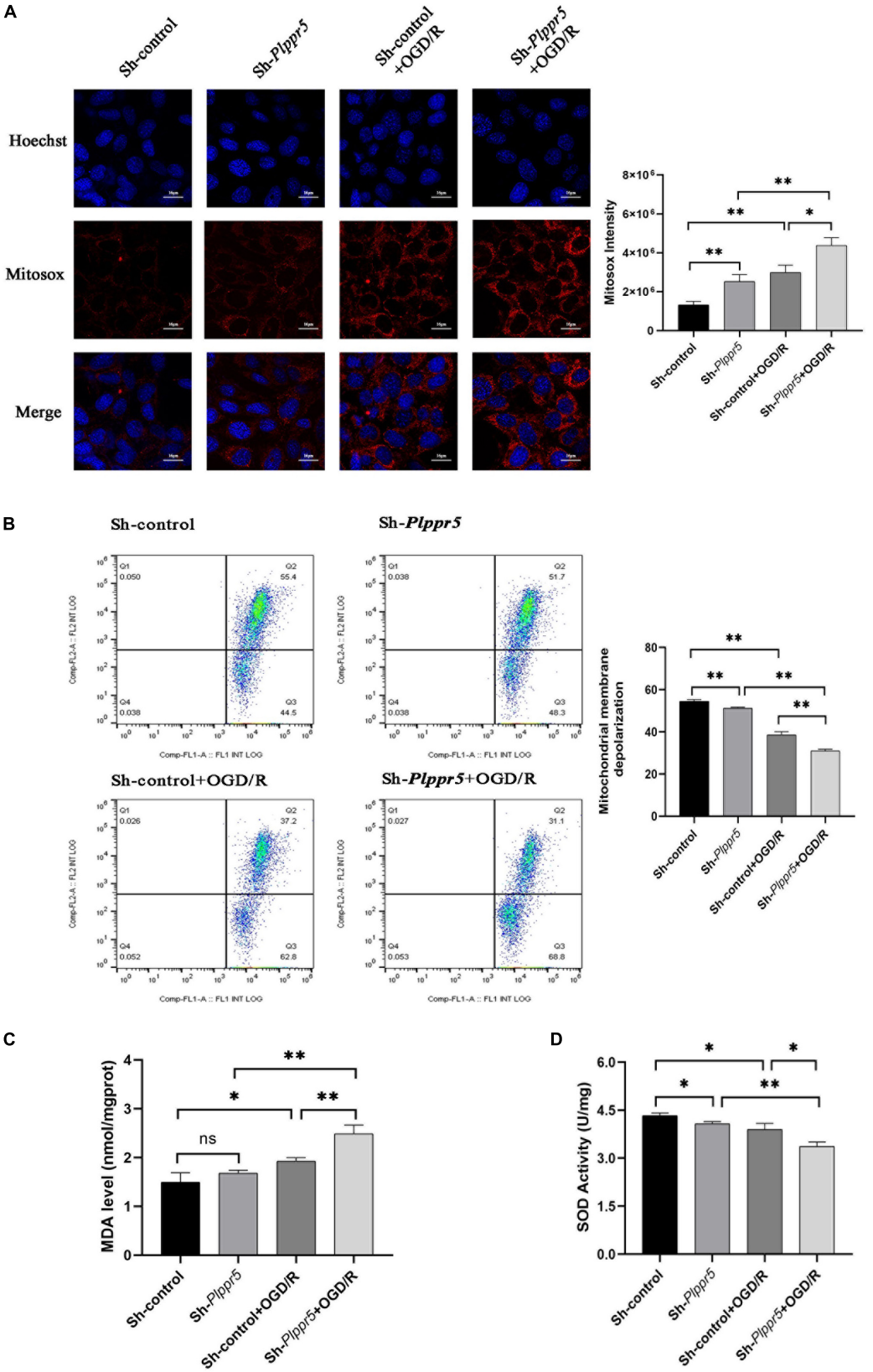

FIGURE 5 | MDA, SOD and ROS MMP levels measurement. **(A)** Mitochondrial ROS content determination and statistics (Red fluorescence: Mitosox; Blue fluorescence Hoechst); **(B)** MMP levels; **(C)** MDA level; **(D)** SOD activity. Error bars represent mean ± SD; ns, not significantly; $^{*}P < 0.05$; $^{**}P < 0.01$ (*t*-test, $n = 3$).

mitochondrial membrane potential. It has been shown that mitochondrial dysfunction-induced high-level release of labile Zn^{2+} from mitochondrial aggravates oxidative stress injury (Horn et al., 2013; Turan and Tuncay, 2021). Meanwhile, loss of enzymes involved in mitochondrial phospholipid biosynthesis can affect the assembly and stability of the mitochondrial protein import machinery and cause abnormal mitochondrial morphology or even lethality (Horvath and Daum, 2013). Combined with the notion that the anti-epileptic effect of ketone bodies is achieved through attenuating the production of mitochondrial reactive oxygen species (ROS) (Kim et al., 2015), thus, our finding, that *Plppr5* silencing leads to increased intracellular zinc ion content, and aggravates the damage of mitochondrial function, support the hypothesis that *Plppr5* knockout precipitates late-onset hypersusceptibility to penicillin-induced juvenile seizures by exacerbating hippocampal zinc signaling-mediated mitochondrial damage.

Here, we also analyzed the role of *Plppr5* in the abnormal sprouting of hippocampal mossy fibers in $Plppr5^{-/-}$ mice, and found that *Plppr5* gene knockout significantly reduced the MFS scores in the hippocampal CA3 area of wild-type mice after hypoxia-ischemia (KO + HIBD vs. WT + HIBD). In addition, compared with the WT + HIBD group, the MFS scores of the hippocampal dentate gyrus of the KO + HIBD group also decreased to a certain extent, suggesting that *Plppr5* gene knockout has a certain inhibitory effect on hippocampal granule cell axon regeneration. This is consistent with the study of Broggini et al. (2010). They found that *Plppr5* promoted the formation of neurites and filopodia of primary neurons, while *Plppr5* silencing weakened the formation and growth of neurites.

It should be pointed out that in this study we found that although $Plppr5^{-/-}$ mice had significantly lower MFS scores in hippocampal CA3 area after HIBD than WT mice, their seizure threshold was also lower than WT mice (KO + HIBD vs WT + HIBD). Sham-operated WT mice and $Plppr5^{-/-}$ mice also have the same phenomenon. This connection between hippocampal MFS and seizure threshold in $Plppr5^{-/-}$ mice is consistent with the recent view that MFS is an active phenomenon, possibly a normal adaptive mechanism that is reversible, which might be related to replacement or restoration of lost synaptic contacts, rather than to the formation of recurrent excitatory circuits in dentate granule cells (Buckmaster, 2014; Bittencourt et al., 2015; Yamawaki et al., 2015; Ni et al., 2019).

Taken together, our findings demonstrate for the first time that *Plppr5*-deficient mouse pups exposed to neuronal hypoxia and ischemia showed aggravated acute brain injury and long-term brain excitability compared with the same treated WT pups, which involves both zinc and mitochondrial-dependent metabolic pathways in the hippocampus. These data support further investigation into novel approaches to target trace element zinc-related mitochondrial homeostasis in neonatal HIE.

DATA AVAILABILITY STATEMENT

The original contributions presented in the study are included in the article/**Supplementary Material**, further inquiries can be directed to the corresponding author/s.

ETHICS STATEMENT

The animal study was reviewed and approved by the University of Soochow University Animal Care and Use Committee.

AUTHOR CONTRIBUTIONS

HN designed the study and wrote the manuscript. YS was the main operator analyzed the data. M-FJ, LL, YL, and DW were the operators of the experiment and were responsible for the statistical analysis of the data. All authors contributed to the article and approved the submitted version.

FUNDING

This work was supported by the National Natural Science Foundation of China (81871024 and 81471337), the key talent's subsidy project in science and education of Department of Public Health of Jiangsu Province (ZDRCC2016008), the Suzhou Science and Technology Development Plan(SYS2018079) and the Postgraduate Research & Practice Innovation Program of Jiangsu Province (KYCX20_ 2722).

SUPPLEMENTARY MATERIAL

The Supplementary Material for this article can be found online at: https://www.frontiersin.org/articles/10.3389/fnins.2022.751489/full#supplementary-material

Supplementary Figure 1 | Figures of Western Blot. **(S1)** Western blotting for the level of ZnT1 in mouse. **(S2)** Western blotting for the level of actin in mouse. **(S3)** Western blotting for the level of ZnT1 in HT22 cell. **(S4)** Western blotting for the level of actin in HT22 cell.

REFERENCES

Adebayo, O. L., Adenuga, G. A., and Sandhir, R. (2016). Selenium and zinc protect brain mitochondrial antioxidants and electron transport chain enzymes following postnatal protein malnutrition. *Life Sci.* 152, 145–155. doi: 10.1016/j.lfs.2016.03.008

Bittencourt, S., Covolan, L., Hamani, C., Longo, B. M., Faria, F. P., Freymuller, E., et al. (2015). Replacement of asymmetric synaptic profiles in the molecular layer of dentate gyrus following cycloheximide in the pilocarpine model in rats. *Front. Psychiatry* 6:157. doi: 10.3389/fpsyt.2015.00157

Bräuer, A. U., and Nitsch, R. (2008). Plasticity-related genes (PRGs/LRPs): a brain-specific class of lysophospholipid-modifying proteins. *Biochim. Biophys. Acta.* 1781, 595–600. doi: 10.1016/j.bbalip.2008.04.004

Broggini, T., Nitsch, R., and Savaskan, N. E. (2010). Plasticity-related gene 5 (PRG5) induces filopodia and neurite growth and impedes lysophosphatidic

acid- and nogo-A-mediated axonal retraction. *Mol. Biol. Cell.* 21, 521–537. doi: 10.1091/mbc.e09-06-0506

Buckmaster, P. S. (2014). Does mossy fiber sprouting give rise to the epileptic state. *Adv. Exp. Med. Biol.* 813, 161–168. doi: 10.1007/978-94-017-8914-1_13

Chen, B., Li, H., Ou, G., Ren, L., Yang, X., and Zeng, M. (2019). Curcumin attenuates MSU crystal-induced inflammation by inhibiting the degradation of IκBα and blocking mitochondrial damage. *Arthritis. Res. Ther.* 21:193. doi: 10.1186/s13075-019-1974-z

Dai, Y., Zhang, H., Zhang, J., and Yan, M. (2018). Isoquercetin attenuates oxidative stress and neuronal apoptosis after ischemia/reperfusion injury via Nrf2-mediated inhibition of the NOX4/ROS/NF-κB pathway. *Chem. Biol. Interact.* 284, 32–40. doi: 10.1016/j.cbi.2018.02.017

Doboszewska, U., Młyniec, K., Wlaź, A., Poleszak, E., Nowak, G., and Wlaź, P. (2019). Zinc signaling and epilepsy. *Pharmacol. Ther.* 193, 156–177. doi: 10.1016/j.pharmthera.2018.08.013

Gluckman, P. D., Wyatt, J. S., Azzopardi, D., Ballard, R., Edwards, A. D., Ferriero, D. M., et al. (2005). Selective head cooling with mild systemic hypothermia after neonatal encephalopathy: multicentre randomised trial. *Lancet* 365, 663–670.

Grabrucker, A. M., Knight, M. J., Proepper, C., Bockmann, J., Joubert, M., Rowan, M., et al. (2011). Concerted action of zinc and ProSAP/Shank in synaptogenesis and synapse maturation. *EMBO J.* 30, 569–581. doi: 10.1038/emboj.2010.336

Grabrucker, S., Jannetti, L., Eckert, M., Gaub, S., Chhabra, R., Pfaender, S., et al. (2014). Zinc deficiency dysregulates the synaptic ProSAP/Shank scaffold and might contribute to autism spectrum disorders. *Brain* 137(Pt 1), 137–152. doi: 10.1093/brain/awt303

Holmes, G. L., Sarkisian, M., Ben-Ari, Y., and Chevassus-Au-Louis, N. (1999). Mossy fiber sprouting after recurrent seizures during early development in rats. *J. Comp. Neurol.* 404, 537–553. doi: 10.1002/(sici)1096-9861(19990222)404:4\<537::aid-cne9\>3.0.co;2-\#

Holtsberg, F. W., Steiner, M. R., Keller, J. N., Mark, R. J., Mattson, M. P., and Steiner, S. M. (1998). Lysophosphatidic acid induces necrosis and apoptosis in hippocampal neurons. *J. Neurochem.* 70, 66–76. doi: 10.1046/j.1471-4159.1998.70010066.x

Horn, A. R., Swingler, G. H., Myer, L., Harrison, M. C., Linley, L. L., Nelson, C., et al. (2013). Defining hypoxic ischemic encephalopathy in newborn infants: benchmarking in a South African population. *J. Perinat. Med.* 41, 211–217. doi: 10.1515/jpm-2012-0107

Horvath, S. E., and Daum, G. (2013). Lipids of mitochondria. *Prog. Lipid. Res.* 52, 590–614.

Hsu, M., and Buzsáki, G. (1993). Vulnerability of mossy fiber targets in the rat hippocampus to forebrain ischemia. *J. Neurosci.* 13, 3964–3979. doi: 10.1523/JNEUROSCI.13-09-03964.1993

Hu, J. J., Yang, X. L., Luo, W. D., Han, S., Yin, J., Liu, W. H., et al. (2017). Bumetanide reduce the seizure susceptibility induced by pentylenetetrazol via inhibition of aberrant hippocampal neurogenesis in neonatal rats after hypoxia-ischemia. *Brain Res. Bull.* 130, 188–199. doi: 10.1016/j.brainresbull.2017.01.022

Jin, M. F., Ni, H., and Li, L. L. (2018). Leptin maintained zinc homeostasis against glutamate-induced excitotoxicity by preventing mitophagy-mediated mitochondrial activation in HT22 Hippocampal Neuronal Cells. *Front. Neurol.* 9:322. doi: 10.3389/fneur.2018.00322

Kim, D. Y., Simeone, K. A., Simeone, T. A., Pandya, J. D., Wilke, J. C., Ahn, Y., et al. (2015). Ketone bodies mediate antiseizure effects through mitochondrial permeability transition. *Ann. Neurol.* 78, 77–87. doi: 10.1002/ana.24424

Martínez-Orgado, J., Villa, M., and Del Pozo, A. (2020). Cannabidiol for the Treatment of Neonatal Hypoxic-Ischemic Brain Injury. *Front. Pharmacol.* 11:584533. doi: 10.3389/fphar.2020.584533

Mitra, S., Bale, G., Mathieson, S., Uria-Avellanal, C., Meek, J., Tachtsidis, I., et al. (2016). Changes in cerebral oxidative metabolism during neonatal seizures following hypoxic-ischemic brain injury. *Front. Pediatr.* 4:83. doi: 10.3389/fped.2016.00083

Ni, H., Jiang, Y. W., Bo, T., Wang, J. M., and Wu, X. R. (2005). c-Fos, N-methyl-d-aspartate receptor 2C, GABA-A-alpha1 immonoreactivity, seizure latency and neuronal injury following single or recurrent neonatal seizures in hippocampus of Wistar rat. *Neurosci. Lett.* 380, 149–154. doi: 10.1016/j.neulet.2005.01.043

Ni, H., Jiang, Y. W., Tao, L. Y., Cen, J. N., and Wu, X. R. (2009a). Effects of penicillin-induced developmental epilepticus on hippocampal regenerative sprouting, related gene expression and cognitive deficits in rats. *Toxicol. Lett.* 188, 161–166. doi: 10.1016/j.toxlet.2009.04.002

Ni, H., Jiang, Y. W., Tao, L. Y., Jin, M. F., and Wu, X. R. (2009b). ZnT-1, ZnT-3, CaMK II, PRG-1 expressions in hippocampus following neonatal seizure-induced cognitive deficit in rats. *Toxicol. Lett.* 184, 145–150. doi: 10.1016/j.toxlet.2008.11.003

Ni, H., Kirschstein, T., Norwood, B. A., and Hsieh, C. L. (2019). Editorial: the developmental seizure-induced hippocampal mossy fiber sprouting: target for epilepsy therapies. *Front. Neurol.* 10:1212. doi: 10.3389/fneur.2019.01212

Omur, A. D., Yildirim, B., Saglam, Y. S., Comakli, S., and Ozkaraca, M. (2019). Activity of resveratrol on the influence of aflatoxin B1 on the testes of Sprague dawley rats. *Pol. J. Vet. Sci.* 22, 313–320. doi: 10.24425/pjvs.2019.129222

Peeva, G. P., Angelova, S. K., Guntinas-Lichius, O., Streppel, M., Irintchev, A., Schütz, U., et al. (2006). Improved outcome of facial nerve repair in rats is associated with enhanced regenerative response of motoneurons and augmented neocortical plasticity. *Eur. J. Neurosci.* 24, 2152–2162. doi: 10.1111/j.1460-9568.2006.05091.x

Pitkänen, A., and Lukasiuk, K. (2009). Molecular and cellular basis of epileptogenesis in symptomatic epilepsy. *Epilepsy. Behav.* 14, 16–25. doi: 10.1016/j.yebeh.2008.09.023

Popescu, G. K. (2015). Zinc transporter found attached to N-methyl-D-aspartate receptors. *J. Neurochem.* 132, 155–158. doi: 10.1111/jnc.13014

Racine, R. J. (1972). Modification of seizure activity by electrical stimulation. II. Motor seizure. *Electroencephalogr. Clin. Neurophysiol.* 32, 281–294. doi: 10.1016/0013-4694(72)90177-0

Rafalo-Ulinska, A., Piotrowska, J., Kryczyk, A., Opoka, W., Sowa-Kucma, M., Misztak, P., et al. (2016). Zinc transporters protein level in postmortem brain of depressed subjects and suicide victims. *J. Psychiatr. Res.* 83, 220–229. doi: 10.1016/j.jpsychires.2016.09.008

Rafało-Ulińska, A., Poleszak, E., Szopa, A., Serefko, A., Rogowska, M., Sowa, I., et al. (2020). Imipramine influences body distribution of supplemental zinc which may enhance antidepressant action. *Nutrients* 12:9. doi: 10.3390/nu12092529

Rakhade, S. N., and Jensen, F. E. (2009). Epileptogenesis in the immature brain: emerging mechanisms. *Nat. Rev. Neurol.* 5, 380–391. doi: 10.1038/nrneurol.2009.80

Rice, J. E. III, Vannucci, R. C., and Brierley, J. B. (1981). The influence of immaturity on hypoxic-ischemic brain damage in the rat. *Ann. Neurol.* 9, 131–141. doi: 10.1002/ana.410090206

Roelofs, B. A., Ge, S. X., Studlack, P. E., and Polster, B. M. (2015). Low micromolar concentrations of the superoxide probe MitoSOX uncouple neural mitochondria and inhibit complex IV. *Free Radic. Biol. Med.* 86, 250–258. doi: 10.1016/j.freeradbiomed.2015.05.032

Sharp, F. R., Sagar, S. M., and Swanson, R. A. (1993). Metabolic mapping with cellular resolution: c-fos vs. 2-deoxyglucose. *Crit. Rev. Neurobiol.* 7, 205–228.

Sigal, Y. J., Quintero, O. A., Cheney, R. E., and Morris, A. J. (2007). Cdc42 and ARP2/3-independent regulation of filopodia by an integral membrane lipid-phosphatase-related protein. *J. Cell Sci.* 120(Pt 2), 340–352. doi: 10.1242/jcs.03335

Sun, Y., Ma, L., Jin, M., Zheng, Y., Wang, D., and Ni, H. (2021). Effects of melatonin on neurobehavior and cognition in a cerebral palsy model of plppr5-/- Mice. *Front. Endocrinol.* 12:598788. doi: 10.3389/fendo.2021.598788

Tang, X., and Brindley, D. N. (2020). Lipid phosphate phosphatases and cancer. *Biomolecules* 10:9.

Tekgul, H., Gauvreau, K., Soul, J., Murphy, L., Robertson, R., Stewart, J., et al. (2006). The current etiologic profile and neurodevelopmental outcome of seizures in term newborn infants. *Pediatrics* 117, 1270–1280. doi: 10.1542/peds.2005-1178

Trimbuch, T., Beed, P., Vogt, J., Schuchmann, S., Maier, N., Kintscher, M., et al. (2009). Synaptic PRG-1 modulates excitatory transmission via lipid phosphate-mediated signaling. *Cell* 138, 1222–1235. doi: 10.1016/j.cell.2009.06.050

Turan, B., and Tuncay, E. (2021). The role of labile Zn(2+) and Zn(2+)-transporters in the pathophysiology of mitochondria dysfunction in cardiomyocytes. *Mol. Cell Biochem.* 476, 971–989. doi: 10.1007/s11010-020-03964-8

Wang, Y., Tu, L., Li, Y., Chen, D., and Wang, S. (2016). Notoginsenoside R1 Protects against neonatal cerebral hypoxic-ischemic injury through estrogen receptor-dependent activation of endoplasmic reticulum stress pathways. *J. Pharmacol. Exp. Ther.* 357, 591–605. doi: 10.1124/jpet.115.230359

Wei, W., Liu, Y., Zhang, Q., Wang, Y., Zhang, X., and Zhang, H. (2017). Danshen-enhanced cardioprotective effect of cardioplegia on ischemia reperfusion injury in a human-induced pluripotent stem cell-derived cardiomyocytes model. *Artif Organs.* 41, 452–460. doi: 10.1111/aor.12801

Wiqas, A., LeSauter, J., Taub, A., Austin, R. N., and Silver, R. (2020). Elevated zinc transporter ZnT3 in the dentate gyrus of mast cell-deficient mice. *Eur. J. Neurosci.* 51, 1504–1513. doi: 10.1111/ejn.14575

Wong, R., Abussaud, A., Leung, J. W., Xu, B. F., Li, F. Y., Huang, S., et al. (2018). Blockade of the swelling-induced chloride current attenuates the mouse neonatal hypoxic-ischemic brain injury in vivo. *Acta Pharmacol. Sin.* 39, 858–865. doi: 10.1038/aps.2018.1

Yamawaki, R., Thind, K., and Buckmaster, P. S. (2015). Blockade of excitatory synaptogenesis with proximal dendrites of dentate granule cells following rapamycin treatment in a mouse model of temporal lobe epilepsy. *J. Comp. Neurol.* 523, 281–297. doi: 10.1002/cne.23681

Yan, X., Yu, A., Zheng, H., Wang, S., He, Y., and Wang, L. (2019). Calycosin-7-O-β-D-glucoside Attenuates OGD/R-induced damage by preventing oxidative stress and neuronal apoptosis via the SIRT1/FOXO1/PGC-1α Pathway in HT22 Cells. *Neural. Plast.* 2019:8798069. doi: 10.1155/2019/8798069

Yang, Y., Jing, X. P., Zhang, S. P., Gu, R. X., Tang, F. X., Wang, X. L., et al. (2013). High dose zinc supplementation induces hippocampal zinc deficiency and memory impairment with inhibition of BDNF signaling. *PLoS One* 8:e55384. doi: 10.1371/journal.pone.0055384

Conflict of Interest: The authors declare that the research was conducted in the absence of any commercial or financial relationships that could be construed as a potential conflict of interest.

Publisher's Note: All claims expressed in this article are solely those of the authors and do not necessarily represent those of their affiliated organizations, or those of the publisher, the editors and the reviewers. Any product that may be evaluated in this article, or claim that may be made by its manufacturer, is not guaranteed or endorsed by the publisher.

frontiers in Neuroscience

ORIGINAL RESEARCH
published: 25 March 2022
doi: 10.3389/fnins.2022.838942

The Changes of Amygdala Transcriptome in Autism Rat Model After Arginine Vasopressin Treatment

Bo Zhou[1,2,3†], Xiaoli Zheng[1,2,3†], Yunhua Chen[4], Xuehui Yan[1,2,3], Jinggang Peng[1,2,3], Yibu Liu[1,2,3], Yi Zhang[1,2,3], Lei Tang[1,2,3] and Min Wen[1,2,3*]*

[1] State Key Laboratory of Functions and Applications of Medicinal Plants, Guizhou Medical University, Guiyang, China, [2] Guizhou Provincial Engineering Technology Research Center for Chemical Drug R&D, Guizhou Medical University, Guiyang, China, [3] College of Pharmacy, Guizhou Medical University, Guiyang, China, [4] College of Basic Medical, Guizhou Medical University, Guiyang, China

OPEN ACCESS

Edited by:
Atsushi Yoshiki, RIKEN BioResource Research Center (BRC), Japan

Reviewed by:
Hidenori Tabata, Aichi Human Service Center, Japan
Mladen-Roko Rasin, Rutgers, The State University of New Jersey, United States

***Correspondence:**
Lei Tang
tlei1974@hotmail.com
Min Wen
670418077@qq.com

† These authors have contributed equally to this work

Specialty section:
This article was submitted to Neurodevelopment, a section of the journal Frontiers in Neuroscience

Received: *18 December 2021*
Accepted: *31 January 2022*
Published: *25 March 2022*

Citation:
Zhou B, Zheng X, Chen Y, Yan X, Peng J, Liu Y, Zhang Y, Tang L and Wen M (2022) The Changes of Amygdala Transcriptome in Autism Rat Model After Arginine Vasopressin Treatment. Front. Neurosci. 16:838942. doi: 10.3389/fnins.2022.838942

Background: Some studies have shown that arginine vasopressin (AVP) can significantly improve the social interaction disorder of autism, but the mechanism remains unclear.

Methods: Female Wistar rats were intraperitoneally injected with VPA or normal saline at embryonic day 12.5 to establish an autism model or normal control in their offspring. Male offspring prenatally exposed to VPA were randomly assigned to two groups: the VPA-induced autism model group and the AVP group. The rats in the AVP group were treated with intranasal AVP at postnatal day (PND) 21 and for 3 weeks. The VPA-induced autism model group was given the same dose of normal saline in the same way. Behavioral responses were evaluated in the open field and three-chambered social test apparatus; the expression levels of AVP in serum were detected by enzyme-linked immunosorbent assay kit, and the gene expression levels on the amygdala were measured by RNA-seq at PND42.

Results: Intranasal administration of AVP can significantly improve the social interaction disorder and elevate the levels of AVP in serum. Transcriptome sequencing results showed that 518 differently expressed genes (DEGs) were identified in the VPA-induced autism model group compared with the control in this study. Gene Ontology biological process enrichment analysis of DEGs showed that the VPA-induced autism model group had significant nervous system developmental impairments compared with the normal group, particularly in gliogenesis, glial cell differentiation, and oligodendrocyte differentiation. Gene Set Enrichment Analysis (GSEA) enrichment analysis also showed that biological process of oligodendrocyte differentiation, axoneme assembly, and axon ensheathment were inhibited in the VPA-induced autism model group. Pathway enrichment analysis of DEGs between the control and VPA-induced autism model group showed that the PI3K/AKT and Wnt pathways were significantly dysregulated in the VPA-induced autism model group. Few DEGs were found when compared with the transcriptome between the VPA-induced autism model group and the AVP treatment group. GSEA enrichment analysis showed deficits in oligodendrocyte development and

function were significantly improved after AVP treatment; the pathways were mainly enriched in the NOTCH, mitogen-activated protein kinase, and focal adhesion signaling pathways, but not in the PI3K/AKT and Wnt pathways. The expression patterns analysis also showed the same results.

Conclusion: AVP can significantly improve the social interaction disorder of VPA-induced autism model, and AVP may target behavioral symptoms in autism by modulating the vasopressin pathways, rather than primary disease mechanisms.

Keywords: autism spectrum disorder, neurodevelopmental, arginine vasopressin, amygdala, oligodendrocyte

INTRODUCTION

Autism spectrum disorder (ASD) is a complex neurodevelopmental disorder primarily characterized by deficits in social interaction and communication as well as repetitive and stereotypic behavior. The current prevalence rate of ASD is 14.7 per 1,000 children in the United States (Christensen et al., 2016) and 7 per 1,000 in China (Zhou et al., 2020). It is more prevalent in males than in females, with reported ratios ranging from 2:1 to 5:1 (Lord et al., 2020). Although many researches have been carried out, the precise molecular mechanisms of ASD are still not fully elucidated, and no medications are currently approved for ameliorating ASD's core social behavior deficits.

Arginine vasopressin (AVP) is a neuropeptide hormone synthesized and secreted by separate neuronal populations in the paraventricular nucleus (PVN) of the hypothalamic (Benarroch, 2013; Sparapani et al., 2021). It has been known for several decades that AVP plays a critical role in promoting the formation of complex mammalian social behavior such as social cognition, social recognition, social exploration, and preference by acting on AVP receptors which mainly located in hippocampus, amygdala, striatum, and other "social brains." In recent years, a growing number of scientific reports have shown that AVP is a crucial factor in neurodevelopmental disorders, including the ASD. Oztan et al. (2018, 2020) (Parker et al., 2018) find that children with ASD have lower cerebrospinal fluid (CSF) AVP concentrations compared with control children and that patients with ASD with the lowest CSF AVP concentrations have the most severe symptoms. Zhang H. F. et al. (2016) find that the plasma AVP levels were associated with repetitive behavior, and ASD children with higher plasma AVP levels tended to have lower levels of repetitive. In addition, lots of researches have shown that correction of vasopressin deficit may ameliorate social deficits of autism (Borie et al., 2021). Parker et al. (2019) presented the safety and efficacy of 4 weeks' intranasal AVP administration to improve social abilities in children with ASD using a double-blind, randomized, placebo-controlled trial design. Wu et al. (2021) studies have shown that infant rats exposed to VPA showed obviously impaired communication and repetitive behaviors with reduced number of AVP-immunoreactive cells in PVN and content of AVP in CSF. The postnatal subcutaneous injection of AVP can alleviate social preference deficits and stereotyped behaviors, accompanied with the increase in AVP concentrations in the CSF. Clearly, AVP signaling pathway may be a promising therapeutic target for autism. Today, the AVP has already entered phase II clinical trials (NCT01962870, NCT03204786) for the treatment of autism. Although intranasally administered AVP will observably achieve behavioral effects, the precise central mechanisms remain elusive.

To explore the potential for AVP as a treatment for autism and to further explore their mechanisms of action, we compared the amygdala transcriptome changes before and after AVP treatment in VPA-induced autism rat model.

MATERIALS AND METHODS

Materials

Chemicals

Valproic acid sodium salt (P4543-10G) was purchased from Sigma-Aldrich Co. (St. Louis, MO, United States). Argipressin (AVP, HY-P0049) was purchased from MedChemExpress. RAT AVP enzyme-linked immunosorbent assay (ELISA) KIT (55R-1951) was purchased from Fitzgerald (United States).

Animals

Male and female Wistar rats weighing 270–290 g were obtained from the Department of Experimental Animal Center of Guizhou Medical University. Animals were housed individually with water and chow freely available under a regulated environment (23°C ± 2°C; 50% ± 10% humidity) with a 12/12-h light–dark cycle. All experiments were approved by the Guizhou Medical University Animal Care and Use Committee.

Methods

Animal Model

As previously described (Schneider and Przewlocki, 2005; Dai et al., 2018), female and male rats were allowed to mate overnight, and the morning when spermatozoa were found was designated as embryonic day 0.5 (E0.5). The pregnant rats were randomly distributed into two groups: VPA group ($n = 10$) and saline group ($n = 5$). On E12.5, rats in the VPA group were intraperitoneally injected with sodium valproate (dose of 600 mg/kg, 250 mg/mL dissolved in physiological saline); the saline groups received the same volume of normal saline at the same time. The day of birth of the offspring was marked as postnatal day 1 (PND1). After weaning at PND21, offspring of the same sex were housed separately, with four to five per cage. To assess the treatment effects of AVP, the offspring of VPA group were randomly divided

FIGURE 1 | Schematic representation of the experimental procedure.

into two groups: VPA-induced autism model groups ($n = 10$) and AVP treatment group ($n = 10$). AVP treatment group received a daily intranasal of AVP (dose of 400 μg/kg, 2.5 mg/mL dissolved in NS) from PND21 to PND42. The offspring of saline groups were marked as control group. The control groups and the VPA-induced autism model group were given the same amount of saline. All experiments were carried out on male offspring. The experimental procedure is shown in **Figure 1**.

Development and Behavioral Tests

Open Eyes Test

To examine the maturation process in the pups, we monitored eye opening status from PND12–16 once daily and scored as follows: 0 = both eyes closed, 1 = one eye open, and 2 = both eyes open.

Swimming Performance

The swimming test measures motor development and integration of coordinated series of reflex responses (Schneider and Przewlocki, 2005). It was conducted on PND8, PND10, PND12, PND14, and PND16. Each animal was put at the center of an container filled with water (28–29°C) and was observed for 5–10 s. Swimming performance was scored as follows: 0 = head and nose below the surface; 1 = nose below the surface; 2 = nose and top of head at or above the surface, but ears still below the surface; 3 = the same as in 2 except that water line was at mid-ear level; and 4 = the same as in 3 except that water line was at the bottom of ears.

Open Field Test

To test for generalized anxiety, the open field test was used at PND42. The tested rat was placed in the center of a squared open field box (80 cm L × 80 cm W × 40 cm H) and allowed to explore freely for 5 min. Locomotion trajectory of the rat was automatically detected and was recorded, and the percentage of the time spent in the central zone in 5 min was calculated.

Three-Chamber Test

The three-chamber test was performed at PND42 as previously described (Rein et al., 2020). A polyvinyl chloride box was divided in three compartments (each chamber is 40 cm L × 40 cm W × 40 cm H), and both side compartments contained an empty perforated cup. First, the tested mouse was allowed to explore freely the whole setting, with all doors open for 10 min (phase 1). After this habituation period, the mouse was restricted in the central compartment, whereas an unfamiliar rat of the same sex (stranger 1) was placed under one of the cups (sides alternated between each rat). The tested mouse was then allowed to explore the whole apparatus for 10 min (phase 2). After that, it was restricted to the central compartment, whereas another unfamiliar rat of the same sex (stranger 2) was placed under the other cup. The tested mouse could then again freely explore the whole apparatus for 10 min (phase 3). In all three phases, time spent in each compartment was manually recorded, and the social preference indexes (Rein et al., 2020) were calculated as follows: social preference indexes = (TS − TNS)/(TS + TNS); TS, social stimulus, the interaction time with strange 1 in phase 2 and the interaction time with strange 2 in phase 3; TNS, non-social stimulus, the interaction time in empty in phase 2 and the interaction time with strange 1 in phase 3. To minimize the impact from residual rat odors, the entire apparatus was thoroughly cleaned with 70% ethanol at the beginning of each trial.

Self-Grooming Test

The procedure of self-grooming was acquired as described previously, to assess the repetitive behavior at PND42 (Mahmood et al., 2020). In brief, a standard cage of the rat was used to measure repetitive behavior in the self-grooming test. The dimensions of cages were 25 cm wide, 45 cm long, and 20 cm high. After a 5-min habituation in the cage, the cumulative grooming time spent for all body parts of each mouse was calculated by using a stopwatch for 5 min.

The Expression Levels of Arginine Vasopressin in Serum

Arginine vasopressin content in the serum was assayed using a commercially available ELISA kit (Fitzgerald, 55R-1951).

RNA-seq

Sampling and RNA Isolation

Rats were decapitated, and the amygdala was quickly dissected and frozen in liquid nitrogen for 2 h. The frozen amygdalae were stored at −80°C until used. Total RNA was extracted and purified using TRIzol reagent (Invitrogen, Carlsbad, CA, United States) following the manufacturer's procedure. The RNA concentration and purity of each sample were quantified using NanoDrop ND-1000 (NanoDrop, Wilmington, DE, United States). RNA quality was measured by Bioanalyzer 2100 (Agilent, Santa Clara, CA, United States). All RNA samples included in the expression analysis had an A260/A280 absorbance ratio greater than 1.8 and RNA integrity number > 7.0.

RNA-seq

An RNA-seq library of each sample was prepared, and 2 × 150-bp paired-end sequencing (PE150) was performed on an Illumina Novaseq^{TM} 6000 (LC-Bio Technology Co., Ltd., Hangzhou, China) following the vendor's recommended protocol.

TABLE 1 | Primer sequences.

Gene	Primer	Sequence (5′–3′)	Polymerase chain reaction products
Rat GAPDH	Forward	ACAGCAACAGGGTGGTGGAC	253 bp
	Reverse	TTTGAGGGTGCAGCGAACTT	
Rat Olig2	Forward	TGAAGAGACTGGTGAGCGAG	165 bp
	Reverse	GAGGGAGGATGGGGTGATG	
Rat SOX10	Forward	GCAGACGATGACAAGTTCCC	189 bp
	Reverse	CTGGTCGGCTAACTTTCTGC	
Rat MBP	Forward	ATGTGTTTGGGGAGGCAGAT	233 bp
	Reverse	TTGGATGGTCTGAAGCTCGT	

Sequence Analysis

Raw data files in FASTQ format were generated from the Illumina Novaseq^{TM} 6000. The reads after quality control and preprocessing were aligned to the reference genome (rattus_norvegicus6.0, v101) using the HISAT2 (Kim et al., 2019) and gene expression quantified using HTSEQ (Anders et al., 2015). The differentially expressed genes (DEGs) were selected with fold changes (FCs) > 1.3 and with statistical significance [false discovery rate (FDR) < 0.05] by DESeq2 (Love et al., 2014); the Gene Ontology (GO) enrichment and Kyoto Encyclopedia of Genes and Genomes (KEGG) enrichment of the DEGs were analyzed using clusterProfiler (Yu et al., 2012). Gene Set Enrichment Analysis (GSEA) was performed to identify the sets of related genes that might be systematically altered in each group by GSEA V4.1.0 (Mootha et al., 2003; Subramanian et al., 2005). The biological process (c5.go.bp.v7.4) and KEGG term (c2.cp.kegg.v7.4) were annotated by Molecular Signatures Database v7.4 (Liberzon et al., 2011, 2015). The significantly enriched gene sets were selected with |NES|>1 (Normalized enrichment score) and with NOM $p < 0.05$ (Nominal p-value). Soft clustering was performed using Mfuzz (Kumar and Futschik, 2007) to mine the expression patterns of genes in three groups. In the clustering analysis, the optimal cluster number was calculated using default parameters. Meanwhile, the min score (membership) threshold was set to 0.6. Each cluster was subsequent functional annotation analysis using the online tool g:Profiler[1] (Raudvere et al., 2019).

Quantitative Reverse Transcription–Polymerase Chain Reaction Confirmation

Total RNA from amygdala was extracted utilizing TRIzol reagent (Invitrogen) and reverse transcribed to cDNA using the Thermo Scientific Revert Aid First Strand cDNA Synthesis Kit (Thermo Fisher Scientific Inc., Waltham, MA, United States). Relative expression level of target mRNA was normalized to GAPDH, and relative expression ratio of a target gene was calculated using the mRNA by the $2^{-\Delta\Delta CT}$ method (Livak and Schmittgen, 2001). The primer sequences used are listed in **Table 1**.

Statistical Analysis

All data are represented as the mean ± SD. Statistical analysis of multiple-group comparisons was performed by one-way analysis of variance, and two-group comparisons were analyzed by the two-tailed Student t test using STATA 14.0 (StataCorp, College Station, TX, United States). Statistical significance was set at $p < 0.05$.

[1]https://biit.cs.ut.ee/gprofiler/gost

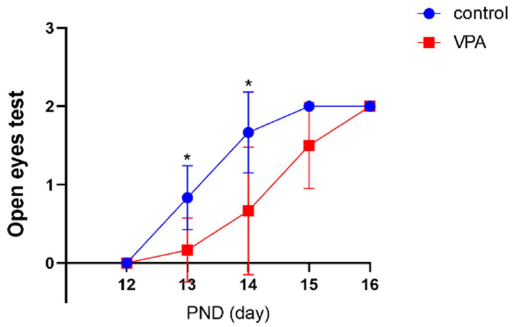

FIGURE 2 | Eye opening test in each group (n = 6 in each group). The eye opening score was significantly delayed in the VPA group on PNDs 13 and 14. Compared with the control group: *$p < 0.05$.

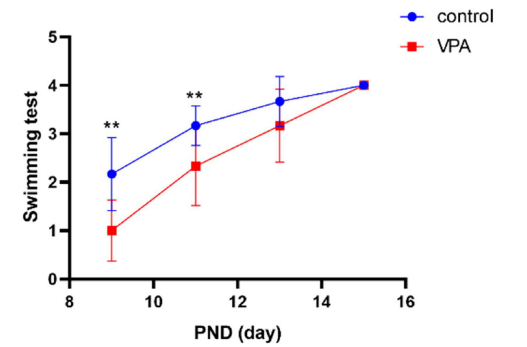

FIGURE 3 | Swimming test in each group (n = 6 in each group). The swimming score was significantly delayed in the VPA group on PND9 and PND11. Compared with the control group: **$p < 0.01$.

RESULTS

Development and Behavioral Tests

Eye Opening

The eye opening scores between the two groups were significantly different on PND13 ($p < 0.05$) and PND14 ($p < 0.05$) with significantly lower eye opening score in the VPA group. On PND12, PND15, and PND16, the eye opening score was similar, and no statistically significant difference was seen between the two groups (**Figure 2**). The results indicate that VPA may significantly delay the maturation of rats.

Swimming Performance

Compared with the control group, the ontogeny of swimming behavior was significantly delayed in VPA rats on PND9 ($p < 0.01$) and PND11 ($p < 0.01$), and no significant differences were found on PND13 and PND15 (**Figure 3**). The results

indicate that VPA may significantly delay motor development and attenuate integration of coordinated series of reflexes.

Open Field Test

When compared with the control group, the anxiety-like behavior was significantly enhanced (it spent more time staying in the edge and corner and less time in the central zone than did the control group) in the VPA-induced autism model group ($p < 0.01$), and the anxiety-like behavior was significantly decreased after the treatment with AVP ($p < 0.01$; **Figure 4**).

Three-Chamber Test

In social preference test (phase2), each group rats spent more time in the side with stranger 1 than in the empty cage ($p < 0.01$). The time in the side with stranger 1 were significantly lower in the VPA-induced autism model group than control ($p < 0.01$) and

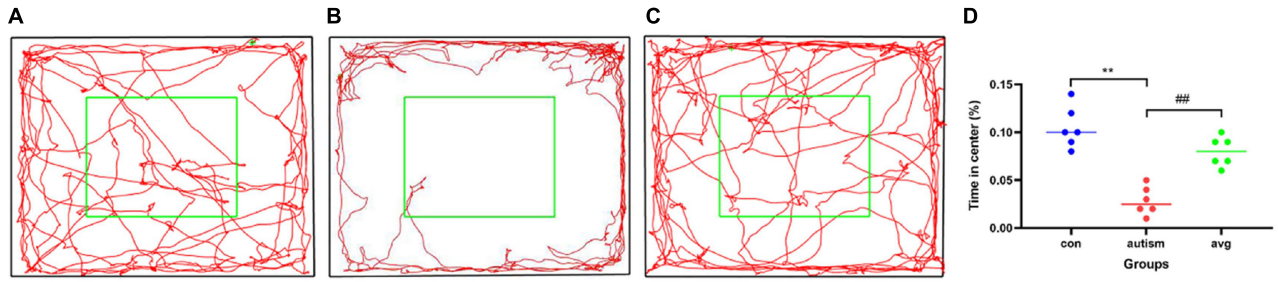

FIGURE 4 | Open field test ($n = 6$ in each group). **(A)** locomotion trajectory of control group, **(B)** locomotion trajectory of VPA-induced autism model group, **(C)** locomotion trajectory of AVP group, **(D)** compare the time spend in center in each group. Compared with the control group: $^{**}p < 0.01$; compared with the VPA-induced autism model group: $\#\#p < 0.01$.

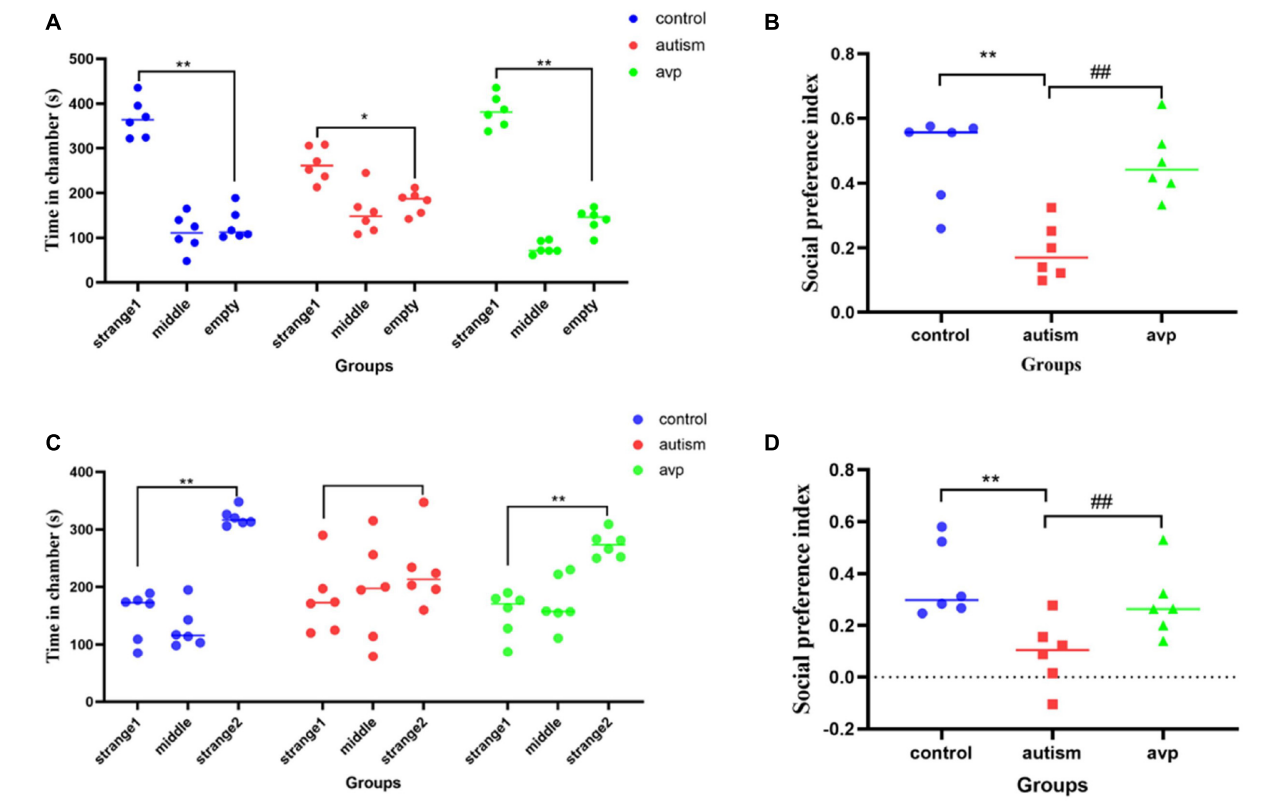

FIGURE 5 | The results of three-chamber test in each group ($n = 6$ in each group). **(A)** The results of social preference test in each group. Comparison of the time spent in the side with stranger 1 vs. the side with empty: $^{*}p < 0.05$, $^{**}p < 0.01$. **(B)** Social preference index in social preference test. Compared with the control group: $^{**}p < 0.01$; compared with the autism group: $\#\#p < 0.01$. **(C)** The results of social novelty test in each group. Comparison of the time spent in the side with stranger 1 vs. the side with stranger 2: $^{*}p < 0.05$, $^{**}p < 0.01$. **(D)** Social preference index in social novelty test. Compared with the control group: $^{**}p < 0.01$; compared with the autism group: $\#\#p < 0.01$.

AVP group ($p < 0.01$; **Figure 5A**). The social preference index in social preference test was significantly decreased in the VPA-induced autism model group compared with the control group ($p < 0.01$) and AVP group ($p < 0.01$; **Figure 5B**). In the social novelty test (phase 3), the control and AVP groups spent more time in the side with stranger 2 than in the side with stranger 1 ($p < 0.01$). The VPA-induced autism rats seemed to lose interest in social novelty with conspecifics, spending a comparable time exploring the cage containing stranger 1 rat and stranger 2 ($p > 0.01$; **Figure 5C**). Furthermore, the social preference index in social novelty test was significantly decreased in the VPA-induced autism model group compared with the control group and AVP group ($p < 0.01$; **Figure 5D**). The results suggest that the social interaction was impaired in the VPA-induced autism model group, and the impairment was significantly improved following AVP treatment.

Self-Grooming Test

To test for repetitive/stereotypic behavior, the self-grooming test was used. When compared with the control group, the cumulative self-grooming time was significantly prolonged in the VPA-induced autism model group ($p < 0.01$), and the cumulative time was significantly shorter in the AVP treatment group ($p < 0.01$) when compared with the VPA-induced autism rats (**Figure 6**).

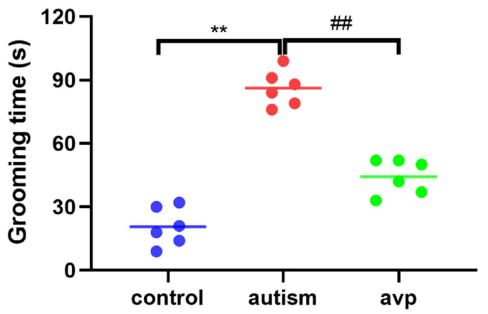

FIGURE 6 | Repetitive/stereotypic behavior test in rats ($n = 6$ in each group). Compared with the control group: $^{**}p < 0.01$; compared with the VPA-induced autism model group: $\#\#p < 0.01$.

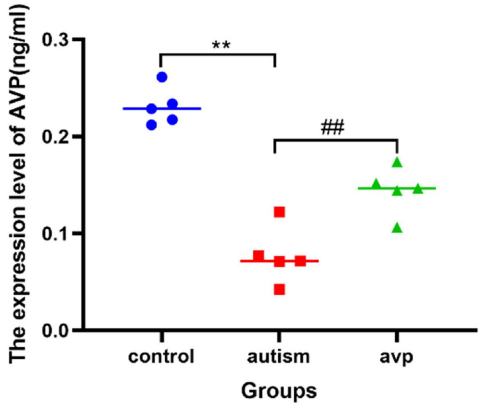

FIGURE 7 | The expression levels of serum AVP in each group ($n = 5$ in each group). Compared with the control group: $^{**}p < 0.01$; compared with the VPA-induced autism model group: $\#\#p < 0.01$.

The Expression Levels of Arginine Vasopressin in Serum

Compared with the control group, the AVP level in the serum significantly decreased in the VPA-induced autism model group ($p < 0.01$). After AVP treatment, the AVP levels in the serum were significantly increased ($p < 0.01$; **Figure 7**).

RNA-seq

Quality Control and Read Mapping

The number of total reads, clean reads, the sequencing error rate, and the percentage of Q20, Q30, and the GC content of all samples met the quality control requirements of sequencing. More than 95% of the clean reads were mapped to the rat genome, and more than 75% of them were mapped to a single genome location.

Differentially Expressed Analysis

There are 518 genes (216 up and 302 down) whose expression was significantly different with an adjusted FDR $p < 0.05$ and FC > 1.3 (only 20 upregulated and 7 downregulated genes were found in FC > 2) in the VPA-induced autism model group compared with the control (the heatmap of the top 50 DEGs are shown in **Figure 8A**). We performed GO biology process (BP) and KEGG pathway functional enrichment analyses to explore the potential biological functions of these differential expression genes. The results of GO BP were significantly enriched in nervous system development, tissue development and remodeling, and extracellular structure organization (**Figures 8B,C**). Clearly, the VPA-induced autism model group had significant developmental impairments compared with the control group, particularly in the nervous system [gliogenesis, glial cell differentiation, and oligodendrocyte (OL) differentiation]. Further analysis showed that neurodevelopmental disorders and tissue developmental disorders were associated with down-regulated genes, whereas extracellular matrix remodeling was associated with up-regulated genes (**Figures 8D,E**). The KEGG pathway enrichment analysis showed that these differential expression genes were significantly enriched in six pathways, such as PI3K-Akt signaling pathway, Wnt signaling pathway, protein digestion and absorption, and so on (**Figure 8F**). We also analyzed the intersection between our differential expression gene list and the list of 1,010 genes that have evidence of genetic association with ASD from the SFARI human gene list[2]. Of 518 differential expression genes, 27 were found in the SFARI database, which are mainly involved in nervous system development, synapse maturation, synapse organization, protein localization to synapse, glial cell migration, and so on.

There are nine genes (seven up and two down) whose expression was significantly different with an adjusted FDR

[2]https://gene.sfari.org/database/human-gene/

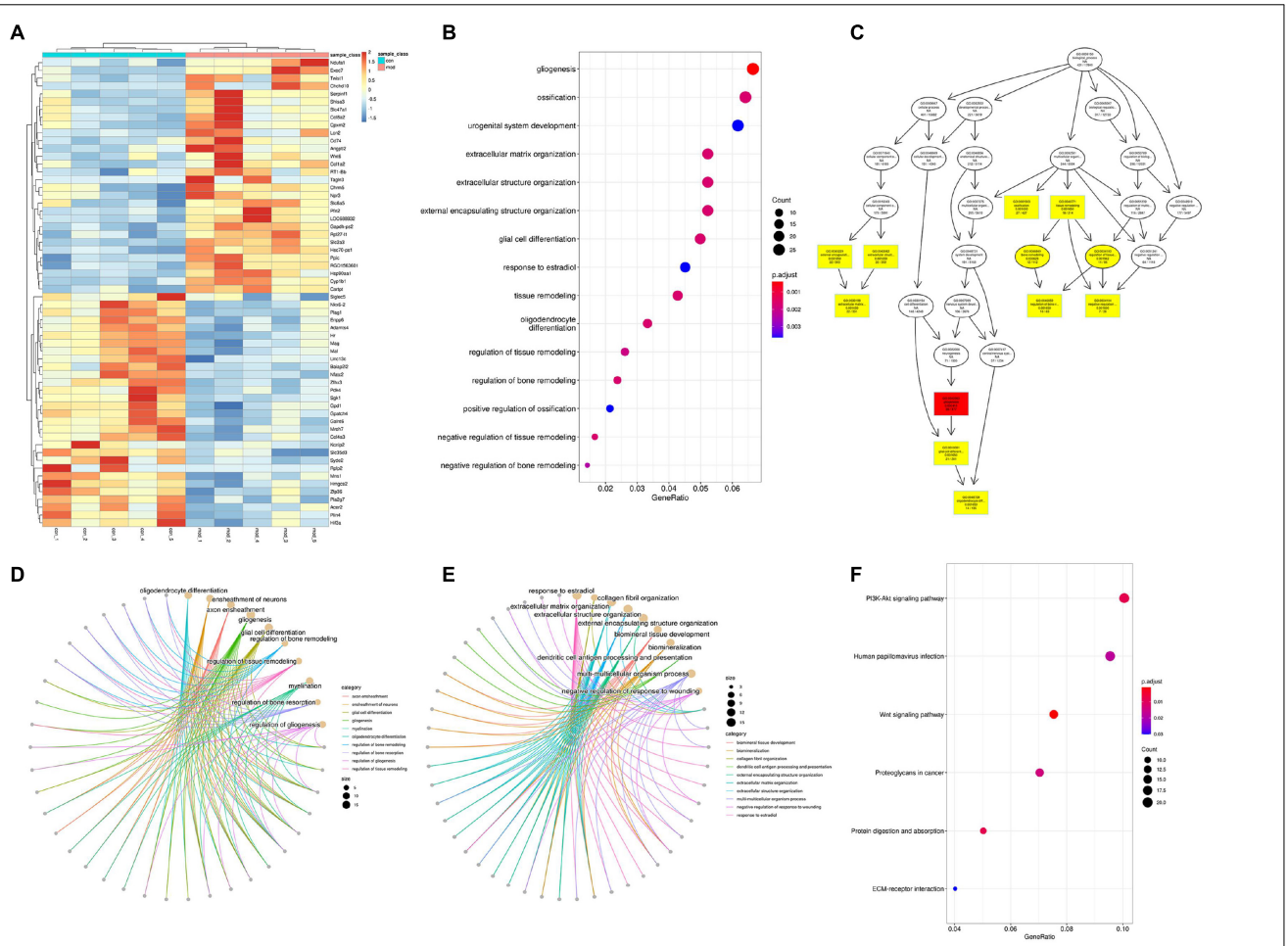

FIGURE 8 | Differentially expressed analysis in autism group compared with the control group (n = 5 in each group). **(A)** Hierarchical clustering heatmap of the top 50 DEGs in the VPA-exposed group compared with the control group. **(B)** GO biology process enrichment analysis of the DEGs. The x axis indicates the enrichment ratio, and the y axis indicates the GO terms. The size of the circle represents the gene number, and the color of the circle indicates the value (adjusted p value). **(C)** Directed acyclic graph of GO biology process in DEGs, the depth of the color represents the degree of enrichment. **(D,E)** GO biology process enrichment analysis of down-regulated and up-regulated genes. The size of the circle represents the gene number, and the color of the line indicates clustering of biological processes **(F)** KEGG enrichment analysis of DEGs. The x axis indicates the enrichment ratio, and the y axis indicates the KEGG terms. The size of the circle represents the gene number, and the color of the circle indicates the value (adjusted p value).

$p < 0.05$ and FC > 1.3 (no significantly different genes were found in FC > 2) in the VPA-induced autism model group compared with the AVP group. The number of DEGs between the VPA-induced autism model and the AVP group was limited and too few for confident GO and KEGG annotation.

Gene Set Enrichment Analysis

Traditional KEGG analysis strategies usually focus on a handful of gene that exhibit differences between two states of interest. Although useful, they are easily affected by the filter threshold (logFC and FDR) and lead to miss some genes with moderate differential expression but important biological significance. To overcome many genes with moderate but meaningful expression changes are discarded by the strict cutoff value, which leads to a reduction in statistical power, we conducted a GSEA (Subramanian et al., 2005). From a biological perspective, GSEA methods are promising because functionally related genes often display a coordinated expression to accomplish their roles in the cell. In the VPA-induced autism model group compared with the control, the results of GSEA GO BP enrichment analysis showed that 239 gene sets are significantly upregulated in the VPA-induced autism model group (NOM $p < 0.05$, $|NES| > 1$). The top 5 terms were significantly enriched in mitochondrial electron transport NADH to ubiquinone, ATP synthesis coupled electron transport, positive regulation of telomerase RNA localization to Cajal body, regulation of cellular amino acid metabolic process, and oxidative phosphorylation. Two hundred eighty-seven gene sets are significantly downregulated in the VPA-induced autism model group (NOM $p < 0.05$, $|NES| > 1$). The top 5 GO terms were significantly enriched in OL differentiation, axoneme assembly, axon ensheathment in central nervous system (CNS), negative regulation of glial cell differentiation, and

microtubule bundle formation. The results of GSEA KEGG enrichment analysis showed that 18 gene sets are significantly upregulated in the VPA-induced autism model group (NOM $p < 0.05$, $|NES| > 1$). The top 5 terms were significantly enriched in proteasome, Parkinson's disease, oxidative phosphorylation, Alzheimer's disease, and Huntington disease. Four gene sets (base excision repair, ether lipid metabolism, notch signaling pathway, and peroxisome proliferator–activated receptor [PPAR] signaling pathway) were significantly downregulated in the VPA-induced autism model group (NOM $p < 0.05$, $|NES| > 1$).

In the VPA-induced autism model group compared with the AVP group, the results of GSEA GO BP enrichment analysis showed that 96 gene sets are significantly upregulated in the VPA-induced autism model group (NOM $p < 0.05$, $|NES| > 1$). The top 5 GO terms were significantly enriched in neuropeptide signaling pathway, γ-aminobutyric acid (GABA) signaling pathway, synaptic transmission GABAergic, chromatin remodeling at centromere, and establishment of mitochondrion localization. Six hundred sixty-six gene sets are significantly downregulated in the VPA-induced autism model group (NOM $p < 0.05$, $|NES| > 1$). The top 5 GO terms were significantly enriched in positive regulation of response to cytokine stimulus, positive regulation of interleukin 4 production, cellular extravasation, cell differentiation involved in metanephros development, and regulation of lymphocyte homeostasis. The results of GSEA KEGG enrichment analysis showed that nine gene sets are significantly upregulated in the VPA-induced autism model group (NOM $p < 0.05$, $|NES| > 1$). The top 5 terms were significantly enriched in neuroactive ligand–receptor interaction, O glycan biosynthesis, aminoacyl tRNA biosynthesis, proteasome, and citrate cycle (tricarboxylic acid cycle). Twenty-seven gene sets are significantly downregulated in the VPA-induced autism model group (NOM $p < 0.05$, $|NES| > 1$). The top 5 pathways were significantly enriched in complement and coagulation cascades, *Leishmania* infection, cytokine–cytokine receptor interaction, prostate cancer, and basal cell carcinoma.

The intersection of the gene expression variation between down in the VPA-induced autism model group (con vs. mod) and up in AVP (mod vs. AVP) was analyzed by Evenn[3]. The results showed that 102 BPs were remarkably downregulated in the VPA-induced autism model group and upregulated in AVP treatment, such as OL differentiation, glial cell differentiation, gliogenesis, and so on (**Figures 9A–F**). Furthermore, some neurodevelopment-related BPs such as glial cell proliferation, glial cell migration, neural tube development, and so on were not changed in the VPA-induced autism model group but remarkably upregulated after AVP treatment. Only notch signaling pathway was found remarkably downregulated in the VPA-induced autism model group and upregulated in AVP treatment. Some neurodevelopment-related pathways, such as mitogen-activated protein kinase (MAPK) signaling pathway, focal adhesion, and so on, were not changed in the VPA-induced autism model group but remarkably upregulated after AVP treatment (**Figures 10A–F**).

[3]http://www.ehbio.com/test/venn/#/

Dynamic Expression Patterns of Genes

The expression trends of genes at each group were analyzed using Mfuzz clustering analysis, and eight clusters with different change trends were screened out (**Figure 11**). Genes in clusters 1 and 8 presented a trend of increasing in the VPA-induced autism model group and decreasing in the AVP group. Genes in clusters 5 and 7 presented a trend of decreasing in the VPA-induced autism model group and increasing in the AVP group. Genes in clusters 2 and 6 presented a trend of gradually declining in the VPA-induced autism model group and AVP group. Genes in clusters 3 and 4 presented a trend of continuous increase in the VPA-induced autism model group and AVP group.

We further analyzed the gene biology function in clusters 5 and 7. A large number of development-related biological processes are enriched in cluster 5, such as neurodevelopment, neurogenesis, gliogenesis, glial cell differentiation, and migration, and these genes all point together to notch signal pathway. In cluster 7, lots of genes were enriched in the cellular developmental process, cell differentiation, cell adhesion, cell migration, and so on, and these genes were mainly involved in the focal adhesion pathway and MAPK pathway. The results of expression trend analysis were basically consistent with those of analysis of GSEA.

The mRNA Levels of Oligodendrocyte and Myelin Development-Related Genes

Compared with the control group, the mRNA levels of OL and myelin development-related genes, such as Sox10 (a transcription factor that directs neural stem cells toward the glial lineage), Olig2 (a transcription factors necessary for OL development), and MBP (a structural component of myelin, expressed exclusively by myelinating glia), were significantly decreased in the VPA-induced autism model group ($p < 0.05$), and the mRNA levels were improved after AVP treatment ($p < 0.05$) (**Figure 12**).

DISCUSSION

Our study showed that rats exposed to VPA at E12.5 had significantly delayed growth development and impaired social behaviors, and the social behaviors were improved significantly by AVP treatment. The results of this study are consistent with previous reports (Wu et al., 2021).

As a hub in the "social brain," the amygdala, which was located within the anterior medial portion of the brain's temporal lobe, maintains diverse connections with the neocortex, basal ganglia, hippocampus, thalamus, and other brain cortical areas *via* a network of white matter tracts, responsible for information processing that subserve emotional learning, social cognition, and social interaction (Baron-Cohen et al., 2000; Zalla and Sperduti, 2013; Ferrara et al., 2021; Raam and Hong, 2021; Xu et al., 2021). A large number of studies have demonstrated that amygdala structural and/or functional abnormalities are associated with social malfunctioning in ASD (Shen et al., 2016; Avino et al., 2018; Herrero et al., 2020; Xu et al., 2020; Seguin et al., 2021; Vitor-Vieira et al., 2021). So, we speculated that the prosocial behavior of AVP may be related

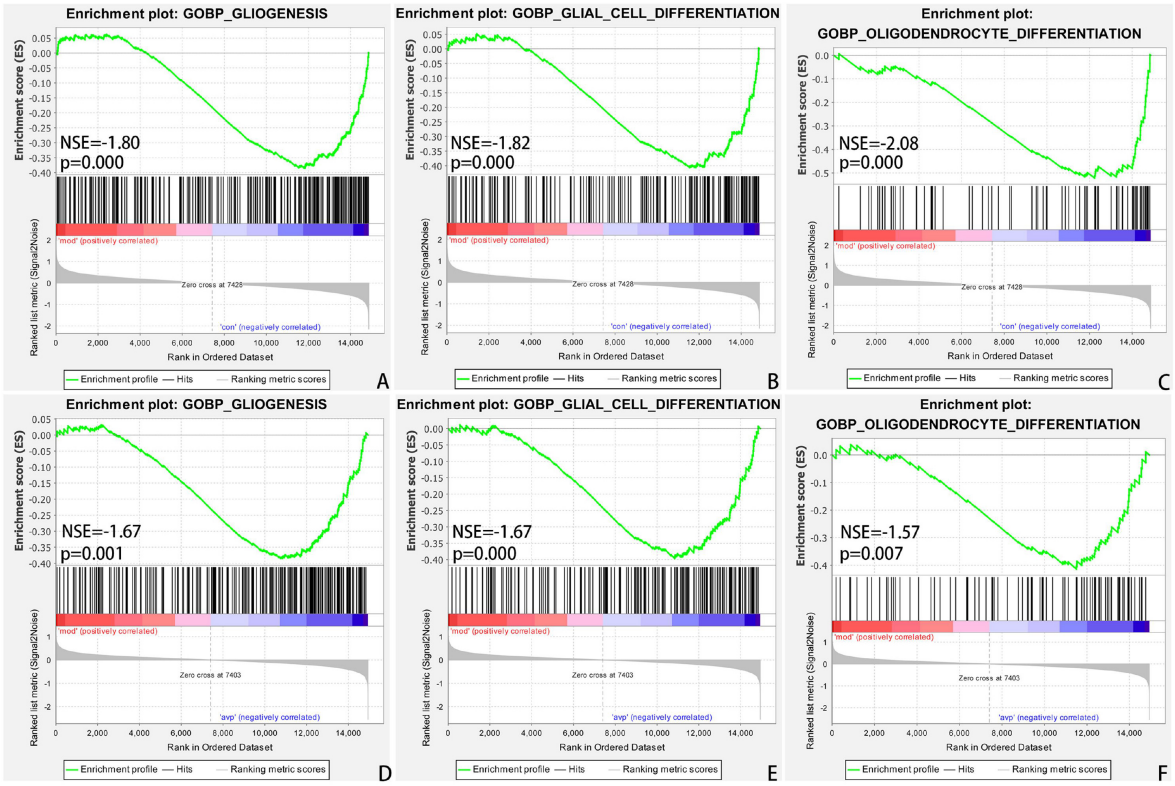

FIGURE 9 | Enrichment of related biological process by GSEA. **(A)** Gliogenesis in control (con) vs. autism (mod), **(B)** glial cell differentiation in control (con) vs. autism (mod), **(C)** oligodendrocyte differentiation in control (con) vs. autism (mod), **(D)** GLIOGENESIS in AVP vs. autism (mod), **(E)** glial cell differentiation in AVP vs. autism (mod), and **(F)** oligodendrocyte differentiation in AVP vs. autism (mod). The significantly enriched gene set was selected with |NES|>1 and with NOM $p < 0.05$.

to the amygdala. In order to further explore its mechanism of action, we focused on transcriptome analysis in the amygdala after AVP treatment.

Deficits in Oligodendrocyte Development and Function Potentially Represent a Common Molecular Pathway Disrupted in Autism Spectrum Disorder

Five hundred eighteen DEGs were identified in the VPA-induced autism model group compared with the control in this study. GO biological process enrichment analysis of DEGs showed that the VPA-induced autism model group had significant nervous system developmental impairments compared with the normal group, particularly in gliogenesis, glial cell differentiation, and OL differentiation. GSEA enrichment analysis also showed that the biological process of OL differentiation, axoneme assembly, and axon ensheathment were inhibited in the VPA-induced autism model group. Further analysis showed that neurodevelopmental disorders were associated with the transcription inhibition of OL development and myelination-related genes. The results were consistent with the research of Zhang X. F. et al. (2020) who found the transcript levels of myelin-related genes were reduced in poly(I:C)-exposed mouse offspring in the MIA model. Obviously, deficits in OL development and function may be one of the core mechanisms of autism. This may be related to VPA directly inhibits histone deacetylase (Kataoka et al., 2013), causing transient hyperacetylation in the brain, inhibiting development-related genes transcription (Kataoka et al., 2013; Taleb et al., 2021), causes a delay in OL differentiation and hypomyelination. In addition, VPA exposure may impairs repair of DNA damage (Servadio et al., 2018), modifies cholesterol/isoprenoid metabolism, and reduces the number of OLs leading to lower myelin and cholesterol levels (Cartocci et al., 2018).

OLs are glial cells in the CNS, responsible for myelin sheath formation, which allows fast signal transmission, provides metabolic support to axons (Cherchi et al., 2021), and contributes to the optimal information processing in complex neural networks to maintaining the functional connectome of the brain. Deficits in OL development and function will lead to demyelination and axonal dysregulation, and disruption in neuron–glia interactions promotes autistic-like features (Bronzuoli et al., 2018; Duncan et al., 2021). Ample evidence has revealed that OL development disorders are closely related to autism. Graciarena et al. (2018) found that reduction in the proliferation of oligodendroglial cells and low levels of myelin basic protein has also been implicated in ASD pathogenesis. The analyses of DEGs highlighted OL dysregulation, which we confirmed in two additional mouse

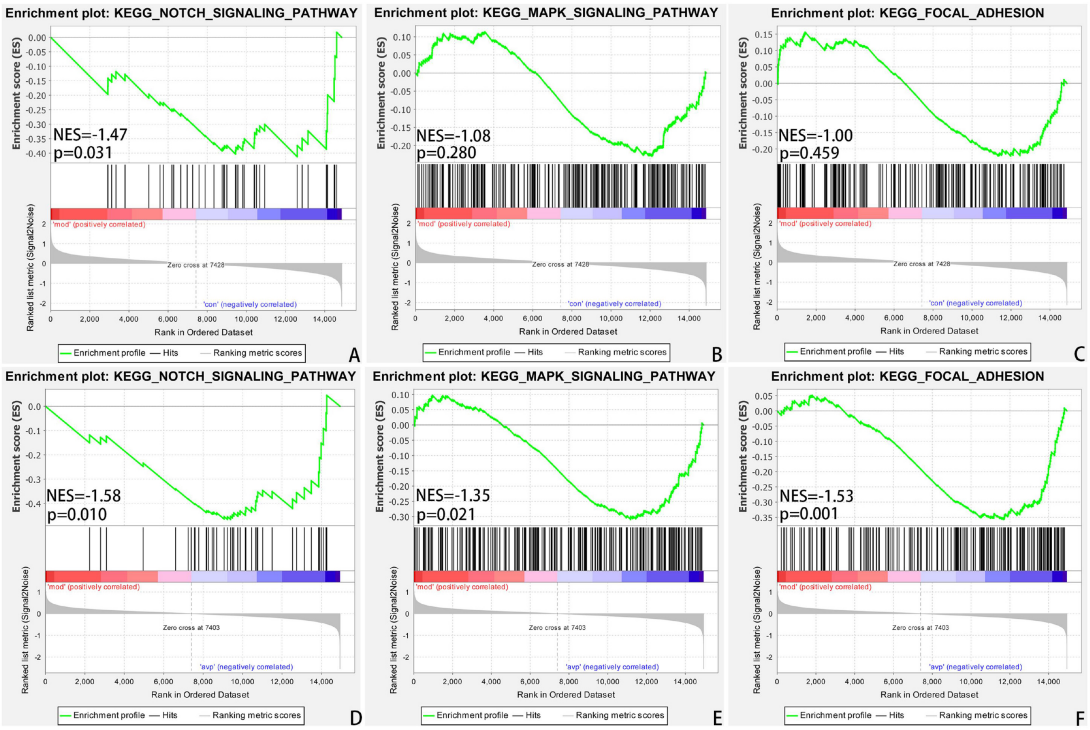

FIGURE 10 | Enrichment of related signaling pathway by GSEA. **(A)** Notch signaling pathway in control (con) vs. autism (mod). **(B)** MAPK signaling pathway in control (con) vs. autism (mod). **(C)** Focal adhesion signaling pathway in control (con) vs. autism (mod). **(D)** Notch signaling pathway in AVP vs. autism (mod). **(E)** MAPK signaling pathway in AVP vs. autism (mod). **(F)** Focal adhesion signaling pathway in AVP vs. autism (mod). The significantly enriched gene set was selected with |NES|>1 and with NOM $p < 0.05$.

models of syndromic ASD (Phan et al., 2020). Zhang X. F. et al. (2020) found oligodendroglia-related gene mRNA, which are critically involved in myelination and OL progenitor differentiation, is significantly decreased in amygdala in maternal immune activation ASD model. Astrocytes and OLs may contribute to neurochemical imbalances described in the autistic brain by disrupting neurotransmission or modifying axonal conduction (Voineagu et al., 2011; Gupta et al., 2014).

PI3K/AKT and Wnt Pathway May Be the Core Mechanism of Autism

Pathway enrichment analysis of DEGs between the control group and VPA-induced autism model group showed that the PI3K/AKT and Wnt pathways were significantly dysregulated in the VPA-induced autism model group.

PI3K/AKT Signaling Pathway Represents an Essential Signaling Mechanism for Mammalian Enzyme-Related Receptors

PI3K/AKT signaling pathway represents an essential signaling mechanism for mammalian enzyme-related receptors in transducing signals or biological processes such as cell development, differentiation, cell survival, protein synthesis, and metabolism (Sharma and Mehan, 2021). Up to now, there is still not a unified conclusion on the expression changes of PI3K/Akt pathway in autism. Nicolini et al. (2015) find that PI3K–AKT–mTOR signaling pathways were downregulated in idiopathic autism fusiform gyrus and in neocortex of valproic acid–induced rat model. Luo et al. (2020) find that the PI3K/Akt pathway was inactivated in BTBR mice; overexpressed moesin significantly restored the activity of PI3K/Akt pathway and improved the autistic-like behaviors. Tylee et al. (2017) found that PI3K–AKT–mTOR and RAS–MAPK signaling cascades were diminished, and ribosomal translation and natural killer cell–related activity increased in ASD blood transcriptome. Conversely, Zhang J. et al. (2016) find that p-PI3K and p-AKT significantly increased in the hippocampus in autism rat model, and inhibition of mTOR by NVP-BEZ235 significantly reduced the activity of PI3K/Akt and improved social interaction in VPA-induced ASD. Zhang W. et al. (2020) find that small GTPase gene RAB39b mutation promotes PI3K–AKT–mTOR activity and alters cortical neurogenesis, leading to macrocephaly and autistic-like behaviors. The inconsistent results may be due to the sample size, different brain regions, different developmental time, and different research methods.

Wnt/β-Catenin Signaling Pathway Plays a Central Role in Neurodevelopment

Wnt/β-catenin signaling pathway plays a central role in neurodevelopment, and perturbation Wnt signaling may trigger

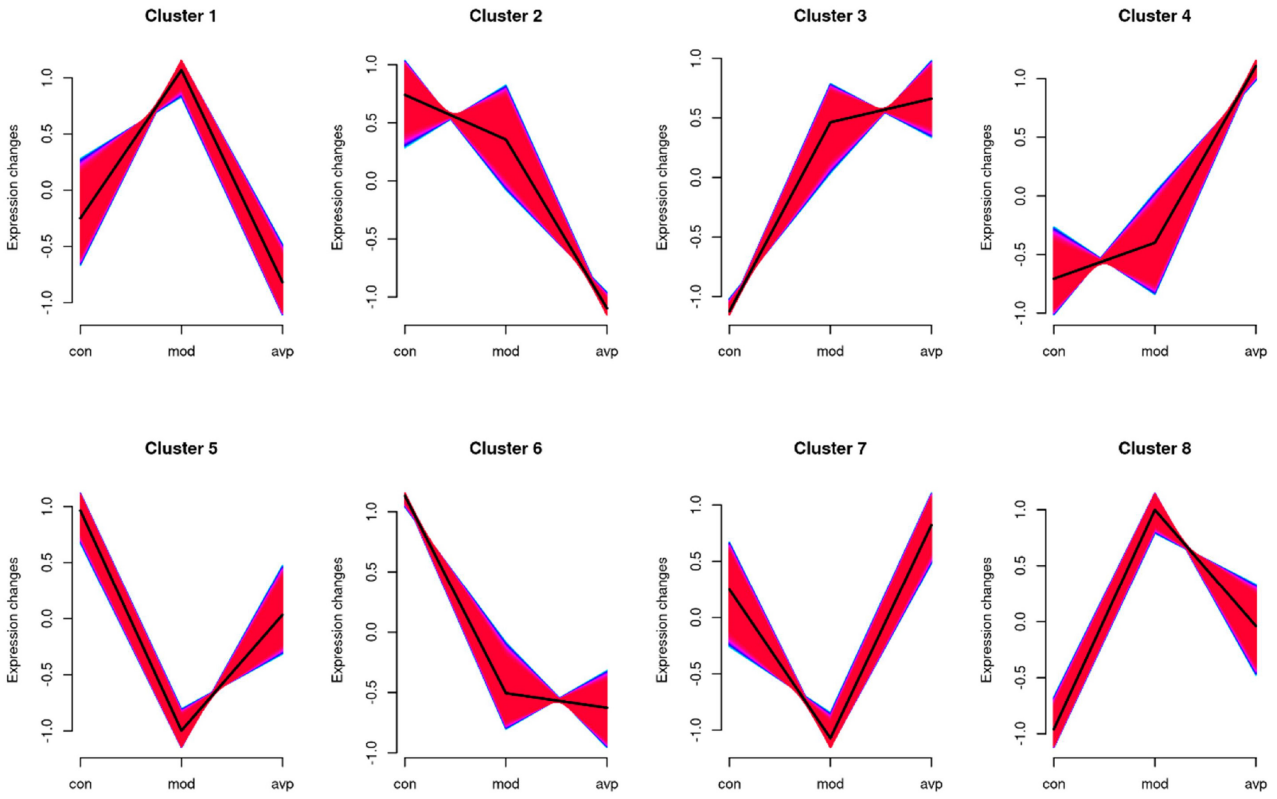

FIGURE 11 | The series of diagrams illustrates the patterns of dynamic changes of gene in each group. Clusters 1 and 8 presented a trend of increasing in the VPA-induced autism model group and decreasing in the AVP group. Clusters 5 and 7 presented a trend of decreasing in the VPA-induced autism model group and increasing in the AVP group. Clusters 2 and 6 presented a trend of gradually declining in the VPA-induced autism model group and AVP group, and clusters 3 and 4 presented a trend of continuous increase in the VPA-induced autism model group and AVP group.

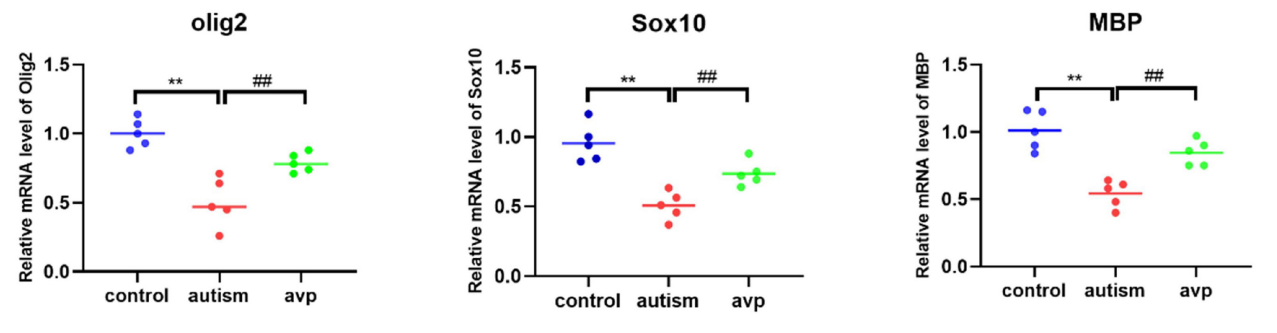

FIGURE 12 | The mRNA levels of oligodendrocyte and myelin development-related genes (n = 5 in each group). Compared with the control group: $^{**}p < 0.01$; compared with the VPA-induced autism model group: $\#\#p < 0.01$.

the advent of disorders related to the structures and functions of the CNS (Inestrosa and Varela-Nallar, 2015; Kumar et al., 2019). Zhang et al. (2012) (Qin et al., 2016; Kuo and Liu, 2018) find that prenatal administration of VPA causes the upregulation of the Wnt/β-catenin signaling pathway, which facilitates susceptibility to autism. Sulindac treatment ameliorates autism-like behavioral phenotypes probably at least in part *via* the downregulation of the canonical Wnt/b-catenin (Zhang et al., 2015). Vallee et al. (2019) found Wnt/β-catenin pathway was upregulated in autism, and PPARγ agonists may play potential treatment for ASD by inhibiting the canonical Wnt/β-catenin pathway. Emery (2010) found the Wnt/β-catenin pathway plays an important role in OL development; mutant mice with elevated Wnt/β-catenin signaling in the OL lineage display blocked differentiation and hypomyelination. It is obvious that the PI3K/AKT and Wnt pathways may be the core mechanism of autism; targeting these pathways can be beneficial for the improvement of autism (Sharma and Mehan, 2021).

Arginine Vasopressin Improves the Autism-Like Behavior Through Non-core Pathways

Although AVP treatment significantly improved social interaction disorders in VPA-induced autism model rats, the mechanism remains unclear. Few DEGs were found when compared with the transcriptome between the VPA-induced autism model group and AVP treatment group. GSEA enrichment analysis showed that deficits in OL development and function were significantly improved after AVP treatment, the pathways were mainly enriched in the NOTCH, MAPK, focal adhesion signaling pathways, but not in the PI3K/AKT and Wnt pathway. The expression patterns analysis also showed the same results. Thus, we speculate that AVP can compensate for the dysregulation of PI3K/AKT and Wnt pathways by regulating the NOTCH, MAPK, and focal adhesion signaling pathways, thus promoting OL development and myelin formation and improving autism-like behavior. A large number of studies have confirmed that activation of NOTCH (Kim et al., 2020; Li et al., 2021), MAPK (Ishii et al., 2016; Lorenzati et al., 2021), and Focal adhesion (Forrest et al., 2009; Lafrenaye and Fuss, 2010) signaling pathway can regulate the proliferation, differentiation, and migration of OL and myelin formation. In addition, crosstalk between these pathways and PI3K/AKT and Wnt pathway has been reported in many neurological or non-neurological disorders (Bai et al., 2019; Ishii et al., 2019, 2021; Worthmuller and Ruegg, 2020; Acar et al., 2021).

CONCLUSION

Collectively, these results demonstrate that AVP can significantly improve the social interaction disorder of VPA-induced autism model, and AVP may target behavioral symptoms in autism by modulating the vasopressin pathways, rather than primary disease mechanisms.

DATA AVAILABILITY STATEMENT

The datasets presented in this study can be found in online repositories. The names of the repository/repositories and accession number(s) can be found in the article/supplementary material.

ETHICS STATEMENT

The animal study was reviewed and approved by Guizhou Medical University.

AUTHOR CONTRIBUTIONS

BZ, LT, and MW: conceptualization, writing, supervision, project administration, and funding acquisition. XZ, JP, and YZ: animal model. XZ, XY, and YL: behavioral tests. BZ and YC: RNA-seq data analysis. All authors read and approved the final manuscript.

FUNDING

This study was supported by Ph.D. research startup foundation of Guizhou Medical University [(2020)008 and (2020)010].

ACKNOWLEDGMENTS

We are grateful to Guizhou Provincial Engineering Technology Research Center for Chemical Drug R&D.

REFERENCES

Acar, A., Hidalgo-Sastre, A., Leverentz, M. K., Mills, C. G., Woodcock, S., Baron, M., et al. (2021). Inhibition of Wnt signalling by Notch via two distinct mechanisms. *Sci. Rep.* 11:9096. doi: 10.1038/s41598-021-88618-5

Anders, S., Pyl, P. T., and Huber, W. (2015). HTSeq–a Python framework to work with high-throughput sequencing data. *Bioinformatics* 31, 166–169. doi: 10.1093/bioinformatics/btu638

Avino, T. A., Barger, N., Vargas, M. V., Carlson, E. L., Amaral, D. G., Bauman, M. D., et al. (2018). Neuron numbers increase in the human amygdala from birth to adulthood, but not in autism. *Proc. Natl. Acad. Sci. U.S.A.* 115, 3710–3715. doi: 10.1073/pnas.1801912115

Bai, C., Zhang, H., Zhang, X., Yang, W., Li, X., and Gao, Y. (2019). MiR-15/16 mediate crosstalk between the MAPK and Wnt/beta-catenin pathways during hepatocyte differentiation from amniotic epithelial cells. *Biochim. Biophys. Acta Gene Regul. Mech.* 1862, 567–581. doi: 10.1016/j.bbagrm.2019.02.003

Baron-Cohen, S., Ring, H. A., Bullmore, E. T., Wheelwright, S., Ashwin, C., and Williams, S. C. (2000). The amygdala theory of autism. *Neurosci. Biobehav. Rev.* 24, 355–364. doi: 10.1016/s0149-7634(00)00011-7

Benarroch, E. E. (2013). Oxytocin and vasopressin: social neuropeptides with complex neuromodulatory functions. *Neurology* 80, 1521–1528. doi: 10.1212/WNL.0b013e31828cfb15

Borie, A. M., Dromard, Y., Guillon, G., Olma, A., Manning, M., Muscatelli, F., et al. (2021). Correction of vasopressin deficit in the lateral septum ameliorates social deficits of mouse autism model. *J. Clin. Invest.* 131:e144450. doi: 10.1172/JCI144450

Bronzuoli, M. R., Facchinetti, R., Ingrassia, D., Sarvadio, M., Schiavi, S., Steardo, L., et al. (2018). Neuroglia in the autistic brain: evidence from a preclinical model. *Mol. Autism* 9:66. doi: 10.1186/s13229-018-0254-0

Cartocci, V., Catallo, M., Tempestilli, M., Segatto, M., Pfrieger, F. W., Bronzuoli, M. R., et al. (2018). Altered brain cholesterol/isoprenoid metabolism in a rat model of autism spectrum disorders. *Neuroscience* 372, 27–37. doi: 10.1016/j.neuroscience.2017.12.053

Cherchi, F., Pugliese, A. M., and Coppi, E. (2021). Oligodendrocyte precursor cell maturation: role of adenosine receptors. *Neural Regen. Res.* 16, 1686–1692. doi: 10.4103/1673-5374.306058

Christensen, D. L., Baio, J., Van Naarden Braun, K., Bilder, D., Charles, J., Constantino, J. N., et al. (2016). Prevalence and characteristics of autism spectrum disorder among children aged 8 years–autism and developmental disabilities monitoring network, 11 Sites, United States, 2012. *MMWR Surveill. Summ.* 65, 1–23. doi: 10.15585/mmwr.ss6802a1

Dai, Y. C., Zhang, H. F., Schon, M., Bockers, T. M., Han, S. P., Han, J. S., et al. (2018). Neonatal oxytocin treatment ameliorates autistic-like behaviors and oxytocin deficiency in valproic acid-induced rat model of autism. *Front. Cell Neurosci.* 12:355. doi: 10.3389/fncel.2018.00355

Duncan, G. J., Simkins, T. J., and Emery, B. (2021). Neuron-oligodendrocyte interactions in the structure and integrity of axons. *Front. Cell Dev. Biol.* 9:653101. doi: 10.3389/fcell.2021.653101

Emery, B. (2010). Regulation of oligodendrocyte differentiation and myelination. *Science* 330, 779–782. doi: 10.1126/science.1190927

Ferrara, N. C., Trask, S., Avonts, B., Loh, M. K., Padival, M., and Rosenkranz, J. A. (2021). Developmental shifts in amygdala activity during a high social drive state. *J. Neurosci.* 41, 9308–9325. doi: 10.1523/JNEUROSCI.1414-21.2021

Forrest, A. D., Beggs, H. E., Reichardt, L. F., Dupree, J. L., Colello, R. J., and Fuss, B. (2009). Focal adhesion kinase (FAK): a regulator of CNS myelination. *J. Neurosci. Res.* 87, 3456–3464. doi: 10.1002/jnr.22022

Graciarena, M., Seiffe, A., Nait-Oumesmar, B., and Depino, A. M. (2018). Hypomyelination and oligodendroglial alterations in a mouse model of autism spectrum disorder. *Front. Cell Neurosci.* 12:517. doi: 10.3389/fncel.2018.00517

Gupta, S., Ellis, S. E., Ashar, F. N., Moes, A., Bader, J. S., Zhan, J., et al. (2014). Transcriptome analysis reveals dysregulation of innate immune response genes and neuronal activity-dependent genes in autism. *Nat. Commun.* 5:5748. doi: 10.1038/ncomms6748

Herrero, M. J., Velmeshev, D., Hernandez-Pineda, D., Sethi, S., Sorrells, S., Banerjee, P., et al. (2020). Identification of amygdala-expressed genes associated with autism spectrum disorder. *Mol. Autism* 11:39. doi: 10.1186/s13229-020-00346-1

Inestrosa, N. C., and Varela-Nallar, L. (2015). Wnt signalling in neuronal differentiation and development. *Cell Tissue Res.* 359, 215–223. doi: 10.1007/s00441-014-1996-4

Ishii, A., Furusho, M., and Bansal, R. (2021). Mek/ERK1/2-MAPK and PI3K/Akt/mTOR signaling plays both independent and cooperative roles in Schwann cell differentiation, myelination and dysmyelination. *Glia* 69, 2429–2446. doi: 10.1002/glia.24049

Ishii, A., Furusho, M., Dupree, J. L., and Bansal, R. (2016). Strength of ERK1/2 MAPK activation determines its effect on myelin and axonal integrity in the adult CNS. *J. Neurosci.* 36, 6471–6487. doi: 10.1523/JNEUROSCI.0299-16.2016

Ishii, A., Furusho, M., Macklin, W., and Bansal, R. (2019). Independent and cooperative roles of the Mek/ERK1/2-MAPK and PI3K/Akt/mTOR pathways during developmental myelination and in adulthood. *Glia* 67, 1277–1295. doi: 10.1002/glia.23602

Kataoka, S., Takuma, K., Hara, Y., Maeda, Y., Ago, Y., and Matsuda, T. (2013). Autism-like behaviours with transient histone hyperacetylation in mice treated prenatally with valproic acid. *Int. J. Neuropsychopharmacol.* 16, 91–103. doi: 10.1017/S1461145711001714

Kim, D., Paggi, J. M., Park, C., Bennett, C., and Salzberg, S. L. (2019). Graph-based genome alignment and genotyping with HISAT2 and HISAT-genotype. *Nat. Biotechnol.* 37, 907–915. doi: 10.1038/s41587-019-0201-4

Kim, H. K., Lee, D. W., Kim, E., Jeong, I., Kim, S., Kim, B. J., et al. (2020). Notch signaling controls oligodendrocyte regeneration in the injured telencephalon of adult zebrafish. *Exp. Neurobiol.* 29, 417–424. doi: 10.5607/en20050

Kumar, L., and Futschik, M. E. (2007). Mfuzz: a software package for soft clustering of microarray data. *Bioinformation* 2, 5–7. doi: 10.6026/97320630002005

Kumar, S., Reynolds, K., Ji, Y., Gu, R., Rai, S., and Zhou, C. J. (2019). Impaired neurodevelopmental pathways in autism spectrum disorder: a review of signaling mechanisms and crosstalk. *J. Neurodev. Disord.* 11:10. doi: 10.1186/s11689-019-9268-y

Kuo, H. Y., and Liu, F. C. (2018). Molecular pathology and pharmacological treatment of autism spectrum disorder-like phenotypes using rodent models. *Front. Cell Neurosci.* 12:422. doi: 10.3389/fncel.2018.00422

Lafrenaye, A. D., and Fuss, B. (2010). Focal adhesion kinase can play unique and opposing roles in regulating the morphology of differentiating oligodendrocytes. *J. Neurochem.* 115, 269–282. doi: 10.1111/j.1471-4159.2010.06926.x

Li, C., Xie, Z., Xing, Z., Zhu, H., Zhou, W., Xie, S., et al. (2021). The notch signaling pathway regulates differentiation of ng2 cells into oligodendrocytes in demyelinating diseases. *Cell Mol. Neurobiol.* doi: 10.1007/s10571-021-01089-0 [Epub ahead of print].

Liberzon, A., Birger, C., Thorvaldsdottir, H., Ghandi, M., Mesirov, J. P., and Tamayo, P. (2015). The molecular signatures database (MSigDB) hallmark gene set collection. *Cell Syst.* 1, 417–425. doi: 10.1016/j.cels.2015.12.004

Liberzon, A., Subramanian, A., Pinchback, R., Thorvaldsdottir, H., Tamayo, P., and Mesirov, J. P. (2011). Molecular signatures database (MSigDB) 3.0. *Bioinformatics* 27, 1739–1740. doi: 10.1093/bioinformatics/btr260

Livak, K. J., and Schmittgen, T. D. (2001). Analysis of relative gene expression data using real-time quantitative PCR and the 2(-Delta Delta C(T)) Method. *Methods* 25, 402–408. doi: 10.1006/meth.2001.1262

Lord, C., Brugha, T. S., Charman, T., Cusack, J., Dumas, G., Frazier, T., et al. (2020). Autism spectrum disorder. *Nat. Rev. Dis. Primers* 6:5.

Lorenzati, M., Boda, E., Parolisi, R., Bonato, M., Borsello, T., Herdegen, T., et al. (2021). c-Jun N-terminal kinase 1 (JNK1) modulates oligodendrocyte progenitor cell architecture, proliferation and myelination. *Sci. Rep.* 11:7264. doi: 10.1038/s41598-021-86673-6

Love, M. I., Huber, W., and Anders, S. (2014). Moderated estimation of fold change and dispersion for RNA-seq data with DESeq2. *Genome Biol.* 15:550. doi: 10.1186/s13059-014-0550-8

Luo, T., Ou, J. N., Cao, L. F., Peng, X. Q., Li, Y. M., and Tian, Y. Q. (2020). The autism-related lncRNA MSNP1AS regulates moesin protein to influence the RhoA, Rac1, and PI3K/Akt pathways and regulate the structure and survival of neurons. *Autism Res.* 13, 2073–2082. doi: 10.1002/aur.2413

Mahmood, H. M., Aldhalaan, H. M., Alshammari, T. K., Alqasem, M. A., Alshammari, M. A., Albekairi, N. A., et al. (2020). The role of nicotinic receptors in the attenuation of autism-related behaviors in a murine BTBR T + tf/J Autistic model. *Autism Res.* 13, 1311–1334. doi: 10.1002/aur.2342

Mootha, V. K., Lindgren, C. M., Eriksson, K. F., Subramanian, A., Sihag, S., Lehar, J., et al. (2003). PGC-1alpha-responsive genes involved in oxidative phosphorylation are coordinately downregulated in human diabetes. *Nat. Genet.* 34, 267–273. doi: 10.1038/ng1180

Nicolini, C., Ahn, Y., Michalski, B., Rho, J. M., and Fahnestock, M. (2015). Decreased mTOR signaling pathway in human idiopathic autism and in rats exposed to valproic acid. *Acta Neuropathol. Commun.* 3:3. doi: 10.1186/s40478-015-0184-4

Oztan, O., Garner, J. P., Constantino, J. N., and Parker, K. J. (2020). Neonatal CSF vasopressin concentration predicts later medical record diagnoses of autism spectrum disorder. *Proc. Natl. Acad. Sci. U.S.A.* 117, 10609–10613. doi: 10.1073/pnas.1919050117

Oztan, O., Garner, J. P., Partap, S., Sherr, E. H., Hardan, A. Y., Farmer, C., et al. (2018). Cerebrospinal fluid vasopressin and symptom severity in children with autism. *Ann. Neurol.* 84, 611–615. doi: 10.1002/ana.25314

Parker, K. J., Garner, J. P., Oztan, O., Tarara, E. R., Li, J., Sclafani, V., et al. (2018). Arginine vasopressin in cerebrospinal fluid is a marker of sociality in nonhuman primates. *Sci. Transl. Med.* 10:eaam9100. doi: 10.1126/scitranslmed.aam9100

Parker, K. J., Oztan, O., Libove, R. A., Mohsin, N., Karhson, D. S., Sumiyoshi, R. D., et al. (2019). A randomized placebo-controlled pilot trial shows that intranasal vasopressin improves social deficits in children with autism. *Sci. Transl. Med.* 11:eaau7356. doi: 10.1126/scitranslmed.aau7356

Phan, B. N., Bohlen, J. F., Davis, B. A., Ye, Z., Chen, H. Y., Mayfield, B., et al. (2020). A myelin-related transcriptomic profile is shared by Pitt-Hopkins syndrome models and human autism spectrum disorder. *Nat. Neurosci.* 23, 375–385. doi: 10.1038/s41593-019-0578-x

Qin, L., Dai, X., and Yin, Y. (2016). Valproic acid exposure sequentially activates Wnt and mTOR pathways in rats. *Mol. Cell Neurosci.* 75, 27–35. doi: 10.1016/j.mcn.2016.06.004

Raam, T., and Hong, W. (2021). Organization of neural circuits underlying social behavior: a consideration of the medial amygdala. *Curr. Opin. Neurobiol.* 68, 124–136. doi: 10.1016/j.conb.2021.02.008

Raudvere, U., Kolberg, L., Kuzmin, I., Arak, T., Adler, P., Peterson, H., et al. (2019). . G:Profiler: a web server for functional enrichment analysis and conversions of gene lists (2019 update). *Nucleic Acids Res.* 47, W191–W198. doi: 10.1093/nar/gkz369

Rein, B., Ma, K., and Yan, Z. (2020). A standardized social preference protocol for measuring social deficits in mouse models of autism. *Nat. Protoc.* 15, 3464–3477. doi: 10.1038/s41596-020-0382-9

Schneider, T., and Przewlocki, R. (2005). Behavioral alterations in rats prenatally exposed to valproic acid: animal model of autism. *Neuropsychopharmacology* 30, 80–89. doi: 10.1038/sj.npp.1300518

Seguin, D., Pac, S., Wang, J., Nicolson, R., Martinez-Trujillo, J., and Duerden, E. G. (2021). Amygdala subnuclei development in adolescents with autism spectrum disorder: association with social communication and repetitive behaviors. *Brain Behav.* 11:e2299. doi: 10.1002/brb3.2299

Servadio, M., Manduca, A., Melancia, F., Leboffe, L., Schiavi, S., Campolongo, P., et al. (2018). Impaired repair of DNA damage is associated with autistic-like

traits in rats prenatally exposed to valproic acid. *Eur. Neuropsychopharmacol.* 28, 85–96. doi: 10.1016/j.euroneuro.2017.11.014

Sharma, A., and Mehan, S. (2021). Targeting PI3K-AKT/mTOR signaling in the prevention of autism. *Neurochem. Int.* 147:105067. doi: 10.1016/j.neuint.2021.105067

Shen, M. D., Li, D. D., Keown, C. L., Lee, A., Johnson, R. T., Angkustsiri, K., et al. (2016). Functional connectivity of the amygdala is disrupted in preschool-aged children with autism spectrum disorder. *J. Am. Acad. Child Adolesc. Psychiatry* 55, 817–824. doi: 10.1016/j.jaac.2016.05.020

Sparapani, S., Millet-Boureima, C., Oliver, J., Mu, K., Hadavi, P., Kalostian, T., et al. (2021). The biology of vasopressin. *Biomedicines* 9:89.

Subramanian, A., Tamayo, P., Mootha, V. K., Mukherjee, S., Ebert, B. L., Gillette, M. A., et al. (2005). Gene set enrichment analysis: a knowledge-based approach for interpreting genome-wide expression profiles. *Proc. Natl. Acad. Sci. U.S.A.* 102, 15545–15550. doi: 10.1073/pnas.0506580102

Taleb, A., Lin, W., Xu, X., Zhang, G., Zhou, Q. G., Naveed, M., et al. (2021). Emerging mechanisms of valproic acid-induced neurotoxic events in autism and its implications for pharmacological treatment. *Biomed. Pharmacother.* 137:111322. doi: 10.1016/j.biopha.2021.111322

Tylee, D. S., Hess, J. L., Quinn, T. P., Barve, R., Huang, H., Zhang-James, Y., et al. (2017). Blood transcriptomic comparison of individuals with and without autism spectrum disorder: a combined-samples mega-analysis. *Am. J. Med. Genet. B Neuropsychiatr. Genet.* 174, 181–201. doi: 10.1002/ajmg.b.32511

Vallee, A., Vallee, J. N., and Lecarpentier, Y. (2019). PPARgamma agonists: potential treatment for autism spectrum disorder by inhibiting the canonical WNT/beta-catenin pathway. *Mol. Psychiatry* 24, 643–652. doi: 10.1038/s41380-018-0131-4

Vitor-Vieira, F., Vilela, F. C., and Giusti-Paiva, A. (2021). Hyperactivation of the amygdala correlates with impaired social play behavior of prepubertal male rats in a maternal immune activation model. *Behav. Brain Res.* 414:113503. doi: 10.1016/j.bbr.2021.113503

Voineagu, I., Wang, X., Johnston, P., Lowe, J. K., Tian, Y., Horvath, S., et al. (2011). Transcriptomic analysis of autistic brain reveals convergent molecular pathology. *Nature* 474, 380–384. doi: 10.1038/nature10110

Worthmuller, J., and Ruegg, C. (2020). The crosstalk between FAK and Wnt signaling pathways in cancer and its therapeutic implication. *Int. J. Mol. Sci.* 21:9107. doi: 10.3390/ijms21239107

Wu, J., Dai, Y. C., Lan, X. Y., Zhang, H. F., Bai, S. Z., Hu, Y., et al. (2021). Postnatal AVP treatments prevent social deficit in adolescence of valproic acid-induced rat autism model. *Peptides* 137:170493. doi: 10.1016/j.peptides.2021.170493

Xu, Q., Zuo, C., Liao, S., Long, Y., and Wang, Y. (2020). Abnormal development pattern of the amygdala and hippocampus from childhood to adulthood with autism. *J. Clin. Neurosci.* 78, 327–332. doi: 10.1016/j.jocn.2020.03.049

Xu, S., Jiang, M., Liu, X., Sun, Y., Yang, L., Yang, Q., et al. (2021). Neural circuits for social interactions: from microcircuits to input-output circuits. *Front. Neural Circuits* 15:768294. doi: 10.3389/fncir.2021.768294

Yu, G., Wang, L. G., Han, Y., and He, Q. Y. (2012). clusterProfiler: an R package for comparing biological themes among gene clusters. *OMICS* 16, 284–287. doi: 10.1089/omi.2011.0118

Zalla, T., and Sperduti, M. (2013). The amygdala and the relevance detection theory of autism: an evolutionary perspective. *Front. Hum. Neurosci.* 7:894. doi: 10.3389/fnhum.2013.00894

Zhang, H. F., Dai, Y. C., Wu, J., Jia, M. X., Zhang, J. S., Shou, X. J., et al. (2016). Plasma oxytocin and arginine-vasopressin levels in children with autism spectrum disorder in china: associations with symptoms. *Neurosci. Bull.* 32, 423–432. doi: 10.1007/s12264-016-0046-5

Zhang, J., Zhang, J. X., and Zhang, Q. L. (2016). PI3K/AKT/mTOR-mediated autophagy in the development of autism spectrum disorder. *Brain Res. Bull.* 125, 152–158. doi: 10.1016/j.brainresbull.2016.06.007

Zhang, W., Ma, L., Yang, M., Shao, Q., Xu, J., Lu, Z., et al. (2020). Cerebral organoid and mouse models reveal a RAB39b-PI3K-mTOR pathway-dependent dysregulation of cortical development leading to macrocephaly/autism phenotypes. *Genes Dev.* 34, 580–597. doi: 10.1101/gad.332494.119

Zhang, X. F., Chen, T., Yan, A., Xiao, J., Xie, Y. L., Yuan, J., et al. (2020). Poly(I:C) challenge alters brain expression of oligodendroglia-related genes of adult progeny in a mouse model of maternal immune activation. *Front. Mol. Neurosci.* 13:115. doi: 10.3389/fnmol.2020.00115

Zhang, Y., Sun, Y., Wang, F., Wang, Z., Peng, Y., and Li, R. (2012). Downregulating the canonical Wnt/beta-catenin signaling pathway attenuates the susceptibility to autism-like phenotypes by decreasing oxidative stress. *Neurochem. Res.* 37, 1409–1419. doi: 10.1007/s11064-012-0724-2

Zhang, Y., Yang, C., Yuan, G., Wang, Z., Cui, W., and Li, R. (2015). Sulindac attenuates valproic acid-induced oxidative stress levels in primary cultured cortical neurons and ameliorates repetitive/stereotypic-like movement disorders in Wistar rats prenatally exposed to valproic acid. *Int. J. Mol. Med.* 35, 263–270. doi: 10.3892/ijmm.2014.1996

Zhou, H., Xu, X., Yan, W., Zou, X., Wu, L., Luo, X., et al. (2020). Prevalence of autism spectrum disorder in china: a nationwide multi-center population-based study among children aged 6 to 12 Years. *Neurosci. Bull.* 36, 961–971. doi: 10.1007/s12264-020-00530-6

Conflict of Interest: The authors declare that the research was conducted in the absence of any commercial or financial relationships that could be construed as a potential conflict of interest.

frontiers | Frontiers in Neuroscience

ORIGINAL RESEARCH
published: 12 May 2022
doi: 10.3389/fnins.2022.885770

Brain Gray Matter Atrophy and Functional Connectivity Remodeling in Patients With Chronic LHON

Qin Tian[1†], *Ling Wang*[1†], *Yu Zhang*[2,3†], *Ke Fan*[4], *Meng Liang*[2,3,5], *Dapeng Shi*[1*], *Wen Qin*[2,3*] *and Hao Ding*[2,3,5*]

[1] Department of Medical Imaging, People's Hospital of Zhengzhou University, Henan Provincial People's Hospital, Zhengzhou, China, [2] Department of Radiology, Tianjin Medical University, Tianjin, China, [3] Tianjin Key Laboratory of Functional Imaging, Tianjin Medical University General Hospital, Tianjin, China, [4] Henan Eye Institute, Henan Eye Hospital, Henan Provincial People's Hospital, Zhengzhou University People's Hospital, Zhengzhou, China, [5] School of Medical Imaging, Tianjin Medical University, Tianjin, China

OPEN ACCESS

Edited by:
Kazuhiko Sawada,
Tsukuba International University, Japan

Reviewed by:
Changzheng Chen,
Renmin Hospital of Wuhan University, China
Daniele Corbo,
University of Brescia, Italy

***Correspondence:**
Dapeng Shi
cjr.shidapeng@vip.163.com
Wen Qin
wayne.wenqin@gmail.com
Hao Ding
dhhere2005@163.com

[†]These authors have contributed equally to this work

Specialty section:
This article was submitted to Neurodevelopment, a section of the journal Frontiers in Neuroscience

Received: 28 February 2022
Accepted: 19 April 2022
Published: 12 May 2022

Citation:
Tian Q, Wang L, Zhang Y, Fan K, Liang M, Shi D, Qin W and Ding H (2022) Brain Gray Matter Atrophy and Functional Connectivity Remodeling in Patients With Chronic LHON. Front. Neurosci. 16:885770. doi: 10.3389/fnins.2022.885770

Purpose: The aim of this study was to investigate the brain gray matter volume (GMV) and spontaneous functional connectivity (FC) changes in patients with chronic Leber's hereditary optic neuropathy (LHON), and their relations with clinical measures.

Methods: A total of 32 patients with chronic LHON and matched sighted healthy controls (HC) underwent neuro-ophthalmologic examinations and multimodel magnetic resonance imaging (MRI) scans. Voxel-based morphometry (VBM) was used to detect the GMV differences between the LHON and HC. Furthermore, resting-state FC analysis using the VBM-identified clusters as seeds was carried out to detect potential functional reorganization in the LHON. Finally, the associations between the neuroimaging and clinical measures were performed.

Results: The average peripapillary retinal nerve fiber layer (RNFL) thickness of the chronic LHON was significantly thinner ($T = -16.421$, $p < 0.001$), and the mean defect of the visual field was significantly higher ($T = 11.28$, $p < 0.001$) than the HC. VBM analysis demonstrated a significantly lower GMV of bilateral calcarine gyri (CGs) in the LHON than in the HC ($p < 0.05$). Moreover, in comparison with the HC, the LHON had significantly lower FC between the centroid of the identified left CG and ipsilateral superior occipital gyrus (SOG) and higher FC between this cluster and the ipsilateral posterior cingulate gyrus ($p < 0.05$, corrected). Finally, the GMV of the left CG was negatively correlated with the LHON duration ($r = -0.535$, $p = 0.002$), and the FC between the left CG and the ipsilateral posterior cingulate gyrus of the LHON was negatively correlated with the average peripapillary RNFL thickness ($r = -0.522$, $p = 0.003$).

Conclusion: The atrophied primary visual cortex of the chronic LHON may be caused by transneuronal degeneration following the retinal damage. Moreover, our findings suggest that the functional organization of the atrophied primary visual cortex has been reshaped in the chronic LHON.

Keywords: LHON, gray matter volume (GMV), functional connectivity (FC), visual cortex (V1), reorganization

INTRODUCTION

Leber's hereditary optic neuropathy (LHON) is a maternally inherited disease, 90% of which is caused by three primary mutation sites, namely, 11778/ND4, 3460/ND1, and 14484/ND6, affecting different subunits of complex I and leading to dysfunction in the mitochondrial respiratory chain (Carelli et al., 2004; Yu-Wai-Man et al., 2009; Giordano et al., 2011). Clinically, the LHON is marked by usually sequential subacute vision loss with bilateral central scotomas that occur most frequently in young men (Ollinger et al., 2001). The retinal ganglia cells (RGCs) and small-caliber fibers of the papillomacular bundle are selectively lost in the early stages of the pathologic process. As the disease progresses, the peripapillary retinal nerve fiber layer (RNFL) becomes thinner and optic nerve atrophy happens (Shulman et al., 2009).

Brain white matter (WM) and gray matter (GM) abnormalities were consistently reported in the chronic LHON, especially along the brain's visual pathways. For example, Barcella et al. reported that the optical radiation was atrophied in the chronic LHON using voxel-based morphometry (VBM) (Barcella et al., 2010). Microstructural changes in the optical radiation in the chronic LHON, as represented by decreased fractional anisotropy (FA) and increased mean diffusivity (MD) and radial diffusivity (RD), were also confirmed by several recent studies (Milesi et al., 2012; Rizzo et al., 2012; Ogawa et al., 2014; Manners et al., 2015; Takemura et al., 2019). Besides the WM changes, VBM also detected decreased GM volume (GMV) in the primary visual cortex (Barcella et al., 2010). Postmortem examination showed a significant neuron loss in both the parvocellular and magnocellular layers of the lateral geniculate nucleus (LGN). These pieces of evidence support the secondary transneuronal degeneration of the visual pathway driven by the primary involvement of the RGCs in the LHON.

Despite the secondary damages, compensatory changes in the brain were also reported in the patients with LHON or carriers. The V2 and V3, two visual association areas, were thicker in the young asymptotic LHON carriers than in the healthy controls (HCs), indicating a potential plastic change in these regions following early retinal involvement (d'Almeida et al., 2013; Mateus et al., 2016). Furthermore, the synchronization of spontaneous blood oxygen level-dependent (BOLD) fluctuations was higher in the high-level visual and auditory networks, which was accompanied by reorganized topology and structural connectivity of the auditory subareas (Rocca et al., 2011). Thus, the damage and compensatory plasticity may coexist in the brain of the LHON. However, it is unknown that the degenerated visual areas also had functional plastic potentials in the chronic LHON. In this study, we hypothesized that the atrophy of the visual cortex in the chronic LHON will lead to functional connectivity (FC) reorganization in the remote brain areas. This hypothesis is based on early studies about the functional impairment and remodeling after blindness by ocular diseases or injuries (Qin et al., 2015). For example, an early study reported that the FC between frontoparietal network and visual cortex was enhanced in the patients with congenital blindness (Qin et al., 2015).

To test this hypothesis, a relatively large sample of patients with chronic LHON and matched sighted control group were recruited to identify the visual areas with decreased GMV in the chronic LHON, to detect the changes in resting-state FC between the atrophied brain areas and the whole brain, and to explore the relationship between structural/functional changes of the brain and clinical measures.

MATERIALS AND METHODS

Participants

A total of 32 patients with chronic LHON (12 women and 20 men, age range: 27.97 ± 11.85 years) and 32 matched sighted HCs (10 women and 22 men, age range: 25.56 ± 9.55 years) were also enrolled from Henan Provincial People's Hospital. The inclusion and exclusion criteria for the LHON cohort were: (1) all patients are genetically confirmed with one of the three primary point mutations of mtDNA (m.3460G > A, m.11778G > A, and m.14484T > C); (2) have a duration after vision loss larger than 1 year; (3) have no history of neurological/psychiatric diseases or substance abuse; (4) have no brain and spinal abnormalities using routine magnetic resonance imaging (MRI); and (5) have no other ophthalmic diseases, such as glaucoma, cataract, and retinopathy. The HCs were enrolled with the same criteria except for the diagnosis of LHON. The detailed demographic information of the recruited subjects is provided in **Table 1**. This study was approved by the local ethics committee, and written consent was obtained from the participants or their guardians for immaturity. The peripapillary RNFL thickness and mean defect of the visual field (MD_{VF}) were measured at enrollment. The average RNFL (360° measure) thicknesses were quantified using a high-resolution spectral-domain Cirrus platform (Carl Zeiss Meditec, Dublin, CA, USA).

MRI Acquisition

The MRI data were obtained on a GE Discovery MR750 3.0T MR scanner (GE Healthcare, Waukesha, WI, USA) with an 8-channel head receiver coil. The routine MRI was initially performed to exclude subjects with brain and spinal abnormalities. High-resolution 3D T1-weighted images were acquired using a brain volume (BRAVO) sequence with parameters as follows: repetition time (TR) = 8.2 ms, echo time (TE) = 3.2 ms, inversion time (TI) = 450 ms, matrix size = 256 × 256, field of view (FOV) = 256 mm × 256 mm, flip angle = 12°, slice thickness = 1 mm, and 176 slices with no gap. The resting-state functional MRI (fMRI) images were obtained using a single-shot gradient-echo echo-planar imaging sequence: TR = 2,000 ms, TE = 30 ms, flip angle = 90 degree, matrix = 64 × 64, FOV = 22 × 22 cm, slice thickness =3.4 mm, gap = 1.0 mm, 33 slices, interleaved transverse slices, and 210 volumes. All subjects were asked to keep awake with eyes closed and heads static during the fMRI scan. One patient with chronic LHON and one sighted control were excluded from the imaging analysis due to poor MRI data quality.

Structural MRI Preprocessing

All 3D T1-weighted structural data were preprocessed using the VBM8 toolbox implemented in the Statistical Parametric

TABLE 1 | Demographic information of the recruited subjects.

	Chronic LHON	HC	Statistics	*P* value
Gender[males /females]	20/11	22/9	$\chi^2 = 0.93$	0.393
Age (range)[years]	27.65 ± 11.93 (13–53)	25.16 ± 9.43(11–44)	t = −0.91	0.177
LHON duration[months]	119.6 ± 129.2	-	-	-
Peripapillary RNFL thickness [μm]	59.62 ±10.93	100.60 ± 6.98	t = −16.42	<0.001
MD_{VF}[%]	17.99 ± 7.91	1.57 ± 1.02	t = 11.28	<0.001

LHON, Leber hereditary optic neuropathy; HC, healthy controls; MD_{VF}, mean defect of visual field; RNFL, retinal nerve fiber layer.

Mapping (SPM) software version 12 (http://www.fil.ion.ucl.ac.uk/spm). During the segmentation, an adaptive maximum *a posterior* technique and a partial volume estimation were applied to estimate the fraction of each pure tissue type present in every voxel. Following the segmentation of GM, WM, and cerebrospinal fluid (CSF), the individual GM and WM components were normalized into the Montreal Neurological Institute (MNI) space using the diffeomorphic anatomical registration through the exponentiated Lie algebra (DARTEL) algorithm based on a study-specific DARTEL template, and re-sliced to a voxel size of 1.5 × 1.5 × 1.5 mm^3. The study-specific DARTEL template was created using the structural data of all recruited subjects based on the standard pipeline provided by SPM12. Then, the relative GMV or WM volume (WMV) maps of each subject were obtained by multiplying the individual's GM or WM component by the non-linear Jacobian determinants derived from the DARTEL deformation parameters to remove the confounding effects of individual global brain volume. Finally, the GMV and WMV maps were smoothed with a full width at half maximum (FWHM) kernel of isotropic 6 mm. After the spatial preprocessing, the normalized and smoothed GMV and WMV maps were used for the following analysis.

Resting-State FMRI Preprocessing

The resting-state fMRI data were preprocessed using the DPARSFA toolbox version 4.3 (rfmri.org/dpabi) and SPM with the following steps: the first 10 volumes of each subject were discarded for removing the effect on the potential fMRI signal dropping caused by incomplete T1 relaxation. The remaining 200 volumes underwent slice-timing to correct the acquisition time delay between slices. Anda rigid spatial realignment was performed to estimate and correct for head motion-induced displacement among scan volumes. All resting-state fMRI data were under the head-motion thresholds with a maximum translation of <2 mm and a maximum rotation of <2.0° in any direction. Considering signal spikes caused by head motion can significantly contaminate the final resting-state fMRI quantification, the frame-wise displacement (FD) was also calculated based on the head motion parameters, representing the volume-by-volume head motion amplitude. The realigned fMRI images of each subject were then linearly co-registered with the individual structural images and were further transformed into the MNI space using the DARTEL deformation field generated during T1 normalization as mentioned above, which were further resampled into a voxel size of 3 × 3 × 3 mm^3. The Friston-24 head motion parameters (six motion parameters and their first-time derivatives, and such 12-corresponding squared items), the volumes with motion spike (FD > 0.5), and the average BOLD signals of the ventricular, WM, and global brain tissue were regressed out from the fMRI data. The regressed fMRI data were subsequently band-pass filtered with a frequency range of 0.01–0.08 Hz to remove high-frequency noises and low-frequency signal drifts. Finally, the filtered fMRI data were smoothed with an FWHM kernel of 6 mm for later quantification.

Voxel-Wise Statistics of the Gray and White Matter Volume

The non-parametric permutation tests (5,000 shuffles) were, respectively, performed to investigate voxel-wise GMV and WMV differences between the chronic LHON and HC groups while controlling for the effects of age and gender using the "randomize" script of FSL 6.0 (https://fsl.fmrib.ox.ac.uk/fsl/fslwiki/). Multiple comparisons were corrected using a threshold-free cluster enhancement (TFCE) family-wise error (FWE) method ($p < 0.05$).

Voxel-Wise Functional Connectivity Calculation and Statistics

The brain regions with intergroup differences in GMV from the VBM step were extracted as the seeds for FC calculation. Specifically, voxels survived during the VBM ($P < 0.05$, FWE corrected) and were within a 9-mm radius sphere that centered at the statistic peak (left calcarine gyrus [CG]: [−10.5, −66, −3]; right CG: [15, −78, 1.5]) were defined as the FC seeds. Regions of interest (ROIs) are a method of marking specific parts of an image. The common approach for investigative ROIs analysis is to create small ROIs at the peak of a threshold cluster (Poldrack, 2007). The spheres are defined by the small radius to ensure that the spheres only include voxels that are more significant. Consistent with the previous studies (Niedtfeld et al., 2010; Li et al., 2017; Zhou et al., 2019), we defined the ROI by a sphere of 9 mm (3 voxels) of radius (about 33 voxels in this sphere) at the peak of group-wise difference clusters based on an isotropic spatial resolution of 3 × 3 × 3 mm^3 for the resting-state fMRI. The mean time series of BOLD signals of the bilateral CGs were then extracted, and the Pearson correlation coefficients between the time series of the seed ROIs and that of each voxel of the whole-brain GM were computed. Later, a Fisher r-to-z transformation algorithm was introduced to convert the correlation coefficient into z-value to increase normality.

Voxel-wise non-parametric permutation tests (5,000 shuffles) were performed to investigate FC differences between the chronic LHON and HC groups while controlling for the effects of age and gender ($p < 0.05$, TFCE-FWE corrected).

Other Statistics

The Kolmogorov–Smirnov tests were first introduced to assess the normality of the variables, including the age, duration, neuro-ophthalmologic assessments, and ROI-wise MRI metrics. The type of ROI-wise MRI metrics was referred to group-wise differences in GMV and FC, including GMV of bilateral CG, and resting-state FC between the left superior occipital gyrus (SOG) and posterior cingulate gyrus. All variables except for the duration were normally distributed. Thus, paired *t*-test was used to test the statistical differences in neuro-ophthalmologic measures between the left and right eyes in the LHON ($p < 0.05$). A two-sample Student's *t*-test was used to test the intergroup differences in neuro-ophthalmologic measures and age ($p < 0.05$). A chi-squared test was used to test the intergroup differences in gender ($p < 0.05$). Finally, the Spearman (non-normality) or Pearson correlation (normality) was used to test the associations between clinical measures and MRI metrics ($p < 0.05$, Bonferroni correction). These statistics were carried out using the SPSS version 19 (https://www.ibm.com/analytics/spss-statistics-software).

RESULTS

Demographic and Clinical Measurements

As shown in **Table 1**, there were no statistical differences in either age (Student's *t*-test, $t = -0.910$, $p = 0.177$) or genders (chi-squared test, $\chi^2 = 0.925$, $p = 0.393$) between the chronic LHON and HC. For the LHON, the duration of visual loss ranged from 13 to 409 months for both eyes. The paired *t*-test showed no statistical differences in mean peripapillary RNFL thickness ($t = 0.824$, $p = 0.417$) and MD_{VF} ($t = 1.662$, $p = 0.107$) between the left and right eyes. Thus, these clinical measures of bilateral eyes were merged for further statistics. Compared with the HC, the Student's *t*-test identified significantly thinner peripapillary RNFL ($t = -16.42$, $p < 0.001$) and higher MD_{VF} ($t = 11.28$, $p < 0.001$) in the chronic LHON.

Intergroup Differences in Neuroimaging Measurements

Compared with the HCs, VBM analysis showed that chronic LHON had significantly lower GMV in the bilateral CG (non-parametric permutation test, $p < 0.05$, TFCE-FWE corrected) (**Figure 1A**, **Table 2**). In addition, VBM analysis showed that chronic LHON had significantly lower WMV in the bilateral optic tracts and optic radiations, and left LGN than those of the HCs (non-parametric permutation test, $p < 0.05$, TFCE-FWE corrected), as shown in **Figure 1B**, **Table 2**. We then defined the ROIs with changed GMV as seeds (left CG and right CG) and then calculated their FC at a voxel-wise level. Voxel-wise non-parametric permutation test identified that the LHON had significantly lower FC between the left CG and ipsilateral SOG and higher FC between left CG and the ipsilateral posterior cingulate gyrus (posterior cingulate cortex [PCC]) ($p < 0.05$, TFCE-FWE corrected) (**Figure 2**, **Table 2**).

Associations Between Neuroimaging Findings and Clinical Measures

The Spearman correlation showed that the GMV of the left CG was negatively correlated with the LHON duration ($r = -0.535$, $p = 0.002$, Bonferroni corrected) (**Figure 3A**). The Pearson correlation identified a negative correlation between the FC of left CG with ipsilateral PCC and the peripapillary RNFL thickness in the chronic LHON ($r = -0.522$, $p = 0.003$, Bonferroni corrected) (**Figure 3B**). There were no statistical differences between the remaining neuroimaging findings and clinical measures ($p > 0.05$).

DISCUSSION

In this study, we aimed to elucidate if the atrophy of the visual cortex in the chronic LHON would cause FC reorganization in the remote brain areas. We found that the GMV of bilateral CGs was significantly lower than the HCs. Taking these atrophied areas as seeds, we further found that the left CG had lower FC with the ipsilateral SOG and had higher FC with the ipsilateral PCC. Finally, besides the negative correlation between disease duration and GMV of left CG, we found a significantly negative correlation between the peripapillary RNFL thickness and the enhanced left CG-PCC FC in the chronic LHON. These findings indicate that the functional organization of the primary visual cortex has been reshaped in the chronic LHON.

Compared with HC subjects, we found that the patients with chronic LHON exhibited decreased GMV in bilateral CGs, which is consistent with the early studies on albinism (von dem Hagen et al., 2005), amblyopia (Mendola et al., 2005), LHON (Barcella et al., 2010), and retinal damage (Kitajima et al., 1997; Boucard et al., 2009). Similar to the LHON, reduced GMV of the visual cortex was also present in the blind people according to visual deprivation (Noppeney et al., 2005; Ptito et al., 2008; Qin et al., 2013; Yang et al., 2014; Jiang et al., 2015). Except for the results of reduced GMV of the primary visual cortex, previous neuroimaging studies have also reported decreased WMV and impaired WM integrity in the optic radiation in the blind and LHON individuals (Barcella et al., 2010; Milesi et al., 2012; Rizzo et al., 2012; Ogawa et al., 2014; Manners et al., 2015). Our study was also consistent with the previous findings, showing decreased fractional anisotropy of the optic radiations in the LHON (Wang et al., 2021). The reduced WMV of LGN and the atrophy of bilateral optic tracts were found in the patients with chronic LHON. In combination with the GM and WM atrophy of the primary visual cortex found in our results, the structural atrophy along the retinofugal pathway may be explained by downstream secondary transneuronal degeneration after the primary involvement of the RGCs in the chronic LHON.

The between-group comparison showed a lower FC between the left CG and the ipsilateral SOG, which might reflect a functional disconnection between the visual cortices in the visual network. As is known, LHON is characterized as RGC

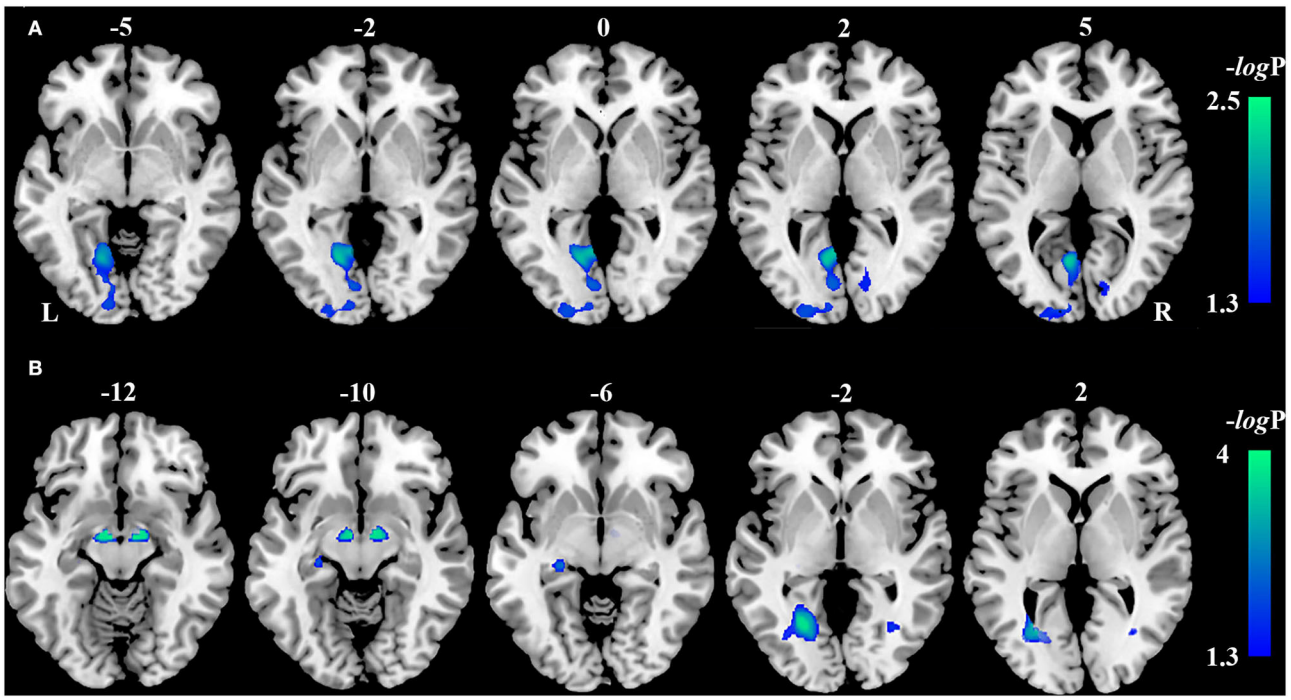

FIGURE 1 | Inter-group differences in gray matter volume (GMV) and white matter volume. **(A)** The difference in GMV between the LHON and HC was tested using a voxel-wise non-parametric permutation test corrected for age and gender ($p < 0.05$, TFCE-FWE corrected). Chronic LHON had significantly lower GMV in the bilateral CG than in the HC (cool color). **(B)** The difference in WMV between the LHON and HC was tested using a voxel-wise non-parametric permutation test corrected for age and gender ($p < 0.05$, TFCE-FWE corrected). Chronic LHON had significantly lower WMV in the bilateral OR, bilateral OT, and left LGN than in the HC (cool color). Color bar represents the -log(p) value. CG, calcarine gyrus; FWE, family-wise error; GMV, gray matter volume; HC, healthy controls; LGN, lateral geniculate nucleus; LHON, Leber's hereditary optic neuropathy; OR, optic radiation; OT, optic tract; TFCE, threshold-free cluster enhancement; WMV, white matter volume.

TABLE 2 | Intergroup differences in gray matter volume, white matter volume and functional connectivity.

Metric	Brain region	Cluster size (ml)	Peak MNI coordinates			*−log10*(p)
			x	y	z	
GMV	Left CG	7.55	−10.5	−66	3	2.28
	Right CG	0.71	13.5	−79.5	0	1.48
WMV	Left OR	1.05	−28.5	−64.5	0	3.70
	Right OR	0.18	34.5	−66	0	2.09
	Left OT	0.20	−13.5	−9	−12	3.70
	Right OT	0.22	6	−9	−10.5	3.70
	Left LGN	0.18	−25.5	−25.5	−7.5	2.80
FC(left CG)	Left SOG	0.32	−12	−96	3	1.43
	Left PCC	1.76	−9	−42	39	1.80

p values are corrected using TFCE-FWE method. FC, functional connectivity; CG, calcarine gyrus; FEW, family-wise error; GMV, gray matter volume; HC, healthy controls; LGN, lateral geniculate nucleus; LHON, Leber hereditary optic neuropathy; OR, optic radiation; OT, optic tract; PCC, posterior cingulate cortex; SOG, superior occipital gyrus; TFCE, threshold-free cluster enhancement; WMV, white matter volume.

degeneration, finally leading to central vision loss (Carelli et al., 2004; Yu-Wai-Man et al., 2009; Giordano et al., 2011). The central vision loss was associated with functional damage to the visual cortex, which is likely secondary to RGC degeneration. Many previous studies have shown FC reduction between the visual cortical areas in patients with amblyopia (Mendola et al., 2018), diabetic retinopathy (Cheng et al., 2021), and retinal damage (Dai et al., 2013), although the coexistence of increased and decreased FC in the visual cortex was also reported (Rocca et al., 2011; Qin et al., 2013). In addition, several studies have reported the degeneration of the visual pathway and the visual cortex after visual deprivation, including a reduced fractional anisotropy in optic radiations (Wang et al., 2013), decreased FC between the visual cortices (Liu et al., 2007), and a decreased FC

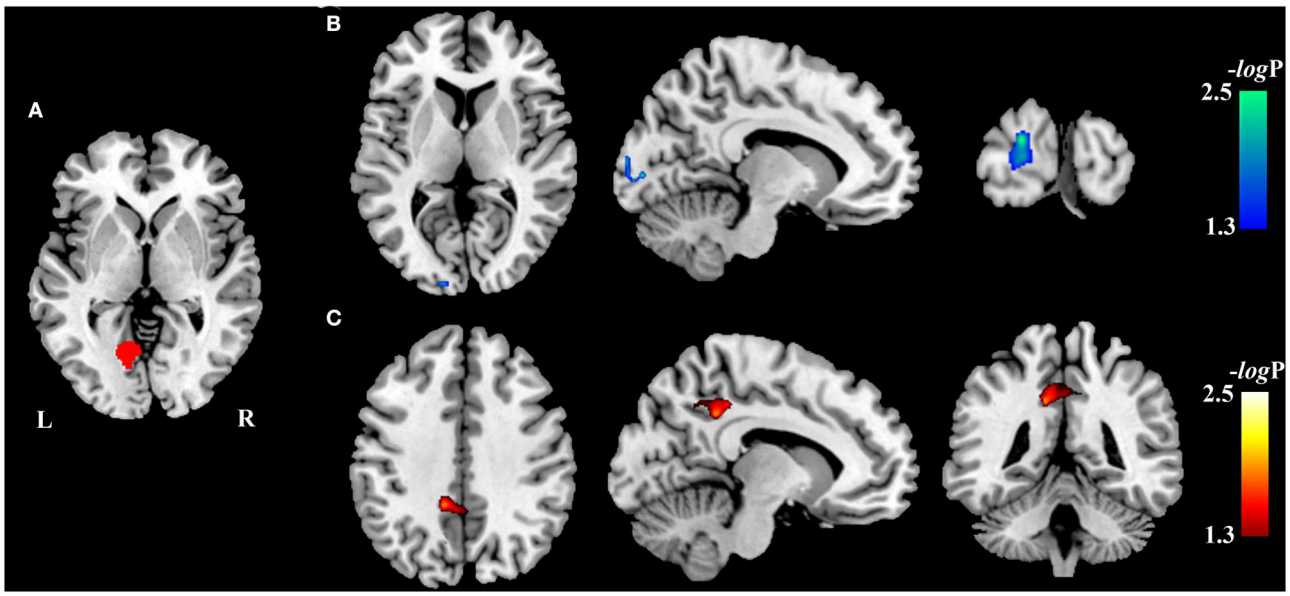

FIGURE 2 | Inter-group differences in resting-state functional connectivity. The difference in FC between the chronic LHON and HC was test using a voxel-wise non-parametric permutation test corrected for age and gender ($p < 0.05$, TFCE-FWE corrected). Color bar represents the -log10(p) value. **(A)** Seeds (left CG) used to calculate the FC, **(B)** brain region (left SOG, cool color) having lower FC with the left CG in the chronic LHON, and **(C)** brain region (left PCC, warm color) having higher FC with the left CG. CG, calcarine gyrus; FC, functional connectivity; FWE, family-wise error; HC, healthy controls; LHON, Leber's hereditary optic neuropathy; PCC, posterior cingulate cortex; SOG, superior occipital gyrus; TFCE, threshold-free cluster enhancement.

density in V1. In combination with the results of these previous studies, we speculated that the degenerative mechanisms may account for functional disconnectivity between the left CG and the ipsilateral SOG in the patients with chronic LHON.

In addition, the most interesting result of our findings was the left CG of the patients with chronic LHON had higher FC with the ipsilateral PCC than the sighted controls. The result was consistent with the previous findings, showing enhanced FC between the PCC and primary visual cortex in patients with type 2 diabetes mellitus (T2DM) (Cheng et al., 2021), increased FC density of the PCC in subjects with peripheral visual deprivation at the late age (Qin et al., 2015), and strengthened FC between the PCC and auditory cortex in the deafness (Malaia et al., 2014). Additional correlation analysis showed that the peripapillary RNFL thickness was negatively correlated to the enhanced FC between the left CG and PCC in the chronic LHON, indicating that more severe visual impairment would cause higher FC enhancement, in line with a prior study, showing patients with T2DM had a positive association between the PCC-calcarine FC and HbA1c, a blood indicator on the severity of T2DM (Cheng et al., 2021). Thus, these studies implied that long-term sensory impairment would remold the FC between the PCC and the deprived sensory area. As indicated by Kravitz et al., the dorsal visual stream can be separated into three major branches outside the occipital areas, including the visual-parieto–prefrontal pathway that mainly processes spatial working memory, the visual-parieto–premotor pathway that participants in visually guided action, and the visual-parieto–medial temporal pathway that is involved in spatial navigation (Kravitz et al., 2011). As a core hub of the visual-parieto–medial temporal pathway, the PCC has been indicated as an important relay between the visual cortex and hippocampus/medial temporal lobe to transport both bottom-up and top-down signals. An early study reported that blind people had increased FC between the posterior hippocampal subregions and PCC (Ma et al., 2016). In cooperation with the findings of enhanced FC between the PCC and deprived visual area, we speculated that top-down neural mechanism might account for functional remodeling of the FC between PCC and visual cortex in the chronic LHON through the dorsal visual stream. Further studies may be preferable to obtain direct evidence using the classical and specific cognitive tasks.

Based on the significant structural impairment of both the GM and WM of the visual cortex and strengthened FC between the PCC and the impaired visual area in patients with chronic LHON, recent studies have reported that the vision of the LHON patients can be restored through gene therapy (Sundaramurthy et al., 2021), and reversing blindness with gene therapy promotes long-term structural plasticity in the visual pathways of Leber's congenital amaurosis (Ashtari et al., 2015). The visual areas with atrophied GM or WM found in this study would be considered as potential targets to evaluate and monitor the therapeutic effects. However, chronic visual deprivation would cause secondary degeneration along the visual pathway, which may hinder the restoration of the visual function even when the frontier visual pathway (e.g., the RGC and optic nerves) is repaired. Thus, it is expected to introduce gene therapy as early as possible. Finally, as reported by early studies, cross-modal plasticity may be maladaptive for sight restoration. They reported persisting cross-modal changes in sight-recovery

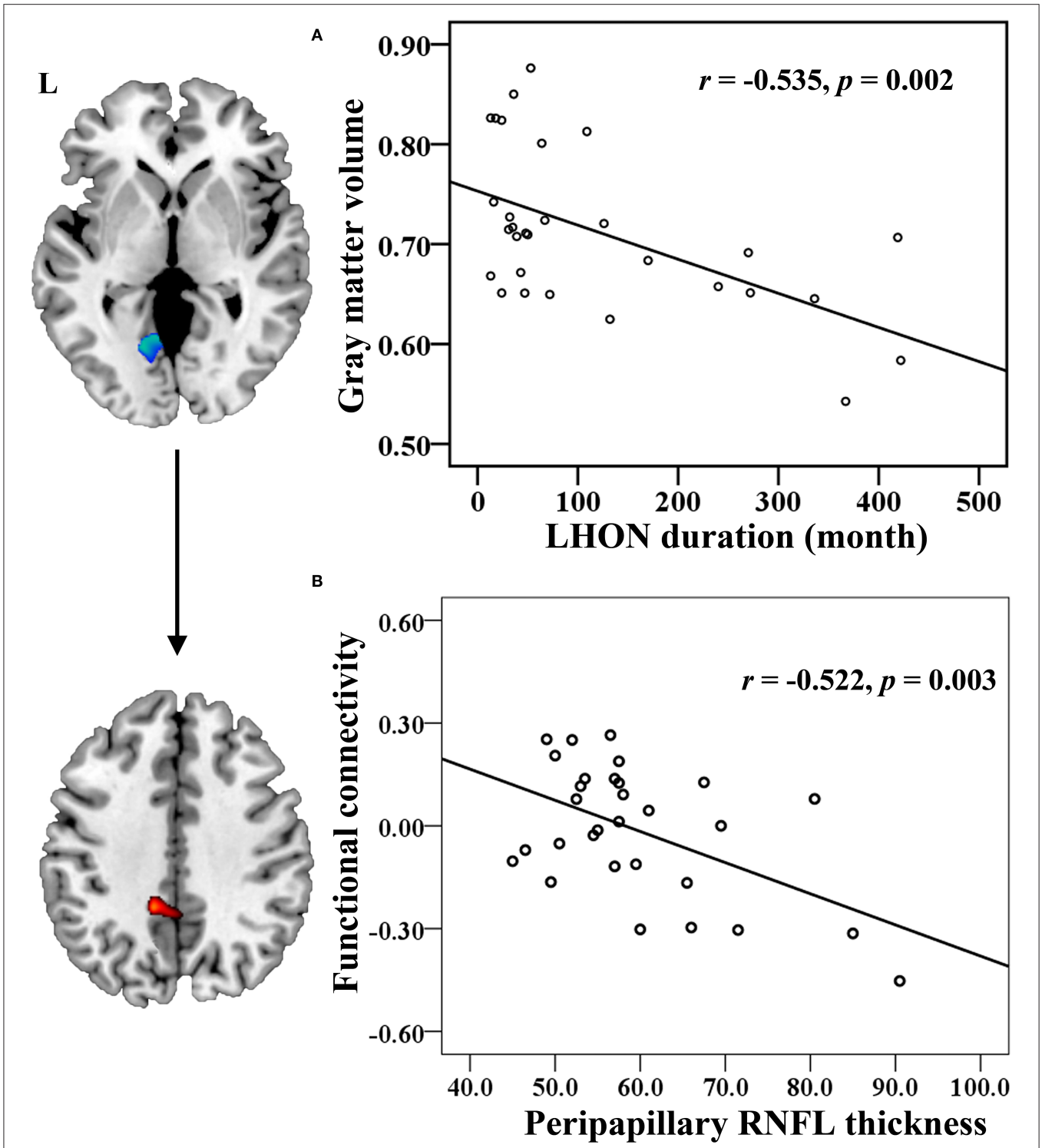

FIGURE 3 | Correlation between the neuroimaging findings and clinical measures in the chronic LHON. **(A)** Spearman correlation coefficient was used to test the association between LHON duration and GMV of left CG, and **(B)** Pearson correlation coefficient was used to test that between peripapillary RNFL thickness and FC between the left CG and left PCC ($p < 0.05$, Bonferroni correction). CG, calcarine gyrus; FC, functional connectivity; GMV, gray matter volume; LHON, Leber's hereditary optic neuropathy; PCC, posterior cingulate cortex; RNFL, retinal nerve fiber layer.

individuals with congenital cataracts (Guerreiro et al., 2016), and limited recovery of the visual function in sight-restored subjects (Fine et al., 2003; McKyton et al., 2015). The enhanced FC between the PCC and visual cortex in chronic LHON may be considered an indicator for the restoration of functional plasticity after therapy.

CONCLUSION

In this study, we found that the GMV of bilateral CGs was atrophied in the chronic LHON. Moreover, the atrophied primary visual cortex was accompanied by functional dysconnectivity with ipsilateral SOG and strengthened connectivity with the default mode network. These findings indicate that the functional organization of the primary visual cortex has been reshaped in the chronic LHON.

DATA AVAILABILITY STATEMENT

The raw data supporting the conclusions of this article will be made available by the authors, without undue reservation.

ETHICS STATEMENT

The studies involving human participants were reviewed and approved by the Ethics Committee of Henan Provincial People's Hospital. The patients/participants provided their written informed consent to participate in this study.

AUTHOR CONTRIBUTIONS

QT designed the study, collected the data, and drafted this article. LW and YZ analyzed the data and visualized result. KF collected the data and revised draft. ML analyzed the data. DS collected the data, supervised the project, and revised the draft. WQ designed the study and revised the draft. HD designed the study, analyzed the data, drafted, and revised this article. All authors contributed to the article and approved the submitted version.

FUNDING

This study was supported by the Natural Science Foundation of China (81971599, 81771818, 81571659, 81271534, and 81601473), the Natural Science Foundation of Tianjin City (19JCYBJC25100 and 17JCYBJC29200), the Postdoctoral Research Foundation of China (2017M611175), and the Science & Technology Development Fund of Tianjin Education Commission for Higher Education (2020KJ207).

REFERENCES

Ashtari, M., Zhang, H., Cook, P. A., Cyckowski, L. L., Shindler, K. S., Marshall, K. A., et al. (2015). Plasticity of the human visual system after retinal gene therapy in patients with Leber's congenital amaurosis. *Sci. Transl. Med.* 7, 296ra110. doi: 10.1126/scitranslmed.aaa8791

Barcella, V., Rocca, M. A., Bianchi-Marzoli, S., Milesi, J., Melzi, L., Falini, A., et al. (2010). Evidence for retrochiasmatic tissue loss in Leber's hereditary optic neuropathy. *Hum. Brain Mapp.* 31, 1900–1906. doi: 10.1002/hbm.20985

Boucard, C. C., Hernowo, A. T., Maguire, R. P., Jansonius, N. M., Roerdink, J. B., Hooymans, J. M., et al. (2009). Changes in cortical grey matter density associated with long-standing retinal visual field defects. *Brain* 132, 1898–1906. doi: 10.1093/brain/awp119

Carelli, V., Ross-Cisneros, F. N., and Sadun, A. A. (2004). Mitochondrial dysfunction as a cause of optic neuropathies. *Prog. Retin. Eye Re.s* 23, 53–89. doi: 10.1016/j.preteyeres.2003.10.003

Cheng, P., Song, S., Li, Y., Zhang, Y., Yi, J., Xu, X., et al. (2021). Aberrant functional connectivity of the posterior cingulate cortex in type 2 diabetes without cognitive impairment and microvascular complications. *Front. Endocrinol.* 12, 722861. doi: 10.3389/fendo.2021.722861

Dai, H., Morelli, J. N., Ai, F., Yin, D., Hu, C., Xu, D., et al. (2013). Resting-state functional MRI: functional connectivity analysis of the visual cortex in primary open-angle glaucoma patients. *Hum. Brain Mapp.* 34, 2455–2463. doi: 10.1002/hbm.22079

d'Almeida, O. C., Mateus, C., Reis, A., Grazina, M. M., and Castelo-Branco, M. (2013). Long term cortical plasticity in visual retinotopic areas in humans with silent retinal ganglion cell loss. *Neuroimage* 81, 222–230. doi: 10.1016/j.neuroimage.2013.05.032

Fine, I., Wade, A. R., Brewer, A. A., May, M. G., Goodman, D. F., Boynton, G. M., et al. (2003). Long-term deprivation affects visual perception and cortex. *Nat. Neurosci.* 6, 915–916. doi: 10.1038/nn1102

Giordano, C., Montopoli, M., Perli, E., Orlandi, M., Fantin, M., Ross-Cisneros, F. N., et al. (2011). Oestrogens ameliorate mitochondrial dysfunction in Leber's hereditary optic neuropathy. *Brain* 134, 220–234. doi: 10.1093/brain/awq276

Guerreiro, M. J. S., Putzar, L., and Roder, B. (2016). Persisting cross-modal changes in sight-recovery individuals modulate visual perception. *Curr. Biol.* 26, 3096–3100. doi: 10.1016/j.cub.2016.08.069

Jiang, A., Tian, J., Li, R., Liu, Y., Jiang, T., Qin, W., et al. (2015). Alterations of regional spontaneous brain activity and gray matter volume in the blind. *Neural. Plast.* 2015, 141950. doi: 10.1155/2015/141950

Kitajima, M., Korogi, Y., Hirai, T., Hamatake, S., Ikushima, I., Sugahara, T., et al. (1997). MR changes in the calcarine area resulting from retinal degeneration. *AJNR Am. J. Neuroradiol.* 18, 1291–1295.

Kravitz, D. J., Saleem, K. S., Baker, C. I., and Mishkin, M. (2011). A new neural framework for visuospatial processing. *Nat. Rev. Neurosci.* 12, 217–230. doi: 10.1038/nrn3008

Li, Y., Zhang, C., Hou, C., Yao, L., Zhang, J., and Long, Z. (2017). Stereoscopic processing of crossed and uncrossed disparities in the human visual cortex. *BMC Neurosci.* 18, 80. doi: 10.1186/s12868-017-0395-7

Liu, Y., Yu, C., Liang, M., Li, J., Tian, L., Zhou, Y., et al. (2007). Whole brain functional connectivity in the early blind. *Brain* 130, 2085–2096. doi: 10.1093/brain/awm121

Ma, G., Yang, D., Qin, W., Liu, Y., Jiang, T., and Yu, C. (2016). Enhanced functional coupling of hippocampal sub-regions in congenitally and late blind subjects. *Front. Neurosci.* 10, 612. doi: 10.3389/fnins.2016.00612

Malaia, E., Talavage, T. M., and Wilbur, R. B. (2014). Functional connectivity in task-negative network of the Deaf: effects of sign language experience. *PeerJ.* 2, e446. doi: 10.7717/peerj.446

Manners, D. N., Rizzo, G., La Morgia, C., Tonon, C., Testa, C., Barboni, P., et al. (2015). Diffusion Tensor Imaging Mapping of Brain White Matter Pathology in Mitochondrial Optic Neuropathies. *AJNR Am. J. Neuroradiol.* 36, 1259–1265. doi: 10.3174/ajnr.A4272

Mateus, C., d'Almeida, O. C., Reis, A., Silva, E., and Castelo-Branco, M. (2016). Genetically induced impairment of retinal ganglion cells at the axonal level is linked to extrastriate cortical plasticity. *Brain Struct. Funct.* 221, 1767–1780. doi: 10.1007/s00429-015-1002-2

McKyton, A., Ben-Zion, I., Doron, R., and Zohary, E. (2015). The limits of shape recognition following late emergence from blindness. *Curr. Biol.* 25:2373–8. doi: 10.1016/j.cub.2015.06.040

Mendola, J. D., Conner, I. P., Roy, A., Chan, S. T., Schwartz, T. L., Odom, J. V., et al. (2005). Voxel-based analysis of MRI detects abnormal visual cortex in children and adults with amblyopia. *Hum. Brain Mapp.* 25, 222–236. doi: 10.1002/hbm.20109

Mendola, J. D., Lam, J., Rosenstein, M., Lewis, L. B., and Shmuel, A. (2018). Partial correlation analysis reveals abnormal retinotopically organized functional connectivity of visual areas in amblyopia. *Neuroimage Clin.* 18, 192–201. doi: 10.1016/j.nicl.2018.01.022

Milesi, J., Rocca, M. A., Bianchi-Marzoli, S., Petrolini, M., Pagani, E., Falini, A., et al. (2012). Patterns of white matter diffusivity abnormalities in Leber's

hereditary optic neuropathy: a tract-based spatial statistics study. *J. Neurol.* 259, 1801–1807. doi: 10.1007/s00415-011-6406-1

Niedtfeld, I., Schulze, L., Kirsch, P., Herpertz, S. C., Bohus, M., and Schmahl, C. (2010). Affect regulation and pain in borderline personality disorder: a possible link to the understanding of self-injury. *Biol. Psychiat.* 68, 383–391. doi: 10.1016/j.biopsych.2010.04.015

Noppeney, U., Friston, K. J., Ashburner, J., Frackowiak, R., and Price, C. J. (2005). Early visual deprivation induces structural plasticity in gray and white matter. *Curr. Biol.* 15, R488–490. doi: 10.1016/j.cub.2005.06.053

Ogawa, S., Takemura, H., Horiguchi, H., Terao, M., Haji, T., Pestilli, F., et al. (2014). White matter consequences of retinal receptor and ganglion cell damage. *Invest. Ophthalmol. Vis. Sci.* 55, 6976–6986. doi: 10.1167/iovs.14-14737

Ollinger, J. M., Corbetta, M., and Shulman, G. L. (2001). Separating processes within a trial in event-related functional MRI. *Neuroimage* 13, 218–229. doi: 10.1006/nimg.2000.0711

Poldrack, R. A. (2007). Region of interest analysis for fMRI. *Soc. Cogn. Affect Neurosci.* 2, 67–70. doi: 10.1093/scan/nsm006

Ptito, M., Schneider, F. C., Paulson, O. B., and Kupers, R. (2008). Alterations of the visual pathways in congenital blindness. *Exp. Brain Res.* 187, 41–49. doi: 10.1007/s00221-008-1273-4

Qin, W., Liu, Y., Jiang, T., and Yu, C. (2013). The development of visual areas depends differently on visual experience. *PLoS ONE.* 8, e53784. doi: 10.1371/journal.pone.0053784

Qin, W., Xuan, Y., Liu, Y., Jiang, T., and Yu, C. (2015). Functional connectivity density in congenitally and late blind subjects. *Cereb. Cortex.* 25, 2507–2516. doi: 10.1093/cercor/bhu051

Rizzo, G., Tozer, K. R., Tonon, C., Manners, D., Testa, C., Malucelli, E., et al. (2012). Secondary post-geniculate involvement in Leber's hereditary optic neuropathy. *PLoS ONE.* 7, e50230. doi: 10.1371/journal.pone.0050230

Rocca, M. A., Valsasina, P., Pagani, E., Bianchi-Marzoli, S., Milesi, J., Falini, A., et al. (2011). Extra-visual functional and structural connection abnormalities in Leber's hereditary optic neuropathy. *PLoS ONE.* 6, e17081. doi: 10.1371/journal.pone.0017081

Shulman, G. L., Astafiev, S. V., Franke, D., Pope, D. L., Snyder, A. Z., McAvoy, M. P., et al. (2009). Interaction of stimulus-driven reorienting and expectation in ventral and dorsal frontoparietal and basal ganglia-cortical networks. *J. Neurosci.* 29, 4392–4407. doi: 10.1523/JNEUROSCI.5609-08.2009

Sundaramurthy, S., SelvaKumar, A., Ching, J., Dharani, V., Sarangapani, S., and Yu-Wai-Man, P. (2021). Leber hereditary optic neuropathy-new insights and old challenges. *Graefes Arch. Clin. Exp. Ophthalmol.* 259, 2461–2472. doi: 10.1007/s00417-020-04993-1

Takemura, H., Ogawa, S., Mezer, A. A., Horiguchi, H., Miyazaki, A., Matsumoto, K., et al. (2019). Diffusivity and quantitative T1 profile of human visual white matter tracts after retinal ganglion cell damage. *Neuroimage Clin.* 23, 101826. doi: 10.1016/j.nicl.2019.101826

von dem Hagen, E. A., Houston, G. C., Hoffmann, M. B., Jeffery, G., and Morland, A. B. (2005). Retinal abnormalities in human albinism translate into a reduction of grey matter in the occipital cortex. *Eur. J. Neurosci.* 22, 2475–2480. doi: 10.1111/j.1460-9568.2005.04433.x

Wang, D., Qin, W., Liu, Y., Zhang, Y., Jiang, T., and Yu, C. (2013). Altered white matter integrity in the congenital and late blind people. *Neural. Plast.* 2013, 128236. doi: 10.1155/2013/128236

Wang, L., Ding, H., Chen, B. T., Fan, K., Tian, Q., Long, M., et al. (2021). Occult primary white matter impairment in Leber hereditary optic neuropathy. *Eur. J. Neurol.* 28, 2871–2881. doi: 10.1111/ene.14995

Yang, C., Wu, S., Lu, W., Bai, Y., and Gao, H. (2014). Anatomic differences in early blindness: a deformation-based morphometry MRI study. *J. Neuroimag.* 24, 68–73. doi: 10.1111/j.1552-6569.2011.00686.x

Yu-Wai-Man, P., Griffiths, P. G., Hudson, G., and Chinnery, P. F. (2009). Inherited mitochondrial optic neuropathies. *J. Med. Genet.* 46, 145–158. doi: 10.1136/jmg.2007.054270

Zhou, Z. W., Lan, X. Q., Fang, Y. T., Gong, Y., Zang, Y. F., Luo, H., et al. (2019). The inter-regional connectivity within the default mode network during the attentional processes of internal focus and external focus: an fMRI study of continuous finger force feedback. *Front. Psychol.* 10, 2198. doi: 10.3389/fpsyg.2019.02198

Conflict of Interest: The authors declare that the research was conducted in the absence of any commercial or financial relationships that could be construed as a potential conflict of interest.

Publisher's Note: All claims expressed in this article are solely those of the authors and do not necessarily represent those of their affiliated organizations, or those of the publisher, the editors and the reviewers. Any product that may be evaluated in this article, or claim that may be made by its manufacturer, is not guaranteed or endorsed by the publisher.

Advantages of publishing in Frontiers

OPEN ACCESS
Articles are free to read for greatest visibility and readership

FAST PUBLICATION
Around 90 days from submission to decision

HIGH QUALITY PEER-REVIEW
Rigorous, collaborative, and constructive peer-review

TRANSPARENT PEER-REVIEW
Editors and reviewers acknowledged by name on published articles

Frontiers
Avenue du Tribunal-Fédéral 34
1005 Lausanne | Switzerland

Visit us: www.frontiersin.org
Contact us: frontiersin.org/about/contact

REPRODUCIBILITY OF RESEARCH
Support open data and methods to enhance research reproducibility

DIGITAL PUBLISHING
Articles designed for optimal readership across devices

FOLLOW US
@frontiersin

IMPACT METRICS
Advanced article metrics track visibility across digital media

EXTENSIVE PROMOTION
Marketing and promotion of impactful research

LOOP RESEARCH NETWORK
Our network increases your article's readership